Etudes par RMN de mécanismes de régulation de la biosynthèse de la paroi bactérienne

Nicolas L Jean

UNIVERSITÉ GRENOBLE ALPES

THÈSE

Pour obtenir le grade de

DOCTEUR DE L'UNIVERSITÉ GRENOBLE ALPES

Spécialité : **Biologie structurale et Nanobiologie**

Arrêté ministériel : 7 août 2006

Présentée par

Nicolas JEAN

Thèse dirigée par **Jean-Pierre SIMORRE** et
codirigée par **Catherine BOUGAULT**

préparée au sein du **groupe de RMN Biomoléculaire, Institut de Biologie Structurale**
dans **l'École Doctorale Chimie et Sciences du Vivant**

Études par RMN de mécanismes de régulation de la biosynthèse de la paroi bactérienne.

Thèse soutenue publiquement le **17 Novembre 2015**,
devant le jury composé de :

Dr. Anne IMBERTY
Directrice de recherche, Centre de Recherche sur les Macromolécules Végétales, Grenoble, Présidente du jury
Dr. Rut CARBALLIDO-LÓPEZ
Directrice de recherche, Institut Micalis, Jouy-en-Josas, Rapporteur
Dr. Sophie ZINN-JUSTIN
Directrice de recherche, Institut de Biologie Intégrative de la Cellule, Gif-sur-Yvette, Rapporteur
Dr. Christophe GRANGEASSE
Directeur de recherche, Institut de Biologie et Chimie des Protéines, Lyon, Examinateur
Pr. Waldemar VOLLMER
Professeur, Université de Newcastle, Examinateur
Dr. Jean-Pierre SIMORRE
Directeur de recherche, Institut de Biologie Structurale, Directeur de thèse
Dr. Catherine BOUGAULT
Maître de conférences, Université Joseph Fourier de Grenoble, Co-encadrante

Acknowledgments

To begin with, I would like to thank the two people who supervised my work during more than three years, Jean-Pierre and Catherine. Thank you for your availability and your kindness. Jean-Pierre, thank you very much for giving me the opportunity to work with you and for your vision of the subject. Thank you also for keeping me focused and efficient, when I was heading in too many directions. If I went that far, it is also thanks to Catherine, which in addition to be my co-supervisor, was an excellent teacher whose determination and teaching skills helped me a lot to improve my oral skills and my writing abilities. I was very lucky to have such good supervisors who taught me so many things, which will be very useful in the coming years to pursue in research.

I am grateful to the whole NMR group, which contributed a lot to my blossoming during this thesis. First, I would like to thank Jérôme for its management of the group, which must not be an easy task when it is constituted by a total of ~ 25 people! I would like to thank Dominique, Paul and Sergio for all the time they dedicated to us, PhD students and post-docs, to teach us patiently NMR theory basics and to be attentive at our questions. I would also like to thank Adrien and Bernhard for all their essential work on spectrometers to create a user-friendly interface, time-saving scripts and the implementation of improved pulse sequences, which played a lot in the recording of spectra with good signal-to-noise ratio. A big thank to you Isabel, who trained me in producing labeled samples and was always, with a smile, answering my interrogations. My thanks to Beate and Cedric for their wise advice on the NMR data analysis software CcpNMR, and on structure calculation, validation and modeling. Without you, structure determination during this thesis would have taken much more time. I would like also to thank those whom I share the office with, particularly since our moving in the Automn 2013, Audrey (thanks for bearing me all of these months!), Karine, Nicholus, Peixiang, Rida (thanks to you, I was rarely the only one in the office at the end of the day), Roberto and *last but not least* Vilius (thank you for your countless friendly jokes!). I will not forget also the other internship and PhD students and post-docs with whom I shared enjoyable times, especially Caroline, Diego, Elisa, Emmanuelle, Guillaume, Hugo, Jia-Ying, Katharina, Lauriane, Mathieu, Rime and Zsofia. I would like also to thank the other members of our group for their good mood, which contributed a lot to the pleasant atmosphere in the lab.

This thesis was also the opportunity to work with Waldemar Vollmer (Newcastle) and Christophe Grangeasse (Lyon). I would like to thank them for the access to unpublished results that they offered during this work and for the enthralling discussions I had with them on peptidoglycan synthesis and cell division. A special thank also to Waldemar and his team (in particular Alex) for their warm welcome in Newcastle during the summer 2014 and for the production of essential NMR samples. I would like also to acknowledge Christophe, Mégane and Sylvie for this nice collaboration, that started last year on MapZ, and the efficient preparations of protein and peptidoglycan. Sylvie, who would have bet, seven years ago, when we were in “L2”, that we will end up working together during our thesis?!

Because they gave me the opportunity to work on this fascinating topic, I would like to acknowledge my funding agencies, the CEA for my 3-year PhD fellowship from the Irtelis program and my 2-month extension by the ANR, through Christophe. Thank you also to the University Joseph Fourier for the grant, which allowed me to work 2 months in Newcastle.

I would like also to sincerely thank the people who accepted to be part of the jury examining this work, Anne Imberty, Christophe Grangeasse and Waldemar Vollmer, and especially my two *rapporteurs*, Rut Carballido-López and Sophie Zinn-Justin for accepting to evaluate it.

Finally, I would like to thank my family for their constant encouragements to study what I wanted and for their support during these three years as well as my friends, especially Achraf, Clément, Delphine, Jérémy, Matthieu, Pan, Sarah and Yoann, for all the good moments we have shared since the university.

General introduction

The use of antibiotics is one of the main strategy to fight bacterial infections. One of the most attractive targets to date has been the bacterial cell envelope, and more especially the biosynthesis of the essential peptidoglycan layer, which surrounds and shapes the bacterial cell in addition to help to support the internal osmotic pressure. However, for several decades bacteria have been developing resistance to several of these drugs (such as penicillin derivatives for example), making the research of new molecules and targets essential. This goal requires first a deep comprehension of how peptidoglycan is generated and of how its growth is spatio-temporally regulated. Indeed, in bacteria like *Escherichia coli* and *Streptococcus pneumoniae*, some peptidoglycan is first synthesized at the lateral wall during cell elongation, before production at mid-cell during division. Second, because structural biology focuses on the atomic scale, it is a powerful tool to decipher the role of biomacromolecules and how they interact with each other in this context.

The work presented here focuses on the regulation of peptidoglycan synthesis dealing with the stimulation of bifunctional peptidoglycan synthases PBP1A and PBP1B by LpoA and LpoB, respectively, in *E. coli.* Due to the poor characterization of these 2 proteins at the atomic level, I used Nuclear Magnetic Resonance (NMR) spectroscopy to determine high-resolution structures, and study their dynamics and some interactions to get a better understanding of their function.

To begin with, an introduction on peptidoglycan summarizes the main knowledge on this macromolecule (Part I). A presentation of this biopolymer (its localization in the cell, 3D architecture and molecular composition) in Chapter 1 is followed by a description of its synthesis, from the generation of its precursors in the cytoplasm to their assembly in the periplasm / extracellular domain (Chapter 2). The peptidoglycan newly synthesized is not inert, but matures through hydrolysis and various modifications, before entering a recycling pathway. These processes are addressed in Chapter 3. Next, two main protein machineries are detailed, which spatio-temporally control the peptidoglycan growth during the two main bacterial cell cycle events, which are elongation and division (Chapter 4). Finally, Chapter 5 focuses on the NMR technique and its interest for the study of peptidoglycan and its related proteins.

Part II of this thesis focuses on the Lpo proteins, essential components of the two molecular complexes involved in peptidoglycan synthesis. After a summary of previous work in Chapter 1, results on LpoA and LpoB are described in Chapter 2 and 3, respectively, through 4 articles published in peer-reviewed journals and personal analyzes. The results present the 3D structures of these two proteins and postulate on their own strategy to interact with their PBP1 target.

Finally, these main results are resumed in a general conclusion, and perspectives on regulation of peptidoglycan synthases by Lpos is briefly discussed.

Contents

List of figures

List of tables

Abbreviations

AFM Atomic Force Microscopy

ADP Adenosine TriPhosphate

ATP Adenosine DiPhosphate

AUC Analytical UltraCentrifugation

CoA Co-enzyme A

CPMAS Cross-Polarization Magic-Angle Spinning

CSP Chemical Shift Perturbation

DNA DeoxyriboNucleic Acid

ECT Electron Cryo-Tomography

EM Electron Microscopy

FAD Flavin Adenine Dinucleotide

FDAA Fluorescent D-Amino Acid

FRET Förster Resonance Energy Transfer

GlcNAc N-Acetyl-Glucosamine

GT GlycosylTransferase

HADDOCK High Ambiguity Driven biomolecular DOCKing

HMW High Molecular Weight

HPLC High-Performance Liquid Chromatography

HSQC Heteronuclear Single Quantum Spectroscopy

Ldt L,D-transpeptidase

LMW Low molecular weight

LPS LipoPolySaccharide

LTA Lipoteichoic Acid

NOESY Nuclear Overhauser Effect correlation SpectroscopY

NCDAA Non-Canonical D-Amino-Acid

NMR Nuclear Magnetic Resonance

MS Mass Spectrometry

MurNAc N-acetyl Muramic acid

NADPH Dihydro-Nicotinamide Adenine Dinucleotide Phosphate

PBP Penicillin-Binding Protein

PEP PhosphoEnolPyruvate

PLP	Pyridoxal 5'-phosphate
RNA	RiboNucleic Acid
rMD	restraint Molecular Dynamics
SANS	Small Angle Neutron Scattering
SAXS	Small Angle X-ray Scattering
SEC-MALS	Size Exclusion-Chromatography – Multi-Angle Light Scattering
TP	TransPeptidase
UDP	Uridine DiPhosphate
UMP	Uridine MonoPhosphate
WTA	Wall Teichoic Acid

Part I
The bacterial cell wall: structure and biosynthesis

Chapter 1
Peptidoglycan as an essential bacterial component

1.A- Main characteristics of the bacterial cell

Bacteria are unicellular organisms which are spread in a wide variety of environments, from our gut (Modi et al., 2014) to the deepest layers of the oceanic crust (Mason et al., 2010). These organisms can adopt a wide variety of shapes, from cocci (the spherical *Staphylococcus aureus*), to bacilli (the rod-like *Escherichia coli*) or even spirilla (the helically coiled *Helicobacter pylori*). According to the classification by Carl Woese in 1990 (Woese et al., 1990), bacteria form one of the two domains which are constituted by prokaryotes (the second one being archaea). As such, bacteria do not have any nucleus and, with the exception of a few species, do not possess any membrane-delimited organelles, unlike eukaryotes. While the latter have a diameter extended usually from 10 to 100 µm, bacteria are in general one order of magnitude smaller, with a size comprised between 1 and 5 µm (although extreme cases exist, like *Thiomargarita namibiensis* which can be detected by naked eyes with a maximum diameter of 750 µm).

A schematic representation of the bacterial cell structure is shown in figure I.1.1, emphasizing on one side the 20- to 530-nm-thick cell envelope (cell wall and capsule) and on another side the cytoplasm, the two parts being delimited by a ~70-Å-thick plasma (or cytoplasmic) membrane which consists of a lipid bilayer containing embedded proteins.

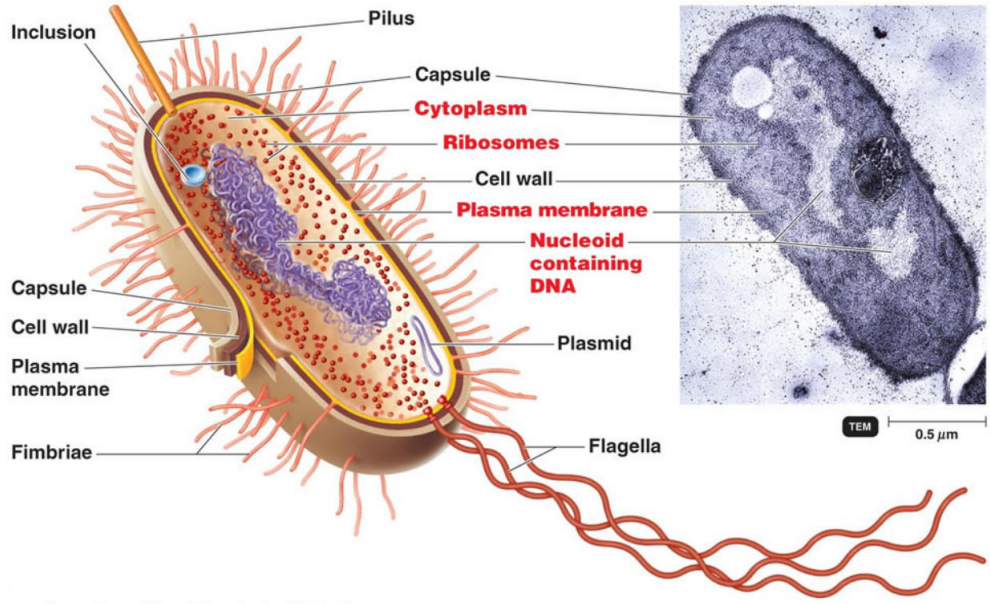

Figure I.1.1: Schematic representation of the bacterial cell. Taken from Tortora et al., 2012.

As bacteria do not have membrane-bound organelles, most of the metabolic reactions occur in the cytoplasm. It is also in this space that the genetic information, DeoxyriboNucleic Acid (DNA), is located. Bacterial DNA is usually present as a single, double-stranded,

circular chromosome. The cell is relatively small comparatively to its genetic material content (about 4.6 million of base pair for 4400 genes for the bacterial model *Escherichia coli*), it is therefore compacted by and with its interaction partners in a poorly defined region called the nucleoid. As there are no compartments in the bacterial cell, transcription of DNA in RiboNucleic Acid (RNA) can be coupled to translation into proteins. This last step is performed by 70S ribosomes (denominated from the value of their sedimentation rate by ultracentrifugation, in Svedberg), which are made of two subunits, 30S and 50S. Each of these is composed of ribosomal RNA (rRNA) complexed to numerous proteins. Interestingly, eukaryotic cells have 80S ribosomes with 40S and 60S subunits, which result from different assemblies. These structural divergences enable the specific targeting of the bacterial ribosome with antibiotics without perturbing the patient's cells. The genome can also be supplemented by one or more smaller circular DNA molecules called plasmids. Contrary to the bacterial chromosome, plasmids are not essential for cell survival but bring additional genes which can be an advantage to cope with environmental stress or to gain resistance (to antibiotics, bacteriophages, and/or chemicals...). This genetic material can be shared rapidly among bacteria by horizontal transfer to promote genetic diversity. This process can occur through three different mechanisms. Some bacteria have the faculty to naturally absorb fragments of DNA which are present in their environment. This competence is called transformation. They can also directly transfer genes from one to another through a sex pilus, an extended surface structure, by conjugation. Finally, genetic material can be acquired by transduction. In this case, DNA can be conveyed by a bacteriophage from a donor bacterium to a recipient cell.

Although the cytoplasm is lacking of complex internal structures, like a nucleus or a Golgi apparatus, bacteria can sometimes present other elementary compartments in addition to the nucleoid, for which a short and non-exhaustive selection is given here. Among them, thylakoids can be found in cyanobacteria, where they are formed by an ensemble of membranes. Similarly to those observed in chloroplasts, these are the home of photosynthesis and respiration processes. Another compartment involved in converting light into chemical energy is the chlorosome, which is bound to the neighboring cytoplasmic membrane in green sulfur bacteria. It contains large pigment assemblies which are absorbing photons with a very high efficiency to deal with poorly light exposed waters, where these cells are living (see Orf & Blankenship, 2013 for more details). Magnetotactic bacteria are characterized by the presence of magnetosomes, lipid bilayers enclosing each a single magnetic mineral such as magnetite (Fe_3O_4) or greigite (Fe_3S_4). The structure obtained is used as a guide for bacteria to follow passively the magnetic field, which may enable these microaerophilic cells (organisms for which oxygen is essential to survive but toxic at atmospheric levels) to find more easily a suitable habitat (for a recent review, see Lower & Bazylinski, 2013). Bacterial organelles can also be only formed by proteins as carboxysomes in cyanobacteria and some other species. These microbodies constitute a shell to likely confine CO_2 and its fixing enzyme, Rubisco, in a small volume to favor the latter's activity (Rae et al., 2013).

The bacterial envelope is made of a cell wall layer (detailed in the following section 1.B) and various extracellular structures, which are mainly implied in virulence. Among them, one can count the viscous polysaccharidic layer, the capsule, that covers the most exposed portion of the bacterial cell. During an infection, this layer enables bacteria to avoid phagocytosis and to resist to antimicrobial peptides and proteins. In addition, the capsule has the faculty to promote adhesion to host cells, other colony individuals, or substrates. This last function can also be fulfilled by excrescences, called pili, and their shorter counterparts fimbriae, which are both resulting from the polymerization of the pilin protein. Flagella are longer hair-like appendages which are anchored in the cytoplasm and serve as a mean of locomotion. They are the result of a complex assembly of more than 30 proteins using the electrochemical potential

difference in protons from both sides of the cytoplasmic membrane to generate motility (reviewed in Morimoto & Minamino, 2014). While these structures are not essential for bacterial survival, the wall delimiting the bacterial cell is fundamental and its chemical structure is highly specific, thus being an attractive target for antibiotics.

1.B- The bacterial cell wall

In 1884, the Danish bacteriologist, Hans Christian Gram, while trying to set up a protocol to stain bacteria for observation under the microscope, developed a technique, which became fundamental to discriminate bacteria according to the composition of their cell wall. Heat-fixed bacterial cells are first treated with a purple dye, gentian violet, which penetrates through the cell wall and plasma membrane, thus staining the cytoplasmic compartment. The addition of iodine, which binds to the violet dye through an ion pair, traps it into the cell. When a decolorizer such as ethanol is added to the fixed cells, two behaviors can be observed, either (i) the purple color is retained, or (ii) the purple color is washed out and a secondary staining with safranin or fuchsin is necessary to give decolorized bacteria a pink or red color for visualization. The permeability of the cells to the decolorizer and the washing-out of the primary dye-iodine complex depends on the architecture of the cell wall. The latter contains an essential and ubiquitous peptidoglycan -or murein- layer, which results from the polymerization of β-1,4-linked N-acetyl-glucosamine (GlcNAc) and N-acetyl-muramic acid (MurNAc) disaccharide units, cross-linked by short peptide stems. If differences in the chemical structure of the individual motifs are rather small, the thickness of the peptidoglycan layer nevertheless drastically differs within bacteria. Bacteria with a thick peptidoglycan layer tend to retain the primary dye of the Gram protocol, while a thin peptidoglycan layer favors the washing-out of the dye-iodine complex. Nevertheless, peptidoglycan is not the exclusive component of the cell wall. Bacteria which give a negative staining in the Gram protocol tend to surrender their thin peptidoglycan layer with a lipid-containing outer-membrane, which is destabilized and washed-out by the addition of the ethanol decolorizer. In contrast, bacteria which give a positive staining in the Gram protocol present a surface layer that tend to be dehydrated upon the ethanol treatment. Some bacteria, such as the genera *Actinomyces*, *Corynebacterium* or *Mycobacterium*, yield a Gram-variable pattern with this protocol. A detailed presentation of the cell wall of typical Gram-positive and Gram-negative bacteria follows, completed by a description of some of these specific Gram-indeterminate bacteria.

1.B.a- Gram-positive bacteria

Gram-positive bacteria encompass organisms such as the rod-shaped model *Bacillus subtilis*, the spheroid *Staphylococcus aureus*, or the ovococcus *Streptococcus pneumoniae*. Because of their thick peptidoglycan layer (figure I.1.2 A), which prevents washing of the gentian violet dye, Gram-positive bacteria appear in purple with Gram-staining. Their wall is further characterized by a single membrane (plasma or inner-membrane) and the presence of different glycopolymers, that are connected either to the peptidoglycan or to lipids of the plasma membrane (for a review, see Weidenmaier & Peschel, 2008). These cell wall glycopolymers thread through the peptidoglycan layers towards the bacterial cell surface, where they can shape physicochemical surface properties and biofilm formation, mediate interaction with host receptors or binding to phages, and initiate innate host defenses and inflammation, T-cell or complement activation, or opsonization. In addition, the surface of Gram-positive bacteria can be covered with protective surface structures, such as capsular polysaccharides or surface layer (S-layer) proteins, which are highly variable among bacterial species and modulate all the previously described activities (see for example Eberhardt et al., 2012 for the attachment of capsular polysaccharides in *S. pneumoniae*).

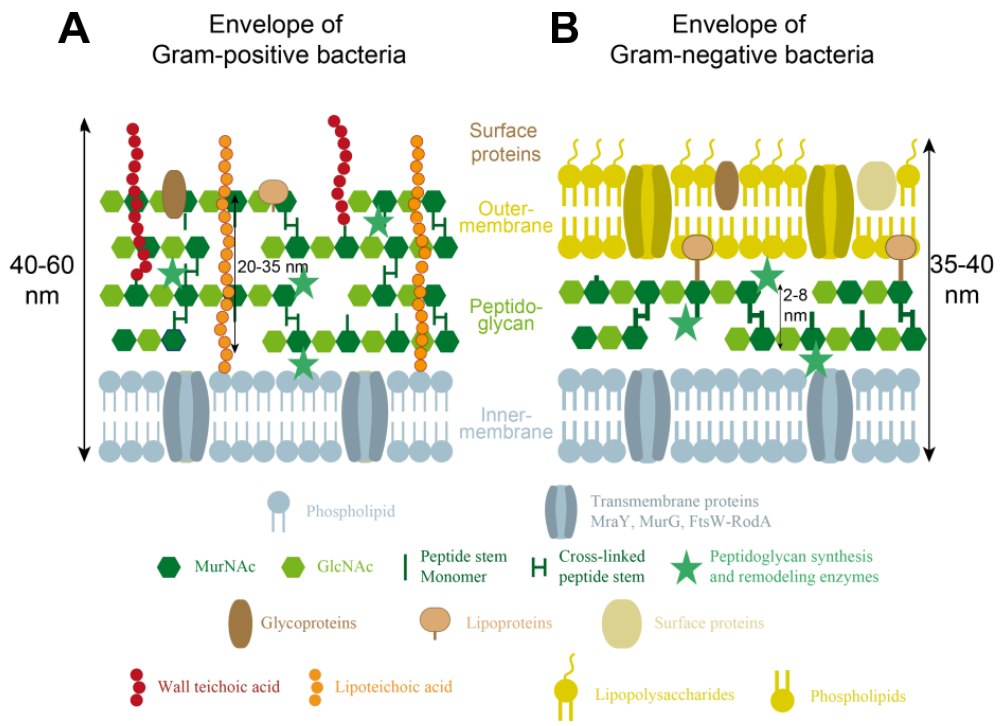

Figure I.1.2: Schematic organization and main components of the bacterial cell-envelope of (A) Gram-positive and (B) Gram-negative bacteria. Details on the typical thicknesses of the cell envelope and constituting layers of different bacterial species can be found in Vollmer & Seligman, 2010. Adapted from Silhavy et al., 2010.

The peptidoglycan-anchored cell wall glycopolymers are usually covalently linked to the peptidoglycan N-acetylmuramic acid through a phosphorylated disaccharide composed of N-acetylglucosamine and another sugar. The glycopolymer itself can be zwitterionic, as in most teichoic acids, anionic as in most teichuronic acids, or neutral when other sugars such as mannose or galactose are involved. Teichoic acids, as in *S. aureus* (Xia et al., 2010), are generally formed by repeats of polyglycerol and/or polyribitol phosphate residues bound by phosphodiesters. Their zwitterionic properties come from the negative charge of their phosphate groups in physiological conditions, balanced with the amino extremities of the D-alanine polyol elements. When D-alanylation is replaced by glycosylation as in *B. subtilis* strain 168 or VKM 501 (Bougault et al., 2012), the teichoic acid becomes anionic. In cases of phosphate starvation, teichuronic acids are produced instead of wall teichoic acids, as in the case of the *B. subtilis* strain 168 (Fritz & Mascher, 2014). The anionic properties of this cell wall glycopolymer then result from the negative charge on the carboxylate group of the glucuronic acid. Alternatively, the secondary cell wall polysaccharides of the *Bacillus cereus* group of Gram-positive bacteria, that includes *Bacillus anthracis*, *B. cereus* and *Bacillus thuringiensis* strains, usually provide a neutral cell wall glycopolymer (Choudhury et al., 2006).

The structure of the membrane anchored glycopolymers is usually less diverse than their peptidoglycan-linked analogs. They usually consist of lipoteichoic acids containing glycerol-phosphate repeating units, that are connected to lipids through a glycerol-disaccharide anchor. However, more complicated lipoteichoic acid structures have also been described, such as the ribitol tetrasaccharide motif of *Streptococcus pneumoniae* (Klein et al., 1996), shown in figure I.1.3.

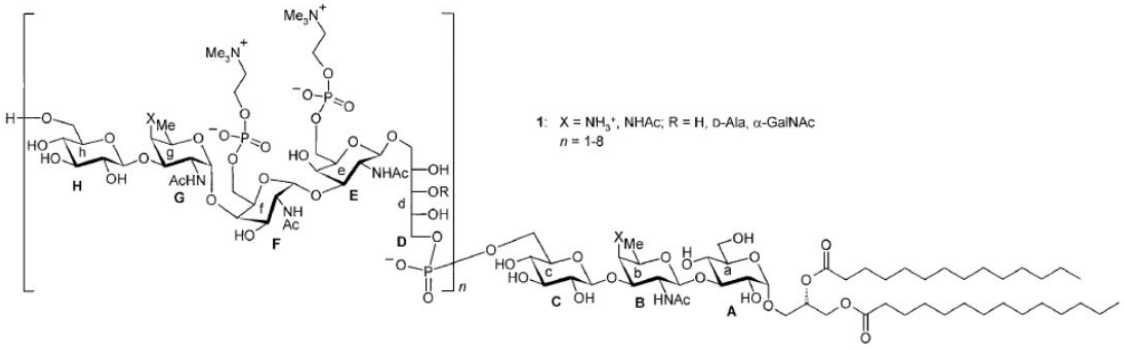

Figure I.1.3: Structure of the lipoteichoic acid (LTA) of *Streptococcus pneumoniae* strain R6. Structure of the wall teichoic acid (WTA) motif in these bacteria is identical (Bui et al., 2012). Taken from Pedersen et al., 2010.

These inner wall zone glycopolymers are essential to Gram-positive bacteria, as their deletion leads to abnormal morphologies and defective division. Variations in the composition of teichoic acids cause changes in local charges that can drastically impact placement of the division site yielding to impairment of the cell-division machinery, but also cation homeostasis, affinity for antimicrobial peptides (Weidenmaier & Peschel, 2008) or autolytic activities (Schlag et al., 2010).

1.B.b- Gram-negative bacteria

Gram-negative bacteria include the well-known *Escherichia coli* or the crescent-shaped model *Caulobacter crescentus.* The lighter color of these bacteria by Gram coloration is due to the inability of these organisms to retain the purple gentian violet dye during the washing step. Indeed, they possess a much thinner peptidoglycan layer than Gram-positive bacteria, but this is enclosed in the periplasmic space between an inner (cytoplasmic) and an outer membrane (figure I.1.2 B, Silhavy et al., 2010). The outer-membrane is an asymmetrical membrane composed of phospholipids and glycolipids (or LipoPolySaccharides; LPS), at the inner and outer leaflets, respectively. The latter molecules consist of a lipid A anchor linked to a core oligosaccharide, that can be extended with an O-antigen polysaccharide of variable length which protects the cell against macrophages and complement system from the innate immune response (Putker et al., 2015). Lipopolysaccharides form an almost impermeable layer at the surface of Gram-negative bacteria, that acts as a protective barrier against antibiotics and other antimicrobial molecules, and more generally hydrophobic molecules.

Embedded in the outer-membrane, proteins can also be found. With a few exceptions, they can be divided in two classes, lipoproteins and β-barrel proteins (Silhavy et al., 2010). The former contain a lipid moiety generally covalently linked to a cysteine residue and are mainly localized in the inner leaflet of the membrane. One of them, the highly abundant Braun's lipoprotein (also known as Lpp), is actually essential in *E. coli* for cell wall integrity as it is covalently linked to peptidoglycan to tether the outer membrane to the murein layer. Alternatively, β-barrel proteins are transmembrane proteins that allow the passive diffusion of small molecules, such as sugars and amino acids, through the outer membrane (porins), or that function as gated channels for the transport of high affinity ligands such as Fe-chelates or vitamins. Some additional proteins, usually specific to the bacterial species can also be found in the outer membrane.

The periplasmic space delimited by the inner- and outer-membranes not only contains the peptidoglycan polymer, but also a high density of various proteins and chaperones, which are

involved in the biosynthesis or maturation of the peptidoglycan and cell envelope polymers, but also in sugar and amino acid transport and chemotaxis (for a review see Silhavy et al., 2010). Secretion systems for example recruit a number of proteins from the cytoplasm to the outer-membrane, that associate to form a dynamical trans-envelope assembly which can release proteins, DNA or toxins in the medium or to prokaryotic or eukaryotic cell (for a review, see for example Costa et al., 2015).

1.B.c- The cell wall of bacteria with intermediate Gram-staining

Although most of bacteria can be classified either as Gram-positive or as Gram-negative, some cases are more complex. For instance, the notorious bacillus *Mycobacterium tuberculosis* is hardly stained by Gram coloration. The cell wall of mycobacteria and other corynebacteria is composed of five layers (figure I.1.4), which are the plasma membrane, the granular layer, the inner wall zone, the medial wall zone and the mycomembrane, when starting the description from the inside to the surface of the cell (Zuber et al., 2008). The plasma membrane is very similar to that of Gram-positive and Gram-negative bacteria. The approximately 8.5-nm thick granular layer is similar to that detected in the Gram-positive Streptococci and is apparently bound to the plasma membrane, while it is absent in Gram-negative bacteria. This is one of the reason why, despite its response to the Gram-staining, mycobacteria and corynebacteria are often classified within the Gram-positive family. The ~15-nm thick inner wall zone is of low density and mainly contains peptidoglycan, while the ~7-nm thick medial wall zone is of intermediate density and contains peptidoglycan covalently bound to arabinogalactan, a glycopolymer composed of 1,4-linked galactose and arabinose. The arabinogalactan is in turn covalently bound to mycolic acids, which are very-long chain of α-branched and β-hydroxylated fatty acids that are specific to the *Corynebacterineae*. The mycolic acids interact with various lipids and glycolipids to form the mycomembrane, which is highly impermeable, similar to the outer-membrane of Gram-negative bacteria (Daffé, 2015). Embedded in this membrane, porins can also be found, which form specific hydrophobic pores in this structure. The outermost layer of the cell envelope represents a capsule-like material mainly composed of polysaccharides and proteins, and eventually in some specific cases specialized glycolipids.

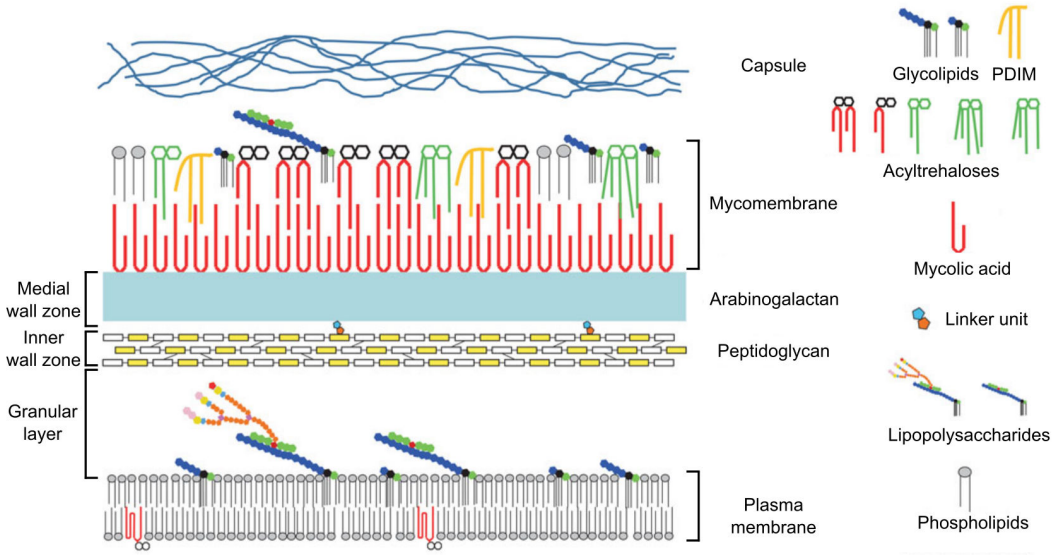

Figure I.1.4: Schematic representation of the mycobacterial cell envelope. The peptidoglycan polymer is represented by yellow (GlcNAc) and white (MurNAc) rectangles, arabinogalactan by a blue region. Trehaloses (in green and red) are non-reducing disaccharides made of glucose. PDIM: phthiocerol dimycocerosate lipid. Adapted from Angala et al., 2014.

Corynebacterieae are not the only example of bacteria with a non conventional cell wall. Until 2014, it was supposed that intracellular pathogens *Chlamydiae* and aquatic *Planctomycetes* phyla did not possess any peptidoglycan layer, although the former were known to be sensitive to antibiotics targeting its synthesis. Using peptidoglycan probes and cryo electron-microscopy, new studies however revealed the presence of a murein layer enclosed between two membranes in some of these organisms (see Pilhofer et al., 2013; Liechti et al., 2014 for *Chlamydiae* and Jeske et al., 2015; van Teeseling et al., 2015 for *Planctomycetes*). These results should trigger a renewal of interest for species from these phyla, as they are currently the only known bacteria with peptidoglycan synthesis machineries totally independent of the usually essential FtsZ division protein (see part I section 4.B).

1.B.d- Peptidoglycan-less bacteria

Interestingly, some bacterial organisms are totally devoid of any bacterial cell wall, therefore lacking peptidoglycan. The most common ones known to date are from the Mollicutes phylum. Indeed, bacteria from their most studied genus, Mycoplasma, are among the tiniest organisms (0.2 to 0.3 µm) and have, excluding viruses, the smallest genome (between 0.6 and 1.35 Mbp), presumably due to a loss of their genes throughout evolution. As a consequence, they are lacking almost all – if not all – the required genes for peptidoglycan synthesis enzymes. Mycoplasma are bound by a single plasma membrane that is made of choline-containing phospholipids, among which phosphatidylcholine and sphingomyelin, cardiolipin and phosphatidylglycerol (Park et al., 2013). The absence of rigid cell wall induces an extreme sensitivity to osmotic pressure, which is the reason why these organisms are depending on the adhesion to the surface of an eukaryotic host cell. More recently, three spherical and chemoheterotrophic Gram-negative bacteria were isolated, affiliated to the genus Cerasicoccus within the phylum 'Verrucomicrobia', and were reported to lack peptidoglycan (Yoon et al., 2010). This suggests that more peptidoglycan-less bacteria may be discovered in the future.

Despite the primary importance of peptidoglycan in bacteria with a cell wall, it has been shown that some Gram-positive and Gram-negative cells can also survive without this structure in a state called L-form. Indeed, such wall-free bacteria can be obtained from the inhibition of cell wall synthesis in osmoprotective conditions (Allan, 1991; Leaver et al., 2009). The generated organisms lose their initial shape, become round, and lose their rigidity. Although still little information is known about bacterial L-forms, it is suggested that they might be implied in diseases (Allan et al., 2009) and it has been hypothesized that they could be a relic of an antique shape existing before the apparition of sacculi (Errington, 2013).

1.C- Macroscopic structure of the peptidoglycan layer

Although the presence of a peptidoglycan network in bacterial cell walls is well-documented, the mechanical properties and architecture of the massive murein sacculus (~3 x 10^9 Da, a repeat of approximately 3.5 x 10^6 moles of monomeric motifs in the Gram-negative *E. coli* as measured by Wientjes et al., 1991) are still poorly understood. Indeed, if it was clear from the early 60's that this bag-shaped exoskeleton surrounding the plasma membrane was essential to maintain the cell shape and to sustain the osmotic pressure originating from the high concentration of solutes in the intracellular compartment, measurement of the elasticity and stiffness of the net had to await developments in Atomic Force Microscopy (AFM) at the end of the 90's. In addition, peptidoglycan flexibility and heterogeneity prevented the determination of large scale architectural features by conventional structural techniques, such as X-ray crystallography and NMR. Due to its limited resolution, negative-staining Transmission Electron Microscopy also failed to provide structural details of the

peptidoglycan 3D superstructure, except maybe for the circumferential orientation of the glycan strands. The absence of key structural data did nevertheless not prevent scientists to build models, with the help of chemical data concerning the average glycan chain length and the percentage of peptide cross-links obtained by High-Performance Liquid Chromatography (HPLC) coupled to mass-spectrometry on enzymatically digested fragments. These models are described in the following paragraphs in the light of the experimental results obtained in the last five years from Electron Cryo-Tomography (ECT), Cryo-Electron Microscopy (Cryo-EM) and/or AFM.

1.C.a- Mechanical properties of the sacculus

The peptidoglycan layer is often seen as a rigid component of the bacterial cell wall, probably because of its functions as a key shape determinant and stress-bearing structure. Yet this appraisal is partial. Actually, sacculi have been shown by low-angle laser light scattering to be able to be stretched up to 3 times their initial surface area by adjustment of the pH and ionic strength condition of the sacculi samples (Koch & Woeste, 1992). This conclusion corroborated previous *in vivo* observations showing that the murein layer undergoes an estimated 45% shrinkage when relaxed (figure I.1.5, left panel) by disruption of cytoplasmic membrane of *E. coli* filaments with a detergent (Koch et al., 1987), and that the peptidoglycan is stretched under the effect of the osmotic pressure (figure I.1.5, middle panel).

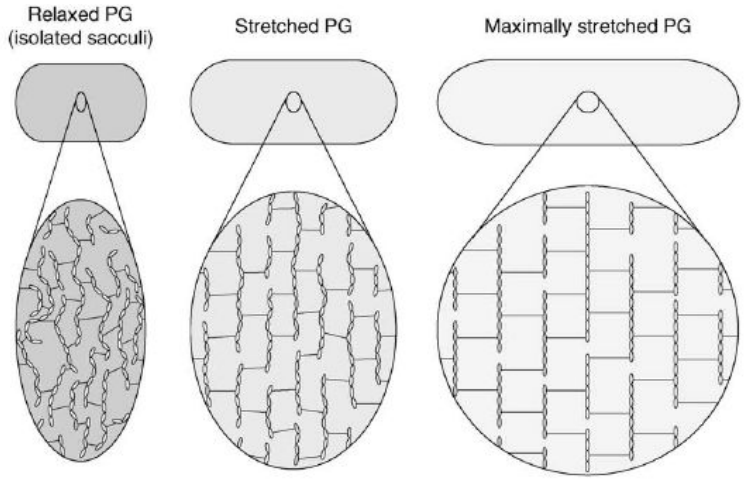

Figure I.1.5: Elasticity of the sacculus. When isolated, sacculi adopt a relaxed conformation (left) while *in vivo*, due to the turgor of the cell, the peptidoglycan layer is stretched (middle). Stronger forces applied to the cell wall can lead to further extension (right). Taken from Vollmer & Seligman, 2010.

AFM is a good method to further probe and quantify peptidoglycan elasticity. AFM principle rests upon the sensing of a surface with a tip mounted on a cantilever, whose deflection can be measured by different methods using piezoelectric effects, optical interferometry or Laser Doppler vibrometry for example. This technique can be used either to acquire topological images of the bacterial surface and isolated sacculi or to measure adhesion forces between the tip and the sample to quantify the cell surface elasticity. With the latter method, Yao and co-workers (Yao et al, 1999) measured a 25 MPa average Young's modulus along the longitudinal axis of the *E. coli* hydrated sacculi, which is increased by a 1.8 factor along the perpendicular axis (figure I.1.5, right panel). The Young's modulus translating the mechanical constraints necessary to extend a material by 100%, the anisotropy of this elasticity was suggested to result from the flexible peptides being rather parallel to the cell longitudinal axis, while the glycan chains would be predominantly perpendicular to it. When hydrated, sacculi were perfectly elastic, springing back to their original position after removal

of the tip, but when dehydrated they proved to be more rigid. With these measurements, the authors estimated that an increase of the turgor pressure by one atmosphere would cause a 12% lengthening and 8% increase in diameter of the bacterium. Similar measurements were performed in the Gram-positive bacteriaium *Staphylococcus aureus* (Loskill et al., 2014) and reported that the stiffness of the peptidoglycan increases with the percentage of cross-linking. As a result, the cell radius and cell wall stiffness are correlated to stress and pressure, thus offering a regulatory mechanism for cell shape changes under environmental conditions.

1.C.b- Mesoscale structural data on peptidoglycan

In addition to mechanical properties, microbiologists soon focused on other physical characteristics of the peptidoglycan layer, including its thickness, the size of pores within it, the average length of the glycan strands or the degree of cross-linking. In Gram-negative bacteria, most of this work was carried out on *E. coli*, while most of the data were collected on *B. subtilis* and *S. aureus* in Gram-positive bacteria. When available, the latter will be complemented with recent data on the pathogenic ovococcus *S. pneumoniae*.

1.C.b.i- Thickness of the peptidoglycan layer

A range of values has been reported for the thickness of the *E. coli* peptidoglycan layer. An initial Small-Angle Neutron Scattering (SANS) study (Labischinski et al., 1991) reported a ~2.5-nm thick single-layered peptidoglycan covering 75 or 80% of the bacterial cell surface and a triple-layered region for the rest in exponentially growing W7 strains. Cryo-EM measurements on *E. coli* confirmed that peptidoglycan was mostly arranged in a layer roughly parallel to the membrane (Gan et al., 2008), with a thickness of approximately 6.35 ± 0.53 nm (Matias et al., 2003). Initial AFM studies (Yao et al., 1999) provided a typical thickness of 3 nm and 6 nm for air-dried and hydrated *E. coli* sacculi, respectively, suggesting that discrepancies between the different measurements may come from the stage of the bacterial cell cycle and conditions used for the preparation of the sample in relation to the experimental technique used for the measurement. An alternative interpretation of the data relates to the number of peptidoglycan layers in *E. coli*, which could vary between 1 and 3 depending on the strain and growth conditions, as a value of 2.41 ± 0.54 nm (Matias et al., 2003) was found for the Gram-negative *Pseudomonas aeruginosa.* This latter value is consistent with the most recent AFM measurement (Turner et al., 2013) in *E. coli* from different bacterial strains and growth phases (2.0 ± 0.3 nm).

Studies in Gram-positive *S. aureus* and *B. subtilis* led to very different observations. As it could be expected for these Gram-positive bacteria, the peptidoglycan layer was shown to be much thicker than in *E. coli*, between 19 ± 4.3 nm and 33.6 ± 4 nm, depending on the species and the conditions, stretched in the cell or relaxed when isolated (Matias & Beveridge, 2005, 2006). Interestingly, the same studies also evidenced the existence of a low-density region between the cytoplasmic membrane and the peptidoglycan, which was interpreted as a periplasmic-like space. Most recent AFM studies suggest that in ovococci like *S. pneumoniae* (Wheeler et al., 2011) or Group B Streptococci (Dover et al., 2015), the layer containing the low- and high-density peptidoglycan is only ~7-to-9 nm thick with a thickness for the isolated peptidoglycan of 4.3 ± 0.8 nm for the former species.

1.C.b.ii- Size of pores in the peptidoglycan layer

Sacculi pore size can be indirectly measured by determining the largest objects that can pass through it. It was studied in the two rod-shaped bacteria *E. coli* and *B. subtilis*, using fluorescein-labeled dextran molecules with a wide range of molecular weights (Demchick & Koch, 1996). In both cases, a similar hole radius was determined, 2.06 nm for the former and

2.12 nm for the latter. From this evaluation in non stress-bearing conditions, it was supposed that a peptidoglycan layer in a relaxed-state should act as a molecular sieve, whith pores large enough for the passage of globular and uncharged proteins reaching up to 22 and 24 kDa respectively. It was further hypothesized that when stretched, globular macromolecules up to 50 kDa should be able to cross the murein network (Vollmer, Blanot et al., 2008). Another study (Vázquez-laslop et al., 2001) showed that proteins up to 100 kDa in size could go through the peptidoglycan of osmotically shocked *E. coli* cells, suggesting that the pore size in stretched peptidoglycan could even go up to 3.1 nm (Vollmer & Höltje, 2004). Larger pores with a 13 ± 5 nm diameter were recently detected by AFM near the poles of the Gram-negative *P. aeruginosa* bacterium, that could accommodate pili or secretion systems (Turner et al., 2013). Pore size could not be measured in Gram-positive bacteria due to the limited resolution of current EM and AFM techniques and the thickness of the peptidoglycan layer.

1.C.b.iii- Average glycan-chain length

High-Performance Liquid Chromatography techniques, eventually coupled to mass spectrometry, afforded key structural data on the glycan chains average length (Boneca et al., 2000). In these studies, peptidoglycan is labeled with N-acetyl[1-^{3}H]glucosamine, purified and digested with the *S. aureus* Atl amidase which cuts the glycan-peptide bonds. The glycan strands are then isolated by chromatography (cation-exchange or gel-filtration chromatography depending on the acetylation of the glucosamine residues). A size-exclusion chromatography is finally used to separate and quantify the different glycan strands according to their molecular weight using a radioactivity monitoring, thus yielding to the distribution of the different chain lengths. Alternatively, the length of glycan strands can be determined through the quantification of the ratio of terminal 1,6-anhydro-N-acetyl-muramic acid with respect to its non-anhydro equivalent (Glauner et al., 1988). In the Gram-negative *E. coli*, average glycan chain length depends on strain, growth condition and the stage of the cell cycle (Vollmer & Seligman, 2010). Approximately 70 to 75% of the glycan strands contain less than 30 disaccharide units with an average of 8.9 units per strand (Harz et al., 1990). The rest contains strands with up to 80 units. These features are quite representative of Gram-negative bacteria. In contrast, a large variability of the glycan strand length occurs in Gram-positive bacteria. The presence of surprisingly long glycan chains was revealed by HPLC in *B. subtilis*, with more than 500 disaccharide units (Hayhurst et al., 2008) for more than 25% of the strands, some of which were even estimated by AFM to measure up to 5 µm, corresponding to approximately 5000 units. Similarly, 44 to 57% of the glycan strands in the ovococcus *S. pneumoniae* contain more than 50 disacccharide units (Wheeler et al., 2011), while in *S. aureus* they have an average of 6 disaccharide units (Boneca et al., 2000).

1.C.b.iv- Degree of cross-linking

Even more than the glycan chain length, the degree of cross-linking highly depends on the bacterial strain, the growth phase and environmental conditions. In *E. coli*, it can easily vary between 31 and 61% (Vollmer & Seligman, 2010). *B. subtilis* also shows different percentages of 56%, 63%, and 3% (Atrih et al., 1996, 1999) in bacilli from exponentially growing, stationary, or sporulation phases, respectively. The percentage of cross-linking is in the high values of 74-92% in *S. aureus* (Vollmer & Seligman, 2010), while it is only 35% in *S. pneumoniae* (Bui et al., 2012). This parameter may nevertheless not be highly determinant in the overall peptidoglycan architecture, and is generally not considered in the design of organizational models. To determine these values, purified sacculi are treated with muramidases, such as mutanolysin, or lysozyme, which break the glycan strands between the disaccharide motifs. The obtained muropeptides are then separated by HPLC on a hydrophobic matrix, to be further analyzed and identified by Matrix Assisted Laser Desorption/Ionization – Time Of Flight Mass Spectrometry (MALDI-TOF MS; Desmarais et

al., 2013). This approach establishes the ratio of each of the monomers (disaccharide bearing tri-, tetra-, or penta-peptides), dimers, trimers and eventually more reticulated material, from which the abundance of cross-linked and un-crosslinked disaccharide peptides can be determined.

A summary of the values for main architectural peptidoglycan parameters discussed in this section regarding *E. coli* and *S. pneumoniae* can be found in table I.1.1

Table I.1.1: Nanoscale architectural data on the peptidoglycan of Gram-negative *E. coli* and Gram-positive *S. pneumoniae.*

	E. coli		*S. pneumoniae*	
	Parameter	Reference	Parameter	Reference
Typical bacterial size	2 µm (longitudinal axis)		1 µm (diameter)	
Elasticity (Young's modulus)	25 Mpa (along glycan strand) 45 Mpa (along peptides) (hydrated sacculi)	Yao et al., 1999	5.3 Mpa (living cells)	Dover et al., 2015
Peptidoglycan thickness	2.0 ± 0.3 nm	Turner et al., 2013	4.3 ± 0.8 nm	Wheeler et al., 2011
Pore size	2.06 nm (fluorescein-labeled dextran); Max 10 nm (AFM)	Demchick & Koch, 1996; Turner et al., 2013	Undetermined	
Glycan strand length	25 - 30% > 30 disaccharides	Harz et al., 1990	44 - 57 % > 50 disaccharides; 8 - 14%> 100 disaccharides	Wheeler et al., 2011
Degree of cross-linking	31 - 61 %	Vollmer and Seligman, 2010	35%	Bui et al., 2012

1.C.c- Models for peptidoglycan organization

Determination of key physical parameters of sacculi enabled the emergence of hypotheses concerning the structural organization of peptidoglycan. Two main models were proposed, the layered and the scaffold models, which are presented in figures I.1.6 A and B, respectively.

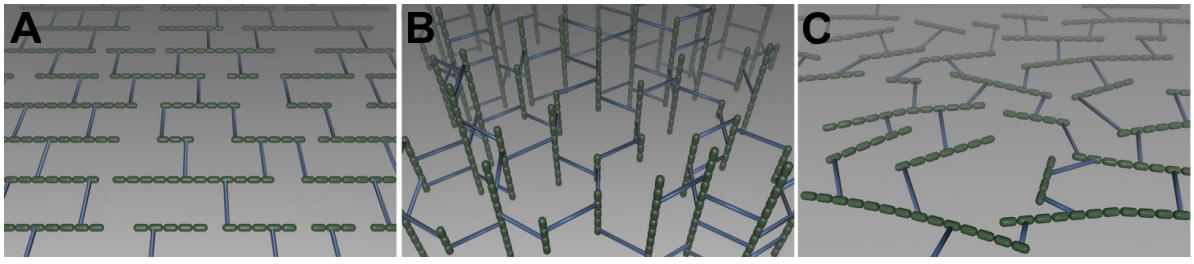

Figure I.1.6: Main models for peptidoglycan organization. (A) The layered-model, (B) the scaffold model. (C) represents a third model derived from the first one, which allows more disorder in the glycan chains positions and is consistent with recent AFM data on *E. coli S. aureus*, and *S. pneumoniae*. Taken from Gan et al., 2008.

In the layered model (figure I.1.6 A), which is currently the most accepted model in the scientific community, glycan strands would be positioned parallel to the cytoplasmic membrane. Because it is generally accepted that glycan chains should rather have a right-

handed helical conformation, with a pitch of 3 or 4 disaccharides per turn (Gumbart et al., 2014; Meroueh et al., 2006), it is thought that peptide stems would be pointing in 3-to-4 alternating different directions. It is therefore suggested that half of them would be in the glycan chain plane, while the other ones would be orthogonal, and available for cross-linking with neighboring peptidoglycan layers. Such an organization could yield to the multi-layered organization in Gram-positive bacteria and could explain the thickness variability observed in some cases in *E. coli*. To explain swelling of the peptidoglycan with the osmotic pressure, it has been put forward that glycans could rather adopt zigzaging conformations, whose cross-linking could give rise to hexagonal pores called tesserae (figure I.1.7 A). The existence of such structures was nevertheless not observed in recent AFM and CET studies (Turner et al., 2013). In *B. subtilis*, a model, which could be associated with a different kind of layered-peptidoglycan organization, proposes that glycan strands could stack circumferentially along the transversal axis of elongated bacilli (figure I.1.7 B) to form 50-nm wide cables, as imaged from recent AFM studies in *B. subtilis* (Hayhurst et al., 2008). The overall organization in the model would be also maintained by the peptide cross-links, oriented along the cell longitudinal axis. Such a model could thus accommodate the current experimental data on elasticity, peptidoglycan thickness, and glycan chain length (Turner et al., 2014).

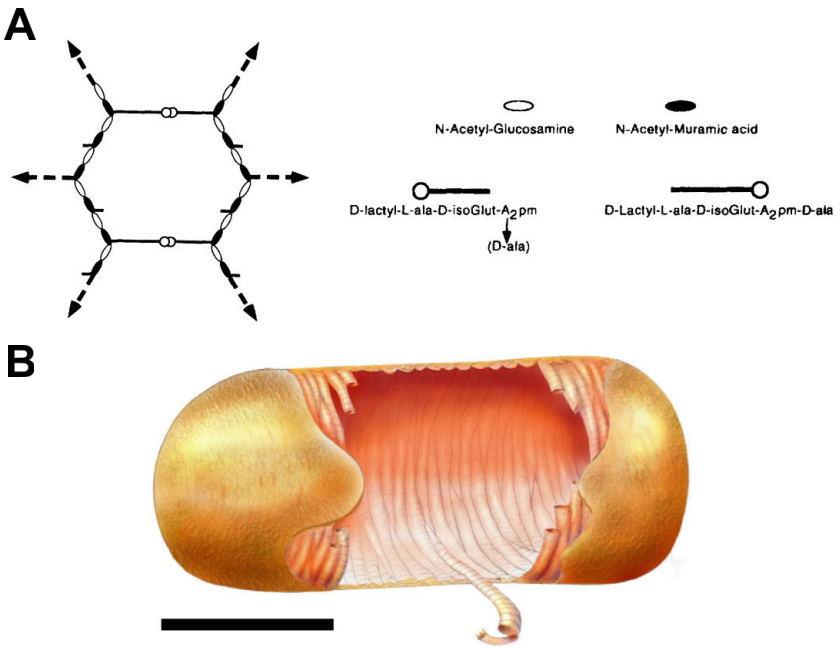

Figure I.1.7: Details of the arrangements proposed in layered-peptidoglycan. (A) Tesserae formed by two facing glycan chains (taken from Koch, 1998). Disaccharide units are represented by a white and black oval couple, while peptides are represented by black lines. (B) Long coiled-peptidoglycan cables as determined from AFM data in *B. subtilis* (taken from Hayhurst et al., 2008). They would be tied to each other through peptide cross-links. The bar in (B) corresponds to a scale of 1 µm.

As for the scaffold model (figure I.1.6 B), it proposes that the glycan strands are perpendicular to the cell envelope, with each of them being cross-linked to the others through their peptide stems (Dmitriev et al., 2004; Meroueh et al., 2006). If this model was rapidly discarded for *E. coli* on the comparison of the average peptidoglycan thickness and glycan strand length, it persisted in Gram-positive bacteria, such as *S. aureus* (Dmitriev et al., 2004). In this context, the further the chains, the older there would be as they are expected to be inserted from close to the cytoplasmic membrane. However, to date, this model has only been supported by computer simulations but was not confirmed experimentally.

Organization of the glycan strands is most probably nevertheless not as regular as

anticipated from the two initial models as suggested in figure I.1.6 C. Indeed, if recent ECT (Gan et al., 2008) and AFM (Turner et al., 2013) data on *E. coli* suggest that tubes of density are mostly in the plane of the sacculus and roughly perpendicular to the cell longitudinal axis, they show heterogeneity. In this respect, the computational model proposed by Gumbart and coworkers (Gumbart et al., 2014), with 12 glycan strands of 17-to-26 disaccharides is in agreement with experimental data on elasticity, thickness and pore radius. Most recent AFM data (Dover et al., 2015) on Group B *Streptococcus* suggest that this situation may not be unique to the peptidoglycan of Gram-negative bacteria, as a net-like structure of bands with a ~25-nm width was imaged in these bacteria. The situation in Gram-positive *S. aureus*, a challenging organism with respect to its peptidoglycan architecture, as this spherical bacterium is dividing sequentially following three different orthogonal plans, is somewhat in between the regular *B. subtilis* structure and the less symmetrical *E. coli* organization. In this organism, it was shown by AFM that equatorial perpendicular peptidoglycan structures encircle the cell, positioned at the previous and new division sites (Turner et al., 2010). Regions of concentric rings and knobbly architectures were also described on sacculi, the former being supposed to be nascent peptidoglycan while the latter are thought to be older matured material (Turner et al., 2010). A comparison of the current peptidoglycan architecture in different species can also be found in Turner et al., 2014.

From these results on a few different bacterial species, it appears that peptidoglycan may adopt a broad diversity of arrangements. However, due to the little quantity of available studies and species investigated, the models trying to describe these observations are to be cautiously considered and await technological developments in high-resolution imaging technology from AFM or optical trapping. While these huge biological macromolecule structures are still puzzling, their atomic chemical composition is much more documented.

1.D- Peptidoglycan molecular structure

1.D.a- Chemical composition

In all bacteria, the glycan strands of peptidoglycan are composed of alternating β-1,4-linked N-acetylglucosamine (GlcNAc) and N-acetylmuramic acid (MurNAc, a variant of GlcNAc with a D-lactate attached to the C-3 by an ether bond) as shown in figure I.1.8. Generally, the obtained strands are terminated at the reducing end by a 1,6-anhydroMurNAc residue, in which the C-1 and C-6 of the sugar backbone are bound through an ether linkage. The unique features of this residue are used to quantify the glycan chain average length, as described in I.1.C.b.iii. The peptide stems are covalently linked to the glycan strands with an amide bond to the carboxyl carbon of the D-lactyl group of the MurNAc. While the chemical composition of the glycans is highly conserved across species, the peptide sequence is more diverse and has the particularity to involve D-amino-acids. In the first position from the lactyl group, an L-alanine (L-Ala) is usually found, and in rare exceptions a Gly or an L-Ser residue. A D-isoglutamic acid (D-iGlu) follows, which is sometimes amidated in Gram-positive bacteria to yield a D-isoglutamine (D-iGln), as in *S. pneumoniae* (Zapun et al., 2013). The γ-carbon of this residue is connected to a third amino acid, that is most probably the most variable within the stem peptide (Vollmer, Blanot et al., 2008). In most Gram-negative species, Gram-positive bacteria of the genus *Bacillus* and mycobacteria, the third amino acid is usually the *meso*-diaminopimelic acid (*m*-A_2pm), while in most-Gram positive species it is usually an L-lysine (L-Lys). The peptide stem is finally terminated by two D-alanines (D-Ala), although different D-amino acids can be found either naturally or by addition of specific amino acids in the growth medium.

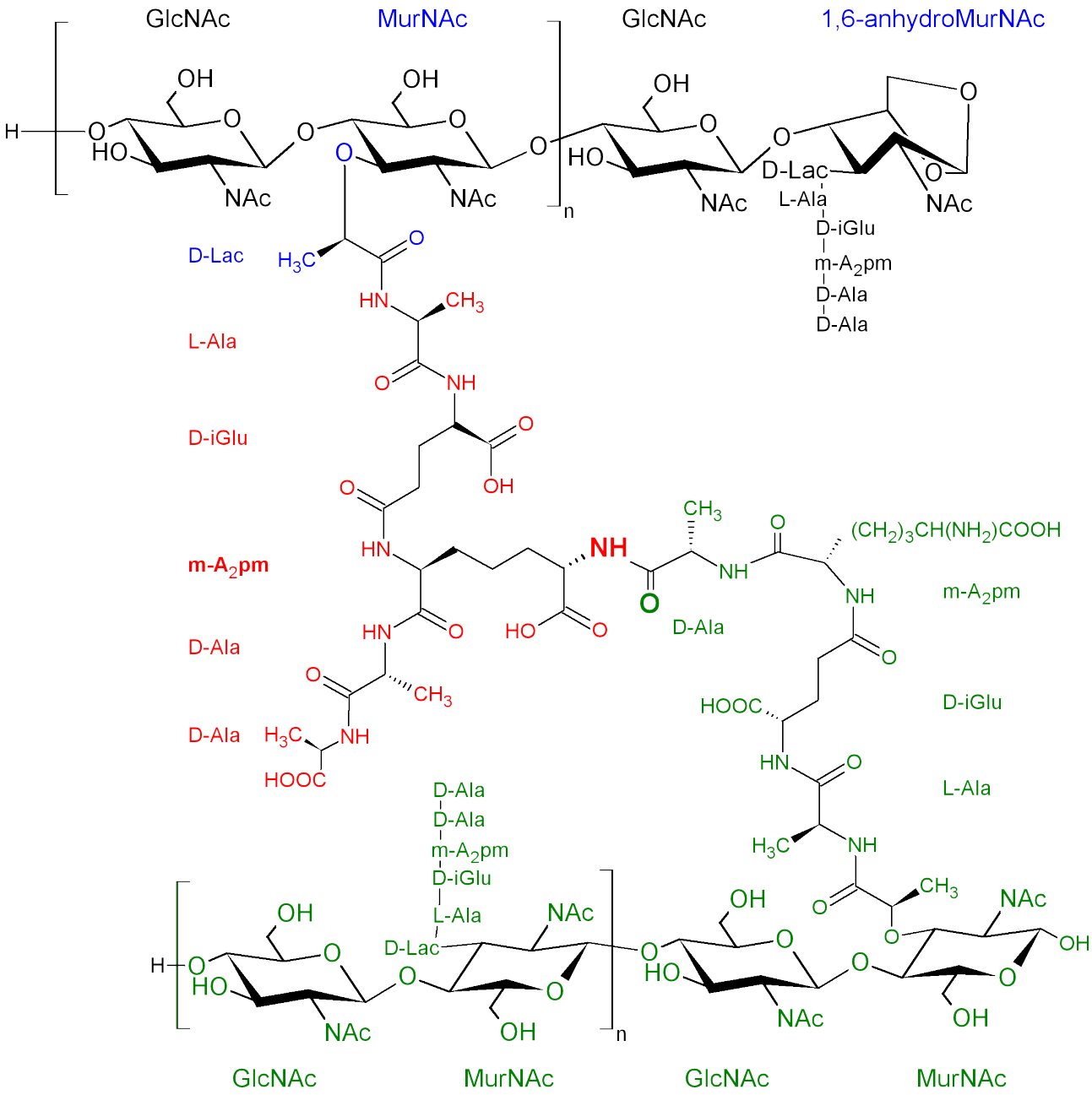

Figure I.1.8: Chemical composition of *E. coli* peptidoglycan. The disaccharide-pentapeptide peptidoglycan motif is shown on the upper left, with GlcNAc in black, MurNAc in black and blue to emphasize the D-lactoyl moiety, and the peptide stem in red. The terminal 1,6-anhydroMurNac is depicted in the upper right portion of the structure. The disaccharide-pentapeptide motifs from another glycan strand are shown in green. One of the peptide stem of this additional strand is cross-linked to the *m*-A_2pm side-chain amino group of the peptide stem of the former glycan strand through the carbonyl of its D-Ala in position 4. Atoms implicated in the peptide bond of the cross-link are shown in bold.

1.D.b- Cross-links at the peptide stems

As discussed in part I section 1.C.b.iv, the percentage of cross-linking in peptidoglycan can be determined by a combination of HPLC and MALDI-TOF MS. Analyzes can be complemented by MS/MS experiments on the individual muropeptides to validate the structure of each individual species by fragmentation. As exposed in part I chapter 5, these analyzes can also be complemented by Nuclear Magnetic Resonance Spectroscopy.

Two main cross-linking strategies have been identified in bacteria up-to-date. The most widespread strategy yields to a 4→3 cross-link, by connecting the amino group of the 3rd

residue (*m*-A_2pm or L-Lys) of the acyl-acceptor stem peptide to the carbonyl moiety of the 4th amino acid (D-Ala) of the acyl-donor stem peptide (figures I.1.8 and I.1.9). This reaction is catalyzed by a D,D-transpeptidase enzyme (among which the Penicillin-Binding Protein (PBP) enzymes), which utilizes disaccharide-pentapeptides as substrate. In this reaction, the D-Ala in position 5 of the acyl-donor peptide stem is thereafter eliminated. An alternative strategy was evidenced in an *in vitro* selected ampicillin-resistant *Enterococcus faecium* strain (Mainardi et al., 2000) and involves a 3→3 cross-link. In this case, transpeptidation occurs between the amino group of the 3rd residue (*m*-A_2pm or L-Lys) of the acyl-acceptor stem peptide and the carbonyl moiety of the 3rd amino acid (*m*-A_2pm or L-Lys) of the acyl-donor stem peptide. This reaction is catalyzed by L,D-transpeptidases (Mainardi et al., 2005) and specifically requires disaccharide-tetrapeptide substrates (figure I.1.9). Although this cross-linking mode is usually in minority, it can become a major strategy in some species, as reported for *M. tuberculosis* (80%; Lavollay et al., 2008). From computer modeling, it was postulated that 3→3 cross-links might induce stiffness in the peptidoglycan, due to the replacement of the D-Ala in position 4 by a the *m*-A_2pm donor in position 3 (de Pedro & Cava, 2015). Nevertheless measurements by solid-state NMR in our research team on 3→3 and 4→3 cross-linked peptidoglycan seem to indicate that the polymer flexibility remains mainly unaffected in the µs-to-ns time-scale dynamical regime (Gansmüller et al., unpublished results). The D,D- and L,D-transpeptidase enzymes responsible for these 4→3 and 3→3 cross-links, respectively, are further discussed in part I section 2.C.b.

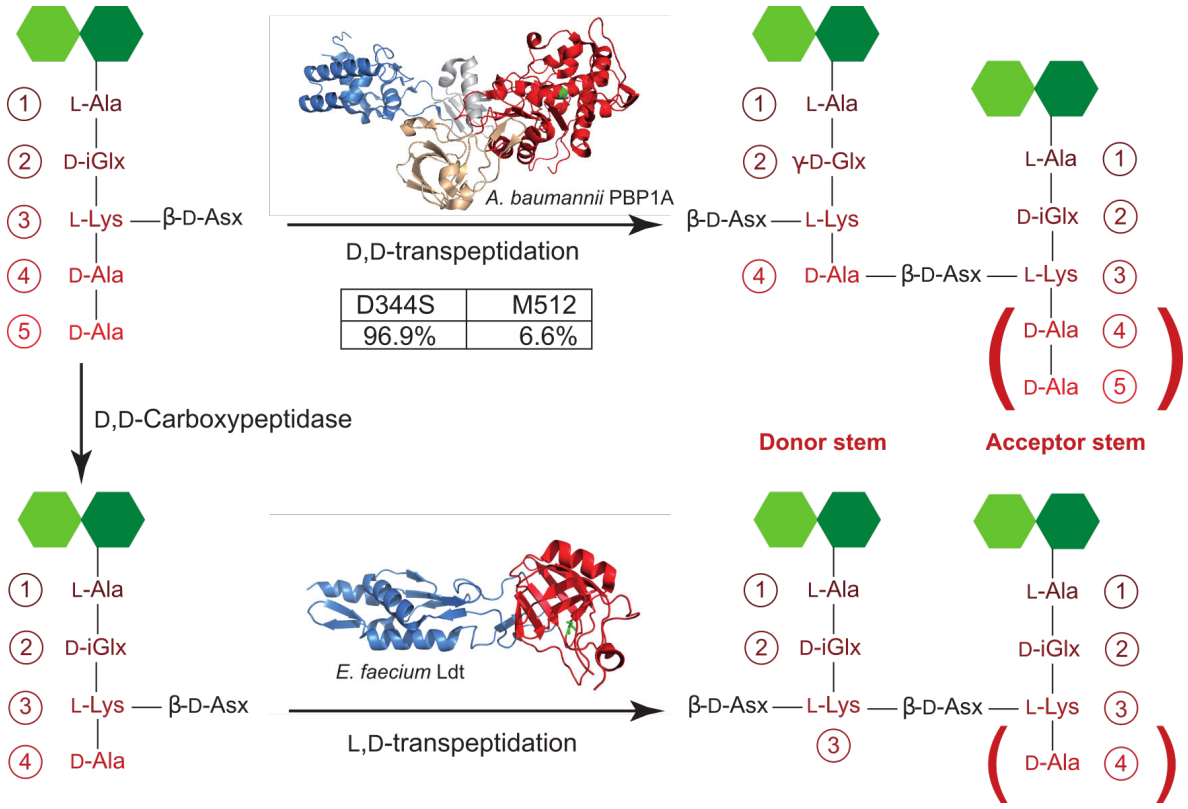

Figure I.1.9: Schematic representation of the 4→3 and 3→3 cross-links in *Enterococcus faecium*. The formation of these cross-links is catalyzed by D,D- and L,D-transpeptidase enzymes, respectively. The light and dark green colors represent the GlcNAc and MurNAc saccharides, respectively. Amino acids are indicated in red with their stereochemistry. Cross-links consist in a peptide bond between the amino group of the amino acid in position 3 of the acceptor peptide stem and the carbonyl group of the amino acid in position 3 or 4 of the donor strand. 96.9% of the cross-links are the usual 4→3 cross-links in the ampicillin-sensitive *E. faecium* strain, D344S, while 6.6% only of these cross-links are present in the M512 ampicillin-resistant strain, yielding to a majority of 3→3 cross-links in this strain (Mainardi et al., 2002).

Additionally to dimeric species, trimers and tetramers can be detected in the analysis of

muropeptides. This is the case if the cross-linking involves one or two more glycan chains. In the case of a trimer, the 4th residue of the acceptor stem in the constitutive dimer can play the role of donor in a new transpeptidation reaction and make a cross-link with the third residue of another acceptor peptide stem. Similarly for a tetramer, the D-Ala of the trimer acceptor peptide stem is connected to a neighboring peptide from another glycan strand. In both cases, these multimerizations produce structural constraints forcing the third and fourth strands to be on distinct plans from the initial peptidoglycan surface (de Pedro & Cava, 2015). One could suggest that such knots, if accumulated locally, are likely to modify peptidoglycan physical properties and would favor a rather disordered net. However, in most species studied until now, trimers are present in limited quantities and tetramers are even much rarer. As an example, trimers and tetramers were only found in less than 10% and 0.25% of the cross-links in *E. coli*, respectively (Glauner et al., 1988). It is hard to determine if these amount are sufficient to impact the sacculus physical properties, especially for the tetramers.

On the contrary to Gram-negative bacteria, it is not rare in Gram-positive organisms to find cross-linking through a bridge. This peptide bridge can be composed of one to seven amino acids and various amino acids can be encountered, which can be connected through their side chains instead of their backbones as the β-D-Asx in *E. faecium* (figure I.1.9). For example, in *S. aureus*, the peptide bridge in the cross-link is made of a succession of five glycines. Such a bridge is also required in the peptidoglycan of corynebacteria, which is specific in cross-linking the α-carboxyl carbon of the D-iGlu in position 2 of one peptide stem (acyl acceptor) to the carbonyl carbon of the D-Ala at position 4 of another peptide stem (acyl donor). Of note, the cross-link in these species is a very unusual $2 \rightarrow 4$ cross-link, whose formation is nevertheless catalyzed by PBPs (see Vollmer, Blanot et al., 2008 for a review).

Cross-linking may also not be uniform across the peptidoglycan as in *S. pneumoniae* (Bui et al., 2012), which contains direct cross-links and cross-linking through L-Ser-L-Ala or L-Ala-L-Ala bridges. Furthermore, peptide cross-linking of the glycan strands is not a process which necessarily happens as soon as the murein is synthesized. Actually, new peptidoglycan has been shown to be less cross-linked than “old” peptidoglycan (Burmant & Park, 1983; de Pedro & Schwarz, 1981). Similarly, the degree of cross-linking can also be impacted by the bacterial stage of growth (Pisabarro et al., 1985) and environmental conditions.

1.D.c- Modification of the peptidoglycan

The peptidoglycan net obtained after polymerization of the glycan strands and cross-linking of the peptide stems rarely remains unaltered. Several chemical modifications have been reported in the glycan strands. These are usually situated on the C-2 and C-6 of MurNAc and/or GlcNAc (figure I.1.10; Vollmer, 2008). One of the most common modifications is the N-deacetylation at the C-2. This deletion occurs on MurNAc, GlcNAc or both, mostly in Gram-positive bacteria. GlcNAc deacetylation gives bacteria resistance to lysozyme (Amano et al, 1977) and autolysins (bacterial lytic peptidoglycan enzymes). Indeed, lysozyme, and probably autolysins, need to recognize N-acetyl groups in order to cleave the GlcNAc-MurNAc glycosidic bond (Vocadlo et al, 2001). Similarly, O-acetylation at C-6 has been observed on MurNAc, and in one case, on GlcNAc (Bernard et al., 2011). Bacteria harboring this pattern show an increased virulence (Bera et al., 2006), due also to a better resistance to the same peptidoglycan lytic enzyme. Less common or bacterial-species specific glycan modifications can also be found, for which more information is given in Vollmer, 2008 and Moynihan et al, 2014.

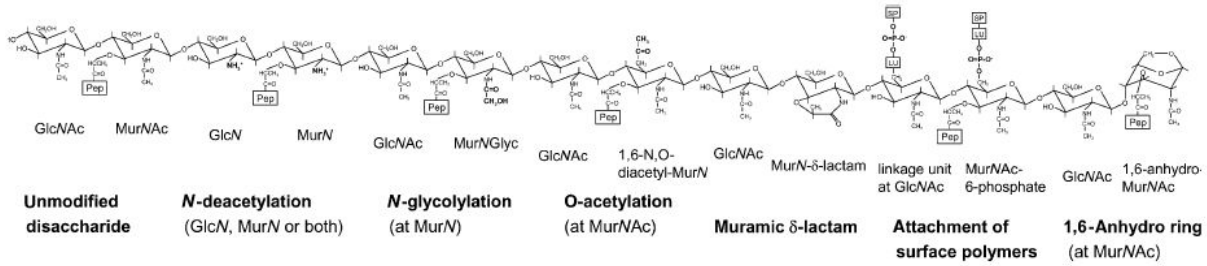

Figure I.1.10: Some of the modifications reported on glycan strands. N-deacetylation and O-acetylation increase bacterial virulence through acquired resistance to lysozyme activity. N-glycolylation is a modification mainly restricted to Mycobacteria which is thought to have a similar function. Muramic acid δ-lactam is limited to spores, where it is a specific target of germination-dedicated hydrolases. Two other common modifications are the attachment to macromolecules (glycopolymers, Lpp...) and the formation of an 1,6-anhydro ring (at the end of the strand). Taken from Vollmer, 2008**.**

The peptide stems can also be the subject of modifications. Some of them include subtle changes of the α- and ε-carboxylic groups of D-iGlu and *m*-A_2pm through amidation, mostly in Gram-positive bacteria. The α-carboxylic group of D-iGlu can also incorporate additional amino acids and hydroxylation of the carbon chain of the third and fourth residues of the stem peptides can occur at high oxygenation levels (see Vollmer, Blanot et al., 2008 for some examples). Others deal with the incorporation of non-canonical D-amino acids (NCDAA), which can be produced by bacteria and released in the extracellular medium. For example, a *Vibrio cholerae* mutant strain inapt to synthesize peptidoglycan was shown to be able to assimilate in its peptidoglycan D-methionine produced by wild type *V. cholerae*. In this process, the incorporated atypical residue is exchanged by L,D-transpeptidases with the D-ala in position 4 or 5 of the stem peptide. This mechanism is thought to be important for the cell to adapt to osmotic pressure and to regulate its amount of peptidoglycan (Cava et al., 2011).

Peptidoglycan can also be modified by the attachment of macromolecules. As discussed in part I section 1.B.a, diverse glycopolymers are exposed at the surface of Gram-positive bacteria, which requires their binding to the peptidoglycan layer. Most of the time, wall teichoic and teichuronic acids are anchored to the murein by a phosphodiester linkage to the hydroxyl group at the C-6 of MurNAc (Vollmer, 2008). In *E. coli*, Lpp is one of the most abundant peptidoglycan-linked (lipo)protein. While its N-terminal end is anchored to the outer-membrane, its C-terminal extremity can be covalently bound to the peptidoglycan layer to ensure outer-membrane integrity (Braun & Rehn, 1969). L,D-transpeptidases were shown to be implied in this reaction, binding the *m*-A_2pm α-carbonyl from a donor peptide stem to the amine group of the side-chain of the Lpp terminal lysine residue (Magnet et al., 2007). Due to the L,D-transpeptidases low specificity with respect to different D-amino acids, this process has been recently adapted *in vitro* to introduce fluorescent D-amino acids (FDAA) in the peptidoglycan and used to label active regions of peptidoglycan synthesis and remodeling *in vivo* (Kuru et al., 2012; Kuru et al., 2015). In Gram-positive bacteria, sortases usually anchor specific proteins to the peptidoglycan and proceed through a transpeptidation reaction between an amino group of the target protein and the peptidoglycan peptide stem. In *S. aureus*, sortase A was shown to be essential for pathogenesis (for a review on sortases see Bradshaw et al., 2015).

Besides these modifications, peptidoglycan can also been reshaped by a high variety of hydrolases which can virtually cleave almost any bond. This aspect is further described in part I section 3.A.a.

Peptidoglycan composition and all of its modifications are accounting for its unique

properties. This enable sacculi to sustain a definite shape for the cell. Most importantly, the rigidity and elasticity of this assembly is essential for bacteria to adapt to the cytoplasmic osmotic pressure and to environmental factors. Due to its role, its unique composition in the living world, and its location outside of the cytoplasmic membrane, peptidoglycan has been and still is an attractive target for antibiotics. However, due to the apparition of resistance to multiple drugs in virtually all bacterial species, it is urgent to develop new strategies (Fischbach & Walsh, 2009). This requires a detailed understanding on the biosynthesis and maturation processes involved in the genesis of this essential and ubiquitous biopolymer.

Résumé en français du chapitre 1 : Le peptidoglycane, composant essentiel de la paroi bactérienne

Les bactéries sont des procaryotes, êtres unicellulaires sans noyau, de taille généralement comprise entre 10 et 100 µm. Les formes de ces organismes sont très variées, allant du bâtonnet (pour la bactérie modèle *Escherichia coli*) à la sphère (comme pour *Staphylococcus aureus*), en passant par l'hélice (*Helicobacter pylori*). La cellule bactérienne est constituée de deux principaux compartiments, le cytoplasme et la paroi bactérienne, séparés par la membrane plasmique. Cette paroi contient un biopolymère essentiel, le peptidoglycane, qui résulte de la polymérisation de disaccharides formés de N-acétylglucosamine (GlcNAc) et d'acide N-acétylmuramique (MurNAc), réticulés via de courtes chaînes peptidiques. La structure obtenue permet à la cellule de résister à la pression osmotique interne et de lui donner sa forme. La coloration de Gram permet d'identifier deux types de bactéries, Gram-positives et Gram-négatives, divergentes par l'organisation et la composition de cette paroi (Figure).

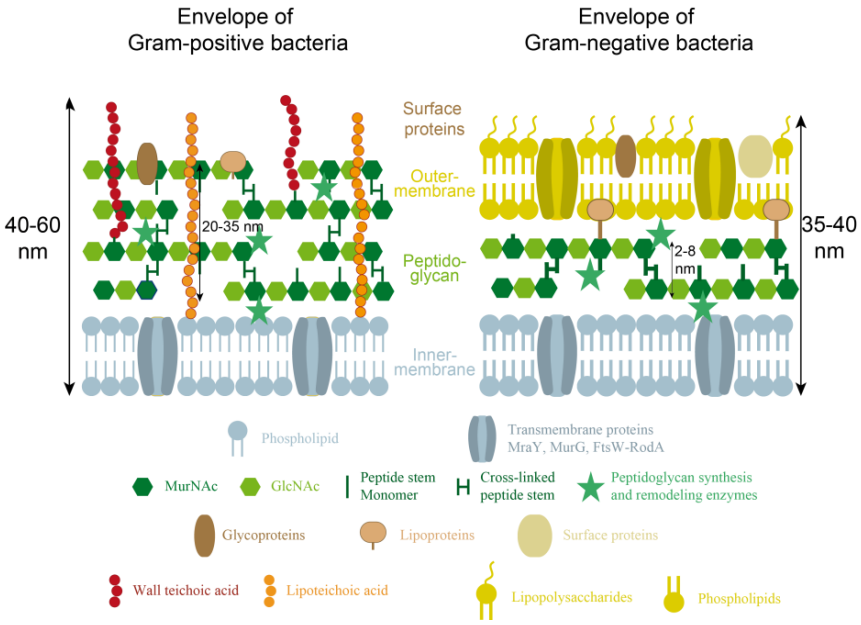

Figure : Organisation schématique de l'enveloppe bactérienne pour les bactéries (A) Gram-positives et (B) Gram-négatives.

Les bactéries Gram-positives, tels que *Bacillus subtilis* ou *Streptococcus pneumoniae*, sont colorées en pourpre, retenant le violet de gentiane utilisé. Leur paroi est composée d'une unique membrane, la membrane plasmique, d'une couche de peptidoglycane épaisse de 20 à 35 nm en général et de divers glycopolymères liés au peptidoglycane ou à la membrane. Ces derniers ont des rôles non négligeables dans la virulence et dans la formation de biofilms par exemple. Trois principaux types de glycopolymères liés au peptidoglycane ont été répertoriés, et classéssuivant leur charge. Les acides téichoïques (zwitterioniques) et les acides teichuroniques (anioniques) sont tous deux constitués de répétition d'unités glycérol et/ou

ribitol phosphate. Ces éléments disposent de charges négatives provenant de leurs groupements phosphates. Le caractère zwitterionique des acides téichoïques provient des charges positives localisées sur la fonction amine libre de l'ester de D-alanine substituant certains des groupements hydroxyles de la chaîne de polyribitol ou polyglycérol. Enfin d'autres glycopolymères, neutres, peuvent également être présents chez certaines espèces, comme *Bacillus cereus par exemple*. Cette diversité de charge se retrouve beaucoup moins chez les glycopolymères covalemment liés à la membrane plasmique, la plupart étant des acides lipotéichoïques constitués de chaînes de glycerol phosphate connectées à la membrane par un disaccharide lié à une unité glycérol. La répartition des charges des glycopolymères liés au peptidoglycane est essentielle pour la bactérie, des variations de composition pouvant causer des divisions défectueuses et perturber l'interaction avec d'autres cellules bactériennes ou des cellules hôtes.

Les bactéries Gram-négatives, comme *E. coli*, apparaissent plus claires à la coloration de Gram, en rose généralement au lieu de pourpre, que les bactéries Gram-positives. Ceci fait suite à leur décoloration après lavage et recoloration par un autre pigment, la safranine ou la fucshine présente dans le colorant de Gram. Leur paroi est constituée de deux membranes, une membrane interne (membrane plasmique analogue à celle des bactéries Gram-positive) et une membrane externe, séparées par un espace périplasmique, où se trouve une fine couche de peptidoglycane d'épaisseur comprise généralement entre 2 et 8 nm. La membrane externe est caractérisée par une composition asymétrique, des phospholipides du côté interne, et des lipopolysaccharides (LPS) sur la face externe. Ces derniers sont constitués d'un lipide A servant d'ancrage, suivi d'un cœur oligosaccharidique, et parfois d'un antigène O permettant à la bactérie d'échapper au système immunitaire de l'hôte. Cette composition est responsable du caractère hautement imperméable de cette membrane. Afin de maintenir son intégrité, la membrane externe est connectée à la couche de peptidoglycane par l'abondante lipoprotéine de Braun.

D'autres organismes sont plus difficiles à classer. C'est notamment le cas des mycobactéries, telles *Mycobacterium tuberculosis*, dont la constitution de la paroi est plus complexe et peut être divisée en 5 couches, dont deux sont constituées de membranes, la membraneplasmique et la mycomembrane. A l'inverse, les mycoplasma, des espèces parasites, sont des organismes dépourvus de paroi. Il a également été démontré que certaines bactéries Gram-positives et -négatives sont capables de survivre sans peptidoglycane, dans des conditions où la pression osmotique est abolie, à savoir dans un état appelé forme L.

Bien que le rôle primordial du peptidoglycane pour la bactérie ait été reconnu dès le début des années 60 et que l'état des connaissances à son sujet n'ait cessé d'augmenter depuis, l'architecture 3D du sacculus, l'enveloppe de peptidoglycane englobant la cellule, reste méconnue. En effet, la cristallographie aux rayons X et la RMN sont toutes deux incapables d'en déterminer la structure exacte à l'échelle atomique, à cause de sa flexibilité et de son hétérogénéité intrinsèques. Les développements en microscopie, microscopie à force atomique (AFM) et microscopie électronique (EM) en particulier, et la mise au point de protocoles basés sur la spectrométrie de masse (MS) alliée à la chromatographie en phase liquide à haute performance (HPLC) ont toutefois permis respectivement l'étude des propriétés mécaniques et de la structure chimique du peptidoglycane ces trois dernières décennies.

Alors que le sacculus est généralement perçu comme une enveloppe rigide, il présente en réalité une élasticité importante, comme l'ont démontré des expériences de diffusion de rayons X aux petits angles et d'AFM. En effet, le sacculus rétrécit lorsqu'il est isolé ou lorsque la membrane cytoplasmique est rompue. Inversement, lorsque la pression osmotique du compartiment cytoplasmique augmente, le sacculus s'étire. De manière intéressante, chez *E. coli*, des mesures par AFM ont montré que l'élasticité de sacculi hydratés était 1,8 fois moins importante le long de l'axe longitudinal que le long de l'axe perpendiculaire. Une explication

avancée pour cette différence d'élasticité est que les chaînes peptidiques, plus flexibles, seraient positionnés dans le sens de la longueur de la cellule alors que les chaînes oligosaccharidiques seraient orientées perpendiculairement à cet axe. La rigidité des sacculi dépend également du taux de réticulation, ce qui connecte directement l'élasticité du peptidoglycane au stress subi par la cellule, en plus de celui imposé par la pression osmotique.

Divers paramètres structuraux ont également pu être déterminés. Parmi ceux-ci, l'épaisseur du peptidoglycane a été estimée comme étant comprise entre 2 et 6 nm chez *E. coli*, suivant les conditions expérimentales (souche, phase de croissance, méthode utilisée, préparation de l'échantillon...), ce qui correspondrait à une à trois couches de chaînes oloigosacchridiques portées par des peptides. Chez les bactéries Gram-positives, cette épaisseur est très variable, atteignant respectivement environ 20 et 35 nm chez *S. aureus* et *B. subtilis*, tandis qu'elle n'est évaluée qu'à 8 nm seulement chez *S. Pneumoniae*.

A l'aide de sondes fluorescentes, la taille des pores formées dans le réseau de peptidoglycane a également pu être mesurée. Un rayon d'environ 2 nm a étédéterminé en absence de stress chez E. coli et *B. subtilis*, ce qui devrait permettre le passage de protéines globulaires d'environ 22 à 24 kDa à travers l'épaisseur du peptidoglycane. En extrapolant à des conditions *in vivo* où le peptidoglycane est étiré, des protéines allant jusqu'à 50 kDa devraient pourvoir traverser la couche de peptidoglycane. Toutefois, la taille de ces pores n'est probablement pas homogène, quelques uns d'entre eux pouvant atteindre jusqu'à 13 nm de rayon chez *P. aeruginosa*.

La combinaison de la chromatographie liquide à haute performance et de la spectrométrie de masse a permis de déterminer un autre paramètre, la longueur des chaînes de glycanes. Pour ce faire, du peptidoglycane marqué radioactivement ^{14}C est purifié, puis digéré par une amidase clivant les liaisons entre le peptide et le MurNAc, avant d'être séparé par chromatographie et analysé par spectrométrie de masse. Le nombre d'unités disaccharidique par chaîne dépend fortement de l'espèce, de la souche bactérienne, mais aussi des conditions de culture et de la phase du cycle cellulaire. Chez *E. coli*, les ¾ des chaînes oligosaccharidiques sont constituées en moyenne de 9 unités disaccharidiques alors que les 25 % restants peuvent comprendre jusqu'à 80 de ces unités. Ces chaînes peuvent toutefois atteindre des longueurs bien plus conséquentes, comme chez *B. subtilis*, où certains d'entre elles semblent être constituées de 5000 unités.

Le degré de réticulation, déterminé à l'aide des mêmes approches, est encore plus variable que la longueur des chaînes oligosaccharidiques. Il peut par exemple fluctuer entre 31 et 61 % chez *E. coli* suivant la souche ou la phase de croissance considérée. De manière similaire, alors qu'elle atteint 56 % chez *B. subtilis* pour des cellules en phase exponentielle, celle valeur chute à 3 % pour des cellules en sporulation. Afin d'obtenir ces données, les sacculi purifiés sont traités avec des muramidases ou du lysozyme afin de rompre les liaisons glycosidiques et d'obtenir des disaccharides plus ou moins réticulés (monomères, dimères, trimères, tétramères...). Les muropeptides obtenus sont ensuite séparés par HPLC et analysés par spectrométrie de masse à source d'ionisation laser assistée par une matrice (MALDI-TOF). Cette approche permet de déterminer le ratio de monomères, dimères, trimères et tétramères, ainsi que la longueur des chaînes peptidiques de chaque constituant.

A partir de l'ensemble des paramètres physico-chimiques ainsi déterminés , deux principaux modèles ont vu le jour pour décrire l'architecture du peptidoglycane. Le modèle le plus accepté dans la communauté scientifique suggère une organisation en couches successives, où les chaînes oligosaccharidiques seraient placées parallèlement à la membrane plasmique. Dans cette configuration, à cause de la conformation en hélice à rotation horaire de la chaîne de glycanes, les peptides seraient orientés à intervalles réguliers dans 3 à 4 directions. Approximativement la moitié d'entre eux seraient alors disponibles pour une réticulation avec d'autre brins dans le même plan, tandis que les autres permettraient de connecter différentes couches, expliquant la variabilité de l'épaisseur de la couche de peptidoglycane d'une espèce bactérienne à une autre. Les chaînes oligosaccharidiques ont

également été prédites pour adopter une conformation en zigzag, ce qui donnerait au final une structure locale en forme d'hexagone, appelée tessera. Cependant cette dernière organisation n'a pas été démontrée expérimentalement pour le moment. Des travaux récents par AFM, chez *B. subtilis* suggèrent que les chaînes de glycanes pourraient se superposer autrement, afin de former une structure hélicoïdale condensée ayant l'allure d'un câble large de 50 nm, parallèle à l'axe transversal. Le second modèle proposé pour l'architecture du peptidoglycane est une organisation en échafaud, où les brins oligosaccharidiques seraient positionnés perpendiculairement à la membrane plasmique et réticulés entre eux par leurs chaînes peptidiques. Toutefois, ce modèle s'adapte très mal aux bactéries Gram-négatives, la longueur des chaînes glycanes étant bien supérieure à l'épaisseur de la couche de peptidoglycane. De plus ce second modèle n'est pour le moment pas étayé par des données expérimentales. La structure du peptidoglycane n'est toutefois sans doute pas aussi régulière qu'initialement conçue. En effet, de récents résultats obtenus par cryo-microscopie électronique et AFM chez *E. coli* et des streptococci semblent indiquer une organisation des chaînes de glycanes approximativement perpendiculaire à l'axe longitudinale, en un réseau hétérogène.

Alors que l'architecture du peptidoglycane reste amplement méconnue, sa composition moléculaire est beaucoup mieux documentée. Les brins oligosaccharidiques sont composés d'une répétition de GlcNAc et MurNAc connectés par une liaison β-1,4-glycosidique. Les chaînes glycanes se terminent généralement par un acide anhydromuramique N-acétylé (1,6-anhydroMurNAc), où les carbones 1 et 6 sont connectés par une liaison éther. La composition de la chaîne peptidique fixé au niveau du D-lactate, est quant à elle, beaucoup plus variable et a la particularité de comporter des acides aminés D. En première position, en partant du lactate, se trouve généralement une L-alanine (L-Ala), suivie d'un acide D-isoglutamique (D-iGlu). Le carbone γ de ce dernier est connecté au 3ème résidu, qui est soit un acide *meso*-diaminopimélique (*m*-A_2pm) chez les bactéries Gram négatives, les bactéries Gram-positives du genre *Bacillus*, et les mycobactéries, soit une L-lysine (L-Lys) chez la plupart des bactéries Gram-positives. Cet chaîne peptidique se termine généralement par deux D-alanines (D-Ala), mais celles-ci peuvent être parfois remplacées par d'autres acides aminés. Afin d'obtenir une structure en réseau, ces peptides peuvent être réticulés par deux types de pontage inter-peptidiques. Le plus répondu est le pontage 4→3, qui connecte le résidu en position 3 du brin accepteur au résidu en position 4 du brin donneur. La réaction de D,D-transpeptidation formant le pontage est catalysée par les protéines liant la pénicilline (PBPs), après clivage du D-Ala en position 5 du brin donneur. Une autre stratégie a également été mise en évidence chez *Mycobacterium tuberculosis* et des souches résistantes d'*Enteroccocus faecium*, le pontage 3→3. Dans ce cas-là, la transpeptidation est réalisée à partir de deux résidus en position 3 par les L,D-transpeptidases. En plus de dimères formés par ce enzymes, des trimères et des tétramères peuvent également être produits en présence de chaînes oligossaccharidiques supplémentaires, mais la proportion de ces deux multimères dépasse rarement 10 %.

Une fois assemblé, le peptidoglycane reste rarement inaltéré, étant la cible de diverses modifications chimiques, généralement sur les carbones 2 et 6 du GlcNAc et du MurNAc. Parmi celles-ci, plusieurs modifications ont pour but de développer une résistance au lysozyme. C'est le cas par exemple des réactions de déacétylation et de O-acétylation (sur le carbone 6). Les brins peptidiques peuvent également être le sujet de modifications ultérieures comme par exemple l'amidation desrésidus D-iGlu et *m*-A_2pm. Certains acides aminés peuvent aussi être remplacés par d'autres résidues non canoniques provenant du milieu extracellulaire, ce qui a récemment été mis à profit pour l'introduction de sondes fluorescentes dans le sacculus afin de suivre sa croissance. Enfin, le peptidoglycane peut être rattaché à d'autres macromolécules. La lipoprotéine de Braun, Lpp, est ainsi covalemment liée au 3ème résidu d'un brin donneur via sa lysine C-terminale. En plus de ces modifications chimiques, il est à noté que la couche de peptidoglycane est constamment remodelée dans les zones de

biosynthèse par des hydrolases.

La composition du peptidoglycane est à l'origine de ses propriétés uniques et de sa capacité à sculpter la cellule. Parce qu'il est restreint aux bactéries, essentiel à leur survie et exposé hors de l'espace cytoplasmique, le peptidoglycane et sa biosynthèse sont des cibles privilégiées pour de nombreux antibiotiques. L'apparition de multiples résistances contraint cependant à la recherche de nouvelles cibles et/ou de nouvelles molécules aux effets thérapeutiques. Cela requiert une compréhension approfondie des étapes de biosynthèse de ce biopolymère et des processus de maturation, phénomènes qui sont décrits dans les chapitres suivants.

Chapter 2
Peptidoglycan biosynthesis

Peptidoglycan synthesis is a long process which requires more than 10 steps and which is performed in two compartments. It begins with the generation of precursors in the cytoplasm. These products are then anchored to a lipid carrier and transferred from the cytoplasm to the periplasm. There, glycan strands are generated and cross-linked to obtain nascent peptidoglycan. As *E. coli* has long been considered as a model in microbiology and as a significant part of the work presented in this thesis relates to some of its proteins, emphasis will be brought on the peptidoglycan biosynthetic system in this organism.

2.A- Synthesis of precursors in the cytoplasm

Peptidoglycan biosynthesis begins in the cytoplasm. The steps occurring in this space start with the synthesis of UDP-GlcNAc and its derivative UDP-MurNAc. Amino-acids are then sequentially added in four steps to the MurNAc to obtain the UDP-MurNAc-pentapeptide compound. Because of the importance of peptidoglycan for the cell, proteins from these steps are highly conserved and essential among diverse bacterial species, with the exception of the D-Ala-D-Ala dipeptide synthesis enzymes.

2.A.a- Biosynthesis of the saccharidic precursors

2.A.a.i- UDP-GlcNAc biosynthesis

Production of UDP-GlucNAc is usually not considered as a step of peptidoglycan biosynthesis, as this compound is involved in several metabolic pathways, among which the formation of other cell wall polymers such as teichoic acids (Brown et al., 2013; Percy & Gründling, 2014). In addition, its production is not unique to bacteria, as it is used in glycoproteins in eukaryotes, although its biosynthesis does not go through the same stages. For these reasons, the generation of UDP-GlcNAc will be only briefly resumed here and the interested reader is invited to refer to the review by Barrateau et al. (Barreteau et al., 2008) for more details.

The synthesis of UDP-GlcNAc from D-fructose-6-phosphate is catalyzed by three enzymes and occurs in four steps (figure I.2.1). First, the glucosamine-6-phosphate synthase GlmS converts D-fructose-6-phosphate into glucosamine-6-phosphate with the use of L-Gln as an ammonia source for the reaction. The structure of GlmS is known and reveals two domains (figure I.2.2 A). The N-terminal glutaminase domain produces L-Glu and ammonia from the L-Gln co-substrate. This latter product is then transferred to the C-terminal isomerase domain through a channel formed upon GlmS dimerization where it is used to generate glucosamine-6-phosphate. Based on crystallographic data on *E. coli* GlmS in the absence and presence of different substrates, Mouilleron and co-authors (Mouilleron et al., 2011) proposed a mechanism in which fructose-6-phosphate binds to the C-terminal domain and opens, thus promoting a conformational change before L-Gln binding in the N-terminal domain and successive events.

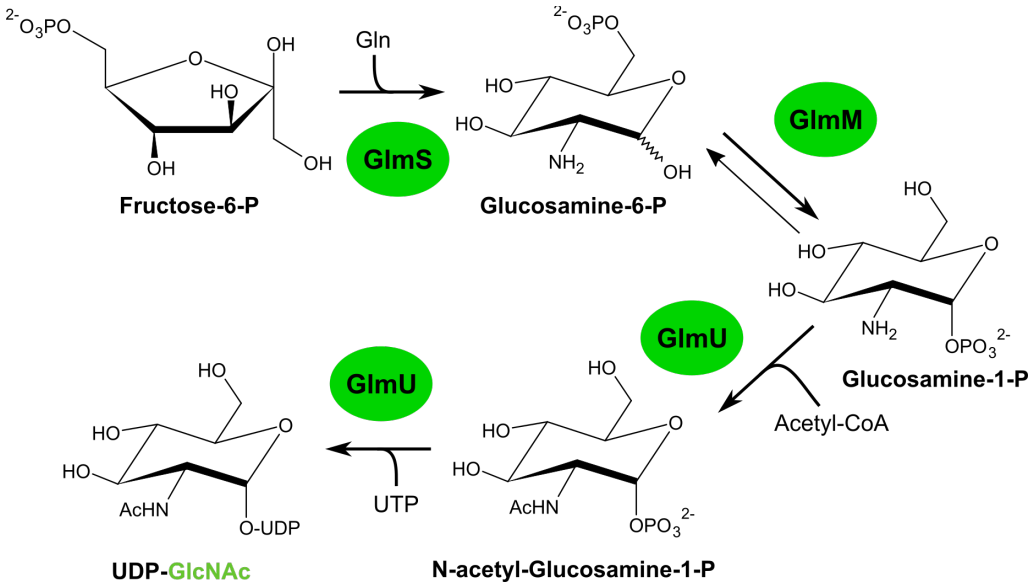

Figure I.2.1: Steps for the biosynthesis of UDP-GlcNAc from D-fructose-6-phosphate. Glucosamine-6-phosphate is generated from D-fructose-6-phosphate by GlmS and then converted to glucosamine-1-phosphate by GlmM. Finally, GlmU catalyzes the formation of UDP-GlcNAc in two steps (acetylation and uridylation). Adapted from Moraes et al., 2015.

The phosphoglucosamine mutase GlmM then catalyzes the interconversion of glucosamine-6-phosphate and glucosamine-1-phosphate (figure I.2.1) through a ping-pong bi-bi mechanism involving glucosamine-1,6-phosphate as an intermediate (Jolly et al., 1999). The protein folds in four domains (figure I.2.2 B) and dimerizes, with the active site located in the center of each monomer where the phosphorylation of a serine is essential in the phosphate group transfer.

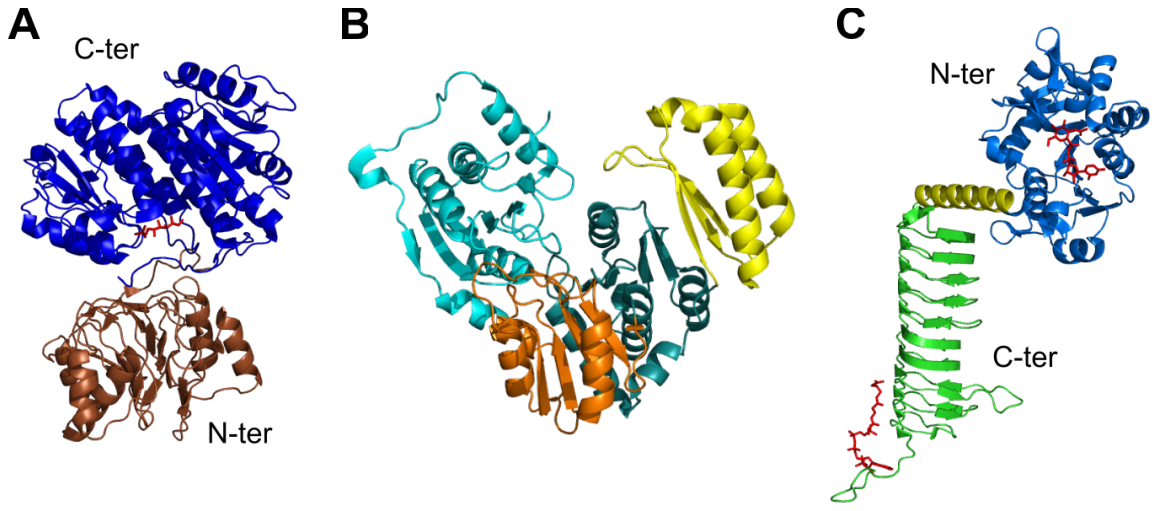

Figure I.2.2: Structures of the three enzymes catalyzing the production of UDP-GlcNAc from fructose 6-phosphate: (A) *E. coli* GlmS (PDB code 1JXA); (B) *Bacillus anthracis* GlmM (PDB code 3PDK); and (C) *E. coli* GlmU (PDB code 2OI5). The GlmS structure shows the glucose-6-phosphate substrate analogue (red) in its binding site. The GlmU structure presents two binding sites, one for the acetyl coenzyme A involved in the acetylation of glucosamine-1-phosphate (C-terminal domain) and one for the product of the uridyltransferase activity (N-terminal domain). Both are represented in red sticks.

The bifunctional N-acetylglucosamine-1-phosphate uridyltransferase enzyme, GlmU, performs the last two required reactions, acetylation and uridylation of the glucosamine (figure I.2.1). Each reaction is performed by an independent domain and in sequential order. The elongated C-terminal domain (figure I.2.2 C, green) catalyzes the acetylation of

glucosamine-1-phosphate with an acetyl coenzyme A cofactor (acetyl CoA). The N-acetylglucosamine-1-phosphate intermediate thus obtained is then transferred to uridine-5'-triphosphate by the N-terminal domain of GlmU (figure I.2.2 C, blue) to form the UDP-GlcNAc precursor and pyrophosphate.

2.A.a.ii- UDP-MurNAc biosynthesis

UDP-MurNAc can then be synthesized from UDP-GlcNAc within two highly conserved steps. First, the enolpyruvate transferase MurA transfers an enolpyruvate group from phosphoenolpyruvate (PEP) to UDP-GlcNAc, yielding to UDP-GlcNAc-enolpyruvate (figure I.2.3).

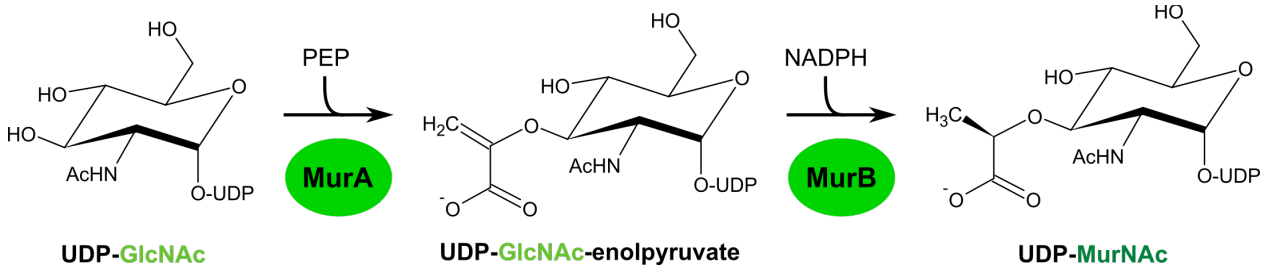

Figure I.2.3: Biosynthesis of UDP-MurNAc from UDP-GlcNAc. The conversion of UDP-GlcNAc into EP-UDP-GlcNAc is catalyzed by MurA, while MurB produces UDP-MurNAc from UDP-GlcNAc-enolpyruvate.

MurA is composed of two similar globular domains. Each of them has six central α-helices surrounded by three four-stranded β-sheets, following a βαβαββ pattern (figure I.2.4). The active site is situated between these two domains. A combination of Small-Angle X-ray Scattering (SAXS) and fluorescence spectroscopy demonstrated that the transition between the open and closed state, which were observed in crystal structures, was triggered by the binding of UDP-GlcNAc (Schönbrunn, et al., 1998). This study also highlighted that this interaction favors the subsequent binding of PEP by an induced-fit mechanism. When MurA is in a closed conformation, the flexible surface-exposed loop (P112-P121, in red in figure I.2.4) folds on the cleft between the two domains to trap the UDP-GlcNAc in this location. Although the exact role of the essential active site residues is still debated (Barreteau et al., 2008), it is largely accepted that the reaction occurs through an addition-elimination mechanism on the hydroxyl group on the C-3 of the GlcNAc, leading to the formation of a tetrahedral phospholactoyl-UDP-GlcNAc intermediate (Marquardt et al., 1993). Interestingly, MurA production of UDP-GlcNAc-enolpyruvate might be inhibited by UDP-MurNAc which is the product of the next step (Mizyed et al., 2005). This would enable the cell to regulate its production of UDP-MurNAc according to its needs and to limit the overconsumption of the UDP-GlcNAc pool.

MurA is the only enzyme from the cytoplasmic step of peptidoglycan synthesis to be the target of a clinically available antibiotic, fosfomycin, which is a molecule naturally produced by *Streptomyces*. This drug competes with the analogous PEP substrate and inactivates MurA by covalent binding with the active site cysteine, which is essential for the enzyme catalysis (Marquardt et al., 1994). Covalent inactivation of MurA by fosfomycin is even increased in the presence of UDP-GlcNAc. Several mechanisms of resistance have nevertheless been identified. For example, mutations of the catalytic cysteine into aspartate in MurA from *M. tuberculosis* impairs fosfomycin binding (Kim et al., 1996). Alternative strategies involve reduced fosfomycin intake, production of drug-degrading enzymes, or overexpression of MurA (see Nikolaidis et al., 2014 for details).

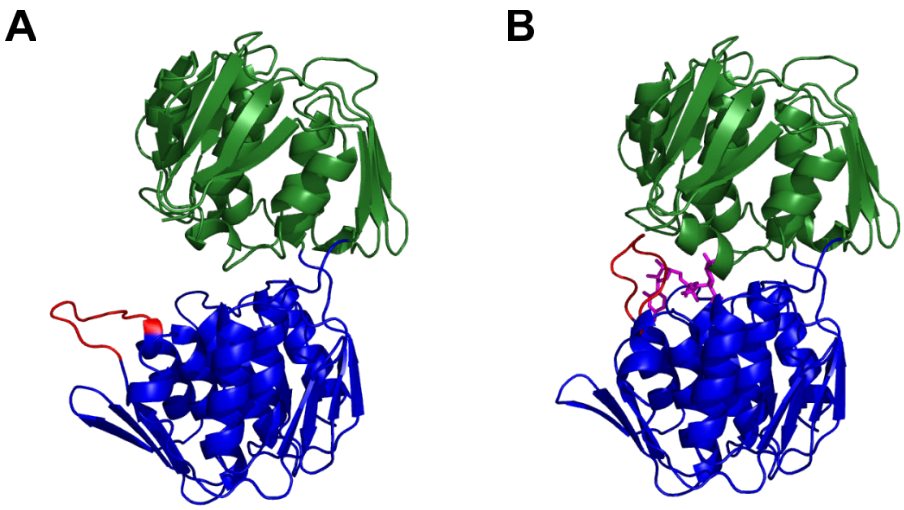

Figure I.2.4: Structures of MurA in the (A) open (PDB code 1NAW) and (B) closed conformations (PDB code 1UAE) from *Enterobacter cloacae* and *E. coli*, respectively. The P112-P121 flexible loop encapsulating the UDP-GlcNAc product (in magenta sticks) is pictured in red. Adapted from Barreteau et al., 2008.

The next stage of the conversion of UDP-GlcNAc into UDP-MurNAc is catalyzed by a flavoprotein, the UDP-N-acetylpyruvyl-glucosamine reductase, MurB (figure I.2.3). The reaction takes place in two steps and is mediated by a Flavin Adenine Dinucleotide (FAD) cofactor. First, the FAD molecule binds at the interface of two of the three α+β domains of MurB (domains 1 and 2 in yellow and orange in figure I.2.5). A Dihydro-Nicotinamide Adenine Dinucleotide Phosphate (NADPH) molecule then binds to the third MurB domain (in red in figure I.2.5), allowing for the reduction of FAD into $FADH_2$ and the release of oxidized $NADP^+$ (Benson et al., 1993). Second, the UDP-GlcNAc-enolpyruvate binds with its UDP moiety replacing the adenine moiety in the previous NADPH binding site (Dhalla et al., 1995). This induces a rotation of domain 3 with respect to the two other domains (Benson et al., 1996), favoring the reduction of the carbon 3 of the enolpyruvyl group by $FADH_2$ through a hydride transfer and a carbanion intermediate. The UDP-MurNAc product is finally released after protonation of carbon 2 of the enolpyruvyl group by a solvent-equilibrated proton (Benson et al., 1993).

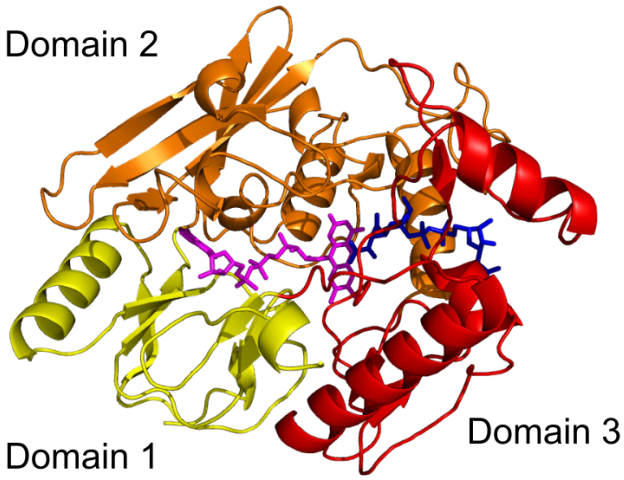

Figure I.2.5: Structure of *E. coli* MurB (PDB code 2MBR). FAD and UDP-GlcNAc-enolpyruvate are shown as sticks in magenta and dark blue, respectively. While FAD binds at the interface of domains 1 and 2, UDP-GlcNAc-enolpyruvate interacts with domain 3, in the same site than the NADPH molecule required in the reaction.

To date, a few molecules targeting MurB have been found (Hrast et al., 2014). However, inhibiting this enzyme could have a two-edged effect, as a decrease in UDP-MurNAc would prevent MurA feedback. This could cause an increase of the produced UDP-GlcNAc-enolpyruvate molecules which could then compete with the drugs (Silver, 2013).

2.A.b- Biosynthesis of the UDP-MurNAc-peptide compound

2.A.b.i- General features of the elongation of the stem peptide

Once UDP-MurNAc is synthesized, the next step is to build the peptide stem from the lactate. This is carried out in the cytoplasm, in four successive steps, each stage consisting in the addition of one or two amino-acid(s). At each stage, the formation of the amide bond is performed by an ATP-dependent Mur ligase, MurC, MurD, MurE or MurF (figure I.2.6). MurC catalyzes the addition of L-Ala to UDP-MurNAc. To date, this is the only one among the four Mur ligases known to adopt, *in vitro*, an equilibrium between monomeric and dimeric forms, although its oligomeric state was not shown to impact its activity (Jin et al., 1996). The next reaction involves MurD, one of the best-understood Mur ligases, which adds a D-Glu amino acid to the stem peptide to yield UDP-MurNAc-L-Ala-D-Glu. Then MurE elongates the peptide stem by binding either *m*-A_2pm or L-Lys to the side-chain carboxylic group of the glutamic acid in most bacterial species. Finally, MurF links the D-Ala-D-Ala dipeptide to UDP-MurNAc-L-Ala-D-iGlu-*m*-A_2pm/L-Lys to obtain UDP-MurNAc-L-Ala-D-iGlu-*m*-A_2pm/L-Lys-D-Ala-D-Ala (figure I.2.6). Despite their modest sequence homologies (10 – 20% between each other; Bugg & Walsh, 1992), these four ligases have conserved motifs and similar 3D structures.

2.A.b.ii- Structural characteristics of the Mur ligases

Mur ligases have been extensively studied and are now well characterized. Structures of all four enzymes were determined by X-ray crystallography, in several organisms including *E. coli* (Smith, 2006). They are organized in three globular domains, an N-terminal (domain 1, green in figure I.2.7), a central (domain 2, blue in figure I.2.7) and a C-terminal (domain 3, red in figure I.2.7) domain, each of them binding a different substrate.

The N-terminal domain 1 is implicated in UDP nucleotide binding, and can adopt two different organizations. In MurC and MurD, domain 1 consists of three-to-five alternating α-helices flanking a parallel β-sheet, yielding to the typically dinucleotide-binding Rossmann fold (Bellamacina, 1996). In these two enzymes, the uridine ring of the UDP-MurNAc(-L-Ala) substrate is sandwiched between two hydrophobic loops (β2-α2 and β4-α4) and one of its aromatic ring nitrogen is anchored to the protein through a hydrogen bond with a conserved residue of the β3-α3 (MurC) or β2-α2 (MurD) loop. The typical nucleotide-binding glycine-rich GxGxxG (loop α1-β1) consensus motif also serves as a diphosphate binding pocket for the substrate (Smith, 2006). In MurE and MurF, domain 1 adopts a different α/β fold with a mixed β-sheet. In MurE, the UDP substrate is stabilized by hydrogen bonds between the uracil and the β1-β2 loop of domain 1, as well as by hydrogen bonds between the pyrophosphate moiety and the β2-α2 loop of the same domain. This compound is further stabilized by additional hydrogen bonds between the N-acetyl-muramic acid and the two other domains (Gordon et al., 2001) in contrast to the MurC and MurD enzymes. Despite the similarity between MurE and MurF apoenzymes, MurF seems to adopt another binding mode for the UDP substrate, as emphasized by a recent UDP-MurF structure in *Acinetobacter baumannii* showing that this nucleotide is interacting with a region astride domains 1 and 2 (Cha et al., 2014). These different strategies from MurC and MurD are likely due to the growing size of the peptide chain in the respective UDP-MurNAc substrates and the requirement in the relative orientation of this binding site with respect to the other two substrate binding sites so

that the ATP-dependent ligation can proceed.

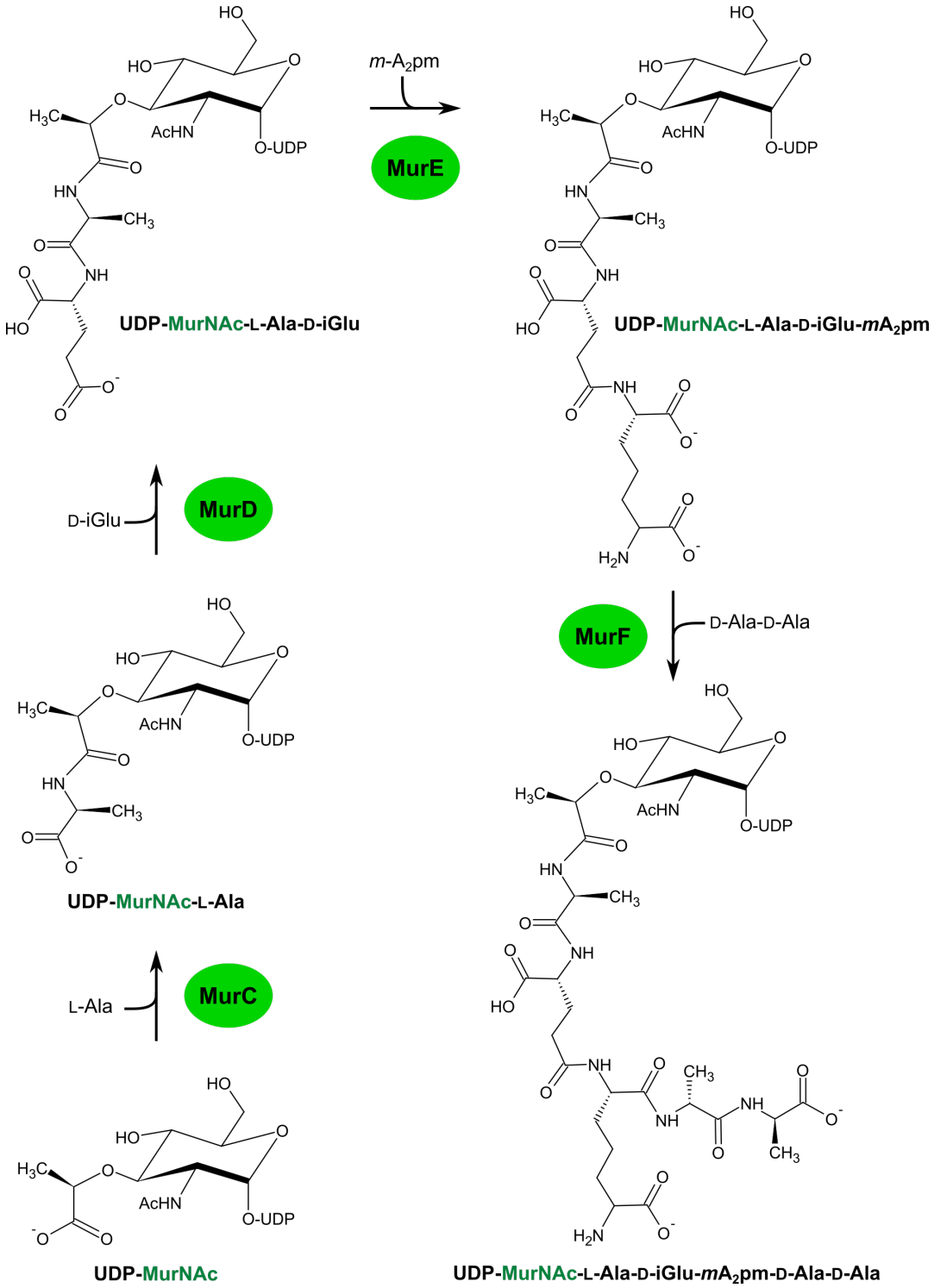

Figure I.2.6: Biosynthesis of UDP-MurNAc-L-Ala-D-iGlu-*m*-A_2pm-D-Ala-D-Ala from UDP-MurNAc by Mur ligases. The UDP-MurNAc-pentapeptide is synthesized in 4 steps, consisting in the sequential addition of L-Ala, D-Glu, *m*-A_2pm (or L-Lys) and D-Ala-D-Ala by MurC, MurD, MurE and MurF, respectively. Adapted from Kouidmi et al., 2014.

The second Mur ligase domain (central domain 2) is also made of a core six- or seven-stranded mostly parallel β-sheet surrounded by four to eight α-helices (Kouidmi et al., 2014) and contains an ATP-binding site. Among the three Mur domains, this one shows the highest degree of sequence identity (22 to 26 %) and homology, as well as structural similarity (Smith, 2006). A possible explanation to this observation is that this domain is the

only one which always accommodates the exactly same substrate. The triphosphate moiety of ATP is hydrogen-bonded to a consensus GxxGKT-T/S motif, similar to the classical mononucleotide-binding P-loop GxxxxGKS/T pattern (Saraste et al., 1990), and establishes additional contacts with a conserved arginine residue and an histidine (in MurC) located in the third domain. Domain 2 also coordinates two Mg^{2+} ions through essentially conserved glutamate and histidine residues. This second ion appears to be essential in the catalysis of the phosphate transfer from ATP to the UDP-MurNAc substrate and its binding site is stabilized by a carbamoylated lysine in all Mur enzymes except MurC, which involves a glutamate close to the first Mg^{2+} binding site. The specificity of the binding site for the adenine triphosphate is conditioned by hydrogen-bonding to the asparagine and pi-stacking to an aromatic residue of a H(/F in MurE)-xxxN consensus motif (Kouidmi et al., 2014).

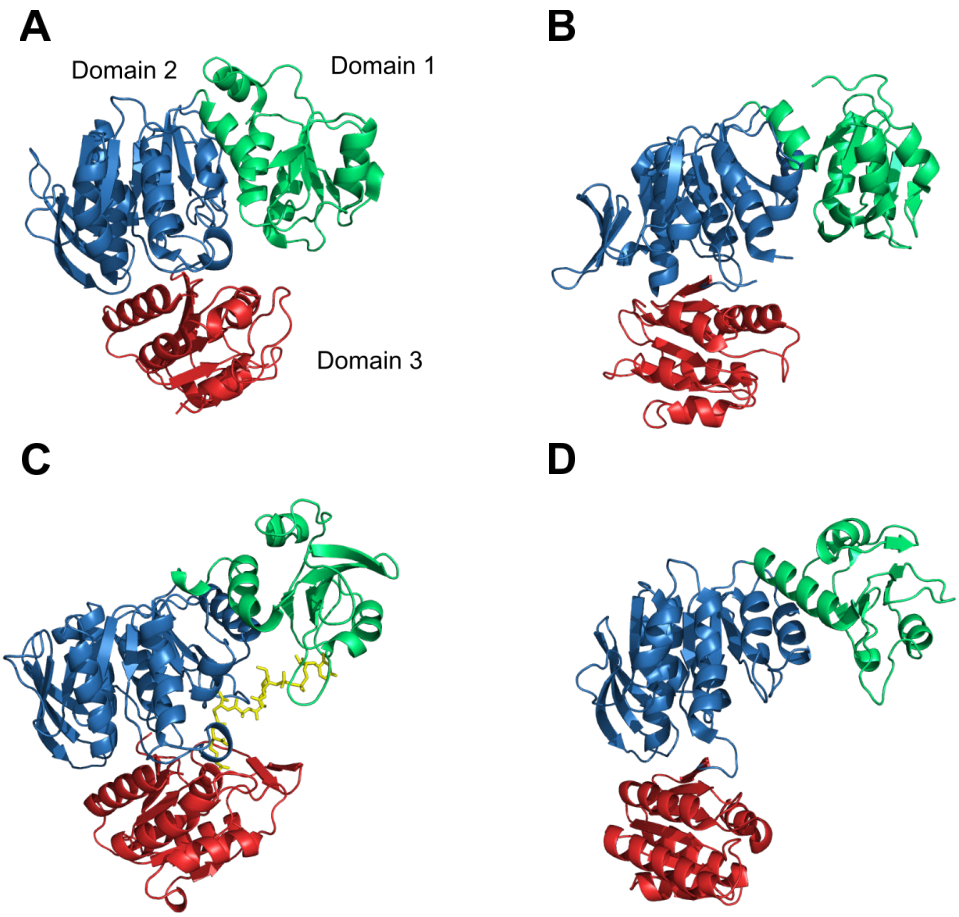

Figure I.2.7: Structures of *E. coli* Mur ligases, (A) MurC (PDB code 2F00), (B) MurD (PDB code 1E0D), (C) MurE (PDB code 1E8C), and (D) MurF (PDB code 1GG4). Mur enzymes consist of three globular domains, domains 1, 2 and 3 from the N-terminus to the C-terminus, which are colored in green, blue and red, respectively. The MurE structure also depicts the UDP-MurNAc-tripeptide product in yellow sticks. Adapted from Smith, 2006.

Similarly to the N-terminal domain, domain 3 has a α/β Rossmann-like fold but does not contain any glycine-rich sequence. This domain is highly likely implicated in amino-acid binding and in further stabilization of the α- and γ-phosphate of the ATP substrate, as well as its ribose. However, in the absence of structures containing the free amino acid or dipeptide involved in the reaction, the binding site is not well characterized. In the case of *E. coli* MurE, the protein residue Arg416 was determined as a key structural determinant for the addition of *m*-A_2pm to the peptide stem, while alanine or asparagine at this position are specific to the addition of L-Lys in the peptide stem (Gordon et al., 2001). Interestingly, it seems that in MurC and MurF ligases, the binding region is not highly specific for their L-Ala and D-Ala-D-Ala substrates. Indeed, MurC was shown to be able to accommodate Gly and L-Ser (Liger et

al., 1991), while MurF can also ligate, among others, D-Ala-D-Lac or D-Ala-D-Ser under the pressure of antibiotics such as vancomycin (van Heijenoort, 2001).

2.A.b.iii- Catalytic mechanism

As a consequence of their structural similarities, all four Mur enzymes follow a common mechanism to ligate the amino acid or dipeptide to the peptidoglycan precursor. This mechanism is well understood and proceeds in three successive steps. First, ATP binds to domain 2 and induces a conformational change from an "open" to a "closed" state, which brings the C-terminal domain 3 closer to the N-terminal domain 1 and central domain 2 (figure I.2.8 A and B). This re-orientational motion is triggered by stabilizing interactions between the triphosphate and ribose of ATP and two motifs in domain 3, respectively. The initial positioning of the ATP substrate is driven by the interaction of a Mg^{2+} ion with the β- and γ-phosphates on one side and protein residues on the other side.

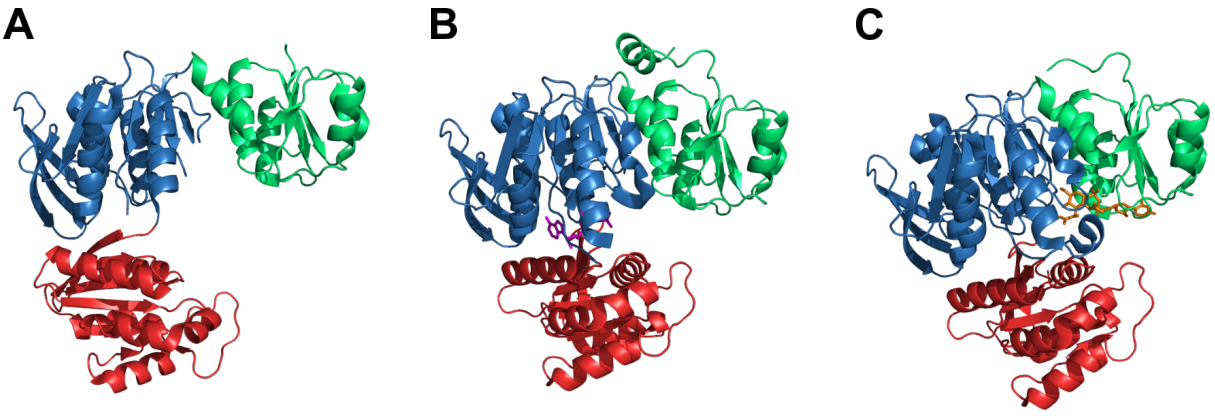

Figure I.2.8: Mur ligases conformations. Mur ligases (here *Haemophilius influenzae* MurC) can adopt an open conformation (A; PDB code 1GQQ) in the apo-enzyme and a closed conformation induced by ATP (B; PDB code 1GQY) and/or UDP-MurNAc (C; PDB code 1P31) binding. Domains 1, 2 and 3 are colored in green, blue and red respectively. The ATP and UDP-MurNAc substrate mimetics are shown as magenta and orange sticks, respectively.

Second, the UDP-MurNAc substrate binds to domain 1. This process is also assisted by one of the Mg^{2+} ions which bridges the terminal carboxylate of the peptide stem and the carbamoylated lysine of domain 2 and may also contribute to the transition between the "open" and "closed" states (figure I.2.8 C). If the timely occurrence of this conformational rearrangement directly after ATP- or UDP-MurNAc binding is still debated (Perdih et al., 2007), the two substrates in the "closed" state are in a correct geometry for phosphate transfer. In this configuration, the C-terminal carboxyl group of the stem peptide of the UDP-MurNAc-peptide substrate is phosphorylated by the ATP γ-phosphate to yield an acyl-phosphate intermediate (upper part of figure I.2.9; Bertrand et al., 1999).

Third, the amino acid or dipeptide to be added on the peptidoglycan precursor peptide stem binds to the Mur ligase domain 3. Its amino group then performs a nucleophilic attack on the carbonyl of the acyl-phosphate intermediate to yield a tetrahedral intermediate (figure I.2.9, lower right), which in turn eliminates the phosphate group to generate the lengthened UDP-MurNAc-peptide$_{n+1}$ product (figure I.2.9, lower left; Kouidmi et al., 2014).

2.A.b.iv- Inhibition

Despite the need to cross two membranes in Gram-negative bacteria to reach them, Mur ligases have been validated as interesting antibiotic targets, and a lot of research is currently performed on this subject (Hrast et al., 2014). Because they have similar mechanism and

structures, these synthases of peptidoglycan precursors appear as attractive enzymes for "broad-range" drugs. Indeed, several lead candidates were isolated in the last years (Antane et al., 2006; Mansour et al., 2007; Sova et al., 2009). Recently, furan-based benzene carboxylic acid derivatives have been optimized by virtual screening, which exhibit multiple MurC-F ligase inhibition in the micromolar range and present promising antibacterial activity against *Staphylococcus aureus* (Perdih et al., 2015).

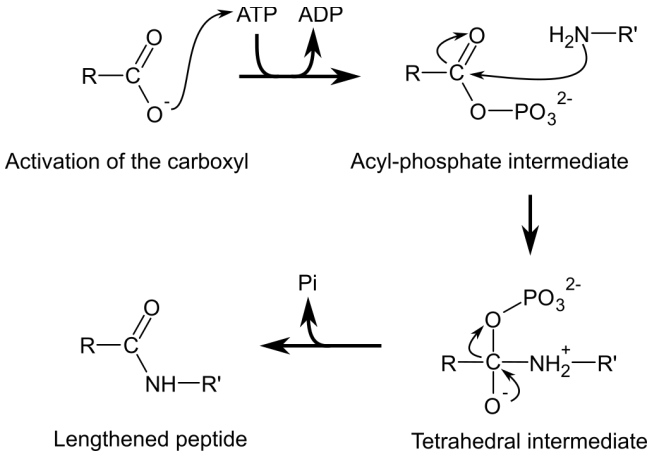

Figure I.2.9: Mechanism of the reaction of elongation of the peptide stem catalyzed by the Mur ligases. In the first step, the γ-phosphate of ATP is transferred to the terminal carboxylic group of the UDP-MurNAc peptidoglycan precursor, to generate the acyl-phosphate intermediate and ADP. In the second step, the free nucleophilic amino group of the amino acid or dipeptide adds to the carbonyl of the acyl intermediate to generate a tetrahedral intermediate. In the third and last step, the phosphate leaving group is released to yield the elongated peptidoglycan precursor. Adapted from Kouidmi et al., 2014**.**

2.A.c- Biosynthesis of unusual amino-acids for peptidoglycan peptide stems

Peptidoglycan peptide stems usually contain three uncommon residues: D-Glu and *m*-A_2pm (mainly in Gram-negative bacteria) in position 2 and 3 respectively, and D-Ala which is added at the extremity of the peptide stem as a D-Ala-D-Ala dipeptide. *m*-A_2pm is the last intermediate in the biosynthesis of L-Lys in bacteria. As such, its production will not be discussed here, but a detailed pathway can be found in Triassi et al., 2014.

2.A.c.i- Biosynthesis of D-Glu

In bacteria, the D-Glu amino acid is mainly found in peptidoglycan and in some Gram-positive bacteria as a poly-gamma-glutamate (PGA) polymer that is anchored to the bacterial cell surface or released in the extracellular medium (Candela & Fouet, 2006). D-Glu can be synthesized following two pathways, either isomerization of L-Glu into D-Glu by a racemase or transamination from D-Ala to α-ketoglutarate.

E. coli can only produce D-Glu with the glutamate racemase MurI. On the contrary to most of the amino-acid racemases, this one does not require any cofactor. MurI has two α/β domains facing each other (figure I.2.10), separated by a pocket where the catalytic and substrate binding sites are found. Two cysteines, one in each domain (in red in figure I.2.10), point towards this site and are implicated in a two-base racemization mechanism (Hwang et al., 1999). It was suggested that the thiolate group of one of these cysteines participates in the deprotonation of the α-carbon of L-Glu, producing a carbanion, which is then reprotonated with the opposite stereochemistry by the second cysteine (Gallo et al., 1993). Unlike the other MurI homologues investigated so far, *E. coli* MurI was reported to require activation by the UDP-MurNAc-L-Ala precursor for glutamate conversion catalysis and increased substrate-binding affinity (Doublet et al., 1993). This activator (in orange, figure I.2.10) binds in a

groove at the interface of the two α/β domains, but on the protein surface, at a remote location from L-Glu and the catalytic cysteines (Lundqvist et al., 2007). The regulation of the MurI L-Glu-to-D-Glu racemase activity by the peptidoglycan precursor enables the cell to produce D-Glu as needed and avoids an excessive consumption and rerouting of L-Glu from the pool devoted to protein synthesis.

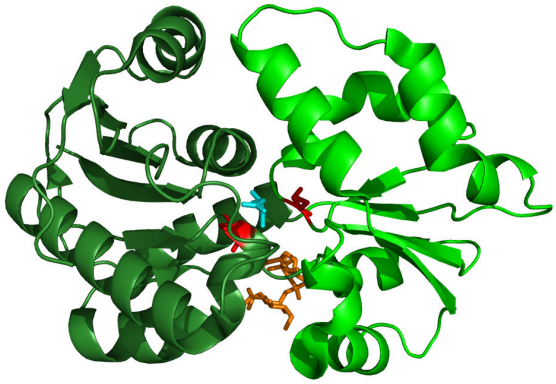

Figure I.2.10: Structure of *E. coli* MurI (PDB code 2JFN) responsible for L-Glu conversion into D-Glu. The two domains are represented in two variants of green. The L-Glu substrate, the UDP-MurNAc-L-Ala activator and the two catalytic cysteine residues are shown as cyan, orange and red sticks, respectively. MurI from other species present a similar fold, although some of them tend to dimerize like the *Helicobacter pylori* protein. MurI from *E. coli* is nevertheless the only glutamate racemase so far with a UDP-MurNac-L-Ala regulated activity.

Some Gram-positive bacteria show an additional D-Glu biosynthetic route. *Staphylococcus haemolyticus* for example (Pucci et al., 1995), shows a D-amino acid aminotransferase (D-AAT) activity in addition to its L-Glu racemase activity. In this transamination pathway, D-AAT is coupled to a pyridoxal 5'-phosphate (PLP) cofactor to produce D-Glu and pyruvate from α-keto-glutarate and D-Ala. The reaction is performed through a ping-pong mechanism and involves a L-Lys as a general acid/base catalytic residue. Both MurI and D-AAT have been considered as interesting targets for “narrow spectrum” antibiotics and a few potent inhibitors have been developed (Keating, 2013).

2.A.c.ii- Biosynthesis of the D-Ala-D-Ala dipeptide

The D-Ala-D-Ala dipeptide is the last compound to be linked to the UDP-MurNAc peptide stem. Its synthesis results from two successive reactions. First, L-Ala is converted into D-Ala by an alanine racemase, which is then mainly used in the biosynthesis of peptidoglycan and teichoic acids of Gram-positive bacteria. Second, two D-Ala residues are condensed by a D-Ala-D-Ala ligase. D-Ala-D-Ala can then be used for UDP-MurNAc-pentapeptide biosynthesis.

The alanine racemase Alr uses PLP as a cofactor for L-Ala conversion. In *E. coli*, it is a dimeric enzyme (Strych & Benedik, 2002), with each monomer displaying an N-terminal domain with an α/β barrel fold and a C-terminal domain mainly composed of β-strands (figure I.2.11). The PLP molecule is localized in the active site between these two domains, where it is bound to a lysine (Shaw et al., 1997). Crystal structures of *Bacillus stearothermophilus* with intermediate analogs revealed that catalysis likely follows a two-base mechanism (Watanabe et al., 2002). First, PLP forms a Schiff base with L-Ala by transaldimination. Then, a reactive tyrosine removes the α-proton from L-Ala and the resulting carbanion gets reprotonated by a lysine on the other side to yield the D-Ala isomer (Watanabe et al., 2002). Finally the D-Ala is released from the enzyme through the formation of an internal aldimine between PLP and the catalytic lysine. In *E. coli* and some other species, a second alanine racemase isozyme named

DadX is also present. While Alr is expressed constitutively, DadX expression is induced by L-Ala (Wild et al., 1985). The reason for this regulation is not very clear, although it has been observed that DadX was expressed when D-Ala was used as a carbon source. It was therefore postulated that DadX activity was important for a D-Ala dehydrogenase (DadA) in the same operon using D-Ala as a substrate for generation of pyruvate and was not particularly involved in peptidoglycan synthesis when Alr is functional (Wasserman et al., 1983).

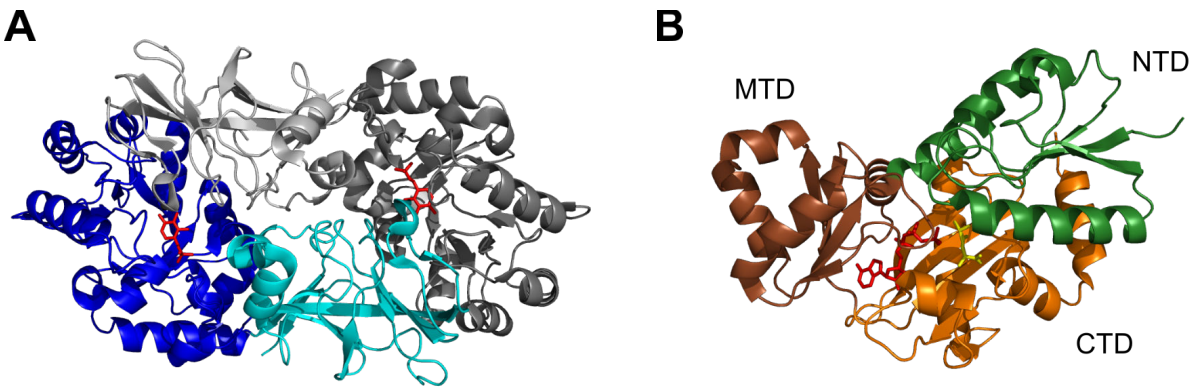

Figure I.2.11: Structure of the two enzymes responsible for D-Ala-D-Ala biosynthesis: (A) *E. coli* alanine racemase Alr (PDB code 2RJG) and (B) *E.coli* D-Ala-D-Ala ligase DdlB (PDB code 4C5C). Alr is represented under its dimeric form, with one monomer in blue, one in grey. The PLP cofactors for Alr, and ATP for DdlB, are displayed in red sticks, while DdlB D-Ala-D-Ala product is in yellow. NTD, MTD, CTD: N-, Middle, and C-terminal domains, respectively.

Once the D-Ala amino acids synthesized, they are assembled in a dipeptide by an ATP-dependent D-Ala-D-Ala ligase (Ddl). Similarly to Alr, two isozymes of Ddl exist in *E. coli*, DdlA and DdlB (Zawadzke et al., 1991), that are composed of three domains (figure I.2.11 B; Fan et al., 1994). While ATP binds between the middle and C-terminal domain, each D-Ala has its own binding site, situated between the N- and C-terminal domains. Biochemical studies highlighted that these two sites have different specificities for D-Ala, the donor site for the N-terminal D-Ala, being the more specific (Neuhaus, 1962). Upon binding of its substrate, Ddl undergoes a conformational change from an “open” to a “closed” state by a rotation of its central domain and a swing motion from a lid loop (Lee et al., 2006). The reaction follows a ter-ter mechanism, which undergoes similar steps as described for the Mur enzymes in figure I.2.9, despite the structural dissimilarity between the two enzymes (Mullins et al., 1990). The D-Ala-D-Ala product generated is a strong inhibitor of the ligase, likely to avoid overproduction of D-Ala which would deplete the L-Ala pool (Mullins et al., 1990). It is noteworthy that in some species, like *Chlamydia*, the reaction is performed by a bifunctional MurC-Ddl enzyme. Although these two activities are independent, it appears that D-Ala-D-Ala ligation requires the full structure (McCoy & Maurelli, 2005).

The D-Ala structural analogue D-cycloserine is one of the most important Alr and Ddl inhibitors. Crystal structure of Alr with this moleculer shows that it forms a stable adduct with the PLP cofactor, inactivating the racemase (Fenn et al., 2003). Although inhibition of Ddl by D-cycloserine has been reported, the mechanism implied in this process is still not fully understood and it is not clear whether lethal phenotypes are due to impairment of one or both enzyme activities (Bruning et al., 2011). Mutations in the D-cycloserine active transporter or overexpression of Alr are some of the bacterial mechanisms described in the literature to limit this drug's effect (Nikolaidis et al., 2014). Another main antibiotic targeting peptidoglycan synthesis is the glycopeptide vancomycin, which binds covalently to the C-terminal carboxyl of the D-Ala-D-Ala dipeptide produced by Ddl. This sequestration prevents cross-linking leading to defects in the peptidoglycan layer. However, resistance to vancomycin arose from biosynthesis of non-canonical D-Ala-D-Lac depsipeptide and D-Ala-D-Ser dipeptide for which

the antibiotic has low affinity (Bugg et al., 1991) and which are produced by proteins from several clusters that can be exchanged by horizontal transfer. In addition to the production of a D-Ala-D-X ligase, these transferred plasmid can encode among others for D,D-peptidases to eliminate D-Ala-D-Ala dipeptides, dehydrogenases to produce D-lactate from pyruvate, or D-serine racemases (Depardieu et al., 2007).

2.B- Biosynthesis of lipid-linked intermediates

The two steps following synthesis of saccharide-peptide precursors in the cytoplasm are performed in close correlation with the cytoplasmic membrane inner leaflet (figure I.2.12). To begin with, UDP-MurNAc-pentapeptide is anchored to a lipid carrier to yield lipid I. Then, GlcNAc is transferred from UDP-GlcNAc onto lipid I, giving lipid II. Inhibitors of these two reactions are under investigation, although the detailed catalytic mechanisms are not completely understood yet.

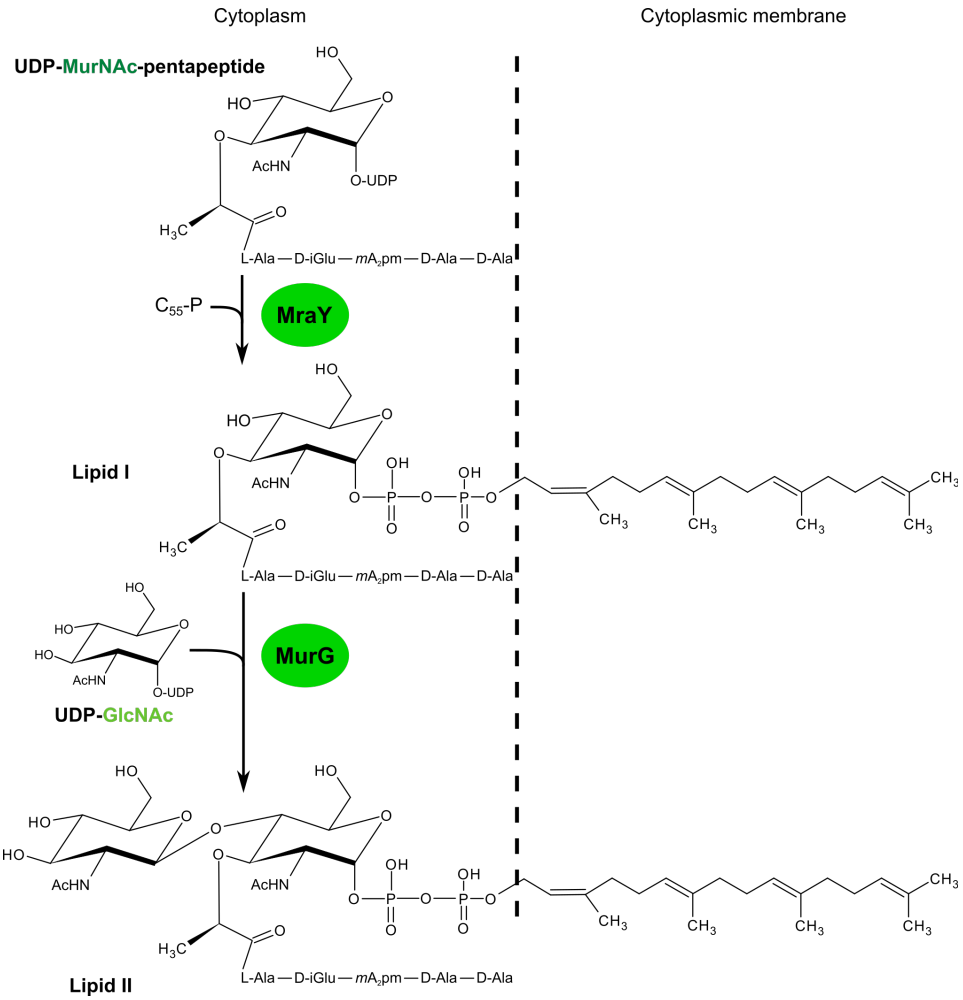

Figure I.2.12: Synthesis of lipid II. Lipid II is synthesized in two steps: first, UDP-MurNAc-pentapeptide is attached to C_{55}-P by MraY to generate lipid I. Then, MurG adds UDP-GlcNAc, leading to the formation of lipid II. Although not displayed here, MraY is inserted in the cytoplasmic membrane while MurG is likely associated to the membrane by a hydrophobic patch.

2.B.a- Biosynthesis of lipid I

The phospho-MurNAc-pentapeptide translocase MraY is the membrane enzyme responsible for the attachment of the UDP-MurNAc-pentapeptide to an undecaprenyl phosphate lipid acceptor (C_{55}-P). The reaction is catalyzed by a Mg^{2+} ion and releases lipid I

and UMP. While MraY has a good specificity for residues in position 1 and 4 of the peptide stem, glycine substitutions showed that the third and fifth positions allowed for more variability, probably in order to deal with the variations (*m*-A_2pm/L-Lys, D-Ala/D-Lac for example) that can exist in these locations in different species (Hammes & Neuhaus, 1974). Because purification of a large amount of this membrane protein has long been challenging, its crystal structure was solved only recently (Chung et al., 2013). MraY appears to be mainly composed of a succession of membrane-inserted α-helices linked by several loops pointing in the periplasm or the cytoplasm (figure I.2.13, left panel), as predicted in 1999 (Bouhss et al., 1999). Because the protein crystallized as a dimer and showed positive results to cross-linking and bacterial two-hybrid studies (White et al., 2010; Chung et al., 2013), it is thought that this is the oligomerization state adopted by the protein *in vivo*. On the inner leaflet side of the cytoplasmic membrane, MraY has a highly conserved cavity shaped by 5 α-helices that is proposed as the active site. To support this hypothesis, a Mg^{2+} catalytic ion was found in this site and four residues (3 Asp and 1 His) in this region were shown to be essential for MraY activity and invariant across species (figure I.2.13, right panel; Chung et al., 2013). The UDP-MurNac-pentapeptide binding site is thought to be trapped between the transmembrane helix α9 and a HHH loop which contains the conserved histidine residue. The undecaprenyl phosphate is likely positioned in an internal hydrophobic groove with its phosphate end pointing towards the Mg^{2+} ion in the active site, maintained in this location by the conserved Asp residues.

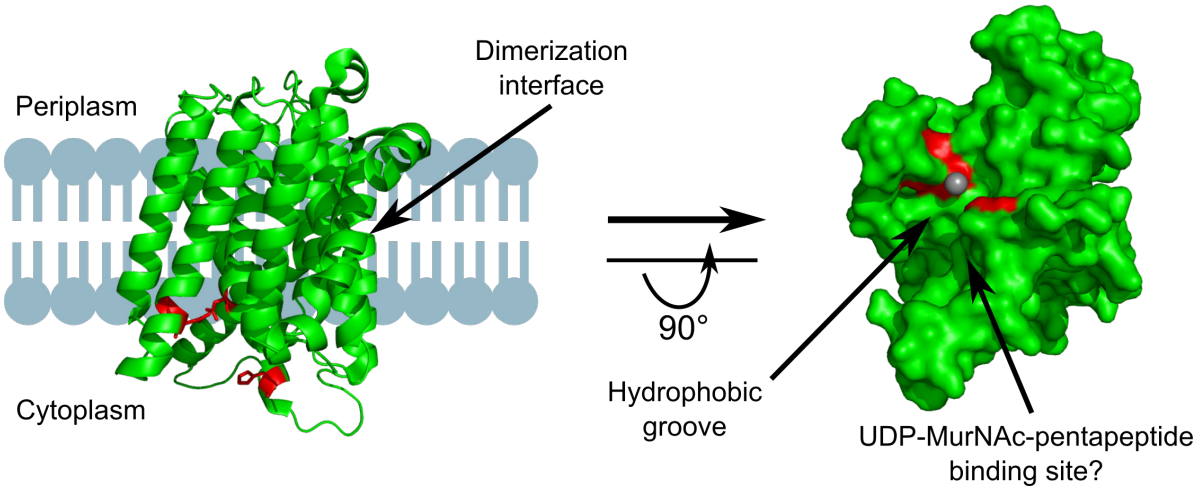

Figure I.2.13: Structure of *Aquifex aeolicus* MraY (PDB code 4J72). Left: Cartoon representation of a monomeric unit of the dimer. In the current representation, the dimerization interface is on the right of the monomeric unit, perpendicular to the membrane. Right: MraY surface representation from the cytoplasm side. Mg^{2+} is represented by a gray ball in the active site cavity. The invariant residues in the active site Asp117, Asp118, Asp265 coordinating the Mg^{2+} ion and His324 from the HHH loop are shown as red sticks. The proposed C_{55}-P (the hydrophobic groove) and UDP-MurNAc-pentapeptide binding sites are each indicated by an arrow.

Although this structure sheds new light on the lipid I synthesis, details of the MraY reaction mechanism are still poorly understood. More than 45 years ago, a two-steps reaction was proposed. First a nucleophilic attack of a protein residue on the UDP-MurNAc-pentapeptide β-phosphate would yield a covalently bound enzyme-phospho-MurNAc-pentapeptide intermediate after the release of UMP. Then, the phosphate of this intermediate would undergo a nucleophilic attack by the oxoanion from the C_{55}-P phosphate group (Heydanek & Neuhaus, 1969). Based on recent mutation studies on pure samples, Al-Dabbagh and co-workers (Al-Dabbagh et al., 2008) proposed a direct mechanism where, after deprotonation by a catalytic aspartate, the phosphate oxygen of the C_{55}-P molecule performs a nucleophilic attack on the β-phosphate of the UDP-MurNAc-pentapeptide substrate. This

scenario is strengthened by the MraY structure where the catalytic aspartate is localized in the C_{55}-P binding site.

2.B.b- Biosynthesis of lipid II

The membrane-associated N-acetyl-glycosyl transferase MurG catalyzes the transfer of GlcNAc from UDP-GlcNAc to lipid I, producing lipid II and releasing UDP. *E. coli* MurG is composed of two structurally homologous α/β domains (figure I.2.14) with a Rossman-like fold, separated by a large cleft (Ha et al., 2000). The UDP-GlcNAc donor molecule binds to the C-terminal domain while the lipid I acceptor binds to the N-terminal domain, close to the cleft. This domain is also involved in interaction with membrane through a hydrophobic patch surrounded by basic residues. The reaction proceeds following an ordered bi-bi mechanism, with UDP-GlcNAc as the first substrate (L. Chen et al., 2002). Upon its binding, MurG adopts a slightly closer conformation (Hu et al., 2003), which likely favors subsequent binding of lipid I. MurG has a high selectivity for UDP-GlcNAc (Sha Ha et al., 1999), UDP fitting perfectly the geometry of the small binding pocket and establishing hydrogen bonds through its 2'- and 3'-hydroxyl groups, as well as through its α-phosphate. GlcNAc is also well discriminated, as the hydroxyl group at position 4 establishes numerous hydrogen bonds with residues of the protein (Hu et al., 2003). The lipid I binding site is much less specific, as MurG accepts *in vitro* multiple analogues with variable chain lengths provided that they mimic the *cis*-conformation of the three first isoprene units in the C_{55} lipid moiety (L. Chen et al., 2002). While no structure with lipid I are currently available, it is predicted that two conserved glycin-rich loops are involved in this interaction. From the study of glycosyl-transferase enzymes from the same superfamily, it is also expected that the MurNAc group of lipid I undergoes a deprotonation on its carbon 4, leading to the formation of an oxyanion, which then does a nucleophilic addition on the GlcNAc carbon 1. The transient oxocarbenium-ion-like compound obtained would then dissociate to release first UDP and then the lipid II product.

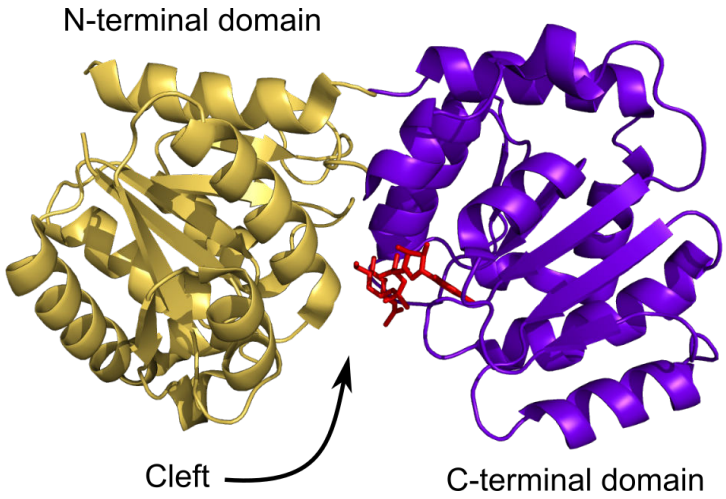

Figure I.2.14: Structure of *E.coli* MurG (PDB code 1NLM). The UDP-GlcNAc substrate is represented in red sticks. Binding site of the lipid I is located on the other face of the cleft, on the N-terminal domain.

2.C- Assembly of the peptidoglycan precursors

Once the lipid II precursor is synthesized, it is flipped from the inner to the outer layer of the cytoplasmic membrane. Peptidoglycan assembly can then proceed through two reactions, the oligomerization of the disaccharide units and the cross-linking of the peptide stems, which involve glycosyltransferase and transpeptidase activities, respectively (figure I.2.15). Most of the proteins implicated in these reactions (are thought to) exist at least in two distinct copies,

conversely to precursor synthesis enzymes.

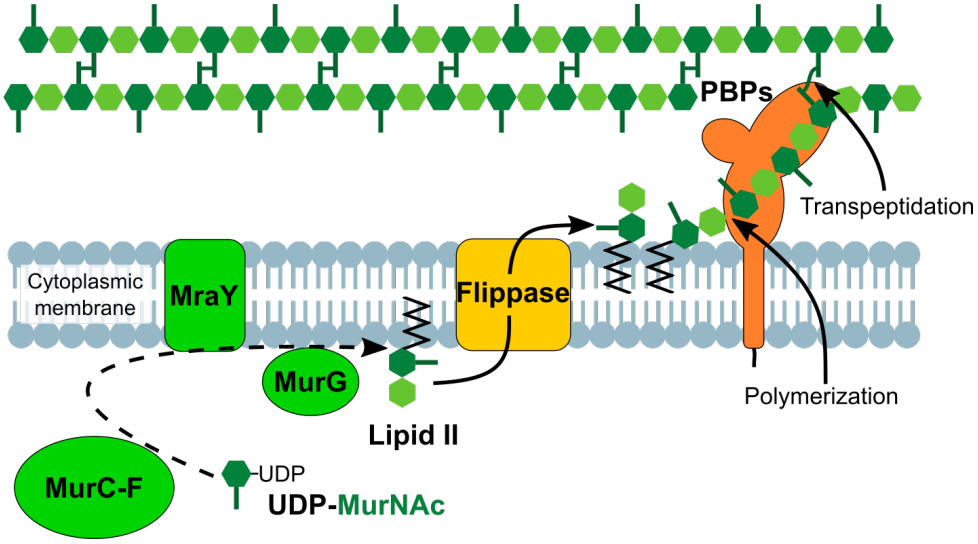

Figure I.2.15: Assembly of peptidoglycan from lipid II intermediate. Lipid II is first translocated from the cytoplasm to the periplasm through an undetermined flippase, likely FtsW/RodA or MurJ in *E. coli*. Glycan strands are then polymerized from the disaccharidic units and cross-linked by PBPs. Although not represented here, transpeptidation can also be performed by Ldts.

2.C.a- Lipid II translocation from the cytoplasm to the periplasm

Peptidoglycan is assembled in the periplasm but the lipid II intermediate is synthesized on the inner leaflet of the plasma membrane. It must therefore "flip" to be available on the other side of the membrane, a process which long remained enigmatic. Fluorescence spectroscopy studies on 7-nitro-2,1,3-benzoxadiazol-4-yl-labeled (NBD-labeled) lipid II showed that translocation is an ATP-independent process, unable to occur spontaneously, highly coupled to the consumption of lipid II in the extra-cytoplasmic space (van Dam et al., 2007). It was thus hypothesized that this step was performed by one or several unknown proteins. However, the identity of the translocase(s) is(are) still, to date, highly controversial.

FtsW and RodA were the first proteins to be suggested to play an active role in lipid II translocation (Ehlert & Höltje, 1996). These essential polytopic membrane proteins are part, with the *B. subtilis* SpoVE protein, of the SEDS (shape, elongation, division, sporulation) superfamily, for which at least one member is found in almost all bacteria possessing a peptidoglycan layer (Henriques et al., 1998). The two proteins are highly homologous (with 31.9% sequence identity in *E. coli*) and are predicted to share a similar topology consisting of 10 transmembrane helical segments and a long periplasmic loop between the α-helices 7 and 8, with the two protein ends in the cytoplasm (Gérard et al., 2002; Lara & Ayala, 2002). FtsW and RodA were thus proposed to play similar functional roles during septal and lateral cell wall synthesis along division and elongation, respectively (Ikeda et al., 1989). In 2011, fluorescence resonance energy transfer (FRET)-based studies performed on *E. coli* membrane vesicles, with NBD-labeled lipid II as a donor and tetramethylrhodamine cadaverine (TMR)-labeled vancomycin as an acceptor, led the authors to the conclusion that FtsW was the long-searched flippase (Mohammadi et al., 2011). The considered vancomycin antibiotic is unable to cross the plasma membrane and can thus only lead to a FRET if lipid II synthesized in the cytoplasm by a reconstituted machinery is translocated to the outer layer. With this tool, the authors demonstrated that lipid II translocation is increased in overexpressing FtsW strains and that purified FtsW was the only transmembrane protein among others to catalyze this process in proteoliposomes. More recently the same authors identified two positively charged key residues, Arg145 and Lys153, in the 4th helix of FtsW and suggested that lipid II transport

is controlled by the size of the FtsW pore (Mohammadi et al., 2014).

In parallel to these studies on SEDS proteins, a genetics (Inoue et al., 2008) and a reductionist bioinformatics approach (Ruiz, 2008) in 2008 proposed the membrane protein of unknown function MurJ (previously known as MviN) as the likely lipid II flippase. MurJ is a member of the MOP (Multidrug/Oligosaccharidyl-lipid/Polysaccharide) exporter family, which is essential in *E. coli*, and whose depletion leads to an accumulation of nucleotide and lipid precursors in the cytoplasm and a defective peptidoglycan synthesis. According to a model that was generated with the I-TASSER server using known structures of other MOP proteins, MurJ is organized in 14 transmembrane α-helices and presents a central solvent-exposed cavity which might accommodate the diphosphate-disaccharide-pentapeptide moiety, similarly to FtsW (Butler et al., 2013; Butler et al., 2014). Lately, an *in vivo* assay was developed to investigate lipid II translocation upon deactivation of MurJ (Sham et al., 2014). In this assay, the colicin M toxin (ColM) is used to cleave periplasmic lipid II and the obtained product are further quantified by HPLC. While wild-type cells yield ColM degraded products, these products are below the detection level when the assay is performed on cells with inactivated MurJ. These results were interpreted by the authors as a proof that MurJ was the flippase.

The statement that MurJ or FtsW are the flippase remains controversial. The pro-FtsW clan objected that the four MurJ homologues in *B. subtilis* proved to be nonessential for cell viability (Fay & Dworkin, 2009). However, recent results demonstrate the existence of another protein in this organism, Amj (formerly YdaH) whose concomitant deletion with MurJ is lethal and whose expression in an *E. coli* ΔmurJ strain re-establishes the wild-type phenotype (Meeske et al., 2015). The pro-MurJ clan argued that purified MurJ was not functional in the FRET-assays that targeted the MurJ-mediated transport activity (Mohammadi et al., 2011) and that accumulation of downstream PG precursors in FtsW-deficient *E. coli* strains (Lara et al., 2005) is in disfavor of a FtsW flippase activity. This is consistent with the fact that no inhibition of the lipid II translocation is observed in *in vivo* assays on a ΔrodA strain with depleted FtsW (Sham et al., 2014). However, FtsW and RodA associate with the essential transpeptidases PBP3 (and maybe PBP1B) and PBP2 during cell division and elongation, respectively (Mercer & Weiss, 2002). It is therefore tempting to assert that if these enzymes were flippases, lipid II transport would be correlated with peptidoglycan synthesis. As a conclusion, the translocation mechanism remains largely uncharacterized and if FtsW/RodA or MurJ/Amj were to play the role of the flippase, the function of the alternative enzymes would have to be further elucidated.

2.C.b- Assembly of the peptidoglycan chains

Once translocated to the extra-cytoplasmic space, lipid II motifs are assembled through two reactions, transglycosylation that elongates a growing glycan strand by the addition of the disaccharide unit from a new lipid II molecule and transpeptidation that performs subsequent cross-linking between peptide ends of two different GlcNAc-MurNAc-pentapeptide motifs (figure I.2.15). In *E. coli*, both reactions are performed by two separate glycosyltransferase (GT) and transpeptidase (TP) domains of class A bifunctional Penicillin-Binding Proteins (PBPs, figure I.2.16), PBP1A, PBP1B, or PBP1C, which take their name from their transpeptidase activity inhibition by the famous penicillin antibiotics. Monofunctional glycosyltransferase (MtgA) and transpeptidases (class B PBPs: PBP2, PBP3) also participate in these reactions. All of these proteins are found in the periplasm, where they are anchored in the inner membrane.

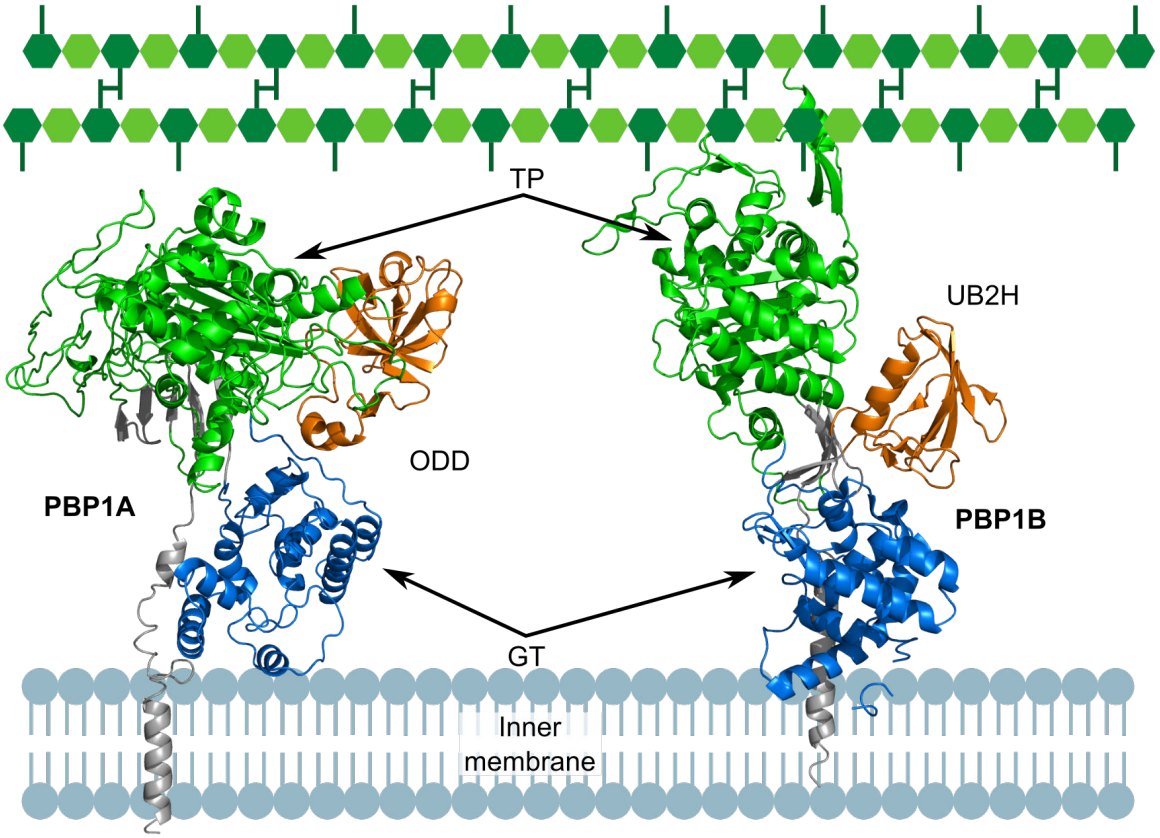

Figure I.2.16: Structural organization of the two *E. coli* main bifunctional PBP1s: PBP1A (model generated by Phyre2), and PBP1B (PDB code 3VMA). The transpeptidase (TP), glycosyltransferase (GT) and non-catalytic domains (ODD and UB2H for PBP1A and PBP1B, respectively) are colored in green, blue, and orange respectively. The transmembrane α-helix and the β-sheet linking these domains are in gray. Note that the relative position of the TP compared to the GT domain in the modeled PBP1A may be different in the real structure.

2.C.b.i- Glycan chain polymerization by glycosyltransferase activity

Lipid II polymerization is performed by a monotopic glycosyltransferase domain. Monofunctional glycosyltransferases and the GT domain of bifunctional PBPs are situated in the periplasm and are anchored to the plasma membrane by an N-terminal α-helix. On the contrary to other glycosyltransferase domains which use a nucleotide-sugar substrate and have an α/β Rossmann fold, the peptidoglycan glycosyltransferase structure presents some fold similarities to the bacteriophage λ-lysozyme that is responsible for breaking the β1,4-glycosidic bond, and is mainly composed of α-helices (figure I.2.17 A), as revealed from structures solved in the last eight years (Lovering et al., 2007; Yuan et al., 2007; Heaslet et al., 2009; Sung et al., 2009; Han et al., 2011; Huang et al., 2012). Secondary structure elements are organized in two sub-domains consisting of a small flexible jaw and a globular head. The jaw is maintained in close proximity or partly embedded in the membrane via hydrophobic residues and positively-charged regions (Lovering et al., 2007; Sung et al., 2009) which may be the reason why its purification even in absence of the N-terminal transmembrane helix requires detergents. These two regions of the GT domain are separated by a cleft, where the active site is located, as revealed by the structures obtained in the presence of moenomycin inhibitor (Lovering et al., 2007; Heaslet et al., 2009; Sung et al., 2009) or lipid II substrate analogs (Huang et al., 2012).

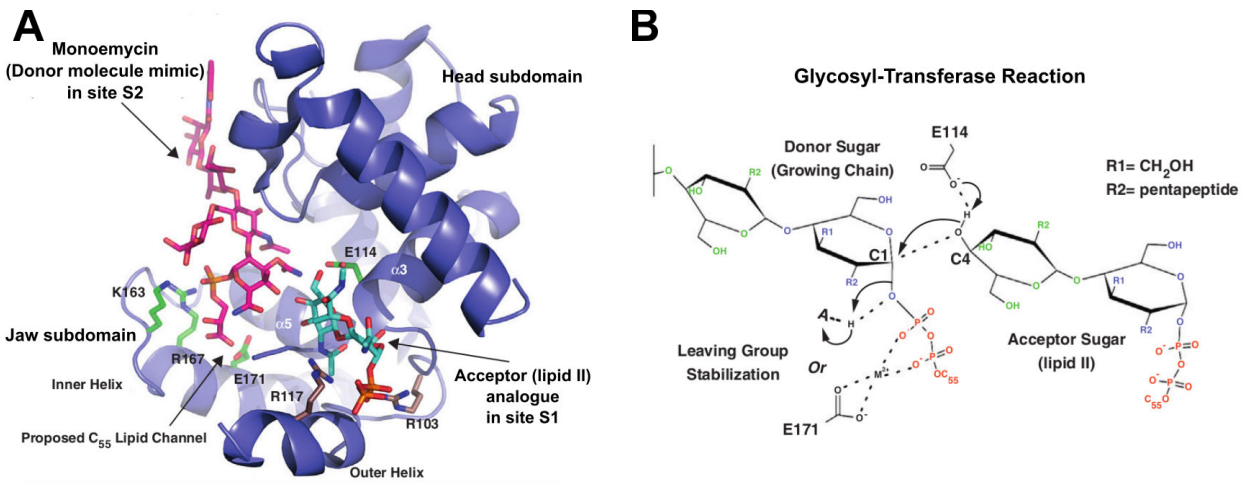

Figure I.2.17: Modeling of the glycosyltransferase activity in *S. aureus* PBP2. (A) Binding sites of the lipid II acceptor molecule (site S1) and the moenomycin inhibitor (donor site S2) that mimics the elongating glycan strand from the neosynthesized peptidoglycan. The two substrates are located in the cleft between the globular and jaw sub-domains which is in close interaction or partly embedded in the plasma membrane. Binding of these substrates involve interactions with five characteristic conserved motifs (Terrak et al., 2008). In this configuration, the C-1 of MurNAc of the donor substrate would face the C-4 of the GlucNac of the lipid II acceptor. (B) Main steps of the mechanism of the glycosyltransfer from the donor substrate to the lipid II acceptor. After deprotonation by a conserved glutamate, the oxygen of the hydroxyl group at position 4 of the GlcNAc exerts a nucleophilic substitution with stereochemistry inversion at the carbon 1 of MurNAc of the donor. The leaving of the pyrophosphate group at this carbon is assisted by its protonation by a general acid catalysis. Adapted from Sobhanifar et al., 2013.

These structures enabled to propose a detailed mechanism for the glycan strand polymerization of the lipid II precursors. The reaction is initiated by the formation of a β-1,4-glycosidic bond between two lipid II molecules, yielding lipid IV. An elongation step follows, where lipid II (glycosyl acceptor) molecules are successively attached to the growing nascent peptidoglycan chain (glycosyl donor). In each of these steps, the lipid II acceptor and the donor molecule (either lipid II or the growing glycan chain phosphorylated at its reducing end) bind in different locations in the cleft, S1 and S2, respectively, which both allow the anchoring of the diphosphate lipid moiety in the plasma membrane. The acceptor lipid II molecule is stabilized in S1 by the coordination of a Mg^{2+} ion bound to a highly conserved glutamate residue, and by additional hydrogen bonds between its hydroxyl or phosphate groups and the backbone or the side chain of pocket residues. The four terminal carbohydrate rings of the donor substrate are superimposed on the moenomycin inhibitor skeleton and its terminal phosphorylated end is maintained in the S2 binding site through hydrogen bonding interaction. In this configuration, the carbon 1 of phosphorylated sugar of the donor and the hydroxyl group at position 4 in the GlcNac of the acceptor are facing each other. The latter hydroxyl is then deprotonated by a catalytic glutamate (E114 in *S. aureus* PBP2) and performs a nucleophilic attack on the donor carbon 1 (figure I.2.17 B). The pyrophosphate moiety of the donor substrate being stabilized by a Mg^{2+} ion or by two basic residues, Arg or Lys, that play the role of general acid catalysts, the C_{55}-pyrophosphate can be released upon formation of the β-1,4-glycosidic bond. Then the product is slightly moved to the donor site through attraction by nearby basic (Lovering et al., 2007) and/or hydrophobic residues (Yuan et al., 2007). Finally a new lipid II substrate enters the cleft so that the reaction can process without release of the elongating product between each cycle.

In *E. coli*, MtgA is the only identified monofunctional glycosyltransferase. However, it is likely that, *in vivo*, transglycosylation is mainly performed by class A bifunctionnal PBPs, as MtgA is not essential (Schiffer & Höltje, 1999) and is unable to rescue peptidoglycan synthesis with monofunctional transpeptidases in PBP1A or PBP1B deletion mutants

(Denome et al., 1999). Interestingly, deletion in *B. subtilis* of all the four enzymes with glycosyltransferase activity is not lethal and does not suppress completely peptidoglycan synthesis. This suggests the existence of an additional glycosyltransferase protein, which remained unidentified when the genome was screened for homologues with the five conserved glycosyltransferase motifs (Mcpherson & Popham, 2003).

2.C.b.ii- Cross-linking of peptide stems by D,D-transpeptidase activity

D,D-transpeptidation consists in cross-linking the D-Ala in position 4 of an acyl-donor peptide stem to the residue in position 3 (*m*-A_2pm or L-Lys) of an acyl-acceptor peptide stem, thus releasing the fifth D-Ala of the donor stem. This reaction is performed by monofunctional transpeptidases or bifunctional PBPs. D,D-transpeptidase domains are composed of two subunits. The first one is made of a five-stranded β-sheet and three α-helices, while the second is exclusively α-helical. Three conserved motifs are delimiting the active site (figure I.2.18 A), which is situated in the cavity between the two sub-domains (Goffin & Ghuysen, 1998). Among the conserved residues, the SXXK motif (motif I) contains the catalytic serine required for transpeptidation and the lysine that acts as a general base to activate the catalytic residue. When the donor strand binds to the transpeptidase domain, the deprotonated γ-oxygen from the activated serine adds to the carbonyl carbon of the D-Ala-D-Ala peptide bond to generate a stabilized oxoanion tetrahedral intermediate. The D-Ala at position 5 is then released, yielding the acyl-enzyme. Then, the side-chain ammonium of the third residue (*m*-A_2pm or L-Lys) of the acceptor peptide stem undergoes a deprotonation probably by a serine from motif II or a lysine from motif III (Sauvage et al., 2008). The generated nucleophilic amine adds to the carbonyl carbon of the acylenzyme, causing deacetylation of the enzyme, and leads to the product which contains a peptide bond between the *m*-A_2pm of the acceptor stem and the D-Ala of the donor stem (figure I.2.18 B). Although the structural aspect of the inhibition of the D,D-transpeptidation by β-lactams has been extensively studied and can mimic the first part of the reaction with the donor stem peptide, the binding site of the acceptor peptide stem is still undefined.

The transpeptidase domain is the target of β-lactam antibiotics, among which is the well-known penicillin. These drugs inhibit transpeptidation activity by the formation of an adduct with the enzyme, mimicking with their β-lactam ring amide bond the D-Ala-D-Ala peptide bond from the acceptor peptide stem (Tipper & Strominger, 1965). The catalytic serine attacks the β-lactam ring carbonyl, opens it and forms a covalent acyl-enzyme with a very low hydrolysis rate at the cell time-scale (Zapun et al., 2008). The cell being unable to cross-link its glycan chains thus undergoes lysis. The exact molecular mechanism leading to this stage is not clear, but it has been proposed lastly that this was caused by induction of futile cycles of peptidoglycan synthesis depleting precursors pools and by degradation of the uncrossed nascent chains (Cho et al., 2014). Resistance to β-lactams can be developed by acquisition of low-affinity PBPs. Several resistant monofunctional D,D-transpeptidases, also called class B PBPs, have been reported to present mutations in their active site, or on residues involved in the stabilization of the drug or in the modification of the active site aperture, inducing resistance. As an example, a PBP2x mutant in the highly penicillin-resistant *S. pneumoniae* strain Sp328 was shown to harbor 92 mutations in total (Dessen et al., 2001), although this is certainly not the only resistance mechanism to β-lactams and their cell-wall targeting antibiotics (Nikolaidis et al., 2014).

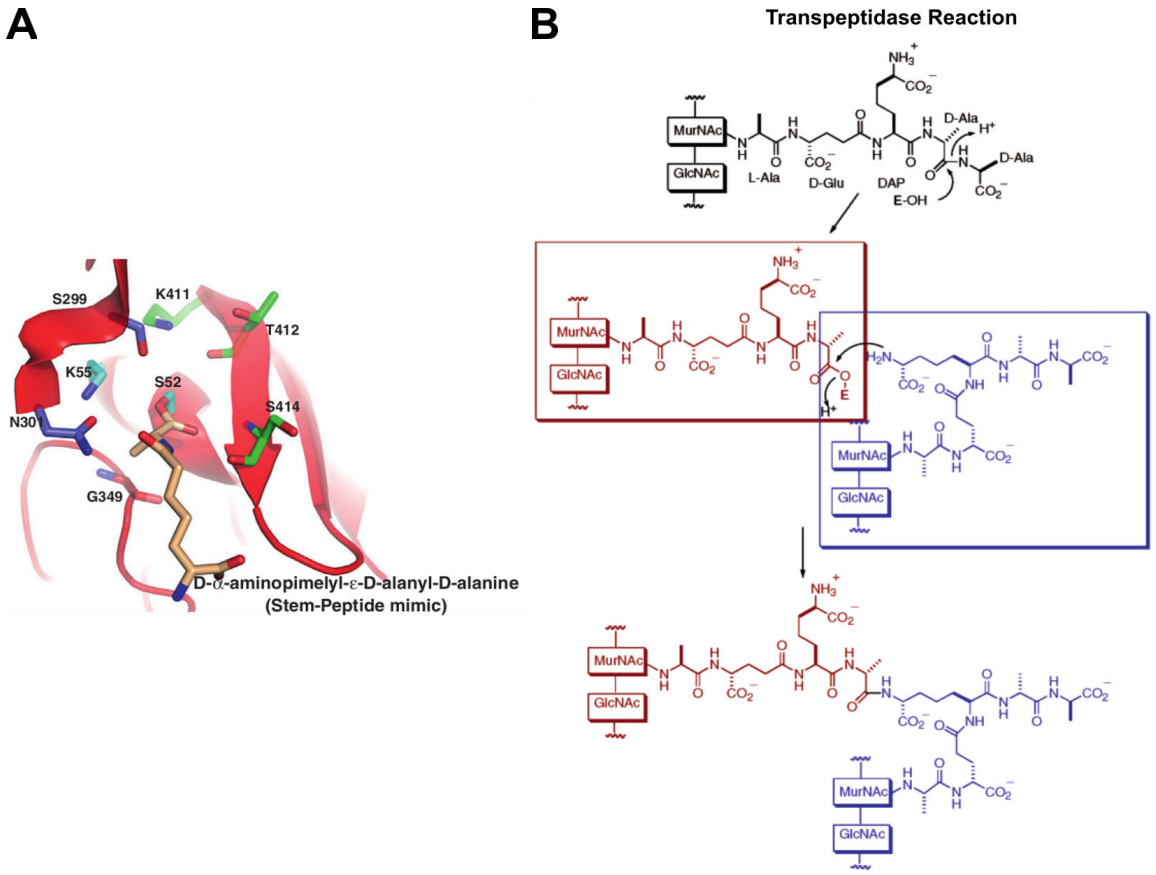

Figure I.2.18: Modeling of the D,D-transpeptidation in *B. subtilis* PBP4A. (A) Structure of the transpeptidase domain active site in red with a *m*-A_2pm-D-Ala-D-Ala peptide in beige sticks, mimicking the peptidoglycan donor stem peptide. The SXXK, SXN and KTG(S/T) motifs (I-III) involved in the formation of the acylenzyme, the departure of the donor stem D-Ala, and the nucleophilicity of the acceptor stem amino group are shown in cyan, violet and green sticks, respectively. Adapted from Sobhanifar et al., 2013. (B) Main step of the transpeptidation mechanism. Nucleophilic addition to the D-Ala-D-Ala of the donor stem by the catalytic serine leads to the formation of an acyl-enzyme (in the red box) and release of the D-Ala in position 5. The amine moiety from the third residue of the acceptor stem, after deprotonation, then adds to the carbonyl carbon of the acyl-enzyme. This induces the deacetylation of the PBP, generating the peptide bond between the *m*-A_2pm (acceptor stem) and the D-Ala (donor stem). Adapted from Lee et al., 2003.

2.C.b.iii- High molecular weight PBPs are the main peptidoglycan synthases

PBPs can be classified in three groups. Class A PBPs are responsible for both transpeptidation and transglycosylation, while class B PBPs only perform transpeptidation. Both classes are part of the high molecular weight PBPs (HMW PBPs) and are anchored to the cytoplasmic membrane by an N-terminal transmembrane helix. The last group, class C, is composed of hydrolases, also known as low molecular weight PBPs (LMW PBPs). Their function is to cleave the peptide bond between the last two D-Ala of the disaccharide-pentapeptide peptidoglycan motif with a similar mechanism to transpeptidases, with water replacing the aminogroup of the acceptor stem peptide as a nucleophile in the second step of the reaction (figure I.2.18). Due to the fact that historically PBPs were numbered according to their migration profile on a sodium dodecylsulfate-polyacrylamide gel electrophoresis (SDS-PAGE), homologous PBPs doe not generally have the same name in different organisms (Sauvage et al., 2008).

In *E. coli*, class A encompasses bifunctional PBP1A, PBP1B and PBP1C. In these PBPs, the N-terminal glycosyltransferase domain is linked to a C-terminal transpeptidation domain through a linker region and a small variable domain (figure I.2.16, in gray and orange, respectively). The latter non-catalytic domain is classified as ODD, Outer-membrane PBP1A

Docking Domain, also named in Pfam as a PCB_OB (for oligonucleotide/oligosaccharide binding) domain, in the case of *E. coli* and *Acinetobacter baumannii* PBP1A (Typas et al., 2010), and as UB2H (UvrB domain 2 homologue) in the case of PBP1B (Sung et al., 2009). The PBP1A and PBP1B enzymes were reported to be able to form homodimers (Zijderveld et al., 1991; Charpentier et al., 2002), although their relevance *in vivo* is uncertain.

The presence of a portion of the N-terminal transmembrane helix in *E. coli* PBP1B, the only *E. coli* HMW PBP of known structure to date, allowed protein orientation relative to the inner membrane. According to this structure, the elongated peptidoglycan nascent chain is growing almost perpendicularly to the bilayer, most probably in direction of the transpeptidase domain (Sung et al., 2009), and it is thought that the TP domain prefers this chain coming out of the GT as a substrate (Terrak et al., 1999; Born et al, 2006). These observations support the hypothesis that both GT and TP activities are probably concerted in bifunctional PBPs.

PBP1A and PBP1B are redundant in *E. coli.* Each of them is not individually essential for the cell, as the remaining PBP in a single deletion mutant can compensate for the deleted protein. Nevertheless, deletion of both PBP1A and PBP1B is lethal (Yousif et al., 1985). In addition to their structural differences, the two PBPs show functional dissimilarities. PBP1B synthesizes longer glycan strands and peptidoglycan cross-linked at a higher ratio (Bertsche et al., 2005) in comparison to PBP1A (Born et al., 2006). Both proteins display slightly different localization patterns. PBP1B is found at the side walls, like PBP1A (Typas et al., 2010), but also at the site of division, the septum (Bertsche et al., 2006). Interestingly, PBP1B exists in three isoforms, α, β and γ. While PBP1B β is an artefactual degradation product of the full-length PBP1B α by the protease OmpT upon cell lysis (Henderson et al, 1994), the γ-isoform is a shorter and functional version of the main PBP1B α, beginning at Met46 due to the use of an alternative start codon (Kato et al., 1984).

PBP1C is the last *E. coli* class A PBP. Its exact role is currently not well understood, as it is not able to compensate for PBP1A/B deletions, even when overexpressed (Schiffer & Höltje, 1999). Although it is considered as a PBP on the basis of sequence homology with the two other bifunctional PBPs, its transpeptidation activity remains uncertain because the corresponding domain does not extensively bind β-lactams and does not show any measurable enzymatic activity, at least *in vitro* (Schiffer & Höltje, 1999).

E. coli has two other HMW PBPs, the monofunctional transpeptidases PBP2 and PBP3. As class B PBPs, they possess an N-terminal non-penicillin binding domain, which probably serves as a pedestal or for interactions (Figure I.2.19). The C-terminal transpeptidase module is similar to its equivalent in class A PBPs. PBP2 is essential for elongation of the cell in rod-shaped bacteria and is selectively inactivated by mecillinam (amdinocillin), yielding to a spherical cell phenotype (Spratt & Pardee, 1975). PBP2 was shown to localize on the lateral walls, but also transiently at the septum (Den Blaauwen et al., 2003). On the contrary, PBP3, also known as FtsI, is required for peptidoglycan synthesis at the septum and is therefore found at mid-cell (Weiss et al., 1997). Its inhibition by the specific aztreonam antibiotic leads to the generation of filamentous cells unable to divide, which suggests a role in cell division for PBP3 (see part I section 4.B.b.ii; Georgopapadakou et al., 1982).

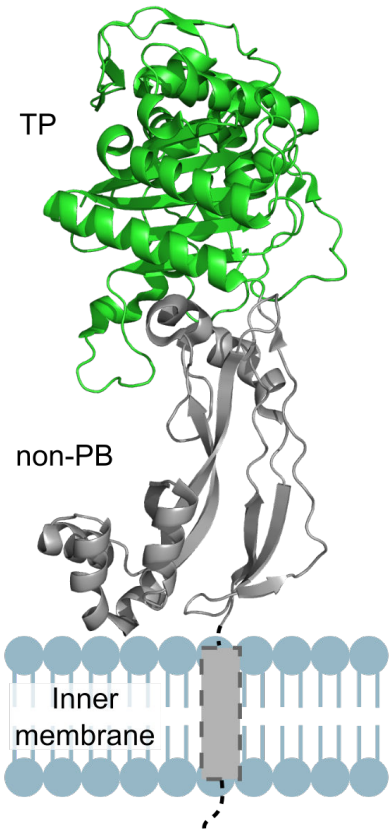

Figure I.2.19: Structure of *Pseudomonas aeruginosa* PBP3 (PDB code 3OC2). The N-terminal α-helix anchoring PB3 to the inner membrane is represented by a dotted rectangle. TP: transpeptidase domain, non-PB: non-penicillin-binding domain.

2.C.b.iv- An alternative cross-linking strategy or the role of L,D-transpeptidases

In 1984, *E. coli* muropeptide analysis by HPLC revealed the existence of a second, minor (< 4%) type of cross-linking connecting two *m*-A_2pm instead of the conventional D-Ala-*m*-A_2pm pattern (figure I.2.20 A; Pisabarro et al., 1985). The peptidoglycan resulting from this new transpeptidation process was later shown later to be abundant in an *in vitro* selected ampicillin insensitive *Enterococcus faecium* strain, suggesting a PBP independent transpeptidation pathway in Gram-positive bacteria (Mainardi et al., 2000). More recently, *M. tuberculosis* cells were shown to naturally present a high percentage (80%) of L,D-transpeptidation in the stationary phase (Lavollay et al., 2008). L,D-transpeptidases (Ldts), the enzymes responsible for this reaction, were identified in 2005 (Mainardi et al., 2005).

Ldt structures obtained to date generally present two domains (sometimes three) in addition to a short transmembrane N-terminal helix. The domains towards the N-terminal end are peptidoglycan recognition folds and vary in different species. It is a LysM domain in *Bacillus subtilis* (Lecoq et al., 2012), an immunoglobulin-like fold in *M. tuberculosis* Ldts (Ldt_{Mt1}, Correale et al., 2013; Ldt_{Mt2}, Kim et al., 2013), or a mixed α/β-fold in *Enterococcus faecium* (Ldt_{fm}, Biarrotte-Sorin et al., 2006). The C-terminal domain, on the contrary, is highly conserved and catalyzes the transpeptidase activity (figure I.2.21).

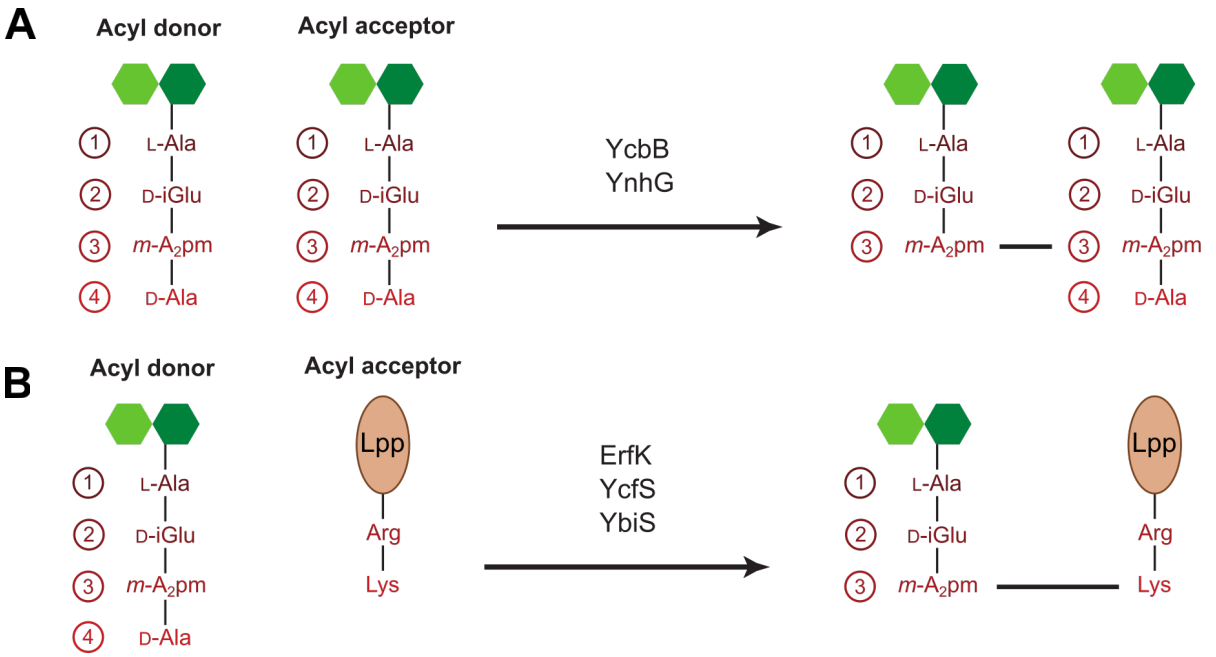

Figure I.2.20: Reactions catalyzed by *E. coli* L,D-transpeptidases. (A) Cross-linking between the carbonyl carbon of residue at position 3 of the donor stem and the amino group of the side-chain of residue at position 3 of the acceptor stem (*m*A_2pm→*m*A_2pm cross-link), by YcnB and YnhG. (B) Anchoring of a Lpp lipoprotein to peptidoglycan by ErfK, YcfS and YbiS.

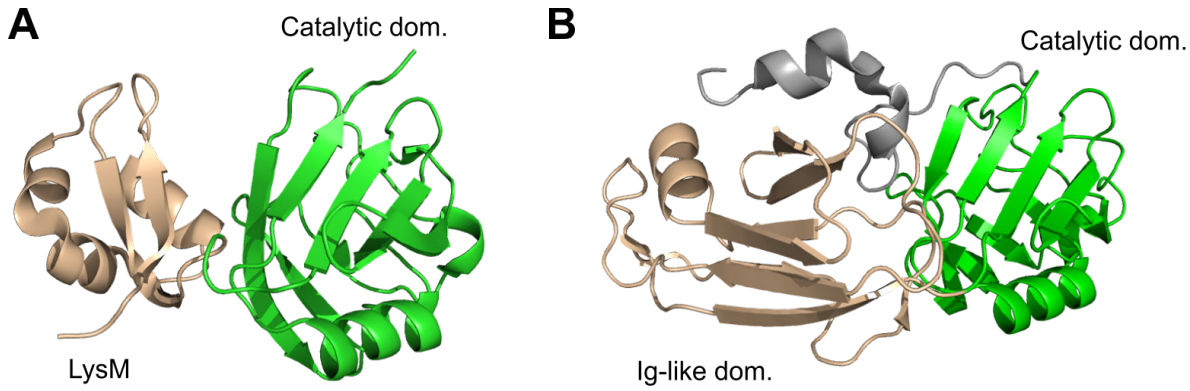

Figure I.2.21: Examples of the bimodular organisation of Ldt structures. (A) *B. subtilis* Ldt_{Bs} (PDB 3ZQD). (B) Extra-cytoplasmic portion of *M. tuberculosis* Ldt_{Mt2} (PDB 4GSQ). Ig-like: Immunoglobulin-like.

Ldts require a tetrapeptide acyl donor substrate for the transpeptidation reaction (Mainardi et al., 2005), which is obtained after cleavage of the D-Ala at position 5 by a β-lactam-insensitive D,D-carboxypeptidase (Mainardi et al., 2002). After binding of the acyl donor in one pocket close to the active site, the thiol of a catalytic triad consisting in a cysteine, an histidine and an aspartate (Biarrotte-Sorin et al., 2006) attacks the carbonyl carbon of the peptide bond between the third and fourth residues of peptide stem (Biarrotte-Sorin et al., 2006). Similarly to the PBP transpeptidation mechanism (figure I.2.18), an acyl-enzyme is formed as an intermediate and the terminal peptide stem residue is released. When the peptide stem of an acyl acceptor binds to a second pocket located on the other side of the catalytic cysteine (figure I.2.22, Triboulet et al., 2015), the nucleophilic side-chain amino group of its residue at position 3 attacks the acyl-enzyme, causing deacetylation and yielding the peptide cross-link. Recently, the interaction of Ldts with peptidoglycan was also studied in *B. subtilis* by solid-state NMR (see part I section 5.C.c). In the resulting model, the glycan strands are thought to interact in a groove between the LysM and catalytic domains, thus positioning the donor peptide stem at the active cysteine. Based on a layered-peptidoglycan

network geometry, another peptide stem from an adjacent glycan strand is also expected to be directed toward this residue to act as an acceptor (Schanda et al., 2014).

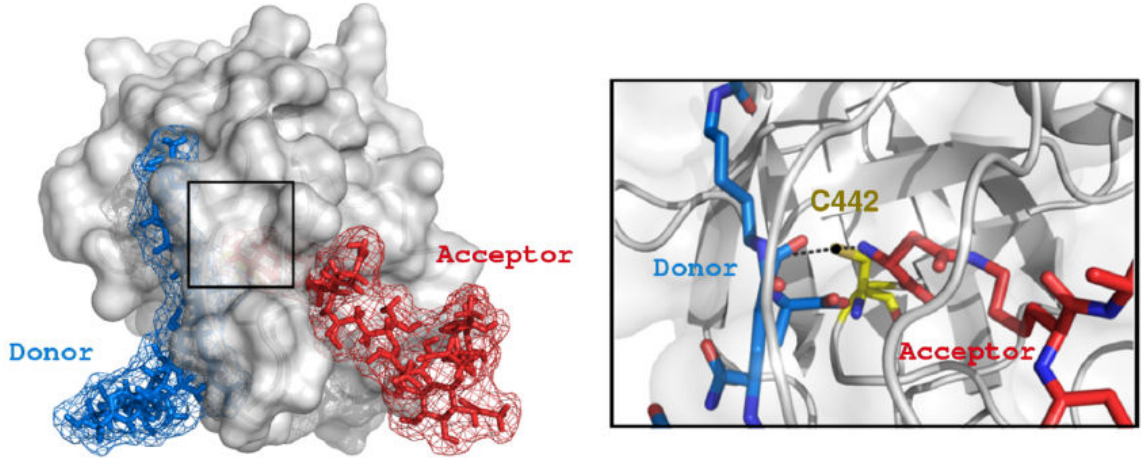

Figure I.2.22: Model of *Enterococcus faecium* Ldt_{fm} in complex with two tetra-muropeptides, calculated by the HADDOCK webserver. Ldt_{fm} (PDB code 1ZAT) is represented in gray. Its catalytic cysteine positioned between the two peptide stems is highlighted in the zoom in the right panel. Taken from Triboulet et al., 2015.

Interestingly, despite the unrelated structural features of PBPs and Ldts and the different stereochemistry of the cleaved peptide bond (L,D- versus D,D-, respectively), β-lactams inhibit to some extent both proteins through acylation of the catalytic residue. In Ldts, carbapenem has proved to be the most efficient to generate a thioester bond with the catalytic cysteine and leads to a stable acylenzyme (Mainardi et al., 2007). In fact, if molecules from other β-lactam families, like penams, were also shown to bind Ldts with similar K_d values (between 44 and 79 mM, Triboulet et al., 2013), the intermediate is formed according to a slower kinetic and is unstable, leading to its hydrolysis.

In *E. coli*, YcbB and YnhG are the two L,D-transpeptidases responsible for 3→3 cross-linking (Magnet et al., 2008). Three other homologous proteins, ErfK, YcfS, and YbiS, were shown to have another specific activity, which concerns anchoring of the outer-membrane lipoprotein Lpp to peptidoglycan (Magnet et al., 2007). In this case, the α-carboxyl of the acyl *m*-A_2pm donor is linked to the side chain amino group of the C-terminal Lpp arginine residue (figure I.2.20 B). As *E. coli* is a Gram-negative bacterium, all these Ldts are found in the periplasm. However, this compartment is known to yield an oxidizing environment favoring formation of disulfide bonds. In the case of Ldts that have a single cysteine, oxidation of this catalytic residue leads to the formation of a sulfonic acid and inactivation of the enzymatic activity. The catalytic cysteine of YbiS, and probably by extension of other *E. coli* Ldts, was thus reported to be maintained in a reduced state by the oxidoreductase DsbG for correct functioning (Depuydt et al., 2009).

Another Ldt activity reported lately is the incorporation of various D-amino acids from the medium into peptidoglycan, through an exchange of the residue in the last position of the tetrapeptide (Cava et al., 2011). This mechanism has been diverted to label sacculi with D-cys (de Pedro et al., 1997) or more recently with fluorescent D-amino acids (FDAA) to observe sites of active peptidoglycan synthesis (Kuru et al., 2012).

Résumé en français du chapitre 2 : La biosynthèse du peptidoglycane

La synthèse du peptidoglycane est un long processus qui débute dans le cytoplasme, avec la formation de précurseurs. Ceux-ci sont ensuite ancrés à un transporteur lipidique avant d'être transféré dans le périplasme pour les bactéries Gram-négatives ou l'espace extracellulaire pour les bactéries Gram-positives. Les muropeptides y sont polymérisés et réticulés, formant alors le peptidoglycane néosynthétisé.

La synthèse des précurseurs dans le cytoplasme débute avec la production d'UDP-GlcNAc et de son dérivé UDP-MurNAc. Les résidus des brins peptidiques sont ensuite ajoutés séquentiellement au MurNAc, afin de générer l'UDP-MurNAc-pentapeptide. Tout d'abord, la synthèse d'UDP-GlcNAc est réalisée à partir de D-fructose-6-phosphate en 4 étapes par 3 enzymes. A partir de D-fructose-6-phosphate et de L-glutamine, la glucosamine-6-phosphate synthase GlmS produit de la glucosamine-6-phosphate et de l'acide L-glutamique. Ensuite, la phophoglucosamine mutase GlmM catalyse l'interconversion entre la glucosamine-6-phosphate et la glucosamine-1-phosphate. Cette dernière sert alors de substrat pour la N-acetylglucosamine-1-phosphate uridyltransferase GlmU, qui réalise son acétylation puis son uridylation, produisant ainsi de l'UDP-GlcNAc.

L'UDP-MurNAc est ensuite synthétisé en deux étapes à partir de l'UDP-GlcNAc. Pour commencer, MurA transfert un groupe énolpyruvate depuis une molécule de phosphoénolpyruvate (PEP) à l'UDP-GlcNAc, libérant en fin de réaction de l'UDP-GlcNAc-énolpyruvate. A l'heure actuelle, cette enzyme est la seule parmi celles impliquées dans la biosynthèse des précurseurs de peptidoglycane dans le cytoplasme à être la cible d'un antibiotique disponible cliniquement, la fosfomycine. En effet, cette molécule, par son analogie avec le PEP, inactive MurA en formant une liaison covalente avec la cystéine de son site actif. L'UDP-N-acétylpyruvyl-glucosamine réductase MurB catalyse ensuite la formation d'UDP-MurNAc à partir d'UDP-GlcNAc-énolpyruvate à l'aide d'un co-enzyme, le nicotinamide adénine dinucléotide phosphate (NADPH), et d'un cofacteur, la flavine adénine dinucléotide (FAD).

Une fois que l'UDP-MurNAc est produit, le brin peptidique est synthétisé en 4 étapes par les ligases Mur, ATP-dépendantes. Chacune de ces enzymes permet l'ajout de un à deux résidus sur le peptide en construction. Ainsi, MurC lie la L-alanine au groupement lactate du MurNAc. MurD catalyse ensuite l'addition de l'acide D- glutamique, puis MurE y attache à son carbone γ la L-lysine ou de l'acide meso-diaminopimélique. Enfin MurF rallonge le peptide en liant un dipeptide composé de deux D-alanine, formant ainsi l'UDP-MurNAc-L-Ala-D-iGlu-*m*-A_2pm/L-Lys-D-Ala-D-Ala. Ces 4 enzymes présentent des structures très similaires, organisées en 3 domaines globulaires (N-terminal, central et C-terminal, également nommé respectivement domaines 1, 2 et 3), chacun d'entre un interagissant avec un substrat différent. Le domaine 1 lie spécifiquement l'UDP du précurseur muropeptidique. Sa structure est la plus variable des 3 modules présents dans les 4 ligases Mur, son architecture chez MurE et MurF étant différente de celle chez MurC et MurD, probablement pour s'accommoder de l'allongement du brin peptidique et le positionner correctement vers les deux autres substrats. A l'inverse, le domaine 2 est le plus conservé, certainement car il est le seul à fixer toujours une même molécule, l'ATP. Enfin, le dernier domaine interagit avec l'acide aminé à rajouter à

l'UDP-MurNAc(-peptide). Dans le cas de MurF, ce domaine présente une spécificité peu élevée pour son substrat, ce qui permet l'addition d'autres dipeptides à la place du D-Ala-D-Ala, cible de l'antibiotique vancomycine. Le mécanisme catalytique des ligases Mur est bien caractérisé, dévoilant un processus en 3 étapes. L'ATP est le premier substrat à interagir avec l'enzyme, ce qui induit un changement conformationnel rapprochant les domaines 1 et 3 (état fermé). L'UDP-MurNAc(-peptide) est ensuite fixé, ce qui pourrait également contribuer à la réorientation des domaines. Cette complexation est suivie par celle de l'acide aminé ou du dipeptide à ajouter. Le mécanisme réactionnel pour les 4 ligases Mur étant similaires, ces enzymes apparaissent comme d'attractives cibles potentielles pour des inhibiteurs à spectre large. Des premières molécules prometteuses ont été récemment isolées.

La biosynthèse de l'UDP-MurNAc-pentapeptide par les ligases Mur requiert trois résidus inhabituels, qui sont l'acide D-glutamique, l'acide *meso*-diaminopimélique et la D-alanine. Alors que l'acide *meso*-diaminopimélique est simplement le dernier intermédiaire de la voie de biosynthèse de la L-lysine, les deux autres résidus requièrent des enzymes spécifiques pour leur formation.

La biosynthèse de l'acide D-glutamique est catalysée par exemple par la glutamate racemase MurI. De façon intéressante, chez *E. coli*, cette enzyme a besoin d'être activée par de l'UDP-MurNAc-L-Ala pour stimuler son activité et son affinité pour le substrat, lui permettant ainsi d'ajuster sa consommation de D-Glu à ses besoins. Chez certaines bactéries Gram-positives, une autre voie de biosynthèse est également disponible, faisant appel à une D-amino acid aminotransférase (D-AAT).

La formation du dipeptide D-Ala-D-Ala résulte de deux réactions successives. Tout d'abord, la L-alanine est convertie en D -alanine par l'alanine racémase Alr. Chez *E. coli* et chez quelques autres espèces, une seconde alanine racémase est aussi présente, DadX. Cependant, son rôle est encore méconnu, son expression n'étant pas constitutive contrairement à celle de Alr. Une fois que la D-alanine est synthétisée, deux D-Ala sont assemblées en dipeptide par la D-Ala-D-Ala ligase Ddl. Celle-ci dispose de deux sites de liaison à cet acide aminé, chacun ayant sa propre spécificité. Le produit obtenu inactivant la ligase, cela permet d'éviter un épuisement du stock de L-alanine. La D-cycloserine est un des plus importants inhibiteurs connu de cette voie métabolique. En effet, par son analogie structurale avec la D-alanine, la D-cycloserine est capable de former un adduit stable avec Alr et semble également être capable d'inactiver Ddl. La vancomycine est aussi un antibiotique notable, mais celui-ci se fixe covalemment au groupement carboxyle C-terminal au lieu d'interagir avec l'enzyme. Toutefois, la formation de dipeptides non canoniques comme le D-Ala-D-lac et D-Ala-D-Ser permet d'échapper à son action.

Une fois l'UDP-MurNAc-pentapeptide synthétisé, les deux étapes suivantes se déroulent à proximité de la membrane plasmique afin d'attacher le précurseur à un transporteur lipidique, formant au final le lipide II. La phospho-MurNAc-pentapeptide translocase MraY catalyse la première de ces deux réactions, la liaison de l'UDP-MurNAc-pentapeptide à un accepteur lipidique, l'undecaprenyl phosphate (C_{55}-P), produisant du lipide I. Cette enzyme membranaire dispose d'une cavité du côté cytoplasmique liant le C_{55}-P et d'un autre site interagissant avec le précurseur. MraY reconnaît davantage spécifiquement les premier et quatrième résidus que ceux en troisième et cinquième positions, probablement car ces derniers sont les plus variables (*m*-A_2pm/L-Lys et D-Ala/D-Lac respectivement). La N-acétyl-glycosyl transférase MurG, associée à la membrane cytoplasmique, catalyse le transfert du GlcNAc de l'UDP-GlcNAc sur le lipide I, générant le lipide II. MurG est constitué de deux domaines fixant chacun l'un des deux substrats, et séparés par une cavité où se déroule la réaction.

Une fois que le lipide II est synthétisé, il est transféré du feuillet interne de la membrane plasmique vers son feuillet externe, où le peptidoglycane pourra être assemblé. Bien qu'il soit

acquis que cette étape ne se déroule pas spontanément et ne requiert pas d'ATP, la (ou les) protéine(s) qui en est (sont) responsable(s) n'a (n'ont) pas pu être déterminée(s) avec certitude à l'heure actuelle, son (leur) identité étant encore largement débattue dans la communauté scientifique.

Les premières protéines suggérées pour le transfert du lipide II de part et d'autre de la membrane plasmique furent FtsW et RodA, deux homologues, membres de la famille des protéines membranaires SEDS (abréviation de Shape, Elongation, Division, Sporulation en anglais) et dont l'une des deux au moins est toujours présente chez les bactéries ayant une couche de peptidoglycane. Alors que RodA semble impliquée dans la synthèse de sacculus durant l'élongation de la cellule bactérienne, FtsW est impliquée dans la formation de peptidoglycane au septum (au milieu de la cellule) durant la division, chez *E. coli*. Récemment, des expériences *in vitro* de transfert d'énergie par résonance de type Förster ont permis de mettre en évidence la capacité de FtsW à transporter le lipide II de la face interne à la la face externe de vésicules. En parallèle, des études génétiques et bioinformatiques ont proposé, à la place, la protéine membranaire MurJ. Un protocole *in vivo* fut développé, dont les résultats furent interprétés comme une activité de transfert de la part de MurJ. Ces résultats sur MurJ et FtsW restent néanmoins controversés, les deux groupes concurrents à 'origine de ces résultats employant des protocoles différents pour lesquels seule leur protéine semblent être la translocase recherchée.

L'assemblage des unités disaccharidiques dans le périplasme à partir de lipide II s'effectue suivant deux réactions, la transglycosylation, qui allonge la chaîne oligosaccharidique naissante, et la transpeptidation, qui réalise ensuite la réticulation de peptides de deux brins différents. Chez *E. coli*, celles-ci sont catalysées par deux domaines distincts des PBPs de classe A, bifonctionnelles, PBP1A, PBP1B et PBP1C. Une glycosyltransférase, MtgA, et deux transpeptidases (PBP de classe B), PBP2 et PBP3, participent également à ces réactions. Toutes ces protéines sont localisées dans le périplasme et ancrées à la membrane interne.

Les domaines glycosyltransférases sont ancrés à la membrane interne par une hélice α. Ils présentent une architecture similaire au lysozyme et divisée en deux sous-domaines : une petite mâchoire flexible, étroitement associée à la membrane, surmontée d'une structure globulaire. Ces deux parties sont séparées par une poche où se situe le site actif. Initialement, une liaison glycosidique β-1,4 est formé entre deux molécules de lipide II, formant un lipide IV. Une étape d'élongation s'ensuit, où les lipides II (accepteurs) sont successivement attachés à la chaîne croissante de glycane (donneur). A chaque étape, l'accepteur et le donneur se lient chacun à un site spécifique, S1 et S2 respectivement, qui les positionnent de manière appropriée pour faciliter la réaction. Une fois la liaison glycosidique β-1,4 formée, un undecaprényl-pyrophosphate est relâché et le produit se déplace dans le site S2. Un nouveau lipide II entre dans le site S1 et la réaction d'élongation peut alors se poursuivre sans libération de la chaîne oligosaccharidique. Bien que MtgA soit la seule glycosyltransférase monofonctionnelle chez *E. coli*, la réaction de transglycosylation est en fait principalement réalisée par les PBPs bifonctionnelles de classe A.

La D,D-transpeptidation (pontage 4→3) consiste en la formation d'une liaison peptidique entre la D-Ala en position 4 d'un brin donneur et le résidu en position 3 d'un brin accepteur (*m*-A_2pm ou L-Lys), accompagnée de la libération de la D-Ala en position 5. Les domaines transpeptidases des PBPs sont également constitués de deux sous-domaines, le site actif se trouvant dans la cavité formée à l'interface entre ces deux parties. Le domaine de D,D-transpeptidation des PBPs est la cible d'antibiotiques, les β-lactames qui forment une liaison covalente avec la sérine catalytique en mimant le brin donneur. Alors que le site de liaison à ces inhibiteurs est bien défini, celui pour le brin accepteur reste toujours à déterminer.

Les PBPs peuvent être classées en 3 classes, dont les PBPs de classe A (bifonctionnelles) et les PBPs de classe B mentionnées précédemment. Celles-ci sont regroupées sous le nom de PBPs à haut poids moléculaires par opposition aux PBPs de classes C, qui sont en réalité des

hydrolases. Ces dernières effectuent une réaction similaire à la D,D-transpeptidation, à la différence que le groupement amine du brin accepteur est remplacé par une molécule d'eau. Il est à noter que suivant les organismes, la numérotation peut varier, étant originellement attribuée d'après leur ordre après migration sur un gel SDS-PAGE. Les PBPs de classe A, PBP1A, PBP1B et PBP1C chez *E. coli*, sont composées d'un domaine glycosyltransférase N-terminal séparé du domaine de transpeptidation C-terminal par une région faisant la jonction entre les deux et par un autre petit domaine, non-catalytique. Ce dernier est hautement variable suivant les espèces et les PBPs. Dans le cas de PBP1A, il s'agit d'un domaine ODD (Outer membrane PBP1A Docking Domain) alors que pour PBP1B, celui-ci se nomme UB2H (UvrB domain 2 homologue). Grâce à la détermination d'une structure de PBP1B avec une partie de son hélice N-terminale, son orientation par rapport à la membrane interne a pu être déterminée. Il semblerait que la chaîne oligosaccharidique s'allongent quasiment perpendiculairement à la membrane, ce qui lui permettrait d'atteindre le domaine de D,D-transpeptidation, en accord avec l'hypothèse que ces deux activités sont connectées.

PBP1A et PBP1B apparaissent comme des PBPs redondantes et essentielles pour la synthèse du peptidoglycane chez *E. Coli.* En effet, la suppression de l'une d'entre elles est compensée par l'autre, alors que leur absence simultanée est létale. Toutefois, ces deux enzymes conduisent à des produits quelque peu différents au niveau de la longueur des chaînes oligosaccharidiques produites et de leur degré de réticulation inter-peptidique. La localisation de ces PBPs varie également, PBP1B se trouvant au septum en plus de leur localisation sur les parois latérales de la cellule où se situe PBP1A. Concernant PBP1C, son rôle exact n'est pas compris, et son activité de transpeptidation reste incertaine. Les deux autres PBPs de haut poids moléculaire d'*E. coli*, PBP2 et PBP3, appartiennent à la classe B. Leur domaine transpeptidase C-terminal est précédé par un domaine N-terminal sans activité catalytique connue, servant probablement de piédestal ou d'interface d'interaction. De part leur localisation et les phénotypes observés lorsqu'elles sont supprimées, PBP2 et PBP3 semblent être impliquées dans la synthèse de peptidoglycane sur les paroislatérales de la cellule (élongation) et au septum (division) respectivement.

Comme évoqué au chapitre 1, un pontage alternatif entre deux résidus en position 3 (pontage 3→3), généralement minoritaire mais pas toujours, existe. Celui-ci est réalisé par les L,D-transpeptidases (Ldts). Les Ldts sont organisées en deux ou trois domaines. Celui (ou ceux) variable(s) situé en N-terminal reconnai(ssen)t généralement des motifs du peptidoglycane avec lequel ils interagissent. Le domaine C-terminal quant à lui est hautement conservé et est responsable de l'activité catalytique. La réaction nécessite un tetrapeptide pour le brin donneur, qui va se fixer dans une première poche. Le peptide du brin accepteur se place ensuite après formation de l'acylenzyme dans une seconde poche pour être lié covalemment au premier. Bien que les PBPs et les Ldts soient différentes structuralement et ne catalysent pas la formation d'un même pontage, ces dernières sont aussi inhibées par un sous-ensemble des β-lactams, les carbapénèmes. D'autres activités ont également été répertoriées chez *E. coli* pour les Ldts, comme l'incorporation de divers acides aminés D en dernière position dans des tetrapeptides ou l'attachement de la lipoprotéine de Braun (ancrée à la membrane externe) au peptidoglycane (nécessaire pour maintenir l'intégrité de la membrane externe).

Chapter 3
Peptidoglycan maturation and recycling

The peptidoglycan network obtained after polymerization of lipid II must not been seen as an inert compound but as an envelope subject to maturation. In fact, at each generation, up to 50 % of the peptidoglycan is degraded by the cell (Goodell, 1985) and then released in the medium or recycled. Furthermore peptidoglycan is the target of several modifications such as N-deacetylation of the disaccharide, O-acetylation and -deacetylation, or replacement of D-amino acids in the peptide stems.

3.A- Peptidoglycan maturation

3.A.a- Peptidoglycan hydrolysis

Bacteria possess a wide variety of peptidoglycan hydrolases able to trim almost any bond in the sacculus. In *E. coli*, more than twenty of them have been identified. Generally, they are not essential, reflecting a – at least – partial redundancy, and some of these enzymes display more than one activity, which makes it difficult to assign a specific role to each of them. Most of them are implicated in sacculus growth, cell septation, peptidoglycan turnover, or autolysis, or create space for macromolecular assemblies. Generally, a common structural feature to hydrolases is the presence of one or more peptidoglycan-binding domain in addition to a catalytic domain.

Hydrolases can be divided in three main groups: glycosidases, N-Acetylmuramyl-L-alanine amidases which cleave the bond between the peptide stem and the glycan chain, and peptidases (figure I.3.1).

3.A.a.i- Glycosidases

E. coli glycosidases are divided into two groups, N-acetyl-β-D-muramidases and N-acetyl-β-D-glucosaminidases (the latter one being only represented by the cytoplasmic NagZ, presented in part I section 3.B.a.i). Some bacteria also possess peptidoglycan N-deacetylases, but none were identified in *E. coli* neither were their activity detected, suggesting their absence in this organism. Two main groups of N-acetyl-β-D-muramidases have been reported: lysozymes and lytic transglycosylases (LTs; Vollmer et al., 2008). Both catalyze hydrolysis of the β-1,4-glycosidic bond between MurNAc and GlcNAc. In addition, the latter group performs a simultaneous intramolecular transglycosylation, to yield a 1,6-anhydro cycle between MurNAc carbons 1 and 6. This modification produces the first intermediate in the peptidoglycan recycling pathway. While lysozymes are absent in *E. coli*, this bacterium has a total of seven periplasmic LTs, which belong to three families (out of four) based on conserved sequence patterns (Blackburn & Clarke, 2001).

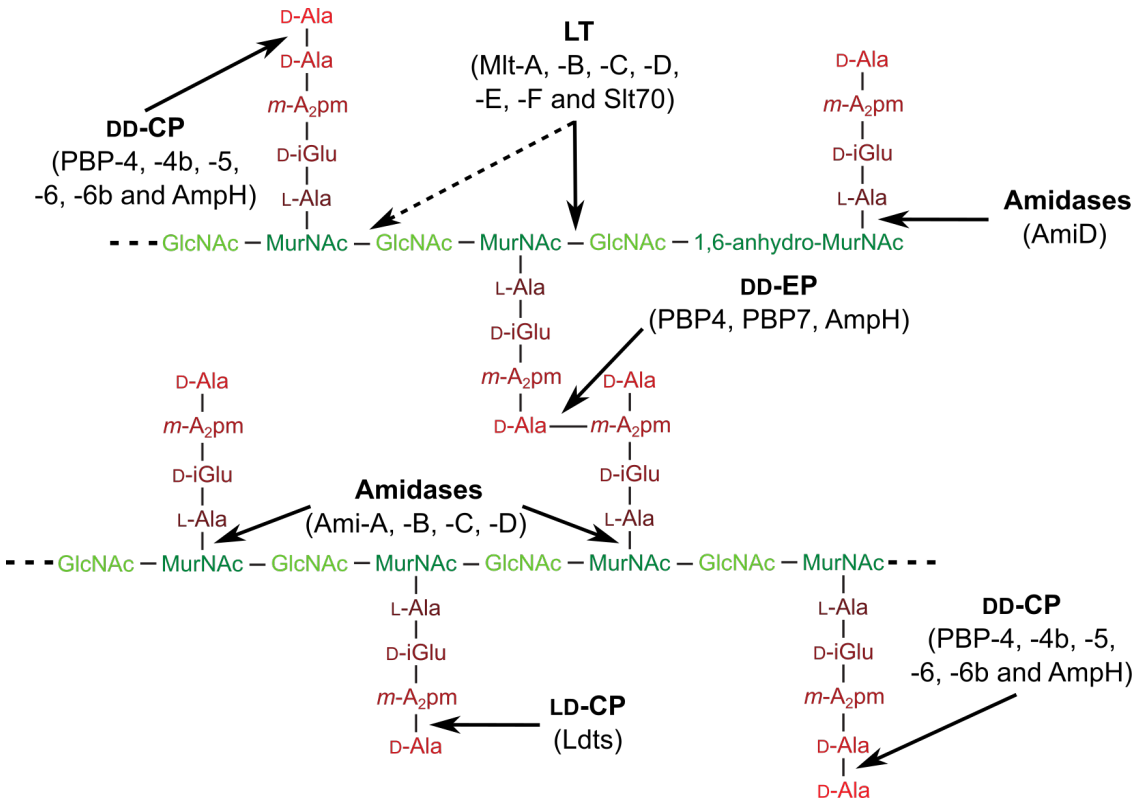

Figure I.3.1: Cleavage sites of periplasmic hydrolases operating on sacculi. LT: lytic transglycosylases; CP: carboxypeptidases. Adapted from (van Heijenoort, 2011; Vollmer, Joris et al., 2008).

Slt70 (soluble lytic transglycosylase), MltC (membrane-bound lytic transglycosylase), MltD, MltE and MltF are members of family 1. With the exception of Slt70, all of them are anchored to the outer-membrane by a lipoyl moiety linked to the cysteine following their N-terminal sequence signal. The structure of these enzymes is usually organized in a variable N-terminal domain and a helical goose-type lysozyme C-terminal domain, which holds the conserved catalytic glutamate specific to LTs (figure I.3.2 A-D). In MltC, the N-terminal domain, annotated in Pfam as DUF3393, is docked onto the catalytic domain and offers an extension of the peptidoglycan binding groove at the proximity of the catalytic glutamate residue (figure I.3.2 A), that is crucial to the processivity of the cleavage of the glycan strand during endolytic or exolytic activity (Artola-Recolons et al., 2014). In MltD the two C-terminal LysM domains are proposed for the interaction with peptidoglycan (Bateman & Bycroft, 2000), while the N-terminal super-helical ring in Slt70 (figure I.3.2 B) is thought to have a similar function (van Asselt et al., 1999). MltF (figure I.3.2 C) does not seem to have a domain dedicated to this function, but has instead an N-terminal region of unknown function that is similar to bacterial amino-acid ABC transporter which plays a role in the modulation of the lytic activity (Madoori & Thunnissen, 2010). MltE (Artola-Recolons et al., 2011) is an exception in this family, as only the lysozyme-like domain is present (figure I.3.2 D). Despite the fact that all enzymes have a lytic transglysosylase activity, the variety of family 1 structural organizations might indicate different specific roles *in vivo*. Interestingly, the conserved patterns of these proteins in the catalytic domain also displays some slight variations, which make each of them representative of a different subfamily (Blackburn & Clarke, 2001).

The two remaining LTs, MltA and MltB, are members of families 2 and 3, respectively. While MltB (Figure I.3.2 E) has a similar catalytic fold to enzymes from family 1 (Jacob et al., 1998), MltA (Figure I.3.2 F) presents its active site in a groove between two domains each composed of β-strands arranged in one β-barrel and α-helices (van Straaten et al., 2005).

Although, both proteins are anchored to the outer-membrane as the other Mlts, MltB has also been found in a soluble form called Slt35 which is a product of proteolytic cleavage (Ehlert et al., 1995). It is currently not known if this observation is an artifact or a regulation mechanism.

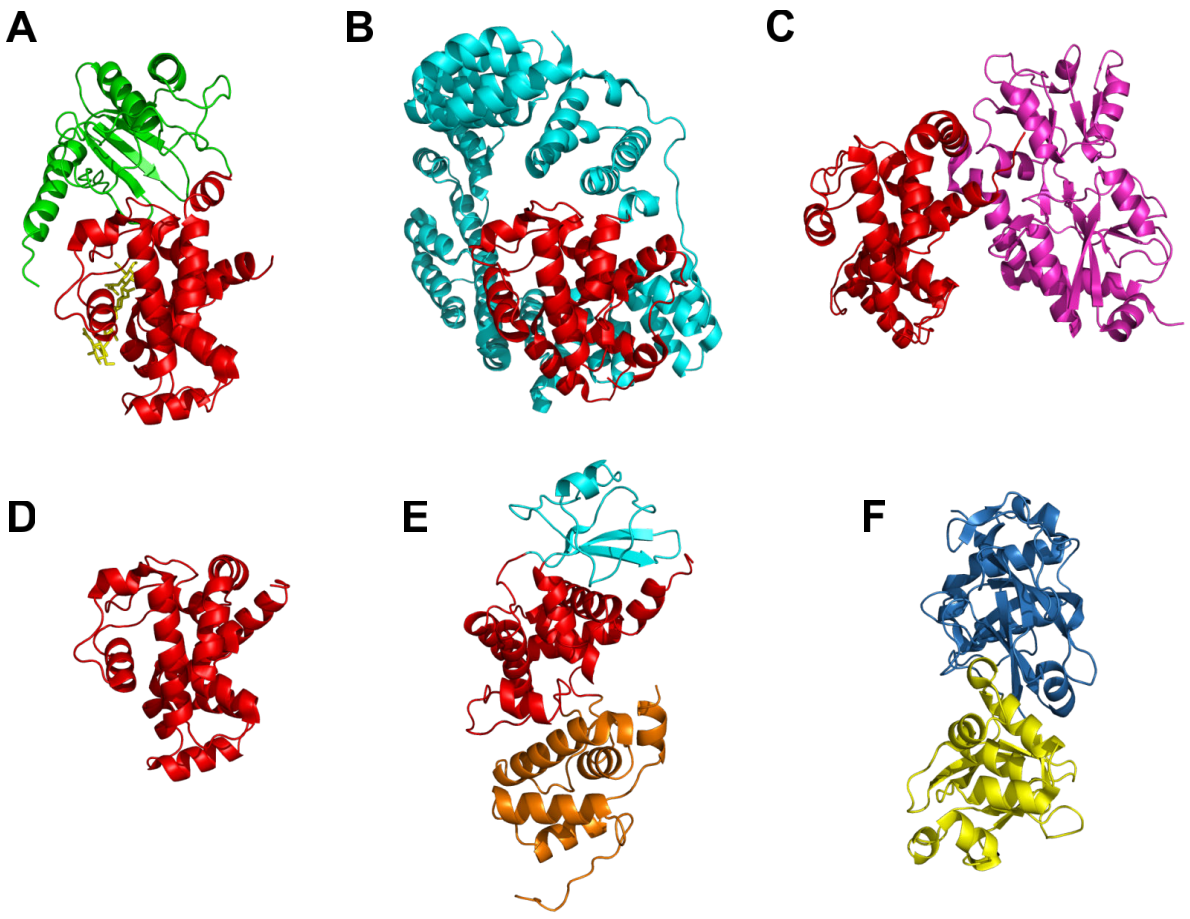

Figure I.3.2: Structures of *E. coli* lytic transglycosylases or orthologues. (A) MltC (PDB code 4CFO) bound to a substrate analogue (yellow sticks), (B) Slt70 (PDB code 1QSA), (C) *Pseudomonas aeruginosa* MltF (PDB code 4P11), (D) MltE (PDB code 2Y8P), (E) MltB (PDB code 1LTM), (F) MltA (PDB code 2AE0). The catalytic domain (lysozyme-like for Mlt-C, E, -F and Slt70, core domain for MltB) is shown in red. In the case of MltA, the active site is located at the interface of the two domains and the substrate is positioned in a groove that extends from the N-terminal into the C-terminal domain to direct the processivity of the glycan strand cleavage.

Some variations in LTs preferred substrates and enzymatic activities have been reported in a recent extensive comparative study (Lee et al., 2013). For this, the authors purified *E. coli* sacculi and exposed them to each of these seven enzymes. The products were then analyzed by liquid chromatography-mass spectrometry (LC/MS) or liquid chromatography-tandem mass spectrometry (LC/MS-MS). Briefly, it appears that the seven LTs have an exolytic activity and that some of them also exhibit an endolytic activity (while MltE was thought before to be the only one not cleaving the terminal disaccharide; Kraft et al., 1998). All LTs were shown to prefer substrates with tetrapeptides and to a lesser extent tripeptides. In addition to non-crosslinked muropeptides, MltA, MltB and MltC can also accommodate cross-linked substrates. Differences between all these enzymes is further demonstrated by the generation by some of them (MltD, MltE, MltF and Slt70) of products without any 1,6-anhydro carbohydrate. This study also evidences differences of several order of magnitude in their specific activity. For example, MltA is 1000 times more active *in vitro* than MltF. In addition to their role in the release of recycling intermediates in the periplasm, it is likely that these enzymes are somehow involved in cell separation by cleavage of the septal

peptidoglycan between the two new daughter cells. Indeed, deletion of all the LTs except MltF results in up to 50% of the cells being undivided and organized in chains of three to eight cells (Heidrich et al., 2002).

3.A.a.ii- Amidases

N-Acetylmuramyl-L-alanine amidases are hydrolases involved in the cleavage of the peptide stem from the sugar units (figure I.3.1). Four of these enzymes, AmiA, AmiB, AmiC and AmiD, have been identified in the periplasm of *E. coli*. They can be further divided into two families on the basis of their sequence homologies (Pennartz et al., 2009). AmiA, AmiB and AmiC belong to the Pfam superfamily amidase_3 and trim the MurNAc-L-Ala bond. They are thought to be implicated in septal peptidoglycan splitting, as simultaneous deletion of all the three of them yields to long chains of unseparated cells (Heidrich et al., 2001). These three amidases have a similar catalytic domain, but different N-terminal domains of unknown function in the case of AmiA and AmiB. In AmiC, the catalytic C-terminal domain is linked to an AmiN N-terminal domain (de Souza et al., 2008), that is essential for septum localization (Bernhardt & de Boer, 2003). A recent study revealed that this domain adopts a peptidoglycan-binding fold composed of two four-stranded β-sheets facing each other (figure I.3.3 A). Each of the two outer-faces of this domain presents two RXXXD/E patterns, which are likely to recognize an undetermined septal peptidoglycan motif (Rocaboy et al., 2013). A similar domain is expected for the other septum localizing amidase, AmiB. The catalytic C-terminal domain of these hydrolases is characterized by the presence of a Zn^{2+} ion in the active site and, most importantly, by an α-helix obstructing access to this cleft (Yang et al., 2012; Rocaboy et al., 2013). This last structure would need to be displaced for being reached by the murein substrate, which indicates that it is probably part of an auto-inhibition mechanism to avoid uncontrolled hydrolase activity. It is likely removed by their EnvC (for AmiA and AmiB) and NlpD (for AmiC) activators.

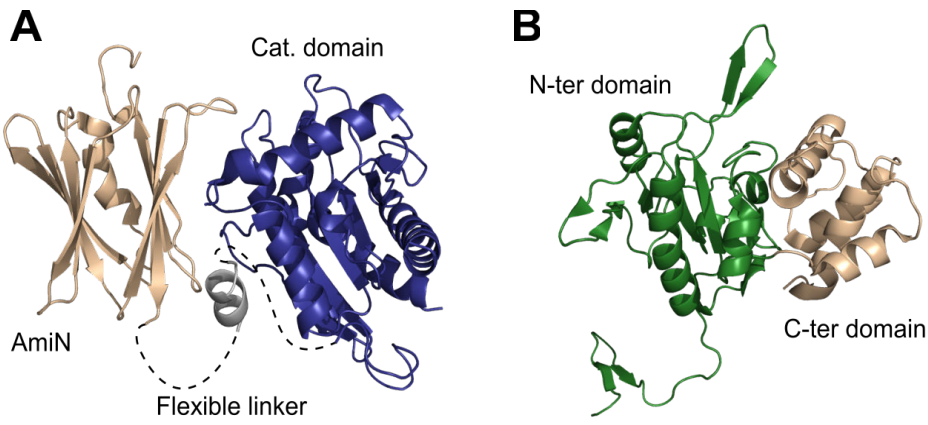

Figure I.3.3: Structure of two *E. coli* amidases. (A) AmiC with its AmiN peptidoglycan-binding domain (PDB code 4BIN). The AmiN and catalytic domains are connected by a ~30 residue linker (dotted line and gray α-helix). (B) AmiD (PDB code 2WKX).

AmiD is the only periplasmic N-Acetylmuramyl-L-alanine amidase member of the Pfam superfamily amidase_2 (Pennartz et al., 2009). Anchored to the outer-membrane, the AmiD lipoprotein cleaves the bond between the MurNAc and its peptide stem in muropeptides or sacculi with a preference for substrates with tri- or tetra-peptides, irrespectively of the presence of a 1,6-anhydro saccharide (Uehara & Park, 2007; Pennartz et al., 2009). The crystal structure of *E. coli* AmiD shows a bimodular organization for this protein (figure I.3.3 B, Kerff et al., 2010). Its N-terminal catalytic domain consists in a mixed α-helix and β-sheet structure, which presents high structural homologies with bacteriophage T7 lysozyme and peptidoglycan recognition proteins. A zinc ion, necessary for the enzymatic activity, is present

in an L-shaped active site. The C-terminal domain, entirely composed of α-helices, is expected to bind peptidoglycan according to its structural homology with domains of lytic transglycosylases from other Gram-negative bacteria. Interestingly, the twenty-eight N-terminal residues (residues 18 to 45) following the cysteine serving as a lipid anchor to the outer-membrane are either not detected or wrapped around a second AmiD molecule, forming an artefactual dimer. This has been interpreted as a case of domain swapping where the N-terminal segment would be in fact at least partially disordered in solution and stabilized in the solid state by crystal packing. The flexibility of this region would thus enable the lipoprotein to increase its radius of action to reach peptidoglycan binding sites.

3.A.a.iii- Peptidases

Finally, peptide stems and cross-links can be trimmed by peptidases. The enzymes can be classified in two groups, low molecular weight PBPs (LMW PBPs) and penicillin-insensitive peptidases.

LMW PBPs, as the previously described PBPs, are characterized by a penicillin-binding domain or structural homologue (Figure I.3.4) with three conserved motifs, one of them displaying a reactive serine essential for the reaction. The reaction mechanism is similar to that described for HMW PBPs, except that the role of the acceptor is played by a water molecule, thus leading to hydrolysis instead of transpeptidation. LMW PBPs can be classified in four subfamilies as proposed in Sauvage et al., 2008, according to what is found in *E. coli*. In this bacterium, type-4 class is represented by PBP4, type-5 by PBP5, PBP6, PBP6b (also called DacD), type-7 by PBP7 and type-AmpH by AmpH and PBP4b.

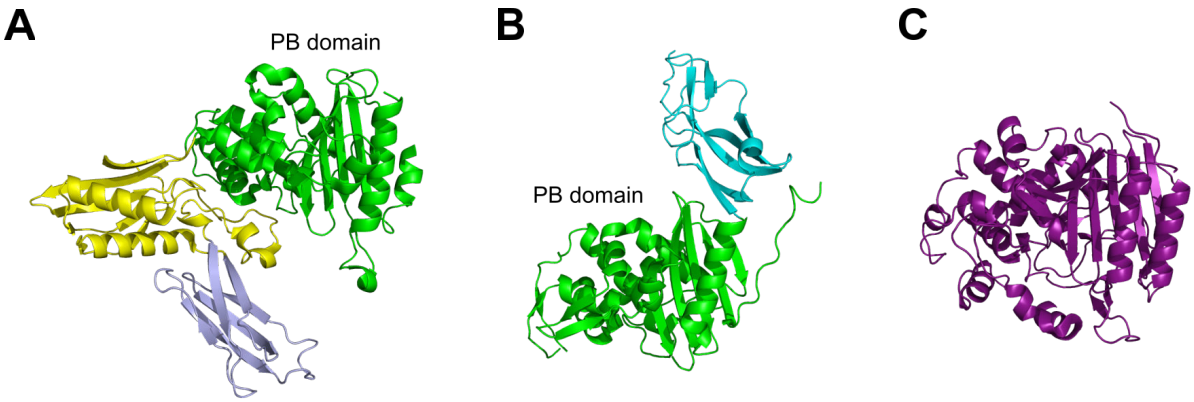

Figure I.3.4: Structures of low molecular weight PBPs (also called class C PBPs) from different subfamilies. (A) *E. coli* PBP4 (PDB code 2EX2), (B) *E. coli* PBP5 (PDB code 1HD8), (C) *Streptomyces* R61 AmpH-type D,D-peptidase (PDB code 3PTE). PB domain: Penicillin binding domain.

PBP4 is a soluble periplasmic protein which might be loosely associated to the inner membrane as it can be found in membrane vesicles (Leidenix et al., 1989). It has three domains which are organized as Russian dolls (figure I.3.4A): the third domain is inserted in the second one, which itself is embedded in the penicillin-binding domain (Kishida et al., 2006). The role of the second and third domains are unknown, but it has been postulated that the second domain could be implicated in interaction with the membrane or with teichoic acids, as its *B. subtilis* homologue PBP4a has a well-oriented positively charged patch (Sauvage et al., 2007). PBP4 was found to have both D,D-carboxypeptidase and D,D-endopeptidase activities. Indeed, this enzyme is able to cleave the D-Ala→*m*-A_2pm peptide bond in cross-links as well as the D-Ala-D-Ala linkage of UDP-MurNAc pentapeptide stem (Korat et al., 1991). Both activities involve recognition of the *m*-A_2pm residue by the active site residues Asp155, Arg361 and Gln422 in *E. coli* (Clarke et al., 2009).

Type-5 PBPs are the most represented class in *E. coli* LMW PBPs. Its members, PBP5, PBP6 and PBP6b are all anchored to the cytoplasmic membrane by a C-terminal amphipathic helix (van Heijenoort, 2011). They consist of the penicillin-binding domain and a perpendicularly oriented, C-terminal, β-stranded module (figure I.3.4 B, Davies et al., 2001; Chen et al., 2009), whose exact function is not understood. All three proteins are D,D-carboxypeptidases, which are specifically cleaving the D-Ala-D-Ala amide bond. PBP5 is one of the most abundant LMW PBPs. Its deletion leads to an increased portion of pentapeptide-containing peptidoglycan (de Pedro et al., 1980) and has an impact on cell morphology (Nelson & Young, 2000). Based on the observation that overexpression of soluble PBP5 was more lethal than that of membrane-attached PBP5, it was proposed that the major role of this protein is to trim only pentapeptides that are directed towards the cytoplasmic envelope, in order to avoid incorrect cross-linkings with newly synthesized chains (Nelson & Young, 2001). PBP6 and PBP6b are PBP5 homologues with 65% and 47% sequence identity, respectively. However, they both exhibit lower D,D-carboxypeptidase activity (Chowdhury et al., 2010; Chowdhury et al., 2012). *In silico* studies suggest that the reduced activity is caused by smaller active site grooves and by different orientations of the key catalytic residues (Chowdhury & Ghosh, 2011; Chowdhury et al., 2012). Deletion of both proteins does not result in morphological defects (Nelson & Young, 2000) on the contrary to PBP5, probably because of a different function in the cell. This conclusion is further supported by the fact that PBP6 is mainly expressed during stationary phase (Buchanan & Sowell, 1982).

As a D,D-endopeptidase, PBP7 cleaves D-Ala → *m*-A_2pm cross-links. It was long confused with PBP8 which is in fact an artefactual product of its degradation (Henderson et al., 1994). Like PBP4, it is not anchored in membranes, but remains loosely associated with them (Romeis & Höltje, 1994). Because deletion of either PBP4 or PBP7 in a PBP5 mutant (but not in a wild-type) leads to a worsening of shape defects (Nelson & Young, 2001) and because they share similar activities, they are suspected to have similar autolysin functions (Sauvage et al., 2008). Nevertheless, the fact that PBP7 accepts only sacculi as substrates (Romeis & Höltje, 1994), while PBP4 requires preferentially muropeptides (Clarke et al., 2009), seems to indicate different tasks *in vivo*.

AmpH and PBP4b are two non-essential proteins (Henderson et al., 1997; Vega & Ayala, 2006) and representatives of the last class C PBP subfamily. They have a single domain adopting the penicillin-binding fold and, as a main feature, are typified by the replacement of the conserved serine in motif II by a tyrosine, as well as by slight modifications in the loops (Sauvage et al., 2008). According to the homologous *Streptomyces* R61 D,D-peptidase structure (figure I.3.4 C, Kelly et al., 1989), type-AmpH LMW PBPs are closely related to β-lactamases. However, AmpH and PBP4b do not display such an activity, but instead have a role of both D,D-carboxypeptidase and D,D-endopeptidase (AmpH, González-Leiza, et al., 2011) or D,D-endopeptidase only (PBP4b, Vega & Ayala, 2006). Similarly to PBP4 and PBP7, AmpH is predicted not to have any membrane-anchoring α-helix, but still remains associated to the cytoplasmic envelope. This enzyme was shown to accept a broad range of peptidoglycan substrates, from various solubilized muropeptides to whole sacculi (González-Leiza et al., 2011). PBP4b is probably anchored in the inner membrane by its uncleaved signal peptide. To date, the lack of knowledge on these two proteins prevents from assigning them to a specific function.

A few non-penicillin-binding peptidases are also identified in *E. coli* periplasm. MepA (figure I.3.5) is a D,D-endopeptidase which cleaves specifically the D-Ala → *m*-A_2pm cross-link between dimeric muropeptides. It has a globular fold organized around a central four-stranded β-sheet (Marcyjaniak et al., 2004). The protein is insensitive to penicillin because of a structure that drastically differs from that of PBPs. It is a member of the LAS family

(Lysostaphin, D-Ala–D-Ala carboxypeptidase, and Sonic hedgehog protein family). As so, it is a metallopeptidase, which contains a Zn^{2+} ion in its active site and presents two conserved motifs involved in its coordination. This Zn^{2+} ion is essential for the folding and catalytic activity of MepA (Firczuk & Bochtler, 2007). Surprisingly, overexpression of this protein does not lead to any significant variations in peptidoglycan cross-linking ratios (Keck et al., 1990). Due to a lack of data on MepA, its role is still unclear.

Figure I.3.5: Structure of *E. coli* penicillin-insensitive D,D-endopeptidase MepA (PDB code 1U10). The zinc ion essential for the folding and activity of the protein is represented by a red ball.

Of note, other non-penicillin-insensitive enzymes are the Ldts that, in addition to their L,D-transpeptidase activity, also act as L,D-carboxypeptidases cleaving the *m*-A_2pm → D-Ala bond (Magnet et al., 2008; Triboulet et al., 2015). A combination of the carboxypeptidase and transpeptidase activities in the extra-cytoplasmic space could also potentially modify amino acids of the peptide stem and favor the formation of bridges instead of the classical cross-links. Most of these modifications are nevertheless most commonly introduced at the level of the biosynthesis of the peptide stem in the cytoplasm or at the level of the lipid II precursors when bound to the inner membrane (see Bouhss et al., 2008; Vollmer, 2008 for a review).

3.A.b- Enzymes responsible for peptidoglycan modifications

Mature peptidoglycan is not only subject to hydrolysis, it is also the target of various modifications, among which the most usual ones are reported in part I section 1.D.c. Here, we focus on the enzymes that are responsible for N-deacetylation, as well as for O-acetylation and -deacetylation.

3.A.b.i- Peptidoglycan N-deacetylases

In some bacteria other than *E. coli*, MurNAc or GlcNAc can be N-deacetylated to yield a δ-lactam ring by intramolecular cyclization with the carboxylic group of the lactyl moiety at position 3 of the MurNAc or to gain resistance towards peptidoglycan hydrolysis by lysozyme for example. This deacetylation is performed by extracytoplasmic peptidoglycan deacetylases that belong to the carbohydrate esterase family 4 (CE4, Vollmer, 2008). Among the five N-deacetylase structures to date for *B. subtilis* PdaA (Blair & Van Aalten, 2004), *S. pneumoniae* PgdA (Blair et al., 2005), *B. anthracis* BaCE4 (Oberbarnscheidt et al., 2007), *Helicobacter pylori* HP0310 (Shaik et al., 2011), and *B. cereus* Bc1960 (PDB 4L1G, 2014), a homologous catalytic domain is found in common. This domain adopts a $(\alpha/\beta)_8$ barrel fold, similar to TIM-barrels, with a groove at the top (figure I.3.6). Conserved residues and a metallic ion (usually Zn^{2+}) are found in this groove at the active site. The O-lactoyl group of the MurNAc saccharide is suspected to be one of the motifs recognized by these proteins, through a positively charged patch (Blair & Van Aalten, 2004). N-deacetylases are thought to generally

require an oligomeric substrate for their activity. They can also show substrate specificity, as for example in the case of *B. subtilis* MurNAc deacetylase PdaA which was shown to be active only on glycan strands bearing no peptides (Fukushima et al., 2005). Another interesting example is the case of *H. pylori* HP0310 deacetylase, which has a much smaller groove than the other deacetylases of known structures (Shaik et al., 2011). It was postulated that this protein could recognize another yet undetermined peptidoglycan component, as it does not show any activity *in vitro* against N-acetylpolysaccharides while being able to deacetylate crude peptidoglycan extracts (Wang et al., 2009).

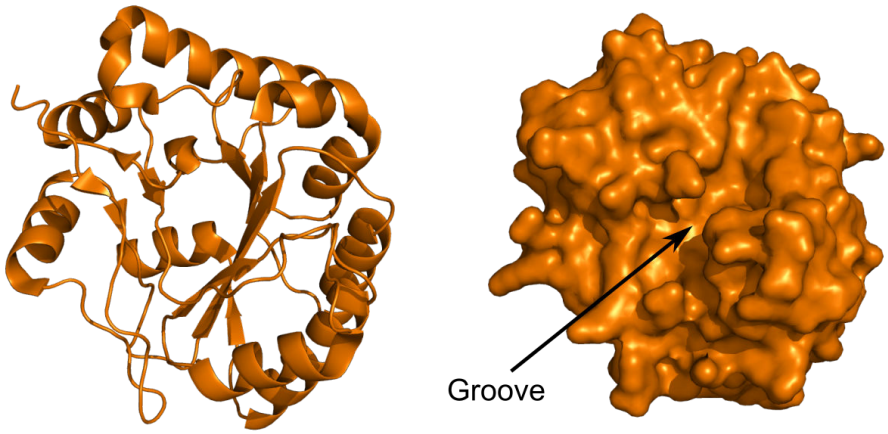

Figure I.3.6: Structure of *B. subtilis* N-deacetylase PdaA (PDB code 1W17). PdaA is represented from the "top", in a cartoon representation on the left highlighting the TIM-barrel homologous structure and in a surface representation (same orientation as in cartoon) on the right showing the groove where is found the active site.

3.A.b.ii- O-acetylation and deacetylation

O-acetylation is also a peptidoglycan post-synthetic modification which contributes to lysozyme resistance. Identification of the enzymes involved in this process is relatively complex, as *in vitro* assays to confirm their activity remained unavailable until 2013 (Moynihan & Clarke, 2013). Since 2005, two main pathways have been identified for the O-acetylation at position 6 of the peptidoglycan MurNAc, which both necessitate most probably the cytoplasmic acetyl-coenzyme A (Ac-CoA) as a source for the acetyl-group (figure I.3.7).

The first of these pathways is the O-acetylation by OatA-type O-acetyltransferases and is found in majority in Gram-positive bacteria. The OatA integral protein was shown in *S. aureus* to be essential for MurNAc O-acetylation in the peptidoglycan (Bera et al., 2005). This protein and its homologues in other bacteria are expected to transport the acetyl group from Ac-CoA from the cytoplasm to the extra-cytoplasmic environment and to transfer this group to the MurNAc oxygen 6 on the peptidoglycan (figure I.3.7 A). No X-ray structure of OatA-type O-acetyltransferases is available to date, but a bimodular organization of the structure has been inferred from the sequence (Vollmer, 2008). The N-terminal domain is predicted to contain eleven transmembrane α-helices, which are likely involved in the translocation of the acetyl moiety. The C-terminal domain is extra-cytoplasmic and is thought to be responsible for the acetyl transfer to the MurNAc residue. These proposals are supported by the importance of an aspartate and a serine residue as putative members of a catalytic triad (Moynihan et al., 2014). Recently, OatA function was shown to be more complex than contributing to peptidoglycan O-acetylation. Indeed, in *Lactobacillus plantarum*, OatA was also demonstrated to be essential for spatio-temporal regulation of the septation (Bernard et al., 2012).

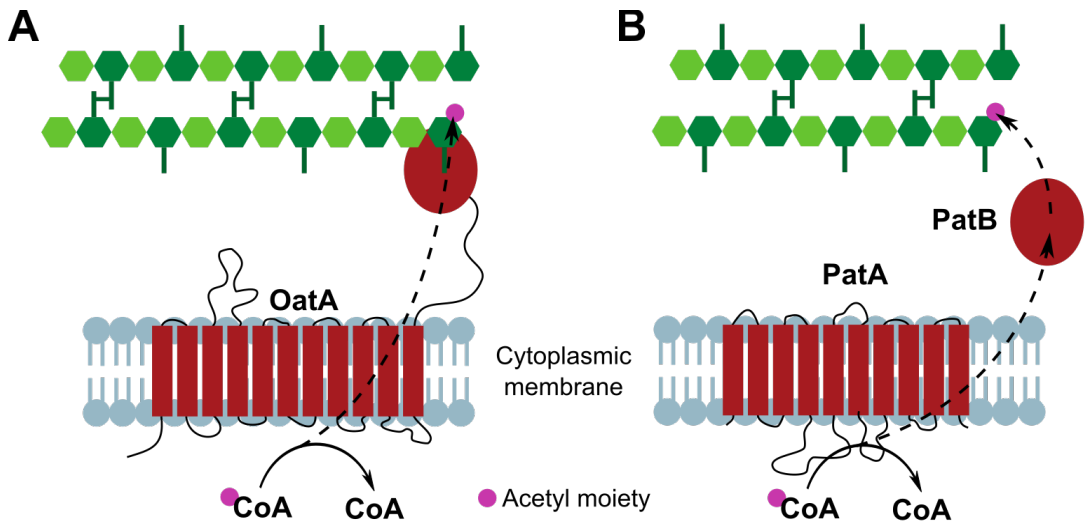

Figure I.3.7: Two different mechanisms have been identified for O-acetylation. (A) The OatA protein performs both transport of the acetyl moiety from the cytoplasm to the extra-cytoplasmic space and transfer to the position 6 of the peptidoglycan MurNAc. This protein is mainly found in Gram-positive bacteria. (B) The Pat pathway, mainly found in Gram-negative bacteria, requires one protein for each stage, PatA for transport across the plasma membrane, and PatB for the transfer to the peptidoglycan.

The second pathway implies two proteins that were first described in *Neisseria gonorrhoeae*: Pat (Peptidoglycan O-AcetylTransferase) A and B (figure I.3.7 B). PatA is a hypothetical single-domain acetyltransferase (Weadge et al., 2005) made of ten transmembrane α-helices. PatB, formerly Ape2, is an extra-cytoplasmic protein, which was proposed to be responsible for the transfer of the acyl group on the MurNAc carbon 6 moiety (Moynihan & Clarke, 2010). While biochemical characterization is still lacking for PatA, PatB activity was confirmed *in vitro* on a GlcNAc polymer, the chitooligosaccharide (Moynihan & Clarke, 2014b). A catalytic triad composed of an aspartate, a histidine and a nucleophile serine were identified as the catalytic residues involved in the transfer on the basis of sequence alignments and biochemical evidences (Moynihan & Clarke, 2014a).

O-deacetylation is required for the cleavage of the modified peptidoglycan by lytic transglycosylases (figure I.3.8). This reaction is performed by Ape, which is an O-AcetylPeptidoglycan Esterase, whose sequence is relatively close to PatB (Moynihan & Clarke, 2010). The recent and so far only X-ray structure of *Neisseria meningitidis* Ape1 (Williams et al., 2014) shows two domains (figure I.3.9). The N-terminal module is a β-sandwich of two antiparallal β-sheets, which is predicted, by structural homology, to bind peptidoglycan. The C-terminal domain is a five-stranded β-sheet surrounded by eleven helices, which adopts the fold of the SGNH hydrolases. As a member of this family, it harbors an active site, here in a pocket, which has, among other conserved residues, a serine, an aspartate and a histidine as a catalytic triad. From the trapping of two reaction intermediates, it was proposed that the substrate activates the serine, which then attacks the carbonyl of the MurNAc acetate group at position 6, forming a tetrahedral intermediate. This falls down, leading to a serine-acylated Ape1 and the release of the de-O-acetylated peptidoglycan. The active site comes back to its initial state by deacetylation of the serine with a water molecule. The ape gene is found, at least in *N. gonorrhoeae*, in the same oap operon as the one coding for PatA and PatB (Weadge & Clarke, 2006). However, the balance between Ape and Pat activities is not known. One hint is the *in vivo* observation that *N. meningitidis* Ape1 is specific for GlcNAc-MurNAc-tripeptides (Veyrier et al., 2013), which might mean that previous action of a carboxypeptidase is required (figure I.3.8). Interestingly, this latter study also correlates de-O-acetylation with cell size.

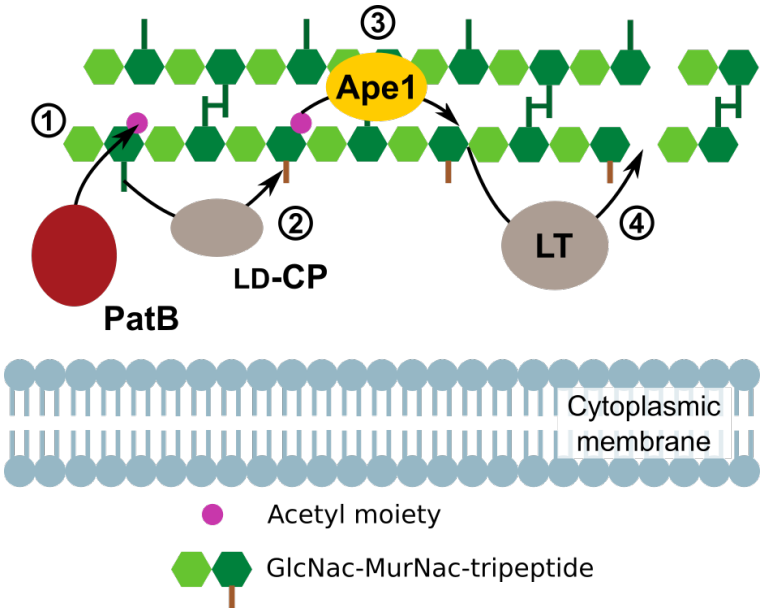

Figure I.3.8: O-deacetylation by Ape proteins is required for peptidoglycan cleavage by lytic transglycosylases. If muro-tetrapeptide are acetylated by PatB (1), a L,D-carboxypeptidase (LD-CP) is required to generate muro-tripeptides (2). The latter muropeptides are the substrates for the O-acetyl-peptidoglycan esterase Ape1, which can remove their O-acetyl moiety at the position 6 of MurNAc (3). This step is essential to enable cleavage of the glycan strand by lytic transglycosylases (4). Adapted from Moynihan & Clarke, 2014b.

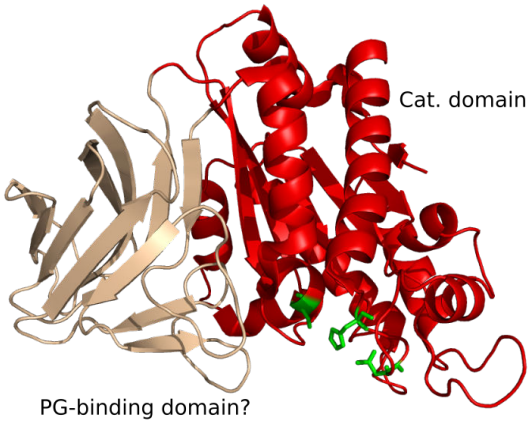

Figure I.3.9: Structure of the O-acetyl-esterase Ape1 from *Neisseria meningitidis* (PDB code 4K40). The active site catalytic residues Ser80, Asp366 and His369 are shown as green sticks and are part of a highly conserved groove in the SGNH catalytic domain. PG: peptidoglycan; Cat: catalytic.

In Gram-positive bacteria and mycobacteria, position 6 of MurNAc and GlcNAc can also be phosphorylated and serve as a platform to anchor other cell wall polymers such as teichoic acids or arabinogalactan. The genetics and enzymology of the enzymes involved in these reactions is nevertheless still enigmatic.

Of note, some modifications have been registered at the position 2 of the peptidoglycan MurNAc, like the N-glycolylation commonly found in Mycobacteria, but these modifications are introduced during the synthesis of the lipid II precursors in the cytoplasm (Raymond et al., 2005).

3.B- Recycling of peptidoglycan and its lipidic precursor

Up to 50% of the peptidoglycan can be replaced in one generation at the lateral walls as shown by peptidoglycan labeling (Burman et al., 1983; de Pedro et al., 1997) and an even more important remodeling with the replacement of up to 60% at each generation has been proposed (Park & Uehara, 2008). However, the muropeptides resulting from peptidoglycan degradation are not lost – this would be a huge waste of energy for the cell – but are either freed in the medium or recycled through a dedicated pathway. This process is constantly tightly regulated, and any imbalance between peptidoglycan synthesis and recycling is sensed by the bacterial organism, triggering β-lactamase induction. In parallel, the undecaprenyl pyrophosphate released by the glycosyltransferase reaction must be dephosphorylated and flipped back to the cytoplasm to act again as a lipidic transporter. As undecaprenyl pyrophosphate recycling is required for the synthesis of other cell wall polysaccharides in addition to peptidoglycan, and as it is still not fully understood, this process will be only briefly exposed here. The interested reader can refer to a detailed report of the current knowledge published on this topic in 2014 (Manat et al., 2014).

3.B.a- Recycling of peptidoglycan (in Gram-negative bacteria)

The GlcNAc-anhydroMurNAc-tetrapeptides generated by hydrolase activity in the periplasm are recycled by the cell in view of saving energy. In this process the muropeptides are first imported in the cytoplasm. Then GlcNAc, MurNAc and peptides are separated, before to be re-incorporated in peptidoglycan precursors or introduced in other metabolic pathways. In many Gram-negative bacteria, recycling intermediates are also cleverly used to sense β-lactams action and trigger resistance mechanisms (figure I.3.10).

3.B.a.i- Disassembly of the disaccharide-peptide unit

Generation of the first intermediates in the peptidoglycan recycling pathway begins in the extra-cytoplasmic space with the degradation of peptidoglycan by lytic transglycosylases. At this stage, the MurNAc of the muropeptide is replaced by a 1,6-anhydro-MurNAc. The next step consists in the transport of muropeptides into the cytoplasm by the major permease AmpG. Topology studies of AmpG suggests that this membrane protein contains ten transmembrane α-helices and two large cytoplasmic loops bearing four hydrophobic segments (Chahboune et al., 2005). Because two of the three reported mutations impairing AmpG function (Lindquist et al., 1993) are found in these latter regions, these loops are likely involved in the transport mechanism. AmpG does not carry any peptidoglycan turnover product. Instead the protein was shown to specifically transport disaccharidic GlcNAc-1,6-anhydro-MurNAc compounds with or without their attached peptides, which are produced by the lytic transglycosylases. In the absence of the GlcNAc residue or of the anhydro modification, the substrate cannot cross the membrane. AmpG transport activity was also shown to be dependent upon proton motive force (Cheng & Park, 2002).

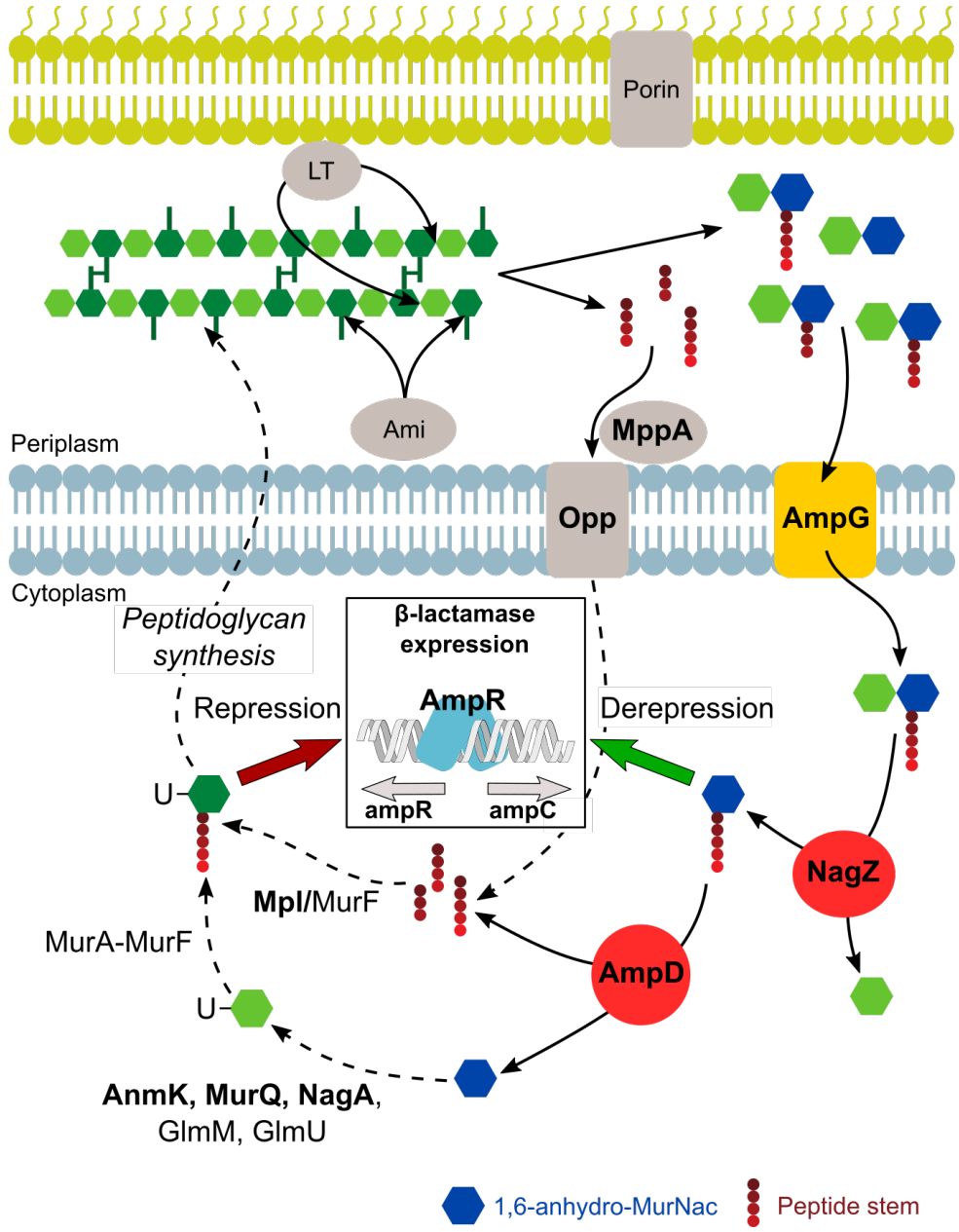

Figure I.3.10: Peptidoglycan recycling pathway and connection with the β-lactamase induction pathway in Gram-negative bacteria. Names of the main enzymes involved in these two processes are written in bold. Light green, dark green and blue hexagons are schematic representations of the GlCNAc, MurNAc and 1,6-anhydro-MurNAc residues. Amino acids of the peptide stems are sketched as red filled circles. UDP moiety is represented by "U-". The text clarifies the role of each enzyme. Adapted from Fisher & Mobashery, 2014**.**

Once in the cytoplasm, the β-1,4-glycosidic bond in the GlcNAc-(1,6-anhydro-MurNAc)-peptide is then cleaved by the N-acetyl-β-D-glucosaminidase NagZ. In *E. coli*, this protein seems to be non redundant as its deletion causes an accumulation of anhydro-disaccharides (Cheng et al., 2000). Although only anhydro-muropeptides are expected to be found in the cytoplasm, NagZ is also able to hydrolase GlcNAc-MurNAc disaccharides (Cheng et al., 2000). The X-ray structure of a NagZ homologue in *Vibrio cholerae (Stubbs et al., 2007)* suggests that the protein adopts a single domain TIM-barrel fold characteristic of glycoside hydrolases, but shows an unusually large open pocket at its surface that binds the substrate (figure I.3.11). Subsequent structural studies revealed an uncommon structural plasticity of the active site to accommodate the disaccharide, that may be crucial to deal with the variability of the peptide stem length and to distort the substrate for an optimal positioning for the catalytic reaction to occur (Bacik et al., 2012).

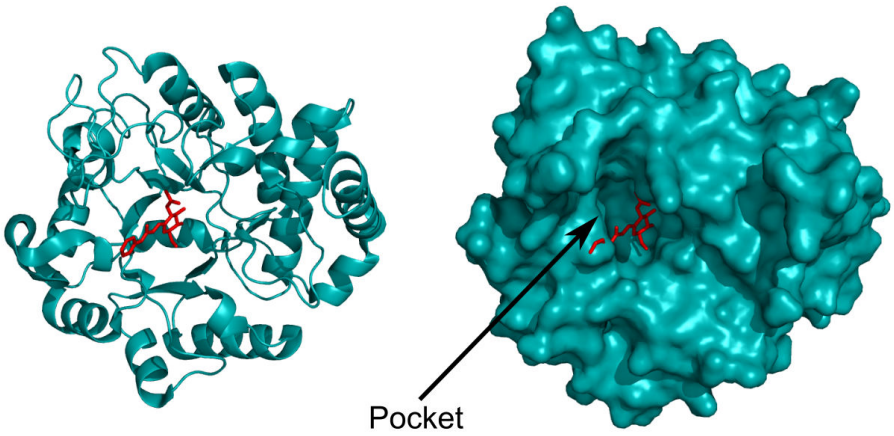

Figure I.3.11: Cartoon and surface representations of *Vibrio cholerae* N-acetyl-β-D-glucosaminidase NagZ (PDB code 2OXN). A NagZ inhibitor, PUGNAc, is represented in red sticks in the active site. The surface representation evidences the largely opened binding pocket for the substrate.

The GlcNAc trimmed by NagZ, the anhydro-MurNAc-peptide D-Lac→L-Ala peptide bond is then cleaved by the N-acetylmuramyl-L-alanine amidase AmpD (Höltje et al., 1994; Jacobs et al., 1995). AmpD is, like the AmiD lipoprotein, a member of the Pfam superfamily amidase_2. As members of the same family, both proteins share 40% sequence identity (Pennartz et al., 2009) and a similar lysozyme-like catalytic fold containing the essential zinc ion for amidase activity (Liepinsh et al., 2003). NMR and X-ray structures determined for AmpD show a "closed" and an "open" conformation, respectively (figure I.5.7 in part I chapter 5), suggesting an activation mechanism (Liepinsh et al., 2003; Carrasco-López et al., 2011). If the existence of these two conformations is not an *in vitro* artifact, the factors triggering this large structural modifications (up to 17 Å) are still unknown. AmpD is highly specific for 1,6-anhydro-MurNAc, but can accommodate for the presence or absence of the GlcNAc residue in the substrate (Jacobs et al., 1995). This amidase is almost ineffective on UDP-MurNAc-peptides with an 85,000 to 100,000 times slower rates, thus avoiding depletion of the peptidoglycan precursor pool in the cytoplasm.

3.B.a.ii- Recycling of the hexosamines GlcNAc and 1,6-anhydro-MurNAc

The GlcNAc and 1,6-anhydro-MurNAc residues obtained from NagZ are both converted in N-Glucosamine-6-Phosphate (GlcN-6-P) through a common N-acetyl-Glucosamine-6-Phosphate intermediate (GlcNAc-6-P), which can finally re-enter the peptidoglycan synthesis pathway (figure I.3.12).

The N-AcetylGlucosamine Kinase, NagK – not to be confused with the N-Acetyl-L-Glutamate Kinase NAGK – first specifically phosphorylates GlcNAc to yield GlcNAc-6-P (Uehara & Park, 2004). In parallel, the Anhydro-N-acetylMuramic acid Kinase AnmK cleaves the 1,6-anhydro-cycle and phosphorylates the 1,6-anhydro-MurNAc substrate to produce N-acetyl-muramic acid-6-phosphate, MurNAc-6-P (Uehara et al., 2005). Both steps require ATP. In the case of AnmK, X-ray crystallography and Small Angle X-ray Scattering (SAXS) allowed detailed structural studies showing that AnmK holds an active site in a cleft located between its two domains (figure I.3.13 A, Bacik et al., 2011; Bacik et al., 2014). Upon binding of ATP and 1,6-anhydro-MurNAc, these two modules undergo an important conformational change by a rotation of up to 32°, which brings the ATP γ-phosphate closer to the 1,6-anhydro-MurNAc carbon 6 oxygen to favor this unusual reaction. The MurNAc-6-P generated is then converted into GlcNAc-6-P by the N-acetylmuramic acid-6-phosphate etherase MurQ with the release of D-lactate (Jaeger et al., 2005). Determination of the high-resolution structure (Hadi et al., 2013) shows that MurQ is composed of two domains connected by a

long flexible linker, one of which adopting a α/β Rossman-fold (figure I.3.13 B). At least in the crystallized form, the reaction seems to be performed in a pocket between two MurQ monomers. A one base mechanism was suggested where a glutamate deprotonates the carbon 2 after opening the MurNAc-6-P ring, and assists in the departure of the D-lactyl-ether group (Hadi et al., 2013). Then the same residue would deprotonate an incoming water molecule to reprotonate the enolate intermediate, forming GlcNAc-6-P.

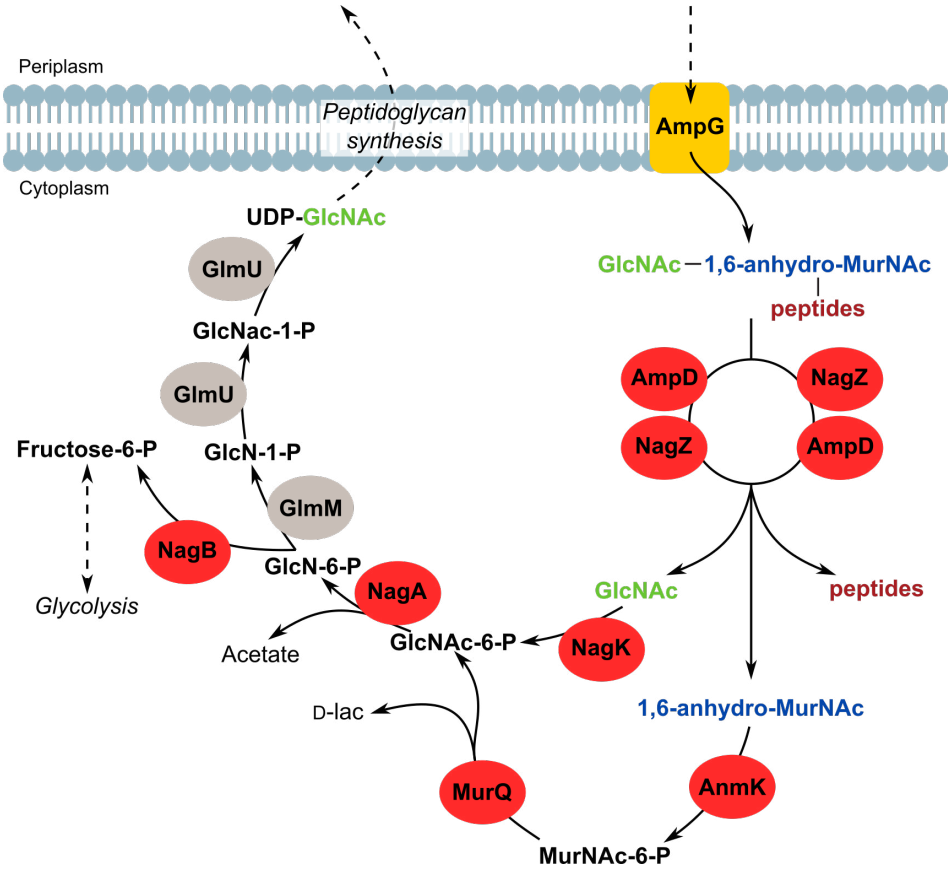

Figure I.3.12: GlcNAc-(1,6-anhydro-MurNAc) disaccharide recycling pathway in the cytoplasm. As shown in figure I.3.10, the disaccharide muropeptides are first trimmed by NagZ and AmpD, which cleave the β-1,4-glycosidic linkage and the D-Lac→L-Ala peptide bond, respectively. The saccharides are then phosphorylated at position 6 before to be converted into UDP-GlcNAc by a cascade of reactions which re-enters the peptidoglycan precursor biosynthesis pathway. Adapted from Park & Uehara, 2008.

Finally, the GlcNAc-6-P produced by NagK and AnmK/MurQ is deacetylated by the N-acetylglucosamine-6-phosphate deacetylase NagA (White & Pasternak, 1967) to produce GlcN-6-P and acetate. The deacetylase has one distorted $(\alpha/\beta)_8$ TIM-barrel domain and a second domain adopting an incomplete β-barrel fold (figure I.3.13 C, Vincent et al., 2004). *In vitro*, *E. coli* NagA forms dimer of dimers, with one active site per subunit located at the bottom the TIM-barrel domain (Hall et al., 2007). A divalent ion in this region is essential for the coordination of a water molecule which, upon activation by a general base, performs a nucleophilic attack on the carbonyl of the GlcNAc-6-P acetamide. The nitrogen of the tetrahedral intermediate is then reprotonated by a general acid, likely played by the same residue that previously served as a general base, and the GlcN-6-P and acetic acid are released (Vincent et al., 2004; Ferreira et al., 2006; Hall et al., 2007). Following this step, GlcN-6-P can be re-used for peptidoglycan synthesis as a substrate for the phosphoglucosamine mutase GlmM (discussed in part I section 2.A.a.i) or be converted to fructose-6-phosphate by the glucosamine-6-P deaminase NagB to enter the glycolysis pathway.

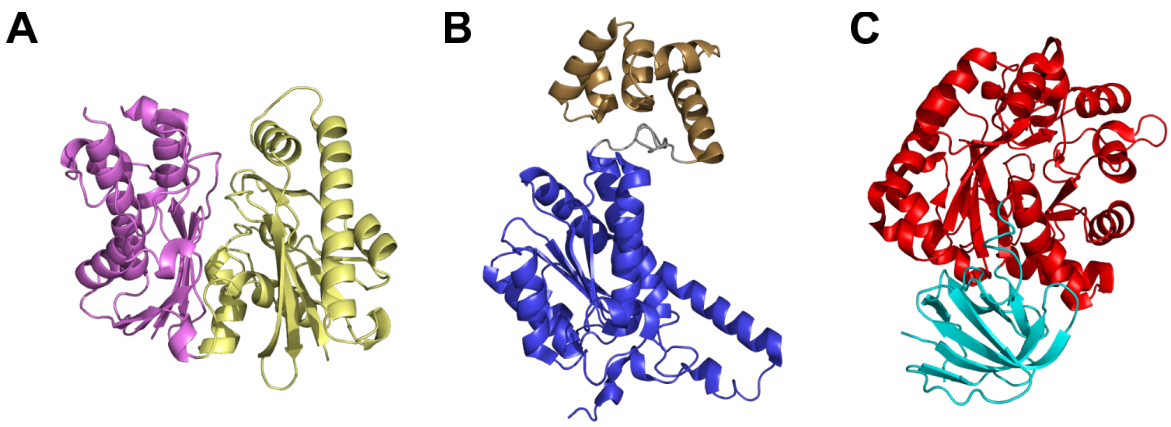

Figure I.3.13: Structures of some of the enzymes involved in GlcNAc-(1,6-anhydro-MurNAc) disaccharide recycling. (A) *Pseudomonas aeruginosa* anhydro-N-acetylmuramic acid kinase AnmK (PDB code 3QBX). The two domains undergo an important reorientation upon ATP and 1,6-AnhydroMurNAc binding at the active site located in the cleft between the two domains. (B) *Haemophilus influenzae* N-acetylmuramic acid-6-phosphate etherase MurQ (PDB code 4M0D). The α/β Rossman-fold domain in blue and the small α-helical domain in brown are connected by a flexible linker in gray. (C) *B. subtilis* N-acetylglucosamine-6-phosphate deacetylase NagA (PDB code 2VHL). The distorted $(\alpha/\beta)_8$ TIM-barrel and incomplete β-barrel domains are shown in red and light blue, respectively.

3.B.a.iii- Recycling of the peptide stem

Peptides obtained from the cytoplasmic AmpD and, to a much minor extent, from extra-cytoplasmic amidases after tripeptide transport to the cytoplasm by the MppA-OppBCDF system (Park et al., 1998; Park & Uehara, 2008) can be recycled in two different ways. They are in majority directly used as substrate for incorporation in precursors but they can also be cleaved into single amino-acids or shorter peptides which are then re-introduced in the precursors or in other metabolic pathways (figure I.3.14).

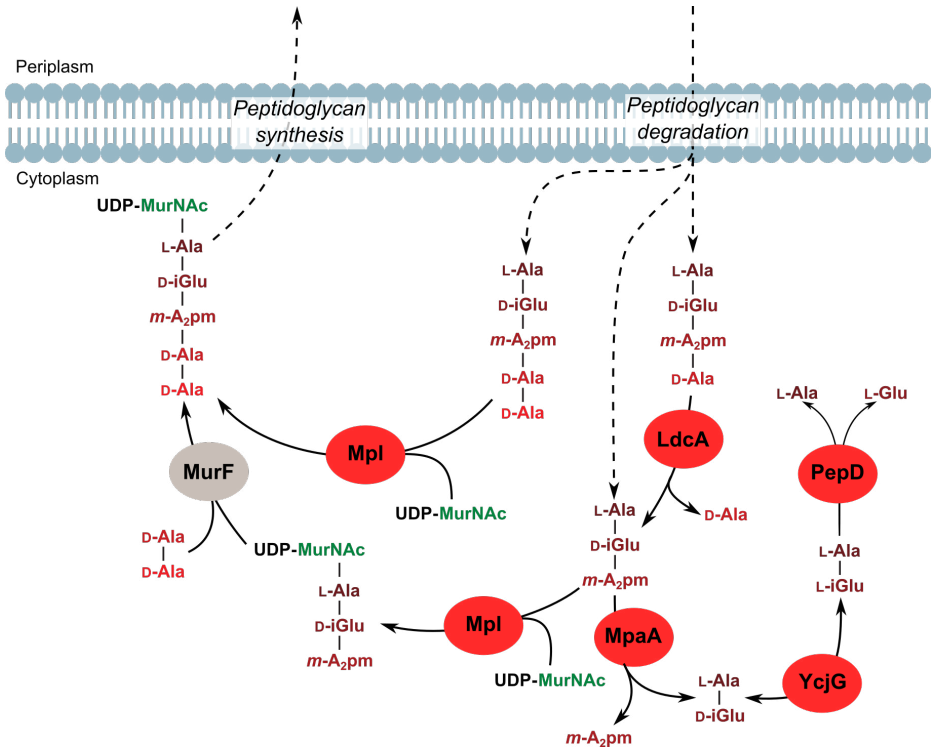

Figure I.3.14: Recycling of peptidoglycan peptide stems in the cytoplasm. Peptide stems can be cleaved into individual amino acids by successive enzymatic degradation by LdcA, MpaA, YcjG and PepD, cleaving one amino acid at a time. Alternatively penta- and tri-peptides can be coupled directly to UDP-MurNAc by Mpl to generate the UDP-MurNAc-pentapeptide peptidoglycan precursor. Adapted from Park & Uehara, 2008.

The murein peptide ligase Mpl is a MurC paralogue (with 28.7% of sequence identity), which catalyzes the attachment of the tripeptide stem to UDP-MurNAc (Mengin-Lecreulx et al., 1996). The X-ray structure of Mpl from *Psychrobacter arcticus* – a permafrost bacterium – presents, as expected from the similar sequences, a fold close to Mur enzymes (figure I.3.15). The three N-terminal, central, and C-terminal domains bind one substrate each, UDP-MurNAc, ATP, and the peptide, respectively (Das et al., 2011). Conservation in Mpl of essential Mur ligase residues for substrate binding and requirement for Mg^{2+} for activity suggest that the catalytic mechanism is the same that in Mur ligases. Nevertheless, the C-terminal domain shows marked variations with Mur enzymes (figure I.3.15), as it displays conserved residues specific to Mpl proteins, likely for adaptation to its substrates.

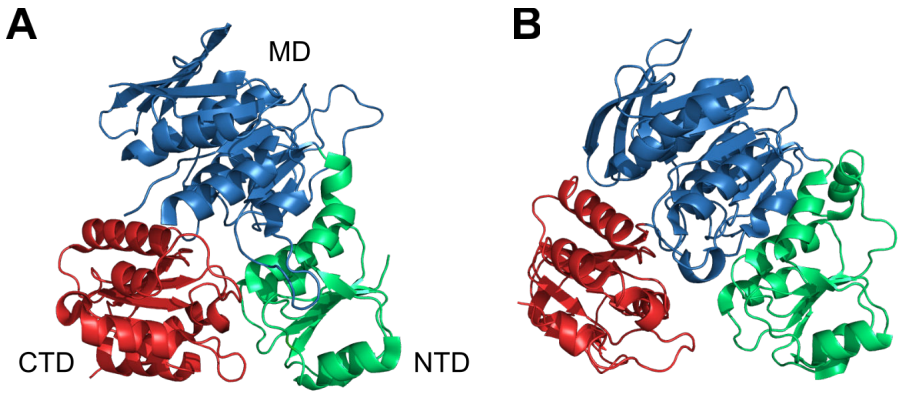

Figure I.3.15: Mpl shows structural homologies with Mur ligases. (A) *Psychrobacter arcticus* Mpl structure (PDB code 3HN7). (B) *E. coli* MurC structure (PDB code 2F00) for comparison. The C-terminal domain of Mpl shows the largest variations in the catalytic residues to MurC. NTD: N-terminal domain; MD: middle domain; CTD: C-terminal domain

Biochemical characterization of *E. coli* Mpl showed that it has a rather broad specificity *in vitro*, as it can ligate tetra- and pentapeptides in addition to tripeptides, with similar efficiency (Hervé et al., 2007). *In vivo*, Mpl probably does not use tetrapeptides, as they are the specific substrates for the L,D-carboxypeptidase LdcA (Templin et al., 1999). This enzyme is responsible for the cleavage of the D-Ala in position 4 of the peptide stem, yielding the L-Ala-D-iGlu-*m*-A_2pm tripeptide. Specificity studies demonstrated that LdcA can use a wide range of substrates such as monomeric muropeptides, free tetrapeptides, and UDP-MurNAc-tetrapeptide, but can not process cross-linked compounds or sacculi (Templin et al., 1999). Its active site contains an essential Ser – His – Glu catalytic triad (Korza & Bochtler, 2005) situated at the interface between the N- and C-terminal domains (figure I.3.16 A). LdcA has the peculiarity to be the only enzyme in the recycling process that is essential in *E. coli*, its deletion resulting in cell lysis during the stationary phase. It was proposed that, when LdcA is inactivated, the accumulating tetrapeptides are incorporated in the muropeptide precursors instead of the classical pentapeptide. The peptidoglycan produced in these conditions would thus contain less strands available as donors for the D,D-transpeptidation, which would explain the measured 23 % decrease of the ratio of cross-linked versus uncross-linked peptide stems (Templin et al., 1999). As this lethal phenotype is not observed during the exponential phase, this suggests an increased role for peptidoglycan recycling during the stationary phase. Therefore, *in vivo* and in presence of LdcA, Mpl might ligate only tripeptide and pentapeptide to UDP-MurNAc, generating substrates for MurF and MraY, respectively.

Another minor pathway exists, which cleaves all the amino-acids from the tripeptide one by one (figure I.3.14). First, the D-iGlu→*m*-A_2pm bond is hydrolyzed by the Murein Peptide Amidase A MpaA (Uehara & Park, 2003). MpaA is specific for tripeptides, but has a four-fold lower affinity for them than Mpl for tetrapeptide. This explains why the Mpl pathway is

favored *in vivo* (Maqbool et al., 2012). As a zinc-dependant carboxypeptidase, MpaA adopts a common eight-stranded β-sheet fold surrounded by α-helices (figure I.3.16 B). On the top of the groove that binds the substrate, a β-hairpin flap is found, which might restrict the accessibility to a given peptide length and give its specificity to MpaA for tripeptides. After removal of the *m*-A_2pm residue, the L-Ala-iGlu epimerase YcjG converts L-Ala-D-iGlu in L-Ala-L-iGlu (Schmidt et al., 2001). The structure of YcjG (Gulick, et al., 2001) reveals a fold close to that of the other members of the enolase family, with a capping domain located above the active site from a $(\beta/\alpha)_7$ β-barrel domain. While the dipeptide is well positioned in the active site by interaction with its L-Ala α-ammonium group, the capping domain participates in the enzyme specificity by forming a salt bridge with the glutamate side chain (Klenchin et al., 2004). The reaction involves a Mg^{2+} ion and a Lys-X-Lys motif serves as a general acid/base catalyst to perform a 1,1-proton transfer. The L-Ala-L-iGlu product is finally hydrolyzed by the PepD metallodipeptidase, an enzyme with a low specificity for its dipeptide substrates (Schroeder et al., 1994).

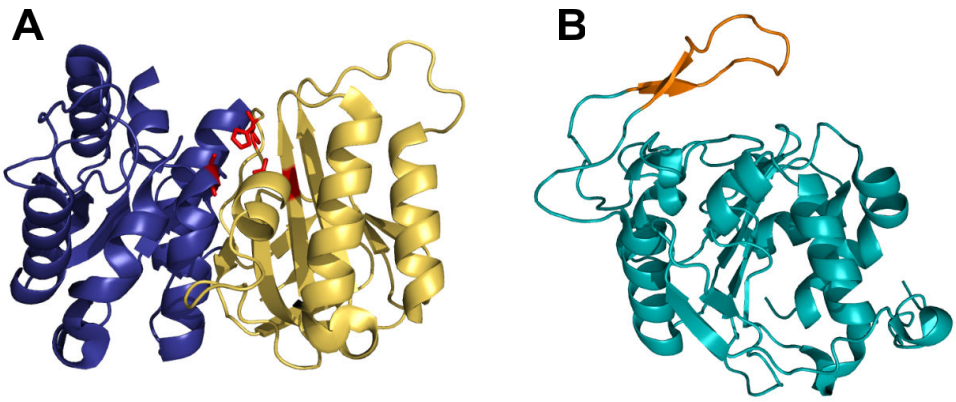

Figure I.3.16: Structures of periplasmic peptide stem carboxypeptidases. (A) *Pseudomonas aeruginosa* LdcA (PDB code 1ZRS). LdcA Ser-His-Glu catalytic triad is shown as red sticks. (B) *Vibrio harveyi* MpaA (PDB code 4AXV), which adopts a typical carboxypeptidase fold. The β-hairpin region suggested to limit access to the binding site is represented in orange.

3.B.a.iv- Induction of β-lactam resistance by cell-wall recycling enzymes

In many Gram-negative bacteria except *E. coli*, AmpG, NagZ and AmpD were quickly shown to be related to β-lactam resistance (figure I.3.10). When AmpG (Lindquist et al., 1993) or NagZ (Vötsch & Templin, 2000) are mutated, the cells present an increased sensitivity to β-lactams. This was rapidly correlated to a defect in the induction of the AmpC β-lactamase, an enzyme which hydrolyzes and thus inactivates the corresponding antibiotic. The expression of AmpC is regulated by the inducer AmpR through its interaction with the intergenic region of the ampC-ampR DNA. In the absence of β-lactams, the UDP-MurNAc-pentapeptide precursor binds to AmpR and the expression of AmpC is repressed (Jacobs et al., 1997). Muropeptides coming from cell wall recycling are able to compete with the UDP-MurNAc-pentapeptide repressor to favor AmpC induction by activation of AmpR. Conversely, inactivation of AmpD results in a semi-constitutive expression of AmpC (Lindberg, et al., 1987). When AmpD is mutated in *Enterobacter cloacae* cells treated with β-lactams, 1,6-anhydro-MurNAc-pentapeptides accumulate in the cytoplasm and the AmpC expression level increases, suggesting that this anhydro derivative is likely the effector (Dietz, et al., 1997). Therefore, induction of AmpC is sensitive to the 1,6-anhydro-MurNAc-pentapeptide:UDP-MurNAc-pentapeptide ratio, which is imbalanced in the presence of β-lactams. Other factors may come into consideration in this pathway, as other molecules, such as pentapeptides and lipid II, are suspected to regulate AmpR (Park & Uehara, 2008).

Because inactivation of AmpG, NagZ or AmpR prevents the cell from stimulating AmpC

production, these three proteins are viewed as attractive drug targets. Depending the species, additional or alternative proteins implicated in AmpC regulation may be considered, such as the two additional AmpD homologues and the cytoplasmic membrane protein of unknown function AmpE in *Pseudomonas aeruginosa* (Johnson et al., 2013) or proteins from *Aeromonas* species that are reviewed in Zeng & Lin, 2013. In Gram-positive bacteria, different pathways were identified. One of the most studied mechanism relies on the sensor and signal transducer protein, BlaR1, which triggers β-lactam resistance by expression of a β-lactamase or of a low drug affinity PBP upon irreversible acylation of BlaR1 with antibiotics. Details on this pathway can be found in Johnson et al., 2013. Recently, this path was shown to induce β-lactam-resistance also from the use of peptidoglycan fragments in the Gram-positive *Bacillus licheniformis* (Amoroso et al., 2012).

3.B.b- Recycling of undecaprenyl pyrophosphate

Polymerization of the glycan chain by HMW PBPs releases undecaprenyl-pyrophosphate, C_{55}-PP. This lipid is recycled in a two-step process to be re-used as a lipid I peptidoglycan precursor. The C_{55}-PP product obtained after consumption of lipid II by the glycosyltransferase is first dephosphorylated by phosphatases (figure I.3.17). Four integral membrane proteins from two different families were identified in *E. coli*. UppP is the major one, as its *in vivo* activity accounts for 75% of the total activity (El Ghachi et al., 2004). It is the sole representative of the BacA (the former name of UppP) family. The three other membrane proteins, YbjG, YeiU and PgpB, belong to the PAP2 family (El Ghachi et al., 2005). Which of these four enzymes is (are) responsible for the dephosphorylation of C_{55}-PP in the extra-cytoplasmic space is not clear to date, as the phosphatase activity is not only required for recycling but also for C_{55}-PP generation from *de novo* synthesis by the UppS enzyme (Manat et al., 2014). However, YbjG and YeiU are the most likely candidates (Tatar et al., 2007). In addition to its importance for C_{55}-PP recycling, the dephosphorylation reaction is a resistance mechanism to the antibacterial peptide bacitracin, which sequestrates C_{55}-PP by completely wrapping its pyrophosphate moiety (Siewert & Strominger, 1967; Economou et al., 2013). Following dephosphorylation, the C_{55}-P product is translocated on the inner leaflet of the cytoplasmic membrane by an unknown protein (figure I.3.17), although the lipid II flippase itself was suggested as a potential translocase (Manat et al., 2014). Once in the cytoplasm, a new cycle begins with the C_{55}-P ready for the transfer to MurNAc-pentapeptide by MraY.

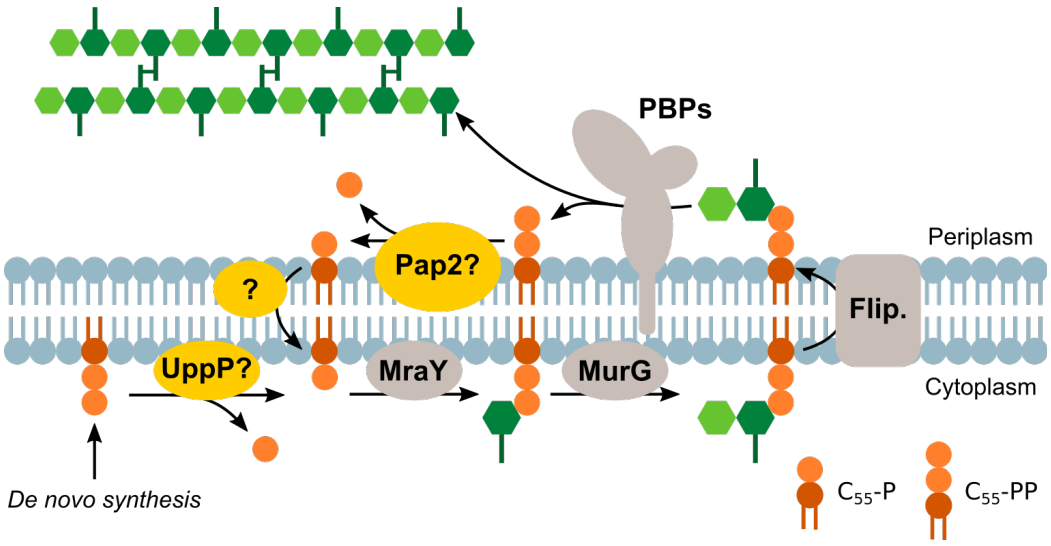

Figure I.3.17: Recycling pathway of the undecaprenyl diphosphate. The GlcNAc, MurNAc, phopshate and undecaprenol moities are sketched as light-green hexagon, dark green hexagon, orange filled circle and dark orange filled circle with antennas, respectively. Adapted from Manat et al., 2014.

Résumé en français du chapitre 3 : Maturation et recyclage du peptidoglycane

Le réseau obtenu après assemblage du peptidoglycane par les PBPs n'est pas une structure inerte, mais est au contraire sujet à maturation. En effet, plus de 50 % du peptidoglycane est dégradé par des hydrolases à chaque génération, et sera ensuite recyclé ou libéré dans le milieu. Il est également la cible de diverses modifications.

Les bactéries disposent d'une vaste palette d'hydrolases (plus de 20) afin d'hydrolyser quasiment n'importe quelle liaison présente dans le sacculus. Ces enzymes disposent souvent de plusieurs activités, qui peuvent être partagées, ce qui complique l'attribution d'une tâche spécifique à chacune d'entre elles. De manière générale, leur fonction est corrélée à la croissance du sacculus, à la division cellulaire, au recyclage du peptidoglycane, à l'autolyse ou à la création d'espace pour des assemblages macromoléculaires. Elles sont généralement caractérisées par une organisation en deux domaines, l'un liant le peptidoglycane, l'autre l'hydrolysant. Suivant la nature du substrat de ce dernier module, elles peuvent être classées en 3 groupes : les glycosidases, les N-acétylmuramyl-L-alanine amidases (clivant la liaison entre le brin peptidique et la chaîne oligosaccharidique), et les peptidases.

Les glycosidases sont représentées dans le périplasme d'*E. coli* par les transglycosylases lytiques (LTs), qui catalysent l'hydrolyse de la liaison glycosidique β-1,4 entre le MurNAc et le GlcNAc et forment simultanément une éthérification intramoléculaire, produisant un dérivé anhydro cyclique entre les carbones 1 et 6 du MurNAc (1,6-anhydroMurNAc). Les 7 LTs d'*E. coli* peuvent être classées en 3 familles parmi les 4 existantes, sur la base de la conservation de séquences consensus. Les membres de la famille 1 sont Slt70 (soluble lytic transglycosylase), une protéine soluble, et MltC (membrane-bound lytic transglycosylase), MltD, MltE et MltF qui sont toutes les 4 ancrées à la membrane externe. Ces protéines présentent un domaine N-terminal variable (à l'exception de MltE) et un domaine C-terminal riche en α-hélices, similaire au lysozyme de blanc d'oeuf d'oie et qui dispose de l'activité catalytique. Les deux autres LTs, MltA et MltB (elles aussi ancrées à la membrane externe) appartiennent aux familles 2 et 3 respectivement. Les LTs ont une activité exolytique et, dans une moindre mesure, une activité endolytique. Elles ont toutes une préférence pour des substrats comportant des tetrapeptides. Des différences peuvent être notées, comme l'acceptation de substrats réticulés pour certaines d'entre elles contrairement à d'autres, comme la formation d'un ratio important de produits comportant un sucre terminal non-anhydro, ou encore comme la présence d'activités spécifiques fortement divergentes. Parce que la suppression concomitante de plusieurs hydrolases provoque la formation de longues chaînes de cellules, les LTs sont probablement impliquées majoritairement dans le clivage du peptidoglycane au septum pour séparer les cellules filles.

Les (N-acétylmuramyl-L-alanine) amidases sont elles impliquées dans le clivage du brin peptidique des muropeptides. Quatre d'entre elles ont été identifiées dans le périplasme d'*E. coli*. Elles ont été classées en 2 groupes sur la base d'homologies de séquence : AmiA, AmiB, et AmiC d'une part, et AmiD d'autre part. Les données disponibles sur AmiA, AmiB et AmiC, telles que leur localisation au septum, la formation chaînes de cellules non séparées lorsqu'elles sont inactivées, suggèrent que ces amidases sont engagées dans le clivage du peptidoglycane durant la division. Elles disposent toutes les trois d'un domaine catalytique C-terminal similaire, dont le site actif est obstrué par une hélice α. Cette structure secondaire fait

probablement partie d'un mécanisme d'auto-inhibition, et pourrait être déplacée par leurs activateurs connus, EnvC (pour AmiA et AmiB) et NlpD (pour AmiC). AmiD quant à elle est la seule des 4 amidases à être ancrée à une membrane, la membrane externe. Elle dispose aussi, contrairement à AmiA, AmiB et AmiC, d'une région désordonnée à l'extrémité N-terminale, dont la flexibilité sert probablement à élargir son rayon d'action.

La cellule bactérienne dispose également d'un ensemble de peptidases, afin de cliver les brins peptidiques et les pontages. La plupart d'entre elles sont des PBPs de faible masse moléculaire (PBPs de classe C), caractérisées par un domaine liant la pénicilline et une sérine comme résidu catalytique. La réaction que ces enzymes catalysent est similaire à la D,D-transpeptidation catalysée par les PBPs de haute masse moléculaire, à l'exception du fait que l'accepteur est une molécule d'eau et non pas un autre brin peptidique. Ces PBPs de classe C peuvent être classées en 4 sous-familles, sur la base de leur architecture chez *E. coli*. La première famille est la classe de type 4, dont le seul membre est PBP4. PBP4 a des activités D,D-carboxypeptidase et D,D-endopeptidase, clivant donc la liaison peptidique entre les D-Ala en position 4 et 5, ainsi que la liaison peptidique des ponts $4 \rightarrow 3$. La seconde famille est constituée des PBPs de type 5, les D,D-carboxypeptidases PBP5 (l'une des PBPs de classe C les plus abondantes), PBP6 et PBP6b, qui sont ancrées à la membrane cytoplasmique. Le rôle des deux dernières PBPs reste encore mal compris, leur activité étant peu élevée et leur suppression ne causant pas de phénotype particulier, à l'inverse de ce qui a lieu pour PBP5. La troisième classe est celle de type 7 et contient PBP7. Cette protéine est une D,D-endopeptidase faiblement associée aux membranes, comme PBP4. Elle diffère cependant de cette dernière par leur substrat, PBP7 acceptant seulement les sacculi tandis que PBP4 préfère des muropeptides. Ce constat suggère que ces deux types de PBPs auraient des fonctions différentes *in vivo*. Enfin, la dernière sous-famille de PBPs de classe C est celle de type AmpH, composée de l'enzyme du même nom et de PBP4b. Bien qu'étroitement liées aux β-lactamases, ces enzymes ne partagent pas leur activité, catalysant à la place des réactions de D,D-carboxypeptidation (AmpH) et/ou D,D-endopeptidation (AmpH, PBP4b). Leur rôle spécifique reste cependant méconnu. D'autres enzymes présentent une activité peptidase dans le périplasme d'*E. coli*, comme MepA, une D,D-endopeptidase ou les Ldts, capables de cliver la liaison peptidique entre les résidus en positions 3 et 4.

Lors du processus de maturation, diverses enzymes modifient également chimiquement le peptidoglycane. Celles responsables de la N-déacétylation et de la O-(dé)acétylation sont les mieux caractérisées. Les structures des N-déacétylases (enzymes absentes chez *E. coli*) connues à ce jour adoptent toutes un repliement similaire en tonneau α/β, avec une cavité à leur sommet contenant le site actif, comme PdaA et PgdA, chez *Bacillus subtilis* et *Streptococcus pneumoniae* respectivement. Le motif du substrat reconnu par l'enzyme n'a pas clairement été déterminé à ce jour. De manière similaire à la N-déacétylation, la O-acétylation contribue également à la résistance au lysozyme. Deux principales voies ont été identifiées pour cette réaction, qui font toutes les deux très probablement appel à l'acétyl-coenzyme A (acétyl-CoA) cytoplasmique comme source de groupement acétyle. La première voie consiste en une O-acétylation par une seule protéine, OatA, et est principalement identifiée chez les bactéries Gram-positives. D'après des analyses bioinformatiques, cette protéine devrait être constituée de deux principaux modules : un domaine membranaire, suspecté de transférer le groupement acétyle du cytoplasme au milieu extra-cytoplasmique, et un domaine extra-cytoplasmique catalysant l'acétylation de l'oxygène 6 du MurNAc. La seconde voie se trouve principalement chez les bactéries Gram-négatives (mais pas chez *E. coli*) et se déroule en deux étapes : la protéine membranaire PatA transporte d'abord l'acétyl-CoA puis PatB, dans le périplasme, le transfère au MurNAc. Les chaînes oligosaccharidiques ainsi O-acétylées ne sont plus la cible du lysozyme ou d'autres hydrolases. Cela peut poser problème à la bactérie, qui ne peut alors plus les cliver si nécessaire. C'est pourquoi elles disposent aussi de O-déacétylases, nommées Ape (AcétylPeptidoglycane Estérase). Ces dernières requièrent

cependant un GlcNAc-MurNAc-tripeptide comme substrat (celui-ci est produit par une L,D-carboxypeptidase), vraisemblablement pour éviter une déacétylation incontrôlée.

Le peptidoglycane dégradé peut être libéré dans le milieu ou recyclé afin que ses constituants soient ré-incorporés dans les précurseurs cytoplasmiques. Les unités disaccharidiques libérées par les hydrolases périplasmiques sont transportées vers le cytoplasme, où le GlcNAc, le MurNAc et les peptides sont séparés. Dans le détail, l'action des transglycosylases lytiques dans le milieu extra-cytoplasmique produit des unités disachharidiques comportant un 1,6-anhydroMurNAc. Ces muropeptides sont alors spécifiquement transportés vers l'espace cytoplasmique par la protéine membranaire AmpG à l'aide d'une force motrice proton-dépendante. Ensuite, une fois dans le cytoplasme, la N-acétyl-β-D-glucosaminidase NagZ catalyse le clivage de la liaison glycosidique β-1,4, séparant le GlcNAc du MurNAc-peptide. Puis la liaison peptidique D-Lac → L-Ala est clivée par AmpD, une amidase similaire à AmiD. Après ces deux réactions, le GlcNAc, le 1,6-anhydroMurNAc et les brins peptidiques sont isolés.

Les hexosamines obtenues après ces deux réactions sont alors convertis en plusieurs étapes en N-glucosamine-6-phosphate (GlcN-6-P). Tout d'abord, la N-AcétylGlucosamine Kinase NagK phosphoryle le GlcNAc pour former du GlcNAc-6-P. En parallèle, le MurNAc est également phosphorylé par l'Anhydro-N-acétylMuramic acid Kinase AnmK, formant du MurNAc-6-P. Ce dernier est converti en GlcNAc-6-P par l'acide N-acétylmuramic-6-phosphate éthérase MurQ avec relargage du D-Lac. Enfin le GlcNAc-6-P obtenu est déacétylé par la N-acétylglucosamine-6-phosphate désacétylase NagA, produisant du GlcN-6-P, qui peut alors servir de substrat pour la phosphoglucosamine mutase GlmM (voir chapitre 2) ou la glucosamine-6-P deaminase NagB pour intégrer la voie de la glycolyse sous la forme de fructose-6-phosphate.

Les peptides produits par AmpD peuvent être recyclés suivant deux voies différentes. La majorité d'entre eux est réutilisée pour la synthèse de précurseurs. Dans ce cas-là, ils sont directement rattaché à un UDP-MurNAc par la muréine peptide ligase Mpl, un paralogue de MurC, dont la structure en est très proche, si ce n'est le domaine C-terminal (ou domaine 3) qui varie davantage. Bien qu'ayant une large spécificité *in vitro*, Mpl ne catalyse probablement *in vivo* que la liaison de tripeptides et de pentapeptides à l'UDP-MurNAc. En effet, la L,D-carboxypeptidase cytoplasmique LdcA, seule enzyme essentielle de la voie de recyclage du peptidoglycane, clive spécifiquement la liaison peptidique entre le résidu en position 3 et la D-Ala en position 4. De ce fait, il ne peut pas y avoir incorporation de tetrapeptides dans les précurseurs, qui ne pourraient pas être réticulés une fois assemblés dans la couche de peptidoglycane. Une voie alternative de recyclage des peptides existe. Elle procède par clivage de tous les acides aminés un à un à partir de tripeptides. La liaison D-iGlu → *m*-A_2pm peut être tout d'abord hydrolysée par la Muréine Peptide Amidase A MpaA, libérant le *m*-A_2pm. Par la suite, l'épimerase YcjG peut alors convertir le dipeptide L-Ala-D-iGlu en L-Ala-L-iGlu, qui sera ensuite clivé par la métallodipeptidase PepD.

Dans de nombreuses bactéries Gram-négatives autres que *E. coli*, le recyclage du peptidoglycane est étroitement lié à la résistance aux β-lactames. En effet, ces organismes sont très sensibles à l'équilibre entre l'UDP-MurNAc-pentapeptide et le 1,6-anhydro-MurNAc-pentapeptide. Le premier réprime l'expression du gène codant la β-lactamase AmpC en inactivant son inducteur AmpR. A l'inverse, le 1,6-anhydro-MurNAc-pentapeptide favorise cette stimulation. Il en résulte, en cas de traitement par les β-lactames, un déplacement de cet équilibre vers le produit du recyclage, déclenchant l'expression de la protéine AmpC.

L'undecaprenyl-pyrophosphate relâché après élongation de la chaîne de peptidoglycane est aussi recyclé, suivant une courte voie métabolique moins bien caractérisée. Après sa déphosphorylation du côté du périplasme, l'undecaprenyl-phosphate obtenu est transporté vers le cytoplasme par une flippase à l'identité inconnue. Il peut alors servir à nouveau de substrat pour MraY (voir chapitre 2).

Chapter 4
Spatio-temporal control of peptidoglycan synthesis

In rod-shaped bacteria like *E. coli*, the cell cycle is generally divided into two phases: elongation of the lateral walls and division at the septum in the center of the cell. Both of these phases require a spatio-temporal regulation of peptidoglycan synthesis, so that precursor production, glycan strand polymerization and peptide stem cross-linking, as well as hydrolysis, are coordinated. This is the only way for the cell to avoid any disruption in the sacculus that would be lethal. During elongation and division, new muropeptides need to be inserted in the existing peptidoglycan network; this process is nevertheless still not well understood. In the 90's, Höltje proposed a “three-for-one” mechanism for both lateral and septal cell wall synthesis (Höltje, 1998). In this model, three glycan strands are inserted replacing a single strand, through coordination of PBPs and hydrolases activities. In the last fifteen years, researchers focused on the identification of the machineries implicated in the peptidoglycan modifications for elongation and division. In this context, proteins were identified and more and more interactions were reported between the key players of peptidoglycan synthesis, describing little by little complex dynamic networks. In *E. coli* and other rod-shaped bacteria, two main trans-envelope complexes extending from the cytoplasm to the periplasm are involved in cell elongation on the one hand and septum synthesis and division on the other hand. Both of them incorporate lipid II into the newly synthesized material. Because of their relative localization, these networks were named elongasome (Nanninga, 1991) and divisome (den Blaauwen et al., 2008), respectively. Each of these machineries is guided by a cytoplasmic cytoskeletal-like protein, MreB during elongation and FtsZ during division, which is connected to regulators and to periplasmic HMW PBPs. Although they do not share the same proteins, both elongasome and divisome have similar features, which were speculated as a possible remnant of a shared origin (Szwedziak & Löwe, 2013). These machineries are described in more details in what follows.

4.A- Peptidoglycan synthesis during elongation

During elongation, peptidoglycan synthesis occurs on the lateral walls, transversely to the long axis of the cell. The peptidoglycan synthases involved in this process are part of the elongasome complex, which is thought to be guided by the cytoskeleton-like MreB protein. The current knowledge on MreB will be exposed before describing the different components of the elongasome and to detail their interaction network.

4.A.a- MreB guides the elongasome complex

MreB is an actin homologue, which is essential for the morphogenesis of most rod-shaped bacteria, but which is generally absent in non-elongated cells, such as cocci. Some MreB-independent alternative mechanisms have also been described through polar growth (Daniel & Errington, 2003), but they are only related to a minor number of the bacterial species studied to date. While *E. coli* has only one copy of the mreb gene, some organisms can have several homologues. *B. subtilis* for example has three of them: MreB, MreBH (MreB homologue) and Mbl (MreB-like). If these paralogues have partially redundant function, they

probably also show specific reactivity (Jones et al., 2001).

In *E. coli*, MreB is essential, as its depletion leads to the formation of spherical cells followed by lysis. The lethality of this mutation can nevertheless be reverted by overexpression of the FtsZ division-specific protein (Kruse et al., 2005). MreB assembles in filaments *in vivo* (Jones et al., 2001) and *in vitro* (van den Ent et al., 2001). The X-ray structure of monomeric *Thermotoga maritima* MreB (van den Ent et al., 2001) reveals a fold homologous to actin (with an r.m.s.d. of 3.7 Å) that is composed of two domains, each of them being further divided in two sub-domains (figure I.4.1). Polymerization of MreB requires hydrolysis of ATP or GTP, in the presence or the absence of magnesium ions. The nucleotide-binding site is found in the cleft between module I and module II at the interface between the four IA, IB, IIA, IIB sub-domains. The structural organization of straight MreB protofilaments was also determined at the atomic level in the same study. In these polymers, the two A sub-domains interact with the two B sub-domains in a head-to-tail intermolecular geometry, leading to a longitudinal spacing of 51 Å between each MreB monomeric unit, a value that was obtained by X-ray and electron microscopy. This value is very similar in actin protofilaments (55 Å), demonstrating once again the intramolecular and intermolecular structural homology between both proteins. Recent structural work established that MreB actually forms antiparallel double filaments. These structures are required for MreB functionality, as *in vivo* disruption of inter- or intra- protofilament contacts in *E. coli* causes the same spherical cell phenotype than its inactivation (van den Ent et al., 2014). These filaments can also adopt a helical geometry to associate laterally with others in order to form large sheets *in vitro* (Popp et al., 2010). The exact role of such super-structures is not known, but they are supposed to confer higher rigidity to the filaments, which could be required to impose the cell shape.

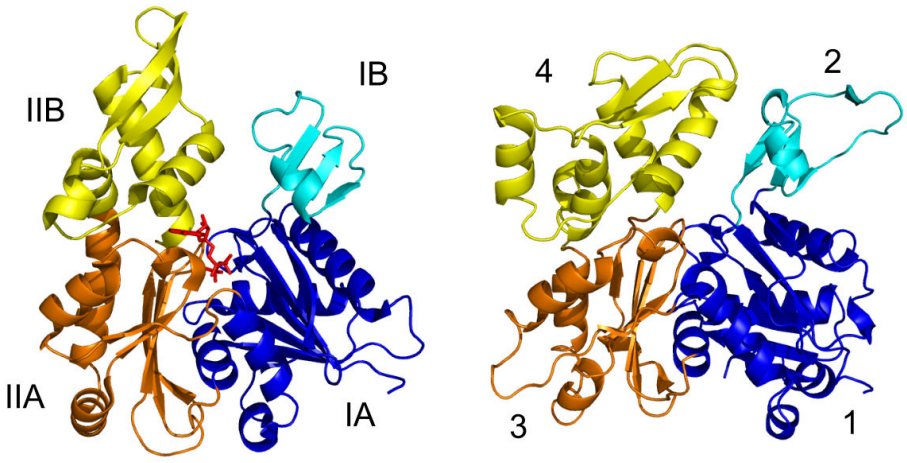

Figure I.4.1: MreB is a structural homologue of actin. Left: structure of *Thermotoga maritima* MreB (PDB code 1JCE). An ATP analogue, AMPPNP is represented in the binding site in red sticks. The intermolecular contacts between two MreB proteins in the protofilaments can be visualized by a 51 Å vertical translation of the represented structure towards the bottom of the page. Right: structure of the *Oryctolagus cuniculus* actin (PDB code 1ATN) for a structural comparison with MreB.

In vivo, MreB is tightly associated with the inner leaflet of the cytoplasmic membrane, generally through either an N-terminal amphipathic α-helix or a hydrophobic loop in Gram-negative and Gram-positive bacteria, respectively (Salje et al., 2011). The exact localization of the MreB filaments within the cell has been the subject of several studies. The first attempts of *in situ* visualization were performed using immunofluorescence (Jones et al., 2001; Figge et al., 2004) or the fluorescence of a GFP-MreB protein fusion (Kruse et al., 2003). In several species including *E. coli*, MreB was shown to form long filaments adopting a helical pattern all along the cell (figure I.4.2 A). These structures were later reported to be

highly dynamic as constant remodeling was observed with FRAPs (Fluorescence Recovery After Photobleaching) experiments (Carballido-Löpez & Errington, 2003). This long helical bundle organization of MreB has been nevertheless challenged lately, as microscopy techniques with better spatial and temporal resolutions describe instead the circumferential motion of short MreB patches (figure I.4.2 B, Domínguez-Escobar et al., 2011; Garner et al., 2011). Experimental conditions were put forward to try to explain the artifactual nature of the long helical filaments, among which the misbehavior of MreB when coupled to fluorescent proteins such as YFP (Swulius & Jensen, 2012), or low resolution of the optical images. In 2013, this debate was revived after new superresolution imaging data of MreB revealed extended filaments with circumferential motion similar to that observed for the shorter patches (figure I.4.2 C) (Olshausen et al., 2013; Reimold et al., 2013). To reconcile all of the obtained results, the group of Errington proposed an hypothesis according to which MreB filaments would be shorter in cells with abnormal morphology (Errington, 2015). In the latter case, elongation of MreB filaments would be modulated in relation with the cell plasma membrane curvature (Ursell et al., 2014).

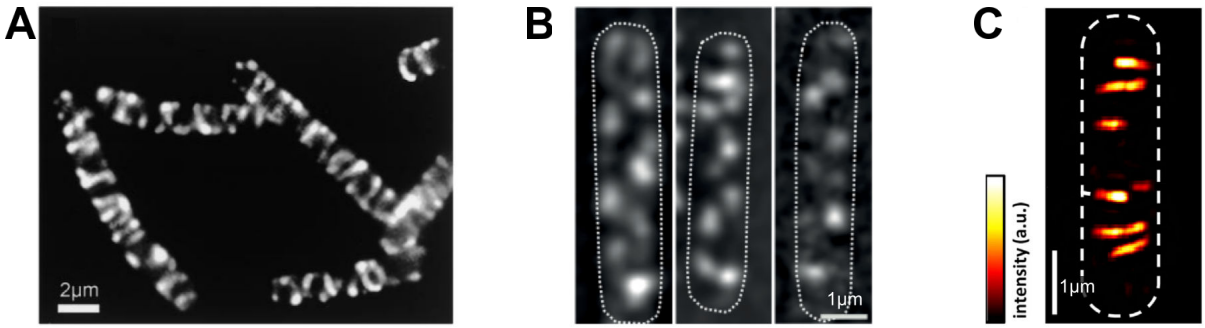

Figure I.4.2: The *in vivo* high order structural organization of MreB under debate. (A) The long helical filaments of Mbl, an *E. coli* MreB homologue in *B. subtilis* as observed by fluorescence microscopy when the protein of interest is fused to GFP at the C-terminus. Taken from Jones et al., 2001. (B) Discrete patches of *E. coli* MreB homologues (MreB, Mbl, MreBH) in *B. subtilis* as visualized by TIRFM (Total Internal Reflection Fluorescence Microscopy) in N-terminal GFP fusion proteins. Taken from Domínguez-Escobar et al., 2011. (C) *B. subtilis* MreB filaments of various lengths found by a combination of TIRF and SIM (Structured Illumination Microscopy). The fluorescence intensity diminished form light colors to darker red colors. Adapted from by Olshausen et al., 2013.

In parallel to these results, the close link between MreB and the peptidoglycan synthesis machinery was confirmed. First, new muropeptides are incorporated into peptidoglycan in a helical pattern (Daniel & Errington, 2003). Second, MreB patches circumferential motility has been quantitatively correlated with cell wall synthesis activity, either by controlling the availability of peptidoglycan precursors (van Teeffelen et al., 2011), or by measuring the activity of peptidoglycan biosynthetic enzymes such as PBPs (Domínguez-Escobar et al., 2011; Garner et al., 2011). In this respect, MreB differs from actin, whose motion is driven by a treadmill mechanism in correlation with the polarization of the protofilament bundles. This is consistent with the absence of polarity in MreB filaments (van den Ent et al., 2014). As a result, MreB patches would allow a limited diffusion of the murein synthetic enzymes, thus orienting correctly peptidoglycan synthesis perpendicularly to the cell longitudinal axis. When organized in long filaments, MreB would alternatively distribute the peptidoglycan synthetic machineries all over the lateral walls to perform a homogeneous growth of the cell wall.

MreB may play additional roles in the three organisms where it has been the more extensively studied, namely *B. subtilis*, *E. coli* and *C. crescentus*. The actin-like protein is indeed essential for initiation of septal peptidoglycan synthesis and cell division (as explained in part I section 4.C, Fenton & Gerdes, 2013). In 2014, MreB was also shown to be able to create fluid lipid domains, which may affect protein distribution in the inner membrane

(Strahl et al., 2014). Cell polarity can furthermore be determined by MreB. In *C. crescentus* for example, positioning of the stalk – a cytoplasmic extension at one cell pole – is dependent on MreB (Gitai et al, 2004). Multiple studies have also raised the possibility that MreB could be implicated in chromosome segregation (to avoid the two DNAs to remain in the septum region, preventing their "beheading" during cytokinesis). These results are nevertheless controversial, as some of them were shown to actually result from side effects of MreB deletion or inhibition (Chastanet & Carballido-López, 2012) and as a similar plasmid partitioning function can be performed by another actin-like protein, ParM (Salje, et al., 2010). In addition to its role in cell wall synthesis, MreB is also implicated in cell motility in *Myxococcus xanthus* through its connection to motility complexes (Mauriello et al., 2010; Treuner-Lange et al., 2015). Lastly, in *Streptomyces coelicolor*, MreB is not involved in vegetative growth, which is based on an apical tip extension mode, but is involved in sporulation (Mazza et al., 2006). If MreB may have multiple regulatory functions within the cell, researchers focused in the last fifteen years to decipher the interaction network, today named elongasome machinery, which connect MreB in the cytoplasmic compartment to the extra-cytoplasmic peptidoglycan assembly by PBPs.

4.A.b- The elongasome complex

The elongasome machinery comprises more than ten proteins and extends from the cytoplasm to the periplasm (figure I.4.3). The main characterization studies performed in *E. coli, C. crescentus* and *B. subtilis* show that it can be arbitrarily split in three parts tightly interplaying with each other: the cytosolic MurC, MurD, MurE, MurF, MraY, and MurG enzymes involved in peptidoglycan precursors synthesis, the membrane-associated MreB, MreC, MreD, RodA, and RodZ proteins, and the peptidoglycan synthases PBP1A and PBP2. A non exhaustive summary of the reported interactions can be found in table A.1 in the annexes. Because of the limited copies of some of these proteins, approximately 50 elongasome complexes are expected to be distributed in the whole cell (den Blaauwen et al., 2008).

Mur enzymes and MraY are tightly linked to the membrane via MreB, and to a lesser extent to MreD. Indeed, both protein families where shown to interact with some of the enzymes implicated in lipid II synthesis. Localization of these enzymes was also shown to be dependent on the presence of long MreB filaments, suggesting the existence of a sub-complex (Divakaruni et al., 2007; White et al., 2010). Interestingly, MurC-F ligases do not seem to interact with each other but rather remain associated through MurG and their common interaction with MreB (Favini-Stabile et al., 2013). This gathering of the peptidoglycan precursor synthetic enzymes at MreB should avoid diffusion of the intermediate products within the cytoplasm and thus participate to the efficiency of the muropeptide precursor synthesis at the elongation site.

The membrane-associated sub-complex encompasses MreB, MreC, MreD, RodA, and RodZ. Although MreC, MreD and RodZ are essential for *E. coli* viability and cell morphogenesis (Kruse et al., 2005; Alyahya et al., 2009; Bendezú et al., 2009), their role is still poorly understood. Both mreC and mreD genes are found in the same operon than that of mreB. MreC has an N-terminal transmembrane α-helix followed by a major periplasmic C-terminal domain made of two β-barrels positioned on each side of a coiled-coil region (figure I.4.4, van den Ent et al., 2006; Lovering & Strynadka, 2007). This module is involved in the asymmetric dimerization of the protein through the coiled coil, thus creating a structure that alternates the first and second β-barrels. By translation, it was postulated that this could lead to the formation of the MreC helical filaments observed *in vivo* (Mark Leaver & Errington, 2005), with the condition that other protein partners stabilize the interface between two MreC

dimers in the absence of exposed coiled-coil regions.

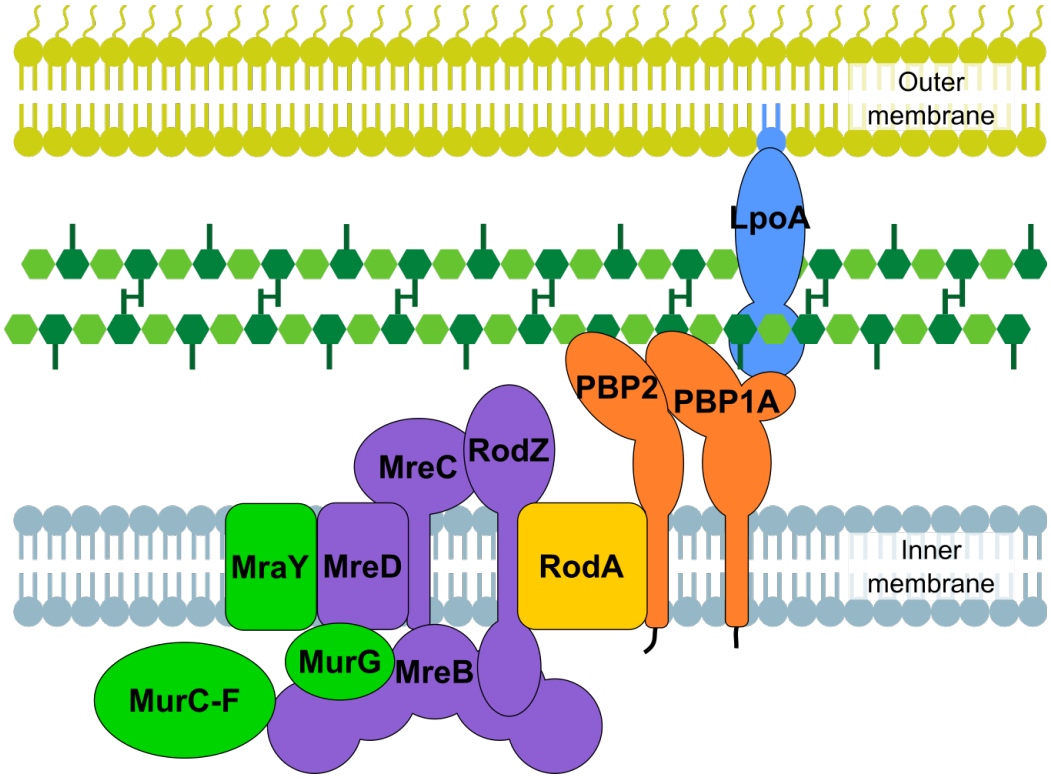

Figure I.4.3: The elongasome is the trans-envelope complex responsible for peptidoglycan synthesis on the lateral walls during cell elongation. It comprises more than ten proteins that can be divided into three families, the peptidoglycan precursor synthetic enzymes, the transmembrane or membrane-associated proteins, and the peptidoglycan synthases sketched in green, purple/yellow and orange, respectively.

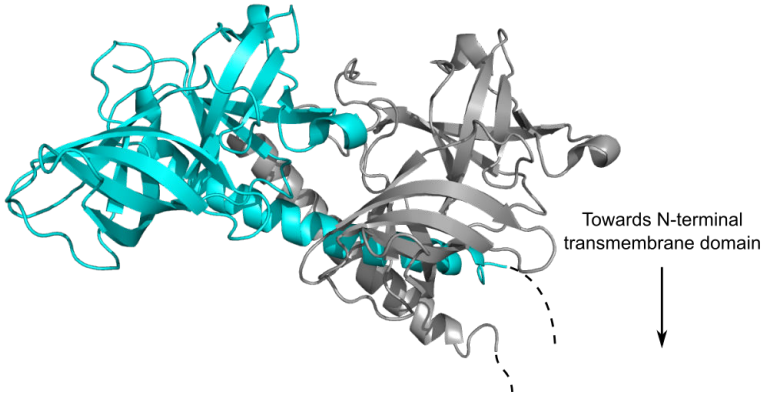

Figure I.4.4: Structure of *Listeria monocytogenes* MreC periplasmic dimer (PDB code: 2J5U). The interaction between two MreC molecules in cyan and gray, respectively, involves the coiled-coil region. MreC might polymerize in the periplasm, in the presence of additional protein partners. Note that the orientation of each MreC monomer with respect to the plasma membrane is not determined.

MreD is probably the least characterized protein from the elongasome, probably because of its integral membrane nature. This small protein (19 kDa) is inserted in the inner membrane and is predicted to have five to six transmembrane α-helices (by the transmembrane prediction servers TMHMM 2.0, (http://www.cbs.dtu.dk/services/TMHMM-2.0/), PredictProtein (https://www.predictprotein.org/) and Tmpred (http://www.ch.embnet.org/software/TMPRED_form.html). Both MreC and MreD are hypothesized to serve as scaffolds for the interaction of the other members of the elongasome

on each side of the plasma membrane. The importance of RodZ in cell wall elongation has only been determined less than ten years ago (Alyahya et al., 2009; Bendezú et al., 2009; Shiomi, Sakai, & Niki, 2008; van den Ent et al., 2010). RodZ is a bitopic membrane protein with a periplasmic domain connected to a cytoplasmic domain through a disordered region and transmembrane segment. As shown in a rare structural characterization of an interaction within the elongasome (van den Ent et al., 2010), the cytoplasmic domain binds to MreB through a helix-turn-helix (HTH) motif (figure I.4.5).

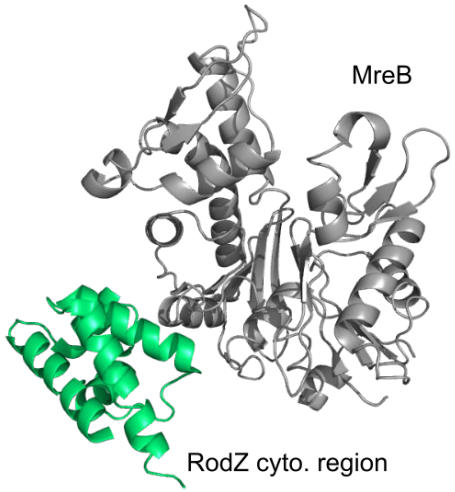

Figure I.4.5: Structural characterization of RodZ cytoplasmic domain, in green, in interaction with MreB, in gray (PDB code 2WUS).

MreB polymerized structures present an inter-dependent localization with the other proteins from the membrane-associated sub-complex it interact with. Indeed, MreC, MreD, and RodZ all exhibit helical distribution patterns that are affected by the absence of MreB (Leaver & Errington, 2005; Shiomi et al., 2008; Alyahya et al., 2009; Bendezú et al., 2009; White et al., 2010). Alternatively, when MreC, MreD, and RodZ are deleted in *E. coli* (Kruse et al., 2005), MreB localization is perturbed and cells adopt a similar phenotype to that observed in the case of cytoskeleton-like protein inactivation. These results point towards an interdependency of MreB and the MreC/MreD/RodZ transmembrane proteins. MreC and RodZ, together with RodA, are in turn involved in interactions with the peptidoglycan synthases in the extra-cytoplasmic compartment, thus connecting the MreB filaments to peptidoglycan assembly. MreC interacts with several class A and B HMW PBPs (Divakaruni et al., 2005; van den Ent et al., 2006). RodA belongs to the same operon than PBP2 and is essential to its elongation specific transpeptidase activity (Ishino et al., 1986). As such, it can be expected that both proteins interact directly or indirectly through a common partner. If RodA is indeed a lipid II translocase (discussed in part I section 2.C.a), this spatial proximity with PBP2 and/or class A PBPs would enable coupling of muropeptide translocation with its polymerization. Lastly, the RodZ periplasmic domain, although its exact function is unclear, was expected to interact with peptidoglycan synthases, as deletion of this region induces formation of spherical cells (Alyahya et al., 2009).

In addition to the monofunctional transpeptidase PBP2, the other main HMW PBP during cell elongation is the bifunctional PBP1A (Banzhaf et al., 2012). Interestingly, PBP2 and PBP1A seem to cooperate while synthesizing peptidoglycan, with PBP2 stimulating PBP1A glycosyltransferase activity, at least *in vitro*. It is nevertheless currently not known if PBP1A directly interacts with Mre and Rod proteins or not.

Cell elongation cannot be performed without hydrolysis of the old glycan strands and

peptide stems before to inject new material. The link between glycan insertion and cell wall hydrolysis is however still poorly characterized in the elongasome. Yet, PBP1A is suspected to be linked to MltA (Vollmer et al., 1999) through an unknown partner and PBP2 likely binds Slt70 (von Rechenberg et al., 1996). These interactions await further characterization to understand if they play a role in the regulation and/or the localization of the peptidoglycan hydrolysis process. Given the high number of hydrolases, numerous other connections between elongasome components and these enzymes can be expected to finely tune their potentially dangerous cell-wall destroying activities.

To conclude, cell elongation is performed by a dedicated machinery in *E. coli* and in most of the rod-shaped bacteria. This macromolecular protein complex closely links periplasmic peptidoglycan synthesis to cytosolic enzymes through MreB filaments and associated membrane proteins. It assists peptidoglycan synthases in the insertion of new glycan strands in a perpendicular orientation with respect to to the cell longitudinal axis. Another machinery is dedicated to peptidoglycan synthesis at the division site, the divisome.

4.B- Septal peptidoglycan synthesis and division

During division of the bacterial cell, peptidoglycan is synthesized at the septum, at the middle of the cell, to create a new pole for each daughter cell. Similarly to what was described for the elongasome, the divisome is tightly associated with the essential cytoskeletal-like cytoplasmic FtsZ protein after its polymerization into a ring. This super-structure is necessary to recruit the other proteins that are implicated in septal peptidoglycan synthesis as well as in cell constriction. In parallel, a second machinery, the Tol-Pal system, is dedicated to outer membrane invagination.

4.B.a- FtsZ assembles in a ring marking the site of division

While MreB is an actin-like protein, FtsZ is a tubulin-homologue GTPase. FtsZ is widely spread in bacteria, although some exceptions exist as in *Chlamydiae* (Pilhofer et al., 2013). This tubulin-like protein was also found to be required for the division of archaea (Vaughan et al., 2004), chloroplasts (TerBush et al., 2013) and, in some cases, eukaryotic mitochondria (Leger et al., 2015). Its deletion in *E. coli* leads to the formation of filamentous cells unable to divide, and which end up lysing (Dai & Lutkenhaus, 1991).

Although their sequence share weak homologies (less than 18% identity), FtsZ and tubulin both have similar structures (Löwe & Amos, 1998). The structure of FtsZ is organized in a globular fold (figure I.4.6) followed by a long C-terminal disordered region. This C-terminal tail is of variable length depending the organisms (Ma & Margolin, 1999) and terminates with a small highly conserved segment involved in interactions with multiple partners. The structured module can be divided in two sub-domains separated by a central α-helix. The N-terminal sub-domain adopts a Rossman fold and contains the GTPase binding site, while the C-terminal sub-domain is responsible for the activation of the GTPase activity through a T7 loop located at the opposite side of the protein.

Upon addition of GTP, FtsZ polymerizes in head-to-tail protofilaments, which brings into contact catalytic residues from the T7-loop C-terminal sub-domain and the GTP binding site, thus allowing GTP hydrolysis (Nogales et al., 1998). It is the binding of the nucleotide or an analogue, but not the enzymatic reaction itself that is required for FtsZ assembly (Mukherjee & Lutkenhaus, 1994). On the contrary, the GTPase activity participates in the instability of the filaments, through the formation of GDP (Erickson et al., 2010). As a result, FtsZ filaments are highly dynamic, with a subunit turnover of 7 to 9 seconds *in vivo* (Anderson et al.,

2004) and *in vitro* (Chen & Erickson, 2005). When reconstituted *in vitro*, these protofilaments are one-subunit thick (Romberg et al., 2001). However, depending on the experimental conditions, these structures can also form higher-order arrangements, such as bundles in which GTPase activity is decreased, stability of the protofilament is increased, and filaments longer than the 30-subunits average form (Chen & Erickson, 2009). Other arrangements such as sheets or mini-rings were also described by electron microscopy (Erickson, et al., 1996). Nevertheless, it is difficult to know if these assemblies are relevant *in vivo*, as the existence of lateral inter-filament contacts, that are not mediated by binding partners, is uncertain (Erickson et al., 2010).

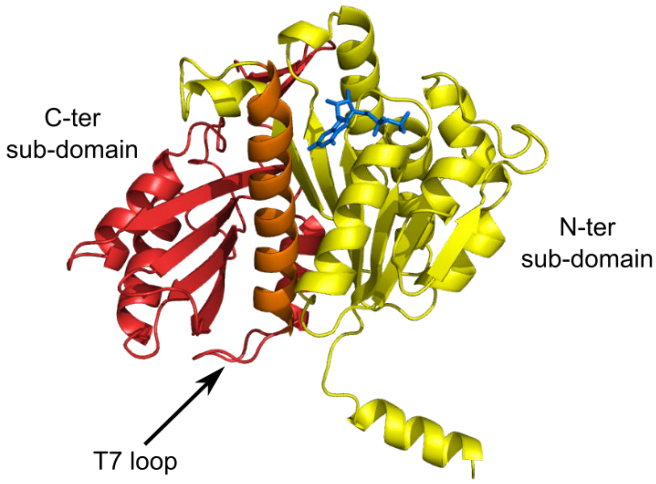

Figure I.4.6: Structure of *Methanococcus jannaschii* FtsZ (PDB code 1FSZ). The N-terminal sub-domain contains the GTPase activity, which is activated by the T7-loop from the C-terminal sub-domain of another FtsZ molecule. The centrak α-helix is represented in orange. The C-terminal disordered region and the ending conserved peptide sequence involved in FtsZ interaction with multiple partners are not shown. The GDP product is represented as blue sticks to evidence the nucleotide binding site.

In the cell, approximately 30% of the total FtsZ pool is mobilized in the ring supra-structure (Stricker et al., 2002). Recent expansion of electron-cryotomography and superresolution microscopy techniques has enabled a more accurate characterization of the FtsZ-ring *in vivo*. Surprisingly, it appears as a heterogeneous structure in *C. crescentus* (Li et al., 2007), *E. coli* (Fu et al., 2010; Si et al., 2013), *B. subtilis* (Jennings et al., 2011; Strauss et al., 2012), and *S. aureus* (Strauss et al., 2012) with minor differences between the four bacteria. In *E. coli*, the Z-ring was proposed to be composed of loose bundles of protofilaments, which randomly overlap with each other in the longitudinal and radial direction as shown in figure I.4.7 A.

Figure I.4.7: Architecture of the Z-ring. (A) Loose bundle of protofilaments randomly overlapping as deduced from the PALM (Photoactivated Localization Microscopy) data analysis in *E. coli*. Taken from Fu et al., 2010. (B) Semi-atomic model of long protofilaments with a slight helical path allowing constriction by sliding in liposomes, as interpreted from tomography results. In this model, *S. aureus* FtsZ monomers (PDB code 3VO8) were mapped in the detected filaments. Taken from Szwedziak et al., 2014.

In addition to its role as a scaffold for the recruitment of proteins from the divisome machinery, the FtsZ-ring was suggested to actively participate in cytokinesis through its contraction after its assembly (Erickson, 1997). *In vitro* experiments with liposomes confirmed that FtsZ can display some constrictive force (Osawa, et al., 2008). Two main models were proposed to explain this ability, which are discussed in details in (Erickson, 2009). The first model is based on a switch from the straight GTP-bound filaments to a bent shape upon nucleotide hydrolysis (Lu et al., 2000). This model is however not completely satisfactory, because these conformational changes in FtsZ still remain uncertain (Oliva et al., 2007). Another model suggests that the required force could be generated by filament sliding through transient lateral interactions (Lan et al., 2009). Lately, long FtsZ filaments associated with their membrane-anchoring partner FtsA (see the following section) were shown, by electron cryotomography, to form slightly helical supra-structures able to constrict liposomes (figure I.4.7 B; Szwedziak et al., 2014). Interestingly, FtsZ starts disassembling before constriction is completed (Erickson et al., 2010; Söderström et al., 2014). This might imply that one or several other process(es) is (are) also responsible for the generation of the septum closure force.

4.B.b- Septal peptidoglycan synthesis by the divisome

In comparison to the elongasome, the divisome is much more characterized. This complex is formed into two steps (Aarsman et al., 2005). It begins with the assembly of the Z-ring and it is then followed by the maturation of the complex, which sequentially recruits the different proteins for septal peptidoglycan synthesis, for divisome regulation and for cell division, just before the constriction (figure I.4.8 A). In the end, the assembly obtained gather together more than thirty proteins (figure I.4.8 B), whose main interactions reported in the literature are resumed in table A.2 in the annexes. Approximately thirty-five such complexes are estimated to operate in parallel for the division of the cell (Vischer et al., 2015).

4.B.b.i- Assembly of the Z-ring

In the first stage of the divisome assembly, the FtsZ-ring is formed by FtsZ polymerization. It is anchored to the inner leaflet of the cytoplasmic membrane and stabilized by various accessory proteins once it localizes at mid-cell. In *E. coli*, ZipA and FtsA are responsible for the attachment of the ring-like super-structure to the membrane and for the recruitment of maturation proteins, such as FtsB, FtsL, FtsQ, FtsK, FtsI, and FtsN (Hale & de Boer, 2002). Both ZipA and FtsA proteins localize in a FtsZ-dependent manner (Addinall & Lutkenhaus, 1996; Hale & de Boer, 1999), through interaction with the C-terminal conserved peptide of the tubulin-homologue. Although only one of these two proteins is sufficient for stabilization of the Z-ring, both of them are required for localization of the maturation proteins (Pichoff & Lutkenhaus, 2002).

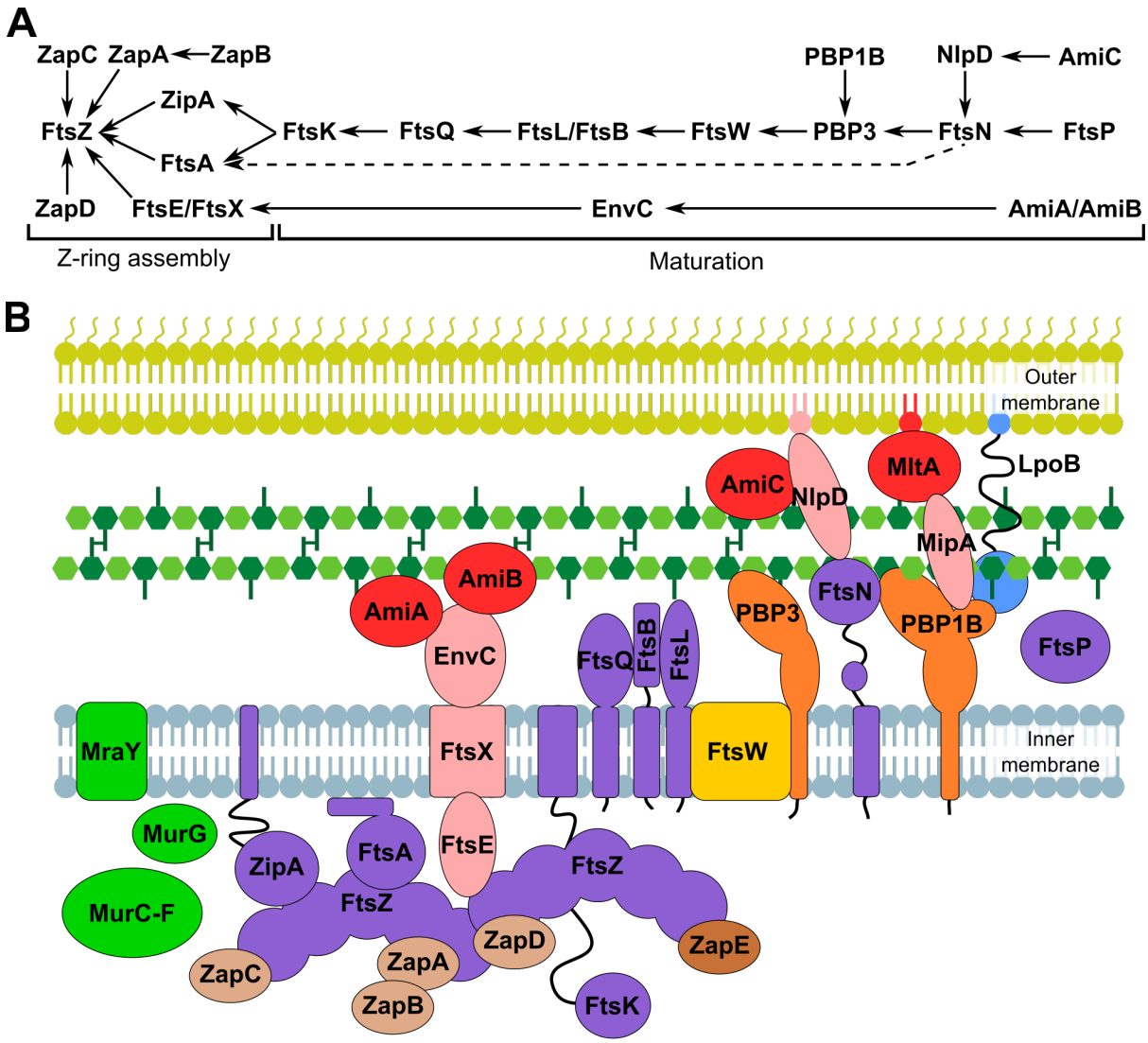

Figure I.4.8: The divisome is the mid-cell complex responsible for septal peptidoglycan synthesis and inner membrane constriction. (A) Sequential recruitment of the main divisome proteins, when known. The starting point is on the left and proteins interact sequentially from the left to the right to form the divisome macromolecular assembly. The dotted line outlines the early recruitment of a few FtsN molecules ahead of an advanced maturation of the divisome. Adapted from Egan et al., 2013. (B) Schematic representation of the matured divisome machinery. Lipid II precursor synthesizing proteins, plasma-membrane associated protein, peptidoglycan synthase, and peptidoglycan hydrolases are shown in green, purple, orange, and red, respectively. Zap proteins in brown stabilize (ZapA, ZapB, ZapC and ZapD) or disassemble (ZapE) the FtsZ ring.

ZipA (Z-Interacting Protein A) is a bitopic protein, whose N-terminal region is embedded in the inner membrane and connected to a globular C-terminal module through a flexible basic linker (Hale & de Boer, 1997). The C-terminal domain (figure I.4.9) consists of a six β-stranded sheet on one face of the protein and three α-helices on the other face, with a βαβ motif reminiscent of RNA-binding proteins (Mosyak et al., 2000; Moy et al., 2000). A hydrophobic pocket is present on the former face and binds FtsZ C-terminal conserved α-helical peptide. *In vitro*, this interaction was shown to bundle FtsZ protofilaments, via an undetermined mechanism (RayChaudhuri, 1999) and is believed to favor assembly of these structures in the cell as well. This specific binding is also important for FtsZ as it protects the cytoskeletal protein from degradation by the ClpP protease (Pazos et al., 2013). As for the N-terminal domain, it appears to have an additional role to membrane anchoring, which likely consists in interacting with other divisome components (Hale et al., 2000).

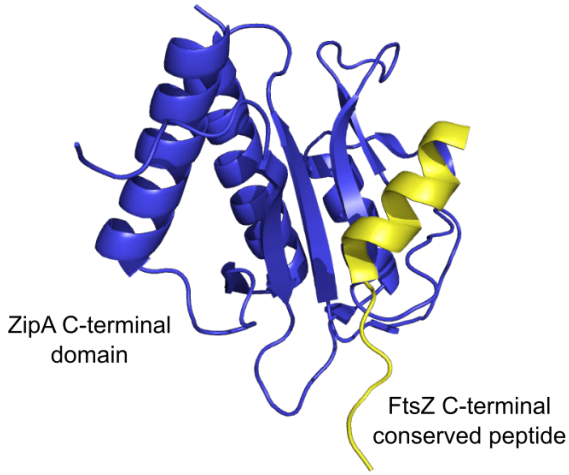

Figure I.4.9: Structure of *E. coli* ZipA C-terminal domain interacting with an FtsZ peptide (PDB code 1F47). ZipA, in dark blue, interacts through hydrophobic contacts from its β-sheet with the conserved peptide at the C-terminus of FtsZ, in yellow,, which adopts an α-helical structure.

On the contrary to ZipA, which is found mainly in γ-proteobacteria, FtsA is widely distributed among bacteria (Adams & Errington, 2009), where it is generally found in the *dcw* cluster, containing several genes involved in peptidoglycan synthesis and cell division (Vicente et al., 1998). FtsA is another actin-homologue, which is bound to the cytoplasmic membrane via a C-terminal amphipathic α-helix (Pichoff & Lutkenhaus, 2005). Like MreB, FtsA is also composed of two domains, which can be each further divided into two sub-domains (van den Ent & Löwe, 2000). The two proteins show a striking structural homology for all of the sub-domains (figure I.4.10), with the exception of sub-domains IC and IB in FtsA and MreB, respectively. This may be explained by the fact that sub-domain IC in FtsA recruits other proteins that are essential for divisome maturation (Rico et al., 2004). Sub-domain IIB interacts with the FtsZ C-terminal peptide (Szwedziak et al., 2012).

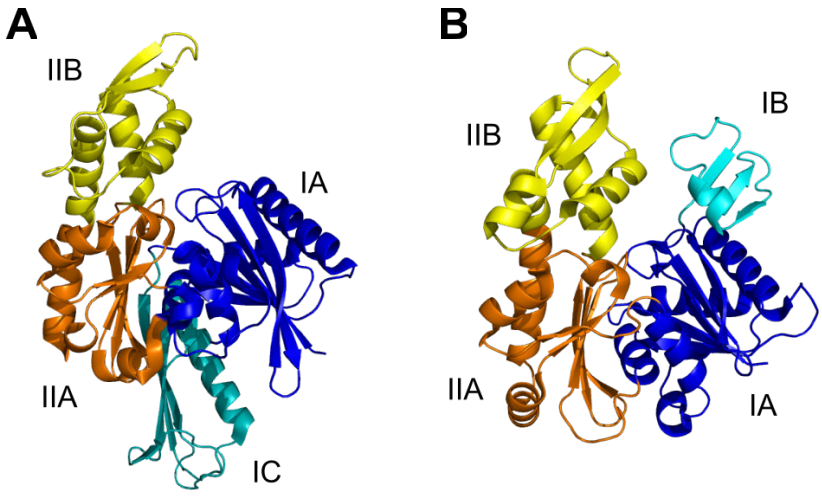

Figure I.4.10: Comparison of *Thermotoga maritima* FtsA (PDB code 1E4F) and MreB (PDB code 1JCE) structures. Homologous sub-domains are represented with the same colour. The main difference stands in sub-domains IB and IC of MreB and FtsA, respectively.

Despite the presence of a nucleotide-binding site, the ability of FtsA to polymerize in protofilaments has long remained unsure. Recent structural studies and *in vivo* mutations tend to indicate that the protein is able to do so, but surprisingly there is no obvious proof of an ATPase activity (Szwedziak et al., 2012). Interestingly, several FtsA mutations impairing its

oligomerization, such as the well studied FtsA* (Arg286Trp), are also known for their ability to bypass ZipA requirement (Pichoff et al., 2012). It is therefore hypothesized that FtsA tend to oligomerize in the cell, thus preventing late divisome protein recruitment due to the implication of sub-domain IC in the monomer-monomer interface. By competition with FtsA for FtsZ binding (figure I.4.11), ZipA might disrupt FtsA oligomers and favor monomers. In this configuration, the sub-domain IC is then free for interaction (Pichoff et al., 2012; Rico et al., 2013). Conversely, the sub-domain IC would be immediately available in the case of FtsA mutants inhibiting self-interaction. This hypothesis is further supported by the observation that the FtsA/FtsZ ratio is important for cell division to occur (Dai & Lutkenhaus, 1992). Recruitment of other divisome protein by ZipA would therefore be indirect and could explain its limited conservation among bacteria.

Overall, FtsA and ZipA play a role of membrane anchoring for the Z-ring. In bacteria lacking FtsA, such as mycobacteria, the SepF protein found in B. subtilis or homologues can reproduce the three main known activities of FtsA, i.e. polymerization, binding to the membrane, as well as anchoring FtsZ (Duman et al., 2013). In *B. subtilis* and many Gram-positive bacteria, EzrA play a role that is similar to that of ZipA in regulating the cytokinetic assembly of FtsZ. The two proteins also share common structural features (Steele et al., 2011). Both SepF and Ezra are present in *S. pneumoniae* (in addition to FtsA), although they are not well characterized in this organism, to date.

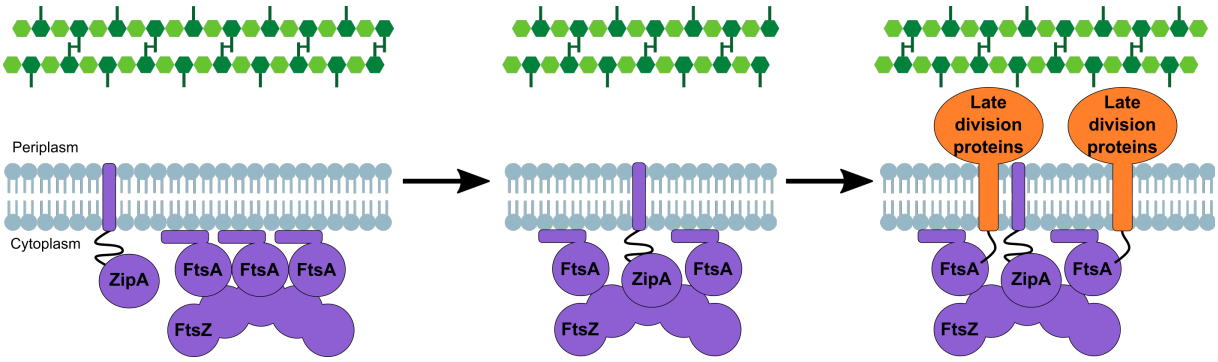

Figure I.4.11: The oligomeric state of FtsA is a regulation mechanism for the maturation of the divisome. FtsA tends to form oligomers bound to FtsZ (left panel). ZipA ability to interact with the tubulin-like protein disrupts these oligomers by competition for FtsZ binding (middle panel). When monomeric, the FtsA binding site (IC domain) becomes available and is therefore able to recruit downstream proteins (right panel). Adapted from Rico et al., 2013.

Zap (FtsZ-Associated Protein) proteins are non-essential members of the divisome (figure I.4.8), which localize in a FtsZ-dependent manner and modulate filaments association and stabilization of the Z-ring. Among the five Zap proteins currently known in *E. coli*, ZapA (Gueiros-Filho & Losick, 2002), ZapB (Ebersbach et al., 2008), ZapC (Durand-Heredia et al., 2011; Hale et al., 2011), and ZapD (Durand-Heredia et al., 2012), are early cell division proteins, which stimulate high-order structures and FtsZ-ring stability. Deletion of one of them leads to slightly more elongated cells but inactivation of several of them causes synergistic defects (Huang et al., 2013). ZapA, ZapC, ZapD and ZapE were shown to interact directly with FtsZ, but only ZapD interacts with its C-terminal peptide. Unlike other Zap proteins, ZapB is bound to the FtsZ-ring through the mediation of ZapA. These two proteins were proposed to work altogether *in vivo* to promote the Z-ring assembly (Buss et al., 2013). Currently, only high-resolution structures of ZapA (Low et al., 2004) and ZapB (Ebersbach et al., 2008) are known. ZapA presents a short double-stranded β-sheet coupled to an α-helix, forming a small globular domain, followed by a long α-helix (figure I.4.12 A). The N-terminal region is implicated in the dimerization of the protein, while the protuberant C-terminal α-helices are the basis of a coiled-coil motif which allow for tetramerization. ZapB also

dimerizes through a coiled coil domain, but does not have any additional region equivalent to the ZapA N-terminal domain (figure I.4.12 B). Interestingly, oligomerization is also found for ZapD (Durand-Heredia et al., 2012), suggesting that this characteristic could be required to stimulate FtsZ bundling. On the contrary to the four other Zap proteins, the lastly discovered ZapE protein localizes at the FtsZ-ring at the end of the cell division process and destabilizes the ring during constriction (Marteyn et al., 2014).

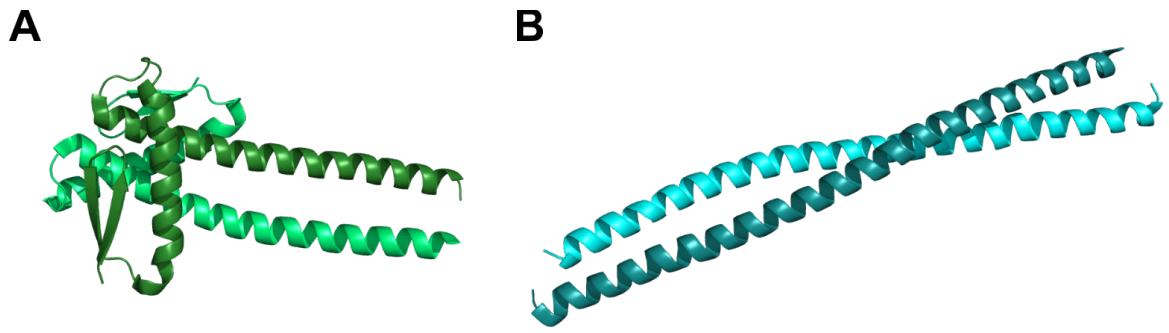

Figure I.4.12: Structures of two Z-ring stabilizing proteins. (A) *Pseudomonas aeruginosa* ZapA dimer (PDB code 1W2E) and (B) *E. coli* ZapB dimer (PDB code 2JEE). In each structure, the two monomeric units are shown in dark and lighter colors.

Finally, the FtsE-FtsX (FtsEX) sub-complex is the last known component of the divisome localizing before maturation. FtsEX forms an ATP-binding cassette (ABC) transporter-like complex, with FtsX as the transmembrane domain and FtsE as the cytoplasmic element. Based on depletion of various division proteins, FtsEX is thought to depend on FtsZ, FtsA and ZipA for mid-cell localization and to be recruited before other division proteins, which are mostly absent from septal rings as a consequence of FtsEX inactivation (Schmidt et al., 2004). Intriguingly, FtsEX is essential only in media of low-osmotic strength, and it was proposed to modulate Z-ring stability (Reddy, 2007). The role of this sub-complex was only revealed a few years ago. Upon ATPase activity of FtsE, a conformational change is induced in FtsX. This structural modification enables the activation of EnvC, which in turn will stimulate the activity of AmiA and AmiB amidases (Yang et al., 2011). As FtsE interacts with FtsZ (Corbin et al., 2007), this mechanism was proposed to be correlated with the state of the Z-ring, in order to trigger peptidoglycan hydrolysis only during Z-ring constriction. More generally, FtsX seems to be able to recruit and activate directly or indirectly different peptidoglycan hydrolases depending on the organism, as shown by recent studies in *S. pneumoniae* (Sham et al., 2011), *B. subtilis* (Meisner et al., 2013) and *M. tuberculosis* (Mavrici et al., 2014).

4.B.b.ii- Maturation of the divisome

The additional proteins that localize at the septum are members of the second step of cell division: the divisome maturation (figure I.4.8). When the cell weight double in 85 minutes, a delay of 16 minutes is observed between the FtsZ-ring assembly and the FtsZ-ring maturation (Aarsman et al., 2005). The localization of the proteins in this second stage happens in a short period.

The first protein to localize downstream of the early division protein is FtsK. FtsK is a multifunctional protein, which can be divided in three segments: an N-terminal domain embedded in the inner membrane with four predicted α-helices (Dorazi & Dewar, 2000), a very long linker of more than 600 residues in the cytoplasm, and a C-terminal domain (Massey et al., 2006). This last module assembles in hexamers in the cytoplasm and forms a ring (figure I.4.13). This structure is involved in chromosome segregation through its DNA translocase activity to resolve dimeric chromosomes and keep away DNA from the septum

(Steiner et al., 1999).

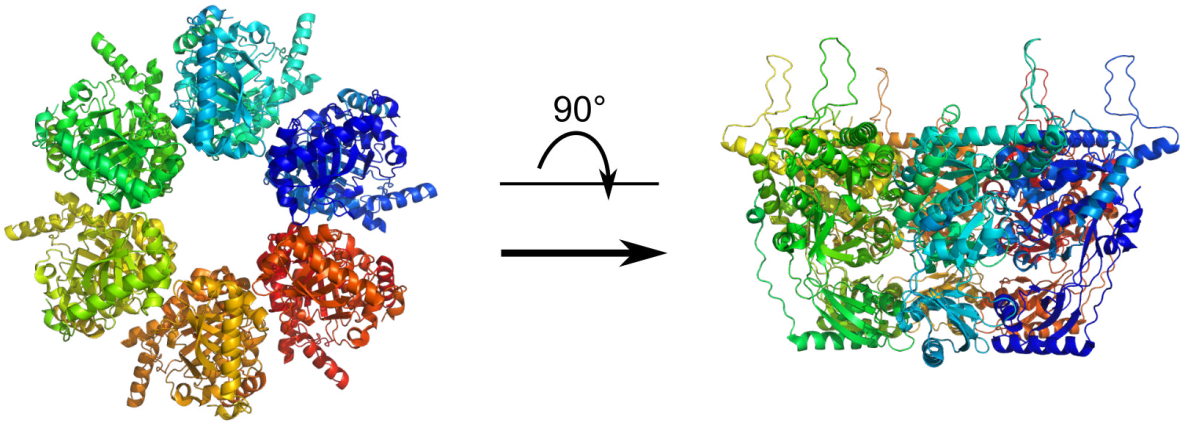

Figure I.4.13: Structure of the hexamer of the FtsK C-terminal cytoplasmic domain (PDB code 2IUU). This domain is involved in chromosome segregation, to keep away DNA from the division site.

Although the N-terminal domain is essential for cell division (Wang & Lutkenhaus, 1998), its function is less obvious. It is probably implicated in divisome stabilization through multiple interactions, as suggested by its bypass by expression of FtsA* or by the phenotypes observed when FtsQ, FtsA, and FtsZ are overexpressed (Geissler & Margolin, 2005). Late results on this N-terminal domain point to a role in the coupling of the invagination of the inner membrane with septal peptidoglycan synthesis and outer-membrane constriction (Berezuk et al., 2014). Recently, a model was proposed where FtsK hexamers coordinate at the same time two divisome complexes, also named synthesis nodes, with the cytoplasmic FtsA-FtsZ cytoskeleton in order to synchronize the synthesis of the two future new poles (Egan & Vollmer, 2015).

FtsQ is the next protein to localize at the division site and recruit FtsL-FtsB (Chen & Beckwith, 2001; Buddelmeijer et al., 2002; Chen et al., 2002) to yield a 1:1:1 sub-complex (Glas et al., 2015). FtsQ, FtsL and FtsB are small bitopic inner membrane proteins, which have a short cytoplasmic N-terminus and a periplasmic C-terminus. The crystal structure of the FtsQ periplasmic region (figure I.4.14) exhibits two domains (van den Ent et al., 2008). The first one, the closest to the membrane, is similar to POTRA (Polypeptide Transport Associated) domains and is necessary for FtsQ localization, while the second module, a nine-stranded β-sheet covered by two α-helices, is required for the recruitment of downstream division proteins. The periplasmic domain of FtsB is a coiled coil domain connected to a transmembrane helix through a likely flexible linker. A recent study (Lapointe et al., 2013) suggests that the coiled coil is stabilized by FtsL, which interacts with the FtsB transmembrane domain. FtsQ could then recruit the FtsB-FtsL complex through binding to their periplasmic regions. Because the FtsQLB sub-complex makes extensive contacts with other divisome components, these three proteins were long been thought to be only required for divisome stability. However, recent work suggests that it could have a decisive role in the activation of septal peptidoglycan synthesis, once stimulated by a feedback mechanism involving FtsN after assembly of the synthesis machinery (Liu et al., 2015; Tsang & Bernhardt, 2015).

Similarly to FtsQLB, the putative FtsW flippase and the septum-specific monofunctional PBP3 (previously presented in part I section 2.C) forms another sub-complex (Fraipont et al., 2011), which requires FtsL to be recruited at the divisome (Mercer & Weiss, 2002). As FtsW and PBP3 both interact with PBP1B, the latter bifunctional PBP might be also part of this sub-complex. Actually, PBP1B requires the presence of PBP3 (but not its activity) to localize at

the division site (Bertsche et al., 2006). Interestingly, the same periplasmic loop of FtsW is expected to interact with PBP3 and PBP1B (Fraipont et al., 2011). This close relationship between FtsW and peptidoglycan synthases underpins its putative role in peptidoglycan synthesis. The interaction of the bifunctional PBP1C and the monofunctional glycosyltransferase MtgA each with PBP3/PBP1B and FtsW/PBP3, respectively, suggest that PBP1C and MgtA are present, at least transiently, in the divisome, although experimental demonstration has not been reported yet. The role of the latter proteins in septal peptidoglycan synthesis remains also to be defined. As PBP1A in the elongasome, PBP1B is also known to be indirectly connected to the lytic transglycosylase MltA, via an identified partnership with the outer-membrane-associated scaffolding protein MipA. In parallel, the transpeptidase activity of PBP3 fosters the recruitment of amidases at the septal ring in the presence of their activators (Peters et al., 2011). Interaction of PBP1B or PBP3 with several hydrolases hint once more to a close link between peptidoglycan synthesis and hydrolysis.

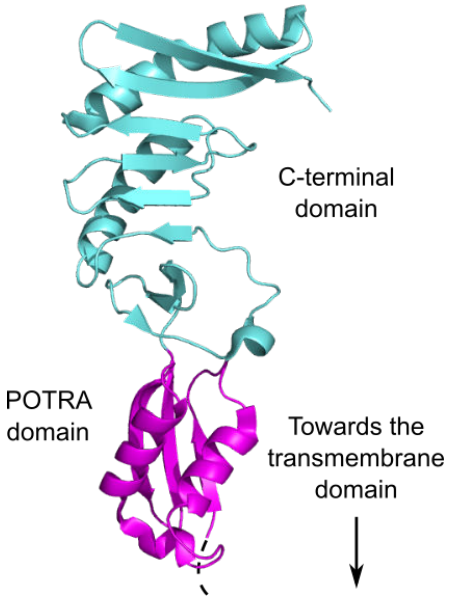

Figure I.4.14: Structure of the periplasmic region of *E. coli* FtsQ (PDB code 2VH1). The POTRA domain (in magenta), the closest to the cytoplasmic membrane, is required for the FtsQ localization to mid-cell. The C-terminal domain (in light blue) recruits the FtsBL sub-complex.

The last essential protein to be recruited is FtsN, a bitopic inner membrane protein involved in triggering cell constriction. It is composed of a short cytoplasmic domain and a periplasmic region. The latter contains three N-terminal transient α-helices (^{E}FtsN), a long proline/glutamate-rich flexible linker, and a C-terminal globular SPOR domain (Yang et al., 2004). The structure of this last module presents a βαββαβ fold (figure I.4.15), which is able to bind peptidoglycan (Ursinus et al., 2004). The localization of individual SPOR domains from FtsN and other proteins (DamX, DedA and RlpA for *E. coli*) to the septum suggests that they specifically bind septal peptidoglycan (Arends et al., 2010; Gerding et al., 2009). This hypothesis was confirmed recently by a fluorescence and phase-contrast microscopy study, showing that GFP-SPOR recognizes glycan strands lacking peptide stems at mid-cell (Yahashiri et al., 2015).

The N-terminal cytosolic region of FtsN is implicated in interaction with the FtsA IC domain (Busiek et al., 2012), thus making one of the rare known connections between early and late divisome proteins. Despite these interactions, the short ^{E}FtsN domain (35 residues) is the only region to be essential for FtsN and it is involved in a self-enhanced accumulation of the protein at mid-cell (Gerding et al., 2009). With the latest experimental results (Liu et al.,

2015; Pichoff, et al., 2015; Tsang & Bernhardt, 2015; Weiss, 2015) a global mechanism starts to emerge that explains the role of FtsN in the activation of septal peptidoglycan synthesis (figure I.4.16). First, a small portion of FtsN is recruited to the Z-ring by FtsA. This occurs once the domain IC of FtsA is freed from FtsZ-binding through competition with ZipA. The interaction of FtsN with FtsA and with the FtsQLB sub-complex in the divisome then switches FtsA and FtsQLB in an "on" state, thus activating or de-repressing peptidoglycan synthesis and triggering constriction. Synthesis of septal peptidoglycan enables the recruitment of FtsN through its SPOR domain, generating a self-enhancing cycle (Gerding et al., 2009). In addition to its essential function as a peptidoglycan synthesis and constriction trigger, FtsN is also involved in stimulation of the hydrolase activity. Indeed, FtsN recruits NlpD, activator of AmiC, and is necessary for its mid-cell localization (Uehara et al., 2010; Peters et al., 2011).

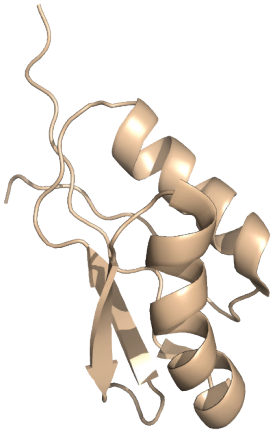

Figure I.4.15: Lowest energy NMR structure of FtsN SPOR domain (PDB code 1UTA). This domain binds glycan chains with no peptide stems, through the recognition of an undetermined motif.

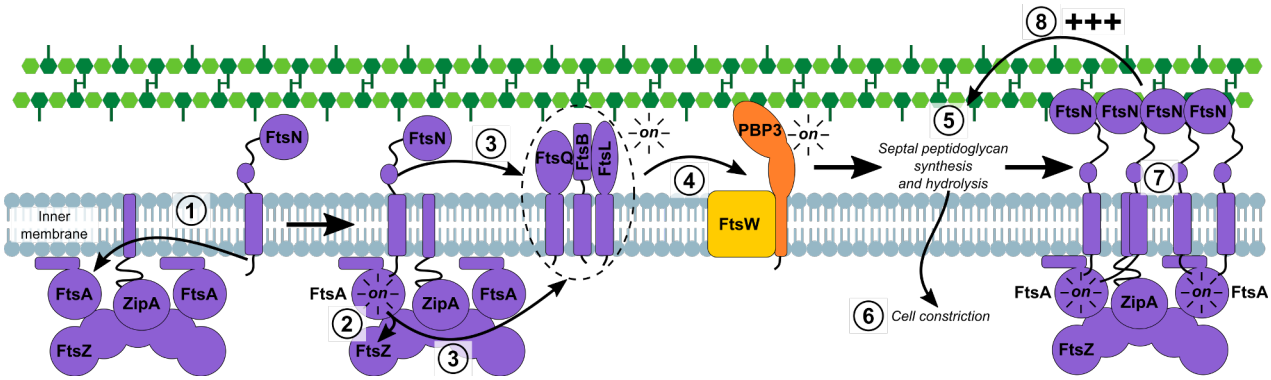

Figure I.4.16: Putative model for the activation of septal peptidoglycan synthesis by FtsN. Once FtsA is mainly monomeric, a few FtsN proteins are recruited by its IC domain (1). The interaction of FtsN with FtsA turns the latter protein in an "on-state", which stabilizes the Z-ring (2). FtsA and FtsN (through its essential region) then signals the divisome assembly state to FtsQLB (3). This sub-complex, in turn, communicates with FtsW and PBP3 to activate (or de-repress) peptidoglycan synthesis, remodeling, and cell constriction (4, 5 and 6). Synthesis of new peptidoglycan recruits more and more FtsN proteins, which bind to the glycan strands through its SPOR domain (7). This triggers a positive feedback loop that stimulates more and more cell wall growth (8). Adapted from Tsang & Bernhardt, 2015.

FtsP is one of the last component of the divisome to locate at the septum, according to our current knowledge. FtsP is a periplasmic protein which requires FtsN for localization at the septum, after the onset of cell constriction (Tarry et al., 2009). Although its function is unknown, FtsP was proposed to ensure stabilization of the divisome under environmental

stress (Samaluru et al., 2007). Its crystal structure (Tarry et al., 2009) revealed a fold homologous to multicopper oxidases protein with three domains, composed each of a β-sandwich (figure I.4.17). Despite structural similarities with the latter enzyme superfamily, FtsP is not expected to have any catalytic oxidase activity, as residues usually required for the four metal-binding sites are not present. Instead, FtsP harbors several conserved residues on a face which was predicted to bind (a) non identified partner(s).

Figure I.4.17: Structure of the late divisome protein FtsP (PDB code 2UXT). FtsP role is unknown, but the protein is thought to be required for divisome stability under stress conditions. Each β-sandwich domain is colored differently.

Although the proteins synthesizing peptidoglycan precursors are required for septal synthesis, their involvement in the divisome assembly has been little investigated. Immunofluorescence studies reported the mid-cell localization of MurG during cell division (Mohammadi et al., 2007; van der Ploeg et al., 2013). However, no MurG binding partner is currently known in the divisome. Presence of murC-G and mraY genes in the same *dcw* cluster than several genes coding for division proteins suggest such connections. Localization of these Mur and MraY proteins during division thus remains to be explored.

4.B.b.iii- Invagination of the outer-membrane by the Tol-Pal system

While inner membrane is constricting and septal peptidoglycan is synthesized, the outer-membrane must also invaginate to allow proper cell separation. A sub-complex connecting the inner-membrane to the outer-membrane is responsible for this process, although its mechanical details are still unclear. Six proteins were identified in this system: the inner-membrane components TolQ, TolR and TolA, the periplasmic TolB and CpoB (YbgF), and the outer-membrane anchored Pal protein (figure I.4.18, interactions reported in annexes, table A.2). Although this complex is not essential for the cell, it is required for outer-membrane integrity, as deletion of Pal or any Tol proteins induce outer-membrane defects (Gerding et al., 2007).

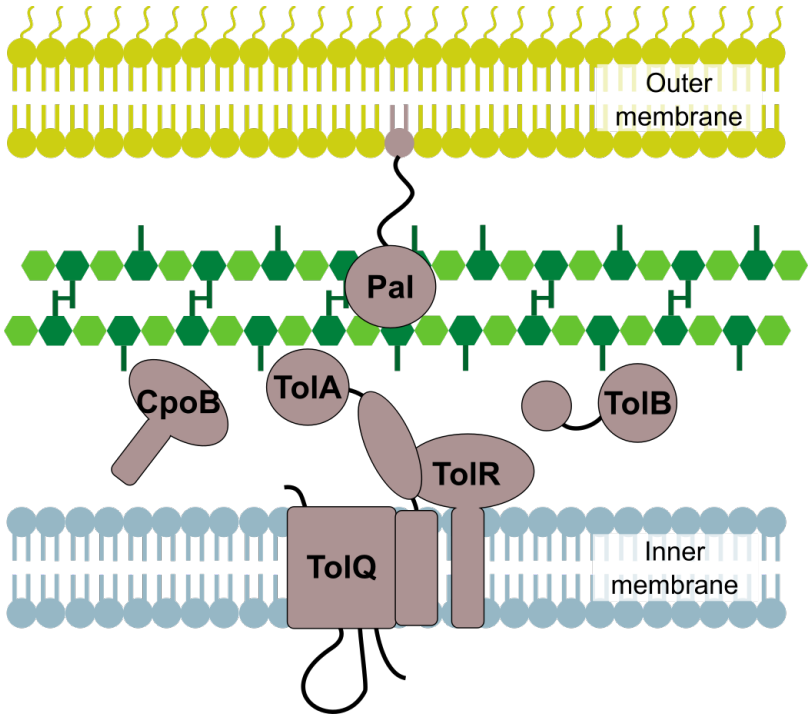

Figure I.4.18: The Tol-Pal system is the complex implicated in outer-membrane invagination. This process is thought to be regulated by an energization state-dependent conformational change of TolA by TolQ-TolR. It induces transient interactions between TolA and its partners (TolB and Pal), which result in outer-membrane invagination.

In the cytoplasmic-membrane, TolQ, TolR and TolA are likely tightly associated. TolQ is an integral protein with three predicted transmembrane segments and two large cytosolic loops (Kampfenkel & Braun, 1993). TolR has one transmembrane α-helix, followed by a periplasmic domain. This last module is composed of a four-stranded β-sheet packed with two α-helices (figure I.4.19 A) and terminates with a tail, which is expected to associate with the membrane (Parsons et al., 2008). TolA transmembrane α-helix (TolAI) is followed by two periplasmic domains, a long α-helix (TolAII) and a globular fold (TolAIII; Witty et al., 2002; Deprez et al., 2005; figure I.4.19 B), which are all linked by flexible regions (Levengood et al., 1991). Under energizing by TolQ and TolR through the use of proton-motive force, TolA undergoes a conformational change, necessary for interactions with some of its partners (Cascales et al., 2000; Lloubès et al., 2001; Gray et al., 2015).

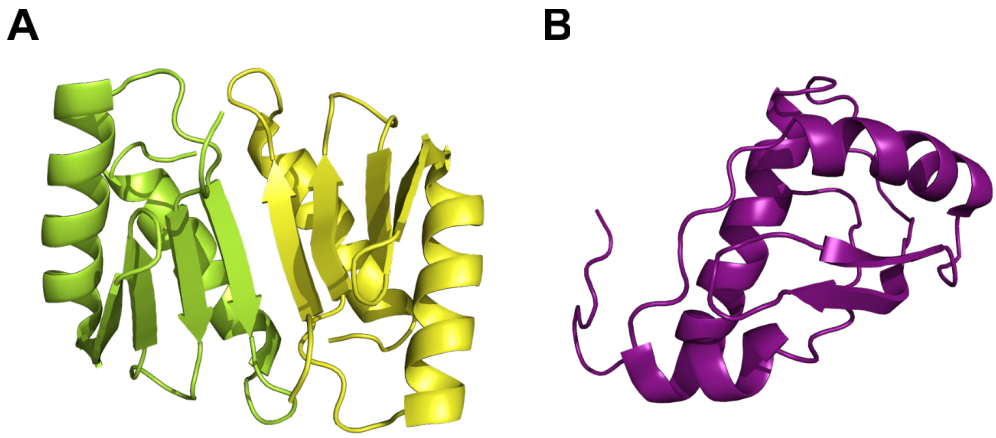

Figure I.4.19: Lowest energy NMR structures of periplasmic domains of inner membrane anchored Tol-Pal system proteins. (A) Dimer of the soluble region of *Haemophilus influenzae* TolR (PDB code 2JWL). (B) *E. coli* TolA domain III (PDB code 1S62).

Pal and TolB are thought to form another complex in the Tol-Pal system. Pal is an outer-membrane lipoprotein (Parsons et al., 2006) with an approximately 40-residue flexible linker (according to prediction from the IUPred server; iupred.enzim.hu/), which precedes a C-terminal domain that folds into an α/β sandwich and that interacts with peptidoglycan (figure I.4.20 A). The periplasmic TolB (Abergel et al., 1999) is a bi-modular protein with a small globular α/β domain followed by a β-propeller structure (figure I.4.20 B). Pal interacts with the latter domain of TolB after substantial conformational changes (Bonsor et al., 2007).

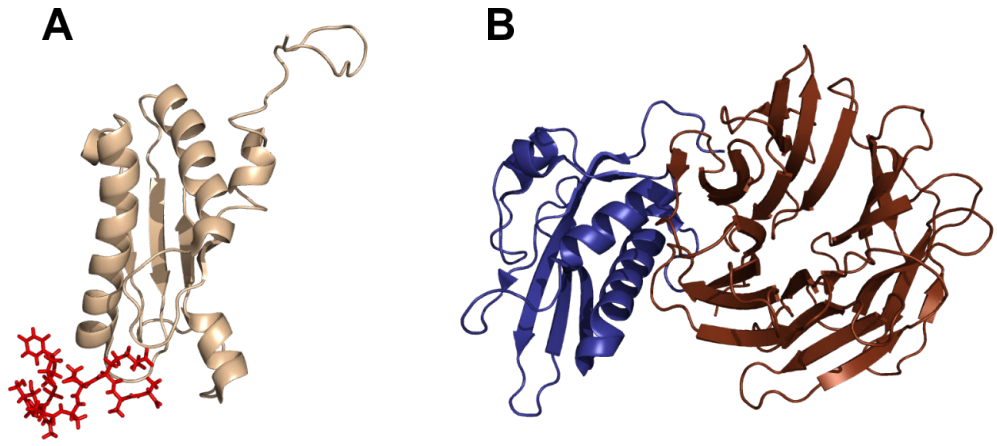

Figure I.4.20: Structures of (A) *Haemophilus influenzae* Pal (PDB code 2AIZ) and (B) *E. coli* TolB (PDB code 1CRZ). The UDP-MurNAc-pentapeptide bound to Pal is shown in red.

TolA, TolB and Pal can all interact with each other, but presumably only one by one (Cascales & Lloubès, 2004; Bonsor et al., 2009). Although the mechanism for membrane invagination is not well understood, it seems to involve cycles of proton motive force-driven TolA-Pal association and dissociation which would generate the required strength (Gerding et al., 2007). When TolA and Pal are not interacting, TolB is thought to compete with peptidoglycan for interaction with Pal, allowing dynamical localization all along the process.

The role of the periplasmic CpoB protein, previously known as YbgF, has long remained unclear. Structures of its two domains were solved by X-ray crystallography (Krachler et al., 2010). Its N-terminal coiled coil region allows trimerization of the protein. The protein extends with a C-terminal TPR (TetratricoPeptide Repeat) domain (figure I.4.21). TPR modules are arrangements of several antiparallel α-helices which are generally used as interaction scaffolds in complexes (Allan & Ratajczak, 2011). This domain is implicated in the binding of TolA, a process which modulates the CpoB oligomerization state. It is not known if the CpoB monomeric and trimeric states have or not different functions, or if they correspond to active and inactive forms.

As the Tol/Pal proteins localize at the onset of constriction to perform outer-membrane invagination during cell division (Gerding et al., 2007), they can be expected to interact with other divisome protein in order to localize at mid-cell and to coordinate their action with the rest of the machinery. Recent work showed indeed that CpoB is actually responsible for linking invagination with septal peptidoglycan synthesis (Gray et al., 2015). This point and resulting deductions will be addressed later regarding results from this thesis (part II section 3.B.b).

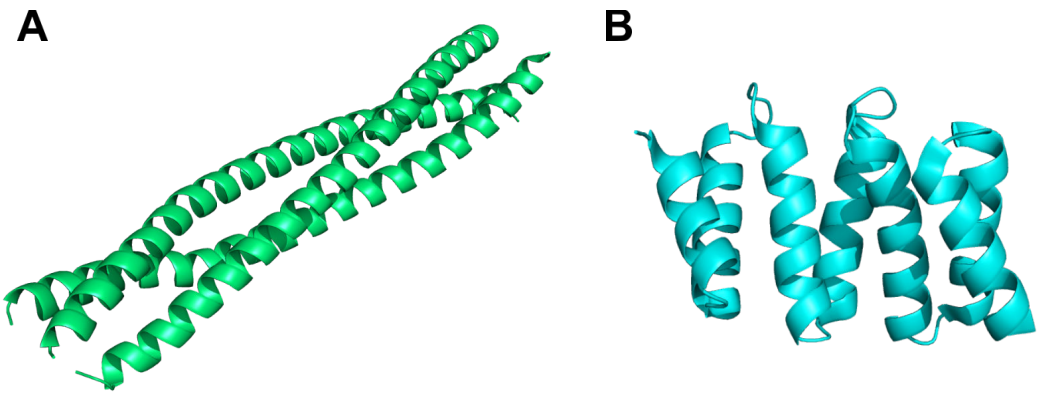

Figure I.4.21: Structure of CpoB. (A) Trimer of *E.coli* N-terminal coiled coil domain (PDB code 2XDJ). (B) *Xanthomonas campestris* C-terminal TPR domain (PDB code 2XEV). Role of the different oligomerization states of CpoB is undetermined.

4.C- Switching from elongation to division

From the observation of these two machineries, one general question remains unsettled: how does the cell switch from one to the other? A solution could be found in the study of a short period of elongation occurring at mid-cell before the divisome maturation stage, guided by FtsZ (Nanninga, 1991; de Pedro et al., 1997). Because in *E. coli* this process does not require PBP3 activity which is essential for septal peptidoglycan synthesis, this was called PBP3-Independent Peptidoglycan Synthesis (PIPS). As it does not either require any late division proteins (Potluri et al., 2012) and as it occurs before septum formation, this process is also referenced as preseptal synthesis. Indeed, among all members of the divisome, only FtsZ and ZipA are essential for this particular growth (Potluri et al., 2012). The nature of the peptidoglycan synthase(s) involved in this process is obscure, but one of the two bifunctional PBPs and the monofunctional PBP2 are suspected to operate. Indeed, the elongation-specific PBP2 transpeptidase was shown to localize at mid-cell at the same time than FtsZ (van der Ploeg et al., 2013). Similarly, MreB co-localizes early with the FtsZ-ring during cell division, but it also interacts directly with the tubulin-homologue (Fenton & Gerdes, 2013). However, if this interaction is impaired, cell elongation is not altered, but division is blocked despite maturation of the divisome, and PBP1B and PBP2 are not recruited at the septum. This suggests that MreB transfers both PBPs to the divisome (as well as potential other proteins such as the Mur enzymes) and that the latter step is an essential requirement for cell division. Preseptal synthesis could thus be an essential process resulting from switching from elongation to division. It is expected to be performed by a mixed complex (figure I.4.22), which contains MreB, FtsZ, ZipA, and some members of the elongasome. However, these proteins could also be implicated transiently in septal synthesis instead (or in addition?), as the late division protein PBP3 interacts with PBP2 and as the former activity is required for the latter mid-cell localization (den Blaauwen et al., 2003; van der Ploeg et al., 2013). Further studies on relationships between the elongasome and the divisome will be required to determine more inter-machineries connections and their precise role.

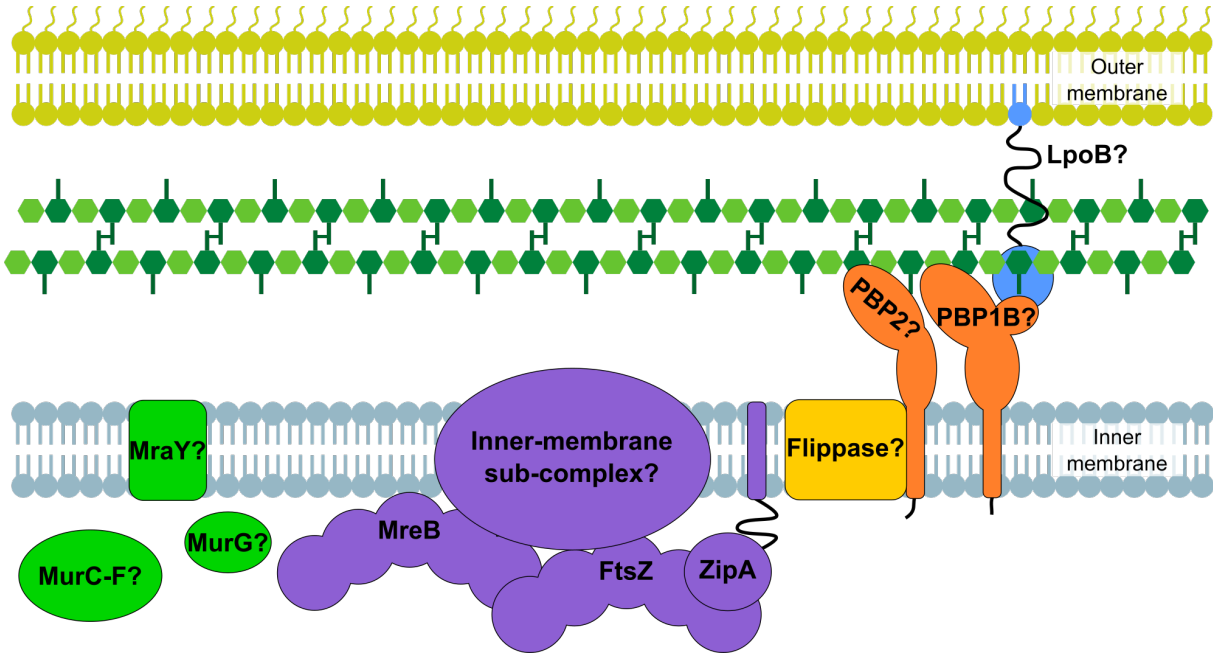

Figure I.4.22: Putative complex involved in preseptal peptidoglycan synthesis. Preseptal peptidoglycan synthesis (or PIPS) is thought to occur before maturation of divisome and to elongate the cell at mid-cell. Proteins suspected to belong to this transiant complex are followed by a question mark.

If tremendous progress have been made in the last fifteen years to disentangle the different mechanisms of peptidoglycan synthesis and maturation, details of the operations of the identified machineries are still missing. Together with a large range of biophysical techniques, integrative structural biology approaches are required and their potential use and limitations have to be analyzed. The next part focuses on one of these methods, Nuclear Magnetic Resonance (NMR), which was used as a central technique, for the work developed in this thesis.

Résumé en français du chapitre 4 : Contrôle spatio-temporel de la synthèse du peptidoglycane

Chez les bactéries en bâtonnets comme *E. coli*, le cycle cellulaire est généralement divisé en deux phases : l'élongation des parois latérales et la division au septum, au milieu de la cellule. Afin d'éviter une rupture du sacculus qui serait létale pour la bactérie, sa synthèse, son assemblage et son hydrolyse doivent être étroitement coordonnées spatio-temporellement afin d'insérer les nouveaux muropeptides dans le réseau de peptidoglycane existant. Bien que ce processus ne soit pas bien compris dans le détail, le modèle de Höltje propose un mécanisme de « 3 brins pour 1 », c'est-à-dire que trois chaînes de glycanes seraient insérées à la fois par les PBPs dans un espace occupé précédemment par une seule chaîne, retirée au préalable par des hydrolases. De nombreux travaux se sont alors concentrés sur l'identification des machineries impliquées dans la synthèse et l'évolution de la couche de peptidoglycane durant l'élongation et la division. Chez *E. coli* et chez d'autres bactéries allongées, deux complexes dynamiques s'étendant du cytoplasme au périplasme ont été mis en évidence, chacun d'entre eux étant dédié à l'une de ces deux phases du cycle cellulaire, leur valant le nom d'élongasome et de divisome, respectivement. Chacun de ces complexes est guidé par une protéine cytoplasmique formant des structures similaires au cytosquelette eucaryote. Ils sont par ailleurs connectés à divers régulateurs et aux PBPs à haut poids moléculaire.

L'élongasome est guidé par MreB, un homologue de l'actine, qui est essentiel à la morphogenèse des bactéries en bâtonnets, mais généralement absent des bactéries sphériques telles que les cocci. Chez *E. coli*, MreB est essentiel, son inactivation menant à la formation de cellules sphériques qui finissent par lyser. *In vivo* et *in vitro*, MreB s'assemble en filaments doubles antiparallèles, via un mécanisme dépendant de l'hydrolyse du GTP ou de l'ATP. Cette super-structure est essentielle pour que MreB soit fonctionnelle, la perturbation des contacts inter- ou intra-filaments résultant également en l'adoption d'une forme sphérique. *In vivo*, MreB est étroitement associée à la membrane. La localisation de ses filaments a été le sujet de nombreuses études, dont les résultats furent sujet à débats. Alors que de premiers travaux en microscopie suggéraient que les filaments de MreB formaient un long motif hélicoïdal le long de la cellule, des observations ultérieures ont mis en évidence une organisation en patch, où les filaments adoptent un mouvement circonférentiel. Les derniers travaux en date semblent indiquer plutôt la formation de filaments étendus, avec la même dynamique que les patchs décrits précédemment. La différence de longueur des polymères de MreB entre ces deux derniers résultats pourrait être due à des morphologies anormales, causant l'assemblage de plus courts filaments, via une variation de la courbure de la membrane. L'étude des zones actives de synthèse de peptidoglycane montrant une forte corrélation avec la localisation de MreB et sa dynamique, il est probable qu'il guide l'élongasome, en limitant la diffusion de ces membres et les répartissant de façon homogène sur les parois latérales de la cellule.

L'élongasome est constitué de plus de 10 protéines qui peuvent être placées arbitrairement dans 3 sous-groupes, les protéines cytoplasmiques, les protéines membranaires et les PBPs, sous-goupes qui interagissent entre eux. Le premier sous-complexe comprend les ligases Mur (MurC-MurF), MraY et MurG. Bien que ne se liant pas entre elles, ces enzymes restent associées ensemble grâce à leur interaction commune avec MreB, évitant ainsi la dispersion des produits intermédiaires. MreB forme un autre ensemble avec plusieurs protéines associées

à la membrane : MreC, MreD, RodA (voir chapitre 2) et RodZ. Le rôle de celles-ci reste cependant mal compris. MreC est constitué d'une hélice α transmembranaire suivie d'un domaine périplasmique. Celui-ci est capable de dimériser et pourrait même former des filaments. MreD quant à elle est l'un des membres de l'élongasome les moins bien caractérisés. Cette petite protéine membranaire et MreC pourraient servir de support pour connecter les autres protéines de l'élongasome de part et d'autre de la membrane interne. Un rôle similaire est attendu pour RodZ, qui présente un domaine cytoplasmique et un domaine périplasmique. L'interdépendance entre la localisation de MreB et celle de ces 3 protéines ainsi que la détermination d'interactions, directes ou indirectes, entre MreC, RodA et RodZ avec les PBPs semblent conforter cette hypothèse. Chez *E. coli*, les 2 principales PBPs de ce complexe sont PBP2 et PBP1A (voir chapitre 2). Bien que la façon dont l'insertion de nouveaux brins est corrélée à l'hydrolyse d'anciens brins soit peu claire, il semblerait que ces PBPs soient connectées, au moins indirectement, à certaines hydrolases. De telles interactions restent toutefois à être caractérisées.

Une seconde machinerie est dédiée à la synthèse du peptidoglycane, mais cette fois-ci durant la division : le divisome. En effet, durant cette phase, les futurs nouveaux pôles des deux cellules filles doivent être synthétisés, et doivent être séparés, en corrélation avec la constriction des membranes interne et externe. Le divisome est guidé par la protéine cytoplasmique FtsZ, un homologue structural de la tubuline à activité GTPase. La liaison avec son substrat provoque la polymérisation de FtsZ sous forme de filaments, tandis que son hydrolyse déstabilise cette super-structure. D'autres assemblages de FtsZ ont également pu être observés *in vitro*, mais leur pertinence *in vivo* reste inconnue. Les études *in vivo* de FtsZ montrent que cette protéine forme une structure en anneau nommé « anneau Z ». Avec le développement de la microscopie super-résolution et de la cryo-tomographie électronique, cet anneau a pu être caractérisé plus en détail. Les deux principales hypothèses évoquent soit une structure hétérogène faite de filaments superposés plus ou moins orientés de la même manière, soit la présence de peu de filaments mais très longs. Dans le dernier cas, cette architecture pourrait permettre facilement la constriction de la membrane interne par coulissement, l'une des fonctions avancées pour FtsZ.

Par rapport à l'élongasome, le divisome est bien mieux caractérisé. Cette machinerie se forme en deux étapes : l'assemblage de l'anneau Z, puis la maturation du complexe, qui consiste en le recrutement séquentiel des différents acteurs nécessaires à la synthèse du peptidoglycane septal, à sa régulation et à la division de la cellule. Durant la phase d'assemblage, l'anneau Z est ancré à la membrane interne et stabilisé par diverses protéines. Chez *E. coli*, cet ancrage est effectué par ZipA et FtsA, qui interagissent spécifiquement avec une région peptidique hautement conservée à l'extrémité C-terminale de FtsZ. FtsA a la particularité d'être un autre homologue de l'actine à la différence d'un sous-domaine qui lui est spécifique (IC), qui est impliqué dans son oligomérisation et dans l'interaction avec des protéines essentielles à la maturation du divisome. Lorsque FtsZ polymérise, FtsA ne peut pas recruter les autres membres de ce complexe, le sous-domaine IC étant à l'interface entre les monomères. ZipA étant en compétition avec FtsA pour l'interaction avec FtsZ, sa liaison à l'homologue de la tubuline devrait déstabiliser la présence d'oligomères de FtsA, dont l'état monomérique serait favorisé. Son sous-domaine IC serait alors disponible pour interagir avec d'autres partenaires. L'assemblage de l'anneau Z est modulé par une famille de protéines appelée Zap (FtsZ-Associated Proteins). Parmi les 5 protéines Zap connues à ce jour, ZapA, ZapB, ZapC, ZapD et ZapE, les 4 premières stabilisent l'assemblage de FtsZ. La dernière, ZapE, ne localise au centre de la cellule qu'à la fin de la division et déstabilise l'anneau Z durant l'étape de constriction. Enfin, le sous-complexe FtsE/FtsX est le dernier composant à se localiser au site de division avant maturation. Il s'agit d'un transporteur ABC (ATP-Binding Cassette) connecté à FtsZ, et dont la fonction est d'activer directement et/ou indirectement des hydrolases du peptidoglycane.

Une fois l'anneau Z et ses partenaires assemblés vient la maturation du divisome. La première protéine à être recrutée est alors FtsK. Elle a la particularité d'avoir un domaine N-terminal membranaire et un domaine C-terminal cytoplasmique reliés entre eux par une très longue région déstructurée. Alors que le rôle du premier domaine est méconnu, le domaine C-terminal s'assemble en hexamère pour former un large anneau repoussant l'ADN du septum. C'est ensuite au tour du sous-complexe FtsQLB formé de protéines insérées dans la membrane interne et présentant une région périplasmique, de se localiser au site de division, FtsQ dans un premier temps, suivi de FtsB-FtsL. Ces protéines, en plus d'être probablement impliquées dans la stabilisation du divisome, ont dernièrement été proposées pour avoir un rôle dans l'activation de la biosynthèse de peptidoglycane septal. La présence de FtsL au septum permet de recruter un autre sous-complexe, constitué de la possible flippase FtsW, de la D,D-transpeptidase PBP3 (voir chapitre 2) et de peut-être la PBP bifonctionnelle PBP1B, dont la participation au sein du divisome est en tout cas avérée. Les synthases MtgA et PBP1C pourraient également être impliquées, au moins transitoirement, dans la croissance du peptidoglycane au site de division, via leurs interactions avec ces protéines. La caractérisation de partenaires de PBP1B et de PBP3 a également permis de mettre en évidence une connexion avec les hydrolases (MltA, amidases), comme prédit par le modèle de Höltje. La dernière protéine essentielle à la division à être recrutée est FtsN, une protéine impliquée dans le déclenchement de la constriction. Son domaine membranaire est précédé d'une courte queue cytoplasmique et est suivi, dans le périplasme, d'une région flexible à structures secondaires transitoires, essentielle à sa fonction, puis d'un domaine liant le peptidoglycane. De récents travaux suggèrent un mécanisme d'activation de la synthèse de peptidoglycane septal faisant appel à FtsN. Tout d'abord, une petite fraction de FtsN serait recrutée en amont par FtsA. Cette interaction ferait passer FtsA puis FtsQLB dans un état activé, qui stimulerait ou déréprimerait à son tour la synthèse de peptidoglycane. Les nouveaux brins oligosaccharidiques seraient alors reconnus par le domaine périplasmique d'autres molécules de FtsN, provoquant un cercle vertueux, où de plus en plus de FtsN se localise au site de division et où l'assemblage de peptidoglycane est de plus en plus stimulé. Tout cela nécessite cependant en amont la présence des enzymes de biosynthèse des précurseurs du peptidoglycane dans le cytoplasme. Cependant, leur connexion avec le divisome reste actuellement indéterminée, bien que l'on sache que certaines se localisent au septum durant la division.

Une fois que l'anneau Z s'est assemblé et que la synthèse de peptidoglycane septal a débuté, la constriction de la membrane interne a lieu, peut-être via une force appliquée par FtsZ. En parallèle, la membrane externe subit également une invagination. Bien que ce mécanisme reste peu clair, les protéines impliquées sont connues et font partie du complexe Tol-Pal. Ce complexe comprend des protéines insérées dans la membrane interne, TolA, TolQ et TolR, ancrées à la membrane externe, Pal et solubles, TolB et CpoB. TolQ et TolR sont sensibles à la force proton motrice, sous l'effet de laquelle ces protéines peuvent énergiser TolA, dont les deux domaines périplasmiques adopteraient alors une conformation étendue. TolA, TolB et Pal interagissant tous les uns avec les autres, mais seulement un par un, il semblerait que la stimulation de Tol par TolQ et TolR provoque des cycles d'association TolA-Pal, responsables de l'invagination de la membrane externe. En absence d'énergisation, Pal interagirait avec TolB et/ou le peptidoglycane, un autre de ses partenaires. Quant à CpoB, de récents travaux semblent montrer que son rôle est de coordonner l'invagination de la membrane externe avec la synthèse de peptidoglycane par PBP1B.

De l'étude des complexes de biosynthèse de peptidoglycane durant l'élongation et la division d'*E. coli*, un point reste non abordé : la transition d'une machinerie à l'autre. Bien que celle-ci soit peu documentée, il semblerait qu'une courte période de synthèse de peptidoglycane préseptal (avant la maturation du divisome), nommé PIPS (Synthèse de Peptidoglycane Indépendante de PBP3) en soit la signature. Parmi les membres de ce complexe transitoire, FtsZ et ZipA sont essentielles, contrairement aux autres protéines du

divisome. L'interaction déterminante de MreB avec FtsZ à ce stade suggère également que PBP2 et/ou PBP1A pourraient jouer un rôle. Davantage d'études de ce processus devraient permettre de révéler si cette machinerie est en effet constituée d'un mélange de protéines de l'élongasome et du divisome.

Chapter 5
NMR as a tool for the study of peptidoglycan and its associated proteins

Determining the atomic organization of peptidoglycan and of proteins involved in its biosynthesis is an essential step towards the understanding of the function and interconnections of these factors in the bacterial cell envelope. This knowledge is crucial to apprehend the complexity of the apparent simple forms of life that bacteria represent and to elaborate new antibiotics on the basis of rational design. Structural biology is the field at the frontier of biology and physics which studies the three-dimensional atomic arrangement of biomacromolecules. The two main techniques for the determination of high-resolution (atomic) structures are X-ray crystallography and Nuclear Magnetic Resonance (NMR) spectroscopy. X-ray crystallography is based on the scattering of X-rays by a monocrystal made of a regular arrangement of a same conformational state of the studied protein. With the development of high-throughput devices for automated crystallization conditions assays, the number of structures solved by X-ray crystallography has been increasing steadily, accounting for nearly 90% of the total number of structures deposited in the Protein Data Bank (PDB). More details on X-ray crystallography principles and applications, with a highlight on amidases can be found in the following reviews, Shi, 2014; Büttner et al., 2015. NMR spectroscopy instead rests upon magnetic properties of the nuclei from the sample, which can be in solution or in the solid state (micro-crystals, non crystalline powder or more or less hydrated paste). Low-resolution methods can also give further insight in macromolecular structures and can be combined with the two previous techniques to obtain additional information. Among them, Small Angle X-ray and Neutron Scattering (SAXS and SANS) methods are able to provide data on the general conformation of a protein or a complex in solution (Mertens & Svergun, 2010; Petoukhov & Svergun, 2013). Molecular envelops can also be observed by cryo-Electron Microscopy (cryo-EM) which is particularly appropriate for the study of macromolecular assemblies (Cheng et al., 2015). Due to recent multiple technical developments, cryo-EM is evolving as a method at the edge between high and low-resolution, allowing atomic resolution (resolution below 5 Å) of more and more macromolecules in the future (Binshtein & Ohi, 2015; Cheng, 2015). The complementarities between all of these techniques is the basis of integrative structural biology, which aims at addressing challenging questions through a combination of the individually developed methods (van den Bedem & Fraser, 2015). In support of all of these experimental techniques, computational simulation can also be decisive to unveil currently inaccessible data, such as transient conformations (Purdy et al., 2014). Additional biophysical techniques can also been combined to structural studies to investigate interactions between different cell wall components and/or to explore protein oligomerization. Among them are Surface Plasmon Resonance (SPR) (Christie et al., 2014), Mass Spectrometry (MS, Boeri Erba & Petosa, 2015; Sinz et al., 2015), Analytical UltraCentrifugation (AUC, Cole et al., 2008; Howlett, Minton, & Rivas, 2006), Size-Exclusion Chromatography – Multi-Angle Light Scattering (SEC-MALS, Sahin & Roberts, 2012). Imaging techniques are not to be forgotten, as for example Atomic Force Microscopy (AFM) that enables to probe surfaces or single proteins (Dufrêne, 2014; Puchner & Gaub, 2009), super-resolution microscopy to detect supramolecular assemblies *in vivo* (Coltharp & Xiao, 2012; Godin et al., 2014); and Förster Resonance Energy Transfer (FRET, Sun et al., 2013) to investigate on interactions in the cell.

5.A- NMR for the study of biomacromolecules

Each nucleus is characterized by an intrinsic parameter called spin, which reflects its properties in a magnetic field (in a spectrometer for example). Some isotopes with a non-zero spin, like ^{1}H, ^{15}N and ^{13}C, behave like a compass and tend to adopt specific orientations in this field. Energy can be associated to each of these orientations and spectroscopy can be operated by detecting the transitions between the different energy levels. In practice, application of a short radio frequency pulse perturbs the equilibrium population. Return to the equilibrium will give rise to a radio frequency signal with a frequency corresponding to the energy difference between the excited and the ground states ($\Delta E = h\gamma B_0/2\pi$, where gamma is also a magnetic property of the nucleus, and B_0 is the static magnetic field). Due to shielding effects coming from neighboring electrons, each nucleus will feel a different local B_0 and then will emit a signal at a specific frequency. This local shielding of the magnetic field will depend on the nature of the environment (bond, structure …). This signal will be detected in a coil and recorded to be processed. After a mathematical operation, called the Fourier transform, the different frequencies emitted by the nuclei are extracted and displayed as a 1D spectrum where the x axis corresponds to the frequency and the y axis to the intensity of the signal (figure I.5.1). However, as these resonance frequencies are field dependent and then spectrometer-dependent, the corresponding chemical shift values, expressed in ppm, are preferred.

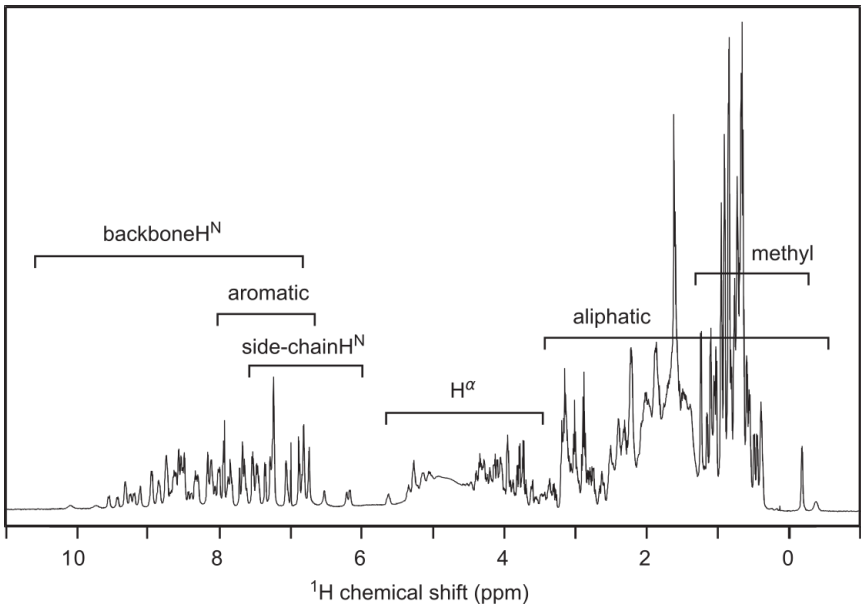

Figure I.5.1: 1D NMR proton spectrum of ubiquitin in 95%H_2O-5%D_2O. Despite the low molecular weight (8.5 kDa) of the protein, multiple resonances already overlap. The types of protons, which can be found at the different chemical shifts values are noted above the signals. Taken from Cavanagh et al., 2007.

In the 1D representation, the position of the peak will correspond to the chemical shift and the linewidth will depend on the relaxation. The relaxation processes are driven by the reorientation of the spins relative to the B_0 magnetic field. This reorientation over the time is a complex function of the global molecular tumbling and the local flexibility. Sharp peaks are obtained when the signal decays (comes back to equilibrium) slowly. In the case of a faster relaxation, the peaks in the spectrum will appear broader, causing a loss of resolution and of intensity in the spectrum. This happens in particular when the molecular tumbling (the free rotation of the molecule in solution) of the protein is decreased via formation of oligomers. Similarly, molecular weight of the protein must also be considered before to start an NMR study, because the higher the molecular weight, the larger the NMR signals as shown in figure I.5.2. Of note, the shape of the macromolecule also influences the linewidth, but to a lesser extent. Taking these factors into consideration, NMR in solution is limited to protein sizes up

to roughly 40 kDa typically, although strategies exist to partially overcome this limitation such as the use of solid-state NMR (see section C), or methyl-specific (Kerfah et al., 2015) or deuterium (Tugarinov, 2013) labelings. Whereas an increase in temperature generally decreases the relaxation by increasing the molecular tumbling, agents such as glycerol are not recommended because of their faculty to affect the viscosity and then the molecular tumbling.

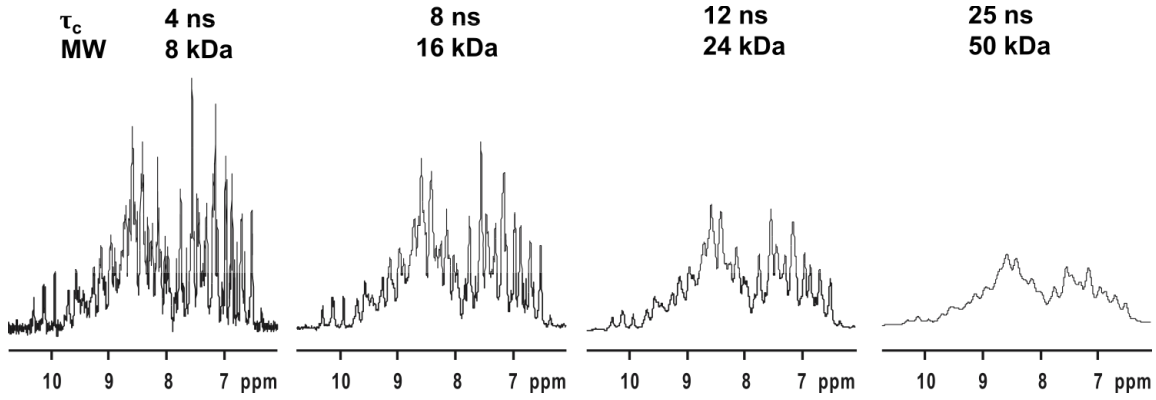

Figure I.5.2: Simulation of a 1D NMR proton spectrum of an 8 kDa protein at different oligomerization states (from monomer to tetramer). As the protein size increases, the correlation time τ_c, which measures the time necessary for the protein to reorient in solution by an angle of 1 radian, also rises, causing the signals to broaden and lose intensity. Taken from Michael Sattler, NMR of large proteins and complexes, EMBO World Practical Course 2009 (http://cwp.embo.org/wpc09-07/sattler_embo2009_large_proteins.pdf).

To extract the NMR information at an atomic resolution it is necessary to identify which resonance belongs to which atom(s). This process is called resonance assignment. In the case of a small molecule, this is a straightforward task, as the number of signals is limited. For a biomacromolecule such as a protein, the spectrum is highly crowded, preventing assignment (figure I.5.1). The strategy to overcome this issue is to transfer the magnetization from one nucleus to one or several others and switch to multi-dimensional spectra (usually 2D and 3D spectra). In the resulting spectrum, each dimension will correspond to the chemical shift of a specific nucleus. For biomolecules, the typical heteronuclear experiments will correlate ^{1}H, ^{15}N and ^{13}C nuclei. Such multidimensional heteronuclear spectra allow macromolecule resonance assignment by reducing signal overlaps, provided that the sample meets some requirements, in labeling in particular. This spectroscopy is possible only for relatively slow relaxation rates, in order to enable the transfer of the magnetization from one nucleus to others.

Except for ^{1}H (also commonly referred as protons) nuclei, the most abundant isotope is not necessarily the most appropriate for NMR. To gain in sensitivity, samples are generally isotopically labeled with ^{15}N and ^{13}C isotopes. For this, bacteria overproducing the protein or other studied molecules are grown in a minimum medium (M9), in which all of the main carbon (glucose) and nitrogen (ammonium chloride) sources are labeled. As NMR is quite an insensitive method, this requires a high quantity of the molecular sample in the volume used for the signal detection (approximately 130 to 450 µL depending on the NMR standard tube used). Although “low” concentrations (20 µM) can be enough for 1D or 2D spectra, much higher concentrations (generally above 500 µM) are needed for acquisition of 3D NMR datasets for structural studies. The sample must furthermore be as pure as possible, as contamination could give rise to additional peaks. Aggregation is also to be avoided for linewidth issues.

The usual 2D-spectrum which is first recorded is a ^{1}H,^{15}N-HSQC (Heteronuclear Single-Quantum Correlation). Two examples of such a spectrum are shown in figure I.5.3. Each peak corresponds to a hydrogen directly bonded to a nitrogen, which represents in most of the cases

amide groups from the backbone for all residues except for prolines which lack amide protons. Additional signals come from the arginine guanidinium and tryptophane indol moieties, as well as from the amide groups present in asparagine and glutamine side-chains. The $^{1}H,^{15}N$-HSQC spectrum is considered as a fingerprint of the macromolecule, because its appearance can readily be informative on the state of the sample, as well as on some structural features. In the case of a folded protein for example, the signals will exhibit a good dispersion (figure I.5.3 A). Some patterns can also be indicative on secondary structures, as for resonances at high proton chemical shifts (> 9 ppm) which generally correspond to amide groups from residues localized in β-sheets. One interesting aspect of the NMR technique is the study of intrinsically disordered proteins (IDP), which have a high flexibility and do not exhibit stable secondary structures (although they may transiently exist or be stabilized by an interaction partner). As all backbone amide protons in disordered molecules have a similar local environment, their chemical shift does not vary significantly from each other. Such samples (figure I.5.3 B) give signals which have the particularity to be poorly dispersed on the ^{1}H axis (in a window ranging from 7.5 to 8.5 ppm). In addition, because of the high tumbling rate of theses regions, the detected peaks are also highly intense. Finally, a protein with a mixture of both disordered and structured region will have some peaks with a narrow distribution, while others will be well dispersed across the spectrum. Although not highlighted in this paragraph, 1D and multidimensional NMR spectra can also be recorded on sugars (like muropeptides) and nucleic acids (which tend to exhibit a smaller signal dispersion).

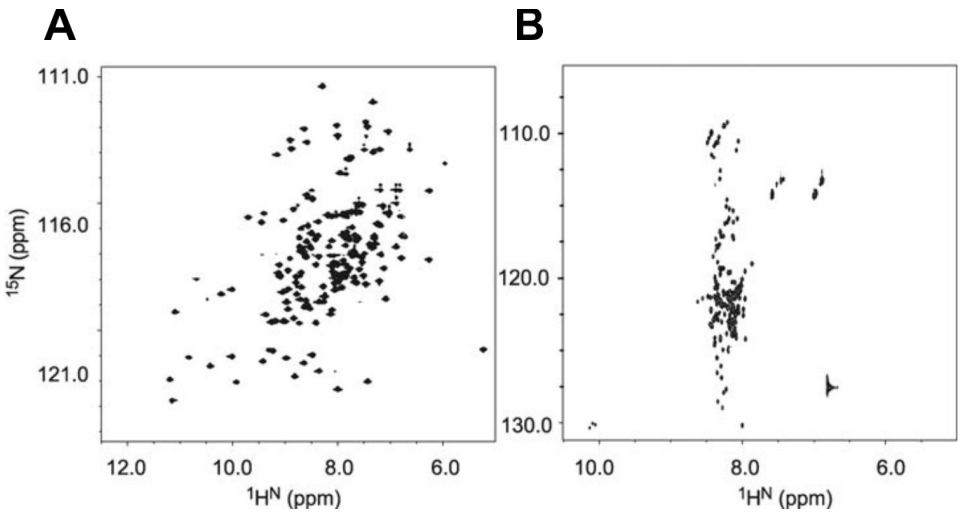

Figure I.5.3: 2D $^{1}H,^{15}N$-HSQC gives a signature of the studied macromolecule. Spectra were recorded on a *Azotobacter vinelandii* flavodoxine in (A) a folded and (B) an unfolded state (in 6 M GuHCl)**.** When unfolded, the signals are poorly dispersed in the ^{1}H dimension, while resonances are well spread when the protein is folded. Taken from Breukels et al., 2011.

5.B- Liquid-state NMR studies of bacterial cell wall proteins

Due to its limitations to small biological macromolecules, liquid-state NMR is not suited for direct studies on sacculi. It is however a valuable technique for the study of the structure and dynamics of proteins involved in its synthesis, maturation, or recycling. It is also well suited to investigate interactions between these key players and other proteins or peptidoglycan material.

5.B.a- NMR assignment process

To connect the information provided by a spectrum to specific residues, resonances must be assigned, that is, linked to the corresponding atoms (actually nuclei) in the protein. In the

case of an interaction or dynamics study, assignment of the backbone (N, H^N, C' carbonyl, C_α and C_β) atoms is sufficient. For structure determination, the assignment of ^1H, ^{13}C and ^{15}N side-chain atoms is also required, which can rapidly overcome a thousand of frequencies to identify. This step is therefore definitively the longest one in the resolution of the structure. It can take up to several months for a 25 – 30 kDa protein. The assignment strategy rests upon the use of several couples of 3D spectra (HNCO/HN(CA)CO, HNCA/HN(CO)CA, HNCACB/HN(CO)CACB...). Each spectrum correlating one N_iH_i amide group (from amino acid i) with carbon atoms from the previous residue in the sequence (i-1) is associated with another spectrum whose amide N_jH_j is linked to carbons of both residues j-1 and j (figure I.5.4). A good match will be considered when j = i-1, thus going downstream of the sequence. Each of these datasets thus enables linking of the backbone amide moieties to each other. Complementary experiments can be collected, which will correlate other backbone and/or side-chain atoms.

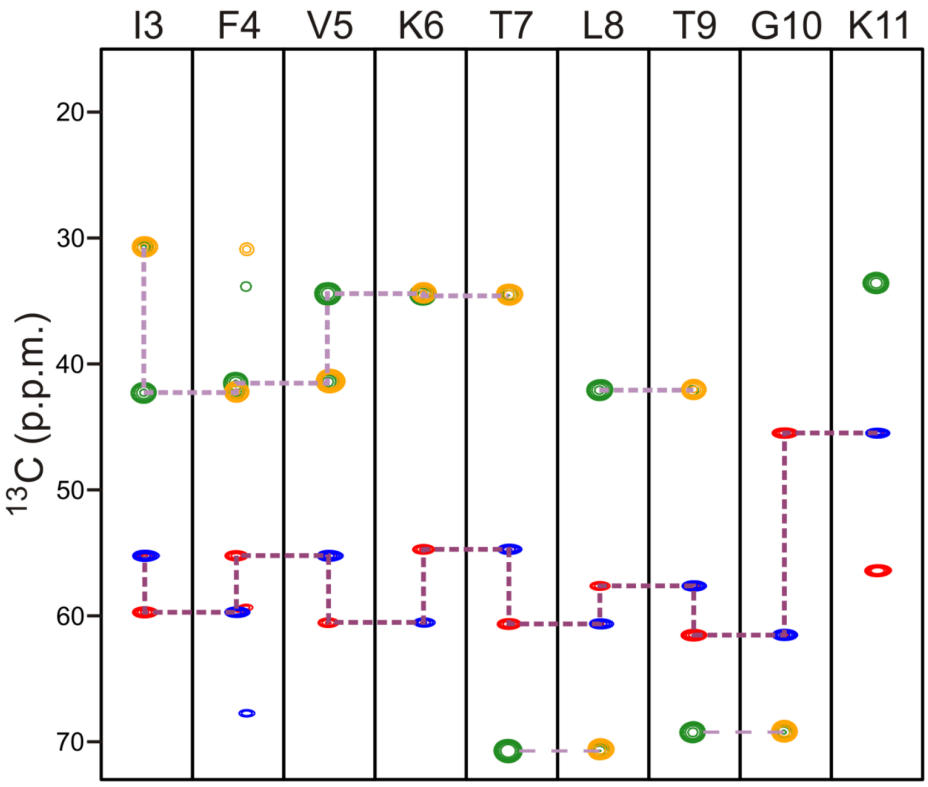

Figure I.5.4: Example of a sequential walk for residues Ile3 to Lys11 in human ubiquitin. Four 3D experiments have been superimposed: (i) the HNCA (peaks in red and blue) that gives correlations between the amide nuclei N_iH_i and Cα nuclei of amino acids i and i-1, (ii) the HN(CO)CA (peaks in blue) that gives correlations between the amide nuclei N_iH_i and Cα nuclei of amino acids i-1, (iii) the HN(CO)CACB (peaks in blue and orange) that gives correlations between the amide nuclei N_iH_i and Cα (blue) and Cβ (orange) nuclei of amino acids i-1, and (iv) the HNCACB (all the peaks) that gives correlations between the amide nuclei N_iH_i and Cα (blue and red) and Cβ (orange and green) nuclei of amino acids i-1 and i, respectively. For each amide, the assignment of a resonance to a carbon and residue type is achieved by the analysis of one dataset or the comparison of two datasets. As an example, the Cα of residue i-1 is readily identified on an HN(CO)CA dataset. A comparison with an HNCA strip for the same amide, leads to assign the additional resonance in this experiment to the Cα of residue i. The sequential ordering of residues is then achieved, when the carbons of residue i-1 show the exact same chemical shift than the carbons of residue j. Identification of a chemical shift pattern particular to a residue type then allows to replace the assigned fragment in the overall sequence. Taken from the Department of Biochemistry at the Albert Einstein College of Medicine, 2012 NMR Course, Introduction to 3D triple resonance experiments (http://www.bioc.aecom.yu.edu/labs/girvlab/nmr/course/COURSE_2012/BackboneAssignment_LectureNotes.pdf)

Assignment of the resonances give already access to some structural information at an atomic resolution. For example, measured chemical shifts can be compared for each residue

with a reference chemical shift determined for each amino acid types in a classical extended structure (Chemical Shift Index CSI). This analysis identifies the presence of stable or partially stable secondary structures. Alternatives to this simple strategy, like TALOS+ (Shen et al., 2009), have been proposed, using data mining of the structural (PDB) and NMR chemical shift (BMRB) databases. This assignment step is indispensable for further analysis of the high resolution structure, local dynamic or specific interactions.

5.B.b- Protein structure determination

To determine the structure of an assigned (backbone and side-chains) protein, structural restraints derived from NMR data are required to be incorporated in a structure calculation protocol software (figure I.5.5). Two main kinds of constraints are generally used: proton-proton distances and dihedral angles (φ and ψ). Distances are extracted from NOESY (Nuclear Overhauser Effect correlation SpectroscopY) spectra, which relies on the detection of NOE signals between two spatially close protons (5 Å or less). A third dimension (^{15}N or ^{13}C) is generally added to diminish overlaps. As the peak volume is inversely proportional to the power of 6 of the distance between the two nuclei, their proximity can be estimated (this number is not very precise due to the presence of multiple spins and spin diffusion effects). Given the high number of NOEs (several thousands), their assignment and distance evaluation is performed by the structure calculation software itself. Regarding dihedral angles, they can be predicted from the comparison of tripeptide backbone chemical shifts with those from multiple similar triplets issued from a database. These values can also be obtained experimentally, but as this requires additional data collection and analysis, the former method is preferred.

Structures are generated through an energy minimization process and a restraint Molecular Dynamics protocol (rMD). Energies are evaluated using a simplified force field and taking into consideration theoretical constraints (bonds lengths, bond angles, charges...) and combine them with the experimental restraints (NOE distances, dihedral angles...) described before. To avoid getting structures trapped in an irrelevant local minimum, the macromolecule folding is performed under simulated annealing. This means that, at the starting point, the system is brought to high temperatures to allow exploration of the conformational space by an ensemble of random structures. The temperature is then slowly cooled down to fold the molecule accordingly to physical and NMR-derived restraints. As the assignment of many NOE peaks can be ambiguous when the structure is not known due to overlapping resonances, a set composed of the best results from the calculation (that is the conformations which violate the less the constraints) is used to re-assign NOE signals, removing some ambiguities among distance restraints. A new cycle of calculation can then be launched. This iterative process is repeated several times to increase the number of unambiguous constraints. Finally, a water refinement step is performed on the best structures, which combines the simplified rMD field with electrostatics forces which would be engendered by the neighboring water molecules.

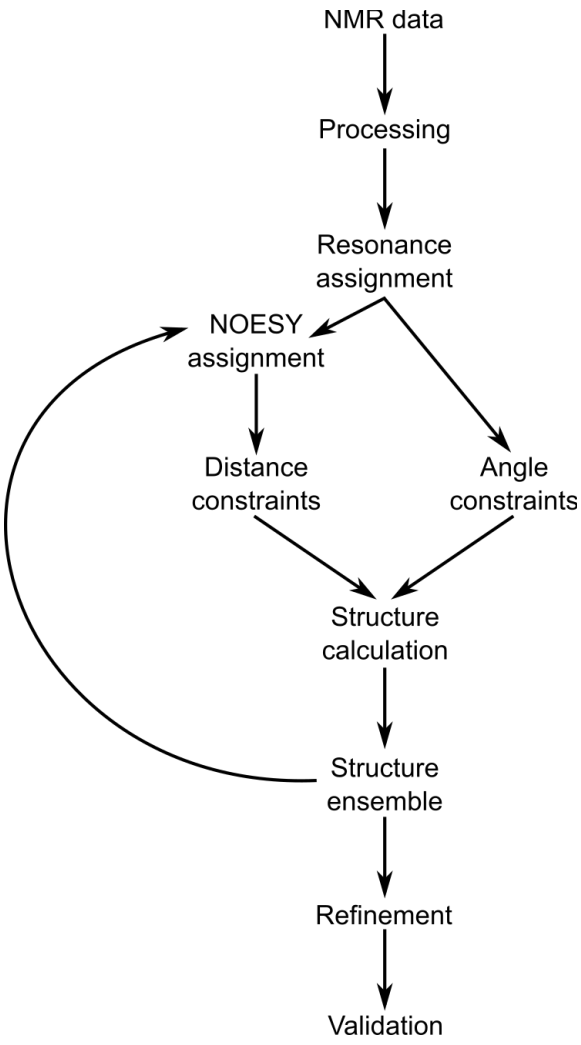

Figure I.5.5: Protocol of structure determination with NMR data. Once the ^{1}H, ^{15}N and ^{13}C nuclei are assigned, dihedral angles and distances can be obtained from the analysis of chemical shifts and assignment of NOESY spectra. These data are extracted by a structure calculation software, which proceeds in an iterative manner to improve at each cycle the NOE assignments and the structure ensembles. The final set of lowest-energy structures is refined in water and can be submitted to the PDB after validation.

Because conformations obtained by NMR are not a direct extraction of the atomic coordinates, but an ensemble of results which respect the inter-atomic distances, their quality cannot be assessed by a "resolution". Instead, the root mean square deviation (r.m.s.d.) is preferred, which is a parameter describing the precision (how the folds are close to each other) but not the accuracy (if the folds are close to the real solution structure). An r.m.s.d lower than 1 Å for the backbone atoms is expected for the final ensemble (usually 20 structures). However, this only concerns rigid parts of the protein. Due to the dynamical motions of flexible regions, no NOE are detected between their atoms (except sometimes intra-residue ones), and thus these regions are not constrained during the calculation, resulting in a high r.m.s.d value due to a poor convergence. To further evaluate the structure ensemble, different software are available to the NMR community to assess the quality of the conformations. These tools check for different physical parameters, such as bond lengths, bond angles, side-chain planarity, as well as the distribution of residues in the Ramachandran plot (which displays residues according to their dihedral angles: φ on abscissa and ψ on ordinate). Figure I.5.6 presents such a plot, with most of the residues in the favored regions (combination of φ and ψ angles commonly found in secondary structures).

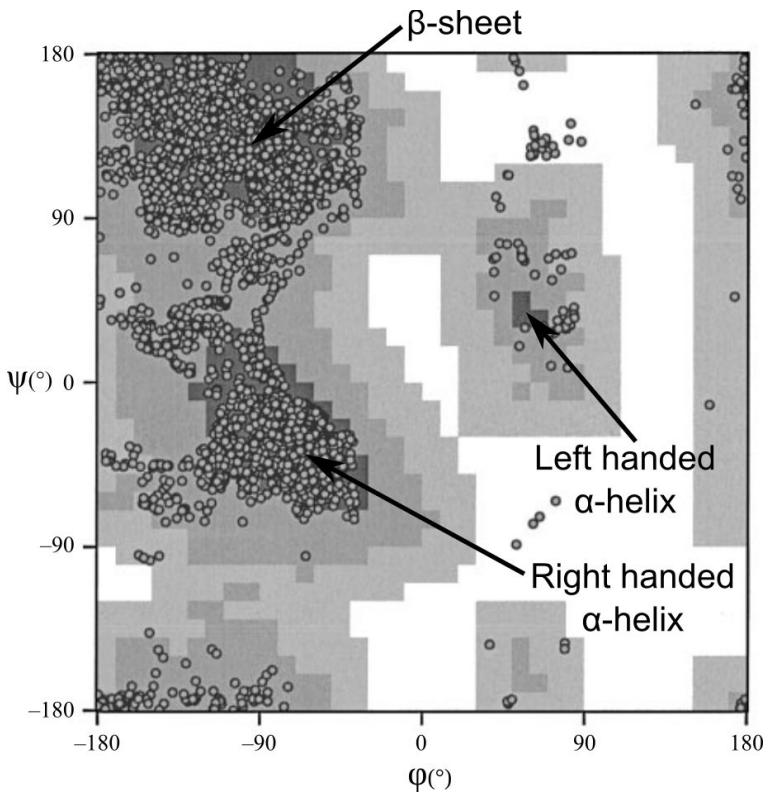

Figure I.5.6: Ramachandran plot of the residues from 20 conformations of the cyclophilin A protein. Each circle represents the φ and ψ dihedral angles of a residue (except glycines). Dark, medium and light gray as well as white areas correspond to most favored, additionally allowed, generously allowed and disallowed regions, respectively. Adapted from Güntert, 1998.

In the context of the bacterial cell wall, several protein structures were reported as solved by liquid-state NMR. NMR can be a powerful technique, in particular when proteins do not crystallize. This is probably the case for the periplasmic domain of TolR, as to date only one structure was published, determined by NMR in 2008 (Parsons et al., 2008). The case of AmpD is an interesting example, as its conformations evidenced by NMR and later by X-ray crystallography display significant variations as can be seen from the superimposition of different structures in Figure I.5.7 (Carrasco-López et al., 2011; Liepinsh et al., 2003). Indeed, four regions around the active site exhibit structural changes, with r.m.s.d. values between the two structures as high as 17 Å for some atoms, leading putatively to the observation of an inactive and active state by NMR and X-ray crystallography, respectively. This interpretation is consolidated by the identification of several inactivating mutations, which are not situated in the active site itself, but instead block the transition between the two forms. A reason could be that crystal packing favored the open conformation, while in solution AmpD adopted its native inactive fold, as the energy barrier between both is expected to be modest. The *in vivo* mechanism allowing switching from the off to the on conformation is currently not known.

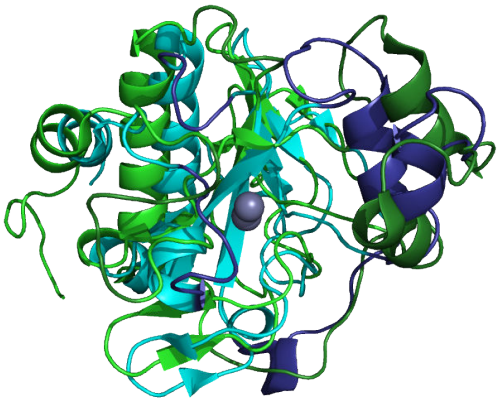

Figure I.5.7: Comparison of *Citrobacter freundii* AmpD structures solved by NMR (green, PDB code 1J3G) and X-ray crystallography (blue, PDB code 2Y2D). Significant structural modification are highlighted in dark green and dark blue on their respective structure (mainly in the right region).

In the case of FtsN, NMR was used to demonstrate that the region preceding the periplasmic C-terminal SPOR domain (separated by a glutamine rich fragment) is disordered (Yang et al., 2004). Indeed, intense peaks with a low ^{1}H dispersion were detected in this region, as emphasized by the $^{1}H,^{15}N$-HSQC spectrum displayed in Figure I.5.8. One of the strengths of the NMR technique is to be able to study further such samples. Analysis of the few NOEs revealed 25 sequential NH_i-NH_{i+1} cross-peaks, but also, more importantly, 5 weak H_i-NH_{i+3} correlations, which are typical of α-helices. The authors therefore were able to conclude on the presence of small transient α-helices (from roughly residues 62 to 67, 80 to 93 and 117 to 123), which were surprisingly in agreement with secondary structure predictions. These helices are likely not trivial, as the $FtsN_{71-105}$ fragment (^{E}ftsN), which is centered on the second helix, was shown to be essential to promote septal peptidoglycan synthesis (Gerding et al., 2009), probably through interaction with (a) divisome partner(s) (Liu et al., 2015; Tsang & Bernhardt, 2015).

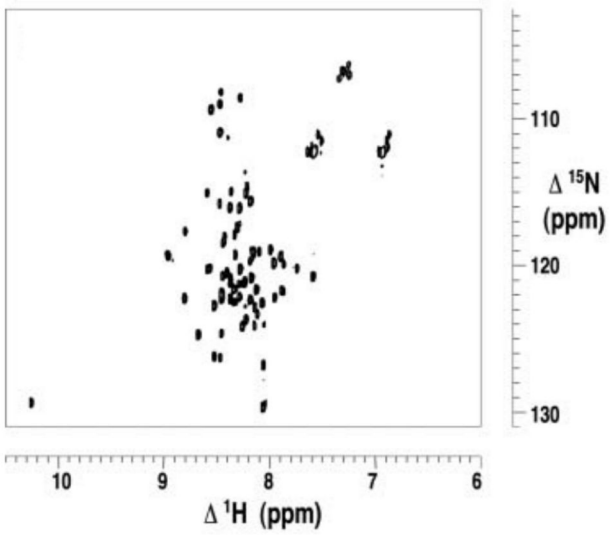

Figure I.5.8: The $^{1}H,^{15}N$-HSQC of the FtsN fragments from residues 58 to 128 represents a disordered region. Taken from Yang et al., 2004.

5.B.c- Protein dynamics

NMR is also a powerful technique for the study of biological macromolecule dynamics, which can give an insight into their flexibility, enzymatic process or transient conformations, for example. This is probably a unique method because it allows such studies at the atomic level on a wide range of time scales. The ps-to-ms internal motions, corresponding to movement of individual inter-nuclear vectors and global molecular rotation of the molecule, as well as correlated motions of disordered regions and loops on larger time scales, can be measured by relaxation experiments through the study of three parameters for each amide groups: the longitudinal and transverse relaxation R_1 and R_2, respectively, and the $\{^1H\}$-^{15}N heteronuclear NOE. Briefly, R_1 is related to the rate at which the excited spins come back to equilibrium along the spectrometer magnetic field and is representative of fast motions (ps-to-ns), while R_2 measures the rate at which the spin coherence is lost (the rate of loss of the common phase with time) in a perpendicular plane to the magnetic field, which correlates with fast motions (ps-to-ns) but also to slower dynamics (up to the ms) due to the contribution of chemical exchange processes. As for $\{^1H\}$-^{15}N heteronuclear NOE, it determines the NOE between the amide proton and its neighboring nitrogen atom, which is mainly sensitive to very fast motions (ps). These data are generally combined to evaluate the correlation time of the molecule τ_c (the time necessary for the protein to reorient by one radian, which is inversely proportional to the molecular tumbling rate) and the local order parameter relative to the reorientation of each H-N vector.

Relaxation studies of the C-terminal domain of TolA (TolAIII), showed for example an unusual high flexibility for loop residues 30 to 39 (and for the N-terminal end) compared to the rest of the protein (figure I.5.9; Deprez et al., 2005). Based on a different conformation observed for this domain when bound to the bacteriophage protein g3p (the Tol-Pal system is hijacked through this interaction by viruses to allow their entry in the bacterial cell), the authors were able to postulate that this flexible loop was the structural element allowing re-positioning of the impacted α-helix.

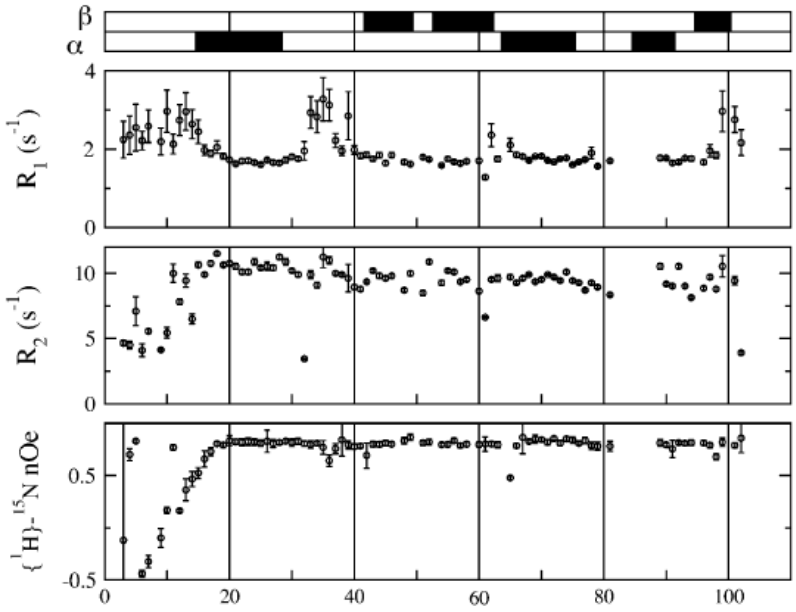

Figure I.5.9: Dynamics study of TolAIII domain based on relaxation measurements. The top panel shows the protein secondary structure. The three graphs below represents the R_1, R_2 and $\{^1H\}$-^{15}N heteronuclear NOE values respectively measured for the amides along the sequence. Variations observed indicates local flexibility at the approximately 17 N-terminal residues (R_2 and $\{^1H\}$-^{15}N heteronuclear NOE drastically decrease) and between residues 30 and 40 (R_1). The discrepancies between the three graphs demonstrate dynamics at different time-scales. Taken from Deprez et al., 2005.

In another study, relaxation data were used to demonstrate that α-helix 3 of the DamX septal peptidoglycan-binding SPOR domain is quite mobile (Williams et al., 2013). As no structure of its complex with peptidoglycan is known, it was hypothesized that α-helix 3 could be implicated in a regulation mechanism and that its motion would be required for the domain to bind peptidoglycan. These relaxation data also enabled calculation of DamX correlation time and demonstrated the monomeric state of the protein, in agreement with dynamic light scattering data.

Another possibility offered by NMR is to specifically study the chemical exchange contribution, to extract more specific information on conformational changes. In the case of a protein undergoing interconversion between two states, different NMR signals can be observed in the spectra depending on the speed of the transition. This phenomenon is called chemical exchange and is illustrated in Figure I.5.10 with one nucleus switching between two states. If the exchange is slow (meaning that the exchange rate k is much slower than the frequency difference between both nuclei conformations), peaks for both nuclei states will be found. Conversely, in a fast exchange regime (when the exchange rate k is much faster than the frequency difference), only one signal at a population-weighted chemical shift is recorded (an “average” state is therefore observed). Finally, if both values are similar (intermediate exchange), the peaks broaden and lose intensity, and can become undetectable.

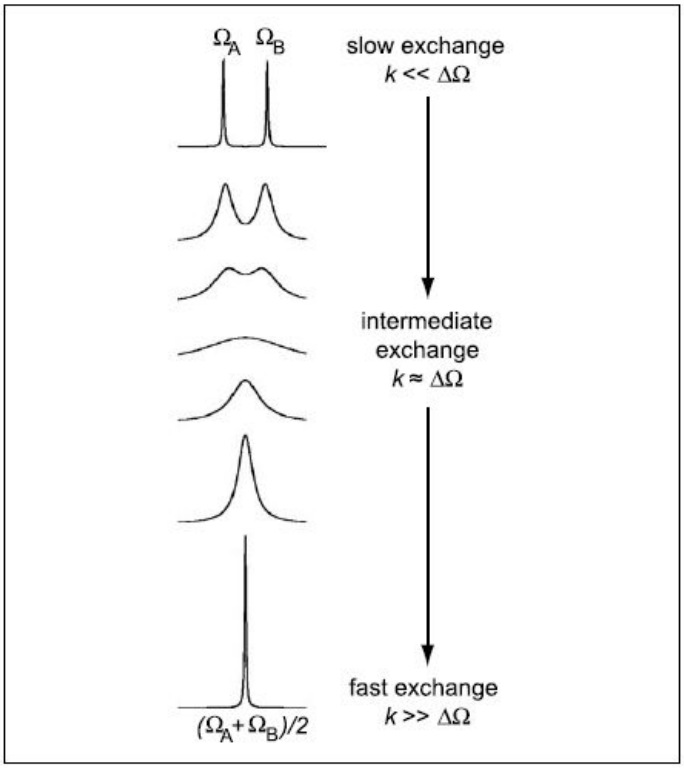

Figure 1.5.10: 1D spectrum for a single nucleus undergoing chemical exchange between two states, at various exchange rates. ΔΩ: chemical shift (or frequency) difference between the two states. Taken from Breukels et al., 2011.

Interestingly, the acylenzyme generated by reaction between *B. subtilis* Ldt (Ldt_{Bs}) and imipenem antibiotics or Ellman's DTNB reagent 5,5'-dithiobis-(2-nitrobenzoic acid) has some signals which exhibit a decreased intensity compared to the apoenzyme, as shown in figure I.5.11 (Lecoq et al., 2012). This observation is the result of an intermediate exchange, this region undergoing conformational dynamics in the ms time-scale range.

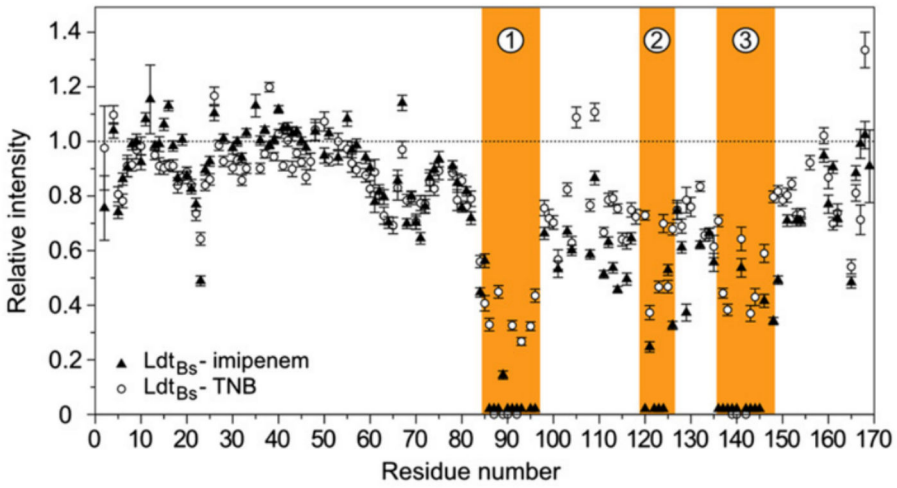

Figure I.5.11: ^{1}H,^{15}N-HSQC peak intensity for the acylenzyme formed by reaction of *Bacillus subtilis* Ldt and imipenem or DTNB relative to the apoenzyme. The three orange regions, which are around the binding site, present a significant intensity decrease manifesting conformational exchange. Taken from Lecoq et al., 2012.

In addition to these two examples (relaxation data and chemical exchange), macromolecular dynamics can be studied by NMR in an extensive number of other ways, which will not be detailed here but can been found summarized in Kleckner & Foster, 2011.

5.B.d- Interaction studies

Liquid-state NMR can also be employed for the study of interactions (involving proteins, nucleic acids, sugars, small ligands...) and complexes. One of its advantage is to be able to carry on experiments even on weakly interacting samples (with a K_d in the mM range).

One of the simplest and direct way to perform such investigations is to accomplish Chemical Shit Perturbations (CSP) experiments. For this, a non-labeled partner is added in several aliquots (if enough quantity is available) to the labeled sample, and spectra, generally ^{1}H,^{15}N- HSQCs, are recorded after each ligand addition. If there is an interaction, the labeled macromolecule nuclei implicated in the binding site will have a different local environment than in the absence of the partner, resulting in shifted signals. However, the sample switching between an unbound and a bound state, the same chemical exchange as for dynamical conformations can also be observed. If this is a fast exchange, one shifted peak is indeed visualized. Upon successive addition of the ligand, this peak will be seen moving linearly in a direction until saturation. Determination of the residues involved in the reaction will be simple, as the assignment can be easily transferred from the initially unbound form. In other cases, identification of these residues can be more tricky. In a slow exchange regime, two peaks would be detected: one for each state. Assignment of the interacting residues may therefore not be straightforward. Finally, if there is an intermediate exchange, the peak will shift and lose intensity at the same time due to broadening, and may re-appear further after sufficient addition of ligand. Figure I.5.12 sums up all of these possible perturbations, which can be met during a CSP experiment. Note that depending on the residues, different chemical exchange regimes can be observed for a same binding assay. Such experiments can be performed to pursue protein-protein interaction studies, but peptidoglycan fragments, muropeptides or even sacculi can be used as the unlabeled partner. However, in the latter case, the molecular weight is so large that the bound state will not be observed (this form will behave as a huge macromolecule, and thus its signals will broaden beyond detection). If the exchange regime is fast, this would lead in the disappearance of the spectrum after addition of the sacculi.

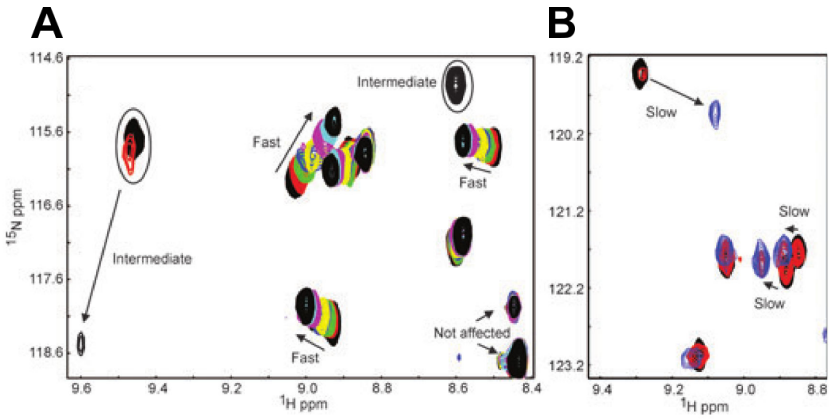

Figure I.5.12: Chemical Shift Perturbations to probe interactions. Two sets of $^{1}H,^{15}N$-HSQC spectra (8 in A, 3 in B) recorded upon interaction between a ^{15}N-labeled protein and a small unlabeled oligosaccharide are represented. (A) Upon addition of the ligand, fast and intermediate exchange are observed, the former being characterized by shift of the peak, while in the second case the peak loses intensity, disappears and may reappear after further ligand additions (as the one at the extreme left). Signals are not affected, as in the bottom right corner of the spectrum, when the nuclei are not in a region implicated in the interaction or undergoing conformational change. From background to foreground, spectra are recorded first in the absence and then in the presence of more and more ligand. (B) Addition of oligosaccharide reveals a slow exchange regime for most of the peaks affected: the signals do not shift but instead can be found at two chemical shift values. This is particularly visible for the two indicated resonances in the middle, where each can been seen as two peaks in the red spectrum. Black: no ligand, red: ligand:protein ratio of 0.5:1, blue: saturation of the protein by the ligand. Taken from Bieri et al., 2011.

Once the residues perturbed by the interaction are determined, the K_d of the interaction can sometimes be calculated by plotting their shifts or intensity variations as a function of the ligand concentration. Due to the sensitivity of NMR, K_d can be correctly determined in the range of few µM to hundred of mM. CSPs can also be mapped on the structure to identify the binding site. However, one must be cautious as the perturbed signals can also result from conformational rearrangements occurring upon interaction. Once significant chemical shift perturbations are established, they can be used as ambiguous restraints for a data-driven docking of the two (or more) partners. Such a calculation can be performed by a software like HADDOCK (High Ambiguity Driven protein-protein DOCKing, van Zundert et al., 2015), which can allow moving of some backbone regions and side chains to favor an interaction model respecting the ambiguous constraints. In addition to CSPs, a wide range of other results can be used as restraints, such as mutagenesis data.

The NMR study of a mixture of labeled ZipA and unlabeled FtsZ C-terminal peptide (Moy et al., 2000) enabled for example to confirm the interaction, through the detection of CSPs in $^{1}H,^{15}N$-HSQC (figure 1.5.13). Mapping of the perturbed residues allowed identification of the ZipA interaction region, a hydrophobic pocket at the surface of its β-sheet.

Recently, Triboulet and coworkers tried to determine which pocket among two binds the muropeptide acceptor for transpeptidation in *Enterococcus faecium* Ldt (Triboulet et al., 2015). The authors began by saturating the donor binding site with the ertapenem antibiotics before adding muropeptides, which therefore could only bind to the acceptor site. Determination of the CSPs and their mapping on the Ldt_{fm} structure showed that most of the impacted residues were found in the neighborhood of pocket 2 (figure I.5.14). Finally, a model calculated by HADDOCK with significant CSPs (twice or more than the standard deviation) was obtained (figure I.5.15), confirming that the acceptor binds to pocket 2 and not in the same pocket than the donor in contradiction with initial proposals suggesting that the

two peptide stems would have to bind the same one to be cross-linked.

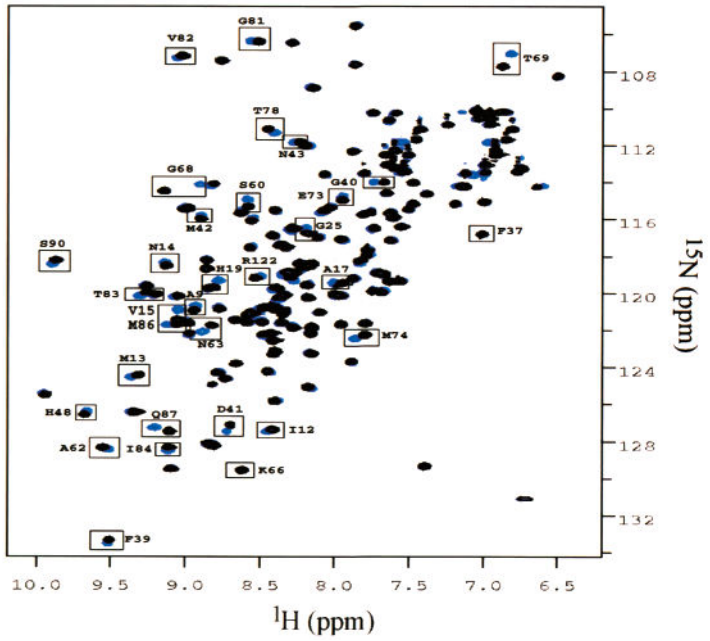

Figure I.5.13: ^{1}H-^{15}N HSQC spectra superimposition of ^{1}H, ^{15}N, ^{13}C ZipA$_{185-328}$ (black) and ^{1}H, ^{15}N, ^{13}C ZipA$_{185-328}$ interacting with FtsZ C-terminal peptide (blue). The resonances shifting upon interaction are boxed. Taken from Moy et al., 2000.

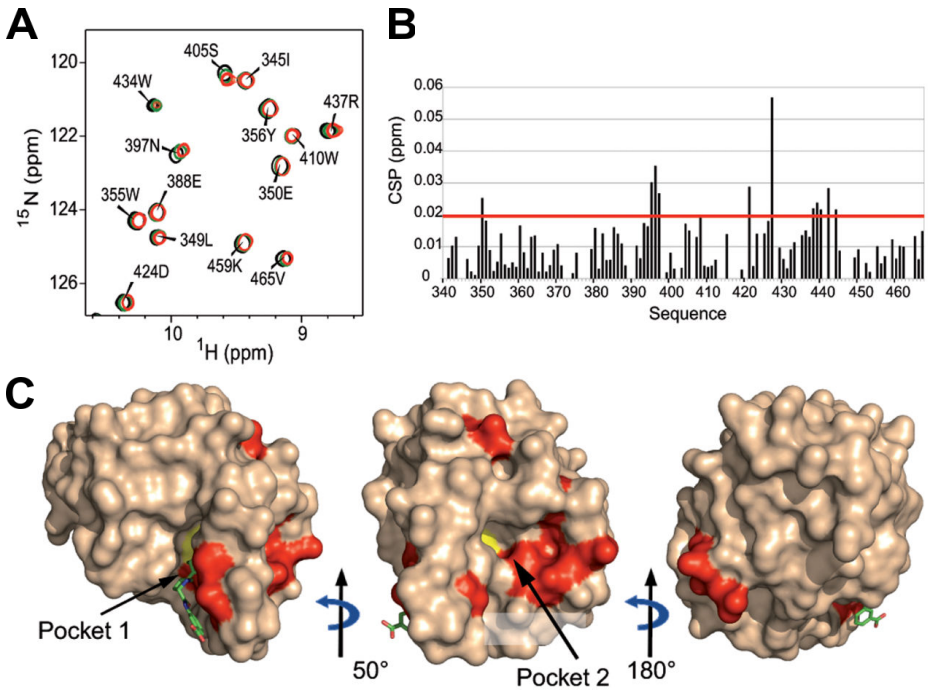

Figure 1.5.14: Structural characterization of the interaction between *Enterococcus faecium* Ldt and muropeptides. (A) The Chemical Shift Perturbation experiment shows a few residues undergoing shifts after several addition of muropeptides (black: no muropeptide, green and red: 25- and 300-fold muropeptide excess, respectively). Only a part of the full ^{1}H,^{15}N-HSQC spectrum is displayed. (B) Histogram of all of the CSPs observed with a 300-fold excess of muropeptides. Only the values above the two standard deviations threshold (red line) were considered as significant. (C) Mapping of the significantly perturbed residues (red) on the surface structure of *E. faecium* Ldt. The yellow amino-acid is the catalytic cysteine, while the ligand in pocket 1 is the ertapenem. Most of the perturbations are found on the other side, around pocket 2. Taken from Triboulet et al., 2015.

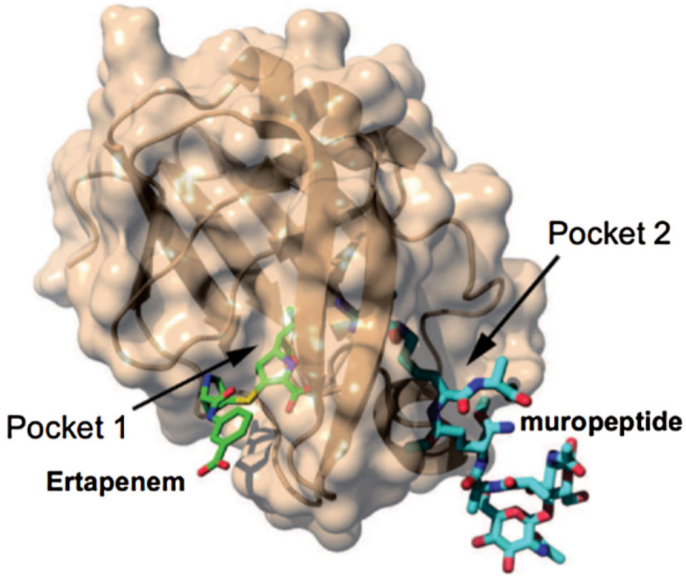

Figure I.5.15: Lowest energy docking model of the *E. faecium* Ldt acylenzyme-muropeptide (disaccharide-tetrapeptide). This model was obtained with HADDOCK, using the most significant CSPs (see figure 1.5.14) as ambiguous restraints. Taken from Triboulet et al., 2015.

Interactions can also be determined and studied extensively by other NMR methods, such as Paramagnetic Relaxation Enhancement (PRE), where a paramagnetic probe is inserted in one of the two macromolecules, leading to a broadening (or even disappearance) of the peaks from residues of the other partner that come in the vicinity of the labeled region. Saturation-Transfer Difference NMR can be used for the screening of drugs by observing ligand signal perturbations, when the spins of the protein partner are saturated, in cases when there is binding. Structure of the complex can also be elucidated by the collection of inter-molecular NOEs. A more detailed insight into these strategies, as well as CSP and other NMR methods for interaction studies can been found in O'Connell et al., 2009.

For further information on liquid-state NMR, the following reviews and book chapters are recommended to the reader: Bieri et al., 2011; Breukels et al., 2011; Kwan et al., 2011; Chou & Sounier, 2013; Marion, 2013. The book from Cavanagh et al. is also suited for a complete detailed explanation of NMR theory and its applications for the study of proteins (Cavanagh et al., 2007).

5.C- Peptidoglycan characterization by solid-state NMR

On the contrary to liquid-state NMR, solid-state NMR is not dependent on the molecular weight of the macromolecule and is able to work with non-solubilized samples. As a consequence, this rising technique suits well for the study of protein aggregates, membrane proteins, big assemblies or biopolymers (detailed example of solid-state NMR applications are discussed in Goldbourt, 2013). Because signals for such species would be too broad for analysis due to their slow molecular tumbling and because of the presence of anisotropic interactions that are not averaged to zero, NMR samples must be spun at high frequency (above 5000 Hz) in a rotor tilted at a particular angle ($\theta = 54.74°$, which corresponds to the cancellation of the 3 $\cos^2\theta$ -1 function responsible for the internuclear dipolar interactions) from the spectrometer magnetic field (figure I.5.16). This method is called Magic-Angle Spinning and is required for the collection of good quality spectra in solid-state NMR (although the resolution is generally lower than in liquid-state NMR). The strategy is then similar to solution studies, ^{13}C and/or ^{15}N labeled sample are required to record multidimensional spectra (to avoid signal overlapping) and assign resonances. Because the

experiments are not based exactly on the same type of transfer, their names differ, but they also show nucleus correlations. However, in solid-state NMR, as proton resonances are less well resolved at standard spin rates, most of the experiments are rather based on ^{13}C, ^{15}N or ^{31}P nuclei. The review from Müller et al. is recommended for a detailed presentation of biomolecular solid-state-NMR (Müller et al., 2013).

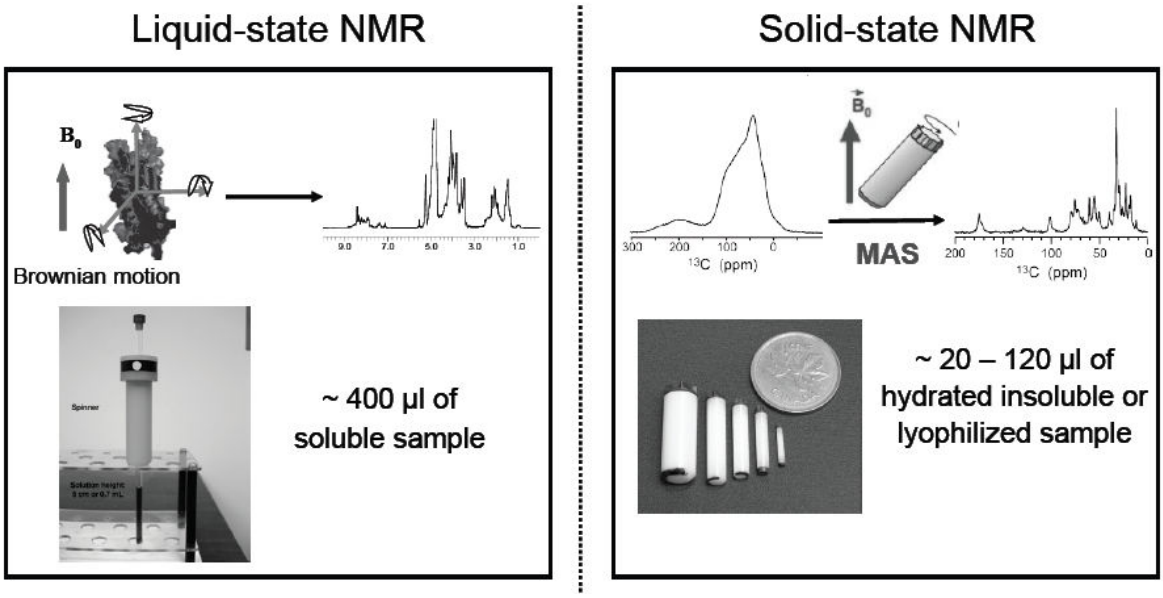

Figure I.5.16: Main differences in liquid and solid-state NMR. While in liquid-state high detection of the well-resolved resonance peaks is possible because of the Brownian motions (fast molecular tumbling) in the sample in solution, the species of interest in solid-state must be rotated at high frequency (several MHz) in a rotor (white elements bellow the coin) to obtain a spectrum of similar resolution. Taken from Bougault et al., 2012.

Due to their high molecular weight, sacculi and whole bacterial cell walls (which also contains wall teichoic acids in Gram-positive bacteria or lipopolysaccharides in Gram-negative bacteria for example) cannot be studied by liquid-state NMR. However, in solid-state, multiple analyzes can be performed to determine peptidoglycan composition, the percentage of cross-links, the average value of the peptide chain length, as well as peptidoglycan dynamics or its interactions with proteins. Although not described here, this technique can also be used to work with other cell wall components, such as wall teichoic acids and to study their relationship with peptidoglycan (Bougault et al., 2012).

5.C.a- Peptidoglycan composition

Composition of peptidoglycan sacculi can be directly studied by ^{13}C 1D spectra or through-bond ^{13}C-^{13}C correlation spectra. For example, chemical modifications can be assessed by solid-state NMR. Indeed, such variations are indirectly observable, because they will cause a modification of the local environment of some of the carbon (and/or nitrogen) atoms detected. This will result in the appearance of two or more peaks for a same assigned nucleus, each one resulting from a different situation. For example, in *E. faecium*, specific ^{15}N-labeling of the peptidoglycan L-Lys ε-nitrogen (figure I.5.17) showed three peaks in a 1D ^{15}N-CPMAS (Cross-Polarization Magic-Angle Spinning) echo spectrum (Patti, Chen, Schaefer, & Gross, 2008). These peaks represent the free amine side chain, the ε-nitrogen bound to a D-Asp/D-Asn (a structural feature of *E. faecium* peptidoglycan is to contain a Lys-Asp/Asn bridge), and its modification to lysyl succinimide (otherwise confirmed by mass spectrometry).

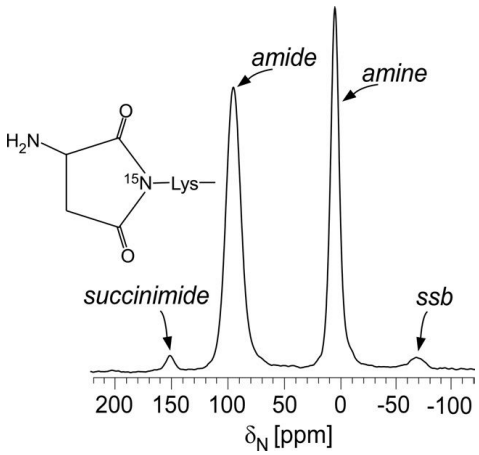

Figure I.5.17: 1D ^{15}N-CPMAS echo-spectrum of a specific ^{15}N L-Lys labeled intact cell wall sample from *E. faecium*. As only the lysine from the peptidoglycan peptide stem is detected, these three signals report directly on modifications on this residue. At 5 ppm is the amine form, when the lysine is not involved in a bridge, while at 95 ppm this residue is engaged in a bridge via an amide group. The small peak at 151 ppm is expected to be lysyl-succinimides. Taken from Patti et al., 2008.

Similarly, the rate of bridge- or cross-links can also be evaluated by specifically labeling the third position residue. In a study in *B. subtilis* for example, Shenouda et al. showed by solid-state NMR that 62% of the peptide stems were cross-linked by comparison of the amide and amine peak integrations in a 1D ^{15}N-CPMAS spectrum (Shenouda et al., 1996). The same experiment performed on peptidoglycan from cells exposed to cephalothin antibiotics allowed direct evaluation of its effect on the biopolymer, showing a decrease in cross-links to 52%. Solid-state NMR therefore appears as a promising technique to probe chemical modifications under various stress conditions (antibiotics, gene deletion, environmental stress...). Comparison of sacculi from various species (*E. coli*, *B. subtilis* and *S. aureus*) was performed by 2D through-bond ^{13}C-^{13}C correlations experiments (Kern et al., 2010). As expected from their similar composition, few differences were observed, which were the result of some known chemical variations (presence of a pentaglycine bridge for *S. aureus*, additional peaks for *B. subtilis m*-A_2pm due to their amidation...). This agrees with the postulate that at the local scale, peptidoglycan structure is highly similar across bacterial species. However, it must be noted that this does not provide information on the general peptidoglycan architecture (such as glycan lengths and 3D structure).

5.C.b- Peptidoglycan dynamics

In a similar manner to liquid-state NMR, sample dynamics can also be studied. Such experiments can enable the investigation of the rigidity of peptidoglycan in regard of its arrangement. Indeed, although they give shape to the cell, hydrated cell walls were shown to be quite flexible. Proton-driven spin diffusion (PDSD) experiments, which determine if neighbored nuclei remained in contact for a long time or not and therefore describes flexibility, indicated that peptide stems display more flexibility than glycan chains (Kern et al., 2008). Another study from Kern and coworkers compared for example peptidoglycan flexibility in hydrated cell walls between the Gram-negative *E. coli* and the Gram-positive *B. subtilis* and *S. aureus* species by measuring longitudinal relaxation time-constant T_1 ($T_1 = 1/R_1$) values (Kern et al., 2010). The results show that, whatever the selected resonances (from the polysaccharide or the peptide stems), peptidoglycan rigidity always ranges in the order *E. coli* (higher dynamics) < *B. subtilis* < *S. aureus* (lower dynamics). Interestingly, peptidoglycan cross-linking rate ranks in the same order for these three species, which suggests that this has a strong role in peptidoglycan dynamics despite the presence of local flexible elements, such as pentaglycine bridges in *S. aureus*. Such studies could help in understanding the dynamics

of the cell wall and identify the situations where dynamics is affected, such as in the case of interactions.

5.C.c- Protein-sacculi interactions

Solid-state NMR being able to focus on sacculi, it is then possible to analyze how this polymer interacts with proteins, an information that is hard to obtain directly by other methods, especially at the atomic level. This approach has also the advantage to allow studying of the binding events in an architecture that is closer to the *in vivo* environment. Furthermore, it can be essential if partners do not recognize small peptidoglycan fragments while they do interact with the complete sacculus. To date, little work has been reported in the literature on sacculi-protein interactions by solid-state NMR. This is probably due to the tight association required to visualize an effect on the several mg of peptidoglycan and to the small chemical shifts perturbations generally observed, which makes its characterization even more difficult. In 2014, Schanda et al. managed to determine the first intact peptidoglycan-protein structural complex (Schanda et al., 2014). CSPs on labeled *B. subtilis* Ldt (Ldt_{Bs}) bound to unlabeled hydrated sacculi were obtained by solid-state NMR and analyzed (in solution, the interaction would lead to disappearance of the protein resonances, as the protein would acquire the solid-like behavior of its partner, preventing complex characterization). The most significant CSPs were used as ambiguous restraints in the HADDOCK docking software, using the Ldt_{Bs} structure and *in silico* generated hexasaccharide-tetrapeptide fragments. In the best model ensemble obtained, the glycan chain is expected to bind in the groove between the Ldt_{Bs} catalytic and the saccharide-binding LysM domains (figure I.5.18). This proposal was strengthened by the determination that a mutation (blue residues in figure I.5.18) on either side of the groove weakens the interaction. Dynamics behavior of peptidoglycan was also investigated, by the measure of dipolar couplings (spin interactions with their close neighbors) and T_1 values. These experiments evidenced an increase in the rigidity of the glycan chain upon addition of Ldt_{Bs}, while no differences were detected in the peptide region. These results are consistent with the predicted tight interaction between the glycan strands and the protein. An interesting observation is that dynamics data also suggest that binding of Ldt_{Bs} proteins caused a general stiffness of sacculi, not only on the glycan chain where it binds but also on the other regions. Characterization of more sacculi-protein interactions by solid-state NMR could improve in the future our knowledge about each protein peptidoglycan recognition pattern and help to determine at the atomic level why some proteins do bind sacculi, while they do not interact strongly enough with murein fragments.

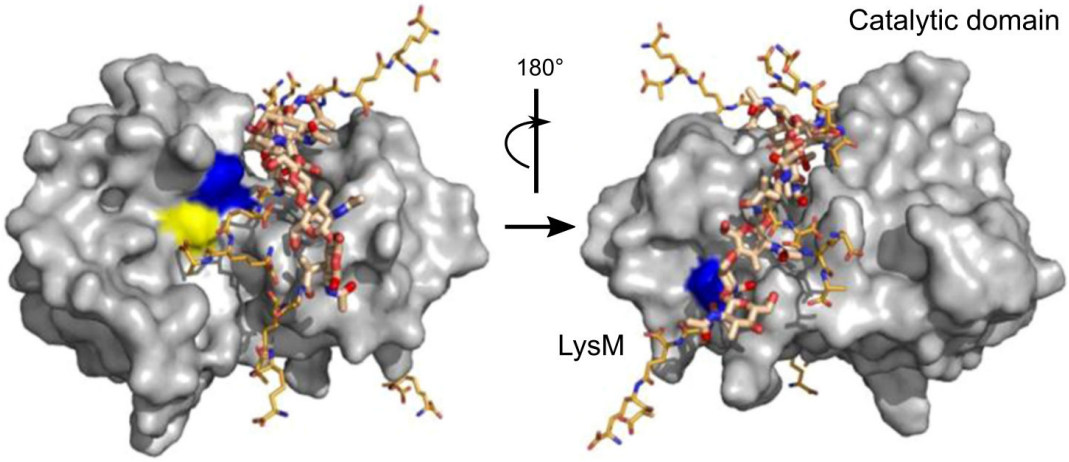

Figure I.5.18: Lowest-energy model generated by HADDOCK for the Ldt_{Bs}-peptidoglycan (hexasaccharide-tetrapeptide fragment) complex. The residues later mutated to prove their implication in the interaction (Val 47 and His 122) are colored in blue while the catalytic cysteine is in yellow. Taken from Schanda et al., 2014.

To conclude, NMR appears as a versatile technique that can yield crucial structural information on proteins implicated in the synthesis or maturation of the peptidoglycan, but that also allow monitoring of protein-protein, as well as protein-peptidoglycan interactions and deciphering of relative binding affinities and geometries.

Résumé en français du chapitre 5 : La RMN en tant que technique pour l'étude du peptidoglycane et des protéines associées

L'étude du peptidoglycane et des protéines qui y sont associées est essentielle d'un point de vue fondamental pour comprendre la complexité de la cellule bactérienne et d'un point de vue appliqué pour le design de nouveaux antibiotiques. La biologie structurale est un domaine à la frontière de la biologie et de la physique qui s'intéresse à l'arrangement tri-dimensionnel des atomes constituant les biomolécules et leur complexes macromoléculaires. Les deux principales techniques utilisées pour la détermination de structure à haute-résolution sont la cristallographie aux rayons X sans aucun doute la technique la plus prolifique, qui nécessite un monocristal fait d'un arrangement régulier d'une conformation donnée de la protéine étudiée, et la Résonance Magnétique Nucléaire (RMN), qui repose sur les propriétés magnétiques des noyaux présents dans l'échantillon biologique, qu'il soit en solution ou en phase solide. Les résultats obtenus par ces méthodes peuvent être combinés à des techniques de plus basse résolution, telles que la diffusion de rayons X ou de neutrons aux petits angles (SAXS et SANS respectivement), qui peuvent permettre la détermination d'une enveloppe pour la molécule ou le complexe étudié(e). A la frontière entre les approches haute et basse résolution se trouve la cryo-microscopie électronique, dont les récents développements techniques lui permettent d'atteindre des résolutions de l'ordre de 4-5 Å. Afin de répondre à des questions biologiques complexes, les données acquises par ces diverses techniques sont de plus en plus analysées conjointement, avec parfois l'appui d'autres méthodes biophysiques expérimentales telles que la résonance plasmonique de surface, la spectrométrie de masse, l'ultracentrifugation analytique, la microscopie à force atomique ou super-resolution, et avec l'aide de simulations sur ordinateur.

La RMN se base sur un paramètre intrinsèque à chaque noyau appelé spin, qui reflète ses propriétés dans un champ magnétique. Dans le cas d'isotopes à spin non nul, ^{1}H, ^{13}C, ^{15}N par exemple, les noyaux se comportent comme des boussoles avec des orientations spécifiques par rapport à ce champ. Une énergie peut être associée à chaque orientation, et les transitions entre ces différents niveaux d'énergie peuvent être déterminés par spectroscopie. Pour ce faire, une impulsion radio-fréquence judicieusement choisie (fréquence de Larmor) change la répartition de la population des divers niveaux d'énergie par rapport à la répartition à l'équilibre. Le retour à la distribution d'équilibre produit un signal radio-fréquence à la fréquence correspondant à la différence d'énergie entre l'état excité et l'état fondamental. Chaque noyau ressentant un champ B_0 (le champ magnétique statique) différent à cause d'effets de blindage par les électrons voisins, chaque noyau aura une fréquence spécifique dépendant de son environnement local. Le signal est alors détecté par une bobine, puis traité via une transformée de Fourier. Les fréquences des différents noyaux sont alors représentées, sous la forme d'un spectre 1D, suivant l'axe x, les intensités étant reportées sur l'axe y. Afin de s'affranchir du champ magnétique duquel elles dépendent, les fréquences de résonance sont exprimées préférablement sous la forme de déplacement chimique, en ppm. L'intensité du signal quant à elle est liée aux différences de population entre les divers états d'énergie et leur évolution temporelle, notamment vis-à-vis du retour à l'équilibre, autrement appelé relaxation. Ce dernier phénomène résulte de la réorientation des spins par rapport au champ B_0 après impulsion, suivant les mouvements browniens et la flexibilité moléculaire locale. Dans le cas

d'une relaxation rapide, par exemple pour des oligomères ou échantillons à haut poids moléculaire, les pics vont s'élargir et perdre en intensité, causant une perte de résolution dans le spectre 1D. C'est pourquoi la RMN est limitée à des macromolécules de 40 kDa ou moins, bien que d'autres stratégies peuvent permettre des études au-delà de cette valeur (RMN du solide, marquage spécifique des méthyles,...). Afin d'obtenir l'information atomique renfermée par chaque pic, l'identification de l'atome à l'origine de la résonance est nécessaire. Cette étape est appelée attribution des résonances RMN. Les spectres 1D étant largement dégénérés à cause du recouvrement de plusieurs résonances, l'aimantation est transférée à d'autres noyaux, permettant de passer à des spectres 2D et 3D corrélant 2 et 3 noyaux respectivement (^{1}H, ^{15}N et/ou ^{13}C généralement), où la diminution de la superposition des signaux favorise leur attribution. Cette approche demande toutefois un échantillon marqué isotopiquement ^{15}N et/ou ^{13}C. Pour la préparation de tels échantillons, les bactéries surexprimant la molécule d'intérêt sont cultivées en milieu minimum M9 avec des sources d'azote et/ou de carbone marquées et parfaitement contrôlées. Les quantités de protéines produites puis purifiées doivent être relativement conséquentes pour permettre une étude structurale, à savoir 130 à 450 µL d'échantillon (suivant le tube utilisé) à une concentration typique d'au moins 500 mM. De plus, afin de limiter la détection de résonances autre que celles de la macromolécule d'intérêt, une pureté élevée est requise. La qualité de l'échantillon est vérifiée par l'acquisition d'un spectre 2D ^{1}H,^{15}N-HSQC, où chaque résonance correspond à une corrélation entre un noyau ^{1}H et un noyau ^{15}N liés covalemment, issus majoritairement des groupes amide du squelette protéique. Ce spectre a la particularité de procurer une « signature » de la biomolécule étudiée. En effet, d'après la distribution des pics suivant les déplacements chimiques en protons, un œil averti saura reconnaître une protéine repliée d'une protéine dépliée, et la présence d'un type particulier de structures secondaires pourra également être suggéré.

La RMN du liquide étant fortement dépendante de la masse moléculaire de la macromolécule étudiée, elle n'est pas adaptée à l'étude de sacculi. Elle peut se révéler par contre fort utile pour la détermination de la structure et de la dynamique de protéines impliquées dans sa biosynthèse, maturation ou recyclage par exemple. Elle peut par ailleurs permettre d'identifier la zone et la force des interactions inter-protéiques ou protéine/peptidoglycane. Afin de résoudre une structure atomique, l'attribution des noyaux de la chaîne principale et des chaînes latérales est requise. Pour cela, divers couples de spectres sont enregistrés. Dans le binôme HNCACB HN(CO)CACB par exemple, un spectre connecte les groupe amides N_iH_i aux carbones α et β du résidu précédent (i-1) (HNCOCACB). L'autre spectre présente des groupes amides N_jH_j corrélés aux carbones α et β des résidus j et j-1 (HNCACB). Le but est alors de retrouver par l'analyse conjointe de ce binôme de spectres, quel atome j correspond à i-1 afin de connecter entre eux des résidus voisins et de remonter peu à peu dans la séquence. A partir de ces attributions, les déplacements chimiques peuvent alors être utilisés pour déterminer la nature et la localisation des structures secondaires. Afin de déterminer la structure d'une protéine attribuée, deux types de contraintes, dérivées des données RMN doivent être incorporées dans le protocole de calcul : les distances protons-protons et les angles dièdres. Les premières sont évaluées à partir des spectres NOESY, où les signaux NOE sont détectés uniquement entre protons proches dans l'espace (moins de 5 Å). Le volume de ces pics étant inversement proportionnel à la distance entre les noyaux à la puissance 6, des contraintes de distances peuvent en être extraites. Quant aux angles dièdres, ils sont prédits par comparaison avec ceux d'atomes, situés au sein de tripeptides de protéines de structures connues, dont les déplacements chimiques sont similaires. A partir de ces contraintes expérimentales et d'autres contraintes physiques, les structures sont générées par un protocole de dynamique moléculaire sous contrainte. Afin d'éviter de rester piégé dans un minimum local, le repliement suit une stratégie de recuit simulé, où le système est amené à des températures élevées avant de refroidir peu à peu. Après plusieurs cycles de recuit simulé et d'amélioration de l'attribution des NOE à partir des conformations intermédiaires obtenues,

une étape d'affinement dans l'eau est réalisée sur les structures de plus basse énergie, celles dont les contraintes sont les moins violées. L'ensemble structural calculé est ensuite validé, sur la base du respect de divers paramètres physiques et du r.m.s.d., qui atteste de la précision de la conformation. Cest selon un protocole similaire que fut déterminé une des structures de l'amidase cyoplasmique AmpD, qui révèle un état différent de celui proposé à partir de la structure cristallographique. Dans le cas de FtsN, la RMN du liquide a permis de mettre en évidence la présence d'hélices α transitoires dans une région cytoplasmique désordonnée essentielle.

La RMN est également une technique puissante pour l'étude de la dynamique moléculaire, sur une large échelle de temps. Par exemple, les mouvements de la ps à la ms peuvent être mesurés par des expériences de relaxation à travers l'étude de 3 paramètres pour chaque groupement amide d'une protéine : les relaxations longitudinale R1 et transversale R2, correspondant respectivement au temps de retour du signal à l'équilibre le long du champ magnétique B_0 et de perte de cohérence, et les NOE hétéronucléaires $\{^{1}H\}$-^{15}N. Dans le cas du domaine SPOR de la protéine DamX, l'étude de sa dynamique a par exemple permis de mettre en évidence la mobilité d'une hélice α empêchant sa liaison au peptidoglyane. Il fut alors suggéré que cette structure secondaire, qui dans certaines situations pourrait être déplacée afin de permettre l'interaction, pourrait être un mécanisme de régulation. La RMN peut également mettre en lumière une interconversion entre deux états (échange conformationnel), ce qui se traduit par la présence de deux pics distincts ou d'un déplacement chimique à une valeurs moyenne de chacune des deux formes correspondantes, selon que la constante de vitesse d'échange entre les deux conformations k est bien inférieure ou bien supérieure à la différence de déplacement chimique entre ces deux états. Dans le cas où ces deux valeurs sont similaires, le pic s'élargit et perd en intensité, jusqu'à parfois disparaître comme observé par exemple dans le cas de la Ldt de *Bacillus subtilis* lorsqu'elle est inhibée par l'imipénème.

Enfin, l'une des autre applications de la RMN du liquide est l'étude d'interactions, étude qui peut être menée même dans des cas où le Kd atteint le mM. L'une des méthodes les plus directes est de réaliser des expériences de perturbation de déplacements chimiques (CSP) où le ligand non marqué est rajouté peu à peu à la macromolécule d'intérêt, dont les signaux sont enregistrés sous la forme de ^{1}H,^{15}N-HSQCs. Cette titration induit, suivant si l'interaction est en échange lent ou non, le déplacement du pic, sa disparition ou l'apparition d'un deuxième pic, de manière similaire à un échange conformationnel. Les résidus les plus perturbés par l'interaction peuvent alors être reportés sur la structure, permettant la proposition d'une interface d'interaction. Un modèle du complexe peut alors être proposé à l'aide de logiciels de « docking » tel que HADDOCK en utilisant ces CSP comme contraintes ambiguës. C'est ainsi que de récents travaux ont démontré que le brin oligosaccharidique donneur se positionne dans une seconde poche différente de celle du brin accepteur chez la Ldt d'*Enterococcus faecium*. Dans les cas favorables, un Kd peut être déterminé par suivi de l'évolution des variations d'intensités ou du déplacement chimique de quelques résonances au cours de la titration.

La RMN du solide, contrairement à la RMN en solution, n'est pas dépendante de la masse moléculaire de la macromolécule et peut être utilisée pour des échantillons non solubles. Elle est donc parfaitement adaptée pour l'étude d'agrégats, de protéines membranaires, de gros assemblages ou de biopolymères. Ici, afin d'obtenir des signaux bien résolus (mais généralement un peu moins bien résolus qu'en RMN du liquide), les échantillons sont placés dans un rotor qui est mis en rotation à haute fréquence et à un angle particulier, l'angle magique (54.74°), par rapport au champ magnétique. Cette méthode est appelée la rotation à l'angle magique. La stratégie appliquée est similaire à celle de la RMN du liquide, à savoir l'utilisation de molécules marqués isotopiquement pour l'enregistrement de spectres multidimensionnels permettant l'attribution des résonances. Toutefois, la RMN du solide donnant lieu à des résonances proton trop larges pour être détectables, la plupart des

expériences sont basées sur les noyaux ^{13}C, ^{15}N ou ^{31}P présents dans les macromolécules biologiques.

Les sacculi, malgré leur masse moléculaire, peuvent être étudiés en RMN du solide, avec ou sans les autres constituants de la paroi cellulaire. La composition du peptidoglycane peut ainsi être examinée par cette technique en 1D ou en 2D. Cela peut permettre par exemple de montrer qu'un résidu existe sous plusieurs formes (modifiées ou non). De manière similaire, le ratio de brins peptidiques réticulés/non réticulés peut aussi être évalué.

La RMN du solide permet aussi des études de dynamique, de manière similaire à la RMN du liquide. Dans le cas de sacculi, cela peut permettre d'évaluer la rigidité du peptidoglycane. La comparaison de la flexibilité de parois cellulaires hydratées d'*E. coli*, *B. subtilis* et *S. aureus* a ainsi mis en évidence une corrélation entre la rigidité du peptidoglycane et son taux de réticulation.

Enfin, des interactions protéines-sacculi peuvent être étudiées. Alors qu'en RMN du liquide, la protéine marquée disparaîtrait lors de l'interaction (car elle se comporterait comme une espèce de la taille du sacculus), il n'en va pas de même en RMN du solide. L'analyse de l'interaction du peptidoglycane avec diverses protéines est donc possible. En 2014, un premier modèle d'une interaction protéine-sacculus a ainsi pu être proposé pour la Ldt de *B. subtilis*. La stratégie appliquée est très proche de celle employée en solution, avec l'observation de CSPs, puis l'identification des résidus impactés par l'interaction et leur cartographie sur la structure, suivi du calcul d'un modèle avec le logiciel HADDOCK.

La RMN apparaît donc comme une technique versatile, qui peut permettre d'obtenir des informations cruciales au niveau atomique sur les protéines impliquées dans la synthèse ou la maturation du peptidoglycane, ainsi que sur leur divers réseaux d'interaction.

Part II
Regulation of peptidoglycan synthesis from the outer-membrane

Introduction

From the studies on protein members of the elongasome and divisome, it clearly appears that peptidoglycan synthesis is tightly tied to the inner-membrane and to the cytoplasm, where proteins required for recruitment and regulation of the peptidoglycan synthases are found. For a long time, among the proteins involved in peptidoglycan growth, hydrolases only were thought to be located outside of the sacculus. However, at the end of 2010, the teams of W. Vollmer and T. Bernhardt independently demonstrated in two striking articles that, in *E. coli*, two lipoproteins anchored to the outer-membrane stimulate peptidoglycan growth (Paradis-Bleau et al., 2010; Typas et al., 2010). These proteins were called Lpos for *L*ipoprotein activators of *P*BP from the *O*uter membrane. With this discovery, regulation of peptidoglycan synthesis is now tightly connected not only to the inner-membrane and cytoplasm, but also to the outer-membrane, allowing for a simultaneous coordination of the growth of the three layers of the Gram-negative cell envelope. Here, I will discuss in more details the Lpo discovery and their initial characterization, before to present in the next chapters the detailed structural and functional study that was the core of the work of this thesis.

Chapter 1
Lpo lipoproteins, outer-membrane regulators essential for peptidoglycan synthesis

As reported previously (in part I section 2.C.b.iii), in *E. coli*, the bifunctionnal PBP1A and PBP1B are partially redundant: deletion of one of them is not lethal for *E. coli* on the contrary to the simultaneous inactivation of both of them (Kato et al., 1985; Yousif et al., 1985). However, based on the analysis of their respective interaction partners and of their *in vivo* localization, each of these PBPs seem to be part of a different macromolecular complex, the elongasome for PBP1A, the divisome for PBP1B (detailed in part I chapter 4). Therefore, to find out potential PBP1 regulators, Paradis-Bleau and coworkers searched for mutants (Paradis-Bleau et al., 2010), which were lethal upon PBP1A or PBP1B deletion (suggesting that the remaining PBP1 was no more as efficient as in a the wild-type strain, but was active enough to maintain viability). In a parallel study, Typas and coworkers (Typas et al., 2010) performed a high-throughput genetic screen in multiple stress conditions to discover mutations of PBP1B that were causing a phenotype similar to that of the PBP1B gene (mrcB) loss (depletion of PBP1B leads to cells with increased sensitivity to β-lactams on the contrary to PBP1A deletion). They also developed a direct binding assay to extract membrane proteins from the outer-membrane with bead-coupled PBP1A or PBP1B. These three methods led to the identification of the outer-membrane lipoprotein LpoA, previously YraM, and LpoB, previously YcfM, as essential components of the peptidoglycan machineries. Subsequent assays showed that Lpo deletion phenotypes mirrored PBP1s, meaning that inactivation of one of the Lpos is tolerated, but that deletion of both induces cell lysis and is lethal. In addition, LpoA was found out to be required in the absence of PBP1B and, similarly, LpoB was demonstrated to be necessary, when PBP1A was not active. Finally, depletion of PBP1A and LpoA on one hand, and of PBP1B and LpoB on the other hand, are not lethal. These results are due to the requirement of PBP1s activation by their cognate Lpos. Each of the Lpos directly and specifically binds one PBP1, PBP1A for LpoA, and PBP1B for LpoB. Although peptidoglycan can be synthesized *in vitro* from lipid II precursors by PBP1A or PBP1B, their activity must be stimulated *in vivo* by their respective Lpo to ensure a wild type phenotype. Indeed, a direct regulation of PBP1A and PBP1B enzymatic reactions was observed *in vitro* (Lpos were for example required to produce muropeptide trimers and tetramers from monomers) and was evidenced from the analysis of mutant cell sacculi. LpoB is thought to stimulate first PBP1B glycosyltransferase activities (Lupoli et al., 2014), enhancing by up to eight-fold its kinetic, and, second its transpeptidase activity by increasing the cross-linking from ~50% to ~70% (Typas et al., 2010; Egan et al., 2014). In contrast, LpoA directly increases the transpeptidase activity, increasing cross-linking from ~40% to ~70%; (Typas et al., 2010), which in turn induces an enhanced glycosyltransferase activity (Lupoli et al., 2014). In addition to these interactions, pull-down experiments suggested that Lpos, especially LpoA, might bind to peptidoglycan.

Immunofluorescence and fluorescence microscopies were performed by Vollmer's and Bernhardt's groups to determine the localization of Lpos. Both proteins displayed a broad distribution on lateral walls. A preferred presence for LpoB over LpoA was observed at the septum in dividing cells, during the maturation of the divisome. In agreement with this latter result, LpoB is unable to be recruited when septal peptidoglycan synthesis is impaired (by

specific inhibition of PBP3 by the aztreonam antibiotics). Interestingly, Lpo recruitment in the peptidoglycan synthesis complexes is not carried out by PBP1A or PBP1B, as deletion of any of these class A PBPs does not hinder localization patterns of the two lipoproteins.

In agreement with this localization at mid-cell, the LpoB-PBP1B couple was also suggested to be implicated in outer-membrane invagination. In *E. coli*, the Tol-Pal system is predicted to be responsible for this process (see part I section 4.B.b.iii), but surprisingly its proteins are not essential, suggesting a functional redundancy. Typas and coworkers demonstrated that LpoB and PBP1B could also be connected to this event, as LpoB and Pal proteins show a negative genetic interaction (phenotype of pal^- mutants is worsened upon inactivation of LpoB) and form a second trans-envelope complex during division. The exact role of PBP1B-LpoB in cell constriction was nevertheless unclear at this time. Since then, recent work has been published and shed a new light on this (Gray et al., 2015; see also part II section 3.B.b).

The region of PBP1A and PBP1B interacting with LpoA and LpoB, respectively, was proposed to be their additional non-enzymatic domain, ODD, inserted at the beginning of the transpeptidase domain in PBP1A, and UB2H, a domain intercalated between the two catalytic domains in PBP1B. Indeed, each of these domains is conserved in the same bacterial lineages than their PBP1 cognate partner, γ-proteobacteria (an important class of Gram-negative bacteria gathering many known pathogens) for ODD/LpoA, enterobacteriaceae (the only family, also commonly known as enterobacteria, of enterobacteriales, one of the main orders of γ-proteobacteria) for UB2H/LpoB. In most cases (but exceptions exist), the absence of these domains correlates with lack of Lpos (Typas et al., 2010). Finally, a construction of PBP1B without UB2H, PBP1BΔUB2H, was unable to cross-link with LpoB, on the contrary to the wild-type PBP1B, further hinting in the possible implication of this domain in mediating the interaction. In the case of LpoA-PBP1A, ODD was overexpressed in PBP1B-LpoB depleted cells, which caused cell lysis. This result was interpreted as LpoA being titrated out by ODD, suggesting a possible interaction of this domain with the lipoprotein.

However, if both Lpos do interact directly with these domains, they have to reach their cognate PBPs on the other side of the 200-Å-wide *E. coli* periplasm (Matias et al., 2003). From the crystal structure of PBP1B (Sung et al., 2009), UB2H is expected to be situated at approximately 50 Å from the inner membrane, below the peptidoglycan layer (figure II.1.1). Similarly, a structural model of *E. coli* PBP1A places ODD at ~ 60 Å from the cytoplasmic membrane. As Lpo proteins are anchored to the outer-membrane, these observations suggest that they have to cross the peptidoglycan network. However, the strategies sat up by these macromolecules to reach their partners through the peptidoglycan molecular sieve were not determined at the time of their discoveries. In addition, LpoA and LpoB do not show any sequence similarities, suggesting different approaches, instead of a single one, to realize this connection.

When this thesis was initiated, very few additional elements had been described in the literature regarding Lpo proteins, and the interaction between Lpos and PBP1A/B remained to be characterized at the atomic level to understand the detailed mechanism leading to PBP1s activity stimulation. I therefore focused my work on the high-resolution structure determination of both *E. coli* Lpos, to pursue then with the study of the UB2H-LpoB interaction. As crystallization of LpoA and LpoB was not productive (W. Vollmer, personal communication), NMR was employed (sometimes in combination with SAXS) to resolve their respective structure. This method also has the advantage to enable at the same time the study of their dynamics and of their interaction in solution.

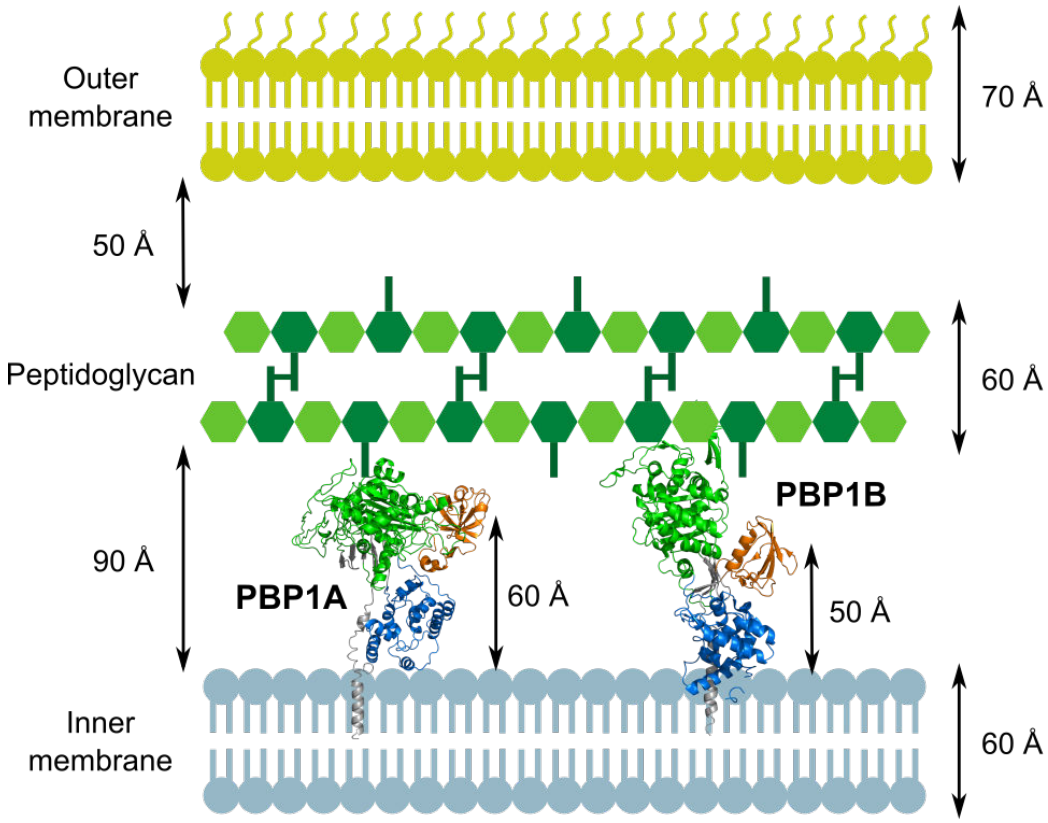

Figure II.1.1: The non-catalytic PBP1A/B domains likely lie below the peptidoglycan layer, at the opposite side of Lpos localization. The structure of *E. coli* PBP1A was modeled with Phyre2, while PBP1B was taken from the PDB (PDB code 3VMA). Periplasmic distances and peptidoglycan width are based on electron microscopy observations by Matias et al., 2003.

Résumé en français du chapitre 1 : Les lipoprotéines Lpos, des régulateurs ancrés à la membrane externe essentiels à la synthèse du peptidoglycane

Suite à l'étude des complexes multi-protéiques de l'élongasome et du divisome, il apparaît clairement que la synthèse du peptidoglycane s'étend du cytoplasme au périplasme et qu'une coordination spatiale et temporelle des diverses étapes biomoléculaires afférentes est nécessaire. Jusqu'à très récemment, seules des hydrolases étaient connues pour leur localisation du côté externe du sacculus. Cependant, les équipes de W. Vollmer et T. Bernhardt ont démontré, indépendamment dans deux articles parus fin 2010, que chez *E. coli* la régulation de la synthèse a également lieu depuis la membrane externe, où sont ancrées deux lipoprotéines. Celles-ci furent appelées Lpos, pour lipoprotéines activatrices des PBPs depuis la membrane externe. Avec cette découverte, la synthèse du peptidoglycane connecte désormais les trois enveloppes de la paroi bactérienne, permettant la coordination de leur croissance.

Les protéines PBP1A et PBP1B étant quasiment inactives in vitro, les auteurs de ces travaux ont recherché de nouveaux partenaires de ces protéines. L'une des stratégies mises en place a reposé sur la redondance partielle de ces deux enzymes. En effet, alors que la suppression de l'une des deux PBP1s est tolérée par la bactérie, l'inactivation des deux protéines est létale. Ainsi, Paradis-Bleau et al. ont analysé les effets de la délétion de divers gènes dans de souches bactériennes ne comportant plus que l'une des deux PBP1s. La recherche de mutations létales a ainsi permis d'identifier des activateurs potentiels de PBPs, en se basant sur le fait que dans ces cas-là la PBP1 restante n'était plus assez active pour maintenir la survie de la bactérie. Dans les travaux de Typas et al., un screen génétique à haut-débit a été effectué afin de trouver des mutants présentant un phénotype similaire à celui causé par la suppression de PBP1B, à savoir une sensibilité accrue aux antibiotiques de type β-lactame. En parallèle des interactants de PBP1A et de PBP1B ont été isolés i*n vitro* à partir d'extraits membranaires de *E. coli* en utilisant des billes sur lesquelles étaient covalemment attachées les PBPs d'intérêt. Ces trois méthodes ont permis l'identification convergente de deux lipoprotéines Lpos, ancrées à la membrane externe. Leur rôle est essentiel pour la bactérie, leur double inactivation étant létale, au même titre que celle des PBPs. Des observations par microscopie de fluorescence ont également confirmé qu'*in vivo* les Lpos étaient colocalisées avec leurs PBP1s correspondantes. Alors que LpoA interagit spécifiquement avec PBP1A, LpoB se lie uniquement à PBP1B, stimulant dans les deux cas les activités enzymatiques de transglycosylation et de transpeptidation de chacune d'entre elles. Le couple PBP1B-LpoB semble également être impliqué dans l'invagination de la membrane externe, ainsi que le suggèrent des expériences d'interactions génétiques négatives avec Pal. Les détails au niveau atomique de l'interaction Lpo-PBP1 étaient inconnus avant le début de cette thèse. Toutefois les domaines non catalytiques ODD et UB2H, respectivement de PBP1A et de PBP1B, étaient proposés comme de bons candidats à l'origine de l'interaction avec les Lpos, sur la base d'études phylogénétiques et de tests préliminaires *in vivo* visant à exprimer PBP1B sans UB2H ou surexprimer ODD seul, en absence de la seconde PBP1. Les domaines UB2H et ODD étant situés uniquement à enniron 50 - 60 Å de la membrane interne,

il semble toutefois que les Lpos aient besoin de traverser la couche de peptidoglycane et une grande partie du périplasme soit environ200 Å pour atteindre leur domaine cible. La question se pose alors de l'approche structurale utilisée par les Lpos pour effectuer leur fonction d'activation.

En l'absence de données structurales à l'échelle atomique sur les Lpos dans la littérature et de données permettant de mieux comprendre le mécanisme de stimulation des synthases de la famille des PBPs de haute masse moléculaire, le travail de cette thèse s'est concentré sur la détermination de structures à haute-résolution de LpoA et de LpoB, ainsi que sur l'étude des interactions entre le domaine UB2H de PBP1B et LpoB. LpoA et LpoB ne cristallisant pas, la RMN fut la principale technique employée.

Chapter 2
Structural characterization of LpoA

LpoA is a 678-residue lipoprotein. As introduced previously, LpoA is anchored at the outer-membrane. The 27 first residues form a signal peptide for the targeting of the protein, which is inserted in the lipidic bilayer through a covalent bond between three fatty acids and the cysteine 27, after removal of the N-terminus (for a recent review on lipoprotein biosynthesis, see Nakayama et al., 2012). The mature LpoA is predicted to have two domains, delimited in figure II.2.1. While the structure of the N-terminal module ($LpoA^N$) was unknown, the fold of the C-terminal domain ($LpoA^C$) was determined for its *Haemophilus influenzae* (not to be confused with the influenza virus) homologue a couple of years before the role of the protein was established (Vijayalakshmi et al., 2008). Actually, the protein was investigated at this time for its essential undetermined function in this pathogen. The C-terminal domain is divided in two sub-domains (figure II.2.2 A). The N-terminal region adopts an α/β fold, with a five-stranded β-sheet surrounded by four α-helices. Another small distant α-helix is also present close to one of the two linkers with the C-terminal part. This C-terminal sub-domain is composed of a seven-stranded β-sheets enclosed by four α-helices. These two folds are positioned in such a way that a large cleft (20-Å-long) clearly appears in the inter-domain space, where several conserved residues are found. Because of the high structural similarities of $LpoA^C$ with periplasmic-solute binding proteins (with for example an r.m.s.d of 4.1 Å with the periplasmic leucine/valine/isoleucine-binding proteins shown in figure II.2.2 B) and other solute-binding proteins, this domain was proposed to similarly bind a partner in this pocket and to undergo a conformational change upon interaction, leading to a putative closed state. Nevertheless, it must be noted that the relevance of a structural change is actually totally unknown. Although $LpoA^C$ was demonstrated by Typas et al. to be the domain interacting with PBP1A, it is unclear if the inter-domain cleft is implicated.

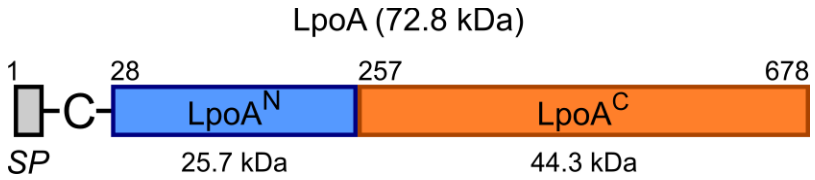

Figure II.2.1: Domain organization of *E. coli* LpoA. SP: Signal Peptide, cleaved to anchor the protein to outer-membrane fatty acids.

The high-resolution structure of $LpoA^C$ being solved (in *H. influenzae*) and its molecular weight being little compatible with liquid-state NMR (44.3 kDa in *E. coli*), I focused my attention on *E. coli* $LpoA^N$ (construct of 28 kDa without the lipid anchor). Its structure revealed a fold exclusively composed of α-helices, organized in a helix-turn-helix pattern similar to tetratricopeptide repeat (TPR) patterns. These modules are generally implicated in protein-protein interactions, suggesting a role for binding unidentified partners. In order to investigate on the spatial organization of $LpoA^N$ and $LpoA^C$ in the full-length protein, with the goal of determining if it could reach PBP1A, I then performed a combination of NMR and SAXS experiments (the latter being able to furnish low-resolution data on the conformation in solution of full-length LpoA). The data showed that the two $LpoA^N$ and $LpoA^C$ domains were rigidly linked and formed an elongated structure. Interestingly, two flexible stretches of unknown function (if they have some) in *E. coli* $LpoA^C$, and absent in the *H. influenzae*

homologue, were found. From the approximate length (~145 Å) and width (~30 Å) of *E. coli* LpoA determined, a model of LpoA crossing the periplasm and the peptidoglycan layer to reach the ODD domain was proposed. The assignment required for the structure calculation of $LpoA^N$ as well as the structural results themselves are presented in the two following articles, published in *J. Biomol. Assign.* and *Structure*, respectively, in 2014 (Jean, Bougault, Derouaux et al., 2014; Jean, Bougault, Lodge et al., 2014). Note that a structure of *H. influenzae* $LpoA^N$ (PDB code 4P29) was released from the Protein Data Bank a few months later by the team of M. Saper, already responsible for the publication of the $LpoA^C$ structure. Although the two proteins show high structural similarities as expected, they display a loop of different length between α-helices 7 and 8 as well as a different inclination of the latter helix, resulting in a different orientation (by 50°) of the second half of the domain.

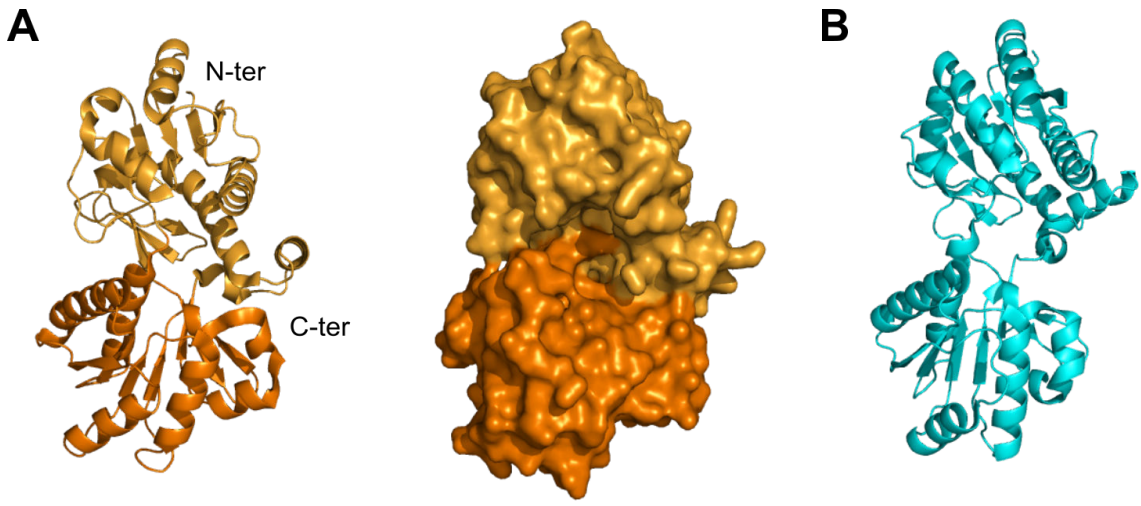

Figure II.2.2: LpoA C-terminal domain is a structural homologue of leucine/valine/isoleucine binding proteins (LVIBP). (A) Cartoon (left) and surface (right) representation of the crystal structure of *Haemophilus influenzae* C-terminal domain of LpoA (residues 257 – 575, corresponding to residues 257 – 678 in *E. coli*; PDB code 3CKM). The two sub-domains are represented in two shades of orange. (B) Structure of LVIBP in an open conformation (PDB code 1Z15).

2.A- Structural characterization of LpoA by NMR and SAXS

Biomol NMR Assign
DOI 10.1007/s12104-014-9546-2

ARTICLE

Backbone and side-chain ^{1}H, ^{13}C, and ^{15}N NMR assignments of the N-terminal domain of *Escherichia coli* LpoA

Nicolas L. Jean · Catherine Bougault · Adeline Derouaux · Gilles Callens · Waldemar Vollmer · Jean-Pierre Simorre

Received: 22 November 2013 / Accepted: 27 January 2014

Abstract The peptidoglycan is a major component of the bacterial cell wall and is essential to maintain cellular integrity and cell shape. Penicillin-Binding Proteins (PBPs) catalyze the final biosynthetic steps of peptidoglycan synthesis from lipid II precursor and are the main targets of β-lactam antibiotics. The molecular details of peptidoglycan growth and its regulation are poorly understood. Presumably, PBPs are active in peptidoglycan synthesizing multienzyme complexes that are controlled from inside the cell by cytoskeletal elements. Recently, two outer-membrane lipoproteins, LpoA and LpoB, were shown to be required in *Escherichia coli* for the function of the main peptidoglycan synthases, PBP1A and PBP1B, by stimulating their transpeptidase activity. However, the mechanism of PBP-activation by Lpo proteins is not known, and the Lpo proteins await structural characterization at atomic resolution. Here we present the backbone and side-chain ^{1}H, ^{13}C, ^{15}N NMR assignments of the N-terminal domain of LpoA from *E. coli* for structural and functional studies.

Keywords Outer-membrane lipoprotein activator of PBP · Bacterial cell wall biogenesis · Cell elongation complex · Peptidoglycan · NMR resonance assignment

Biological context

The peptidoglycan sacculus is a major component of the cell envelope in most bacteria and is essential for maintaining cell shape. Made of long polysaccharide chains cross-linked by short peptides the net-like sacculus forms a thin layer with unique physical properties: it is both, elastic and porous, and has the strength to resist the osmotic pressure (turgor) to protect the cell from busting. The main steps of peptidoglycan biosynthesis and the structures of key enzymes have been elucidated (for reviews see Typas et al. 2012; Matteï et al. 2010): (1) synthesis of the building blocks in the cytoplasm by the Mur enzymes, (2) covalent binding to a polyprenol lipid for transport across the

N. L. Jean · C. Bougault · J.-P. Simorre
Institut de Biologie Structurale Jean-Pierre Ebel, 41 rue Jules Horowitz, 38027 Grenoble, France

N. L. Jean · C. Bougault · J.-P. Simorre
Univ. Grenoble Alpes, Institut de Biologie Structurale (IBS), 38000 Grenoble, France

N. L. Jean · C. Bougault · J.-P. Simorre
CNRS, IBS, 38000 Grenoble, France

N. L. Jean · C. Bougault · J.-P. Simorre
CEA, DSV, IBS, 38000 Grenoble, France

A. Derouaux · G. Callens · W. Vollmer
Centre for Bacterial Cell Biology, Institute for Cell and Molecular Biosciences, Newcastle University, Richardson Road, Newcastle upon Tyne NE2 4AX, UK

Present Address:
A. Derouaux
Centre d'Ingénierie des Protéines, Université de Liège, B6a Allée de la Chimie, Sart Tilman, 4000 Liège, Belgium

Present Address:
G. Callens
Eurogentec S.A., 5 rue du Bois Saint-Jean, 4102 Seraing, Belgium

J.-P. Simorre (✉)
Institut de Biologie Structurale, EPN Campus, 6 rue Jules Horowitz, 38000 Grenoble, France
e-mail: jean-pierre.simorre@ibs.fr

Published online: 04 February 2014

cytoplasmic membrane, and (3) polymer assembly outside the cytoplasm by the Penicillin-Binding Proteins (PBPs) which are the principal targets of β-lactam antibiotics like penicillin. Bi-functional PBPs have two peptidoglycan synthesis activities catalyzing both the glycosyltransferase reaction to polymerize the glycan chains and the trans-peptidation to cross-link the peptides.

Although isolated PBPs can polymerize the peptidoglycan precursors in vitro, in the cell they require additional factors to synthesize peptidoglycan and to maintain a particular cell shape. This is in part due to the permanent remodeling of the peptidoglycan layer that involves a subtle balance between the insertion of newly synthesized peptidoglycan and the removal of old material by hydrolases. Furthermore, peptidoglycan growth must be spatially and temporarily synchronized with the growth of the other cell envelope layers, like the outer membrane in Gram-negative species, and coordinated with cell elongation and division in rod-shaped bacteria (Margolin 2009). Results from protein–protein interaction studies support a model according to which PBPs act within multi-protein complexes together with peptidoglycan hydrolases and cell morphogenesis proteins linked to cytoskeletal proteins (such as MreB and FtsZ), consistent with the essential role of the cytoskeleton in directing or organizing peptidoglycan growth from inside the cell (for reviews see Typas et al. 2012; Egan and Vollmer 2013).

Two novel outer-membrane anchored lipoproteins, LpoA and LpoB, are essential for the functioning of the main peptidoglycan synthases, PBP1A and PBP1B, respectively, in *Escherichia coli* (Typas et al. 2010, Paradis-Bleau et al. 2010). PBP1A and PBP1B have partially redundant functions in cell elongation and division, but the cell requires at least one of these synthases together with its cognate Lpo protein for growth. Purified LpoA (YraM) interacts with PBP1A and stimulates its transpeptidase activity in vitro, and purified LpoB (YcfM) interacts with PBP1B and stimulates both, glycosyltransferase and transpeptidase activities (Typas et al. 2010, Paradis-Bleau et al. 2010). Both Lpo proteins interact with their cognate PBPs in the cell (Typas et al. 2010), presumably forming *trans*-envelope complexes through the periplasm. PBP1B and LpoB are enriched at the cell division site where, presumably together with PBP3, they catalyze the synthesis of septal peptidoglycan (Typas et al. 2010).

PBP1A and LpoA appear to participate mainly in cell elongation together with PBP2 (Typas et al. 2010; Banzhaf et al. 2012). However, the structure of the PBP1A/LpoA complex and the mechanism by which LpoA stimulates PBP1A's transpeptidase activity is not known. The X-ray crystal structure of the C-terminal domain of LpoA from *Haemophilus influenzae* has been solved (Vijayalakshmi et al. 2008). The structure and function of the N-terminal domain has remained unknown. Here we report the essentially complete backbone and side-chain resonance assignments (^{1}H, ^{13}C, ^{15}N) and identify the secondary structure elements of the N-terminal domain of *E. coli* LpoA protein (LpoA^{N}) comprising amino acid residues 28–256.

Expression and purification of LpoA^{N}

Recombinant, ^{13}C, ^{15}N-labeled LpoA^{N} lacking the membrane anchoring signal peptide and containing an N-terminal oligo-histidine tag [MGSSH$_6$SSGLVPRGSHM-LpoA(G28-T256)] was produced from *E. coli* BL21(DE3) pET28LpoA^{N} (Typas et al. 2010). Cells were grown overnight at 37 °C in 100 mL of M9 minimal medium containing 3 g/L [^{13}C]-D-glucose, 1 g/L [^{15}N]-NH_4Cl (Goss Scientific, Cheshire, UK), 50 μg/mL kanamycin and 2 mM thiamine. The cells were harvested by centrifugation, resuspended in 1 L of fresh growth medium and grown at 37 °C to an OD_{600} of 0.6. IPTG (1 mM) was added and the cells were incubated further for 3 h at 37 °C for LpoA^{N} overproduction. The cells were harvested by centrifugation (8,650×*g*, 15 min, 4 °C) resuspended in 40 mL of 25 mM Tris/HCl, 20 mM imidazole, 10 % glycerol, 200 mM NaCl, pH 7.5 (buffer A). Few milligrams of DNase and 1 mM of phenylmethylsulfonylfluoride (PMSF) were added and the cells were disrupted by sonication (5 pulses of 1 min at 40 %, Branson Digital Sonifyer). The insoluble material was removed by ultracentrifugation (80,000×*g* for 1 h at 4 °C) and the supernatant was incubated with 7 mL of Ni–NTA-agarose beads (Qiagen) for 2 h at 4 °C. The beads were washed two times with 50 mL of buffer A and loaded into a gravity column. After washing with 50 mL of buffer A LpoA^{N} was eluted with 20 mL of 25 mM Tris/HCl, 400 mM imidazole, 10 % glycerol, 200 mM NaCl, pH 7.5. The sample was dialyzed against 20 mM Tris/HCl, 250 mM NaCl, pH 8.0 (buffer B) and concentrated to 10 mL. Half of the sample was loaded on a 120 mL-Superdex-75 gel filtration column equilibrated with buffer B followed by elution with buffer B at 1 mL/min. Fractions containing LpoA^{N} were pooled, dialyzed against 100 mM sodium acetate, pH 4.5 and concentrated using a Vivaspin-20 spin column (Sartorius).

NMR spectroscopy

All NMR data were collected at 323 K on a 2.5 mM sample of ^{13}C,^{15}N-labeled LpoA^{N} in 100 mM sodium acetate buffer, pH 4.5 containing 10 % D_2O. Spectra for backbone and side-chain assignment (except aliphatic and aromatic ^{13}C-NOESY-HSQCs) were recorded on Agilent spectrometers

equipped with cryogenic triple ^{1}H, ^{13}C, ^{15}N resonance probes operating at 600 and 800 MHz ^{1}H NMR frequencies. Aliphatic and aromatic ^{13}C-NOESY-HSQCs were collected on the Imagif national platform on a Bruker US^{2} spectrometer operating at 950 MHz ^{1}H NMR frequency equipped with a cryogenic triple ^{1}H, ^{13}C, ^{15}N resonance probe. Assignment of the sequential backbone resonances was achieved by using [^{1}H,^{15}N]-HSQC, 3D Best-TROSY-HNCA (with 50, 16.7, and 14.3 Hz resolution in ^{13}C, ^{15}N, and ^{1}H dimensions, respectively, for a total experimental time of 58.8 h), 3D Best-TROSY-HNCACB (with 65, 20, and 7.6 Hz in ^{13}C, ^{15}N, and ^{1}H for 29 h), 3D Best-TROSY-HN(CO)CACB (with 100, 20.8, and 14.3 Hz in ^{13}C, ^{15}N, and ^{1}H for 61.2 h), 3D Best-TROSY-HNCO (with 10.1, 20, and 14.3 Hz in ^{13}C, ^{15}N, and ^{1}H for 34.2 h), and 3D Best-TROSY-(HN)CO(CA)NH (with 14.7, 20.8, and 14.3 Hz in ^{13}C, ^{15}N, and ^{1}H for 61.2 h) (Lescop et al. 2010). Side-chains were assigned using aliphatic and aromatic [^{1}H,^{13}C]-CT-HSQCs, a methyl-selective [^{1}H,^{13}C]-CT-HSQC, a 3D H(C)CH-TOCSY (with 95.2, 143.6, and 12.5 Hz in indirect ^{1}H, ^{13}C, and direct ^{1}H for 68.7 h), a 3D (H)C(CCO)NH (with 100.5, 19.4, and 10.1 Hz in ^{13}C, ^{15}N, and ^{1}H for 56.7 h), a 3D H(CCCO)NH (with 41.6, 19.4, and 10.1 Hz in indirect ^{1}H, ^{15}N, and direct ^{1}H for 56.2 h), and a 3D ^{15}N-NOESY-HSQC (with 14.3, 20.8, and 12.5 Hz in indirect ^{1}H, ^{15}N, and ^{1}H for 83.7 h) with 120 ms mixing time, as well as 3D aliphatic, aromatic and methyl-^{13}C-NOESY-HSQC experiments with mixing times of 120, 145, and 160 ms and total experimental times of 93.8 h (resolution 24.3 × 95.5 × 11.9 Hz for indirect ^{1}H × ^{13}C × ^{1}H), 42.5 h (resolution 24.3 × 115.6 × 11.9 Hz for indirect ^{1}H × ^{13}C × ^{1}H), and 39.3 h (resolution 50 × 50 × 14.3 Hz for indirect

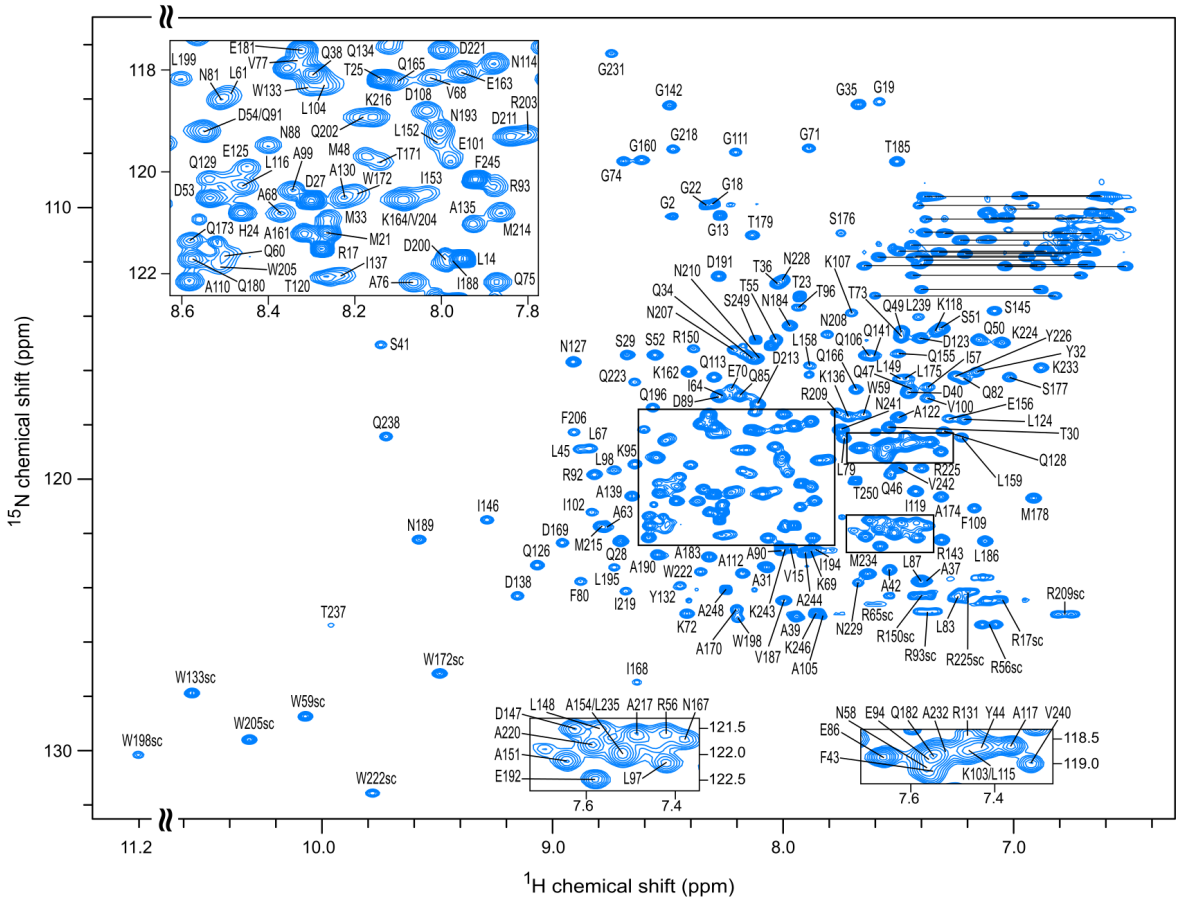

Fig. 1 Fully assigned 2D [^{1}H,^{15}N]-HSQC spectrum of 2.5 mM LpoA^{N} in 100 mM sodium acetate buffer, pH 4.5, at 323 K. Each backbone amide resonance is labeled with the amino acid type (*one-letter code*) and position in the sequence. Amine groups from tryptophan (Hε1–Nε1) and arginine (Hε–Nε) side chains are labeled with "sc". Assigned amide groups from glutamine and asparagine side chains are outlined with *horizontal lines*

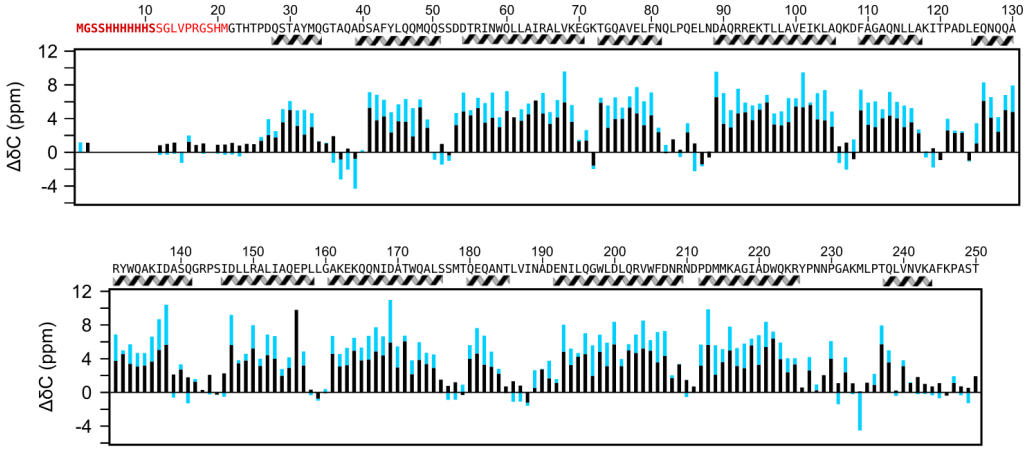

Fig. 2 Amino acid sequence and secondary structure of LpoA^N. Residues in *red* in the sequence correspond to the N-terminal oligo-histidine tag and are irrelevant to wild-type LpoA. The first eleven residues in *bold* and *darker characters* in this tag remain mainly unassigned. The secondary structure elements, 13 α-helices represented below the sequence, were predicted using TALOS+ according to the experimental backbone chemical shifts. Chemical shift deviations from random coil values (in ppm) were calculated for Cα and CO for each residue within the CcpNmr Analysis 2.2 software using the approach developed by Schwarzinger et al. in 2001 (see CcpNmr online manual for further details). These Cα and CO values are reported as *black* and *blue histograms*, respectively

^{1}H × ^{13}C × ^{1}H), respectively. NMR data were processed with NMRPipe (Delaglio et al. 1995) and analyzed using the CcpNmr Analysis 2.2 software (Vranken et al. 2005).

Extent of assignments and data deposition

LpoA^N gives rise to a well-resolved 2D [^{1}H,^{15}N]-HSQC spectrum at 323 K (Fig. 1). The first eleven residues from the N-terminal [MGSSH$_6$SSGLVPRGSHM] oligo-histidine tag remained unassigned with the exception of the amide group and Cα of G2, due to extensive amino acid type redundancy and fast H/D exchange leading to the absence of the corresponding amide resonance in the [^{1}H,^{15}N]-HSQC spectrum. These residues are excluded from the subsequent statistical analysis. Backbone assignment from all other protein residues is complete with the exception of S12/S19/H20, S12/S19/H20/L62/R65, S19/T25/L61/I64/L83/T120/R143/E156/D211/Y226/N229/L235/K246, S19, and S19/E156 for H$_N$ (98.7 % for non-proline residues), N (97.8 % for non-proline residues), CO (94.1 %), Cα (99.6 %) and Cβ (99.1 %) resonances, respectively. Concerning the side-chains, 98.8, 92.9, 76.2, and 87.1 % of the Hα, Hβ, aromatic and other aliphatic protons were assigned, respectively. ^{13}C assignments were completed to 77.1 and 73.7 % for aliphatic and non-quaternary aromatic carbons, respectively.

Analysis of the backbone chemical shifts by TALOS+ (Shen et al. 2009) and of the Cα and CO chemical shift deviations from random coil values concurrently suggest that LpoA^N is highly structured with 13 α-helices separated by short loops (Fig. 2). Unusual chemical shifts have been observed for one of the S29 Hβs, Q47 Hβs and Hγs, Q60 Nε and Hε, one of the L62 Hβs, K107 Hα, Y132 Hδs and Hεs, A154 Hβs, T171 Hγs, W172 Hζ, S176 Hβs, G197 Hα, L201 Hδs, R209 Hδs, W222 Hζ, one of the Y226 Hβs, and L239 Hγ and Hδs with standard deviations of 0.25–0.44 ppm for ^{1}H and of 1.72 ppm for ^{15}N upfield of the expected chemical shifts. The relatively high content of LpoA^N in aromatic residues suggests that ring current shielding effects from such vicinal residues could explain these unusual chemical shifts. The validation of this hypothesis awaits the resolution of the atomic structure of LpoA^N.

All ^{1}H, ^{13}C and ^{15}N chemical shifts have been deposited in the BioMagResBank (http://www.bmrb.wisc.edu) under the accession number 18853.

Acknowledgments Financial support by the French TGIR-RMN-THC FR3050 CNRS for conducting the research on the 950 MHz spectrometer of the Imagif Facility and on the 800 MHz spectrometer of the IBS Facility is gratefully acknowledged. This work was further supported by a Ph.D. fellowship to NLJ (Contrat de Formation par la Recherche) from the Commissariat à l'Energie Atomique et aux Energies Alternatives, an EMBO long-term fellowship to AD and the EU Commission through the DIVINOCELL project to WV.

Conflict of interest The authors declare that they have no conflict of interest.

References

Banzhaf M, van den Berg van Saparoea B, Terrak M, Fraipont C, Egan A, Philippe J, Zapun A, Breukink E, Nguyen-Distèche M, den Blaauwen T, Vollmer W (2012) Cooperativity of

peptidoglycan synthases active in bacterial cell elongation. Mol Microbiol 85:179–194

Delaglio F, Grzesiek S, Vuister GW, Zhu G, Pfeifer J, Bax A (1995) NMRPipe: a multidimensional spectral processing system based on UNIX pipes. J Biomol NMR 6:277–293

Egan AJF, Vollmer W (2013) The physiology of bacterial cell division. Ann NY Acad Sci 1277:8–28

Lescop E, Kern T, Brutscher B (2010) Guidelines for the use of band-selective radiofrequency pulses in heteronuclear NMR: example of longitudinal-relaxation-enhanced BEST-type ^{1}H–^{15}N correlation experiments. J Magn Reson 203:190–198

Margolin W (2009) Sculpting the bacterial cell. Curr Biol 19:R812–R822

Matteï PJ, Neves D, Dessen A (2010) Bridging cell wall biosynthesis and bacterial morphogenesis. Curr Opin Struct Biol 20:749–755

Paradis-Bleau C, Markovski M, Uehara T, Lupoli TJ, Walker S, Kahne DE, Bernhardt TG (2010) Lipoprotein cofactors located in the outer membrane activate bacterial cell wall polymerases. Cell 143:1110–1120

Shen Y, Delaglio F, Cornilescu G, Bax A (2009) TALOS+: a hybrid method for predicting protein backbone torsion angles from NMR chemical shifts. J Biomol NMR 44:213–223

Typas A, Banzhaf M, van den Berg van Saparoea B, Verheul J, Biboy J, Nichols RJ, Zietek M, Beilharz K, Kannenberg K, von Rechenberg M, Breukink E, den Blaauwen T, Gross CA, Vollmer W (2010) Regulation of peptidoglycan synthesis by outer-membrane proteins. Cell 143:1097–1109

Typas A, Banzhaf M, Gross CA, Vollmer W (2012) From the regulation of peptidoglycan synthesis to bacterial growth and morphology. Nat Rev Microbiol 10:123–136

Vijayalakshmi J, Akerley BJ, Saper MA (2008) Structure of YraM, a protein essential for growth of *Haemophilus influenzae*. Proteins 73:204–217

Vranken WF, Boucher W, Stevens TJ, Fogh RH, Pajon A, Llinas M, Ulrich EL, Markley JL, Ionides J, Laue ED (2005) The CCPN data model for NMR spectroscopy: development of a software pipeline. Proteins 59:687–696

Structure
Short Article

Elongated Structure of the Outer-Membrane Activator of Peptidoglycan Synthesis LpoA: Implications for PBP1A Stimulation

Nicolas L. Jean,[1,2,3] Catherine M. Bougault,[1,2,3] Adam Lodge,[4] Adeline Derouaux,[4,6] Gilles Callens,[4,7] Alexander J.F. Egan,[4] Isabel Ayala,[1,2,3] Richard J. Lewis,[5] Waldemar Vollmer,[4,*] and Jean-Pierre Simorre[1,2,3,*]
[1]University Grenoble Alpes, Institut de Biologie Structurale, F-38027 Grenoble, France
[2]CEA, DSV, Institut de Biologie Structurale, F-38027 Grenoble, France
[3]CNRS, Institut de Biologie Structurale, F-38027 Grenoble, France
[4]The Centre for Bacterial Cell Biology, Institute for Cell and Molecular Biosciences, Newcastle University, Richardson Road, Newcastle upon Tyne NE2 4AX, UK
[5]Institute for Cell and Molecular Biosciences, Newcastle University, Framlington Place, Newcastle upon Tyne NE2 4HH, UK
[6]Present address: Centre d'Ingénierie des Protéines, Université de Liège, allée de la Chimie, B6a, Sart Tilman, 4000 Liège, Belgium
[7]Present address: Eurogentec S.A., 5 rue du Bois Saint Jean, 4102 Seraing, Belgium
*Correspondence: w.vollmer@ncl.ac.uk (W.V.), jean-pierre.simorre@ibs.fr (J.-P.S.)
http://dx.doi.org/10.1016/j.str.2014.04.017

SUMMARY

The bacterial cell envelope contains the stress-bearing peptidoglycan layer, which is enlarged during cell growth and division by membrane-anchored synthases guided by cytoskeletal elements. In *Escherichia coli*, the major peptidoglycan synthase PBP1A requires stimulation by the outer-membrane-anchored lipoprotein LpoA. Whereas the C-terminal domain of LpoA interacts with PBP1A to stimulate its peptide crosslinking activity, little is known about the role of the N-terminal domain. Herein we report its NMR structure, which adopts an all-α-helical fold comprising a series of helix-turn-helix tetratricopeptide-repeat (TPR)-like motifs. NMR spectroscopy of full-length LpoA revealed two extended flexible regions in the C-terminal domain and limited, if any, flexibility between the N- and C-terminal domains. Analytical ultracentrifugation and small-angle X-ray scattering results are consistent with LpoA adopting an elongated shape, with dimensions sufficient to span from the outer membrane through the periplasm to interact with the peptidoglycan synthase PBP1A.

INTRODUCTION

Most bacteria surround their cytoplasmic membrane with a peptidoglycan (PG) sacculus, which maintains cell shape and protects the cell from lysis due to turgor. The PG sacculus is an elastic, net-like molecule composed of glycan chains that are connected by short peptides (Vollmer et al., 2008). Gram-negative bacteria, such as *Escherichia coli*, have a thin, mainly single-layered PG and an outer membrane containing lipopolysaccharide.

Growing and dividing cells polymerize the PG precursor lipid II and insert it into the existing PG layer by the combined actions of PG synthases and hydrolases, which presumably form dynamic, membrane-attached multienzyme complexes (Vollmer et al., 2008). *E. coli* has six cytoplasmic-membrane-anchored PG synthases. PBP1A and PBP1B are the major (and semi-redundant) bifunctional glycosyltransferase-transpeptidases, with well characterized in vitro activities (Banzhaf et al., 2012; Bertsche et al., 2005; Born et al., 2006). PBP2 and PBP3 are transpeptidases that are essential for cell elongation and division, respectively.

PG synthesis and hydrolysis are regulated from inside the cell by cytoskeletal elements (Typas et al., 2012). In *E. coli* and presumably in other Gram-negative bacteria, PG synthesis is also regulated from outside the sacculus. PBP1A and PBP1B both require cognate outer-membrane-anchored lipoproteins (LpoA and LpoB, respectively) for function (Paradis-Bleau et al., 2010; Typas et al., 2010). LpoA and LpoB are unrelated in amino acid sequence, but both attach to the inner leaflet of the outer membrane by an N-terminal lipid modification. The C-terminal domain of LpoA interacts with PBP1A to stimulate its transpeptidase activity by an as yet unknown mechanism, whereas LpoB interacts with the noncatalytic UB2H domain of PBP1B to stimulate its glycosyltransferase and transpeptidase activities. In the cell, the Lpo proteins must reach through pores in the PG net to interact with their cognate PG synthase. Therefore, it has been proposed that the Lpo-mediated activation of PBPs occurs in response to the properties of the pores in the elastic PG layer to adjust the rate of PG growth with the rate of cell growth (Typas et al., 2010, 2012). Supporting this model, a previous study showed that both outer-membrane-anchored Lpo proteins could be crosslinked to their cognate cytoplasmic membrane-anchored PBP in the cell (Typas et al., 2010). However, in the absence of structural data for full-length LpoA and LpoB, it has remained unclear whether both proteins are long enough to span a distance of at least 110 Å from the outer membrane through the PG layer to interact with their cognate PBP.

The crystal structure of the C-terminal domain of *Haemophilus influenzae* LpoA ($LpoA^C$, residues 257–573) reveals two subdomains that adopt a fold commonly found in periplasmic substrate-binding proteins (Vijayalakshmi et al., 2008). *E. coli* $LpoA^C$

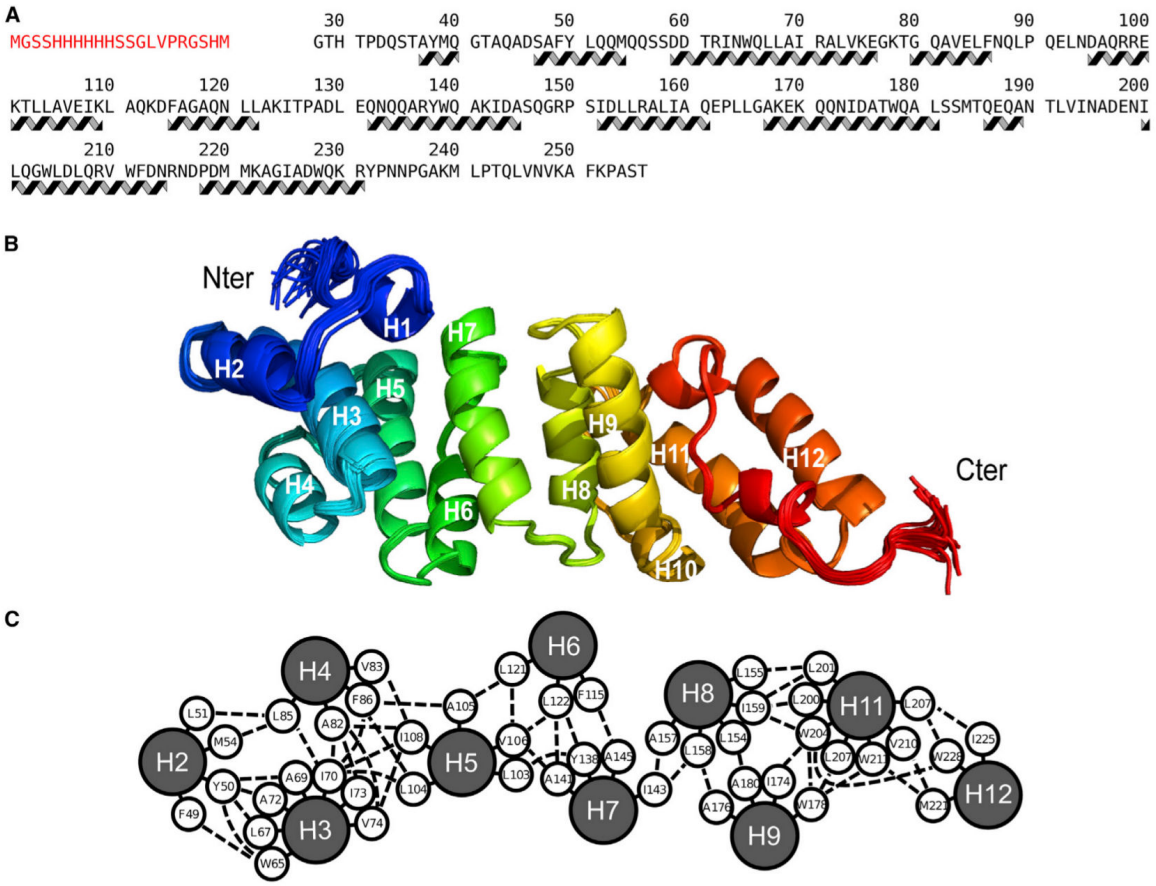

Figure 1. LpoA^N Has a TPR Domain-like Structure

(A) Amino acid sequence of the LpoA^N construct used for structure determination and secondary structure elements (α helices). The residues of the oligohistidine tag are shown in red.

(B) Cartoon representation of the 20 lowest-energy structures of LpoA^N, as determined by NMR spectroscopy, emphasizing the spatial arrangement of the 12 α-helices, which are numbered from the N to C terminus.

(C) LpoA^N is stabilized by numerous interhelical hydrophobic contacts. The ten α helices with more than four residues are shown as circles and labeled according to the description in (B). Interhelical hydrophobic contacts are represented with dashed lines, and short plain lines connect each of the residues to its corresponding helix.

See also Figure S1.

has two additional stretches of 67 and 39 amino acids, respectively, that are missing in the *H. influenzae* ortholog. The role of the N-terminal domain (LpoA^N) is not clear, as it does not interact with PBP1A (Typas et al., 2010).

In this work, we present the structure of LpoA^N determined by NMR spectroscopy. LpoA^N is almost completely made of α-helices that form helix-turn-helix motifs similar to tetratricopeptide repeat (TPR) motifs, which are commonly used as a scaffold underpinning protein/protein complexes. We also provide evidence from NMR spectroscopy that LpoA^C contains flexible (unstructured) regions and that the two domains of LpoA are connected by a rather rigid linker. Further biophysical characterization by analytical ultracentrifugation (AUC) and small-angle X-ray scattering (SAXS) showed that full-length LpoA has an elongated molecular shape, supporting the hypothesis that LpoA has the capacity to span the distance from the outer membrane to its cognate cytoplasmic-membrane-anchored PG synthase, PBP1A.

RESULTS

The N-Terminal Domain of LpoA Adopts a TPR-Domain-like Fold

We purified the N-terminal domain of *E. coli* LpoA lacking its signal peptide sequence and outer-membrane lipid anchor (LpoA^N, residues 28–256) fused to an N-terminal oligohistidine tag (Figure 1A and Figure S1A available online). ^{1}H-^{15}N heteronuclear single quantum coherence (^{1}H-^{15}N-HSQC) NMR spectra were recorded from ^{13}C,^{15}N-LpoA^N samples at different temperatures (5°C–50°C) and at different pH values (4.5–7.5), and

Table 1. Structural Statistics for the Ensemble of 20 NMR Structures of LpoA^N

NMR Distance and Dihedral Constraints	Number/Parameter
Distance Constraints	
Total unambiguous NOE restraints	5,210
Intraresidue	1,826
Interresidue	3,384
Sequential ($\|i-j\|=1$)	1,141
Medium-range ($\|i-j\|\leq 5$)	1,225
Long-range ($\|i-j\|>5$)	1,018
Total ambiguous NOE restraints	440
Total Dihedral Angle Restraints	426
Backbone Φ	213
Backbone Ψ	213
Structure Calculation Statistics[a]	
Restraints Violations	
Distance (>0.3 Å, >0.5 Å)	41.95, 4.5
Dihedral (>5°, >6°)	13, 0
Average pairwise root-mean-square deviation (Å)[b]	
Backbone atoms	0.44 ± 0.06
All heavy atoms	0.63 ± 0.05
Ramachandran Analysis[b]	
Residues in most favored regions (%)	85.2
Residues in additional allowed regions (%)	13.6
Residues in generously allowed regions (%)	1.0
Residues in disallowed regions (%)	0.2

[a]Pairwise deviations were calculated among 20 refined structures.
[b]These values were calculated on residues 28–256 (according to numbering in wild-type LpoA).

showed that the global fold of the protein remained unchanged (Figure S1B). For structure determination, NMR spectra were recorded at 50°C and pH 4.5, and chemical shifts were assigned (Jean et al., 2014). The structure of LpoA^N (Figures 1B and 1C) was subsequently determined. Relevant structural and statistical data are reported in Table 1.

LpoA^N is made up of 12 α-helices (H1–H12) of variable length linked together through short turns or rigid loops (Figure 1B). Two additional short stretches of three residues at the C terminus also adopt a characteristic 3_{10}-helix conformation (residues 236–238 and 246– 248). There are numerous interhelical hydrophobic contacts (Figure 1C) favored by the high percentage (24%) of long-chain hydrophobic amino acids and few additional side-chain hydrogen bonds, which explains the stability of the structure over wide pH and temperature ranges (Figure S1B).

LpoA^N has a striking structural similarity to protein domains formed by TPR motifs, as revealed by DALI (Holm and Rosenström, 2010), consistent with the repetition of helix-turn-helix motifs found in these proteins and LpoA^N. The highest score (Z = 9.3) was obtained with a 170-residue stretch of the G protein signaling regulator 2 (Protein Data Bank [PDB] code 3SF4), but both structures had a relatively high root-mean-square deviation (RMSD) value of 5.7 Å. Searching the LpoA^N sequence for canonical TPR repeats (Zeytuni and Zarivach, 2012), TPRpred (Biegert et al., 2006) recognized a TPR sequence pattern only in the I63-A96 fragment comprising H3 and H4, although H4 is shorter than the typical α-helices in TPR motifs. H11/H12 shows a substantial structural similarity to TPR motifs, but was not classified as a TPR motif by TPRpred because long-chain hydrophobic residues replace the conserved alanine residues at positions 8, 20, and 27. The similarity between LpoA^N and TPR domains thus seems limited to the presence of a series of helix-turn-helix motifs with short hydrogen-bonded turns between the two helices (H3/H4, H5/H6, H8/H9, and H11/H12) rather than to the presence of canonical TPR repeats with their characteristic hydrophobic contacts. As in most TPR domains, the individual helices in LpoA^N are organized into a superhelical structure; however, the curvature of this structure is too small to generate the concave and convex surfaces often seen in TPR domains. Instead, LpoA^N shows an overall prolate spheroid shape with a width of ~30 Å and a height of ~70 Å. The protein surface contains three grooves. Two of these grooves localize between the central helices H7 and H8, and the third localizes between H3 and H5. Interestingly, these grooves contain highly conserved residues and are therefore potential interaction sites with proteins or other ligands (Figure S1C).

Full-Length LpoA Has Flexible Regions in the C-Terminal Domain

We next sought to determine the overall molecular shape for full-length LpoA and the relative orientation of the two domains. The N-terminally oligohistidine-tagged protein (Figure S1A) was mostly monomeric (~85%) and contained ~10% dimers. This ratio was similar for all three protein concentrations (6, 2, and 0.2 mg/ml) used in AUC experiments, suggesting that monomers and dimers are not in dynamic exchange. The f/f_{min} ratio of 1.5 and hydrodynamic radius of 4.1 nm, determined from the sedimentation coefficient extrapolated to infinite dilution, s_0 = 4.16 S, are characteristic of an elongated molecular shape and/or a flexible molecule.

Full-length LpoA (see Figure 2 for LpoA^C) has a molecular weight of >70 kDa and therefore is too large for structure determination by NMR spectroscopy. Nonetheless, a ^{1}H-^{15}N band-selective excitation short-transient transverse optimized spectroscopy (^{1}H-^{15}N-BEST-TROSY) NMR spectrum of full-length ^{13}C,^{15}N-LpoA showed ~100 intense and tightly dispersed signals (Figure S2A). The signals seen in LpoA^N were all absent in this spectrum, suggesting that the molecular tumbling of the large anisotropic LpoA molecule prevents the NMR observation of structured (or nonflexible) regions and that only residues in disordered (or flexible) parts of the molecule could be seen. LpoA^N is well structured and therefore most of the signals obtained from full-length LpoA should come from disordered regions in the C-terminal domain. To investigate this possibility, we assigned the detected ^{1}H, ^{13}C, and ^{15}N resonances of a full-length ^{13}C,^{15}N-LpoA sample. HNCACB and BEST-TROSY-(H)N(COCA)NH experiments unambiguously identified stretches of contiguous residues that all reside within the two regions of the *E. coli* LpoA sequence that are absent in *H. influenzae* LpoA (Figure 2). These assignments included backbone resonances from 30 residues between N285 and P351 (region 1) and from 16 residues between S493 and N531 (region 2; Figure S2B). Amino acid types were obtained from Cα and Cβ carbon chemical shifts

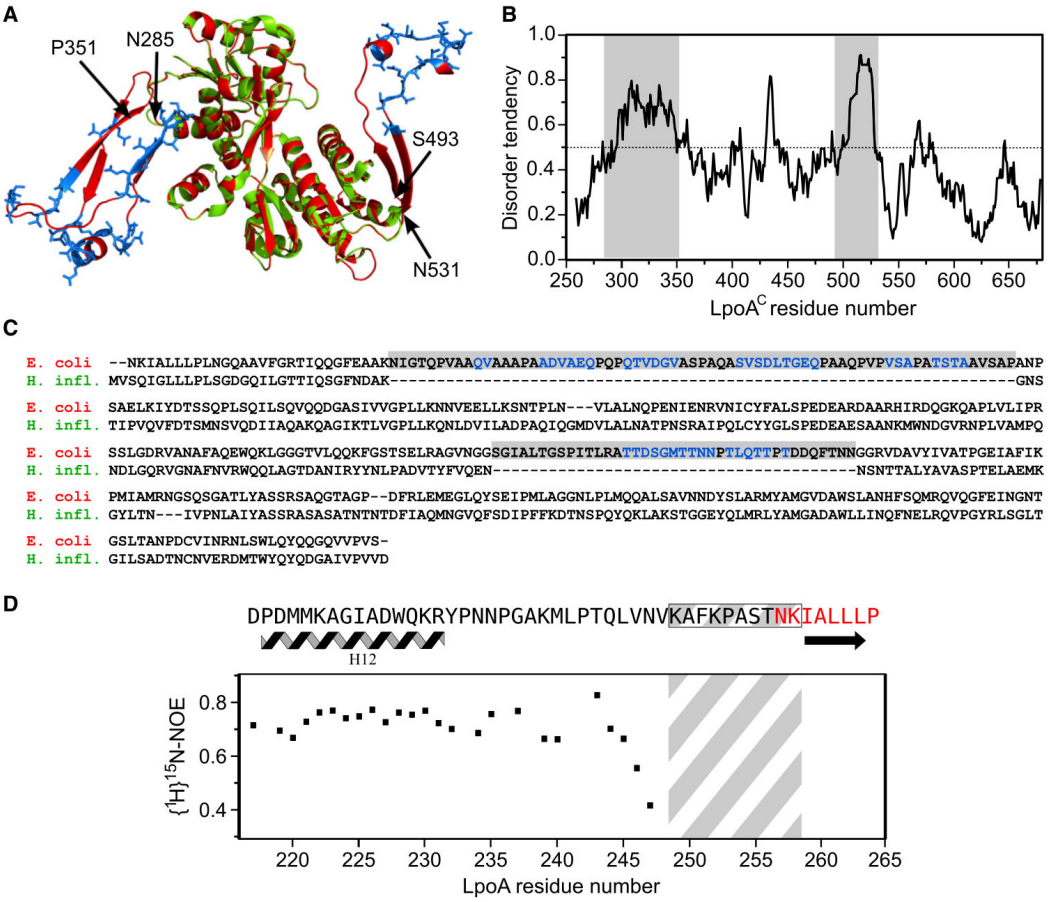

Figure 2. Comparison of LpoA^C from *E. coli* and *H. influenzae*

(A) Superimposition of the X-ray structure of *H. influenzae* LpoA^C (green, PDB code 3CKM) and the structure of *E. coli* LpoA^C predicted by PHYRE (red). Regions 1 (residues N285–P351) and 2 (residues S493–N531) are present in LpoA^C from *E. coli*, but not from *H. influenzae*. Flexible residues for which backbone resonances have been assigned by NMR spectroscopy are sketched as blue sticks.

(B) Disorder in *E. coli* LpoA^C predicted by IUPred. The two main regions absent from the *H. influenzae* LpoA sequence (in gray) are predicted as being mostly unstructured by IUPred (score > 0.5).

(C) Sequence alignment of *H. influenzae* and *E. coli* LpoA^C, where the two *E. coli* inserts are highlighted in gray. NMR-assigned residues are shown in blue.

(D) The linker between LpoA^N and LpoA^C (in gray and white hashes) starts at K249 and ends at K258. The criteria used to define this linker included the structuring of the N-terminal domain as quantified by the $\{^1H\}^{15}N$-NOE measured in LpoA^N (black) and the definition of the first secondary-structure element in the C-terminal domain (red) of LpoA as modeled by PHYRE.

See also Figure S2.

for 36 additional resonances (leaving only eight resonances completely unassigned) and agreed with the expected unassigned amino acids in the two considered regions. In line with these data, regions 1 and 2 were predicted to be unfolded by IUPred (http://iupred.enzim.hu/) with scores higher than 0.5 (Figure 2B).

We subsequently built a structural model of *E. coli* LpoA^C using PHYRE (Kelley and Sternberg, 2009) with the *H. influenzae* LpoA^C structure as a template (Vijayalakshmi et al., 2008; PDB code 3CKM). The superimposition of the *H. influenzae* structure and the *E. coli* model (Figure 2A) emphasizes the presence of extended loops in the flexible regions 1 and 2. To evaluate this model in the light of experimental data, we analyzed chemical shifts from assigned residues in regions 1 and 2, and observed marked dynamics and low secondary-structure propensities at these positions (see Supplemental Experimental Procedures). As a result, region 1 might be more flexible and/or disordered than suggested by the model. In addition to the established loop in region 2, the PHYRE-predicted β sheet (formed by S493-G499 and D525-N531) could not be confirmed by NMR spectroscopy due to incomplete sequence-specific assignments.

LpoA Has a Limited Interdomain Flexibility

If there is a highly flexible linker between the N- and C-terminal domains, full-length $^{13}C,^{15}N$-LpoA should give rise to NMR

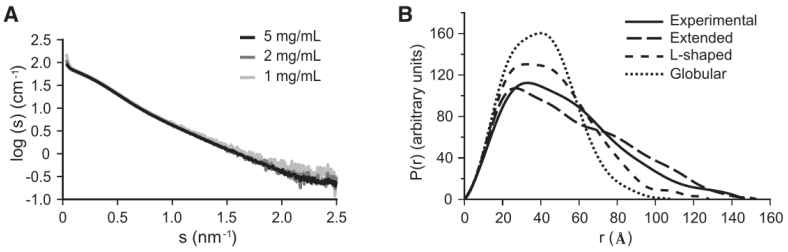

Figure 3. Full-Length LpoA Has an Extended Structure

(A) SAXS curves of LpoA at concentrations of 1, 2, and 5 mg/ml.

(B) Experimental distance distribution function, P(r), calculated from SAXS data collected on a 5 mg/ml ^{15}N-LpoA sample (black) and theoretical P(r) function calculated for molecular models with three different, arbitrarily chosen orientations of the N- and C-terminal domains (....., globular model; ----, L-shaped model; – – –, extended model; see also Figure S3C). The theoretical R_g values extracted from these curves are 3.11 nm for the globular model, 3.58 nm for the L-shaped model, and 4.44 nm for the extended model. The experimental R_g value, 4.22 ± 0.01 nm, fits best to the extended model.

signals corresponding to a sum of the signals observed for the separate domains. However, characteristic LpoA^N resonances remained undetected in this sample after an increase of the signal-to-noise ratio by a factor of 2. Only the virtually complete perdeuteration of full-length LpoA and the spectroscopic advantage of the TROSY effect allowed the detection of LpoA^N and LpoA^C amide resonances (Figure S2C). The structured regions of full-length LpoA, comprising most of the N- and C-terminal domains, thus behave as a highly anisotropic single structural entity without significant flexibility between the domains. This hypothesis was further confirmed by the similar heteronuclear multiple quantum coherence (HMQC) versus HSQC intensity ratios (Tugarinov et al., 2003) for ^{1}H-^{13}C correlations of alanine methyl groups in a U-[^{2}H, ^{12}C, ^{15}N], Val-[^{13}C^{1}H$_3$]$^{pro\text{-}S}$, Ala-[^{13}C^{1}H$_3$]-LpoA sample (Figure S2D), indicating a correlated rotational motion of the two domains. A strong, rather rigid interaction between LpoA^N and LpoA^C also agrees with the low disorder score of <0.38 calculated by IUPred for the linker region.

Full-Length LpoA Has an Elongated Molecular Shape

We used SAXS to determine the overall molecular shape of full-length LpoA (Figure 3). The estimated molecular weights of LpoA by SAXS (66.7 kDa, 64.9 kDa, and 68.2 kDa) were similar for each concentration tested (5, 2, and 1 mg/ml, respectively), showing that the scattering intensities recorded came mostly from the monomeric form of the protein and confirming the largely monomeric and monodisperse behavior of LpoA (Figure 3A). The distance distribution function P(r) was calculated from the SAXS data recorded at the highest protein concentration (Figure 3B) and yielded a radius of gyration (R_g) of 4.22 ± 0.01 nm, which is similar to the R_g of 4.17 ± 0.02 nm calculated by the Guinier approximation (Figure S3A).

We next built hypothetical models of full-length LpoA with different relative orientations of the N- and C-terminal domains using the structure of LpoA^N and the previously built *E. coli* LpoA^C homology model (Figure S3C) (Svergun, 1992), and calculated their theoretical P(r) and R_g values. The elongated putative LpoA model had a theoretical R_g that was close to the experimental value (4.44 nm versus 4.22 nm), whereas the putative globular and L-shaped models had lower theoretical R_g values (3.11 nm and 3.58 nm, respectively). The observed P(r) is typical of an oblate shape and is similar to the curve calculated for the elongated model (Figure 3B). The calculated D_{max} (the longest distance between two points in the protein) of 146.8 Å is also consistent with an elongated arrangement of the two domains, as LpoA^N and LpoA^C have domain lengths of ~70 Å and ~60 Å, respectively. Thus, although the presence of extended flexible regions (regions 1 and 2) in the C-terminal domain (Figure S3B) prevented us from building a higher-resolution model of LpoA, the SAXS data are consistent with an elongated structure.

DISCUSSION

In this work, we determined the structure of the N-terminal domain of LpoA and showed that it adopts a TPR-like fold. Proteins containing TPR domains (or modules) are ubiquitous and are present in organisms belonging to all kingdoms of life (Zeytuni and Zarivach, 2012). It is generally accepted that TPR modules do not exhibit an enzymatic activity, but rather serve as interaction modules in multiprotein assemblies or for protein dimerization (Allan and Ratajczak, 2011). For example, the TPR domain of BamD, an essential component of the outer-membrane β-barrel assembly machinery in Gram-negative bacteria, interacts with the N-terminal, unstructured region of BamC (Kim et al., 2011; Sandoval et al., 2011).

The analysis of 63 unique LpoA^N sequences revealed two conserved patches on the protein surface, which could represent potential interaction sites (Figure S1C). PBP1A interacts with LpoA^C, but not with LpoA^N (Typas et al., 2010), and LpoA and LpoA^N exist predominantly as monomers, suggesting that the TPR-like motifs do not promote self-interaction. Rather, LpoA^N may interact with one or more as yet unknown protein(s). Studies to identify the interaction partners of LpoA^N are currently under way.

Full-length LpoA yielded NMR signals that originate from two flexible regions in the C-terminal domain. Other species, such as *H. influenzae*, either lack these stretches or have different stretches at the same or a different position in the LpoA^C sequence (Vijayalakshmi et al., 2008). The functions of the two flexible regions in *E. coli* LpoA^C are currently unknown. It is possible that they fold into rigid structures under certain conditions, perhaps during the formation of new protein-protein interactions.

The NMR analysis of full-length LpoA also indicated that LpoA^N is not capable of moving independently of LpoA^C. Instead, both domains must be connected rather rigidly, consistent with the absence of any flexible stretch in this region. NMR,

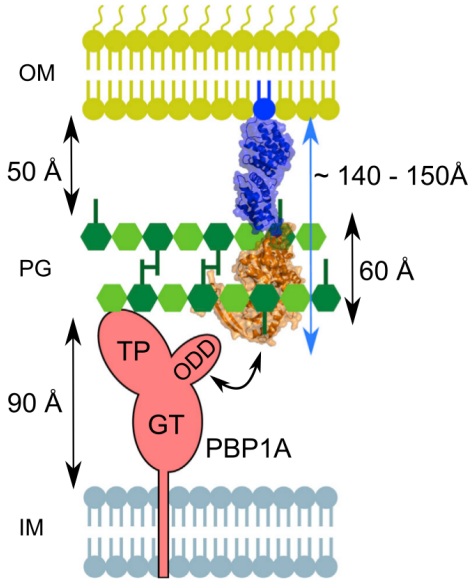

Figure 4. Schematic Representation of PBP1A Activation by LpoA
The N-terminal domain of LpoA (blue) anchors to the outer membrane, whereas the C-terminal domain (orange) interacts with the outer-membrane PBP1A docking domain (Typas et al., 2010). LpoA has an estimated total width of ~30 Å and length of ~145 Å. These dimensions should enable the protein to reach PBP1A through the periplasm and cross the ~60-Å-thick PG layer, which has ~40- to 60-Å-wide pores (Demchick and Koch, 1996). TP, transpeptidase domain; GT, glycosyltransferase domain; IM, inner membrane; OM, outer membrane.

AUC, and SAXS measurements support an elongated molecular shape of LpoA with a length of ~145 Å. With this length, LpoA would be capable of spanning from the outer membrane through the periplasm and PG layer to reach a bifunctional PG synthase, such as PBP1A, whose TPase domain is up to ~100 Å away from the cytoplasmic membrane (Sung et al., 2009; Figure 4). The PG layer is elastic and has pores with a diameter of ~40 Å in the relaxed state, allowing the diffusion of globular proteins of up to 25 kDa (Demchick and Koch, 1996; Vollmer and Höltje, 2004). The pores in stretched PG may have a diameter of ~60 Å and allow the diffusion of proteins of up to ~100 kDa (Demchick and Koch, 1996; Vázquez-Laslop et al., 2001). Hence, LpoA with a width of ~30 Å should be able to penetrate the pores present in PG. Therefore, our data on the molecular dimensions and shape of LpoA are consistent with the observed crosslinking of LpoA with PBP1A in intact cells (Typas et al., 2010).

The synthesis of new PG and its incorporation into the existing cell wall in growing and dividing bacteria is a well-regulated process, ensuring that the growth of all cell envelope layers is coordinated with cell growth. We are only beginning to understand the complexity of these processes and still lack insights into crucial molecular details of PG growth. PG synthases engage in multiple interactions with other PG enzymes, and the cytoskeletal proteins FtsZ and MreB with associated proteins are essential to guide PG growth (Typas et al., 2012). Presumably, these proteins form large multiprotein complexes for PG synthesis during cell elongation and division, called the elongasome and divisome, respectively (Szwedziak and Löwe, 2013). Bifunctional PG synthases with both glycosyltransferase and transpeptidase activities are part of these complexes and play a major role in PG growth, but only few structures of these important enzymes are known (Han et al., 2011; Lovering et al., 2007; Sung et al., 2009). Hence, we need more structural data on PG enzymes and their interacting proteins. In this report, we have presented data on LpoA that form the structural basis for understanding the activation of PG synthases by outer-membrane proteins.

EXPERIMENTAL PROCEDURES

Protein Purification

BL21(DE3) strains harboring pET28LpoA or pET28LpoA^N (Typas et al., 2010) were used to produce soluble full-length LpoA or LpoA^N (lipid anchor replaced by an oligohistidine tag) with different isotopic labeling schemes (details in Supplemental Experimental Procedures).

NMR Spectroscopy

NMR data were collected on a 2.5 mM [^{13}C, ^{15}N]-LpoA^N sample in 100 mM sodium acetate buffer, pH 4.5, containing 10% D_2O at 323 K. Backbone and side-chain resonances were assigned as previously described (Jean et al., 2014). For the assignment of backbone resonances of flexible regions of full-length LpoA, a 3D HNCACB and a 3D BEST-TROSY-(H)N(COCA)NH (Solyom et al., 2013) were collected at 293 K on a 0.75 mM [^{13}C, ^{15}N]-LpoA sample in 50 mM HEPES, 100 mM NaCl, pH 6.5, containing 10% D_2O (buffer I), on Bruker spectrometers operating at 700 and 950 MHz ^{1}H NMR frequency, equipped with triple ^{1}H, ^{15}N, ^{13}C-resonance cryoprobes. 2D ^{1}H-^{15}N-BEST-TROSY and 2D-methyl-HMQC/HSQC (Tugarinov et al., 2003) spectra were recorded on the 950-MHz Bruker spectrometer on a 72 μM U-[^{2}H, ^{12}C, ^{15}N], Val-[^{13}C^{1}H$_3$]$^{pro\text{-}S}$, Ala-[^{13}C^{1}H$_3$]-LpoA, or 297 μM U-[^{2}H, ^{12}C, ^{15}N]-LpoA sample in buffer I at 293 K. Details regarding the data analysis are reported in Supplemental Experimental Procedures.

Extraction of Structural Restraints and Structure Calculation

Distance restraints from 3D ^{15}N-NOESY-HSQC, and 3D aliphatic, aromatic ^{13}C-NOESY-HSQC experiments were obtained by using UNIO'10 version 2.0.2 (Guerry and Herrmann, 2012). Additional distance constraints were extracted from peak volumes from a methyl-^{13}C-NOESY-HSQC experiment assigned manually. TALOS+ was used to determine phi/psi dihedral angle restraints from chemical shifts (Shen et al., 2009). The structure of LpoA^N was calculated with Aria 2.3.1 (Rieping et al., 2007) and 100 structures were calculated in each iteration, except in the last cycle when 700 structures were calculated. The 20 lowest-energy structures underwent explicit water refinement. The structures were visualized graphically and all figures were made with the Pymol Molecular Graphics System, version 1.5.0.4 (Schrödinger, LLC).

AUC

Sedimentation velocity experiments were performed on an analytical ultracentrifuge XLI (Beckman Coulter) operating at 293 K with a rotor speed of 42,000 rpm. Three ^{15}N-labeled LpoA samples (6, 2, and 0.2 mg/ml) in 50 mM HEPES, 100 mM NaCl, pH 6.5, were loaded on double-sector centerpieces in the Anti-50 rotor with optical path lengths of 1.5, 3 and 12 mm, respectively (Nanolytics). The data were acquired at 280 nm using interference optics and analyzed with SEDFIT 14.1 (Schuck, 2000).

SAXS

SAXS data were collected on beamline BM29 at the European Synchrotron Radiation Facility (Grenoble, France). Scattering data were collected on three ^{15}N-LpoA samples with concentrations of 5, 2, and 1 mg/ml, in the same buffer conditions as in the AUC experiments. Each sample was positioned at 2.87 m from a Pilatus detector and ten frames of 1 s were recorded at a

wavelength of 0.99 Å. After normalization to the intensity of the transmitted beam, frames were merged for each sample. Subtraction of the buffer's contribution to the scattering and further processing steps were performed with PRIMUS from the ATSAS 2.5.1 program package (Svergun, 1992). The radius of gyration, R_g, forward scattering intensity, I(0), maximum particle dimension, D_{max}, and distance distribution function, P(r) were evaluated with GNOM. The R_g was also estimated using the Guinier approximation in the Autorg software (Petoukhov et al., 2007). The NMR structure of $LpoA^N$ and a model structure of *E. coli* $LpoA^C$, predicted by PHYRE (Kelley and Sternberg, 2009) from its homolog in *H. influenzae*, were used to calculate the R_g and P(r). Globular, L-shaped, and elongated models of full-length LpoA were created using different dihedral angles in the linker. Scattering curves were then simulated on these models by CRYSOL. Their respective distance distribution function and the parameters R_g and D_{max} were calculated by GNOM.

ACCESSION NUMBERS

The coordinates of 20 structures and chemical shifts of $LpoA^N$ have been deposited in the Protein Data Bank and the BioMagResBank under accession codes 2MHK and 18853, respectively.

SUPPLEMENTAL INFORMATION

Supplemental Information includes Supplemental Experimental Procedures and three figures and can be found with this article online at http://dx.doi.org/10.1016/j.str.2014.04.017.

ACKNOWLEDGMENTS

We thank L. Signor, A. Le Roy, C. Ebel, and the staff of the ESRF and EMBL-Grenoble for assistance, support, and access to the Mass Spectrometry Facility, the Analytical Ultracentrifugation Platform, and beamline BM29. We thank J. Boisbouvier, B. Brutscher, D. Marion, and P. Schanda for stimulating discussions, and NMR-Bio for the kind gift of deuterated alanine and acetolactate precursors. W.V. and R.J.L. were supported by the BBSRC (BB/I020012/1). W.V. was also supported by the EC DIVINOCELL (HEALTH-F3-2009-223431). A.D. was supported by an EMBO long-term fellowship and N.L.J. was supported by a PhD fellowship (CFR) from the CEA. This work used the platforms of the Grenoble Instruct Centre (ISBG; UMS 3518 CNRS-CEA-UJF-EMBL) with support from FRISBI (ANR-10-INSB-05-02) and GRAL (ANR-10-LABX-49-01) within the Grenoble Partnership for Structural Biology (PSB). Financial support was also provided by the IR-RMN-THC FR3050 CNRS to conduct the NMR research.

Received: December 3, 2013
Revised: April 25, 2014
Accepted: April 28, 2014
Published: June 19, 2014

REFERENCES

Allan, R.K., and Ratajczak, T. (2011). Versatile TPR domains accommodate different modes of target protein recognition and function. Cell Stress Chaperones *16*, 353–367.

Banzhaf, M., van den Berg van Saparoea, B., Terrak, M., Fraipont, C., Egan, A., Philippe, J., Zapun, A., Breukink, E., Nguyen-Distèche, M., den Blaauwen, T., and Vollmer, W. (2012). Cooperativity of peptidoglycan synthases active in bacterial cell elongation. Mol. Microbiol. *85*, 179–194.

Bertsche, U., Breukink, E., Kast, T., and Vollmer, W. (2005). *In vitro* murein peptidoglycan synthesis by dimers of the bifunctional transglycosylase-transpeptidase PBP1B from *Escherichia coli*. J. Biol. Chem. *280*, 38096–38101.

Biegert, A., Mayer, C., Remmert, M., Söding, J., and Lupas, A.N. (2006). The MPI Bioinformatics Toolkit for protein sequence analysis. Nucleic Acids Res. *34*, W335–W339.

Born, P., Breukink, E., and Vollmer, W. (2006). In vitro synthesis of cross-linked murein and its attachment to sacculi by PBP1A from *Escherichia coli*. J. Biol. Chem. *281*, 26985–26993.

Demchick, P., and Koch, A.L. (1996). The permeability of the wall fabric of *Escherichia coli* and *Bacillus subtilis*. J. Bacteriol. *178*, 768–773.

Guerry, P., and Herrmann, T. (2012). Comprehensive automation for NMR structure determination of proteins. Methods Mol. Biol. *831*, 429–451.

Han, S., Caspers, N., Zaniewski, R.P., Lacey, B.M., Tomaras, A.P., Feng, X., Geoghegan, K.F., and Shanmugasundaram, V. (2011). Distinctive attributes of β-lactam target proteins in Acinetobacter baumannii relevant to development of new antibiotics. J. Am. Chem. Soc. *133*, 20536–20545.

Holm, L., and Rosenström, P. (2010). Dali server: conservation mapping in 3D. Nucleic Acids Res. *38*, W545–W549.

Jean, N.L., Bougault, C., Derouaux, A., Callens, G., Vollmer, W., and Simorre, J.P. (2014). Backbone and side-chain ^1H, ^{13}C, and ^{15}N NMR assignments of the N-terminal domain of *Escherichia coli* LpoA. Biomol. NMR Assign. Published online February 4, 2014. http://dx.doi.org/10.1007/s12104-014-9546-2.

Kelley, L.A., and Sternberg, M.J. (2009). Protein structure prediction on the Web: a case study using the Phyre server. Nat. Protoc. *4*, 363–371.

Kim, K.H., Aulakh, S., and Paetzel, M. (2011). Crystal structure of β-barrel assembly machinery BamCD protein complex. J. Biol. Chem. *286*, 39116–39121.

Lovering, A.L., de Castro, L.H., Lim, D., and Strynadka, N.C. (2007). Structural insight into the transglycosylation step of bacterial cell-wall biosynthesis. Science *315*, 1402–1405.

Paradis-Bleau, C., Markovski, M., Uehara, T., Lupoli, T.J., Walker, S., Kahne, D.E., and Bernhardt, T.G. (2010). Lipoprotein cofactors located in the outer membrane activate bacterial cell wall polymerases. Cell *143*, 1110–1120.

Petoukhov, M.V., Konarev, P.V., Kikhney, A.G., and Svergun, D.I. (2007). ATSAS 2.1—towards automated and web-supported small-angle scattering data analysis. J. Appl. Cryst. *40*, 223–228.

Rieping, W., Habeck, M., Bardiaux, B., Bernard, A., Malliavin, T.E., and Nilges, M. (2007). ARIA2: automated NOE assignment and data integration in NMR structure calculation. Bioinformatics *23*, 381–382.

Sandoval, C.M., Baker, S.L., Jansen, K., Metzner, S.I., and Sousa, M.C. (2011). Crystal structure of BamD: an essential component of the β-Barrel assembly machinery of Gram-negative bacteria. J. Mol. Biol. *409*, 348–357.

Schuck, P. (2000). Size-distribution analysis of macromolecules by sedimentation velocity ultracentrifugation and lamm equation modeling. Biophys. J. *78*, 1606–1619.

Shen, Y., Delaglio, F., Cornilescu, G., and Bax, A. (2009). TALOS+: a hybrid method for predicting protein backbone torsion angles from NMR chemical shifts. J. Biomol. NMR *44*, 213–223.

Solyom, Z., Schwarten, M., Geist, L., Konrat, R., Willbold, D., and Brutscher, B. (2013). BEST-TROSY experiments for time-efficient sequential resonance assignment of large disordered proteins. J. Biomol. NMR *55*, 311–321.

Sung, M.T., Lai, Y.T., Huang, C.Y., Chou, L.Y., Shih, H.W., Cheng, W.C., Wong, C.H., and Ma, C. (2009). Crystal structure of the membrane-bound bifunctional transglycosylase PBP1b from *Escherichia coli*. Proc. Natl. Acad. Sci. USA *106*, 8824–8829.

Svergun, D.I. (1992). Determination of the regularization parameter in indirect-transform methods using perceptual criteria. J. Appl. Cryst. *25*, 495–503.

Szwedziak, P., and Löwe, J. (2013). Do the divisome and elongasome share a common evolutionary past? Curr. Opin. Microbiol. *16*, 745–751.

Tugarinov, V., Hwang, P.M., Ollerenshaw, J.E., and Kay, L.E. (2003). Cross-correlated relaxation enhanced 1H-13C NMR spectroscopy of methyl groups in very high molecular weight proteins and protein complexes. J. Am. Chem. Soc. *125*, 10420–10428.

Typas, A., Banzhaf, M., van den Berg van Saparoea, B., Verheul, J., Biboy, J., Nichols, R.J., Zietek, M., Beilharz, K., Kannenberg, K., von Rechenberg, M., et al. (2010). Regulation of peptidoglycan synthesis by outer-membrane proteins. Cell *143*, 1097–1109.

Typas, A., Banzhaf, M., Gross, C.A., and Vollmer, W. (2012). From the regulation of peptidoglycan synthesis to bacterial growth and morphology. Nat. Rev. Microbiol. *10*, 123–136.

Vázquez-Laslop, N., Lee, H., Hu, R., and Neyfakh, A.A. (2001). Molecular sieve mechanism of selective release of cytoplasmic proteins by osmotically shocked *Escherichia coli*. J. Bacteriol. *183*, 2399–2404.

Vijayalakshmi, J., Akerley, B.J., and Saper, M.A. (2008). Structure of YraM, a protein essential for growth of *Haemophilus influenzae*. Proteins *73*, 204–217.

Vollmer, W., and Höltje, J.-V. (2004). The architecture of the murein (peptidoglycan) in Gram-negative bacteria: vertical scaffold or horizontal layer(s)? J. Bacteriol. *186*, 5978–5987.

Vollmer, W., Blanot, D., and de Pedro, M.A. (2008). Peptidoglycan structure and architecture. FEMS Microbiol. Rev. *32*, 149–167.

Zeytuni, N., and Zarivach, R. (2012). Structural and functional discussion of the tetra-trico-peptide repeat, a protein interaction module. Structure *20*, 397–405.

SUPPLEMENTAL INFORMATION

The elongated structure of the outer-membrane activator of peptidoglycan synthesis LpoA: implications in PBP1A-stimulation

Nicolas L. Jean, Catherine M. Bougault, Adam Lodge, Adeline Derouaux, Gilles Callens, Alexander J. F. Egan, Isabel Ayala, Richard J. Lewis, Waldemar Vollmer,* Jean-Pierre Simorre*

Inventory of Supplemental Information

Supplemental Experimental Procedures

Expression and purification of LpoA versions.

Unlabeled LpoA and LpoA^N. BL21(DE3) strains harboring plasmids pET28LpoA or pET28LpoA^N were used to purify soluble full-length LpoA or LpoA^N (lipid anchor replaced by an oligohistidine tag). Three liters of LB medium (10 g/L tryptone, 5 g/L yeast extract, 10 g/L NaCl) containing 50 µg/mL kanamycin were inoculated 1 in 50 with a corresponding overnight culture and incubated at 37°C until the OD_{578} reached 0.4 – 0.6. Overexpression of recombinant *lpoA* genes was induced by the addition of 1 mM IPTG and further incubation for 3 h at 30°C. Cells were harvested by centrifugation (10,000 × g, 15 min, 4°C) and the pellet was resuspended in 40 mL of buffer I (25 mM Tris/HCl, 10 mM $MgCl_2$, 500 mM NaCl, 20 mM imidazole, 10% glycerol, pH 7.5). DNase, protease inhibitor cocktail (Sigma) (1 to 1000 dilution) and 100 µM phenylmethylsulfonylfluoride (PMSF) was added before cells were disrupted by sonication using a Branson digital sonicator. The lysate was centrifuged (130,000 × g, 60 min, 4°C) and the supernatant was applied at a 1 mL/min flow rate to a 5 mL HisTrap HP column (GE Healthcare) attached to an ÄKTA PrimePlus (GE Healthcare) FPLC. The column was washed with 4 volumes of buffer I before step-wise elution of bound proteins with buffer II (25 mM Tris/HCl, 10 mM $MgCl_2$, 500 mM NaCl, 400 mM imidazole, 10% glycerol, pH 7.5). If a second purification step was required, proteins were dialyzed against IEX buffer A (20 mM Tris/HCl, pH 8.0) and applied to a 5 mL HiTrap Q HP column (GE healthcare) at a flow rate of 0.5 mL/min using an ÄKTA PrimePlus FPLC system. The column was washed with 85% IEX buffer A and 15% IEX buffer B (20 mM Tris/HCl, 500 mM NaCl, pH 8.0) for 10 column volumes at 2 mL/min before a linear gradient from 15% to 100% B over 150 mL was applied at 2 mL/min. The eluted LpoA protein was pooled and concentrated to 4 – 5 mL for application to a Superdex200 HiLoad 16/600 column at 1 mL/min for size exclusion chromatography in a buffer containing 25 mM Tris/HCl, 10 mM $MgCl_2$, 500 mM NaCl, 10% glycerol at pH 7.5. In the case of LpoA^N the second purification step (ion exchange chromatography) was omitted.

U-^{15}N-LpoA, U-[^{13}C, ^{15}N]-LpoA and U-[^{13}C, ^{15}N]-LpoA^{N}. For the production of ^{15}N- or ^{13}C,^{15}N-isotopically labeled versions, 2 L M9 growth medium (5.29 g/L Na_2HPO_4, 3 g/L KH_2PO_4, 0.5 g/L NaCl, 1 g/L NH_4Cl, 2 mM thiamine, 1 mM $MgSO_4$, 0.1 mM $CaCl_2$, 0.3% glucose, pH 6.8 – 7.2) containing 50 µg/mL kanamycin were used. For single labeled protein [^{15}N]-NH_4Cl was used, for double labeled protein both [^{15}N]-NH_4Cl and [^{13}C]-glucose were used (Cambridge isotope laboratories Inc, USA). Cells were grown overnight in 100 mL M9 medium per liter of final culture, harvested by centrifugation (3,000 × g, 20 min, RT) and resuspended in 2 × 1 mL of fresh M9 medium which was used to inoculate the remaining 900 mL M9 medium containing the desired isotopically labelled compound(s). Purification proceeded by affinity and gel filtration chromatography as described above.

Perdeuterated LpoA samples. The U-[^{2}H, ^{15}N, ^{12}C], Val-[2,3-$^{2}H_2$; 1,2,3-$^{12}C_3$; [^{12}C^{2}H$_3$]$^{pro\text{-}R}$/[^{13}C^{1}H$_3$]$^{pro\text{-}S}$], Ala-[2-^{12}C^{2}H; 3-^{13}C^{1}H$_3$]-LpoA sample (labeled in short U-[^{2}H, ^{15}N, ^{12}C], Val-[^{13}C^{1}H$_3$]$^{pro\text{-}S}$], Ala-[^{13}C^{1}H$_3$]-LpoA) was prepared according to our published protocols (Ayala et al., 2009; Mas et al., 2013). *E. coli* BL21(DE3) carrying the LpoA plasmid were progressively adapted in three stages over 24 h to an enriched M9/D_2O medium containing 5.3 g/L Na_2HPO_4, 3 g/L KH_2PO_4, 0.5 g/L NaCl, 1 g/L $^{15}NH_4Cl$, 1 mM thiamine, 1 mM $MgSO_4$, 0.1 mM $CaCl_2$, 50 µM $ZnSO_4$, 100 µM $FeCl_3$, 30 mg/L kanamycin, a vitamin cocktail, and 2 g/L D-glucose-d_7 ($^{12}C_6{}^{1}H_5{}^{2}H_7O_6$, Isotec) at pH 6.8 – 7.2. Two 500 mL cultures in enriched M9/D_2O medium were inoculated and grown at 37°C. When the OD_{600} reached 0.6 to 0.8, solutions of [2-^{12}C^{2}H; 3-^{13}C^{1}H$_3$]-L-alanine (NMR-Bio), *pro-S* acetolactate-^{13}C (2-hydroxy-2-[^{13}C]methyl-3-oxo-4,4,4-tri-[^{2}H]butanoate, NMR-Bio) and L-leucine-d_{10} (Sigma-Aldrich) in D_2O were added to final concentrations of 500 mg/L, 240 mg/L and 30 mg/L, respectively. After one hour, protein expression was induced by the addition of 1 mM IPTG and the culture was incubated at 20°C overnight. Cells were harvested by centrifugation (5,000 × g, 10 min, 4°C) and the pellet was resuspended in 40 mL of buffer I (25 mM Tris/HCl, 100 mM NaCl, pH 7.5). Purification proceeded through affinity and gel filtration chromatography steps as described above. To prevent LpoA sample degradation, purification steps were led at 4°C in

presence of Complete™ protease inhibitor cocktail (Roche).

The U-[^{2}H, ^{15}N, ^{12}C]-LpoA sample was prepared according to the protocol described by Rasia et al. in 2009. *E. coli* BL21(DE3) bacterial cells harboring the LpoA plasmid were grown in M9/H_2O medium containing 10 g/L $Na_2HPO_4.7H_2O$, 3 g/L KH_2PO_4, 0.5 g/L NaCl, 1 g/L $^{15}NH_4Cl$, 1 mM thiamine, 1 mM $MgSO_4$, 0.1 mM $CaCl_2$, 50 μM $ZnSO_4$, 100 μM $FeCl_3$, 30 mg/L kanamycin, a vitamin cocktail, and 2 g/L D-glucose-d_7 ($^{12}C_6{}^{1}H_5{}^{2}H_7O_6$, Isotec) at 37°C. When the OD_{600} reached 0.5 to 0.6, the medium was supplemented with 3 g/L -[^{2}H, ^{15}N, ^{12}C]-ISOGRO™ powder (Isotec). After one hour, 1 mM IPTG was added and the culture was incubated at 20°C overnight. The purification protocol was identical to the one described just above. Due to the presence of H_2O instead of D_2O in the culture medium, all the water exchangeable nuclei remained protonated, in contrast to the previous sample.

Both perdeuterated protein samples were characterized by gel electrophoresis and the HPLC profile from the gel filtration chromatography and showed identical properties as the U-[^{1}H, ^{13}C, ^{15}N] sample.

Secondary structure propensities in the flexible regions 1 and 2 of full-length LpoA.

The ^{1}H, ^{15}N and ^{13}C chemical shifts from assigned residues in the flexible regions 1 (N285 – P351) and 2 (S493 – N531) of full-length LpoA have been analyzed to determine secondary structure propensity. Chemical shift differences with respect to random coil values corrected with sequence-dependent effects (Schwarzinger et al., 2001) failed to identify secondary structure elements. The SSP software (Marsh et al., 2006) computed 10.5% and 1.4% β-structure and 0.1% and 1.0% α-helical propensity for regions 1 and 2, respectively. MICS (Shen and Bax, 2012) and TALOS+ (Shen et al., 2009) showed marked dynamics for regions 1 and 2 with S^2 values of 0.449 ± 0.091 and 0.458 ± 0.105. These predictions are consistent with the either positive and below 0.2 or negative {^{1}H}-^{15}N-NOE values measured for the sequence specifically assigned residues. The latter programs predicted a higher uniformly distributed β-structure propensity in regions 1 and 2

(28% and 24%, respectively). Delta2D (Camilloni et al., 2012), developed specifically for the analysis of disordered proteins, gave 6.1% and 7.5% β-structure and 87.5% and 83.8% coil propensity for regions 1 and 2, respectively. Consequently, regions 1 and 2 appear disordered or dynamic, at least for the assigned residues, which include a large portion of region 1 and the loop region of region 2. The secondary structure in these regions cannot be determined conclusively from the different programs used because of the discrepancies of their outputs, which may in part be correlated to the incompleteness of the specific resonance assignments for these regions.

NMR data processing and analysis.

NMR data were processed with NMRPipe (Delaglio et al., 1995) and analyzed using the CcpNmr Analysis 2.2 software (Vranken et al., 2005). To estimate correlation times of the N-terminal and C-terminal domain of full-length LpoA, the intensity of ^{1}H-^{13}C correlations of methyl groups for alanine residues in the HMQC (I_{HMQC}) and HSQC (I_{HSQC}) spectra were determined, after fitting of the individual lineshapes with a Gaussian function within the CcpNmr software. Intensity ratios I_{HMQC}/I_{HSQC} were calculated for each individual methyl group. Similar ratios (average value 1.3) were obtained for resolved alanine correlations arising from the N-terminal and C-terminal domains, suggesting a similar correlation time for the two domains. These ratios were drastically different and showed a systematic enhancement with respect to ratios calculated for residues arising from the flexible regions 1 and 2 in the C-terminal domain.

Supplemental References

Ashkenazy, H., Erez, E., Martz, E., Pupko, T., and Ben-Tal, N. (2010). ConSurf 2010: calculating evolutionary conservation in sequence and structure of proteins and nucleic acids. Nucleic Acids Res. *38*, W529-W533.

Ayala, I., Sounier, R., Usé, N., Gans, P., and Boisbouvier, J. (2009). An efficient protocol for the complete incorporation of methyl-protonated alanine in perdeuterated protein. J Biomol NMR, *43*, 111-119.

Camilloni, C., De Simone, A., Vranken, W., and Vendruscolo,, M. (2012). Determination of secondary structure populations in disordered states of proteins using NMR chemical shifts. Biochemistry *51*, 2224-2231.

Delaglio, F., Grzesiek, S., Vuister, G.W., Zhu, G., Pfeifer, J., and Bax, A. (1995). NMRPipe: a multidimensional spectral processing system based on UNIX pipes. J Biomol NMR *6*, 277-293.

Marsh, J.A., Singh, V.K., Jia, Z. and Forman-Kay, J.D. (2006). Sensitivity of secondary structure propensities to sequence differences between α- and γ-synuclein: Implications for fibrillation. Protein Science *15*, 2795–2804.

Mas, G., Crublet, E., Hamelin, O., Gans, P., and Boisbouvier, J. (2013). Specific labeling and assignment strategies of valine methyl groups for NMR studies of high molecular weight proteins. J Biomol NMR, *57*, 251-262.

Rasia, R.M., Noirclerc-Savoye, M., Bologna, N.G., Gallet, B., Plevin, M.J., Blanchard, L., Palatnik, J.F., Brutscher, B., Vernet, T., and Boisbouvier, J. (2009). Parallel screening and optimization of protein constructs for structural studies. Protein Sci *18*, 434-439.

Shen, Y., Delaglio, F., Cornilescu, G., and Bax, A. (2009). TALOS+: a hybrid method for predicting protein backbone torsion angles from NMR chemical shifts. J Biomol NMR *44*, 213-223.

Shen, Y., and Bax, A. (2012). Identification of helix capping and beta-turn motifs from NMR chemical shifts. J. Biomol. NMR *52*, 211-232.

Schwarzinger, S., Kroon, G.J.A., Foss, T.R., Chung J., Wright, P.E., and Dyson, H.J. (2001). Sequence-dependent correction of random coil NMR chemical shifts. J Am Chem Soc *123*, 2970-2978.

Vranken, W.F., Vriend, G., and Vuister, G.W. (2012). CING: an integrated residue-based structure validation program suite. J Biomol NMR *54*, 267-283.

Figure S1

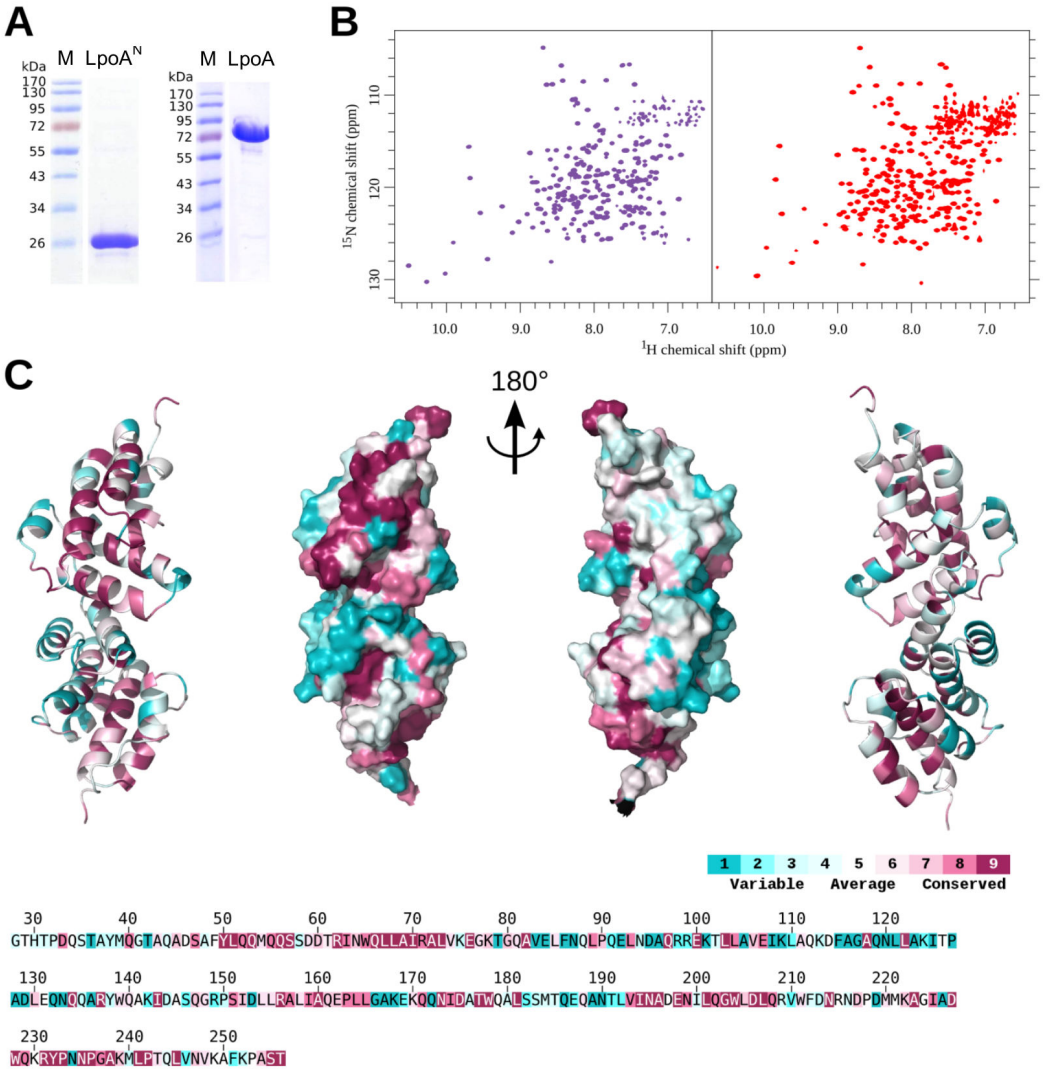

Figure S1, related to Figure 1: Characterization of LpoA^N and full-length LpoA in different conditions. (A) SDS-PAGE analysis of purified LpoA^N and LpoA. The purified proteins were separated by SDS-PAGE before the gels were stained with Coomassie Blue. The molecular weight of the protein markers shown in lanes M is listed. (B) The stability of LpoA^N in different temperature and pH conditions was evaluated by NMR. ^{1}H-^{15}N-BEST-TROSY spectrum recorded at 50°C and pH 4.5 in 150 mM sodium acetate buffer is shown in the left panel (purple). The equivalent spectrum recorded at 25°C and pH 7.0 after dialysis of the same LpoA^N sample in 20 mM HEPES buffer is shown in the right panel (red). Additional conditions (10 mM TRIS buffer at pH 7.5 and 25°C, 20 mM HEPES buffer containing 100 mM NaCl at pH 7.0 and 25°C, 100 mM

MOPS at pH 6.9 and 25°C, 100 mM MES buffer at pH 6.3 and 35°C, 200 mM sodium acetate buffer at pH 4.5 and 35°C) were investigated (data not shown). $LpoA^N$ was stable from 5 to 50°C and on the [4.5 – 7.5] pH range, as emphasized from the characteristic NMR peak pattern. The signal-to-noise ratio in the NMR spectra is increased at elevated temperature and acidic pH. (C) Conserved residues in $LpoA^N$ identified by the Consurf server (Ashkenazy et al., 2010). Multiple sequence alignment was built for $LpoA^N$ (residues 28 to 256) from 63 unique protein sequences using MAFFT and sequences from homologues were obtained from the UNIREF90 database and the CSI-BLAST algorithm. Conservation scores obtained from this alignment were used to color residues on a cartoon and a surface representation of the $LpoA^N$ structure. Two orientations rotated by 180° are shown for the two types of representations. On the bottom part of this panel, the conservation scores are reported on the primary sequence of the $LpoA^N$ protein.

Figure S2

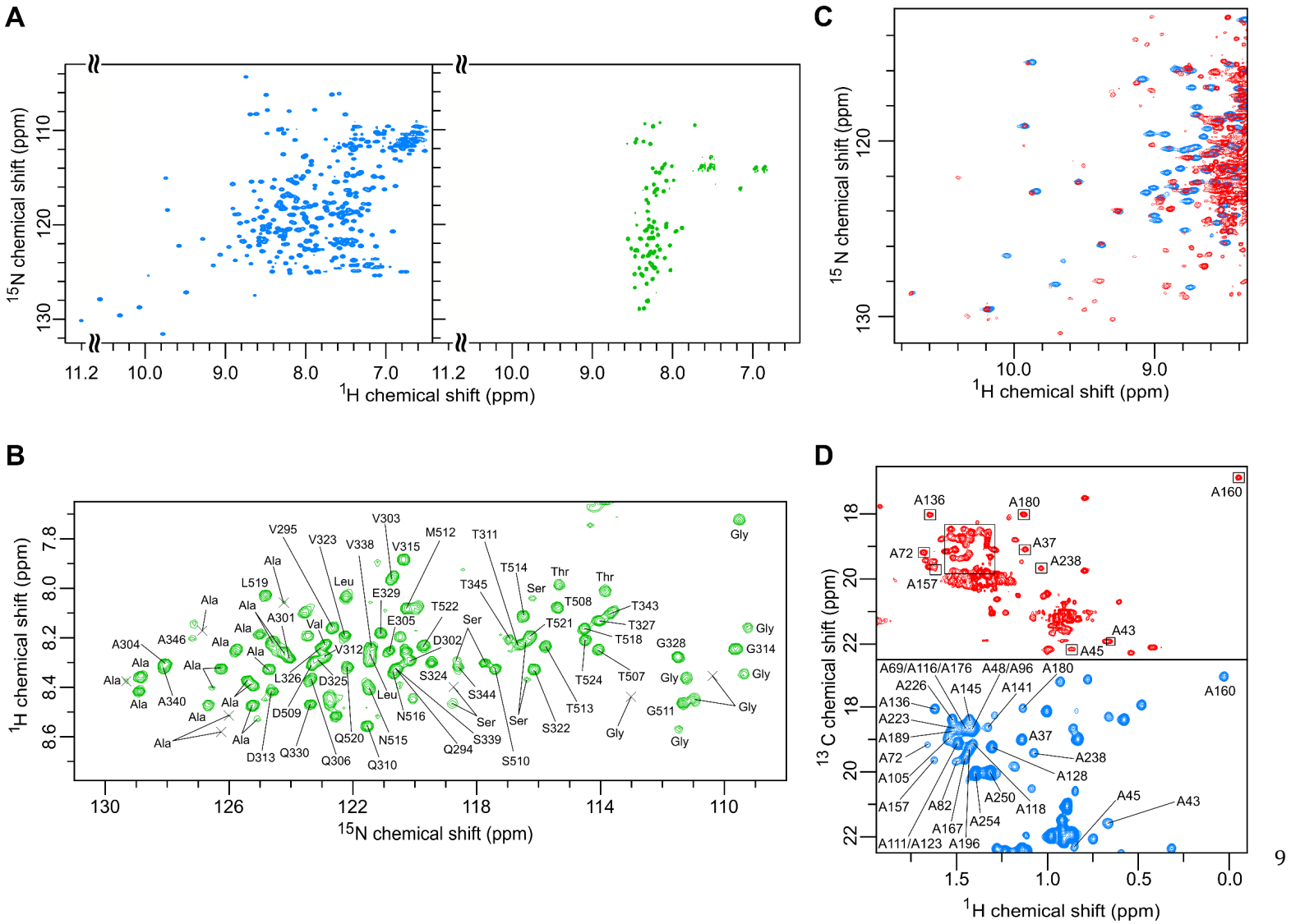
A
B
C
D
^{15}N chemical shift (ppm)
^{1}H chemical shift (ppm)
^{13}C chemical shift (ppm)

Figure S2, related to Figure 2. Characteristic spectroscopic signatures of $LpoA^N$ and full-length LpoA. (A) The ^{1}H-^{15}N-HSQC spectrum (left, blue) on $LpoA^N$ was recorded at 50°C and pH 4.5 in a 100 mM sodium acetate buffer. The ^{1}H-^{15}N-BEST-TROSY spectrum (right, green) on ^{13}C,^{15}N-LpoA was recorded at 20°C and pH 6.5 in a 50 mM HEPES, 100 mM NaCl buffer. In this spectrum, only the amide resonances of residues located in flexible portions (mainly additional regions 1 and 2) were detected. (B) Portion of the LpoA spectrum shown in the previous right panel after rotation of the axes. Assignment of the resonances of disordered residues in LpoA was pursued with the collection of 3D HNCACB and BEST-TROSY-(H)N(COCA)NH. Residues sequentially assigned are indicated with the amino acid numbering of the wild-type LpoA protein. For the residues not sequentially assigned, the residue type obtained from the Cα and Cβ chemical shifts (for 36 resonances among which 19 Ala, which fits reasonably well with the 14 unassigned Ala in region 1 and the 2 Ala in region 2) is indicated by the name of the corresponding amino acid. Peaks observable only at lower threshold are marked with a cross. When the protein sample was stored for a few weeks at 4°C, the full-length ^{13}C,^{15}N-LpoA sample showed degradation of the C-terminal domain (as confirmed by gel electrophoresis and mass spectrometry) and reappearance of the signature of $LpoA^N$. At 20°C, the sample showed significant degradation within 48 h. (C) The left panel shows an overlay of the resolved portion of the 2D ^{1}H-^{15}N-BEST-TROSY (red) and ^{1}H-^{15}N-HSQC (blue) amide region collected on 72 μM U-[^{2}H, ^{12}C, ^{15}N], Val-[$^{13}C^{1}H_3$]$^{pro\text{-}S}$, Ala-[$^{13}C^{1}H_3$]-LpoA and 200 μM ^{13}C,^{15}N- $LpoA^N$ samples, respectively, in 50 mM HEPES, 100 mM NaCl containing 10% D_2O at pH 6.5 and 293 K. This spectrum readily allows the identification of the N-terminal domain resonances in the full-length LpoA sample. ^{1}H-^{15}N correlations exclusively present in the full-length LpoA sample arise from the folded C-terminal domain for the main part, while missing correlations may arise from the partial reprotonation of amide positions as the sample was produced in a D_2O medium. (D) The top spectrum (red) shows a portion of the ^{1}H-^{13}C-methyl selective HMQC collected on the U-[^{2}H, ^{12}C, ^{15}N], Val-[$^{13}C^{1}H_3$]$^{pro\text{-}S}$, Ala-[$^{13}C^{1}H_3$]-LpoA sample in 50 mM HEPES, 100 mM NaCl containing 10% D_2O at pH 6.5 at 293K. Assignments of 27 out of

the 29 resonances of the N-terminal domain of LpoA could be transferred from the bottom spectrum (blue). This spectrum corresponds to a portion of the ^{1}H-^{13}C-CT-HSQC recorded at 50°C and pH 4.5 on the $LpoA^{N}$ sample in a 100 mM sodium acetate buffer. In the latter spectrum only Ala β resonances are labeled; Ile γ2, Val γ1 and γ2, and Thr γ resonances are kept unlabeled for clarity.

Figure S3

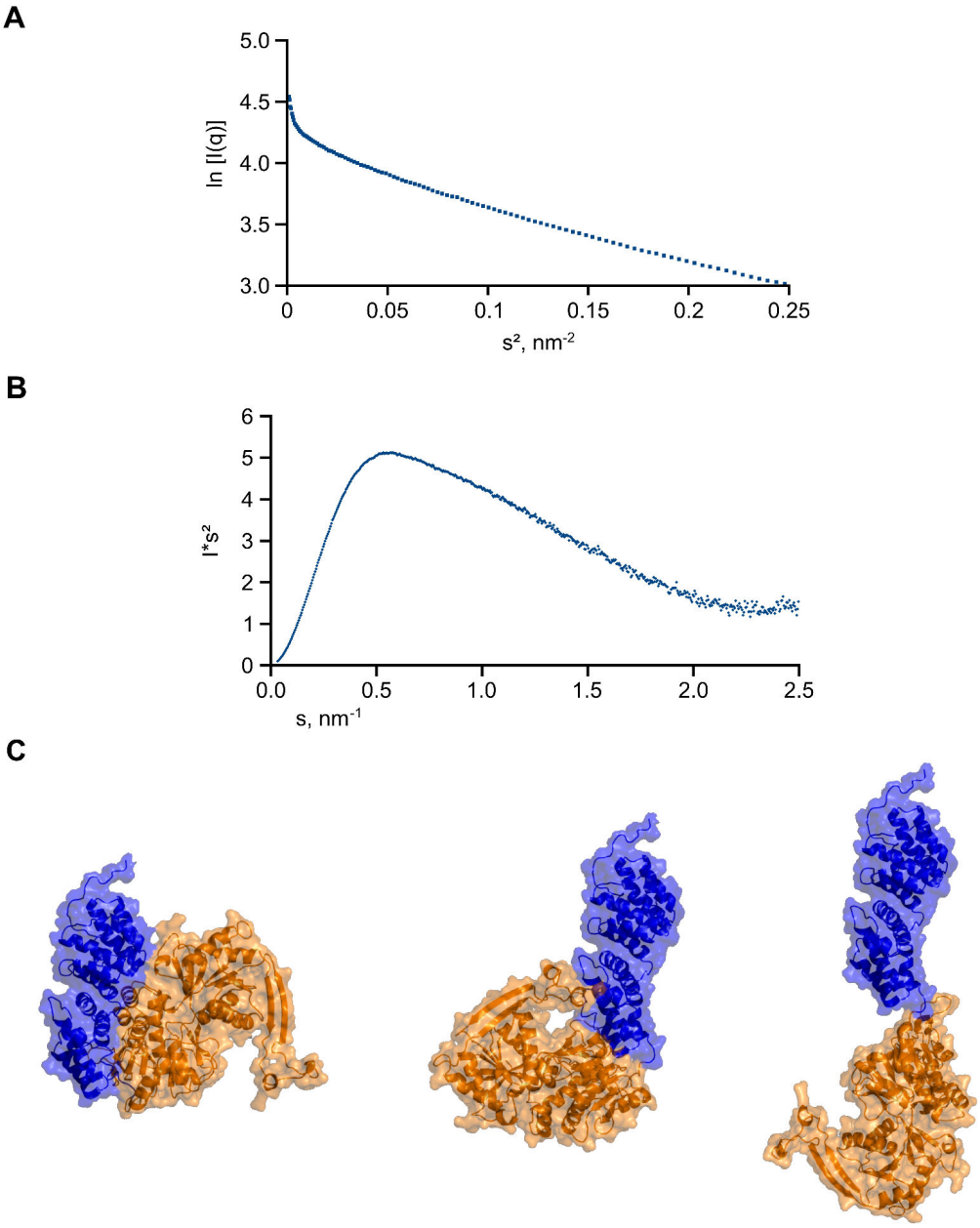

Figure S3, related to Figure 3. Complementary analysis of SAXS data collected on a 5 mg/mL LpoA sample. (A) The Guinier plot calculated from these data is consistent with a 73.4 kDa monomeric protein. (B) The Kratky profile is consistent with a partially unfolded protein, consistent

with AUC and NMR data discussed in the main text. (C) Ribbon representation of the globular (left), L-shaped (middle) and elongated (right) molecular models of LpoA (used to calculate the P(r) curves shown in Figure 3B). These models were built from the *E. coli* $LpoA^N$ NMR structure (blue) and the *E. coli* $LpoA^C$ structure (orange, modeled from the crystal structure of *H. influenzae* $LpoA^C$ (PDB code 3CKM) with PHYRE) by using different dihedral angles in the linker (Figure 2D).

2.B- Discussion

In addition to the issues discussed in the *Structure* article, the determination of the high-resolution structure of $LpoA^N$ and its adoption of an elongated structure to bind PBP1A does not answer all of the questions on its function. It even raises new interrogations, such as the potential partners of its N-terminal domain (and the potential role for those interactions) and the molecular basis of the PBP1A-$LpoA^C$ interaction.

2.B.a- $LpoA^N$ as an interaction platform

As stated in Jean, Bougault, Lodge et al., 2014, $LpoA^N$ has a TPR-like fold. As this conformation is usually implicated in interactions, it seems reasonable to assume that it may enable the binding of LpoA to partners (other than PBP1A) likely members of the elongasome or transiently co-localizing with it. In *Vibrio cholerae* for example, Dörr et al. recently reported the discovery of a new partner for LpoA, the periplasmic CsiV (Cell shape integrity Vibrio, previously named as vc1887), a protein of unknown function (Dörr et al., 2014). CsiV was demonstrated to modulate peptidoglycan synthesis through direct interaction with LpoA (yet the implicated lipoprotein domain was not studied). The protein is thought to favor LpoA ability to stimulate PBP1A transpeptidase activity. If the atomic mechanism of this process and its general aim were not determined, this interaction can be proposed to enable coordination with other processes. Although CsiV is restricted to *Vibrio*, one can think that (an)other protein(s) could play a similar function in *E. coli* and bind to $LpoA^N$ for example. Another interesting observation is that targeting of LpoA to the inner-membrane is lethal in PBP1B-depleted conditions (Paradis-Bleau et al., 2010), suggesting either that PBP1A was not activated by the inner-membrane bound Lpo, or that anchoring to the outer-membrane is required for another essential function, which went unnoticed due to PBP1A and PBP1B redundancies. In the latter case, one can suggest that outer-membrane anchoring could be necessary so that the TPR-like domain remains at proximity of its partner(s). This partner would preferentially be another outer-membrane lipoprotein, such as the AmiD amidase, or one of the Mlt lytic transglycosylases. Such an hypothesis is attractive, as in this context LpoA would directly be linked to both peptidoglycan synthesis and hydrolysis, allowing a concomitant regulation of both events to facilitate glycan strands insertion in the sacculus in a similar manner to Höltje's three-for-one model. Finally, recent work on CpoB established an unexpected redundant role between this protein and $LpoA^N$ (Gray et al., 2015). As CpoB mediates coordination of septal peptidoglycan synthesis with membrane invagination, $LpoA^N$ can be proposed to bridge PBP1A with one of the Tol-Pal elements. This can be surprising as LpoA-PBP1A was stated to be part of the elongasome, but it must be reminded that (i) PBP1A is able to perform septal peptidoglycan synthesis as the single deletion of PBP1B is viable, (ii) LpoA was shown to localize transiently to mid-cell, although in lower proportions than LpoB. Unfortunately, the conditions for PBP1A-LpoA implications in cell division in wild-type cells remain unclear. If we retain the assumption of another lipoprotein partner, then Pal appears as an ideal target. Otherwise, if the ligand is not anchored to the outer-membrane, TolB could be the most promising possibility with the periplasmic domain II and/or III of TolA (despite the fact that no interaction between $LpoA^N$ and TolA were detected, but this may depend on the energized state of TolA, Gray et al., 2015). As for TolQ and TolR, they are likely too far away from this domain to interact with it. How $LpoA^N$ could link outer-membrane constriction to PBP1A activity through one of these putative binding partners remains to be investigated.

Although the importance of possible interactions of $LpoA^N$ were mainly presented here as a way to coordinate different events, another additional likely purpose is the recruitment of LpoA to the elongation sites. Indeed, as briefly reported before, LpoA localization patterns are conserved in the absence of PBP1A. This implies that LpoA either localizes upon interaction

with another elongasome partner, or recognizes a specific peptidoglycan motif (in a similar way to the FtsN SPOR domain). Because $LpoA^N$ length (70 Å) is long enough to reach the peptidoglycan layer, it could indeed mediate this interaction. If the second hypothesis is valid, the specific peptidoglycan motif may be under-represented in the sacculi of *E. coli* collected at the end of the exponential growth, as a first pull-down experiment that I performed with these *E. coli* sacculi and $LpoA^N$ did not evidence any strong interaction (unpublished data).

2.B.b- Stimulation of PBP1A by LpoA

Five years after its discovery, the mode of action of LpoA to stimulate PBP1A still remains obscure. Although the C-terminal domain of LpoA is known to mediate the interaction, the region(s) involved has(have) still not been elucidated. Its most obvious binding interface for an interaction with PBP1A is the cleft between the two C-terminal sub-domains, as it contains several surface conserved residues, and as it is also implicated in interaction with small periplasmic ligands in its structural homologues. This last point raises the question of the nature of the partner binding to this cleft. Is it really interacting with PBP1A or could it be interacting with another molecule? If the cleft is not binding the peptidoglycan synthase, the murein peptide stems or glycan strands appear as an interesting possibility (in agreement with pull-down experiments showing a weak binding of $LpoA^C$ with peptidoglycan). Such an hypothesis is consistent with the relatively high structural similarity of $LpoA^C$ with periplasmic solute-binding proteins, which bind small ligands. However, it is difficult to see what positive effects $LpoA^C$ binding to the peptidoglycan peptide moiety could have, as it would prevent transpeptidase activity by steric clash. The other possibility, recognition of the glycan strand, would have the advantage to maybe orient peptidoglycan in such a way that transpeptidation is facilitated. These hypotheses must be considered with care, as structural homology does not always implicate a same function or partnership. Other interesting regions of *E. coli* $LpoA^C$ deal with its two long disordered stretches, which are likely protruding from two different sides of the protein. Sequence alignments show that, although their sequences are in general little conserved across bacterial species, these extensions are present in similar positions in several organisms, such as *Yersinia pestis* or *Salmonella typhimurium* (Vijayalakshmi et al., 2008). However, these two fragments have different conservation patterns. The first one (residues N285 to P351) is highly variable in sequence (with the exception of the astonishingly well conserved T327) and length, as different organisms present different insertions in this fragment (67 residues in *E. coli* compared to 101 in *Tatumella morbirosei* for example as emphasized in the sequence alignment of figure II.2.3). In contrast, the second stretch (residues S493 to N531) has much less sequence variability and has even several highly conserved residues, such as G499, P501 and Q520. These observations suggest that if these two fragments have indeed a role, the second one is probably involved in a mechanism that is more conserved across γ-proteobacteria. The fact that one of these flexible parts can be found in absence of the other one as in *Pseudomonas aeruginosa* also suggests two separate roles (figure II.2.3). It is not rare to see disordered regions mediating interactions, but a hypothetical binding of these regions to PBP1A remains highly uncertain, as they are entirely absent from $LpoA^C$ in *H. influenzae*, a bacterium which has a PBP1A (albeit the interaction between both remains to be confirmed in this organism).

Molecular characterization of the LpoA-PBP1A interaction could enable to better understand the role of all these noteworthy regions of $LpoA^C$ reported here, but the high dynamics of these two flexible fragments, as well as the high 44-kDa molecular weight of this LpoA domain might partially hinder structural studies by X-ray crystallography and NMR, respectively. Indeed only the two disordered stretches are observed on a $LpoA^C$ $^1H,^{15}N$-NHSQC spectrum, similarly to what was presented in the full-length LpoA spectrum in figure

S2A from the *Structure* article.

Figure II.2.3: Length and sequence diversity in the two disordered stretches of LpoA^{C}. While *H. influenzae* LpoA^{C} does not contain any long disordered region, *P. aeruginosa* has one (the second stretch), and *E. coli* and *Salmonella typhimurium* have two. As illustrated by these last two examples, length of the first stretch can vary significantly. The two disordered stretches (N285 – P351 and S493 – N531 in *E. coli*) are highlighted in gray. Alignments were performed with the T-coffee EBI server.

LpoA interaction with its cognate PBP stimulates its transpeptidase activity (the glycosyltransferase activity was also recently proposed to be enhanced, Lupoli et al., 2014). To determine how this could affect PBP1A, determination of its binding interface is necessary, but unfortunately this is still not defined with certainty. Although as explained earlier, it has been predicted by sequence co-occurrence and by overexpression-inducted lysis in PBP1A-LpoA dependent cells that the ODD domain mediates this interaction, there is still to date no direct evidence available for this function. As an additional non-catalytic domain restricted to one bacterial phylum, it is tempting indeed to define ODD as an interaction platform, similarly to UB2H which interacts at least with LpoB, CpoB (Gray et al., 2015) and likely MipA (Sung et al., 2009). Modeling with Phyre2 of *E. coli* PBP1A based on structures of macromolecules of similar sequences suggests that ODD (R317 to V422) adopts an oligonucleotide/oligosaccharide-binding (OB) fold (figure II.2.4), similarly to the *Acinetobacter baumannii* (Han et al., 2011) and *P. aeruginosa* (Starr et al., 2014) PBP1A determined structures (PDB codes 3UDF and 4OON, respectively). As indicated by its name, this structure is often found implicated in interactions with saccharides and nucleotides, but also with proteins. The OB fold consists of five antiparallel β-strands forming a tight barrel (Arcus, 2002). The face of the barrel composed by the second and third strands, β2 and β3, is generally the surface implicated in interactions, together with the loops of variable lengths located after the first, second and fourth strands (loops L1, L2 and L4, respectively on figure II.2.4 A) which give its specificity. In the case of the ODD model, this region is well solvent-exposed, suggesting that it might have retained the binding function. Interestingly, sequence comparison and structure modeling show that in *H. influenzae*, loop 3 is halved in comparison to its *E. coli*, *A. baumannii* and *P. aeruginosa* homologues (see the bottom of figure II.2.4 B). Whether this loop has an importance for interactions with LpoA or other undetermined

partners is currently unknown.

As LpoA stimulates PBP1A transpeptidase activity, three main hypotheses can be considered for the interaction between the two partners: either LpoA binds only ODD, or only the transpeptidase domain, or an astride region. While the former possibility rather implies a long-range conformation modification (~45 Å), the two latter suggest that the Lpo protein might in addition or instead directly contribute to a modified orientation of the acyl-donor or -acceptor strand, favoring transpeptidation.

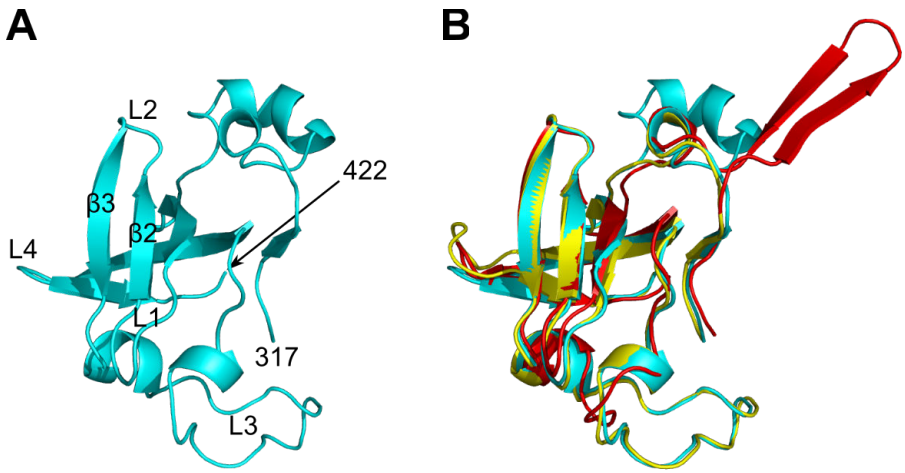

Figure II.2.4: The ODD domain adopts an OB fold. (A) Predicted structure of *E. coli* ODD (R317 – V422). Secondary structure elements discussed in the text are annotated. (B) Comparison of the *E. coli* ODD domain (in cyan) with the equivalent domains from *A. Baumannii* PBP1A structure (R323 – V416, in yellow; PDB code 3UDF) and *H. influenzae* ODD (R317 – I 409, in red). *E. coli* and *H. influenzae* structures were extracted from models of PBP1A generated by Phyre2 for these two organisms. Note that the N-terminal secondary structure ahead of the OB fold itself (an α-helix in *E. coli* and a β-hairpin in *H. influenzae*) must be taken with caution for these models, as their respective sequence is rather similar in this region.

To conclude, the TPR-like domain of the LpoA N-terminal domain can be considered as an interaction platform with partners that remain to be identified. Likely candidates at this stage are proteins that modulate peptidoglycan synthesis like CsiV, or hydrolases like AmiD or Mlts, or proteins of the Tol/Pal system, or peptidoglycan. In contrast, the C-terminal domain of LpoA interacts with PBP1A to activate its transpeptidase activity, which in turn impacts its transglycosylase activity. Likely regions proposed for the $LpoA^{C}$/PBP1A interaction are the cleft between the two C-terminal sub-domains of $LpoA^{C}$ or its two disordered regions, and the ODD and/or transpeptidase domain of PBP1A. These interactions need nevertheless further investigations to yield a detailed understanding of the activation of PBP1A by LpoA and to explain the potential implication of LpoA in the bacterial elongation and division stages.

Résumé en français du chapitre 2 : Caractérisation structurale de LpoA

LpoA est une lipoprotéine de 678 résidus (73 kDa), ancrée à la membrane externe via la cystéine contenue dans un peptide signal. La protéine mature (sans la séquence signal) est composée de deux domaines N- et C-terminal. La structure de ce dernier ($LpoA^C$) était connue pour un homologue de LpoA chez *Haemophilus influenzae* au début de mes travaux. Elle présente un repliement en deux sous-domaines séparés par un sillon, similaire aux protéines liant des solutés périplasmiques. Mes travaux se sont donc tout d'abord focalisés sur la détermination du repliement du domaine N-terminal de LpoA d'*E. coli* ($LpoA^N$) par RMN, en absence de son ancre lipidique. $LpoA^N$ étant stable sur une large gamme de température, les données furent enregistrées à haute température (50 °C) afin de diminuer la superposition des résonances. Ceci permit un taux d'attribution élevé (plus de 95 et 85 % des noyaux ^1H, ^{15}N et ^{13}C du squelette et des chaînes latérales, respectivement). L'analyse des déplacements chimiques ainsi déterminés suggéra rapidement une structure majoritairement composée d'hélices α en l'absence de tout brin β. Ces résultats préliminaires furent l'objet d'un premier article dans le journal *Biomolecular NMR Assignments* (voir article page 157). L'obtention supplémentaire de contraintes structurales, contraintes de distance par attribution des signaux NOE et contraintes angulaires (angles dièdres) par comparaison des déplacements chimiques du squelette avec ceux d'une base de donnée, a permis la détermination de la structure de $LpoA^N$, publiée dans la revue *Structure* (voir article page 162). Ce domaine est composé d'une succession de 12 hélices α et d'une hélice 3_{10} reliées par des boucles. Son organisation structurale est très proche de celle des motifs TPR (TetratricoPeptide Repeat), lui donnant une forme fortement anisotrope. Ces arrangements structuraux étant généralement impliqués dans des interactions, il est probable que le rôle de $LpoA^N$ est de servir de plate-forme d'interaction pour des partenaires qui restent à ce jour non identifiés et qui pourraient être des membres importants de l'élongasome. Étant donné la proximité de $LpoA^N$ à la membrane externe, des lipoprotéines telles que l'amidase AmiD ou les transglycosylases lytiques Mlts pourraient être de tels partenaires. De récents travaux ayant mis en évidence une interaction génétique négative entre LpoA et CpoB, protéine coordonnant la biosynthèse du peptidoglycane et l'invagination de la membrane externe, des membres du système Tol-Pal, tels que Pal ou TolB, pourraient également interagir avec $LpoA^N$.

Mon travail s'est ensuite concentré sur la caractérisation structurale de LpoA entière. Un modèle de $LpoA^C$ ayant pu être généré par homologie avec la structure de $LpoA^C$ d'*H. influenzae*, il restait à définir l'orientation des deux domaines de LpoA l'un par rapport à l'autre. La masse moléculaire de LpoA (environ 70 kDa) est un obstacle majeur à son étude par RMN, provoquant un élargissement des signaux des régions structurées. Toutefois, la collection de spectres ^1H,^{15}N-BEST-TROSY a mis en évidence la présence d'une petite centaine de résonances intenses et faiblement dispersées. Leur répartition étant très différente de celle observée pour $LpoA^N$, une hypothèse selon laquelle les résidus observés provenaient de régions désordonnées du domaine C-terminal a été émise. L'attribution partielle de ces signaux confirma cette hypothèse, montrant qu'ils provenaient de deux régions de $LpoA^C$ absentes chez *H. influenzae* et situées entre les résidus N285 – P351 et S493 – N531. Ce résultat est en accord avec les prédictions bioinformatiques basées sur la séquence (serveur IUPred) qui prédisaient une flexibilité significative pour ces deux fragments. La fonction de ces deux régions reste toutefois inconnue. Un alignement de séquences avec des homologues de LpoA chez d'autres espèces bactériennes met en évidence cependant une plus grande

variabilité de séquence et de longueur pour la première région désordonnée que la deuxième, suggérant des fonctions indépendantes s'ils en est.

L'absence de résonances provenant de $LpoA^N$ et des régions structurées de $LpoA^C$ dans les spectres de LpoA entière suggère que les deux domaines se comportent comme un ensemble unique et que le région charnière les reliant serait donc rigide. Pour confirmer ceci, le marquage spécifique des groupes méthyles, dont les signaux sont beaucoup plus intenses, ProS des valines et des alanines fut effectué, notamment afin de déterminer le temps de corrélation rotationnel de chacun des domaines. Pour les résonances de chaque domaine, le ratio des variations des intensités des pics entre les spectres HMQC (Heteronuclear Multiple Quantum Coherence) et HSQC (Heteronuclear Single Quantum Coherence) calculé fut similaire. Ceci indique un temps de corrélation, temps de réorientation d'un angle d'un radian pour le domaine concerné, très proche pour chacun des domaines, renforçant l'hypothèse d'une connexion rigide entre $LpoA^N$ et $LpoA^C$. Afin de déterminer la forme globale adoptée par LpoA, des expériences de SAXS (diffraction de rayons X aux petits angles) furent menées. L'analyse des courbes de diffraction aux petits angles a permis l'évaluation du rayon de gyration R_G à environ 4,2 nm et le calcul de la fonction de distribution des distances P(r). Étant donné la présence des deux régions flexibles dans $LpoA^C$, une enveloppe de LpoA respectant les données expérimentales ne put être modélisée. Au lieu de cela, trois modèles de LpoA, un modèle globulaire, un modèle coudé en forme de L, et un modèle étendu, furent élaborés sur la base de la structure RMN de $LpoA^N$ et de celle de $LpoA^C$ déterminée par homologie. Les fonctions de distribution de distances théoriques de ces 3 modèles furent calculées et comparées à celle obtenue pour l'échantillon de LpoA en solution. Le modèle de LpoA étendu ayant la courbe la plus proche et un R_G très similaire (4,4 nm environ), il fut conclu que LpoA adopte une conformation plutôt allongée en solution, atteignant une longueur maximale d'environ 145 Å, conforme à la valeur maximale D_{max} de la courbe P(r) déterminée à partir des données expérimentales. La distance entre la membrane externe et le domaine ODD de PBP1A ancrée à la membrane interne étant estimée à environ à un peu plus de 130 Å, LpoA apparaît comme suffisant longue pour atteindre ce domaine. De plus, le diamètre maximal de 30 Å de LpoA devrait être suffisamment faible pour que la protéine puisse traverser les pores du peptidoglycane. Le mécanisme moléculaire selon lequel $LpoA^C$ stimule PBP1A n'est à ce jour pas connue, les interfaces d'interaction sur les deux protéines n'étant pas encore déterminées. Du coté de $LpoA^C$, le sillon en son milieu pourrait être impliqué, puisqu'il lie des substrats de type acides aminés chez les homologues structuraux que sont les protéines liant les solutés périplasmiques. Si tel est le cas, les chaînes peptidiques du peptidoglycane pourraient être suggéré comme un partenaire d'interaction en plus du domaine ODD de PBP1A. Le rôle des extensions désordonnées de PBP1A de *E. coli* étant inconnu, celles-ci pourraient aussi avoir un rôle dans l'interaction, bien qu'elles puissent être absentes comme chez *H. influenzae* par exemple. Concernant PBP1A, ODD pourrait comporter la région liant LpoA comme reporté dans le chapitre 1 de cette partie sur la base de sa conservation. D'après des structures d'homologues de PBP1A, ODD semble adopter un repliement de liaison aux oligonucléotides/oligosaccharides, OB, qui est généralement impliqué dans des interactions avec ces composés ou avec des protéines. En absence de preuves directes d'une interaction de LpoA avec ODD, le domaine transpeptidase de PBP1A doit également rester une hypothèse à considérer.

Ces travaux ont donc permis de déterminer la première structure haute-résolution de $LpoA^N$, qui adopte un repliement similaire à celui des domaines TPR, et pourrait donc être impliqué dans l'interaction avec d'autres partenaires, tels que les transglycosylases lytiques ou des protéines du systèmes Tol-Pal. Ce domaine serait rigidement lié au module C-terminal, donnant à LpoA entière une forme fortement allongée, assez longue pour atteindre PBP1A. Bien que l'interaction entre ces deux protéines ne soit pas caractérisée au niveau moléculaire, le sillon entre les deux sous-domaines de $LpoA^C$ ou ses deux régions désordonnées pourraient

interagir avec PBP1A. Du côté de cette enzyme, ODD apparaît comme une région intéressante, mais le domaine transpeptidase pourrait également être impliqué dans l'interaction.

Chapter 3
Structural characterization of LpoB and interaction with PBP1B

As LpoA, LpoB is anchored to the outer-membrane by covalent bonds between membrane lipids and a cysteine (C20), after cleavage of its preceding signal peptide. From sequence analysis, LpoB seems to be quite different from LpoA. While LpoA is a 72.9 kDa protein (before anchoring), LpoB is only 22.5 kDa (213 residues). In addition, the protein displays a 52-residues low-complexity region containing alanine, glutamate, glutamine, proline and valine which account for more than 77% of the total amino-acid composition, with proline alone representing 30% of this fragment. This N-terminal region is followed by a C-terminal core domain (figure II.3.1). All of these initial observations point to a very different topology from LpoA and suggest that LpoB adopts another strategy than the elongated bi-modal architecture of LpoA to reach the inner-membrane anchored PBP1B. However, at the beginning of this thesis, the structure of LpoB had not been resolved and could not be predicted by homology. Furthermore, its interaction with UB2H was uncharacterized at the atomic level.

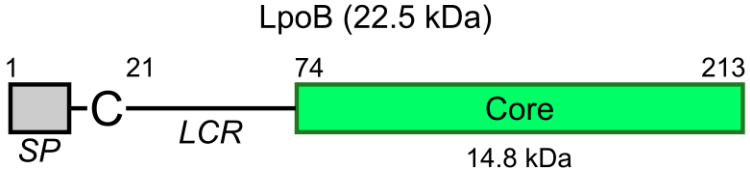

Figure II.3.1: Domain organization of *E. coli* LpoB. SP: Signal Peptide, cleaved to anchor the protein to outer-membrane fatty acids. LCR: Low-Complexity Region.

Similarly to LpoA, mature full-length LpoB crystallization appeared highly challenging (W. Vollmer, personal communication) whereas its high solubility and small molecular weight were positive properties for a study by solution-state NMR. I therefore worked on the high-resolution structure determination of mature LpoB with this technique. LpoB was shown to consist in an N-terminal highly flexible tail (highlighted by NMR dynamics experiments), followed by a globular domain. Interaction with the small non-catalytic PBP1B domain, UB2H, was also investigated by NMR and confirmed. From the chemical shift perturbations recorded, a first atomic model of the interaction of a bifunctional PBP with its activator was proposed. These results were the subject of an article published in *PNAS* in 2014, alongside a description of LpoB assignment in *J. Biomol. Assign*. (Egan et al., 2014; Jean, Bougault, Egan et al., 2014). In parallel to this structure of LpoB, two others (from *E. coli* and *Salmonella enterica*, with PDB code 4Q6Z and 4Q6L, respectively) were published simultaneously in *J. Biol. Chem.* (King et al., 2014). Comparison of these X-ray structures with the solution NMR structure does not show any significant difference, except eventually for the orientation of α-helix 3, which is tilted by 20° in our publication. Whether this slight conformational change between the NMR and X-ray structure represents two significant states or whether this is an artifact due to crystal packing or a lack of some distance restraints in the NMR structure has not been determined yet. However, I carefully checked the 3D NOESY spectra to search for unassigned or misassigned correlations yielding to new distance restraints, which may explain the differences this helix tilt in the protein structure but did not find any significant one.

3.A- Atomic characterization of the LpoB structure and of its interaction with PBP1B by NMR

Biomol NMR Assign
DOI 10.1007/s12104-014-9557-z

ARTICLE

Solution NMR assignment of LpoB, an outer-membrane anchored Penicillin-Binding Protein activator from *Escherichia coli*

Nicolas L. Jean · Catherine M. Bougault · Alexander J. F. Egan · Waldemar Vollmer · Jean-Pierre Simorre

Received: 29 January 2014 / Accepted: 25 March 2014

Abstract Bacteria surround their cytoplasmic membrane with the essential heteropolymer peptidoglycan (PG), which is made of glycan chains cross-linked by short peptides, to maintain osmotic stability and cell shape. PG is assembled from lipid II precursor by glycosyltransferase and transpeptidase reactions catalyzed by PG synthases, which are anchored to the cytoplasmic membrane and are controlled from inside the cell by cytoskeletal elements. Recently, two lipoproteins, LpoA and LpoB, were shown to be required in *Escherichia coli* for activating the main peptidoglycan synthases, Penicillin-Binding Proteins 1A and 1B, from the outer membrane. Here we present the backbone and side-chain assignment of the ^{1}H, ^{13}C and ^{15}N resonances of LpoB from *E. coli*. We also provide evidence for a two-domain organization of LpoB and a largely disordered, 64 amino acid-long N-terminal domain.

Keywords Outer-membrane lipoprotein activator of PBP · Bacterial cell wall biogenesis · Cell division complex · Peptidoglycan · NMR resonance assignment

N. L. Jean · C. M. Bougault · J.-P. Simorre (✉)
Institut de Biologie Structurale Jean-Pierre Ebel, Université Grenoble Alpes, EPN Campus, 6 rue Jules Horowitz, 38027 Grenoble, France
e-mail: jean-pierre.simorre@ibs.fr

N. L. Jean · C. M. Bougault · J.-P. Simorre
CNRS, IBS, 38027 Grenoble, France

N. L. Jean · C. M. Bougault · J.-P. Simorre
CEA, DSV, IBS, 38027 Grenoble, France

A. J. F. Egan · W. Vollmer
Centre for Bacterial Cell Biology, Institute for Cell and Molecular Biosciences, Newcastle University, Richardson Road, Newcastle upon Tyne NE2 4AX, UK

Biological context

Peptidoglycan (PG) is a bacterial cell wall polymer made of glycan chains cross-linked by peptide stems. It forms a net-like, elastic layer ('sacculus') completely surrounding the cytoplasmic membrane to maintain cell shape and to prevent bursting of the cell due to its turgor. Gram-negative bacteria, such as *Escherichia coli*, have in their periplasm a mainly single-layered sacculus that is tightly connected to the outer membrane via interactions with abundant outer membrane proteins, such as Braun's lipoprotein (Lpp), OmpA and Pal.

During the cell cycle, the PG sacculus grows by the incorporation of new material produced by glycosyltransferases (GTases), which polymerize lipid II precursor into glycan chains, and D,D-transpeptidases (TPases), which cross-link the peptide stems (Typas et al. 2012). Sacculus growth is accompanied by the release of a significant amount of old PG (~40 % per generation) by PG hydrolases. PG synthases and hydrolases presumably form dynamic, inner membrane-anchored multi-enzyme complexes. These are controlled from inside the cell by cytoskeletal elements, including the actin-like MreB and the tubulin-like FtsZ. *Escherichia coli* carries three bifunctional PG synthases with GTase and TPase activities (PBP1A, PBP1B and PBP1C), one monofunctional GTase (MgtA) and two monofunctional TPases (PBP2 and PBP3). PBP2 is essential for cell elongation and interacts with PBP1A (Banzhaf et al. 2012). PBP3 is essential for cell division and interacts with PBP1B (Bertsche et al. 2006). *Escherichia coli* requires at least one of the main bifunctional enzymes, PBP1A and PBP1B, for survival.

Recent work showed that in *E. coli*, and presumably in other Gram-negative bacteria, PG synthesis is regulated by outer-membrane anchored lipoproteins (Paradis-Bleau

Published online: 02 April 2014

et al. 2010; Typas et al. 2010). LpoA and LpoB interact in vitro and in the cell with their cognate PG synthases, PBP1A and PBP1B, respectively, presumably forming *trans*-envelope complexes through the periplasm. The synthases require their cognate Lpo protein for function and, hence, the cell cannot survive without LpoA and LpoB. In vitro, LpoA (YraM) stimulates the TPase activity of PBP1A, and LpoB (YcfM) stimulates both, the GTase and TPase activities of PBP1B (Paradis-Bleau et al. 2010; Typas et al. 2010).

The X-ray structure of PBP1B revealed the presence of a small, non-catalytic domain, called UB2H, which resides between the GTase and TPase domains and is unique to this synthase (Sung et al. 2009). Based mostly on genetic evidence, UB2H was suggested to be the docking site for LpoB (Typas et al. 2010). However, there are currently no structural data at atomic resolution on LpoB, and the interface of PBP1B and LpoB is not known. As a first step towards the elucidation of the mechanism by which LpoB stimulates PBP1B, we report here the essentially complete backbone and side-chain ^{1}H, ^{13}C, ^{15}N resonance assignment of LpoB from *E. coli*. In our LpoB construct the N-terminal outer-membrane lipid anchor of the native protein [diacylglycerol-(acyl)cysteine] is replaced by four extra amino acid residues (GSHM) that were left upon cleavage of an oligohistidine-tag introduced for purification purposes. The assignment of chemical shifts and a first structural characterization provide evidence of a disordered N-terminal region from residues 1 to 64 and a well-structured C-terminal domain from residues 65 to 197.

Sample preparation

Soluble recombinant ^{13}C, ^{15}N-labeled LpoB, in which the N-terminal membrane anchoring signal peptide was replaced by an oligohistidine tag, [MGSSH$_6$SSGLVPRGSHM-LpoB(V21-Q213)] was produced from an *E. coli* BL21(DE3) strain harboring the pET28LpoB plasmid (Typas et al. 2010). Cells were grown overnight at 37 °C in 100 mL of M9 minimal medium containing 3 g/L [^{13}C]-D-glucose, 1 g/L [^{15}N]-NH_4Cl (Cambridge Isotope Laboratories, Tewksbury MA, USA), 50 µg/mL kanamycin and 2 mM thiamine from a preculture in rich medium. The cells were harvested by centrifugation, resuspended in 1 L of fresh M9 growth medium and grown at 30 °C to an OD_{578} of 0.6. IPTG (1 mM) was added and the cells were incubated further for 3 h at 30 °C for LpoB overproduction. Cells were harvested by centrifugation (10,000×*g*, 15 min, 4 °C) and the pellet was resuspended in 40 mL of 25 mM Tris/HCl, 10 mM $MgCl_2$, 500 mM NaCl, 20 mM imidazole, 10 % glycerol, pH 7.5 (buffer A). A small amount of DNase, protease inhibitor cocktail (Sigma, 1/1,000 dilution) and 100 µM of phenylmethylsulfonylfluoride (PMSF) were added before cells were disrupted by sonication (Branson Digital Sonifier). The insoluble material was removed by ultracentrifugation (130,000×*g*, 1 h, 4 °C) and the supernatant was loaded onto a 5 mL HisTrap HP column (GE healthcare), attached to an ÄKTA Prime$^+$ (GE Healthcare). The column was washed with 4 volumes of buffer A before elution of bound proteins with 25 mM Tris/HCl, 10 mM $MgCl_2$, 500 mM NaCl, 400 mM imidazole, 10 % glycerol, pH 7.5 (buffer B) at a flow rate of 1 mL/min. To remove the oligohistidine tag, 50 U/mL of restriction grade Thrombin (Novagen) was added to LpoB and left to react for 18 h at 4 °C. The mixture was then dialyzed against 2 L of 25 mM Tris/HCl, 100 mM NaCl, 10 % glycerol, pH 8.3, before it was applied to a 5 mL HiTrap Q HP column (GE healthcare) attached to an ÄKTA Prime$^+$ (GE Healthcare). LpoB was collected in the flow-through with a buffer flow-rate of 0.5 mL/min. The LpoB sample was concentrated to 4–5 mL using a VivaSpin-6 column (MW cut-off 5,000 Da) and loaded onto a Superdex200 HiLoad 16/600 column for size exclusion chromatography. LpoB eluted after ~85 min in 25 mM HEPES/NaOH, 1 M NaCl, 10 % glycerol, pH 7.5 at a flow rate of 1 mL/min. LpoB was finally dialyzed against 100 mM sodium acetate buffer at pH 4.5 and concentrated using a VivaSpin-6 spin column (Sartorius).

NMR spectroscopy

All NMR data were collected at 308 K on a 0.8 mM sample of ^{13}C,^{15}N-labeled LpoB in 100 mM sodium acetate buffer, pH 4.5 containing 10 % D_2O. All of the NMR experiments for backbone and side-chain assignment were performed on Agilent spectrometers operating at 600 or 800 MHz ^{1}H NMR frequencies with the exception of an aliphatic ^{13}C-NOESY-HSQC, which was recorded on the French national platform on a 950 MHz Bruker US^2 spectrometer. All of the spectrometers were equipped with a cryogenic triple ^{1}H, ^{13}C, ^{15}N resonance probe. Backbone chemical shifts were assigned in a sequential manner from the following experiments: 2D [^{1}H,^{15}N]-HSQC, 2D Pro-HN(COCAN) and Pro-iHN(CAN) (Solyom et al. 2013), 3D (H)N(COCA)NH, 3D BEST-HNCACB and BEST-HN(CO)CACB (Lescop et al. 2010), 3D HNCO and 3D HN(CA)CO. Side-chains were assigned using 2D aliphatic and aromatic [^{1}H,^{13}C]-CT-HSQCs, a 2D methyl-selective [^{1}H,^{13}C]-CT-HSQC (Van Melckebeke et al. 2004), a 2D [^{1}H,^{15}N]-HMQC experiment optimized for the detection of $^{2}J_{NH}$ couplings in imidazole rings (Pelton et al. 1993), a 3D H(C)CH-TOCSY, a 3D (H)C(CCO)NH, a 3D H(CCCO)NH, and a 3D ^{15}N-NOESY-HSQC with 150 ms mixing time, as well as 3D aliphatic, aromatic and methyl-^{13}C-NOESY-HSQC (Van Melckebeke et al. 2004) experiments with mixing times of 120, 130, and 160 ms, respectively. NMR data were processed using

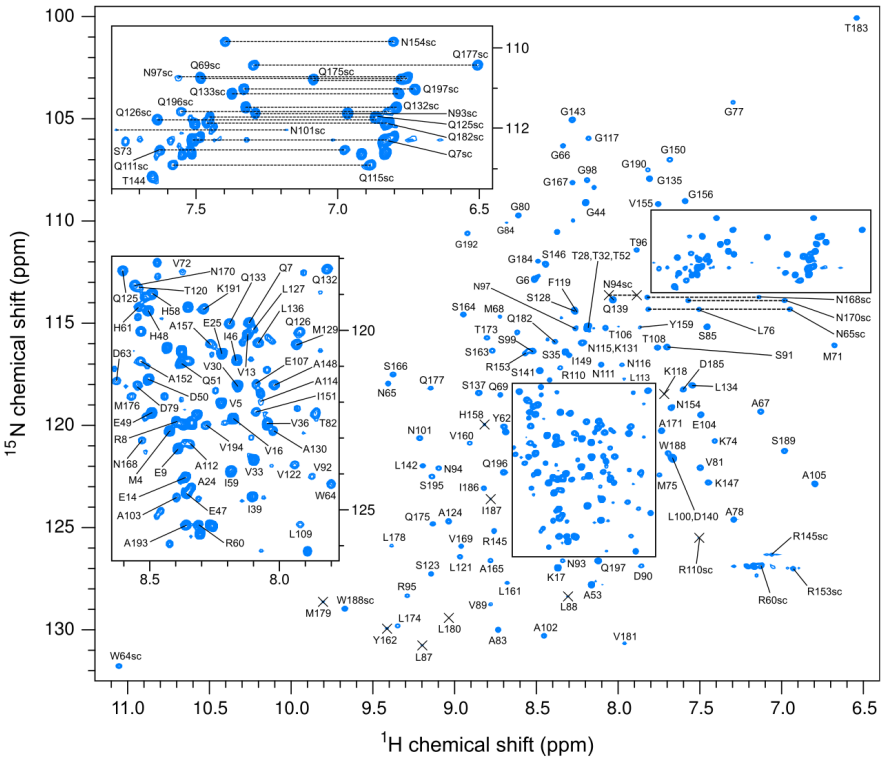

Fig. 1 Fully assigned 2D [^{1}H,^{15}N]-HSQC spectrum of a 0.8 mM sample of ^{13}C,^{15}N-labeled LpoB in 100 mM sodium acetate buffer, pH 4.5, containing 10 % D_2O at 308 K. Each backbone amide resonance is labeled with the amino acid type (one-letter code) and position in the sequence. Amino groups from tryptophan (Hε1-Nε1) and arginine (Hε-Nε) side chains are labeled with "sc". Assigned amide groups from glutamine and asparagine side chains are outlined with *horizontal dotted lines* and labeled with "sc". The position of the resonance of amino acids for which the signal intensity is below the threshold contour level is indicated with a *cross* (×). The sensitivity of the three experiments was sufficient in 3D experiments to assign the corresponding residues with standard procedures together with the other residues

NMRPipe (Delaglio et al. 1995) and analyzed using the CcpNmr Analysis 2.2 software (Vranken et al. 2005). Dihedral angles and secondary structure predictions were obtained using the program TALOS+ (Shen et al. 2009) and the secondary structure chart tool of CcpNmr, respectively. The latter calculates the difference between observed and random coil Cα, Cβ, CO and Hα chemical shifts taking into account sequence-dependent effects according to a protocol described (Schwarzinger et al. 2001).

Extent of assignments and data deposition

Figure 1 shows an assigned 2D ^{13}C-decoupled [^{1}H, ^{15}N]-HSQC spectrum of ^{13}C, ^{15}N-labeled LpoB at pH 4.5 and 308 K. In addition to well-dispersed signals, the center of the spectrum is buried with very intense and sharp resonances, some of which remain unassigned. Analysis of the sequential backbone experiments afforded the identification and sequence specific assignments for 166 out of the 177 expected backbone ^{1}H and ^{15}N amide resonances (93.2 %) (not counting the 19 Pro residues and the N-terminal amino acid). Starting from the assigned amide resonances, we were able to complete the assignment of 90.3, 90.4, and 90.0 % of CO, Cα, and Cβ resonances, respectively, over the whole protein construct. Missing assignments affect exclusively the N-terminal proline-rich region (27 %) defined by the first 60 residues: residues G1 to S3, P10 to A11, P18 to Q22, P26 to P31, P40 to Q42, and P54 to A56. In this protein region, the specific assignment procedure was hindered by the extensive redundancy of short sequences, such as the three PXXP sequences with X = Gln or Glu. Despite these unassigned residues at the N-terminus, 87.4, 83.9, 79.3, and 79.1 % of the Hα, Hβ, aromatic and other aliphatic side-chain protons, respectively, could be assigned over the complete protein construct. Side-chain ^{13}C assignments (from Cγ on) were completed to 70.6 and 79.3 % for aliphatic and non-quaternary aromatic carbons, respectively. Unusual chemical shifts

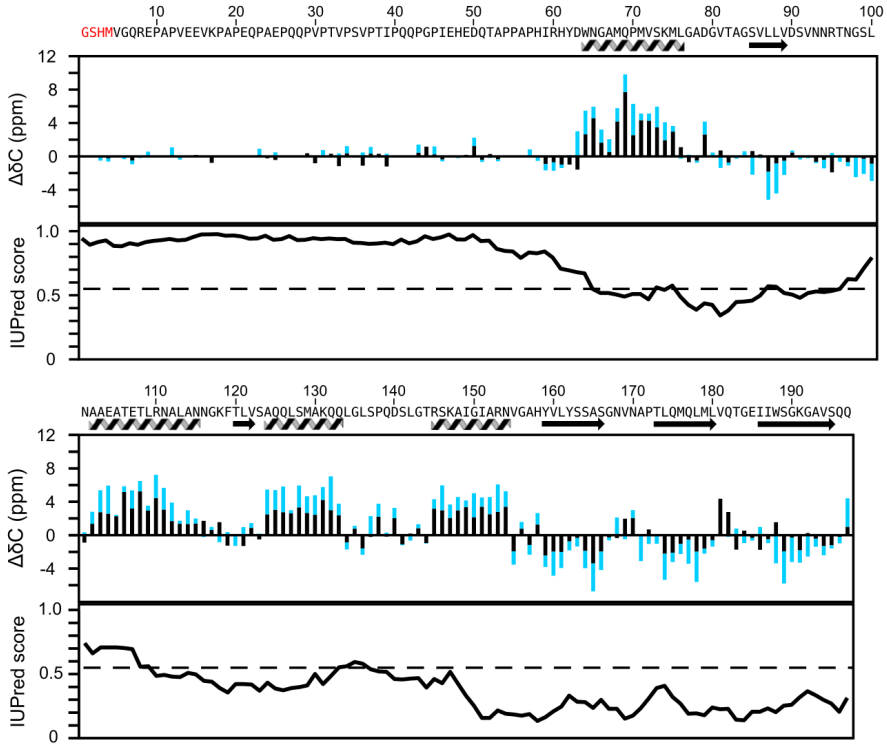

Fig. 2 Amino acid sequence and secondary structure of LpoB. The N-terminal GSHM sequence (*red*) remained after cleavage of the oligohistidine tag by thrombin. The secondary structure elements, 4 α-helices and 5 β-strands shown below the sequence, were predicted using TALOS+ according to the experimental backbone chemical shifts. Chemical shift deviations from random coil values (in ppm) were calculated for Cα and CO for each residue within the CcpNmr Analysis 2.2 software as published (Schwarzinger et al. 2001). These Cα and CO values are shown as *black* and *blue histograms*, respectively. IUPred scores were calculated from the sequence to predict highly disordered regions (IUPred scores for the corresponding residues higher than 0.55, i.e. above the *dotted line* in the graph). The absence of Cα and CO significant chemical shift deviations and the high IUPred scores in the first 64 residues consistently suggest a highly disordered N-terminal region

have been observed for a restricted set of nuclei, i.e. Y62 Hβs, M75 Hα and Hβ1, A105 Hα and Hβs and T183 N. These nuclei are upfield shifted compared with the expected values, suggesting that they are stacked onto aromatic rings and thus experience ring current shifts.

The secondary structure of LpoB was predicted using the Cα and CO chemical shift deviations from random coil values (Schwarzinger et al. 2001) and the empirical determination of phi/psi by TALOS+ from measured backbone chemical shift data (Shen et al. 2009) (Fig. 2). In agreement with the presence of 27 % Pro residues, the G1 to W64 segment is largely unstructured with Cα and CO chemical shifts close to random coil values and IUPred scores larger than 0.55. This unstructured N-terminal region was predicted by IUPred (http://iupred.enzim.hu/) based on the primary sequence (Fig. 2). IUPred also predicted an unfolded region from N97 to L109 which, however, is limited to residues N97 to N101, as TALOS+ and Cα/CO chemical shift deviations indicate an α-helical structure from A102. The analysis of chemical shift data thus suggests that LpoB contains a N-terminal disordered tail and a globular domain consisting of 3 α-helices and 5 β-strands. Based on this assignment we aim to determine the 3D structure of LpoB at atomic resolution with the detailed structural organization of the globular domain, to gain insights into the activation mechanism of PBP1B.

All ^{1}H, ^{13}C and ^{15}N chemical shifts and their assignment have been deposited in the BioMagResBank (http://www.bmrb.wisc.edu) under the accession number 19681.

Acknowledgments Financial support by the French TGIR-RMN-THC FR3050 CNRS for conducting the research on the 950 MHz spectrometer (ICSN, Gif-sur-Yvette) and on the 800 MHz spectrometer (IBS, Grenoble) is gratefully acknowledged. This work was further supported by a PhD fellowship to NLJ (Contrat de Formation par la Recherche) from the Commissariat à l'Energie Atomique et aux Energies Alternatives. WV was supported by the European Commission (DIVINOCELL) and the BBSRC (BB/I020012/1).

Conflict of interest The authors declare that they have no conflict of interest.

References

Banzhaf M, van den Berg van Saparoea B, Terrak M, Fraipont C, Egan A, Philippe J, Zapun A, Breukink E, Nguyen-Distèche M, den Blaauwen T et al (2012) Cooperativity of peptidoglycan synthases active in bacterial cell elongation. Mol Microbiol 85:179–194

Bertsche U, Kast T, Wolf B, Fraipont C, Aarsman MEG, Kannenberg K, von Rechenberg M, Nguyen-Distèche M, den Blaauwen T, Holtje J-V et al (2006) Interaction between two murein (peptidoglycan) synthases, PBP3 and PBP1B, in *Escherichia coli*. Mol Microbiol 61:675–690

Delaglio F, Grzesiek S, Vuister GW, Zhu G, Pfeifer J, Bax A (1995) NMRPipe: a multidimensional spectral processing system based on UNIX pipes. J Biomol NMR 6:277–293

Lescop E, Kern T, Brutscher B (2010) Guidelines for the use of band-selective radiofrequency pulses in hetero-nuclear NMR: example of longitudinal-relaxation-enhanced BEST-type ^{1}H–^{15}N correlation experiments. J Magn Reson 203:190–198

Paradis-Bleau C, Markovski M, Uehara T, Lupoli TJ, Walker S, Kahne DE, Bernhardt TG (2010) Lipoprotein cofactors located in the outer membrane activate bacterial cell wall polymerases. Cell 143:1110–1120

Pelton JG, Torchia DA, Meadow ND, Roseman S (1993) Tautomeric states of the active-site histidines of phosphorylated and unphosphorylated III Glc, a signal-transducing protein from *Escherichia coli*, using two-dimensional heteronuclear NMR techniques. Protein Sci 2:543–558

Schwarzinger S, Kroon GJA, Foss TR, Chung J, Wright PE, Dyson HJ (2001) Sequence-dependent correction of random coil NMR chemical shifts. J Am Chem Soc 123:2970–2978

Shen Y, Delaglio F, Cornilescu G, Bax A (2009) TALOS+: a hybrid method for predicting protein backbone torsion angles from NMR chemical shifts. J Biomol NMR 44:213–223

Solyom Z, Schwarten M, Geist L, Konrat R, Willbold D, Brutscher B (2013) BEST-TROSY experiments for time-efficient sequential resonance assignment of large disordered proteins. J Biomol NMR 55:311–321

Sung M-T, Lai Y-T, Huang C-Y, Chou L-Y, Shih H-W, Cheng W-C, Wong C-H, Ma C (2009) Crystal structure of the membrane-bound bifunctional transglycosylase PBP1b from *Escherichia coli*. Proc Natl Acad Sci USA 106:8824–8829

Typas A, Banzhaf M, van den Berg van Saparoea B, Verheul J, Biboy J, Nichols RJ, Zietek M, Beilharz K, Kannenberg K, von Rechenberg M et al (2010) Regulation of peptidoglycan synthesis by outer-membrane proteins. Cell 143:1097–1109

Typas A, Banzhaf M, Gross CA, Vollmer W (2012) From the regulation of peptidoglycan synthesis to bacterial growth and morphology. Nat Rev Micro 10:123–136

Van Melckebeke H, Simorre J-P, Brutscher B (2004) Amino acid-type edited NMR experiments for methyl–methyl distance measurement in ^{13}C-labeled proteins. J Am Chem Soc 126:9584–9591

Vranken WF, Boucher W, Stevens TJ, Fogh RH, Pajon A, Llinas M, Ulrich EL, Markley JL, Ionides J, Laue ED (2005) The CCPN data model for NMR spectroscopy: development of a software pipeline. Proteins 59:687–696

Outer-membrane lipoprotein LpoB spans the periplasm to stimulate the peptidoglycan synthase PBP1B

Alexander J. F. Egan[a,1], Nicolas L. Jean[b,c,d,1], Alexandra Koumoutsi[e,1], Catherine M. Bougault[b,c,d], Jacob Biboy[a], Jad Sassine[a], Alexandra S. Solovyova[f], Eefjan Breukink[g], Athanasios Typas[e,2], Waldemar Vollmer[a,2], and Jean-Pierre Simorre[b,c,d,2]

[a]Centre for Bacterial Cell Biology, [f]Institute for Cell and Molecular Biosciences, Newcastle University, Newcastle upon Tyne NE2 4AX, United Kingdom; [b]Institut de Biologie Structurale, Université Grenoble Alpes, F-38027 Grenoble, France; [c]Institut de Biologie Structurale, Direction des Sciences du Vivant, Commissariat à l'Energie Atomique, F-38027 Grenoble, France; [d]Institut de Biologie Structurale, Centre National de la Recherche Scientifique, F-38027 Grenoble, France; [e]European Molecular Biology Laboratory, Genome Biology Unit, 69117 Heidelberg, Germany; and [g]Department of Biochemistry of Membranes, Bijvoet Center for Biomolecular Research, University of Utrecht, 3584 CH, Utrecht, The Netherlands

Edited by Caroline S. Harwood, University of Washington, Seattle, WA, and approved April 14, 2014 (received for review January 8, 2014)

Bacteria surround their cytoplasmic membrane with an essential, stress-bearing peptidoglycan (PG) layer. Growing and dividing cells expand their PG layer by using membrane-anchored PG synthases, which are guided by dynamic cytoskeletal elements. In *Escherichia coli*, growth of the mainly single-layered PG is also regulated by outer membrane-anchored lipoproteins. The lipoprotein LpoB is required for the activation of penicillin-binding protein (PBP) 1B, which is a major, bifunctional PG synthase with glycan chain polymerizing (glycosyltransferase) and peptide cross-linking (transpeptidase) activities. Here, we report the structure of LpoB, determined by NMR spectroscopy, showing an N-terminal, 54-aa–long flexible stretch followed by a globular domain with similarity to the N-terminal domain of the prevalent periplasmic protein TolB. We have identified the interaction interface between the globular domain of LpoB and the noncatalytic UvrB domain 2 homolog domain of PBP1B and modeled the complex. Amino acid exchanges within this interface weaken the PBP1B–LpoB interaction, decrease the PBP1B stimulation in vitro, and impair its function in vivo. On the contrary, the N-terminal flexible stretch of LpoB is required to stimulate PBP1B in vivo, but is dispensable in vitro. This supports a model in which LpoB spans the periplasm to interact with PBP1B and stimulate PG synthesis.

Peptidoglycan (PG) is an essential component of the bacterial cell envelope, required for cell shape and stability. It is composed of glycan chains that are connected by short peptides, and forms a net-like, elastic structure, called the sacculus, which encases the cytoplasmic/inner membrane (IM) (1). In Gram-negative bacteria, such as *Escherichia coli*, the sacculus is mainly single-layered and is firmly attached to the outer membrane (OM) by abundant OM proteins. Some of the most effective antibiotic agents, such as the β-lactams and glycopeptides, inhibit PG biosynthesis, resulting in cell lysis.

Bacteria enlarge their sacculus by polymerizing new PG from lipid II precursor at the outer face of the IM and incorporating the newly made material into the existing PG layer. At the same time, a significant amount of old material is released. For synthesis and hydrolysis to be coupled, the corresponding enzymes have to be tightly regulated and coordinate their actions (2). How does this happen? The current view is that PG synthases [penicillin-binding proteins (PBPs)] and hydrolases form membrane-anchored multienzyme complexes, which are driven by cytoskeletal elements. More recently, it was established that dedicated regulators tightly control the activities of PG synthases and hydrolases and/or couple it to other cell envelope processes (3–6).

PG synthesis requires glycosyltransferases (GTases) to polymerize the glycan chains and transpeptidases (TPases) to form peptide cross-links. Most bacteria carry several PG synthases, which can perform one or both enzymatic reactions. In *E. coli*, the bifunctional GTase/TPases PBP1A and PBP1B provide the main PG synthesis activity, and the cell needs one of them to survive. *E. coli* has also two monofunctional TPases, PBP2 and PBP3, which have essential roles in cell elongation and division, respectively. Recent localization and biochemical data suggest that PBP1A works mainly together with PBP2 during cell elongation (7), when PG synthesis is guided by the actin-like MreB. On the contrary, PBP1B and PBP3 interact with each other, as well as with other essential cell division proteins, such as FtsW and FtsN (8–10), and they colocalize at the division site. They are both part of the divisome, a large protein complex, which is nucleated by the tubulin-like FtsZ during cell division to synthesize and split the cell envelope layers, including the PG, and produce new cell poles (11).

Recent work showed that, in *E. coli*, and presumably other Gram-negative bacteria, PG synthesis is also regulated from outside the sacculus by OM-anchored lipoproteins. LpoA and LpoB interact with their cognate PG synthase, PBP1A and PBP1B, respectively, and stimulate their activity, which is essential for the function of the PBPs in vivo (3, 5). This suggests that the OM-anchored Lpo proteins have to penetrate the elastic sacculus net before reaching their cognate, cytoplasmic

Significance

Bacteria surround their cytoplasmic membrane with an essential heteropolymer, the peptidoglycan (PG) sacculus, to maintain osmotic stability and cell shape. Cells enlarge their sacculus by using cytoplasmic membrane-anchored PG synthases, which are guided by cytoskeletal elements. Gram-negative bacteria have a thin, mainly single-layered sacculus, connected to the outer membrane. Outer-membrane–anchored lipoproteins were recently found to be essential for PG growth. Here, we present the structure of the outer membrane protein LpoB of *Escherichia coli*, which is required for the function of the major PG synthase PBP1B. LpoB has a long, flexible N-terminal stretch enabling it to span the periplasm and reach its docking site in PBP1B, the noncatalytic UvrB domain 2 homolog domain, to stimulate PG growth.

Author contributions: A.J.F.E., N.L.J., A.K., C.M.B., A.S.S., A.T., W.V., and J.-P.S. designed research; A.J.F.E., N.L.J., A.K., C.M.B., J.B., J.S., A.S.S., A.T., and J.-P.S. performed research; E.B. contributed new reagents/analytic tools; A.J.F.E., N.L.J., A.K., C.M.B., J.B., A.S.S., A.T., W.V., and J.-P.S. analyzed data; and A.J.F.E., N.L.J., A.K., C.M.B., A.S.S., A.T., W.V., and J.-P.S. wrote the paper.

The authors declare no conflict of interest.

This article is a PNAS Direct Submission.

Freely available online through the PNAS open access option.

Data deposition: The atomic coordinates have been deposited in the Protein Data Bank, www.pdb.org (PDB ID code 2MII). The NMR chemical shifts have been deposited in the BioMagResBank, www.bmrb.wisc.edu (accession no. 19681).

[1]A.J.F.E., N.L.J., and A.K. contributed equally to this work.

[2]To whom correspondence may be addressed. E-mail: typas@embl.de, w.vollmer@ncl.ac.uk, or jean-pierre.simorre@ibs.fr.

This article contains supporting information online at www.pnas.org/lookup/suppl/doi:10.1073/pnas.1400376111/-/DCSupplemental.

membrane-anchored PBP. We have postulated that this allows the cell to control the rate of PG synthesis in response to the local pore size of the sacculus. This hypothesis couples PG growth with overall cell growth, allowing for PG synthesis to rapidly adjust to environmental cues (2, 5).

The crystal structure of PBP1B has been determined (12). In addition to the GTase and TPase domains, PBP1B harbors a small, noncatalytic UvrB domain 2 homolog (UB2H) domain (Pfam 14814), which is unique to this synthase. Based mostly on genetic evidence, we previously suggested that the UB2H domain acts as a docking domain for LpoB (5). In this work, we have determined the structure of a soluble version of LpoB by NMR spectroscopy. LpoB has a 54-aa–long unstructured and flexible stretch at its N terminus, followed by a globular domain, which interacts with the purified UB2H domain. We have mapped the interface between the two proteins by NMR spectroscopy, providing, to our knowledge, the first structural characterization of an interaction between a PG-related enzyme and its regulator. Targeted substitutions in amino acids within the PBP1B–LpoB interface impaired PBP1B activation by LpoB in vivo and in vitro. LpoB versions that partially or completely lack the flexible N terminus could interact with and fully stimulate PBP1B in vitro, but were nonfunctional in the cell. This supports a model in which the OM-anchored LpoB has to reach through the PG mesh to interact with the UB2H domain of PBP1B and stimulate PG synthesis.

Results

LpoB Interacts with PBP1B and Stimulates both of Its Activities. To gain mechanistic and structural insights into the PBP1B–LpoB interaction, we purified both proteins and tested them in surface plasmon resonance (SPR) experiments. PBP1B was covalently bound to a chip surface with immobilized ampicillin. A soluble version of LpoB lacking the N-terminal lipid modification, LpoB(sol) (*SI Appendix*, Table S1), bound to immobilized PBP1B with rapid on/off rates, approaching binding saturation at a concentration of 4 μM, and with a K_d of 0.81 ± 0.08 μM (Fig. 1*A*). Binding of LpoB(sol) to a control surface without PBP1B was negligible (*SI Appendix*, Fig. S1*A*).

LpoB was previously shown to moderately enhance consumption of lipid II by PBP1B (1.5-fold) (3, 13) and to stimulate the TPase activity of PBP1B, yielding a highly peptide cross-linked PG (5, 13) (*SI Appendix*, Fig. S1*B*). As the effect of LpoB on the GTase activity of PBP1B does not require an active TPase, and reduces the average length of glycan strands (3), Lupoli et al. (13) proposed that the dominant effect of LpoB is on the GTase activity of PBP1B (*Discussion*). To more accurately monitor the rate of GTase activity, we used a continuous assay with a fluorescently labeled dansyl-lipid II as a substrate (7). In this assay, LpoB(sol) increased the maximal GTase rate of PBP1B 8-fold (Fig. 1*B*; see Fig. 4*C*). The noncognate LpoA, which specifically interacts with PBP1A, had no effect on the GTase activity of PBP1B. As expected, this activity was completely inhibited by the antibiotic moenomycin. Interestingly, LpoB significantly stimulated the GTase activity of PBP1B even at pH 4.5, at which PBP1B alone was virtually inactive (*SI Appendix*, Fig. S1*C*), suggesting that LpoB might induce conformational changes in the GTase domain to maintain the catalytic Glu233 residue in an active, unprotonated state even at this low pH.

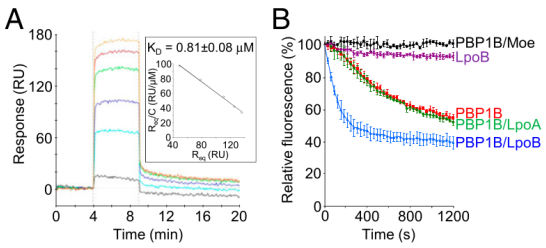

Fig. 1. LpoB interacts with PBP1B and enhances the rate of its GTase activity. (*A*) LpoB–PBP1B interaction dynamics measured by SPR. LpoB was injected at concentrations of 0 (black line), 0.5 (light blue), 1 (dark blue), 2 (green), 3 (red), and 4 (orange) μM to a chip surface with immobilized PBP1B (*SI Appendix*, Fig. S1*A* shows control). The response at equilibrium R_{eq}, normalized to the injected concentration C (R_{eq}/C), plotted against R_{eq}, yields a straight line with a slope of $-K_d^{-1}$ (*Inset*). The average K_d value ± SD was determined from three independent experiments. (*B*) Continuous GTase assay for PBP1B, measuring consumption of fluorescently labeled substrate (dansyl-lipid II). PBP1B activity (red) is stimulated by LpoB (blue) but not by LpoA (green). The antibiotic moenomycin (Moe) inhibits PBP1B GTase activity (black). LpoB alone (purple) shows no activity. Each measurement is shown as mean ± SD of three independent experiments.

Structure of LpoB. Purified LpoB(sol) eluted as a single peak in size-exclusion chromatography with a calculated molecular weight of 45.5 ± 3.3 kDa, which is more than double the theoretical value of 20.3 kDa (*SI Appendix*, Fig. S2*A*). However, this peak remained the same at a wide range of NaCl concentrations (0.1–2 M), arguing against LpoB multimerization. A single monomer peak with a sedimentation coefficient of 1.754 S (*SI Appendix*, Fig. S2*B*) could be seen in analytical ultracentrifugation, which is unusually high for a protein of this size, indicating that LpoB(sol) has an elongated molecular shape and/or extended flexible regions.

We opted to use NMR spectroscopy to determine the structure of LpoB(sol), as the presence of large disordered regions often prevents the crystallization of proteins. NMR data were recorded on a [^{13}C,^{15}N]LpoB(sol) sample and the backbone and side-chain ^{1}H,^{13}C,^{15}N-resonances were assigned by using conventional and targeted experiments to identify the residues in the proline-rich region in the N terminus (14). Automatically and manually assigned unambigous distance restraints (N = 3,849) and ϕ/ψ dihedral angles (N = 248) were derived from Nuclear Overhauser Effect (NOE) data and chemical shifts, respectively, and used for further structure calculation. LpoB(sol) has two structurally distinct parts, a disordered region near the N terminus (up to Pro73) and a well-folded globular domain (His74 to Gln213; Fig. 2*A*). The N terminus contains 27.7% Pro residues and is predicted as disordered by IUPred (15). The high structural flexibility from Val21 to Pro73 was confirmed by (*i*) medium- to long-range NOE correlations being absent, (*ii*) a negative {^{1}H}-^{15}N relaxation NOE value for Val21 to Ala69 amide resonances (Fig. 2*B*), and (*iii*) an inability to identify any secondary structure elements between Val21 and Pro73 when entering ^{1}H, ^{13}C, and ^{15}N-backbone chemical shifts into the δ2D software (16). This large disordered region has an estimated maximal length of ∼145 Å, which explains the high analytical ultracentrifugation sedimentation coefficient.

After refinement, the 20 lowest-energy high-resolution structures of LpoB(sol) were selected and the rmsd values to the average structure were calculated for the backbone (0.18 ± 0.03 Å) and heavy (0.44 ± 0.06 Å) atoms of the globular domain (His74 to Gln213; Fig. 2*A* and *SI Appendix*, Table S2). LpoB comprises a three-stranded antiparallel β-sheet (β2, 175–183; β3, 189–196; and β4, 200–209), which is flanked by a short two-stranded parallel β-sheet (β1, 102–105; β2, 175–178) and four α-helices (H1, 79–93; H2, 118–132; H3, 140–150; H4, 161–171). H3 and H4 are tightly linked with the parallel β-sheet by a hydrophobic core involving H3–β1, H4–β1, and H4–β2 contacts. H1 and H2 are stabilized at the antiparallel β-sheet through hydrophobic contacts between H1, H2, β2, and, in part, β4.

The globular domain of LpoB has a large positively charged patch on the three-stranded β-sheet with an extension toward α-helix H4, and a smaller positive patch between H1 and H2 on the other side of the molecule (*SI Appendix*, Fig. S3*A*). Interestingly, the large positive patch contains highly conserved residues in the three-stranded β-sheet (β2, 175–179; β3, 192–195; and β4, 200–206), as determined by aligning 68 distinct LpoB sequences (*SI Appendix*, Fig. S3 *B–D*). We reasoned that this

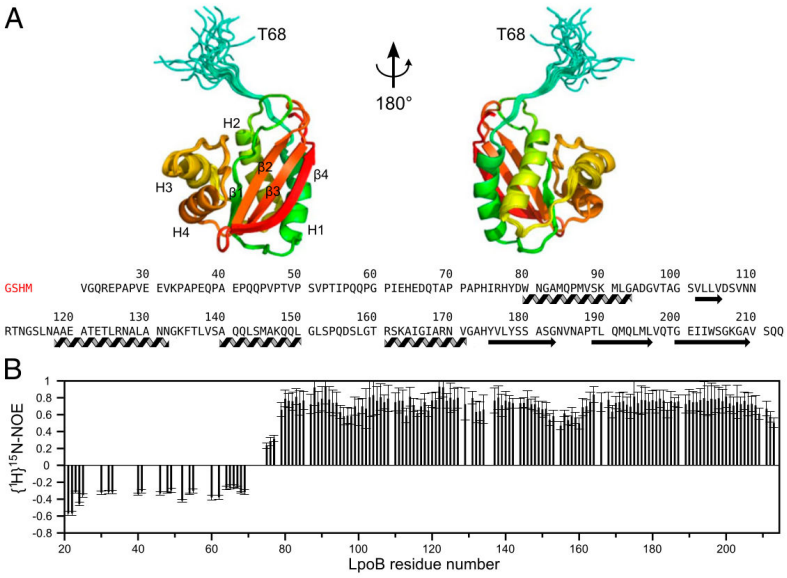

Fig. 2. LpoB structure shows a globular domain with a flexible N-terminal region. (*A*) Ensemble of the 20 lowest-energy structures of LpoB(sol) (from Thr68 for clarity) determined by NMR spectroscopy (colors from cyan to red are from N to C terminus). The position of α-helices (H1–H4) and β-strands (β1–β4) are indicated on the structure and on the sequence below (helices and arrows). (*B*) Heteronuclear $\{^1H\}$-^{15}N-NOE values calculated from the intensity ratio between the saturated and the reference experiments. Errors on the intensity ratio were calculated from the signal-to-noise ratio of the NMR signal in each spectrum. The numbering begins at Val21. High, low, and negative values indicate low, medium, and high flexibility, respectively.

conserved and rather concave surface could potentially serve as an interaction site with PBP1B.

LpoB–UB2H (PBP1B) Interaction. LpoB has coevolved with the small noncatalytic UB2H domain of PBP1B (5), which is situated between its GTase and TPase domains (12). LpoB can be chemically cross-linked to PBP1B in vivo, but not to a version that lacks UB2H (5). We purified an oligohistidine-tagged UB2H domain (His-UB2H) (12), which, as expected, bound to LpoB, but not LpoA (*SI Appendix*, Fig. S4*A*). To map more precisely the LpoB–PBP1B interaction site, spectra from an $[^1H,^{15}N]$-BEST-TROSY-HSQC experiment were recorded on $[^{13}C,^{15}N]$LpoB (sol) alone and with a 2-fold molar excess of unlabeled His-UB2H. Superimposition of the spectra revealed 45 perturbed LpoB amide resonances (*SI Appendix*, Fig. S4 *B* and *C*). When LpoB was progressively added to the LpoB–UB2H sample, changing the ratio of the two proteins, the LpoB resonances shifted closer to their original positions in the free LpoB spectrum. This suggests an intermediate-to-fast exchange regime between the two protein forms, which is fully consistent with a K_d in the micromolar range for LpoB(sol):PBP1B (Fig. 1*A*). Chemical shift and resonance intensity perturbations were mapped on the LpoB (sol) structure (Fig. 3*A*) and were found to concentrate on a conserved region, which included β2, β3, and the tip of H4 (*SI Appendix*, Fig. S3 *B–E*). Incorporating this information into the docking software HADDOCK (17), we could identify two possible interfaces in the UB2H domain of PBP1B, involving a common stretch (167–176) and two exclusive stretches (147–152 and 188–193; *SI Appendix, Supplemental Materials and Methods*). Further biochemical and phenotypic analysis (Fig. 4 and *SI Appendix*, Table S3) supported the latter interface, allowing us to refine the docking model. In the resulting most populated ensemble of LpoB–UB2H structures (Fig. 3*B*), the short β-turn (187–188)–β-strand (190–191) of UB2H stacks between β2 and H4 of LpoB(sol).

The LpoB–UB2H Interaction Is Required for the Function of PBP1B. We constructed a number of PBP1B and LpoB alleles carrying single Ala, multiple Ala, or charge-reversing substitutions in amino acids predicted to be part of the LpoB–UB2H interface, and tested them for binding and activity. PBP1B interface variants carrying single or double amino acid substitutions were only partially active in vivo (Fig. 4*A* and *SI Appendix*, Fig. S5*B*; cefsulodin targets mainly PBP1A, leaving cells dependent on PBP1B) and did not suffice for cell growth without PBP1A (*SI Appendix*, Table S3). PBP1B R190D lost nearly all in vivo activity, but we had to introduce multiple Ala substitutions in PBP1B for such a strong effect (Fig. 4*A* and *SI Appendix*, Fig. S5). These results were mirrored when we measured K_d values of the LpoB–PBP1B interaction (Fig. 4*B* and *SI Appendix*, Fig. S6) and in vitro GTase and

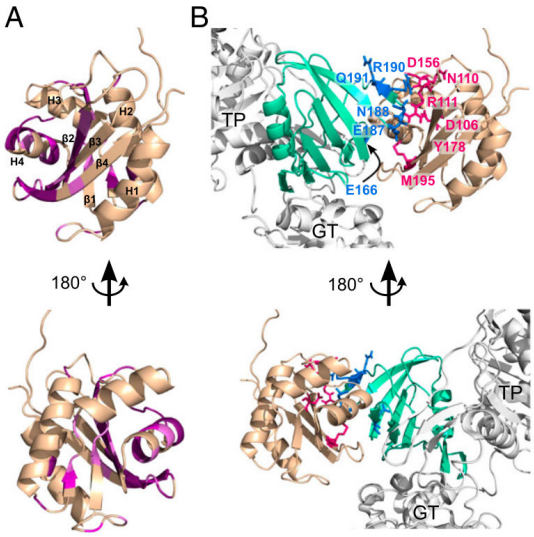

Fig. 3. LpoB interacts with the UB2H domain of PBP1B. (*A*) Residues showing a significant perturbation upon His-UB2H addition are mapped on the cartoon representation of the LpoB(sol) structure. Residues showing chemical shift perturbations higher than 0.05 ppm are shown in pink, and residues for which the $[^1H,^{15}N]$ correlation showed intensity changes upon interaction are in dark purple (*SI Appendix*, Fig. S4*C*). (*B*) Final HADDOCK model of the LpoB–PBP1B complex after addition of ambiguous restraints from NMR perturbations, and biochemical/functional data (Fig. 4). Residues changed to Ala, or reverse-charge amino acids in the activity assays, are represented as sticks in blue (UB2H domain) or magenta (LpoB). Cartoon representation of LpoB and UB2H domain are shown in wheat and green, respectively. Additional domains in PBP1B are shown in gray.

MICROBIOLOGY

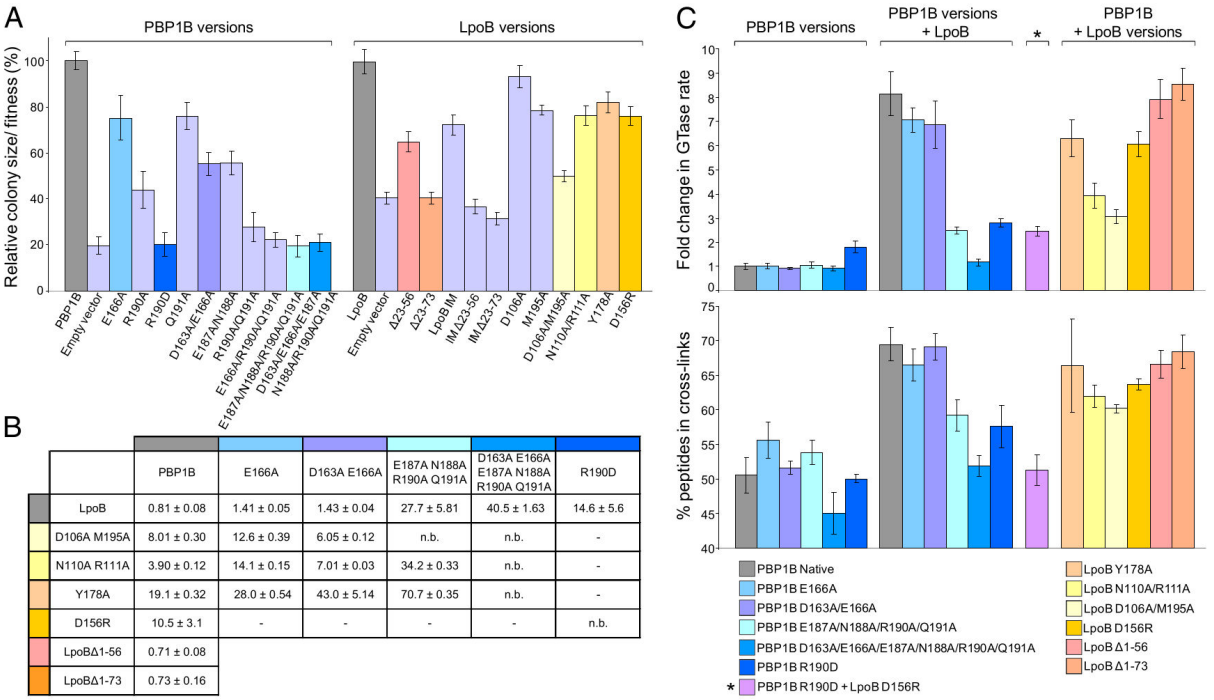

Fig. 4. Dissecting the LpoB–PBP1B interaction and its relevance for PBP1B function. (*A*) In vivo activity of PBP1B and LpoB versions as measured by cellular fitness under cefsulodin treatment (12 and 24 μg/mL for PBP1B and LpoB versions, respectively). Cefsulodin targets primarily PBP1A, increasing the cell's dependence on PBP1B. The colony size is used as proxy of cellular fitness, and the colony size relative to cells expressing the WT protein is plotted here (mean ± SD; $n > 12$). (*B*) K_d values in μM determined by SPR of the PBP1B–LpoB interaction by using different PBP1B and LpoB versions (mean ± SD, $n = 3$). n.b., insufficient binding for determination of K_d; -, not tested. (*C*) GTase or TPase activity assays for PBP1B using different PBP1B and LpoB versions. The GTase rate is compared with the mean rate of PBP1B alone (mean ± SD; $n = 3–6$). The TPase activity is shown as percentages of cross-linked peptides in PG (mean ± SD; $n = 3–4$).

TPase activities of some of the PBP1B mutant in the presence and absence of LpoB (Fig. 4*C* and *SI Appendix*, Figs. S7 and S8). PBP1B R190D and the quadruple PBP1B Ala mutant with a defected interface between 187 and 191 had ∼20- and 30-fold weaker interaction to LpoB, respectively (Fig. 4*B* and *SI Appendix*, Fig. S6), and could only be basally activated by LpoB in vitro, although they were as active as WT PBP1B when assayed without LpoB (Fig. 4*C* and *SI Appendix*, Figs. S7 and S8). A PBP1B version with two further substitutions (D163A and E166A) was completely insensitive to LpoB activation in vivo and in vitro (Fig. 4 and *SI Appendix*, Figs. S7 and S8).

LpoB versions with single, and especially double, Ala substitutions in D106, N110, R111, and M195, and a D156R charge reversal version, were less active in vivo (Fig. 4*A* and *SI Appendix*, Fig. S5*B*) and would not suffice for the cell to survive only with PBP1B (*SI Appendix*, Table S3; the substitutions did not affect the overall folding; *SI Appendix*, Fig. S9). In agreement with D106A and M195A having the strongest effect in vivo, this double mutant showed a strong increase in K_d (∼10-fold; Fig. 4*B* and *SI Appendix*, Fig. S6) and the most severe defect in stimulation of GTase rate and TPase activity (Fig. 4*C* and *SI Appendix*, Figs. S7 and S8). The combination of the charge-reversed versions PBP1B R190D and LpoB D156R did not yield a functional pair in the cell and in vitro (Fig. 4*C* and *SI Appendix*, Fig. S5*B*), although these residues lie within direct interaction proximity. This points to an important role of R190 in PBP1B in the stimulation mechanism. Interestingly, an Ala substitution in Y178, lying within β2 of LpoB, significantly decreased the interaction with PBP1B (∼25-fold; presumably by affecting the interface to amino acids 187–191 of PBP1B, as the quadruple PBP1B mutant showed a suppressive interaction with LpoB Y178A; Figs. 3*B* and 4*B* and *SI Appendix*, Fig. S6), but only moderately affected the in vivo or in vitro activation of PBP1B (Fig. 4 *A* and *C*). This suggests that binding is required but not sufficient for PBP1B activation by LpoB, and supports further a model in which LpoB activates PBP1B by inducing conformational changes in its catalytic domain(s).

Overall, these data indicate that PBP1B and LpoB interact through a large interface that involves several amino acids in both proteins, which is consistent with the NMR data and molecular docking simulations.

The N-Terminal Flexible Region of LpoB Is Vital for Its Function in Vivo. The NMR data preclude any secondary structure elements in the N-terminal region of LpoB, which suggests it could be a long flexible linker that anchors LpoB to the OM. We constructed LpoB versions with a truncated or absent N-terminal region (LpoBΔ1–56 and LpoBΔ1–73, respectively). Both interacted with PBP1B with a similar K_d as native LpoB (Fig. 4*B* and *SI Appendix*, Fig. S6), and were capable of fully stimulating its GTase and TPase activities in vitro (Fig. 4*C* and *SI Appendix*, Figs. S7 and S8), indicating that the flexible region is dispensable for activation of PBP1B in a purified-component assay. In contrast, the partial or complete lack of the flexible region rendered LpoB nonfunctional (i.e., no linker) or partially functional (i.e., truncated LpoB) in the cell (Fig. 4*A* and *SI Appendix*, Fig. S5 and Table S3). We have previously shown that full-length LpoB that is retained in the IM supports cell growth, even in the absence of LpoA–PBP1A (5). When retained in the IM, both LpoB versions with truncated or deleted N termini were nonfunctional (Fig. 4*A* and *SI Appendix*, Fig. S5). In toto, the long N-terminal linker is vital for LpoB in vivo, as it presumably allows it to reach PBP1B from afar (OM; *Discussion*). This region may have additional

roles, as it is still required in the IM-anchored LpoB, although UB2H now lies closer.

Discussion

Activation of PG Synthases from the OM. LpoA and LpoB are OM-anchored lipoproteins that share no homology to each other, and interact with discrete docking domains in their cognate PBP. Up to now, no structural information has been available on these activators and/or their interaction with the PG synthase. By using data from NMR spectroscopy and small-angle X-ray scattering, we have recently modeled the structure of LpoA, which has a rigid, elongated shape with a total length of 145 Å (18). The LpoB structure reported here is clearly distinct: a flexible N-terminal region as long as 145 Å, followed by a ∼30-Å-long globular domain. However, both proteins use different architectural features to achieve the same goal: to span more than two thirds of the 210-Å-wide periplasm (19) and reach their cognate IM-anchored PBP (Fig. 5 shows LpoB). The globular domain of LpoB and the rigid body of LpoA both have a diameter of ∼30 Å, allowing them to traverse the PG layer, which has ∼40–60-Å-wide pores depending on turgor (20, 21). As interlayer distances have been measured only for the lateral part of the *E. coli* envelope, length constraints and membrane separation could be different in the leading edge of the inward growing septum, where PBP1B–LpoB predominantly localizes and acts. This could explain why OM-anchored LpoB was still somewhat functional when the flexible region was significantly shortened by 34 aa (removal of residues 23–56), although not to a degree that would allow cells to survive only on PBP1B/LpoB. When in the IM, LpoB lies closer to UB2H, yet a truncation or removal of its flexible linker was not tolerated. This suggests that the N terminus of LpoB may not merely be a linker but may have additional roles, e.g., interaction with other proteins. Efforts to elucidate its function are under way.

PBP1B interacts with the essential, IM-anchored cell division proteins PBP3 and FtsN (8, 10). FtsN also stimulates the activity of PBP1B, presumably by stabilizing its dimeric form, which is more active in in vitro assays (22). FtsN has a long flexible stretch of ∼120 aa, which allows it to reach and bind to the PG via its C-terminal SPOR domain (23, 24). It is interesting that both proteins stimulating PBP1B, LpoB and FtsN, share long flexible stretches, albeit anchored to different membranes. Such structural flexibility may be vital for dynamic multiprotein envelope complexes and may provide access for controlling the complex activity even from afar.

Globular Domain of LpoB Has Structural Similarity to TolB. The Dali server (25) identifies several structural homologs for the globular domain of LpoB. The top hits are a lipoprotein of unknown function, GNA1162 from *Neisseria meningitidis* [Protein Data Bank (PDB) ID code 4HRV (26); Z = 7.4, rmsd = 2.2 Å], and the N-terminal domain of *E. coli* TolB [TolB_N; PDB ID code 1CRZ (27); Z = 6.2, rmsd = 2.9 Å; *SI Appendix*, Fig. S10]. Interestingly, LpoB has the inverse orientation from TolB_N, with α-helix H1 of LpoB corresponding to the last α-helix of TolB_N. As a member of the Tol–Pal system, TolB participates in OM constriction during cell division, and the first 12 residues of its N-terminal domain interact with the IM protein TolA (28); LpoB lacks this TolA-binding motif. We have previously reported that PBP1B–LpoB and Tol–Pal complexes interact genetically and colocalize at constriction sites, implying that the two systems may have overlapping and/or interlinked functions during cell division (5). The structural similarity between LpoB and TolB_N points further toward a connection between the two machineries. TolB_N domains are found in most proteobacteria and chlamydiae, with many species carrying multiple periplasmic proteins with this domain, often in a Tol–Pal unrelated-genomic context. Interestingly, GNA1162 is part of the DUF799 family, which shows strong genomic co-occurrence and neighborhood with a TolB_N-containing protein (STRING). It is tempting to speculate that the two structurally related domains, TolB_N and DUF799, may work in concert in multiple contexts in the bacterial cell envelope.

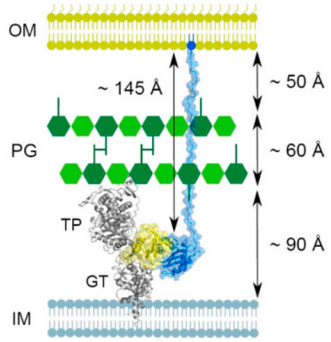

Fig. 5. Model of the stimulation of PBP1B by LpoB in the bacterial envelope. LpoB (blue) uses its ∼145-Å-long, flexible N-terminal region to span the periplasm and places its globular domain in position to interact with the UB2H domain of PBP1B (yellow). The thickness of the PG layer and distances to the IM and OM are according to previous studies (19).

How Does LpoB Activate PBP1B? We have identified amino acid residues in LpoB and the UB2H domain of PBP1B that are important for the PBP1B–LpoB interaction and the in vitro and in vivo function of PBP1B. In both proteins, often more than one amino acid had to be replaced by Ala to observe a measureable effect, and several amino acids had to be targeted to completely break the PBP1B–LpoB interaction. This is consistent with the NMR results, and points to an extended interface between the two proteins. Interestingly, in all PBP1B and LpoB versions with perturbed interface and/or activation, the GTase and TPase activities were affected in similar ways. This suggests that the two activities are interdependent, which is consistent with previous data (5, 13, 22). It may also mean that LpoB primarily activates one of the two PBP1B activities, and the second is affected as a result of the interlinking. As LpoB is capable of stimulating the GTase activity of PBP1B even at pH 4.5, it is likely that LpoB induces conformational changes in PBP1B that impact the environment of the catalytic Glu233 residue within the GTase domain. Such long-range allosteric effects on PBP activity are not without precedent. Recently, the binding of the antibiotic ceftaroline or PG fragments to an allosteric site was shown to open the catalytic TPase site of PBP2a from a methicillin-resistant *Staphylococcus aureus* strain over a distance of ∼60 Å (29). Further experiments are required to determine exactly how LpoB stimulates PBP1B. In any case, the quick on/off rates measured by SPR for the PBP1B–LpoB interaction suggest a highly dynamic interaction. This could be necessary for proper regulation of PBP1B by LpoB within a dynamic divisome.

Materials and Methods

Chemicals and Proteins. [^{14}C]GlcNAc-labeled and dansylated lipid II were prepared as published (22). [^{15}N]NH_4Cl and [^{13}C]glucose were purchased from Cambridge Isotope Labs. All other chemicals were from Sigma. The following proteins were prepared as previously described: PBP1B and versions of it with amino acid exchanges (8) and oligohistidine-tagged soluble LpoA [His-LpoA(sol)] (5). Soluble versions of LpoB with or without the oligohistidine-tag [His-LpoB(sol) and LpoB(sol)] and a His-tagged version of the UB2H domain of PBP1B (His-UB2H) were prepared as described in *SI Appendix, Supplemental Materials and Methods*. Antisera against PBP1B and LpoB (Eurogentec) were purified over an antigen column as described previously (8). VIM-4 β-lactamase was a gift from Adeline Derouaux (Centre for Bacterial Cell Biology, Newcastle University, Newcastle upon Tyne, United Kingdom). Cellosyl was provided by Hoechst.

Bacterial Strains and Growth Conditions. *E. coli* strains and plasmids used in this work are listed in *SI Appendix*, Table S1. For in vivo assays, cells were

grown aerobically at 37 °C in Luria Bertani (LB) Lennox, and, where appropriate, antibiotics/inducers were added: ampicillin (100 μg/mL), kanamycin (30 μg/mL), chloramphenicol (20 μg/mL), and arabinose (10 mM). For protein purification, cells with the appropriate plasmids were grown in LB or M9 minimal medium with 0.3% glucose, pH 6.8–7.2. For ^{15}N uniformly labeled or $^{15}N/^{13}C$ uniformly NMR samples, cells were grown with M9 medium containing [^{15}N]NH_4Cl or [^{15}N]NH_4Cl and [^{13}C]glucose, respectively.

Complementation Experiments for PBP1B and LpoB Versions. All PBP1B versions tested were expressed from the pET28a vector at levels similar or slightly higher than that of the endogenous PBP1B; the only exception was the version with six point mutations, which was less stable in vivo and expressed at significantly lower levels than the endogenous PBP1B. LpoB versions were expressed from the pBAD30 vector, and induction was required to reach endogenous LpoB levels. All LpoB versions were at levels similar or higher than that of the endogenous LpoB and were correctly folded (*SI Appendix*, Fig. S9). Δ*mrcB* and Δ*lpoB* cells, carrying the different PBP1B and LpoB versions, were robotically arrayed on agar plates in a 384-array format, with each variant being present 24 times. Plates were replicate-pinned on new agar plates containing the stress (cefsulodin or A22) and 10 mM arabinose (LpoB variants), incubated overnight, and imaged. Colony sizes were assessed with in-house software.

Protein Interaction and Activity Assays. SPR experiments were performed with slight modifications to a previously described protocol (30), as described in *SI Appendix, Supplemental Materials and Methods*. Continuous fluorescence GTase assays were performed as described previously (7). Radiolabeled lipid II was used as described before to measure TPase activity in an in vitro PG synthesis assay (22).

NMR Spectroscopy. All NMR spectra were collected on Agilent spectrometers operating at 600 or 800 MHz ^1H NMR frequencies, except for an aliphatic ^{13}C-NOESY-HSQC experiment, which was recorded on a 950-MHz Bruker US spectrometer. All spectrometers were equipped with cryogenic triple-resonance probes. Steady-state {^1H}-^{15}N-NOE experiments with a 3-s proton presaturation period were collected at 600-MHz proton frequency (31). For structure determination, NMR spectra were recorded on a 0.8-mM [^{13}C,^{15}N]LpoB(sol) sample in 100 mM sodium acetate, pH 5.0, containing 10% (vol/vol) D_2O at 308 K (14). A 3D ^{15}N-NOESY-HSQC (150 ms mixing time) and 3D aliphatic, aromatic, and methyl-^{13}C-NOESY-HSQC (32) experiments (mixing times of 120, 130, and 160 ms) were used to access experimental structural information. Distance restraints were extracted and analyzed by using UNIO'10 as described in *SI Appendix, Supplemental Materials and Methods*. Interaction studies were performed at pH 7.5 and 298 K on a mixture of 150 μM [^{15}N,^{13}C]LpoB(sol) and 300 μM His-UB2H in a buffer containing 10 mM Tris·HCl, 10 mM $MgCl_2$, 100 mM NaCl, and 10% (vol/vol) D_2O. Models of LpoB docked onto the UB2H domain of PBP1B were built with the HADDOCK Web server for data-driven biomolecular docking of HADDOCK2.1 (17) as described in *SI Appendix, Supplemental Materials and Methods*.

ACKNOWLEDGMENTS. We thank Natalie Strynadka for communicating unpublished results and Che Ma for plasmid pET15bUB2H. This work was supported by Biotechnology and Biological Sciences Research Council BB/I020012/1 and European Commission DIVINOCELL HEALTH-F3-2009-223431 (to W.V.); French Infrastructure for Integrated Structural Biology ANR-10-INSB-05-02, Grenoble Alliance for Integrated Structural Biology ANR-10-LABX-49-01, and Très Grande Infrastructure de Recherche–Résonance Magnétique Nucléaire–Très Haut Champ (TGIR-RMN-THC) FR3050 from the Centre National de la Recherche Scientifique (CNRS) (to J.-P.S.); the Sofja Kovalevskaja award (to A.T.); and European Molecular Biology Laboratory (EMBL) funding (A.K.). N.L.J. holds a PhD fellowship (Contrat de Formation par la Recherche) from the Commissariat à l'Energie Atomique et aux Energies Alternatives. Part of this work was conducted by using the platforms of the Grenoble Instruct center (Integrated Structural Biology; Unité Mixte de service 3518, funded by CNRS, Commissariat à l'Energie Atomique, Université Joseph Fourier, and EMBL).

1. Vollmer W, Blanot D, de Pedro MA (2008) Peptidoglycan structure and architecture. *FEMS Microbiol Rev* 32(2):149–167.
2. Typas A, Banzhaf M, Gross CA, Vollmer W (2012) From the regulation of peptidoglycan synthesis to bacterial growth and morphology. *Nat Rev Microbiol* 10(2): 123–136.
3. Paradis-Bleau C, et al. (2010) Lipoprotein cofactors located in the outer membrane activate bacterial cell wall polymerases. *Cell* 143(7):1110–1120.
4. Sham LT, Barendt SM, Kopecky KE, Winkler ME (2011) Essential PcsB putative peptidoglycan hydrolase interacts with the essential FtsXSpn cell division protein in *Streptococcus pneumoniae* D39. *Proc Natl Acad Sci USA* 108(45):E1061–E1069.
5. Typas A, et al. (2010) Regulation of peptidoglycan synthesis by outer-membrane proteins. *Cell* 143(7):1097–1109.
6. Yang DC, et al. (2011) An ATP-binding cassette transporter-like complex governs cell-wall hydrolysis at the bacterial cytokinetic ring. *Proc Natl Acad Sci USA* 108(45): E1052–E1060.
7. Banzhaf M, et al. (2012) Cooperativity of peptidoglycan synthases active in bacterial cell elongation. *Mol Microbiol* 85(1):179–194.
8. Bertsche U, et al. (2006) Interaction between two murein (peptidoglycan) synthases, PBP3 and PBP1B, in *Escherichia coli*. *Mol Microbiol* 61(3):675–690.
9. Fraipont C, et al. (2011) The integral membrane FtsW protein and peptidoglycan synthase PBP3 form a subcomplex in *Escherichia coli*. *Microbiology* 157(pt 1):251–259.
10. Müller P, et al. (2007) The essential cell division protein FtsN interacts with the murein (peptidoglycan) synthase PBP1B in *Escherichia coli*. *J Biol Chem* 282(50): 36394–36402.
11. Egan AJF, Vollmer W (2013) The physiology of bacterial cell division. *Ann N Y Acad Sci* 1277:8–28.
12. Sung MT, et al. (2009) Crystal structure of the membrane-bound bifunctional-transglycosylase PBP1b from *Escherichia coli*. *Proc Natl Acad Sci USA* 106(22): 8824–8829.
13. Lupoli TJ, et al. (2014) Lipoprotein activators stimulate *Escherichia coli* penicillin-binding proteins by different mechanisms. *J Am Chem Soc* 136(1):52–55.
14. Jean NL, Bougault CM, Egan AJF, Vollmer W, Simorre JP (2014) Solution NMR assignment of LpoB, an outer-membrane anchored Penicillin-Binding Protein activator from *Escherichia coli*. *Biomol NMR Assign*, 10.1007/s12104-014-9557-z.
15. Dosztányi Z, Csizmok V, Tompa P, Simon I (2005) IUPred: Web server for the prediction of intrinsically unstructured regions of proteins based on estimated energy content. *Bioinformatics* 21(16):3433–3434.
16. Camilloni C, De Simone A, Vranken WF, Vendruscolo M (2012) Determination of secondary structure populations in disordered states of proteins using nuclear magnetic resonance chemical shifts. *Biochemistry* 51(11):2224–2231.
17. de Vries SJ, van Dijk M, Bonvin AM (2010) The HADDOCK web server for data-driven biomolecular docking. *Nat Protoc* 5(5):883–897.
18. Jean NL, et al. (2014) The elongated molecular structure of the outer-membrane activator of peptidoglycan synthesis LpoA: Implications for PBP1A-stimulation. *Structure*, in press.
19. Matias VR, Al-Amoudi A, Dubochet J, Beveridge TJ (2003) Cryo-transmission electron microscopy of frozen-hydrated sections of *Escherichia coli* and *Pseudomonas aeruginosa*. *J Bacteriol* 185(20):6112–6118.
20. Demchick P, Koch AL (1996) The permeability of the wall fabric of *Escherichia coli* and *Bacillus subtilis*. *J Bacteriol* 178(3):768–773.
21. Vázquez-Laslop N, Lee H, Hu R, Neyfakh AA (2001) Molecular sieve mechanism of selective release of cytoplasmic proteins by osmotically shocked *Escherichia coli*. *J Bacteriol* 183(8):2399–2404.
22. Bertsche U, Breukink E, Kast T, Vollmer W (2005) *In vitro* murein peptidoglycan synthesis by dimers of the bifunctional transglycosylase-transpeptidase PBP1B from *Escherichia coli*. *J BiolChem* 280(45):38096–38101.
23. Ursinus A, et al. (2004) Murein (peptidoglycan) binding property of the essential cell division protein FtsN from *Escherichia coli*. *J Bacteriol* 186(20):6728–6737.
24. Yang JC, Van Den Ent F, Neuhaus D, Brevier J, Löwe J (2004) Solution structure and domain architecture of the divisome protein FtsN. *Mol Microbiol* 52(3):651–660.
25. Holm L, Rosenström P (2010) Dali server: Conservation mapping in 3D. *Nucleic Acids Res* 38(Web server issue):W545-9.
26. Cai X, et al. (2013) Structure of *Neisseria meningitidis* lipoprotein GNA1162. *Acta Crystallogr Sect F Struct Biol Cryst Commun* 69(pt 4):362–368.
27. Abergel C, et al. (1999) Structure of the *Escherichia coli* TolB protein determined by MAD methods at 1.95 Å resolution. *Structure* 7(10):1291–1300.
28. Bonsor DA, et al. (2009) Allosteric beta-propeller signalling in TolB and its manipulation by translocating colicins. *EMBO J* 28(18):2846–2857.
29. Otero LH, et al. (2013) How allosteric control of *Staphylococcus aureus* penicillin binding protein 2a enables methicillin resistance and physiological function. *Proc Natl Acad Sci USA* 110(42):16808–16813.
30. Vollmer W, von Rechenberg M, Höltje J-V (1999) Demonstration of molecular interactions between the murein polymerase PBP1B, the lytic transglycosylase MltA, and the scaffolding protein MipA of *Escherichia coli*. *J BiolChem* 274(10):6726–6734.
31. Farrow NA, et al. (1994) Backbone dynamics of a free and phosphopeptide-complexed Src homology 2 domain studied by ^{15}N NMR relaxation. *Biochemistry* 33(19): 5984–6003.
32. Van Melckebeke H, Simorre JP, Brutscher B (2004) Suppression of artifacts induced by homonuclear decoupling in amino-acid-type edited methyl ^1H-^{13}C correlation experiments. *J Magn Reson* 170(2):199–205.

SUPPLEMENTARY INFORMATION

The outer-membrane lipoprotein LpoB spans the periplasm to stimulate the peptidoglycan synthase PBP1B

Alexander J. F. Egan[a,1], Nicolas L. Jean[b,c,d,1], Alexandra Koumoutsi[e,1], Catherine M. Bougault [b,c,d], Jacob Biboy[a], Jad Sassine[a], Alexandra S. Solovyova[f], Eefjan Breukink[g], Athanasios Typas[e,2], Waldemar Vollmer[a,2], Jean-Pierre Simorre [b,c,d,2]

[a] The Centre for Bacterial Cell Biology, Institute for Cell and Molecular Biosciences, Newcastle University, Richardson Road, Newcastle upon Tyne, NE2 4AX, United Kingdom.
[b] Univ. Grenoble Alpes, Institut de Biologie Structurale (IBS), F-38027 Grenoble, France.
[c] CEA, DSV, IBS, F-38027 Grenoble, France.
[d] CNRS, IBS, F-38027 Grenoble, France.
[e] European Molecular Biology Laboratory Heidelberg, Genome Biology Unit, Meyerhofstraße 1, 69117 Heidelberg, Germany.
[f] Institute for Cell and Molecular Biosciences, Newcastle University, Richardson Road, Newcastle upon Tyne, NE2 4AX, United Kingdom.
[g] Bijvoet Center for Biomolecular Research, Department of Biochemistry of Membranes, University of Utrecht, Padualaan 8, 3584 CH Utrecht, The Netherlands.

[1]Authors contributed equally to the work.

[2]Correspondence:
Jean-Pierre Simorre: Institut de Biologie Structurale, 71 avenue des Martyrs, CS10090, 38044 Grenoble Cedex 9, France. Email: jean-pierre.simorre@ibs.fr; phone: +33 (0) 457 428 555; fax: +33 (0) 476 501 890.

Waldemar Vollmer: The Centre for Bacterial Cell Biology, Newcastle University, Richardson Road, Newcastle upon Tyne, NE2 4AX, United Kingdom. Email: w.vollmer@ncl.ac.uk; phone: +44 (0) 191 208 3216; fax: +44 (0) 191 208 3205.

Athanasios Typas: European Molecular Biology Laboratory, Genome Biology Unit, Meyerhofstraße 1, Heidelberg 69117, Germany. Email: typas@embl.de; phone: +49 (0) 6221 3878156; fax: +49 (0) 6221 3878518.

Content

1. Supplemental Materials and Methods

Protein overproduction and purification. BL21(DE3) strains harboring plasmids pET28LpoB [for the purification of LpoB; signal sequence and lipid anchor of LpoB replaced by an oligohistidine tag, LpoB(sol) (1)], or pET15bUB2H [for the purification of PBP1B; residues 108-200 with an N-terminal oligohistidine tag (2)] were grown in 3 l of LB medium with appropriate supplements at 30˚C to an OD_{578} of 0.5 - 0.6. Recombinant genes were overexpressed by induction with 1 mM IPTG and further incubation for 3 h at 30˚C. Cells were harvested by centrifugation (10,000 × *g*, 15 min, 4˚C) and the pellet was resuspended in buffer I (25 mM Tris/HCl, 10 mM $MgCl_2$, 500 mM NaCl, 20 mM imidazole, 10% glycerol, pH 7.5). A small amount of DNase, protease inhibitor cocktail (Sigma, 1/1000 dilution) and 100 µM phenylmethylsulfonylfluoride (PMSF) was added before cells were disrupted by sonication (Branson digital). The lysate was centrifuged (130,000 × *g*, 1 h, 4˚C) and the supernatant applied to a 5 ml HisTrap HP column (GE healthcare), attached to an ÄKTA Prime$^+$ (GE Healthcare), at 1 ml/min. The column was washed with 4 volumes buffer I before step-wise elution of bound proteins with buffer II (25 mM Tris/HCl, 10 mM $MgCl_2$, 500 mM NaCl, 400 mM imidazole, 10% glycerol, pH 7.5). To remove the oligohistidine tag from His-LpoB(sol), 50 U/ml of restriction grade thrombin (Novagen) was added and the protein was dialyzed against 2 l of 25 mM Tris/HCl, 100 mM NaCl, 10% glycerol, pH 8.3 for 18 h at 4˚C, before it was applied to a 5 ml HiTrap Q HP column (GE healthcare) attached to an ÄKTA Prime$^+$ (GE Healthcare) at 0.5 ml/min. LpoB(sol) was collected in the flow-through. The LpoB(sol), His-LpoB(sol) or His-UB2H samples were concentrated to 4 - 5 ml using a VivaSpin column (MW cut-off 6,000 Da) and applied to a Superdex200 HiLoad 16/600 column at 1 ml/min for size exclusion chromatography in 25 mM HEPES/NaOH, 1 M NaCl, 10% glycerol, pH 7.5. Finally, proteins were dialyzed against storage buffer (25 mM HEPES/NaOH, 500 mM NaCl, 10% glycerol, pH 7.5). The same procedure was used for LpoB versions with amino acid exchanges. Recombinant PBP1B (pDML924; the functional, short PBP1Bγ version, starting from amino acid 46) and point-mutant alleles, as well as His-LpoA were purified as described previously (1, 3).

Analytical size exclusion chromatography. His-LpoB(sol), His-LpoA(sol) (250 µM), His-UB2H (330 µM) or mixtures of these proteins were diluted into high salt buffer (25 mM Tris/HCl, 10 mM $MgCl_2$, 1 M NaCl, pH 7.5) and incubated at 4°C for 30 minutes before samples were dialyzed overnight against running buffer (25 mM Tris/HCl, 100 mM NaCl, pH 7.5). Size exclusion chromatography was performed with an ÄKTA Prime$^+$, using a 24 ml Superdex-75 or Superdex-200 column (GE Healthcare) and measuring the absorbance at 280 nm. The column was washed with 1.5-fold column volume of H_2O followed by equilibration with 1.5-fold volume running buffer. Chromatography was performed at a flow-rate of 0.5 ml/min, with 1 ml fractions collected.

Fractions were analyzed by SDS-PAGE. Protein standards of known molecular weight, albumin, carbonic anhydrase and cytochrome C (Sigma), were used to produce a standard curve for the calculation of the approximate molecular weight of proteins.

Analytical ultracentrifugation (AUC). Sedimentation velocity (SV) experiments were carried out in a Beckman Coulter ProteomeLab XL-I analytical ultracentrifuge at a rotation speed of 48,000 rpm. The density and viscosity of the buffer at experimental temperature (4°C) were calculated using program SEDNTERP (4). The partial specific volume ($\bar{v}$) of protein was calculated as an additive sum of $\bar{v}$ values of constituent amino acids, using the SEDNTERP program, and adjusted for the experimental temperature (5). Sedimentation velocity profiles were treated using size-distribution c(s) model implemented in the program SEDFIT (6). Each peak on the distribution plot was integrated in order to obtain the weight-averaged values for sedimentation coefficient and molecular mass. Integrated values of sedimentation coefficient (s) obtained at experimental conditions were converted to the standard conditions ($s_{20,w}$) (which is the value of sedimentation coefficient in water at 20°C).

Surface plasmon resonance (SPR). SPR experiments were performed with slight modifications to a previously described protocol (7) using a BioRad ProteOn XPR36 system and associated software (BioRad) with a GLC amine coupling sensorchip. Briefly, ampicillin (10 mg/ml) was immobilized on the chip surface by general amine coupling as per the manufacturers' instructions. PBP1B (3 µg/ml) was immobilized to the ampicillin surface at a flow rate of 30 µl/min for a period of 5 min at 35°C. As a control, an identical ampicillin surface was exposed to PBP1B buffer. The surface was rinsed with regeneration buffer (10 mM Tris/Maleate, 1 M NaCl, 0.05% Triton X-100, pH 7.5) before digestion of free ampicillin with 1 µM β-lactamase VIM-4. LpoB versions were injected at various concentration series (0, 0.5, 1, 2, 3, and 4 µM; 0, 2, 4, 8, 12 and 16 µM; or 0, 5, 10, 20, 30 and 40 µM) in running buffer. Assays were performed in triplicate at 25°C, at a flow rate of 75 µl/min and with an injection time of 5 minutes. Kinetic calculations (Scatchard plot) were performed as described previously (7).

Hydrodynamic calculations. The hydrodynamic parameters were calculated using program SOMO, part of the ULTRASCAN platform (8, 9) for all 20 lowest energy LpoB structures obtained by NMR spectroscopy.

NMR spectroscopy. NMR spectra were collected on Agilent spectrometers operating at 600 or 800

MHz ^{1}H NMR frequencies and an aliphatic ^{13}C-NOESY-HSQC experiment was recorded on a 950 MHz Bruker US spectrometer. All the spectrometers were equipped with cryogenic triple resonance probes. Resonance assignments have been deposited in the BMRB (accession number 19681). NMR data were processed with NMRPipe (10) and analyzed using the CcpNmr Analysis 2.2 software (11). For the LpoB:His-UB2H interaction, two types of behaviors were observed for the LpoB resonances when comparing the [^{1}H,^{15}N]-BEST-TROSY-HSQC spectra collected on a 250 µM [^{15}N,^{13}C]-LpoB(sol) sample to that collected on the LpoB(sol)-His-UB2H mixture: (i) chemical shift perturbations, which were calculated using the following formula;

$$\varnothing\delta = \sqrt{\left(\delta_{H,UB2H-LpoB} - \delta_{H,LpoB}\right)^2 + \left(0{,}1 * \left(\delta_{N,UB2H-LpoB} - \delta_{N,LpoB}\right)\right)^2}$$

(ii) disappearance of resonances due to intermediate exchange (Fig. S4B). The amide resonance perturbation upon complex formation with His-UB2H is reported for each of the LpoB residues in Fig. S4C.

Extraction of structural restraints and structure calculation. Distance restraints from 3D ^{15}N-NOESY-HSQC, as well as 3D aliphatic and aromatic ^{13}C-NOESY-HSQC experiments, were obtained after automatic peak picking and assignment performed by UNIO'10 version 2.0.2 (12). Additional distance constraints were extracted from peak volumes from a methyl-^{13}C-NOESY-HSQC experiment (13) assigned manually. TALOS+ was used to determine φ and ψ dihedral angle restraints from chemical shifts (14). The structure of LpoB was calculated with Aria 2.3.1 (15) using 100 structures for each of the 8 iterations, with the exception of the last cycle where 750 structures were calculated. The 20 lowest energy structures from the last iteration underwent explicit water refinement in the NMR module of the Crystallography and NMR System (CNS) (16). Final structures were deposited in the PDB under the accession code 2MII after validation by iCing (https://nmr.cmbi.ru.nl/icing/; (17)). Structures were visualized and figures were prepared with Pymol Molecular Graphics System, Version 1.5.0.4 Schrödinger, LLC.

HADDOCK calculations. LpoB residues that showed amide chemical shift perturbations larger than 0.05 ppm in the complex (residues 96, 104-107, 127, 137, 139, 155, 156, 166, 169-170, 177, 180-181, 194, 197 and 205, see residues in black in Fig. S4C) or for which the corresponding resonance disappeared in the complex (residues 98, 109-110, 117, 129, 133, 136, 153, 158-160, 162-163, 167-168, 176, 178-179, 193, 195-196, 198, 200-203, see residues in red in Fig. S4C) were considered as perturbed by the UB2H interaction. An initial HADDOCK run was performed with these NMR restraints to search for an interaction surface on the UB2H domain of PBP1B. In this calculation, only residues 113-116, 120-122, 125-126, 129, 133-138, 140, 144-156, 161, 163-182,

184, 185, 187-196 of the UB2H domain are considered as accessible to LpoB, *i.e.* surface exposed residues that are not already involved in an interaction with the TPase or GTase domains of PBP1B. This initial run produced 2 different families of structures with HADDOCK scores significantly lower than the other solutions. In both families, residues 167 to 176 of the UB2H domain interacted with LpoB residues identified by NMR perturbations. Additional interaction sites on the UB2H domain nevertheless differed significantly: one family of structures proposed residues 137-138, 147-152, and 177-178 of UB2H as involved in the interaction, while the other family alternatively proposed residues 164-166 and 188-193 of UB2H as interaction sites. To discriminate between these two UB2H interaction surfaces, we designed targeted amino acid exchanges in both binding partners.

Residues 106, 110, 111, 156, 178 and 195 in LpoB and residues 166, 187, 188, 190, and 191 in PBP1B were experimentally verified to play a role in the PBP1B-LpoB interaction and PBP1B activation (Fig. 4, S6-S8). These residues were thus considered as part of the interaction site in the second stage of the docking procedure. A final HADDOCK calculation included the NMR perturbed residues on LpoB(sol) and residues 166, 187, 188, 190 and 191 on UB2H, which were obtained from the *in vivo* and *in vitro* assays. Two clusters with low HADDOCK scores (-80.4 ± 1.7 and -77.8 ± 2.2 a.u.) were obtained. The most populated cluster with 65 members out of 200 models generated has a well-defined electrostatic (-381.8 ± 22.2 kcal mol^{-1}) and Van der Waals (-57.9 ± 3.4 kcal mol^{-1}) energy. The docking occurred with a minimal conformational rearrangement of the partners. The lowest energy model in the latter cluster is presented in Fig. 3B. Only in this model, residues D156 of LpoB and R190 of the UB2H domain are in close contact (1.65 Å average distance between the O of the D156 carboxylate and the proton of the R190 guanidinium of PBP1B). The *in vivo* and *in vitro* data show a drastic impact of the substitution of these residues, reducing the activation of PBP1B by LpoB (Fig. 4, S6-S8), supporting the proposed model. In the other HADDOCK model, the residues D156 of LpoB and R190 of the UB2H domain are ~ 20 Å apart, and D156 of LpoB does not interact with residues in the UB2H domain. Therefore, this model is not in agreement with the *in vivo* data.

2. Table S1. List of *E. coli* strains and plasmids.

Strain/Plasmid	Genotype/Properties	Notes/Reference
Strain		
BL21(DE3)	Expression strain F^- *ompT*, *dcm*, *hsdS* (rB^- mB^-) *gal* λ(DE3)	Novagen
BW25113	*rrnB3* Δ*lacZ4787 hsdR514* Δ(*araBAD*)567 Δ(*rhaBAD*)568 *rph*-1	KEIO collection parental strain (18)
KEIO single mutants	*lpoB::kan*, *mrcB::kan*	KEIO collection (18)
Plasmid		
pET28LpoB	*lpoB* region encoding the soluble part of LpoB cloned between NdeI and HindIII. Expressed thrombin-cleavable fusion protein: MGSSH_6SSGLVPRGSHM-LpoB(V21-Q213). All LpoB point mutants and truncations for *in vitro* experiments were made in this plasmid.	(1)
pBAD30-LpoB	*lpoB* cloned between EcoRI and SphI. All LpoB point mutants and truncations for *in vivo* experiments were made and tested in this plasmid. The LpoB IM variants carried a different lipoprotein sorting signal (D+2, E+3).	(1)
pDML924	pET28a with oligohistidine-tagged PBP1Bγ (residues 46-642 of PBP1B). All PBP1B point mutants for *in vitro* and *in vivo* experiments were made in this plasmid; basal activity (no inducer) can complement an *mrcB* mutation.	(19)
pET15bHis-UB2H	*mrcB* region encoding the UB2H domain of PBP1B cloned between NdeI and BamHI; expressed fusion protein MGSSH_6SSGLVPRGSHM-UB2H (G108 – R200) + GSGC	(2)

3. Table S2. Structural statistics for the ensemble of 20 NMR structures of LpoB.

NMR distance and dihedral constraints	**Number / parameter**
Distance constraints	
Total unambiguous NOE restraints	3849
Intra-residue	1255
Inter-residue	2594
Sequential ($\|i - j\| = 1$)	779
Medium-range ($\|i - j\| \leq 5$)	575
Long-range ($\|i - j\| > 5$)	1240
Total ambiguous NOE restraints	1289
Total dihedral angle restraints	248
Backbone φ	124
Backbone ψ	124
Structure calculation statistics	
Restraints violations	
Distance (> 0.3 Å, > 0.5 Å)	44.25, 3.35
Dihedral (> 5°)	8.1
Average pairwise root mean square deviation (Å)[a,b]	
Backbone atoms	0.18 ± 0.03
All heavy atoms	0.44 ± 0.06
Ramachandran analysis[b]	
Residues in most favored regions (%)	85.9
Residues in additional allowed regions (%)	12.8
Residues in generously allowed regions (%)	0.8
Residues in disallowed regions (%)	0.5

[a] Pairwise r.m.s. deviation was calculated among the 20 refined structures of lowest energy.
[b] These values were calculated on residues 74 to 213 (globular domain).

4. Table S3. Complementation of PBP1B and LpoB function. Complementation of PBP1B and LpoB function in a *mrcA*$^{-}$*mrcB*$^{-}$ and *mrcA*$^{-}$*lpoB*$^{-}$ background, respectively. *mrcA::kan* was transduced with P1 to ∅*mrcB* pET28a-PBP1B versions or ∅*lpoB* pBAD30-LpoB versions in the presence/absence of 10 mM Ara. When many or no transducants were obtained, complementation was deemed successful (+) or non-successful (-). In the few cases where only a few transducants were isolated, we further tested them by PCR and all of them were false positive (duplications).

Plasmid	Complementation
A. PBP1B versions	
pET28a	-
pET28a-PBP1B (pDML942)	+
pET28a-PBP1B N150A	+
pET28a-PBP1B E153A	+
pET28a-PBP1B N150A+E153A	+
pET28a-PBP1B E166A	-
pET28a-PBP1B D163A+E166A	-
pET28a-PBP1B E187A+N188A	-
pET28a-PBP1B R190A	-
pET28a-PBP1B R190D	-
pET28a-PBP1B Q191A	-
pET28a-PBP1B R190A+Q191A	-
pET28a-PBP1B E166A+R190A+ Q191A	-
pET28a-PBP1B E187A+N188A+ R190A+Q191A	-
pET28a-PBP1B D163A+E166A+ E187A+N188A+R190A+Q191A	-
pET28a-PBP1B R196A	+
B. LpoB versions	
pBAD30	-
pBAD30-LpoB	+
pBAD30-LpoB IM	+
pBAD30-LpoB ∅23-56	-
pBAD30-LpoB ∅23-73	-
pBAD30-LpoB IM ∅23-56	-
pBAD30-LpoB IM ∅23-73	-
pBAD30-LpoB D106A	-
pBAD30-LpoB R111A	+
pBAD30-LpoB N110A R111A	-
pBAD30-LpoB D156R	-
pBAD30-LpoB T160A	+
pBAD30-LpoB R161A	+
pBAD30-LpoB Y178A	-
pBAD30-LpoB R111A+R161A	+
pBAD30-LpoB S180A	+
pBAD30-LpoB R161A+S180A	+
pBAD30-LpoB M195A	-
pBAD30-LpoB D106A+M195A	-

5. Supplemental References

1. Typas, A., Banzhaf, M., van den Berg van Saparoea, B., Verheul, J., Biboy, J., Nichols, R. J., Zietek, M., Beilharz, K., Kannenberg, K., von Rechenberg, M., *et al.* (2010) Regulation of peptidoglycan synthesis by outer-membrane proteins. *Cell* **143,** 1097-1109.
2. Sung, M. T., Lai, Y. T., Huang, C. Y., Chou, L. Y., Shih, H. W., Cheng, W. C., Wong, C. H., & Ma, C. (2009) Crystal structure of the membrane-bound bifunctional transglycosylase PBP1b from *Escherichia coli*. *Proc Natl Acad Sci U S A* **106,** 8824-8829.
3. Bertsche, U., Breukink, E., Kast, T., & Vollmer, W. (2005) In vitro murein peptidoglycan synthesis by dimers of the bifunctional transglycosylase-transpeptidase PBP1B from *Escherichia coli*. *J Biol Chem* **280,** 38096-38101.
4. Laue, T. M., Shah, B. D., Ridgeway, T. M., & Pelletier, S. (1992) in *Analytical ultracentrifugation in Biochemistry and polymer science* (Redwood Press Ltd, Melksham), pp. 90-125.
5. Durchschlag, H. (1986) in *Thermodynamic Data for Biochemistry and Biotechnology*, ed. Hinz, H. J. (Springer - Verlag, Berlin-Heidelberg-New York-Tokyo), pp. 45-128.
6. Schuck, P. (1998) Sedimentation analysis of noninteracting and self-associating solutes using numerical solutions to the Lamm equation. *Biophys.J.* **75,** 1503-1512.
7. Vollmer, W., von Rechenberg, M., & Höltje, J.-V. (1999) Demonstration of molecular interactions between the murein polymerase PBP1B, the lytic transglycosylase MltA, and the scaffolding protein MipA of *Escherichia coli*. *J Biol Chem* **274,** 6726-6734.
8. Brookes, E., Demeler, B., Rosano, C., & Rocco, M. (2010) The implementation of SOMO (SOlution MOdeller) in the UltraScan analytical ultracentrifugation data analysis suite: enhanced capabilities allow the reliable hydrodynamic modeling of virtually any kind of biomacromolecule. *Eur Biophys J* **39,** 423-435.
9. Rai, N., Nollmann, M., Spotorno, B., Tassara, G., Byron, O., & Rocco, M. (2005) SOMO (SOlution MOdeler) differences between X-Ray- and NMR-derived bead models suggest a role for side chain flexibility in protein hydrodynamics. *Structure* **13,** 723-734.
10. Delaglio, F., Grzesiek, S., Vuister, G. W., Zhu, G., Pfeifer, J., & Bax, A. (1995) NMRPipe: a multidimensional spectral processing system based on UNIX pipes. *J Biomol NMR* **6,** 277-293.
11. Vranken, W. F., Boucher, W., Stevens, T. J., Fogh, R. H., Pajon, A., Llinas, M., Ulrich, E. L., Markley, J. L., Ionides, J., & Laue, E. D. (2005) The CCPN data model for NMR spectroscopy: development of a software pipeline. *Proteins* **59,** 687-696.
12. Guerry, P. & Herrmann, T. (2012) Comprehensive automation for NMR structure

determination of proteins. *Methods in molecular biology (Clifton, N.J* **831,** 429-451.

13. Van Melckebeke, H., Simorre, J. P., & Brutscher, B. (2004) Amino acid-type edited NMR experiments for methyl-methyl distance measurement in ^{13}C-labeled proteins. *J Am Chem Soc* **126,** 9584-9591.
14. Shen, Y., Delaglio, F., Cornilescu, G., & Bax, A. (2009) TALOS+: a hybrid method for predicting protein backbone torsion angles from NMR chemical shifts. *J Biomol NMR* **44,** 213-223.
15. Rieping, W., Habeck, M., Bardiaux, B., Bernard, A., Malliavin, T. E., & Nilges, M. (2007) ARIA2: automated NOE assignment and data integration in NMR structure calculation. *Bioinformatics (Oxford, England)* **23,** 381-382.
16. Brunger, A. T., Adams, P. D., Clore, G. M., DeLano, W. L., Gros, P., Grosse-Kunstleve, R. W., Jiang, J. S., Kuszewski, J., Nilges, M., Pannu, N. S.*, et al.* (1998) Crystallography & NMR system: A new software suite for macromolecular structure determination. *Acta Crystallogr D Biol Crystallogr* **54,** 905-921.
17. Doreleijers, J. F., Sousa da Silva, A. W., Krieger, E., Nabuurs, S. B., Spronk, C. A., Stevens, T. J., Vranken, W. F., Vriend, G., & Vuister, G. W. (2012) CING: an integrated residue-based structure validation program suite. *J Biomol NMR* **54,** 267-283.
18. Baba, T., Ara, T., Hasegawa, M., Takai, Y., Okumura, Y., Baba, M., Datsenko, K. A., Tomita, M., Wanner, B. L., & Mori, H. (2006) Construction of *Escherichia coli* K-12 in-frame, single-gene knockout mutants: the Keio collection. *Mol Sys Biol* **2,** 2006 0008.
19. Terrak, M., Ghosh, T. K., van Heijenoort, J., Van Beeumen, J., Lampilas, M., Aszodi, J., Ayala, J. A., Ghuysen, J. M., & Nguyen-Disteche, M. (1999) The catalytic, glycosyl transferase and acyl transferase modules of the cell wall peptidoglycan-polymerizing penicillin-binding protein 1b of *Escherichia coli*. *Mol Microbiol* **34,** 350-364.

6. Supplemental Figures S1 - S10.

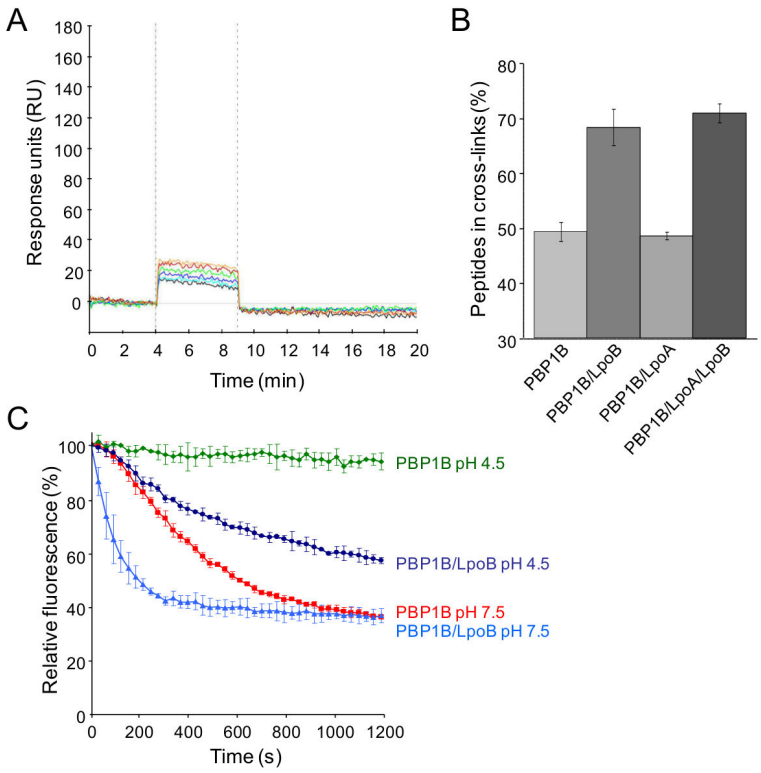

Fig. S1. LpoB interacts with PBP1B and stimulates its GTase and TPase activities. (*A*) LpoB does not significantly interact with a chip surface lacking PBP1B; control experiment for Fig. 1A. LpoB was injected at concentrations of 0 (black line), 0.5 (light blue), 1 (dark blue), 2 (green), 3 (red), and 4 (orange) µM. (*B*) LpoB stimulates TPase activity of PBP1B. PBP1B was incubated with radioactive lipid II substrate with/without LpoA and/or LpoB. The resulting PG was digested with the muramidase cellosyl, followed by reduction with sodium borohydrate and separation of the muropeptides by HPLC. The percentage of peptides in cross-links, which are produced by TPase activity, was calculated as 100% - % monomeric (uncross-linked) muropeptides. LpoB stimulated the TPase activity of PBP1B whereas LpoA did not, in the presence or absence of LpoB. The values are the mean ± standard deviation of three independent experiments. (*C*) LpoB stimulates the GTase activity of PBP1B at low pH (4.5) at which PBP1B alone is virtually inactive. The continuous GTase assay shows the consumption of dansylated lipid II substrate as reduction in relative fluorescence. The proteins are indicated at the curves. The values are the mean ± SD of three independent experiments.

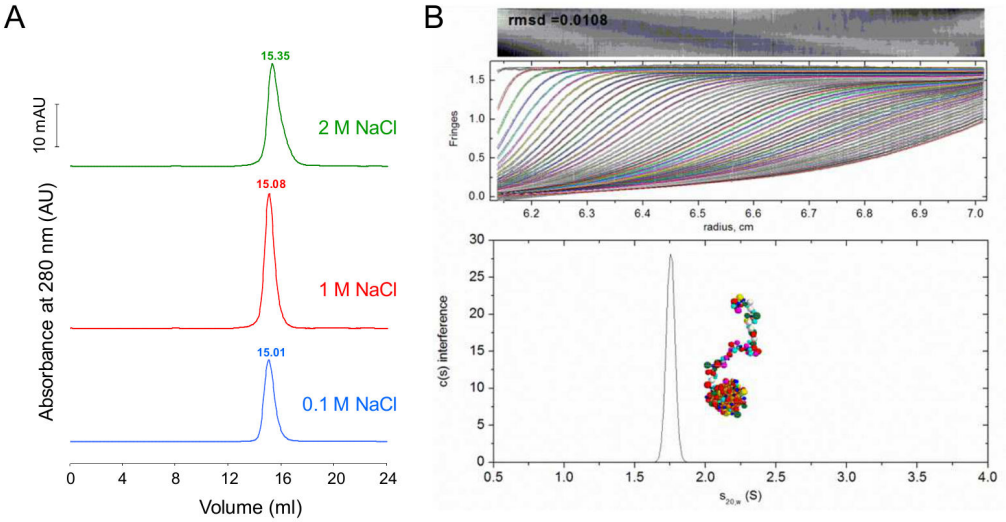

Fig. S2. LpoB is monomeric and has an elongated molecular shape with flexible regions. (*A*) UV chromatograms of LpoB(sol) in SEC resolved in buffers of increasing ionic strength in a 24 ml Superdex-200 column. Retention volume is shown at the top of each peak in ml. No significant shift in the retention of LpoB(sol) was observed from 0.1 to 2 M NaCl. Comparing to known standards, the MW was calculated to be 45.5 ± 3.3 kDa (n = 2), more than double of the theoretical MW of 20.3 kDa. (*B*) AUC results of a sedimentation velocity experiment: sedimentation boundaries (top panel) fitted with c(s) size-distribution model accompanied by hydrodynamic model of plausible solution conformation of the LpoB molecule. The results represent a single species with a MW of 22.6 kDa and a sedimentation coefficient of 1.76 S; the calculated sedimentation coefficient for the model is 1.74 S.

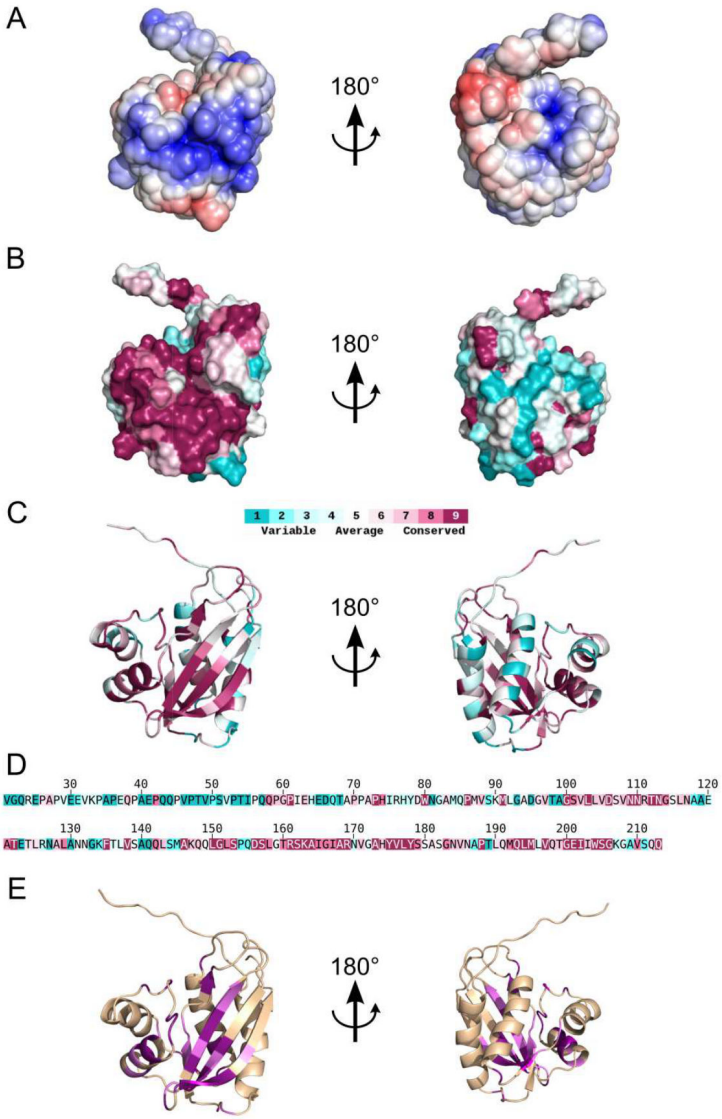

Fig. S3. Structural characteristics of LpoB and its interaction with UB2H. (*A*) Electrostatic surface representation of LpoB structure. Positively and negatively charged residues are shown in blue and red, respectively. LpoB shows a large positive patch at the three-stranded β-sheet site (left) and a smaller positive patch between H1 and H2 (right). (*B*) Surface and (*C*) ribbon representations of LpoB structure showing conserved residues in 68 unique sequences identified by Consurf (13). (*D*) Amino acid sequence conservation. Color coding is the same for panels B-D. (*E*) Cartoon of the structure of LpoB with residues that are subject to chemical shift perturbations and intensity changes upon interaction with UB2H, colored with same code as in Fig. 3A.

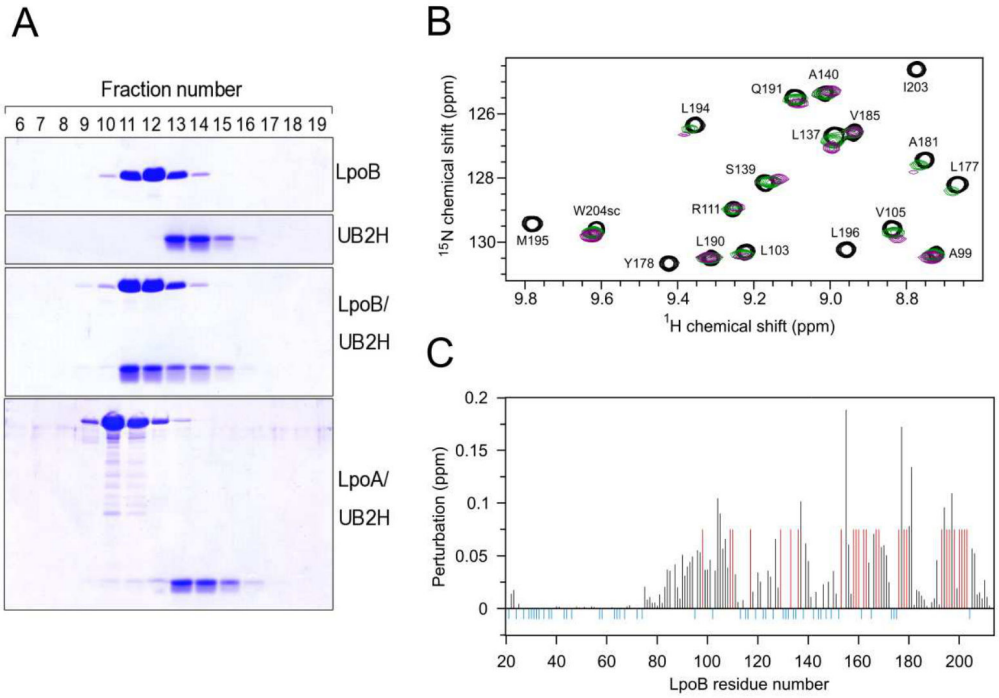

Figure S4. LpoB interacts with the UB2H domain of PBP1B. (*A*) Oligohistidine tagged versions of UB2H, LpoB and LpoA were applied alone or in combinations to a size exclusion chromatography column (24 ml Superdex-75). Fractions of 1 ml were collected and analyzed by SDS-PAGE followed by staining of the gel by Coomassie blue. In the LpoB/UB2H mixture both proteins co-eluted in earlier fractions compared to the proteins alone, indicating complex formation. UB2H did not interact with LpoA. (*B*) Superimposition of a portion of the [^{1}H,^{15}N]-BEST-TROSY spectra of [^{15}N,^{13}C]-LpoB(sol) in the absence (black) and presence of 0.5 (green) and 2 (purple) molar equivalents of His-UB2H. LpoB chemical shift perturbations or resonance intensity decrease indicate complex formation between LpoB(sol) and His-UB2H. LpoB assignments are reported for each of the [^{1}H,^{15}N] correlations; sc, side chain. (*C*) Residue-per-residue histogram of the perturbation detected on the [^{1}H,^{15}N] correlations of LpoB in a BEST-TROSY experiment collected after addition of His-UB2H in a 1:2 ratio (sample conditions: 10 mM Tris/HCl, 10 mM $MgCl_2$, 100 mM NaCl Buffer containing 10% D_2O at pH 7.5 and 25°C). Residues for which the [^{1}H,^{15}N] resonance has been identified in the LpoB alone sample and in the LpoB:UB2H complex are shown in black. For these residues, the chemical shift perturbation (CSP, $\varnothing\delta$ in ppm) was calculated as described in the Supplemental Materials and Methods. When the [^{1}H,^{15}N] resonance was detected in the LpoB sample but not in the complex, residues were labeled in red and assigned an arbitrary +0.075 ppm perturbation. When the [^{1}H,^{15}N] resonance remained unassigned in both samples, residues were labeled in blue and assigned an arbitrary -0.01 ppm perturbation value.

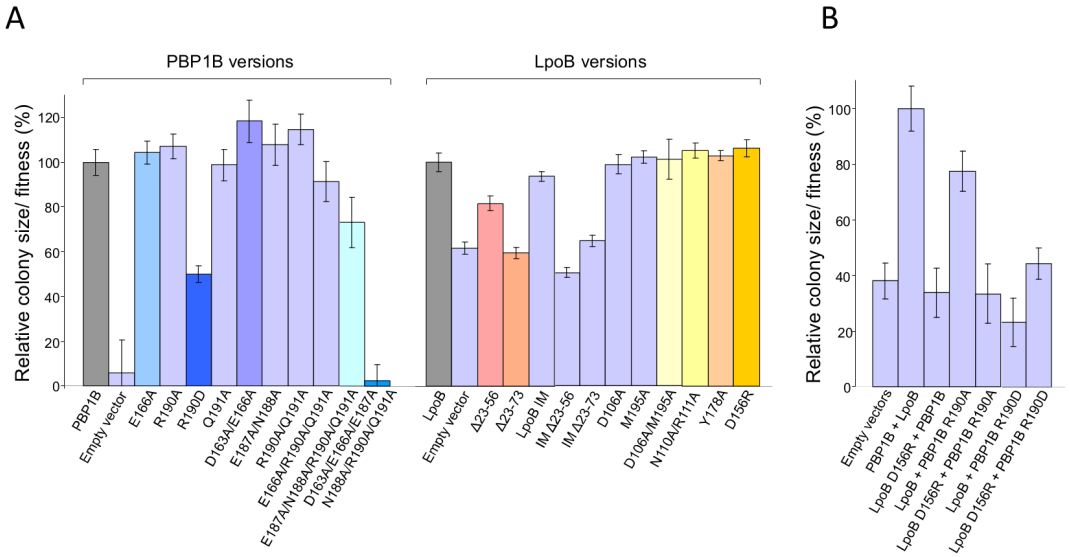

Figure S5. Complementation of PBP1B and LpoB alleles during A22 or cefsulodin treatment. (*A*) *mrcB* and *lpoB* mutants are more sensitive to A22, which targets MreB, and therefore cell elongation. Fitness of cells carrying PBP1B and LpoB alleles at or above wild-type levels was measured under A22 treatment. Colony size was used as proxy of cellular fitness, and the colony size relative to cells expressing the wild-type protein is plotted here (mean ± SD, n > 12). In contrast to Fig. 4A, only the most severe LpoB and PBP1B mutants cannot complement the A22 sensitivity, implying that basal PBP1B activity is sufficient to recover wild-type A22 sensitivity. (*B*) *In vivo* activity of PBP1B and LpoB charge-reversal versions as measured by cellular fitness under cefsulodin treatment (24 µg/ml). Cefsulodin targets primarily PBP1A, increasing the cell's dependence on PBP1B. Colony size is used as proxy of cellular fitness, and the colony size relative to cells expressing the wild-type protein is plotted here (mean ± SD, n>12).

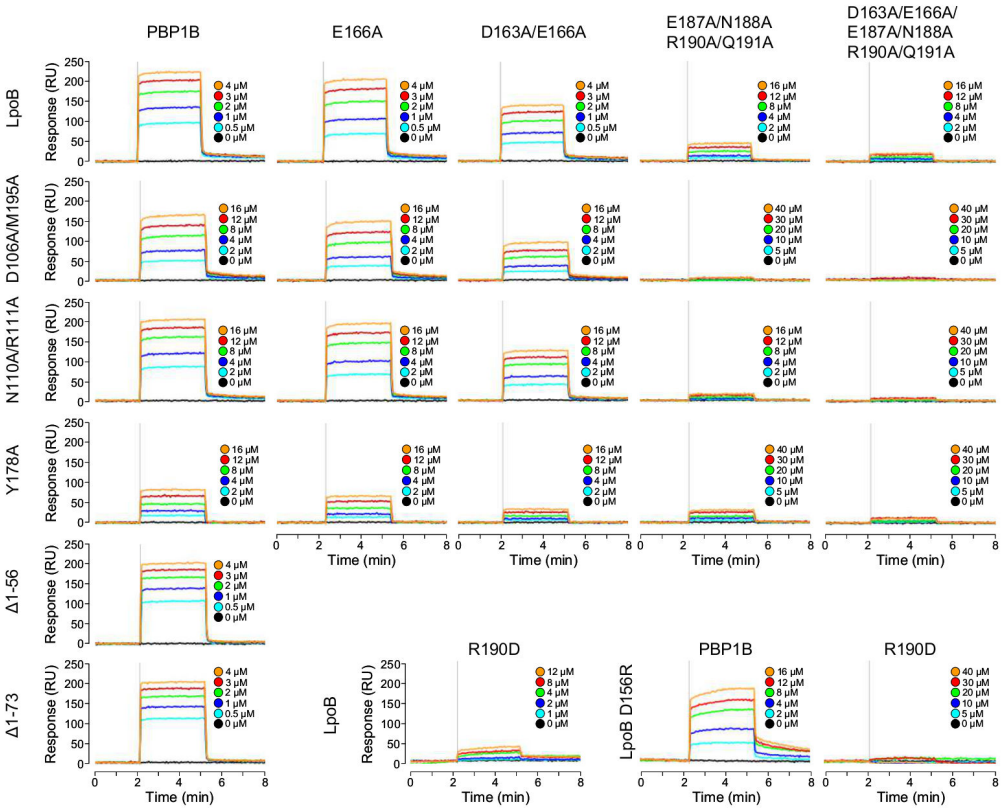

Figure S6. PBP1B or LpoB amino acid substitutions affect their interaction. Representative examples of SPR sensorgrams for the interaction between PBP1B and LpoB versions (corresponding to Fig. 4B). PBP1B versions were immobilized on the chip surface. LpoB versions were injected at the concentration indicated. The signals obtained from the control surface without PBP1B were subtracted.

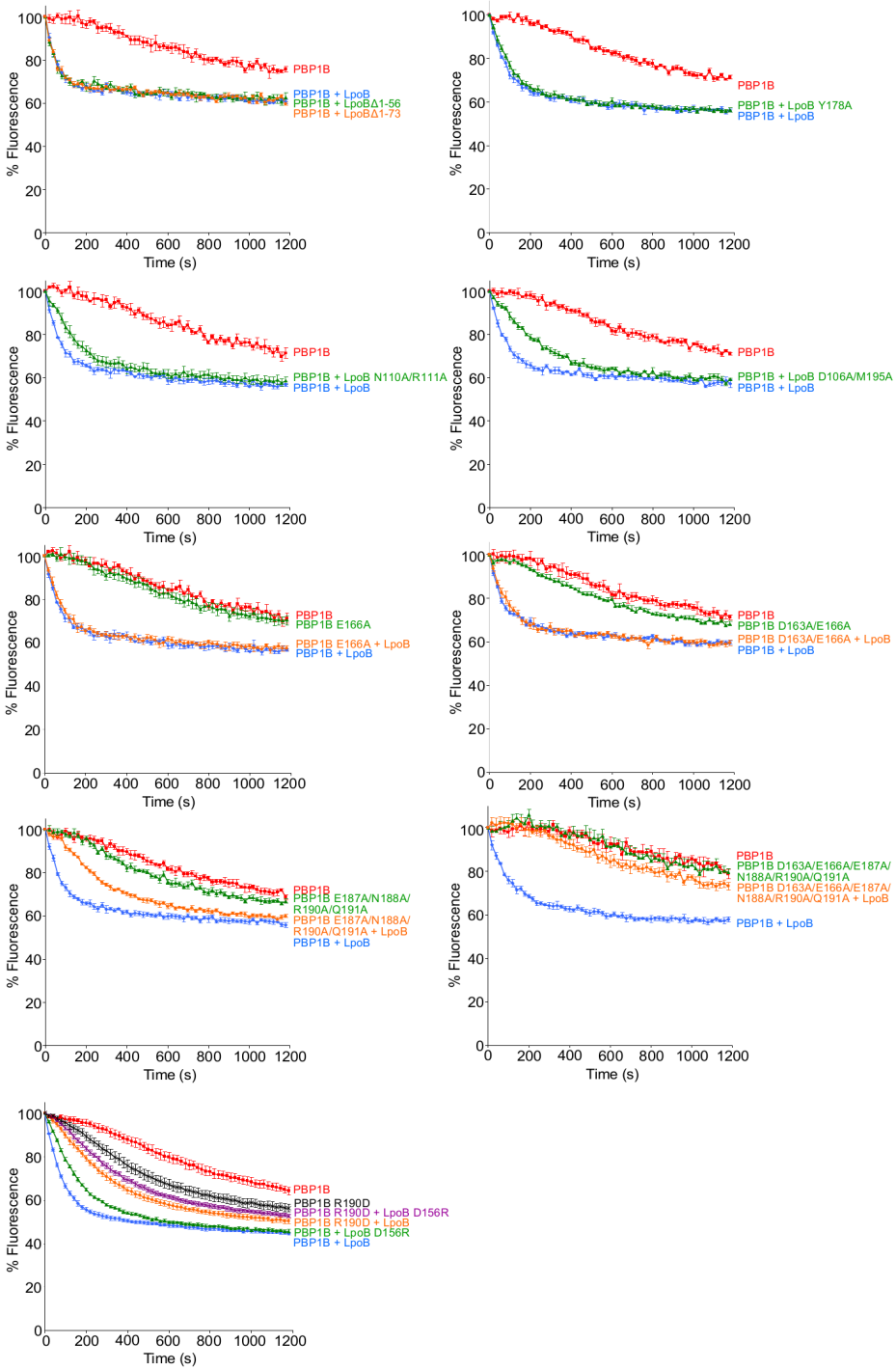

Fig. S7. PBP1B GTase assay; effect of amino acid exchanges in PBP1B or LpoB. Corresponding continuous GTase assays for data shown in Fig. 4C. Proteins present in each reaction are shown next to their corresponding curves in the same color. Each measurement is shown as mean ± SD of three to six independent experiments.

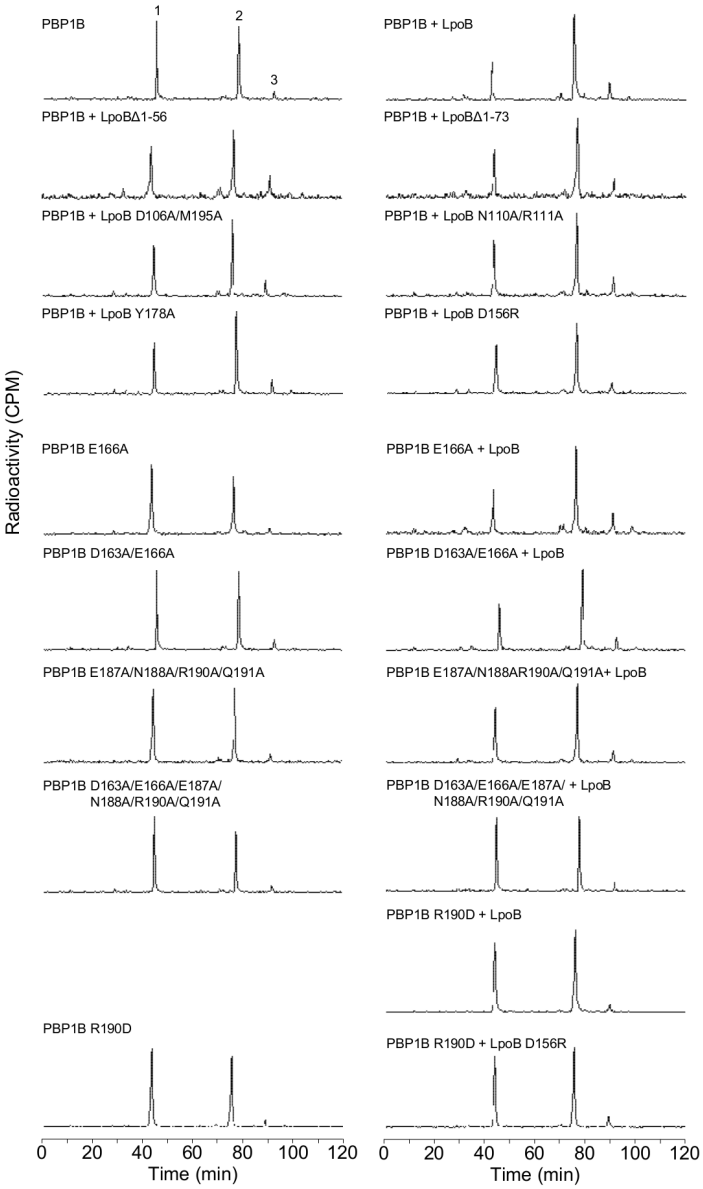

Fig. S8. PBP1B TPase assay; effect of amino acid exchanges in PBP1B or LpoB. Representative examples of HPLC chromatograms for TPase data shown in Fig. 4C. PBP1B versions were incubated with radioactive lipid II substrate in the presence or absence of LpoB versions. The resulting PG was digested with the cellosyl and the muropeptides were reduced with sodium borohydrate and separated by HPLC. The percentage of peptides in cross-links was calculated as 100% - % monomeric (uncross-linked) disaccharide pentapeptide (peak 1). Peak 2 corresponds to bis-disaccharide tetrapentapeptide, peak 3 to tris-disacchride tetratetrapentapeptide. Specific proteins present in each reaction are shown above their corresponding chromatograms.

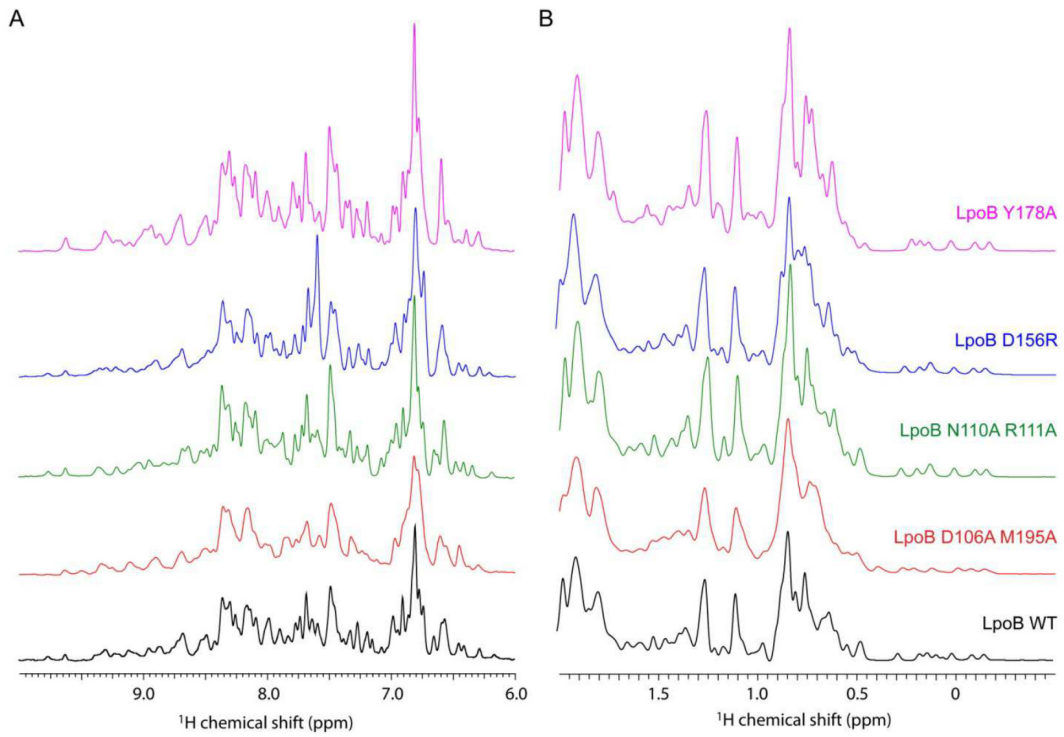

Fig. S9. NMR structural characterization of LpoB versions. 1D ^{1}H NMR spectra of wild-type (WT) LpoB and LpoB versions were collected at 25°C in 25 mM HEPES buffer containing 10 mM $MgCl_2$, 500 mM NaCl, 10% glycerol, pH 7.5. (*A*) The amide region shows well-dispersed signals and a similar signature. (*B*) The methyl region shows similar pattern for the upfield-shifted signals (below 0 ppm). The amide region has a vertical scaling factor of 4 with respect to the methyl region. These data suggest that all LpoB mutants adopt a similar folding as the wild-type protein.

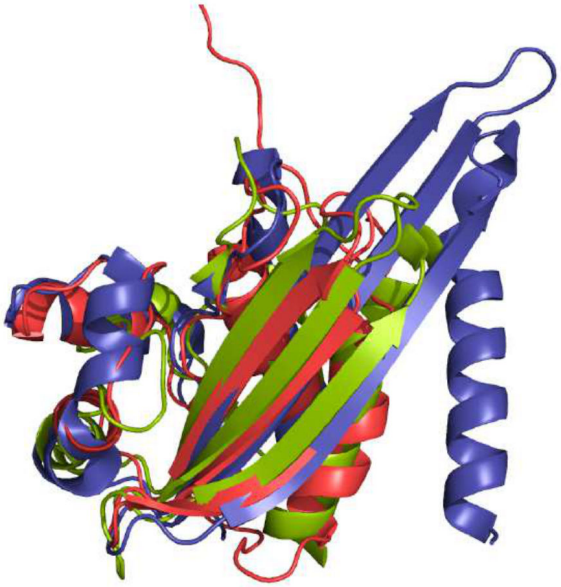

Fig. S10. Structural similarity of the globular domain of LpoB with the N-terminal domain of TolB and GNA1162. LpoB, TolB_N (PDB code 1CRZ), and GNA1162 (PDB code 4HRV) are shown in red, green and dark blue, respectively.

3.B- Discussion

3.B.a- A disordered tail to reach PBP1B

As expected from its sequence, LpoB adopts a completely different architecture from LpoA to reach its cognate PBP1A, although their initial situation is the same, i.e. reaching a partner below the peptidoglycan layer, while being anchored to the outer-membrane. While a rigid extended conformation is exhibited by LpoA, LpoB has a long (54 residues) flexible N-terminal stretch. This is not the first time that such a strategy is described for an outer-membrane lipoprotein involved in peptidoglycan synthesis or maturation. Indeed, among the Mlt lytic transglycosylases (discussed in part I section 3.A.a.i), MltC was shown to have such an N-terminal disordered region (Artola-Recolons et al., 2014) although much restricted (from residues 17 to 29). Moreover, the IUPred server also predicts such an unfolded domain for MltB through disorder scores higher than 0.5 (from residues 19 to 56 or 68, which could be an easy target for proteases, leading to the observed soluble form Slt35). From these three proteins, the flexible tail of LpoB is apparently the longest, in agreement with the hypothesis that the protein is long enough to reach PBP1B when the two others only need to attain the peptidoglycan layer (the short MltC tail can also be a regulation mechanism to act only on local multilayered peptidoglycan or to remain away from the sacculus before membrane release by proteases).

In the divisome, apart from PBP1B-LpoB, another trans-envelope complex is formed by TolA-Pal. In this case, a IUPred prediction expects a 40-amino-acid long disordered region (from residues 22 to 61) at the N-terminal extremity of Pal following the anchored cysteine, in agreement with reported observations of hindered protein crystallization when constructs have this region (Abergel et al., 2001). Although distance of TolAIII (the domain interacting with Pal when TolA adopts its energized conformation) from the outer-membrane is unknown, this module was postulated to reach through the peptidoglycan network to interact with Pal (Gerding et al., 2007). The long N-terminal flexible stretch might thus enable the outer-membrane anchored protein to explore the conformational space, promoting in the end interaction with nearby partners. One might object that, with a length of ~145 Å when extended, LpoB is unlikely to bind PBP1B, as the required extension of its disordered tail for the interaction (UB2H is expected to be more than 110 Å away from the outer-membrane) is entropically unfavorable. A solution to this possible issue would be that this N-terminal region might be stabilized in such a conformation by binding with undetermined partners. Interestingly, putative interactions could also be important for other undetermined reasons, as an inner-membrane targeted LpoB is not able to fully complement the wild type protein (Egan et al., 2014).

3.B.b- Stimulation of PBP1B by LpoB

In our PNAS article, LpoB was shown to interact through a large interface mainly located between the top of α-helix 4, and the β-strands 2 and 3 (see figures 2 and 3 of the *PNAS* article). For UB2H, we proposed, from modeling of the docking complex by HADDOCK and mutations weakening the interaction, that the region formed by the loop and the following small β-strand (residues 187 to 191, residues in red sticks on the right in figure 8.2) was one of the main binding sites. Mutations on the long loop (D163A and E166A, also in red in the lower part of Figure II.C.2) between UB2H β-strands 2 and 3 also suggested an implication from this part of the domain. As this interaction stimulates both the transglycosylase and transpeptidase activities in an apparent interdependent manner (Lupoli et al., 2014), one might expect a conformational change to occur in one or both PBP1B catalytic domains upon interaction. The whole PBP1B protein being a challenging enzyme to work with at concentrations required for structural studies, I focused subsequent work on the UB2H

domain (PBP1B residues 108 to 200) to study its behavior at the atomic level upon interaction with LpoB. Although it shows a propensity for degradation over time at room temperature and seems to barely tolerate concentrations higher than ~350 µM, UB2H has the advantage of a small molecular weight (13.1 kDa for a histidine-tagged construct) which allows collection of NMR data. I performed preliminary experiments to begin the assignment of labeled UB2H and to record chemical shift perturbations upon binding with a construct of LpoB depleted of its N-terminal tail, LpoB Δ1-73 (to reduce its molecular weight, this region not being implicated in the interaction). A first analysis of the results seems to confirm the UB2H binding site predicted by the docking model. However, given that most of the resonances significantly perturbed seem at first glance to be from residues located at the interface (this must be validated after full backbone assignment), it is likely that the interaction does not induce strong conformational changes in UB2H (no secondary structures modifications for example). One hypothesis could be that LpoB binding to UB2H induces only slight structural modifications that are limited to the central β-sheet region linking the three domains (see the three stranded β-sheet structure on the left of the green UB2H domain in figure II.3.2). Conformational change in this region could have a huge impact on the rest of the protein as it may re-position the two catalytic domains relatively to each other in order to enhance their cooperativity for example, and/or to "transfer" the LpoB-binding signal up to their active site. With this long distance conformational rearrangement, these active sites would then adopt a state favoring the reaction. This proposition is in agreement with the finding by the team of T. Bernhardt, that several PBP1B mutants entirely or partially bypass the requirement for LpoB to activate their transpeptidase and transglycosylase functionality (Markovski, 2012). In particular, four isolated mutations were shown to be located at proximity of the growing glycan chain exit or in the region between UB2H and the β-sheet domain linker.

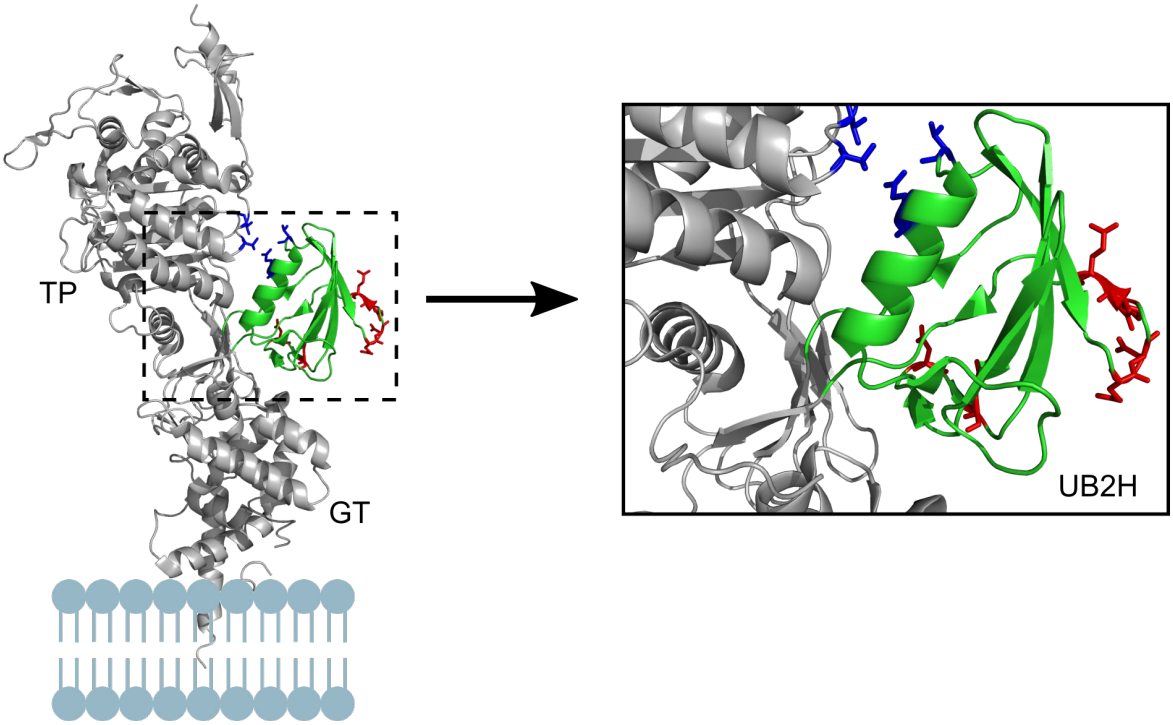

Figure II.3.2: The UB2H module (in green), located between the PBP1B transpeptidase (TP) and glycosyltransferase (GT) domains serves for multiple interactions. Residues thought to interact with LpoB (on the basis of the structural LpoB/PBP1B docking model and of mutations impairing the binding (Egan et al., 2014)) and CpoB (based on *in vivo* cross-linking data (Gray et al., 2015)) are represented in sticks and colored in red and dark blue, respectively.

Recent work by Gray and coworkers suggest that actually PBP1B stimulation by LpoB is

only a partial view of a more complex peptidoglycan synthesis regulating pathway (Gray et al., 2015). From their results, PBP1B was proposed to interact with two proteins from the Tol-Pal system, TolA (probably through their respective transmembrane regions) and CpoB (through a cleft located between UB2H and the transpeptidase domain as suggested by positive cross-linkings experiments whose residues are indicated on figure II.3.2). CpoB binding was shown to specifically prevent transpeptidation stimulation by LpoB. Whether CpoB also interacts with LpoB in this situation remains unclear. On the contrary, TolA seems to repress the inhibitory function of CpoB, in addition to enhance glycosyltransferase activity with LpoB. However, in an interesting manner, TolA effect on CpoB is dependent upon its energization by its TolQ and TolR partners. Figure II.3.3 presents a model for the tertiary CpoB-PBP1B-LpoB complex, as well as a summary of the PBP1B activities regulation pathway proposed. According to Gray et al., CpoB would therefore enable the coordination of peptidoglycan synthesis with outer-membrane constriction, via modulation of the LpoB-stimulated PBP1B activities in accordance with the energized state of the Tol-Pal system.

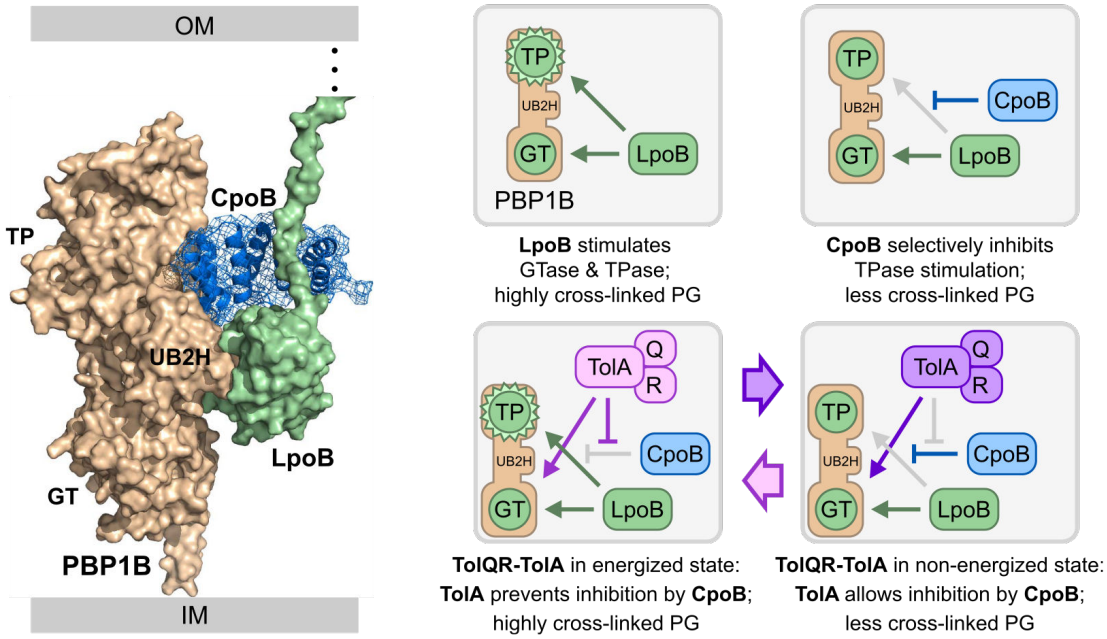

Figure II.3.3: Regulation of LpoB-stimulated PBP1B activities by the Tol-Pal system. Left: Structural model for the CpoB-PBP1B-LpoB tripartite complex based on PBP1B-LpoB docking (Egan et al., 2014) and cross-linking results between PBP1B and CpoB (Gray et al., 2015). LpoB N-terminal tail is partially represented for clarity. Right: *In vivo* PBP1B regulation scheme by LpoB, CpoB and TolA, in function of the latter energized state. Taken from Gray et al., 2015.

To conclude, LpoB reaches the UB2H domain of its cognate PBP1B through an N-terminal 52-residue long flexible tail, which presents the C-terminal globular domain in a position favorable for the interaction. A first atomic model of the interaction between the UB2H and LpoB domains, which evidences the interaction interface, has been obtained on the basis of NMR chemical shift perturbation and mutations impacting the *in vitro* and *in vivo* affinity between the two proteins. Subsequent NMR experiments suggest that this interaction does not cause significant conformational changes in the UB2H domain itself. As a consequence, the activation of the transpeptidase reaction in PBP1B seems to be due to a reorientation of the transpeptidase with respect to the transglycosylase domain rather than to a rearrangement in the UB2H domain itself. This process could imply a reorganization of the three stranded β-sheet at the interface between the two catalytic domains. The LpoB/PBP1B complex seem to be implicated not only in the enhancement of the activities of peptidoglycan synthesis at the septum, but also in a larger regulation mechanism, which implies CpoB and

the Tol-Pal system.

Résumé du chapitre 3 en français : Caractérisation structurale de LpoB et de son interaction avec PBP1B

De manière similaire à LpoA, LpoB est ancrée à la membrane externe via une cystéine après clivage de son peptide signal. Sa séquence est très différente de celle de LpoA et sa masse moléculaire est bien inférieure (22,5 kDa). A l'extrémité N-terminale de LpoB se trouve une région de faible complexité de séquence, c'est-à-dire un fragment constitué de peu d'acides aminés différents, étant prédite comme ayant une grande flexibilité. Cette région est suivie en C-terminal par un domaine non homologue à ceux de LpoA. Ces observations suggéraient que LpoB adoptait une architecture différente de celle de LpoA. Sa structure étant inconnue, une partie de cette thèse s'est donc tout d'abord concentrée sur sa détermination, par RMN, avant d'étudier son interaction avec le domaine UB2H de PBP1B.

Les premiers spectres $^{1}H,^{15}N$-HSQC de LpoB ont mis en évidence des signaux dispersés et d'autres plus intenses et concentrés dans une région entre 8 et 8,5 ppm. L'attribution des résonances du squelette et des chaînes latérales confirma que la partie N-terminale est déstructurée, avec l'aide d'expériences spectroscopiques adaptées à des séquences riches en prolines, alors que la région C-terminale forme un domaine replié. Ces premiers résultats furent publiés dans le journal *Biomolecular NMR Assignments* (voir article page 193).

A partir des contraintes déterminées sur la base des déplacements chimiques (contraintes angulaires) et des intensités des signaux NOE (contraintes de distance), une structure pour LpoB entière fut obtenue. Les résidus 21 à 73 forment une longue extrémité N-terminale non structurée, à la flexibilité importante comme attendu, cette dernière caractéristique ayant été démontrée par l'analyse d'expériences de dynamique enregistrées par RMN. Ce n'est pas la première fois qu'une région déstructurée est observée à l'extrémité N-terminale pour une lipoprotéine ancrée à la membrane externe et impliquée dans la biogenèse de la paroi bactérienne, une telle stratégie ayant déjà été décrite pour quelques transglycosylases lytiques ainsi que pour la protéine Pal. Le reste de LpoB forme un domaine globulaire composé d'un feuillet β central, encadré de 4 hélices α et d'un autre petit feuillet β. Cette structure en solution, présentée dans un article du périodique *Proceedings of the National Academy of Sciences of the United States of America* (voir article page 198), est en accord avec une structure obtenue par cristallographie aux rayons X par l'équipe de N. Strynadka publiée dans la revue *Journal of Biological Chemistry* à la même période. De manière surprenante, ce domaine a un repliement très similaire au module N-terminal de TolB, à l'exception d'une courte région nécessaire à l'interaction de ce dernier avec TolA. La structure de la protéine entière obtenue, ayant une région N-terminale déstructurée pouvant atteindre jusqu'à 145 Å et un domaine globulaire d'environ 30 Å de longueur, est capable de s'étendre sur une longue distance et d'atteindre le domaine UB2H de PBP1B ancrée à la membrane interne.

La RMN fut ensuite employée afin d'étudier l'interaction directe entre LpoB et UB2H (PBP1B entière étant une protéine membranaire peu stable et de masse moléculaire élevée, ce qui rend une étude par RMN compliquée). Des études préliminaires dans l'équipe de notre collaborateur W. Vollmer avaient en effet montré l'interaction entre LpoB et ce seul domaine de PBP1B par des expériences de pull-down. L'enregistrement de spectres $^{1}H,^{15}N$-BEST-TROSY-HSQC sur ^{13}C, ^{15}N-LpoB seule puis après ajout de deux équivalents molaires d'UB2H montra clairement la perturbation d'un nombre non négligeable (45) de résonances

provenant du domaine replié, dans un régime d'échange intermédiaire ou rapide. Le report des résidus les plus impactés, soit au niveau de leur déplacement chimique, soit au niveau de leur intensité, sur la structure de LpoB mis en évidence une région à cheval sur le feuillet β central et une hélice α adjacente. Ces résidus ont alors été utilisés comme contraintes ambiguës pour le calcul d'une structure modèle du complexe par le logiciel HADDOCK, qui utilise les contraintes ambigües pour l'arrimage des deux molécules. Sur la base du modèle ainsi obtenu, nos collaborateurs (les équipes de W. Vollmer et A. Typas) ont muté *in vitro* et *in vivo* les acides aminés de LpoB et/ou de PBP1B,prédits comme faisant partie de l'interface d'interaction. En accord avec nos résultats, ces mutants ont montré une diminution d'affinité de LpoB ou PBP1B pour leur partenaire d'interaction (mesures de K_D par SPR) et une stimulation de PBP1B amoindrie. La façon dont LpoB stimule PBP1B reste toutefois encore mal comprise, bien qu'un changement conformationnel de l'enzyme suite à l'interaction reste l'hypothèse privilégiée sur la base de ce modèle. Si tel est le cas, des modifications structurales au niveau du feuillet β situé à l'interface des trois domaines pourraient permettre une réorientation des deux domaines catalytiques et ainsi favoriser la coopérativité entre ceux-ci et/ou repositionner certains résidus impliqués dans les réactions de transpeptidation et/ou transglycosylation. Les mécanismes menant à la stimulation de ces deux activités sont toutefois probablement indépendants l'un de l'autre, puisque de récents travaux ont montré que CpoB, qui coordonne l'invagination de la membrane externe avec la synthèse de peptidoglycane lors de la division, était capable de sélectivement inhiber l'activation du domaine transpeptidase en interagissant sur une région entre le domaine transpeptidase et UB2H.

La structure haute-résolution de LpoB révèle donc une stratégie totalement différente de celle de LpoA pour atteindre et stimuler sa PBP1 partenaire. Au lieu d'une architecture bi-modulaire, LpoB ne dispose que d'un seul domaine, précédé toutefois d'une très longue extrémité flexible et déstructurée. L'interaction directe avec UB2H a également été confirmée et un modèle structural – le premier concernant une PBP et un de ses activateurs – a été proposé. Le mécanisme de stimulation de PBP1B par LpoB reste à déterminer, mais un changement conformationnel au niveau d'un feuillet β central est proposé comme étant à l'origine de la propagation du signal jusqu'au site actif des domaines de transglycosylation et de transpeptidation.

General conclusion

From the results obtained during this PhD work, a first structural description of the Lpo outer-membrane peptidoglycan synthesis regulators was performed. Both lipoproteins, while remaining anchored outside the sacculus, adopt a different strategy to go through the peptidoglycan pores and reach their cognate PBP1 partners located at the inner-membrane. While LpoA has a bi-modular rigid extended structure, LpoB is constituted of a long tail which brings its small globular core domain at proximity of PBP1B. In both cases, the requirement of an outer-sacculus stimulus for peptidoglycan synthesis might regulate PBP1A and PBP1B activities depending on the physical state of the peptidoglycan network. The more stretched the peptidoglycan would be, the wider the pores, which means that in such a situation Lpo proteins would go through more easily. Conversely, a relaxed or multi-layered sacculus would prevent Lpo binding to PBP1s. In the end, this mechanism could be one among several for the organism to homogenize peptidoglycan density all around its cell surface. My work enabled to propose a first structural model of a PBP1 in complex with its Lpo regulator, which is a first step toward the elucidation of the mechanism of the stimulation of PBPs by these factors. Understanding of this process is essential to comprehend the tight and complex tunings ruling cell wall biosynthesis and to later design new antibiotics that could disturb it. In addition to be key elements for PBP1 activities, it is likely that Lpos have also supplemental functions, as suggested by the requirement for the LpoB tail even when the protein is targeted to the inner-membrane in a closer proximity to the corresponding PBP. The TPR-like fold of $LpoA^N$ or the negative genetic interaction between $LpoA^N$ and CpoB also have to find rational explanations. These first hints promise hopefully new exciting discoveries in the coming years and a better understanding of the general mechanisms regulating peptidoglycan synthesis and maturation. Further work on ODD and UB2H might also lead to the discovery of new partners, making the interaction network between all of the cell wall growth protagonists even more complex. Last but not least, published work on Lpos, since the discovery of their stimulation function, have been mainly performed to date on *E. coli*, which is only one among so many other Gram-negative species. Interestingly, ODD and UB2H are not always coming with a Lpo, such as in *Nitrosomonas europaea*, an LpoA-deficient organism, whose PBP1A has an ODD domain (its structure is available under the PDB code 3D0F). Conversely, it could be interesting to see also if some bacteria have an Lpo, but did not retain their cognate binding domain. Such species may have a Lpo protein that is losing its PBP1 stimulation ability, but that may conserve or gain other functions, for example. Several class A PBPs were found to have one or two different non-catalytic domain in other bacteria, where LpoA and/or LpoB are not present, pointing to the existence of alternative regulation mechanisms (Typas et al., 2012). It would therefore be interesting to see if PBP activation is also performed from the outside of the sacculus in other Gram-negative bacteria and if these regulators are known proteins, which would harbor this additional function or, like in *E. coli*, if these new proteins are restricted to a few phyla.

Conclusion générale

Chez *E. coli*, les PBPs bifonctionnelles doivent être activées par les lipoprotéines ancrées à la membrane externe que sont LpoA et LpoB. Les travaux réalisés au cours de cette thèse ont permis de déterminer la structure à haute résolution des ces protéines et de proposer un premier modèle d'interaction entre une PBP et une protéine activatrice. Ces résultats ont conduit à mettre en évidence deux architectures différentes, mais qui dans les deux cas permettent à ces lipoprotéines d'atteindre leurs PBPs partenaires situées de l'autre coté de la couche de peptidoglycane. Cette localisation des Lpos a alors l'avantage de connecter la stimulation des PBPs à l'état physique du sacculus, les pores permettant le passage des Lpos se réduisant dans le cas d'une couche de peptidoglycane trop dense par exemple, ce qui empêche ces lipoprotéines d'activer leurs PBPs partenaires. Il est également possible que les Lpos aient des fonctions additionnelles, comme le suggère la découverte récente d'une interaction génétique négative entre LpoA et CpoB. Ceci impliquerait une complexité de la stimulation des PBPs bien plus importante que celle initialement anticipée. Le fait que le domaine UB2H de PBP1B interagit également avec d'autres partenaires (tel que CpoB) implique également la recherche d'autres interactants protéiques avec ce domaine ou avec ODD, interactants qui pourraient avoir également un rôle dans la stimulation des activités enzymatiques des PBPs. Enfin, à ce jour, l'activation des PBPs a surtout été étudiée chez *E. coli*, qui n'est probablement pas un cas général. En effet, d'autres domaines non catalytiques ont été reportés chez d'autres bactéries Gram-négatives, pour lesquelles les PBPs de classe A n'ont ni domaine ODD ni domaine UB2H. Un point intéressant serait alors d'établir si l'activation de ces PBPs se fait également depuis la membrane externe, et si une telle activation est effectuée par des protéines connues ayant une fonction additionnelle chez ces organismes ou par des protéines spécifiques dédiées à cette tâche.

Bibliography

Aarsman, M. E. G., Piette, A., Fraipont, C., Vinkenvleugel, T. M. F., Nguyen-Distèche, M., & den Blaauwen, T. (2005). Maturation of the Escherichia coli divisome occurs in two steps. *Molecular Microbiology*, *55*(6), 1631–45. http://doi.org/10.1111/j.1365-2958.2005.04502.x

Abergel, C., Bouveret, E., Claverie, J. M., Brown, K., Rigal, A., Lazdunski, C., & Bénédetti, H. (1999). Structure of the Escherichia coil TolB protein determined by MAD methods at 1.95 Å resolution. *Structure*, *7*(10), 1291–1300. http://doi.org/10.1016/S0969-2126(00)80062-3

Abergel, C., Walburger, A., Chenivesse, S., & Lazdunski, C. (2001). Crystallization and preliminary crystallographic study of the peptidoglycan-associated lipoprotein from Escherichia coli. *Acta Crystallographica Section D: Biological Crystallography*, *57*(2), 317–319. http://doi.org/10.1107/S0907444900019739

Adams, D. W., & Errington, J. (2009). Bacterial cell division: assembly, maintenance and disassembly of the Z ring. *Nature Reviews Microbiology*, *7*(9), 642–653. http://doi.org/10.1038/nrmicro2198

Addinall, S. G., & Lutkenhaus, J. (1996). FtsA is localized to the septum in an FtsZ-dependent manner. *Journal of Bacteriology*, *178*(24), 7167–7172. http://doi.org/10.1016/j.fct.2004.09.005

Al-Dabbagh, B., Henry, X., El Ghachi, M., Auger, G., Blanot, D., Parquet, C., … Bouhss, A. (2008). Active site mapping of MraY, a member of the polyprenyl-phosphate N-acetylhexosamine 1-phosphate transferase superfamily, catalyzing the first membrane step of peptidoglycan biosynthesis. *Biochemistry*, *47*(34), 8919–8928. http://doi.org/10.1021/bi8006274

Allan, E. J. (1991). Induction and cultivation of a stable L-form of Bacillus subtilis. *The Journal of Applied Bacteriology*, *70*(4), 339–343.

Allan, E. J., Hoischen, C., & Gumpert, J. (2009). *Bacterial L-forms. Advances in applied microbiology* (1st ed., Vol. 68). Elsevier Inc. http://doi.org/10.1016/S0065-2164(09)01201-5

Allan, R. K., & Ratajczak, T. (2011). Versatile TPR domains accommodate different modes of target protein recognition and function. *Cell Stress & Chaperones*, *16*(4), 353–67. http://doi.org/10.1007/s12192-010-0248-0

Alyahya, S. A., Alexander, R., Costa, T., Henriques, A. O., Emonet, T., & Jacobs-Wagner, C. (2009). RodZ, a component of the bacterial core morphogenic apparatus. *Proceedings of the National Academy of Sciences of the United States of America*, *106*(4), 1239–1244. http://doi.org/10.1073/pnas.0810794106

Amano, K., Hayashi, H., Araki, Y., & Ito, E. (1977). The action of lysozyme on peptidoglycan with N-unsubstituted glucosamine residues. Isolation of glycan fragments and their susceptibility to lysozyme. *European Journal of Biochemistry / FEBS*, *76*(1), 299–307.

Amoroso, A., Boudet, J., Berzigotti, S., Duval, V., Teller, N., Mengin-Lecreulx, D., … Joris, B. (2012). A peptidoglycan fragment triggers β-lactam resistance in Bacillus licheniformis. *PLoS Pathogens*, *8*(3), e1002571. http://doi.org/10.1371/journal.ppat.1002571

Anderson, D. E., Gueiros-Filho, F. J., & Erickson, H. P. (2004). Assembly dynamics of FtsZ rings in Bacillus subtilis and Escherichia coli and effects of FtsZ-regulating proteins. *Journal of Bacteriology*, *186*(17), 5775–5781. http://doi.org/10.1128/JB.186.17.5775-5781.2004

Angala, S. K., Belardinelli, J. M., Huc-Claustre, E., Wheat, W. H., & Jackson, M. (2014). The cell envelope

glycoconjugates of Mycobacterium tuberculosis. *Critical Reviews in Biochemistry and Molecular Biology*, *9238*, 1–39. http://doi.org/10.3109/10409238.2014.925420

Antane, S., Caufield, C. E., Hu, W., Keeney, D., Labthavikul, P., Morris, K., … Yang, Y. (2006). Pulvinones as bacterial cell wall biosynthesis inhibitors. *Bioorg. Med. Chem. Lett.*, *16*(1), 176–80. http://doi.org/10.1016/j.bmcl.2005.09.021

Arcus, V. (2002). OB-fold domains: A snapshot of the evolution of sequence, structure and function. *Current Opinion in Structural Biology*. http://doi.org/10.1016/S0959-440X(02)00392-5

Arends, S. J. R., Williams, K., Scott, R. J., Rolong, S., Popham, D. L., & Weiss, D. S. (2010). Discovery and characterization of three new Escherichia coli septal ring proteins that contain a SPOR domain: DamX, DedD, and RlpA. *Journal of Bacteriology*, *192*(1), 242–255. http://doi.org/10.1128/JB.01244-09

Artola-Recolons, C., Carrasco-López, C., Llarrull, L. I., Kumarasiri, M., Lastochkin, E., Martínez De Ilarduya, I., … Hermoso, J. a. (2011). High-resolution crystal structure of MltE, an outer membrane-anchored endolytic peptidoglycan lytic transglycosylase from Escherichia coli. *Biochemistry*, *50*(13), 2384–2386. http://doi.org/10.1021/bi200085y

Artola-Recolons, C., Lee, M., Bernardo-Garcia, N., Blazquez, B., Hesek, D., Bartual, S. G., … Hermoso, J. A. (2014). Structure and Cell Wall Cleavage by Modular Lytic Transglycosylase MltC of Escherichia coli. *ACS Chemical Biology*, *9*, 2058–2066.

Atrih, A., Bacher, G., Allmaier, G., Williamson, M. P., & Foster, S. J. (1999). Analysis of peptidoglycan structure from vegetative cells of Bacillus subtilis 168 and role of PBP 5 in peptidoglycan maturation. *Journal of Bacteriology*, *181*(13), 3956–3966.

Atrih, A., Zöllner, P., Allmaier, G., & Foster, S. J. (1996). Structural analysis of Bacillus subtilis 168 endospore peptidoglycan and its role during differentiation. *Journal of Bacteriology*, *178*(21), 6173–83. Retrieved from http://www.pubmedcentral.nih.gov/articlerender.fcgi?artid=178487&tool=pmcentrez&rendertype=abstract

Bacik, J. P., Whitworth, G. E., Stubbs, K. a., Vocadlo, D. J., & Mark, B. L. (2012). Active site plasticity within the glycoside hydrolase NagZ underlies a dynamic mechanism of substrate distortion. *Chemistry and Biology*, *19*(11), 1471–1482. http://doi.org/10.1016/j.chembiol.2012.09.016

Bacik, J. P., Whitworth, G. E., Stubbs, K. a., Yadav, A. K., Martin, D. R., Bailey-Elkin, B. a., … Mark, B. L. (2011). Molecular basis of 1,6-anhydro bond cleavage and phosphoryl transfer by Pseudomonas aeruginosa 1,6-anhydro-N-acetylmuramic acid kinase. *Journal of Biological Chemistry*, *286*(14), 12283–12291. http://doi.org/10.1074/jbc.M110.198317

Bacik, J.-P., Tavassoli, M., Patel, T. R., McKenna, S. a., Vocadlo, D. J., Khajehpour, M., & Mark, B. L. (2014). Conformational Itinerary of Pseudomonas aeruginosa 1,6-Anhydro- N -acetylmuramic Acid Kinase during Its Catalytic Cycle. *Journal of Biological Chemistry*, *289*(7), 4504–4514. http://doi.org/10.1074/jbc.M113.521633

Banzhaf, M., van den Berg van Saparoea, B., Terrak, M., Fraipont, C., Egan, A., Philippe, J., … Vollmer, W. (2012). Cooperativity of peptidoglycan synthases active in bacterial cell elongation. *Molecular Microbiology*, *85*(1), 179–194. http://doi.org/10.1111/j.1365-2958.2012.08103.x

Barreteau, H., Kovač, A., Boniface, A., Sova, M., Gobec, S., & Blanot, D. (2008). Cytoplasmic steps of peptidoglycan biosynthesis. *FEMS Microbiology Reviews*, *32*(2), 168–207. http://doi.org/10.1111/j.1574-6976.2008.00104.x

Bateman, A., & Bycroft, M. (2000). The structure of a LysM domain from E. coli membrane-bound lytic murein transglycosylase D (MltD). *Journal of Molecular Biology*, *299*(4), 1113–1119. http://doi.org/10.1006/jmbi.2000.3778

Bellamacina, C. R. (1996). The nicotinamide dinucleotide binding motif: a comparison of nucleotide binding

proteins. *The FASEB Journal*, *10*(11), 1257–1269.

Bendezú, F. O., Hale, C. A., Bernhardt, T. G., & de Boer, P. A. J. (2009). RodZ (YfgA) is required for proper assembly of the MreB actin cytoskeleton and cell shape in E. coli. *The EMBO Journal*, *28*(3), 193–204. http://doi.org/10.1038/emboj.2008.264

Benson, T. E., Marquardt, J. L., Marquardt, A. C., Etzkorn, F. A., & Walsh, C. T. (1993). Overexpression, purification, and mechanistic study of UDP-N-acetylenolpyruvylglucosamine reductase. *Biochemistry*, *32*(8), 2024–2030. http://doi.org/10.1021/bi00059a019

Benson, T. E., Walsh, C. T., & Hogle, J. M. (1996). The structure of the substrate-free form of MurB, an essential enzyme for the synthesis of bacterial cell walls. *Structure (London, England : 1993)*. http://doi.org/10.1016/S0969-2126(96)00008-1

Bera, A., Biswas, R., Herbert, S., & Götz, F. (2006). The presence of peptidoglycan O-acetyltransferase in various staphylococcal species correlates with lysozyme resistance and pathogenicity. *Infection and Immunity*, *74*(8), 4598–4604. http://doi.org/10.1128/IAI.00301-06

Bera, A., Herbert, S., Jakob, A., Vollmer, W., & Götz, F. (2005). Why are pathogenic staphylococci so lysozyme resistant? The peptidoglycan O-acetyltransferase OatA is the major determinant for lysozyme resistance of Staphylococcus aureus. *Molecular Microbiology*, *55*(3), 778–787. http://doi.org/10.1111/j.1365-2958.2004.04446.x

Berezuk, a. M., Goodyear, M., & Khursigara, C. M. (2014). Site-directed fluorescence labeling reveals a revised N-terminal membrane topology and functional periplasmic residues in the Escherichia coli cell division protein FtsK. *Journal of Biological Chemistry*, *289*(34), 0–28. http://doi.org/10.1074/jbc.M114.569624

Bernard, E., Rolain, T., Courtin, P., Guillot, A., Langella, P., Hols, P., & Chapot-Chartier, M. P. (2011). Characterization of O-acetylation of N-acetylglucosamine: A novel structural variation of bacterial peptidoglycan. *Journal of Biological Chemistry*, *286*(27), 23950–23958. http://doi.org/10.1074/jbc.M111.241414

Bernard, E., Rolain, T., David, B., André, G., Dupres, V., Dufrêne, Y. F., … Hols, P. (2012). Dual Role for the O-Acetyltransferase OatA in Peptidoglycan Modification and Control of Cell Septation in Lactobacillus plantarum. *PLoS ONE*, *7*(10). http://doi.org/10.1371/journal.pone.0047893

Bernhardt, T. G., & de Boer, P. A. J. (2003). The Escherichia coli amidase AmiC is a periplasmic septal ring component exported via the twin-arginine transport pathway. *Molecular Microbiology*, *48*(5), 1171–1182. http://doi.org/10.1046/j.1365-2958.2003.03511.x

Bertrand, J. A., Auger, G., Martin, L., Fanchon, E., Blanot, D., Le Beller, D., … Dideberg, O. (1999). Determination of the MurD mechanism through crystallographic analysis of enzyme complexes. *Journal of Molecular Biology*, *289*(3), 579–590. http://doi.org/10.1006/jmbi.1999.2800

Bertsche, U., Breukink, E., Kast, T., & Vollmer, W. (2005). In vitro murein (peptidoglycan) synthesis by dimers of the bifunctional transglycosylase-transpeptidase PBP1B from Escherichia coli. *Journal of Biological Chemistry*, *280*(45), 38096–38101. http://doi.org/10.1074/jbc.M508646200

Bertsche, U., Kast, T., Wolf, B., Fraipont, C., Aarsman, M. E. G., Kannenberg, K., … Vollmer, W. (2006). Interaction between two murein (peptidoglycan) synthases, PBP3 and PBP1B, in Escherichia coli. *Molecular Microbiology*, *61*(3), 675–690. http://doi.org/10.1111/j.1365-2958.2006.05280.x

Biarrotte-Sorin, S., Hugonnet, J. E., Delfosse, V., Mainardi, J. L., Gutmann, L., Arthur, M., & Mayer, C. (2006). Crystal Structure of a Novel β-Lactam-insensitive Peptidoglycan Transpeptidase. *Journal of Molecular Biology*, *359*(3), 533–538. http://doi.org/10.1016/j.jmb.2006.03.014

Bieri, M., Kwan, A. H., Mobli, M., King, G. F., MacKay, J. P., & Gooley, P. R. (2011). Macromolecular NMR spectroscopy for the non-spectroscopist: Beyond macromolecular solution structure determination. *FEBS Journal*, *278*(5), 704–715. http://doi.org/10.1111/j.1742-4658.2011.08005.x

Binshtein, E., & Ohi, M. D. (2015). Cryo-Electron Microscopy and the Amazing Race to Atomic Resolution. *Biochemistry*, *54*, 3133–3141. http://doi.org/10.1021/acs.biochem.5b00114

Blackburn, N. T., & Clarke, A. J. (2001). Identification of four families of peptidoglycan lytic transglycosylases. *Journal of Molecular Evolution*, *52*(1), 78–84. http://doi.org/10.1007/s002390010136

Blair, D. E., Schüttelkopf, A. W., MacRae, J. I., & van Aalten, D. M. F. (2005). Structure and metal-dependent mechanism of peptidoglycan deacetylase, a streptococcal virulence factor. *Proceedings of the National Academy of Sciences of the United States of America*, *102*(43), 15429–15434. http://doi.org/10.1073/pnas.0504339102

Blair, D. E., & Van Aalten, D. M. F. (2004). Structures of Bacillus subtilis PdaA, a family 4 carbohydrate esterase, and a complex with N-acetyl-glucosamine. *FEBS Letters*, *570*(1-3), 13–19. http://doi.org/10.1016/j.febslet.2004.06.013

Boeri Erba, E., & Petosa, C. (2015). The emerging role of native mass spectrometry in characterizing the structure and dynamics of macromolecular complexes. *Protein Science*, *24*, 1176–1192. http://doi.org/10.1002/pro.2661

Boneca, I. G., Huang, Z. H., Gage, D. a., & Tomasz, A. (2000). Characterization of Staphylococcus aureus cell wall glycan strands, evidence for a new β-N-acetylglucosaminidase activity. *Journal of Biological Chemistry*, *275*(14), 9910–9918. http://doi.org/10.1074/jbc.275.14.9910

Bonsor, D. a, Hecht, O., Vankemmelbeke, M., Sharma, A., Krachler, A. M., Housden, N. G., … Kleanthous, C. (2009). Allosteric beta-propeller signalling in TolB and its manipulation by translocating colicins. *The EMBO Journal*, *28*(18), 2846–2857. http://doi.org/10.1038/emboj.2009.224

Born, P., Breukink, E., & Vollmer, W. (2006). In vitro synthesis of cross-linked murein and its attachment to sacculi by PBP1A from Escherichia coli. *Journal of Biological Chemistry*, *281*(37), 26985–26993. http://doi.org/10.1074/jbc.M604083200

Bougault, C., Hediger, S., & Simorre, J. (2012). Solid-state NMR of the Bacterial Cell Wall. In H. S. Press (Ed.), *Bacterial Glycomics: Current research, technology and applications*.

Bouhss, A., Mengin-Lecreulx, D., Le Beller, D., & Van Heijenoort, J. (1999). Topological analysis of the MraY protein catalysing the first membrane step of peptidoglycan synthesis. *Molecular Microbiology*, *34*(3), 576–585. http://doi.org/10.1046/j.1365-2958.1999.01623.x

Bouhss, A., Trunkfield, A. E., Bugg, T. D. H., & Mengin-Lecreulx, D. (2008). The biosynthesis of peptidoglycan lipid-linked intermediates. *FEMS Microbiology Reviews*, *32*(2), 208–233. http://doi.org/10.1111/j.1574-6976.2007.00089.x

Bradshaw, W. J., Davies, A. H., Chambers, C. J., Roberts, A. K., Shone, C. C., & Acharya, K. R. (2015). Molecular features of the sortase enzyme family. *FEBS Journal*, *282*(11), 2097–2114. http://doi.org/10.1111/febs.13288

Braun, V., & Rehn, K. (1969). Chemical characterization, spatial distribution and function of a lipoprotein (murein-lipoprotein) of the E. coli cell wall. The specific effect of trypsin on the membrane structure. *European Journal of Biochemistry / FEBS*, *10*(3), 426–438. http://doi.org/10.1111/j.1432-1033.1969.tb00707.x

Breukels, V., Konijnenberg, A., Nabuurs, S. M., Doreleijers, J. F., Kovalevskaya, N. V, & Vuister, G. W. (2011). Overview on the use of NMR to examine protein structure. In *Current Protocols in Protein Science* (Vol. Chapter 17, pp. 17.5.1–17.5.44). http://doi.org/10.1002/0471140864.ps1705s64

Brown, S., Santa Maria, J. P., & Walker, S. (2013). Wall teichoic acids of gram-positive bacteria. *Annual Review of Microbiology*, *67*, 313–36. http://doi.org/10.1146/annurev-micro-092412-155620

Bruning, J. B., Murillo, A. C., Chacon, O., Barletta, R. G., & Sacchettini, J. C. (2011). Structure of the Mycobacterium tuberculosis D-alanine:D-alanine ligase, a target of the antituberculosis drug D-

cycloserine. *Antimicrobial Agents and Chemotherapy*, *55*(1), 291–301. http://doi.org/10.1128/AAC.00558-10

Buchanan, C. E., & Sowell, M. O. (1982). Synthesis of penicillin-binding protein 6 by stationary-phase Escherichia coli. *Journal of Bacteriology*, *151*(1), 491–494.

Buddelmeijer, N., Judson, N., Boyd, D., Mekalanos, J. J., & Beckwith, J. (2002). YgbQ, a cell division protein in Escherichia coli and Vibrio cholerae, localizes in codependent fashion with FtsL to the division site. *Proceedings of the National Academy of Sciences of the United States of America*, *99*(9), 6316–6321. http://doi.org/10.1073/pnas.092128499

Bugg, T. D., & Walsh, C. T. (1992). Intracellular steps of bacterial cell wall peptidoglycan biosynthesis: enzymology, antibiotics, and antibiotic resistance. *Natural Product Reports*, *9*(3), 199–215. http://doi.org/10.1039/np9920900199

Bugg, T. D., Wright, G. D., Dutka-Malen, S., Arthur, M., Courvalin, P., & Walsh, C. T. (1991). Molecular basis for vancomycin resistance in Enterococcus faecium BM4147: biosynthesis of a depsipeptide peptidoglycan precursor by vancomycin resistance proteins VanH and VanA. *Biochemistry*, *30*(43), 10408–10415. http://doi.org/doi:10.1021/bi00107a007

Bui, N. K., Eberhardt, A., Vollmer, D., Kern, T., Bougault, C., Tomasz, A., … Vollmer, W. (2012). Isolation and analysis of cell wall components from Streptococcus pneumoniae. *Analytical Biochemistry*, *421*(2), 657–666. http://doi.org/10.1016/j.ab.2011.11.026

Burman, L. G., Raichler, J., & Park, J. T. (1983). Evidence for diffuse growth of the cylindrical portion of the Escherichia coli murein sacculus. *Journal of Bacteriology*, *155*(3), 983–988.

Burmant, L. G., & Park, J. T. (1983). Changes in the Composition of Escherichia coli Murein as It Ages During Exponential Growth. *Journal of Bacteriology*, *155*(2), 447–453.

Busiek, K. K., Eraso, J. M., Wang, Y., & Margolin, W. (2012). The Early Divisome Protein FtsA Interacts Directly through Its 1c Subdomain with the Cytoplasmic Domain of the Late Divisome Protein FtsN. *Journal of Bacteriology*, *194*(8), 1989–2000. http://doi.org/10.1128/JB.06683-11

Buss, J., Coltharp, C., Huang, T., Pohlmeyer, C., Wang, S. C., Hatem, C., & Xiao, J. (2013). In vivo organization of the FtsZ-ring by ZapA and ZapB revealed by quantitative super-resolution microscopy. *Molecular Microbiology*, *89*(6), 1099–1120. http://doi.org/10.1111/mmi.12331

Butler, E. K., Davis, R. M., Bari, V., Nicholson, P. a., & Ruiz, N. (2013). Structure-function analysis of MurJ reveals a solvent-exposed cavity containing residues essential for peptidoglycan biogenesis in Escherichia coli. *Journal of Bacteriology*, *195*(20), 4639–4649. http://doi.org/10.1128/JB.00731-13

Butler, E. K., Tan, W. B., Joseph, H., & Ruiz, N. (2014). Charge Requirements of Lipid II Flippase Activity in Escherichia coli. *Journal of Bacteriology*, *196*(23), 4111–4119. http://doi.org/10.1128/JB.02172-14

Büttner, F. M., Renner-Schneck, M., & Stehle, T. (2015). X-ray crystallography and its impact on understanding bacterial cell wall remodeling process. *J. Med. Microbiol. International Journal of Medical Microbiology*. http://doi.org/10.1016/j.ijmm.2014.12.018

Candela, T., & Fouet, A. (2006). Poly-gamma-glutamate in bacteria. *Molecular Microbiology*, *60*(5), 1091–1098. http://doi.org/10.1111/j.1365-2958.2006.05179.x

Carballido-Löpez, R., & Errington, J. (2003). The bacterial cytoskeleton: In vivo dynamics of the actin-like protein Mbl of Bacillus subtilis. *Developmental Cell*, *4*(1), 19–28. http://doi.org/10.1016/S1534-5807(02)00403-3

Carrasco-López, C., Rojas-Altuve, A., Zhang, W., Hesek, D., Lee, M., Barbe, S., … Hermoso, J. A. (2011). Crystal structures of bacterial peptidoglycan amidase AmpD and an unprecedented activation mechanism. *Journal of Biological Chemistry*, *286*(36), 31714–31722. http://doi.org/10.1074/jbc.M111.264366

Cascales, E., Gavioli, M., Sturgis, J. N., & Lloubes, R. (2000). Proton motive force drives the interaction of the inner membrane TolA and outer membrane Pal proteins in Escherichia coli. *Molecular Microbiology*, *38*(4), 904–915. http://doi.org/10.1046/j.1365-2958.2000.02190.x

Cascales, E., & Lloubès, R. (2004). Deletion analyses of the peptidoglycan-associated lipoprotein Pal reveals three independent binding sequences including a TolA box. *Molecular Microbiology*, *51*(3), 873–885. http://doi.org/10.1046/j.1365-2958.2003.03881.x

Cava, F., de Pedro, M. A., Lam, H., Davis, B. M., & Waldor, M. K. (2011). Distinct pathways for modification of the bacterial cell wall by non-canonical D-amino acids. *The EMBO Journal*, *30*(16), 3442–3453. http://doi.org/10.1038/emboj.2011.246

Cavanagh, J., Fairbrother, W. J., Palmer, A. G., & Skelton, N. J. (2007). *Protein NMR Spectroscopy, Principles and Practice, 2nd Edition*. *Elsevier Academic Press*. Retrieved from http://yadda.icm.edu.pl/yadda/element/bwmeta1.element.elsevier-5d0736f1-03f2-34a3-acf3-9e1e94839edf/c/main.pdf

Cha, S.-S., An, Y. J., Jeong, C.-S., Yu, J. H., & Chung, K. M. (2014). ATP-binding mode including a carbamoylated lysine and two Mg2+ ions, and substrate-binding mode in Acinetobacter baumannii MurF. *Biochemical and Biophysical Research Communications*, *450*(2), 1045–1050. http://doi.org/10.1016/j.bbrc.2014.06.108

Chahboune, A., Decaffmeyer, M., Brasseur, R., & Joris, B. (2005). Membrane topology of the Escherichia coli AmpG permease required for recycling of cell wall anhydromuropeptides and AmpC ??-lactamase induction. *Antimicrobial Agents and Chemotherapy*, *49*(3), 1145–1149. http://doi.org/10.1128/AAC.49.3.1145-1149.2005

Charpentier, X., Chalut, C., Rémy, M. H., & Masson, J. M. (2002). Penicillin-binding proteins 1a and 1b form independent dimers in Escherichia coli. *Journal of Bacteriology*, *184*(13), 3749–3752. http://doi.org/10.1128/JB.184.13.3749-3752.2002

Chastanet, A., & Carballido-López, R. (2012). The actin-like MreB proteins in Bacillus subtilis: a new turn. *Frontiers in Bioscience*, *S4*(4), 1582. http://doi.org/10.2741/S354

Chen, J. C., & Beckwith, J. (2001). FtsQ, FtsL and Ftsl require FtsK, but not FtsN, for co-localization with FtsZ during Escherichia coli cell division. *Molecular Microbiology*, *42*(2), 395–413. http://doi.org/10.1046/j.1365-2958.2001.02640.x

Chen, J. C., Minev, M., & Beckwith, J. (2002). Analysis of ftsQ mutant alleles in Escherichia coli: Complementation, septal localization, and recruitment of downstream cell division proteins. *Journal of Bacteriology*, *184*(3), 695–705. http://doi.org/10.1128/JB.184.3.695-705.2002

Chen, L., Men, H., Ha, S., Ye, X. Y., Brunner, L., Hu, Y., & Walker, S. (2002). Intrinsic lipid preferences and kinetic mechanism of Escherichia coli MurG. *Biochemistry*, *41*(21), 6824–6833. http://doi.org/10.1021/bi0256678

Chen, Y., & Erickson, H. P. (2005). Rapid in vitro assembly dynamics and subunit turnover of FtsZ demonstrated by fluorescence resonance energy transfer. *Journal of Biological Chemistry*, *280*(23), 22549–22554. http://doi.org/10.1074/jbc.M500895200

Chen, Y., & Erickson, H. P. (2009). FtsZ filament dynamics at steady state: Subunit exchange with and without nucleotide hydrolysis. *Biochemistry*, *48*(28), 6664–6673. http://doi.org/10.1021/bi8022653

Chen, Y., Zhang, W., Shi, Q., Hesek, D., Lee, M., Mobashery, S., & Shoichet, B. K. (2009). Crystal structures of penicillin-binding protein 6 from Escherichia coli. *Journal of the American Chemical Society*, *131*(40), 14345–14354. http://doi.org/10.1021/ja903773f

Cheng, Q., Li, H., Merdek, K., & Park, J. T. (2000). Molecular characterization of the beta-N-acetylglucosaminidase of Escherichia coli and its role in cell wall recycling. *Journal of Bacteriology*,

182(17), 4836–4840. http://doi.org/10.1128/JB.182.17.4836-4840.2000.Updated

Cheng, Q., & Park, J. T. (2002). Substrate specificity of the AmpG permease required for recycling of cell wall anhydro-muropeptides. *Journal of Bacteriology*, *184*(23), 6434–6436. http://doi.org/10.1128/JB.184.23.6434-6436.2002

Cheng, Y. (2015). Single-Particle Cryo-EM at Crystallographic Resolution. *Cell*, *161*(3), 450–457. http://doi.org/10.1016/j.cell.2015.03.049

Cheng, Y., Grigorieff, N., Penczek, P. A., & Walz, T. (2015). A Primer to Single-Particle Cryo-Electron Microscopy. *Cell*, *161*(3), 438–449. http://doi.org/10.1016/j.cell.2015.03.050

Cho, H., Uehara, T., & Bernhardt, T. G. (2014). Beta-Lactam Antibiotics Induce a Lethal Malfunctioning of the Bacterial Cell Wall Synthesis Machinery. *Cell*, *159*(6), 1300–1311. http://doi.org/10.1016/j.cell.2014.11.017

Chou, J. J., & Sounier, R. (2013). Solution Nuclear Magnetic Resonance Spectroscopy. In *Methods in Molecular Biology* (pp. 495–517).

Choudhury, B., Leoff, C., Saile, E., Wilkins, P., Quinn, C. P., Kannenberg, E. L., & Carlson, R. W. (2006). The structure of the major cell wall polysaccharide of Bacillus anthracis is species-specific. *Journal of Biological Chemistry*, *281*(38), 27932–27941. http://doi.org/10.1074/jbc.M605768200

Chowdhury, C., & Ghosh, A. S. (2011). Differences in active-site microarchitecture explain the dissimilar behaviors of PBP5 and 6 in Escherichia coli. *Journal of Molecular Graphics and Modelling*, *29*(5), 650–656. http://doi.org/10.1016/j.jmgm.2010.11.009

Chowdhury, C., Kar, D., Dutta, M., Kumar, A., & Ghosh, A. S. (2012). Moderate deacylation efficiency of DacD explains its ability to partially restore beta-lactam resistance in *Escherichia coli* PBP5 mutant. *FEMS Microbiology Letters*, *337*(1), 73–80. http://doi.org/10.1111/1574-6968.12009

Chowdhury, C., Nayak, T. R., Young, K. D., & Ghosh, A. S. (2010). A weak dd-carboxypeptidase activity explains the inability of PBP 6 to substitute for PBP 5 in maintaining normal cell shape in Escherichia coli. *FEMS Microbiology Letters*, *303*(1), 76–83. http://doi.org/10.1111/j.1574-6968.2009.01863.x

Christie, M. P., Toth, I., & Simerska, P. (2014). Biophysical characterization of lectin-glycan interactions for therapeutics, vaccines and targeted drug-delivery. *Future Medicinal Chemistry*, *6*(18), 2113–2129.

Chung, B. C., Zhao, J., Gillespie, R. a, Kwon, D.-Y., Guan, Z., Hong, J., … Lee, S.-Y. (2013). Crystal structure of MraY, an essential membrane enzyme for bacterial cell wall synthesis. *Science*, *341*(6149), 1012–6. http://doi.org/10.1126/science.1236501

Clarke, T. B., Kawai, F., Park, S.-Y., Tame, J. R. H., Dowson, C. G., & Roper, D. I. (2009). Mutational analysis of the substrate specificity of Escherichia coli penicillin binding protein 4. *Biochemistry*, *48*(12), 2675–83. http://doi.org/10.1021/bi801993x

Cole, J. L., Lary, J. W., P. Moody, T., & Laue, T. M. (2008). Analytical Ultracentrifugation: Sedimentation Velocity and Sedimentation Equilibrium. *Methods in Cell Biology*, *84*(07), 143–179. http://doi.org/10.1016/S0091-679X(07)84006-4

Coltharp, C., & Xiao, J. (2012). Superresolution microscopy for microbiology. *Cellular Microbiology*, *14*(12), 1808–1818. http://doi.org/10.1111/cmi.12024

Corbin, B. D., Wang, Y., Beuria, T. K., & Margolin, W. (2007). Interaction between cell division proteins FtsE and FtsZ. *Journal of Bacteriology*, *189*(8), 3026–3035. http://doi.org/10.1128/JB.01581-06

Correale, S., Ruggiero, A., Capparelli, R., Pedone, E., & Berisio, R. (2013). Structures of free and inhibited forms of the l,d-transpeptidase LdtMt1 from Mycobacterium tuberculosis. *Acta Crystallographica Section D: Biological Crystallography*, *69*(9), 1697–1706. http://doi.org/10.1107/S0907444913013085

Costa, T. R. D., Felisberto-Rodrigues, C., Meir, A., Prevost, M. S., Redzej, A., Trokter, M., & Waksman, G.

(2015). Secretion systems in Gram-negative bacteria: structural and mechanistic insights. *Nature Reviews Microbiology*, *13*(6), 343–359. http://doi.org/10.1038/nrmicro3456

Daffé, M. (2015). The cell envelope of tubercle bacilli. *Tuberculosis*, *95*, 155–158. http://doi.org/10.1016/j.tube.2015.02.024

Dai, K., & Lutkenhaus, J. (1991). ftsZ is an essential cell division gene in Escherichia coli. *Journal of Bacteriology*, *173*(11), 3500–3506.

Dai, K., & Lutkenhaus, J. (1992). The proper ratio of FtsZ to FtsA is required for cell division to occur in Escherichia coli. *Journal of Bacteriology*, *174*(19), 6145–6151.

Daniel, R. a., & Errington, J. (2003). Control of cell morphogenesis in bacteria: Two distinct ways to make a rod-shaped cell. *Cell*, *113*(6), 767–776. http://doi.org/10.1016/S0092-8674(03)00421-5

Das, D., Hervé, M., Feuerhelm, J., Farr, C. L., Chiu, H. J., Elsliger, M. A., … Wilson, I. a. (2011). Structure and function of the first full-length murein peptide ligase (Mpl) cell wall recycling protein. *PLoS ONE*, *6*(3), 20–25. http://doi.org/10.1371/journal.pone.0017624

Davies, C., White, S. W., & Nicholas, R. a. (2001). Crystal structure of a deacylation-defective mutant of penicillin-binding protein 5 at 2.3-Å resolution. *Journal of Biological Chemistry*, *276*(1), 616–623. http://doi.org/10.1074/jbc.M004471200

de Pedro, M. A., & Cava, F. (2015). Structural constraints and dynamics of bacterial cell wall architecture. *Frontiers in Microbiology*, *6*(May), 1–10. http://doi.org/10.3389/fmicb.2015.00449

de Pedro, M. A., Quintela, J. C., Höltje, J. V., & Schwarz, H. (1997). Murein segregation in Escherichia coli. *Journal of Bacteriology*, *179*(9), 2823–2834.

de Pedro, M. A., & Schwarz, U. (1981). Heterogeneity of newly inserted and preexisting murein in the sacculus of Escherichia coli. *Proceedings of the National Academy of Sciences of the United States of America*, *78*(9), 5856–5860. http://doi.org/10.1073/pnas.78.9.5856

de Pedro, M. A., Schwarz, U., Nishimura, Y., & Hirota, Y. (1980). On the biological role of penicillin-binding proteins 4 and 5. *FEMS Microbiology Letters*, *9*(3), 219–221. http://doi.org/10.1111/j.1574-6968.1980.tb05640.x

de Souza, R. F., Anantharaman, V., de Souza, S. J., Aravind, L., & Gueiros-Filho, F. J. (2008). AMIN domains have a predicted role in localization of diverse periplasmic protein complexes. *Bioinformatics*, *24*(21), 2423–2426. http://doi.org/10.1093/bioinformatics/btn449

Demchick, P., & Koch, A. L. (1996). The permeability of the wall fabric of Escherichia coli and Bacillus subtilis. *Journal of Bacteriology*, *178*(3), 768–773.

den Blaauwen, T., Aarsman, M. E. G., Vischer, N. O. E., & Nanninga, N. (2003). Penicillin-binding protein PBP2 of Escherichia coli localizes preferentially in the lateral wall and at mid-cell in comparison with the old cell pole. *Molecular Microbiology*, *47*(2), 539–547. http://doi.org/10.1046/j.1365-2958.2003.03316.x

den Blaauwen, T., de Pedro, M. A., Nguyen-Distèche, M., & Ayala, J. A. (2008). Morphogenesis of rod-shaped sacculi. *FEMS Microbiology Reviews*, *32*(2), 321–344. http://doi.org/10.1111/j.1574-6976.2007.00090.x

Denome, S. A., Elf, P. K., Henderson, T. A., Nelson, D. E., & Young, K. D. (1999). Escherichia coli mutants lacking all possible combinations of eight penicillin binding proteins: …. *Journal Of Bacteriology*, *181*(13), 3981–3993. Retrieved from http://jb.asm.org/cgi/content/abstract/181/13/3981\npapers2://publication/uuid/73A10687-6DE2-44D3-86DB-A909BC434E4E

Depardieu, F., Podglajen, I., Leclercq, R., Collatz, E., & Courvalin, P. (2007). Modes and modulations of antibiotic resistance gene expression. *Clinical Microbiology Reviews*, *20*(1), 79–114. http://doi.org/10.1128/CMR.00015-06

Deprez, C., Lloubès, R., Gavioli, M., Marion, D., Guerlesquin, F., & Blanchard, L. (2005). Solution structure of the E. coli TolA C-terminal domain reveals conformational changes upon binding to the phage g3p N-terminal domain. *Journal of Molecular Biology*, *346*(4), 1047–1057. http://doi.org/10.1016/j.jmb.2004.12.028

Depuydt, M., Leonard, S. E., Vertommen, D., Denoncin, K., Morsomme, P., Wahni, K., … Collet, J.-F. (2009). A Periplasmic Reducing System Protects Single Cysteine Residues from Oxidation. *Science*, *326*, 1109–1111. http://doi.org/10.1038/nmat2382

Desmarais, S. M., de Pedro, M. A., Cava, F., & Huang, K. C. (2013). Peptidoglycan at its peaks: How chromatographic analyses can reveal bacterial cell wall structure and assembly. *Molecular Microbiology*, *89*(1), 1–13. http://doi.org/10.1111/mmi.12266

Dessen, A., Mouz, N., Gordon, E., Hopkins, J., & Dideberg, O. (2001). Crystal structure of PBP2x from a highly penicillin-resistant Streptococcus pneumoniae clinical isolate: A mosaic framework containing 83 mutations. *Journal of Biological Chemistry*, *276*(48), 45106–45112. http://doi.org/10.1074/jbc.M107608200

Dhalla, A. M., Yanchunas, J., Ho, H. T., Falk, P. J., Villafranca, J. J., & Robertson, J. G. (1995). Steady-state kinetic mechanism of Escherichia coli UDP-N-acetylenolpyruvylglucosamine reductase. *Biochemistry*, *34*(16), 5390–5402. http://doi.org/10.1021/bi00016a010

Dietz, H., Pfeifle, D., & Wiedemann, B. (1997). The signal molecule for β-lactamase induction in Enterobacter cloacae is the anhydromuramyl-pentapeptide. *Antimicrobial Agents and Chemotherapy*, *41*(10), 2113–2120.

Divakaruni, A. V., Baida, C., White, C. L., & Gober, J. W. (2007). The cell shape proteins MreB and MreC control cell morphogenesis by positioning cell wall synthetic complexes. *Molecular Microbiology*, *66*(1), 174–188. http://doi.org/10.1111/j.1365-2958.2007.05910.x

Divakaruni, A. V., Loo, R. R. O., Xie, Y., Loo, J. a, & Gober, J. W. (2005). The cell-shape protein MreC interacts with extracytoplasmic proteins including cell wall assembly complexes in Caulobacter crescentus. *Proceedings of the National Academy of Sciences of the United States of America*, *102*(51), 18602–18607. http://doi.org/10.1073/pnas.0507937102

Dmitriev, B. A., Toukach, F. V, Holst, O., Rietschel, E. T., & Ehlers, S. (2004). Tertiary Structure of Staphylococcus aureus Cell Wall Murein. *Journal of Bacteriology*, *186*(21), 7141–7148. http://doi.org/10.1128/JB.186.21.7141

Domínguez-Escobar, J., Chastanet, A., Crevenna, A. H., Fromion, V., Wedlich-Söldner, R., & Carballido-López, R. (2011). Processive movement of MreB-associated cell wall biosynthetic complexes in bacteria. *Science*, *333*(6039), 225–228. http://doi.org/10.1126/science.1203466

Dorazi, R., & Dewar, S. J. (2000). Membrane topology of the N-terminus of the Escherichia coli FtsK division protein. *FEBS Letters*, *478*(1-2), 13–18. http://doi.org/10.1016/S0014-5793(00)01820-2

Dörr, T., Lam, H., Alvarez, L., Cava, F., Davis, B. M., & Waldor, M. K. (2014). A Novel Peptidoglycan Binding Protein Crucial for PBP1A-Mediated Cell Wall Biogenesis in Vibrio cholerae. *PLoS Genetics*, *10*(6). http://doi.org/10.1371/journal.pgen.1004433

Doublet, P., Heijenoort, J. Van, Bohin, J.-P., & Mengin-Lecreulx, D. (1993). The murI Gene of Escherichia coli Is an Essential Gene That Encodes a Glutamate Racemase Activity. *Journal of Bacteriology*, *175*(10), 2970–2979.

Dover, R. S., Bitler, A., Shimoni, E., Trieu-Cuot, P., & Shai, Y. (2015). Multiparametric AFM reveals turgor-responsive net-like peptidoglycan architecture in live streptococci. *Nature Communications*, *6*(May), 7193. http://doi.org/10.1038/ncomms8193

Dufrêne, Y. F. (2014). Atomic Force Microscopy in Microbiology : New Structural and Functional Insights into

the Microbial Cell Surface. *mBio*, *5*(4), 1–14. http://doi.org/10.1128/mBio.01363-14.Updated

Duman, R., Ishikawa, S., Celik, I., Strahl, H., Ogasawara, N., Troc, P., … Hamoen, L. W. (2013). Structural and genetic analyses reveal the protein SepF as a new membrane anchor for the Z ring. *Proceedings of the National Academy of Sciences*, *110*(48), E4601–E4610. http://doi.org/10.1073/pnas.1313978110

Durand-Heredia, J. M., Rivkin, E., Fan, G., Morales, J., & Janakiraman, A. (2012). Identification of ZapD as a cell division factor that promotes the assembly of FtsZ in Escherichia coli. *Journal of Bacteriology*, *194*(12), 3189–3198. http://doi.org/10.1128/JB.00176-12

Durand-Heredia, J. M., Yu, H. H., De Carlo, S., Lesser, C. F., & Janakiraman, A. (2011). Identification and characterization of ZapC, a stabilizer of the FtsZ ring in Escherichia coli. *Journal of Bacteriology*, *193*(6), 1405–1413. http://doi.org/10.1128/JB.01258-10

Eberhardt, A., Hoyland, C. N., Vollmer, D., Bisle, S., Cleverley, R. M., Johnsborg, O., … Vollmer, W. (2012). Attachment of capsular polysaccharide to the cell wall in Streptococcus pneumoniae. *Microbial Drug Resistance*, *18*(3), 240–55. http://doi.org/10.1089/mdr.2011.0232

Ebersbach, G., Galli, E., Møller-Jensen, J., Löwe, J., & Gerdes, K. (2008). Novel coiled-coil cell division factor ZapB stimulates Z ring assembly and cell division. *Molecular Microbiology*, *68*(3), 720–735. http://doi.org/10.1111/j.1365-2958.2008.06190.x

Economou, N. J., Cocklin, S., & Loll, P. J. (2013). High-resolution crystal structure reveals molecular details of target recognition by bacitracin. *Proceedings of the National Academy of Sciences of the United States of America*, *110*(35), 14207–12. http://doi.org/10.1073/pnas.1308268110

Egan, A. J. F., Jean, N. L., Koumoutsi, A., Bougault, C. M., Biboy, J., Sassine, J., … Simorre, J.-P. (2014). Outer-membrane lipoprotein LpoB spans the periplasm to stimulate the peptidoglycan synthase PBP1B. *Proceedings of the National Academy of Sciences of the United States of America*. http://doi.org/10.1073/pnas.1400376111

Egan, A. J. F., & Vollmer, W. (2015). The stoichiometric divisome: a hypothesis. *Frontiers in Microbiology*, *6*(May), 1–6. http://doi.org/10.3389/fmicb.2015.00455

Ehlert, K., & Höltje, J. V. (1996). Role of Precursor Translocation in Coordination of Murein and Phospholipid Synthesis in Escherichia coli. *Journal of Bacteriology*, *178*(23), 6766–6771.

Ehlert, K., Höltje, J. V., & Templin, M. F. (1995). Cloning and expression of a murein hydrolase lipoprotein from Escherichia coli. *Molecular Microbiology*, *16*(4), 761–768. http://doi.org/10.1111/j.1365-2958.1995.tb02437.x

El Ghachi, M., Bouhss, A., Blanot, D., & Mengin-Lecreulx, D. (2004). The bacA gene of Escherichia coli encodes an undecaprenyl pyrophosphate phosphatase activity. *Journal of Biological Chemistry*, *279*(29), 30106–30113. http://doi.org/10.1074/jbc.M401701200

El Ghachi, M., Derbise, A., Bouhss, A., & Mengin-Lecreulx, D. (2005). Identification of multiple genes encoding membrane proteins with undecaprenyl pyrophosphate phosphatase (UppP) activity in Escherichia coli. *Journal of Biological Chemistry*, *280*(19), 18689–18695. http://doi.org/10.1074/jbc.M412277200

Erickson, H. P. (1997). FtsZ, a tubulin homologue in prokaryote cell division. *Trends in Cell Biology*, *7*(9), 362–367. http://doi.org/10.1016/S0962-8924(97)01108-2

Erickson, H. P. (2009). Modeling the physics of FtsZ assembly and force generation. *Proceedings of the National Academy of Sciences of the United States of America*, *106*(23), 9238–9243. http://doi.org/10.1073/pnas.0902258106

Erickson, H. P., Anderson, D. E., & Osawa, M. (2010). FtsZ in bacterial cytokinesis: cytoskeleton and force generator all in one. *Microbiology and Molecular Biology Reviews : MMBR*, *74*(4), 504–528. http://doi.org/10.1128/MMBR.00021-10

Erickson, H. P., Taylor, D. W., Taylor, K. a, & Bramhill, D. (1996). Bacterial cell division protein FtsZ assembles into protofilament sheets and minirings, structural homologs of tubulin polymers. *Proceedings of the National Academy of Sciences of the United States of America*, *93*(1), 519–523. http://doi.org/10.1073/pnas.93.1.519

Errington, J. (2013). L-form bacteria, cell walls and the origins of life. *Open Biology*, *3*(1), 120143. http://doi.org/10.1098/rsob.120143

Errington, J. (2015). Bacterial morphogenesis and the enigmatic MreB helix. *Nature Reviews Microbiology*, *13*(4), 241–248. http://doi.org/10.1038/nrmicro3398

Fan, C., Moews, P. C., Walsh, C. T., & Knox, J. R. (1994). Vancomycin Resistance : Structure of D-Alanine : D-Alanine Ligas at 2.3 A Resolution. *Science*, *266*(5184), 439–443.

Favini-Stabile, S., Contreras-Martel, C., Thielens, N., & Dessen, A. (2013). MreB and MurG as scaffolds for the cytoplasmic steps of peptidoglycan biosynthesis. *Environmental Microbiology*, *15*(12), 3218–3228. http://doi.org/10.1111/1462-2920.12171

Fay, A., & Dworkin, J. (2009). Bacillus subtilis homologs of MviN (MurJ), the putative Escherichia coli lipid II flippase, are not essential for growth. *Journal of Bacteriology*, *191*(19), 6020–6028. http://doi.org/10.1128/JB.00605-09

Fenn, T. D., Stamper, G. F., Morollo, A. a., & Ringe, D. (2003). A side reaction of alanine racemase: Transamination of cycloserine. *Biochemistry*, *42*(19), 5775–5783. http://doi.org/10.1021/bi027022d

Fenton, A. K., & Gerdes, K. (2013). Direct interaction of FtsZ and MreB is required for septum synthesis and cell division in Escherichia coli. *The EMBO Journal*, *32*(13), 1953–65. http://doi.org/10.1038/emboj.2013.129

Ferreira, F. M., Mendoza-Hernandez, G., Castañeda-Bueno, M., Aparicio, R., Fischer, H., Calcagno, M. L., & Oliva, G. (2006). Structural Analysis of N-acetylglucosamine-6-phosphate Deacetylase Apoenzyme from Escherichia coli. *Journal of Molecular Biology*, *359*(2), 308–321. http://doi.org/10.1016/j.jmb.2006.03.024

Figge, R. M., Divakaruni, A. V., & Gober, J. W. (2004). MreB, the cell shape-determining bacterial actin homologue, co-ordinates cell wall morphogenesis in Caulobacter crescentus. *Molecular Microbiology*, *51*(5), 1321–1332. http://doi.org/10.1111/j.1365-2958.2003.03936.x

Firczuk, M., & Bochtler, M. (2007). Mutational analysis of peptidoglycan amidase MepA. *Biochemistry*, *46*(1), 120–128. http://doi.org/10.1021/bi0613776

Fischbach, M. a, & Walsh, C. T. (2009). Antibiotics for emerging pathogens. *Science*, *325*(5944), 1089–93. http://doi.org/10.1126/science.1176667

Fisher, J. F., & Mobashery, S. (2014). The sentinel role of peptidoglycan recycling in the beta-lactam resistance of the Gram-negative Enterobacteriaceae and Pseudomonas aeruginosa. *Bioorganic Chemistry*, *56*, 41–48. http://doi.org/10.1016/j.bioorg.2014.05.011

Fraipont, C., Alexeeva, S., Wolf, B., Der Ploeg, R., Schloesser, M., Den Blaauwen, T., & Nguyen-Distèche, M. (2011). The integral membrane FtsW protein and peptidoglycan synthase PBP3 form a subcomplex in Escherichia coli. *Microbiology*, *157*(1), 251–259. http://doi.org/10.1099/mic.0.040071-0

Fritz, G., & Mascher, T. (2014). A balancing act times two: sensing and regulating cell envelope homeostasis in Bacillus subtilis. *Molecular Microbiology*, *94*(6), 1201–1207. http://doi.org/10.1111/mmi.12848

Fu, G., Huang, T., Buss, J., Coltharp, C., Hensel, Z., & Xiao, J. (2010). In Vivo structure of the E. coli FtsZ-ring revealed by photoactivated localization microscopy (PALM). *PLoS ONE*, *5*(9), 1–16. http://doi.org/10.1371/journal.pone.0012680

Fukushima, T., Kitajima, T., & Sekiguchi, J. (2005). A polysaccharide deacetylase homologue, PdaA, in Bacillus subtilis acts as an N-acetylmuramic acid deacetylase in vitro. *Journal of Bacteriology*, *187*(4), 1287–1292.

http://doi.org/10.1128/JB.187.4.1287-1292.2005

Gallo, K. A., Tanner, M. E., & Knowles, J. R. (1993). Mechanism of the reaction catalyzed by glutamate racemase. *Biochemistry*, *32*(15), 3991–3997.

Gan, L., Chen, S., & Jensen, G. J. (2008). Molecular organization of Gram-negative peptidoglycan. *Proceedings of the National Academy of Sciences of the United States of America*, *105*(48), 18953–18957. http://doi.org/10.1073/pnas.0808035105

Garner, E. C., Bernard, R., Wang, W., Zhuang, X., Rudner, D. Z., & Mitchison, T. (2011). Coupled, circumferential motions of the cell wall synthesis machinery and MreB filaments in B. subtilis. *Science*, *333*(6039), 222–225. http://doi.org/10.1126/science.1203285

Geissler, B., & Margolin, W. (2005). Evidence for functional overlap among multiple bacterial cell division proteins: Compensating for the loss of FtsK. *Molecular Microbiology*, *58*(2), 596–612. http://doi.org/10.1111/j.1365-2958.2005.04858.x

Georgopapadakou, N. H., Smith, S. A., & Sykes, R. B. (1982). Mode of action of azthreonam. *Antimicrobial Agents and Chemotherapy*, *21*(6), 950–956. http://doi.org/10.1128/AAC.21.6.950

Gérard, P., Vernet, T., & Zapun, A. (2002). Membrane Topology of the FtsW Division Protein. *Journal of Bacteriology*, *184*(7), 1925–1931. http://doi.org/10.1128/JB.184.7.1925

Gerding, M. a, Ogata, Y., Pecora, N. D., Niki, H., & de Boer, P. A. J. (2007). The trans-envelope Tol-Pal complex is part of the cell division machinery and required for proper outer-membrane invagination during cell constriction in E. coli. *Molecular Microbiology*, *63*(4), 1008–25. http://doi.org/10.1111/j.1365-2958.2006.05571.x

Gerding, M. a., Liu, B., Bendezú, F. O., Hale, C. A., Bernhardt, T. G., & de Boer, P. A. J. (2009). Self-enhanced accumulation of FtsN at division sites and roles for other proteins with a SPOR domain (DamX, DedD, and RlpA) in Escherichia coli cell constriction. *Journal of Bacteriology*, *191*(24), 7383–7401. http://doi.org/10.1128/JB.00811-09

Gitai, Z., Dye, N., & Shapiro, L. (2004). An actin-like gene can determine cell polarity in bacteria. *Proceedings of the National Academy of Sciences of the United States of America*, *101*(23), 8643–8648. http://doi.org/10.1073/pnas.0402638101

Glas, M., van den Berg van Saparoea, H. B., McLaughlin, S. H., Roseboom, W., Liu, F., Koningstein, G. M., … Luirink, J. (2015). The Soluble Periplasmic Domains of E. coli Cell Division Proteins FtsQ/FtsB/FtsL form a Trimeric Complex with Sub-micromolar Affinity. *Journal of Biological Chemistry*, jbc.M115.654756. http://doi.org/10.1074/jbc.M115.654756

Glauner, B., Holtje, J. V., & Schwarz, U. (1988). The composition of the murein of Escherichia coli. *Journal of Biological Chemistry*, *263*(21), 10088–10095.

Godin, A. G., Lounis, B., & Cognet, L. (2014). Super-resolution Microscopy Approaches for Live Cell Imaging. *Biophysical Journal*, *107*(8), 1777–1784. http://doi.org/10.1016/j.bpj.2014.08.028

Goffin, C., & Ghuysen, J. M. (1998). Multimodular penicillin-binding proteins: an enigmatic family of orthologs and paralogs. *Microbiology and Molecular Biology Reviews : MMBR*, *62*(4), 1079–1093.

Goldbourt, A. (2013). Biomolecular magic-angle spinning solid-state NMR: Recent methods and applications. *Current Opinion in Biotechnology*, *24*(4), 705–715. http://doi.org/10.1016/j.copbio.2013.02.010

González-Leiza, S. M., de Pedro, M. A., & Ayala, J. a. (2011). AmpH, a bifunctional DD-endopeptidase and DD-carboxypeptidase of Escherichia coli. *Journal of Bacteriology*, *193*(24), 6887–6894. http://doi.org/10.1128/JB.05764-11

Goodell, E. W. (1985). Recycling of murein by Escherichia coli. *Journal of Bacteriology*, *163*(1), 305–310.

Gordon, E., Flouret, B., Chantalat, L., Van Heijenoort, J., Mengin-Lecreulx, D., & Dideberg, O. (2001). Crystal

Structure of UDP-N-acetylmuramoyl-L-alanyl-D-glutamate: meso-Diaminopimelate Ligase from Escherichia Coli. *Journal of Biological Chemistry*, *276*(14), 10999–11006. http://doi.org/10.1074/jbc.M009835200

Gray, A. N., Egan, A. J., van't Veer, I. L., Verheul, J., Colavin, A., Koumoutsi, A., … Vollmer, W. (2015). Coordination of peptidoglycan synthesis and outer membrane constriction during *Escherichia coli* cell division. *eLife*, *4*, 1–29. http://doi.org/10.7554/eLife.07118

Gueiros-Filho, F. J., & Losick, R. (2002). A widely conserved bacterial cell division protein that promotes assembly of the tubulin-like protein FtsZ. *Genes and Development*, *16*(19), 2544–2556. http://doi.org/10.1101/gad.1014102

Gulick, a. M., Schmidt, D. M. Z., Gerlt, J. a., & Rayment, I. (2001). Evolution of enzymatic activities in the enolase superfamily: Crystal structures of the L-Ala-D/L-Glu epimerases from Escherichia coli and Bacillus subtilis. *Biochemistry*, *40*(51), 15716–15724. http://doi.org/10.1021/bi011641p

Gumbart, J. C., Beeby, M., Jensen, G. J., & Roux, B. (2014). Escherichia coli Peptidoglycan Structure and Mechanics as Predicted by Atomic-Scale Simulations. *PLoS Computational Biology*, *10*(2). http://doi.org/10.1371/journal.pcbi.1003475

Güntert, P. (1998). Structure calculation of biological macromolecules from NMR data. *Quarterly Reviews of Biophysics*, *31*(2), 145–237. Retrieved from http://www.ncbi.nlm.nih.gov/pubmed/9794034

Ha, S., Chang, E., Lo, M.-C., Men, H., Park, P., Ge, M., & Walker, S. (1999). The Kinetic Characterization of Escherichia coli MurG Using Synthetic Substrate Analogues. *J Am Chem Soc*, *121*(37), 8415–8426. http://doi.org/10.1021/ja991556t

Ha, S., Walker, D., Shi, Y., & Walker, S. (2000). The 1.9 A crystal structure of Escherichia coli MurG, a membrane-associated glycosyltransferase involved in peptidoglycan biosynthesis. *Protein Science*, *9*(6), 1045–1052. http://doi.org/10.1110/ps.9.6.1045

Hadi, T., Hazra, S., Tanner, M. E., & Blanchard, J. S. (2013). The Structure of MurNAc 6-Phosphate Hydrolase (MurQ) from Haemophilus influenzae with Bound Inhibitor. *Biochemistry*, *52*(51), 9358–9366. http://doi.org/10.1016/j.biotechadv.2011.08.021.Secreted

Hale, C. A., & de Boer, P. A. J. (1997). Direct binding of FtsZ to ZipA, an essential component of the septal ring structure that mediates cell division in E. coli. *Cell*, *88*(2), 175–185. http://doi.org/10.1016/S0092-8674(00)81838-3

Hale, C. A., & de Boer, P. A. J. (1999). Recruitment of ZipA to the Septal Ring of Escherichia coli Is Dependent on FtsZ and Independent of FtsA. *Journal of Bacteriology*, *181*(1), 167–176.

Hale, C. A., & de Boer, P. A. J. (2002). ZipA is required for recruitment of FtsK, FtsQ, FtsL, and FtsN to the septal ring in Escherichia coli. *Journal of Bacteriology*, *184*(9), 2552–2556. http://doi.org/10.1128/JB.184.9.2552-2556.2002

Hale, C. A., Rhee, A. C., & de Boer, P. A. J. (2000). ZipA-induced bundling of FtsZ polymers mediated by an interaction between C-terminal domains. *Journal of Bacteriology*, *182*(18), 5153–5166. http://doi.org/10.1128/JB.182.18.5153-5166.2000

Hale, C. A., Shiomi, D., Liu, B., Bernhardt, T. G., Margolin, W., Niki, H., & de Boer, P. A. J. (2011). Identification of Escherichia coli ZapC (YcbW) as a component of the division apparatus that binds and bundles FtsZ polymers. *Journal of Bacteriology*, *193*(6), 1393–1404. http://doi.org/10.1128/JB.01245-10

Hall, R. S., Brown, S., Fedorov, A. a., Fedorov, E. V., Xu, C., Babbitt, P. C., … Raushel, F. M. (2007). Structural diversity within the mononuclear and binuclear active sites of N-acetyl-D-glucosamine-6-phosphate deacetylase. *Biochemistry*, *46*(27), 7953–7962. http://doi.org/10.1021/bi700544c

Hammes, W. P., & Neuhaus, F. C. (1974). On the Specificity of Phospho-N-acetylmuramyl- pentapeptide Translocase. *Journal of Biological Chemistry*, *249*(10), 3140–3150.

Han, S., Caspers, N., Zaniewski, R. P., Lacey, B. M., Tomaras, A. P., Feng, X., … Shanmugasundaram, V. (2011). Distinctive attributes of β-lactam target proteins in Acinetobacter baumannii relevant to development of new antibiotics. *Journal of the American Chemical Society*, *133*(50), 20536–20545. http://doi.org/10.1021/ja208835z

Harz, H., Burgdorf, K., & Höltje, J. V. (1990). Isolation and separation of the glycan strands from murein of Escherichia coli by reversed-phase high-performance liquid chromatography. *Analytical Biochemistry*, *190*(1), 120–128. http://doi.org/10.1016/0003-2697(90)90144-X

Hayhurst, E. J., Kailas, L., Hobbs, J. K., & Foster, S. J. (2008). Cell wall peptidoglycan architecture in Bacillus subtilis. *Proceedings of the National Academy of Sciences of the United States of America*, *105*(38), 14603–14608. http://doi.org/10.1073/pnas.0804138105

Heaslet, H., Shaw, B., Mistry, A., & Miller, A. A. (2009). Characterization of the active site of S. aureus monofunctional glycosyltransferase (Mtg) by site-directed mutation and structural analysis of the protein complexed with moenomycin. *Journal of Structural Biology*, *167*(2), 129–135. http://doi.org/10.1016/j.jsb.2009.04.010

Heidrich, C., Templin, M. F., Ursinus, A., Merdanovic, M., Schwarz, H., & de Pedro, M. A. (2001). Involvement of N -acetylmuramyl- L -alanine amidases in cell separation and antibiotic-induced autolysis of Escherichia coli. *Molecular Microbiology*, *41*(1), 167–178.

Heidrich, C., Ursinus, A., Berger, J., Schwarz, H., & Höltje, J. V. (2002). Effects of multiple deletions of murein hydrolases on viability, septum cleavage, and sensitivity to large toxic molecules in Escherichia coli. *Journal of Bacteriology*, *184*(22), 6093–6099. http://doi.org/10.1128/JB.184.22.6093-6099.2002

Henderson, T. a., Dombrosky, P. M., & Young, K. D. (1994). Artifactual processing of penicillin-binding proteins 7 and 1b by the OmpT protease of Escherichia coli. *Journal of Bacteriology*, *176*(1), 256–259.

Henderson, T. A., Young, K. D., Denome, S. A., & Elf, P. K. (1997). AmpC and AmpH, proteins related to the class C β-lactamases, bind penicillin and contribute to the normal morphology of Escherichia coli. *Journal of Bacteriology*, *179*(19), 6112–6121.

Henriques, a O., Glaser, P., Piggot, P. J., & Moran, C. P. (1998). Control of cell shape and elongation by the rodA gene in Bacillus subtilis. *Molecular Microbiology*, *28*(2), 235–247.

Hervé, M., Boniface, A., Gobec, S., Blanot, D., & Mengin-Lecreulx, D. (2007). Biochemical characterization and physiological properties of Escherichia coli UDP-N-acetylmuramate:L-alanyl-gamma-D-glutamyl-meso-diaminopimelate ligase. *Journal of Bacteriology*, *189*(11), 3987–3995. http://doi.org/10.1128/JB.00087-07

Heydanek, M. G., & Neuhaus, F. C. (1969). The initial stage in peptidoglycan synthesis. IV. Solubilization of phospho-N-acetylmuramyl-pentapeptide translocase. *Biochemistry*, *8*(4), 1474–1481. http://doi.org/10.1021/bi00832a024

Höltje, J. V. (1998). Growth of the stress-bearing and shape-maintaining murein sacculus of Escherichia coli. *Microbiology and Molecular Biology Reviews : MMBR*, *62*(1), 181–203. Retrieved from http://www.pubmedcentral.nih.gov/articlerender.fcgi?artid=98910&tool=pmcentrez&rendertype=abstract

Höltje, J. V., Kopp, U., Ursinus, A., & Wiedemann, B. (1994). The negative regulator of beta-lactamase induction AmpD is a N-acetyl-anhydromuramyl-L-alanine amidase. *FEMS Microbiology Letters*, *122*(1-2), 159–164. http://doi.org/10.1111/j.1574-6968.1994.tb07159.x

Howlett, G. J., Minton, A. P., & Rivas, G. (2006). Analytical ultracentrifugation for the study of protein association and assembly. *Current Opinion in Chemical Biology*, *10*(5), 430–436. http://doi.org/10.1016/j.cbpa.2006.08.017

Hrast, M., Sosič, I., Šink, R., & Gobec, S. (2014). Inhibitors of the peptidoglycan biosynthesis enzymes MurA-F. *Bioorganic Chemistry*, *55*, 2–15. http://doi.org/10.1016/j.bioorg.2014.03.008

Hu, Y., Chen, L., Ha, S., Gross, B., Falcone, B., Walker, D., … Walker, S. (2003). Crystal structure of the MurG:UDP-GlcNAc complex reveals common structural principles of a superfamily of glycosyltransferases. *Proceedings of the National Academy of Sciences of the United States of America*, *100*(3), 845–849. http://doi.org/10.1073/pnas.0235749100

Huang, C.-Y., Shih, H.-W., Lin, L.-Y., Tien, Y.-W., Cheng, T.-J. R., Cheng, W.-C., … Ma, C. (2012). Crystal structure of Staphylococcus aureus transglycosylase in complex with a lipid II analog and elucidation of peptidoglycan synthesis mechanism. *Proceedings of the National Academy of Sciences*, *109*(17), 6496–6501. http://doi.org/10.1073/pnas.1203900109

Huang, K. H., Durand-Heredia, J. M., & Janakiraman, A. (2013). FtsZ ring stability: Of bundles, tubules, crosslinks, and curves. *Journal of Bacteriology*. http://doi.org/10.1128/JB.02157-12

Hwang, K. Y., Cho, C. S., Kim, S. S., Sung, H. C., Yu, Y. G., & Cho, Y. (1999). Structure and mechanism of glutamate racemase from Aquifex pyrophilus. *Nature Structural Biology*, *6*(5), 422–426. http://doi.org/10.1038/8223

Ikeda, M., Sato, T., Wachi, M., Jung, H. K., Ishino, F., Kobayashi, Y., & Matsuhashi, M. (1989). Structural similarity among Escherichia coli FtsW and RodA proteins and Bacillus subtilis SpoVE protein, which function in cell division, cell elongation, and spore formation, respectively. *Journal of Bacteriology*, *171*(11), 6375–6378.

Inoue, A., Murata, Y., Takahashi, H., Tsuji, N., Fujisaki, S., & Kato, J. I. (2008). Involvement of an essential gene, mviN, in murein synthesis in Escherichia coli. *Journal of Bacteriology*, *190*(21), 7298–7301. http://doi.org/10.1128/JB.00551-08

Ishino, F., Park, W., Tomioka, S., Tamaki, S., Takase, I., Kunugita, K., … Spratt, B. G. (1986). Peptidoglycan synthetic activities in membranes of Escherichia coli caused by overproduction of penicillin-binding protein 2 and RodA protein. *Journal of Biological Chemistry*, *261*(15), 7024–7031.

Jacob, J., Krafft, C., Welfle, K., Welfle, H., & Saenger, W. (1998). Melting points of lysozyme and ribonuclease A crystals correlated with protein unfolding: A Raman spectroscopic study. *Acta Crystallographica Section D: Biological Crystallography*, *54*(1), 74–80. http://doi.org/10.1107/S0907444997010330

Jacobs, C., Frère, J. M., & Normark, S. (1997). Cytosolic intermediates for cell wall biosynthesis and degradation control inducible β-lactam resistance in gram-negative bacteria. *Cell*, *88*(6), 823–832. http://doi.org/10.1016/S0092-8674(00)81928-5

Jacobs, C., Joris, B., Jamin, M., Klarsov, K., Van Beeumen, J., Mengin-Lecreulx, D., … Frère, J. M. (1995). AmpD, essential for both β-lactamase regulation and cell wall recycling, is a novel cytosolic N-acetylmuramyl-L-alanine amidase. *Molecular Microbiology*, *15*(3), 553–559. http://doi.org/10.1111/j.1365-2958.1995.tb02268.x

Jaeger, T., Arsic, M., & Mayer, C. (2005). Scission of the lactyl ether bond of N-acetylmuramic acid by Escherichia coli “etherase.” *Journal of Biological Chemistry*, *280*(34), 30100–30106. http://doi.org/10.1074/jbc.M502208200

Jean, N. L., Bougault, C., Derouaux, A., Callens, G., Vollmer, W., & Simorre, J.-P. (2014). Backbone and side-chain 1H, 13C, and 15N NMR assignments of the N-terminal domain of Escherichia coli LpoA. *Biomolecular NMR Assignments*. http://doi.org/10.1007/s12104-014-9546-2

Jean, N. L., Bougault, C. M., Egan, A. J. F., Vollmer, W., & Simorre, J.-P. (2014). Solution NMR assignment of LpoB, an outer-membrane anchored Penicillin-Binding Protein activator from Escherichia coli. *Biomolecular NMR Assignments*. http://doi.org/10.1007/s12104-014-9557-z

Jean, N. L., Bougault, C. M., Lodge, A., Derouaux, A., Callens, G., Egan, A. J. F., … Simorre, J.-P. (2014). Elongated structure of the outer-membrane activator of peptidoglycan synthesis LpoA: Implications for PBP1A stimulation. *Structure*, *22*(7), 1047–1054. http://doi.org/10.1016/j.str.2014.04.017

Jennings, P. C., Cox, G. C., Monahan, L. G., & Harry, E. J. (2011). Super-resolution imaging of the bacterial cytokinetic protein FtsZ. *Micron*, *42*(4), 336–341. http://doi.org/10.1016/j.micron.2010.09.003

Jeske, O., Schüler, M., Schumann, P., Schneider, A., Boedeker, C., Jogler, M., … Jogler, C. (2015). Planctomycetes do possess a peptidoglycan cell wall. *Nature Communications*, *6*(May), 7116. http://doi.org/10.1038/ncomms8116

Jin, H., Emanuele, J. J., Fairman, R., Robertson, J. G., Hail, M. E., Ho, H. T., … Villafranca, J. J. (1996). Structural studies of Escherichia coli UDP-N-acetylmuramate:L-alanine ligase. *Biochemistry*, *35*(5), 1423–1431. http://doi.org/10.1021/bi952334k

Johnson, J. W., Fisher, J. F., & Mobashery, S. (2013). Bacterial cell-wall recycling. *Annals of the New York Academy of Sciences*, *1277*(1), 54–75. http://doi.org/10.1111/j.1749-6632.2012.06813.x

Jolly, L., Ferrari, P., Blanot, D., Van Heijenoort, J., Fassy, F., & Mengin-Lecreulx, D. (1999). Reaction mechanism of phosphoglucosamine mutase from Escherichia coli. *European Journal of Biochemistry*, *262*(1), 202–210. http://doi.org/10.1046/j.1432-1327.1999.00373.x

Jones, L. J. F., Carballido-López, R., & Errington, J. (2001). Control of cell shape in bacteria: Helical, actin-like filaments in Bacillus subtilis. *Cell*, *104*(6), 913–922. http://doi.org/10.1016/S0092-8674(01)00287-2

Kampfenkel, K., & Braun, V. (1993). Membrane topologies of the TolQ and TolR proteins of Escherichia coli: Inactivation of TolQ by a missense mutation in the proposed first transmembrane segment. *Journal of Bacteriology*, *175*(14), 4485–4491.

Kato, J., Suzuki, H., & Hirota, Y. (1984). Overlapping of the coding regions for alpha and gamma components of penicillin-binding protein 1 b in Escherichia coli. *Molecular & General Genetics*, *196*(3), 449–457. http://doi.org/10.1007/BF00436192

Kato, J., Suzuki, H., & Hirota, Y. (1985). Dispensability of either penicillin-binding protein-1a or -1b involved in the essential process for cell elongation in Escherichia coli. *Molecular & General Genetics*, *200*(2), 272–277. http://doi.org/10.1007/BF00425435

Keating, T. A. (2013). Resistance mechanism to an uncompetitive inhibitor of a single-substrate, single-product enzyme: a study of Helicobacter pylori glutamate racemase. *Future Medicinal Chemistry*, *5*(11), 1203–14. http://doi.org/10.4155/fmc.13.94

Keck, W., van Leeuwen, a M., Huber, M., & Goodell, E. W. (1990). Cloning and characterization of mepA, the structural gene of the penicillin-insensitive murein endopeptidase from Escherichia coli. *Molecular Microbiology*, *4*(2), 209–219. http://doi.org/10.1111/j.1365-2958.1990.tb00588.x

Kelly, J. a, Knox, J. R., Zhao, H., Frère, J. M., & Ghaysen, J. M. (1989). Crystallographic mapping of beta-lactams bound to a D-alanyl-D-alanine peptidase target enzyme. *Journal of Molecular Biology*, *209*(2), 281–295. http://doi.org/10.1016/0022-2836(89)90277-5

Kerfah, R., Plevin, M. J., Sounier, R., Gans, P., & Boisbouvier, J. (2015). Methyl-specific isotopic labeling: a molecular tool box for solution NMR studies of large proteins. *Current Opinion in Structural Biology*, *32*, 113–122. http://doi.org/10.1016/j.sbi.2015.03.009

Kerff, F., Petrella, S., Mercier, F., Sauvage, E., Herman, R., Pennartz, A., … Charlier, P. (2010). Specific Structural Features of the N-Acetylmuramoyl-l-Alanine Amidase AmiD from Escherichia coli and Mechanistic Implications for Enzymes of This Family. *Journal of Molecular Biology*, *397*(1), 249–259. http://doi.org/10.1016/j.jmb.2009.12.038

Kern, T., Giffard, M., Hediger, S., Amoroso, A., Giustini, C., Bui, N. K., … Simorre, J.-P. (2010). Dynamical characterization of fully hydrated bacterial cell walls by solid-state NMR - evidence for cooperative binding of metal ions. *Journal of the American Chemical Society*, *132*(7), 10911–10919.

Kern, T., Hediger, S., Müller, P., Giustini, C., Joris, B., Bougault, C., … Simorre, J.-P. (2008). Toward the Characterization of Peptidoglycan Structure and Protein− Peptidoglycan Interactions by Solid-State NMR

Spectroscopy. *Journal of the American Chemical Society*, *130*(17), 5618–5619. http://doi.org/10.1021/ja7108135

Kim, D. H., Lees, W. J., Kempsell, K. E., Lane, W. S., Duncan, K., & Walsh, C. T. (1996). Characterization of a Cys115 to Asp substitution in the Escherichia coli cell wall biosynthetic enzyme UDP-GlcNAc enolpyruvyl transferase (MurA) that confers resistance to inactivation by the antibiotic fosfomycin. *Biochemistry*, *35*(15), 4923–4928. http://doi.org/10.1021/bi952937w

Kim, H. S., Kim, J., Im, H. N., Yoon, J. Y., An, D. R., Yoon, H. J., … Suh, S. W. (2013). Structural basis for the inhibition of *Mycobacterium tuberculosis* <scp>L</scp> , <scp>D</scp> -transpeptidase by meropenem, a drug effective against extensively drug-resistant strains. *Acta Crystallographica Section D Biological Crystallography*, *69*(3), 420–431. http://doi.org/10.1107/S0907444912048998

King, D. T., Lameignere, E., & Strynadka, N. C. J. (2014). Structural insights into the lipoprotein outer membrane regulator of penicillin-binding protein 1B. *Journal of Biological Chemistry*, *289*(27), 19245–19253. http://doi.org/10.1074/jbc.M114.565879

Kishida, H., Unzai, S., Roper, D. I., Lloyd, A., Park, S.-Y. Y., & Tame, J. R. H. (2006). Crystal structure of penicillin binding protein 4 (dacB) from Escherichia coli, both in the native form and covalently linked to various antibiotics. *Biochemistry*, *45*(3), 783–92. http://doi.org/10.1021/bi051533t

Kleckner, I. R., & Foster, M. P. (2011). An introduction to NMR-based approaches for measuring protein dynamics. *Biochimica et Biophysica Acta - Proteins and Proteomics*, *1814*(8), 942–968. http://doi.org/10.1016/j.bbapap.2010.10.012

Klein, R. a., Hartmann, R., Egge, H., Behr, T., & Fischer, W. (1996). The aqueous solution structure of a lipoteichoic acid from Streptococcus pneumoniae strain R6 containing 2,4-diamino-2,4,6-trideoxy-galactose: evidence for conformational mobility of the galactopyranose ring. *Carbohydrate Research*, *281*(1), 79–98. http://doi.org/16/0008-6215(95)00336-3

Klenchin, V. a., Schmidt, D. M., Gerlt, J. a., & Rayment, I. (2004). Evolution of enzymatic activities in the enolase superfamily: Structure of a substrate-liganded complex of the L-Ala-D/L-Glu epimerase from Bacillus subtilis. *Biochemistry*, *43*(32), 10370–10378. http://doi.org/10.1021/bi049197o

Koch, A. L. (1998). Orientation of the peptidoglycan chains in the sacculus of Escherichia coli. *Research in Microbiology*, *149*, 678–701.

Koch, A. L., Lane, S. L., Miller, J. A., & Nickens, D. G. (1987). Contraction Of Filaments Of Escherichia-Coli After Disruption Of Cell-Membrane By Detergent. *Journal of Bacteriology*, *169*(5), 1979–1984.

Koch, A. L., & Woeste, S. (1992). Elasticity Of The Sacculus Of Escherichia-coli. *Journal of Bacteriology*, *174*(14), 4811–4819.

Korat, B., Mottl, H., & Keck, W. (1991). Penicillin-binding protein 4 of Escherichia coli: molecular cloning of the dacB gene, controlled overexpression, and alterations in murein composition. *Molecular Microbiology*, *5*(3), 675–684.

Korza, H. J., & Bochtler, M. (2005). Pseudomonos aeruginosa LD-carboxypeptidase, a serine peptidase with a Ser-His-Glu Triad and a nucleophilic elbow. *Journal of Biological Chemistry*, *280*(49), 40802–40812. http://doi.org/10.1074/jbc.M506328200

Kouidmi, I., Levesque, R. C., & Paradis-Bleau, C. (2014). The biology of Mur ligases as an antibacterial target. *Molecular Microbiology*, *94*(2), 242–253. http://doi.org/10.1111/mmi.12758

Krachler, A. M., Sharma, A., Cauldwell, A., Papadakos, G., & Kleanthous, C. (2010). TolA Modulates the Oligomeric Status of YbgF in the Bacterial Periplasm. *Journal of Molecular Biology*, *403*(2), 270–285. http://doi.org/10.1016/j.jmb.2010.08.050

Kraft, A. R., Templin, M. F., & Höltje, J. V. (1998). Membrane-bound lytic endotransglycosylase in Escherichia coli. *Journal of Bacteriology*, *180*(13), 3441–3447.

Kruse, T., Bork-Jensen, J., & Gerdes, K. (2005). The morphogenetic MreBCD proteins of Escherichia coli form an essential membrane-bound complex. *Molecular Microbiology*, *55*(1), 78–89. http://doi.org/10.1111/j.1365-2958.2004.04367.x

Kruse, T., Møeller-Jensen, J., Løbner-Olesen, A., & Gerdes, K. (2003). Dysfunctional MreB inhibits chromosome segregation in Escherichia coli. *EMBO Journal*, *22*(19), 5283–5292. http://doi.org/10.1093/emboj/cdg504

Kuru, E., Hughes, H. V., Brown, P. J., Hall, E., Tekkam, S., Cava, F., … Vannieuwenhze, M. S. (2012). In situ probing of newly synthesized peptidoglycan in live bacteria with fluorescent D-amino acids. *Angewandte Chemie - International Edition*, *51*(50), 12519–12523. http://doi.org/10.1002/anie.201206749

Kuru, E., Tekkam, S., Hall, E., Brun, Y. V., & Van Nieuwenhze, M. S. (2015). Synthesis of fluorescent D-amino acids and their use for probing peptidoglycan synthesis and bacterial growth in situ. *Nature Protocols*, *10*(1), 33–52. http://doi.org/10.1038/nprot.2014.197

Kwan, A. H., Mobli, M., Gooley, P. R., King, G. F., & MacKay, J. P. (2011). Macromolecular NMR spectroscopy for the non-spectroscopist. *FEBS Journal*, *278*(5), 687–703. http://doi.org/10.1111/j.1742-4658.2011.08004.x

Labischinski, H., Goodell, E. W., Goodell, a., & Hochberg, M. L. (1991). Direct proof of a “more-than-single-layered” peptidoglycan architecture of Escherichia coli W7: A neutron small-angle scattering study. *Journal of Bacteriology*, *173*(2), 751–756. http://doi.org/0021-9193/91

Lan, G., Daniels, B. R., Dobrowsky, T. M., Wirtz, D., & Sun, S. X. (2009). Condensation of FtsZ filaments can drive bacterial cell division. *Proceedings of the National Academy of Sciences of the United States of America*, *106*(1), 121–126. http://doi.org/10.1073/pnas.0807963106

Lapointe, L. M., Taylor, K. C., Subramaniam, S., Khadria, A., Rayment, I., & Senes, A. (2013). Structural organization of FtsB, a transmembrane protein of the bacterial divisome. *Biochemistry*, *52*(15), 2574–2585. http://doi.org/10.1021/bi400222r

Lara, B., & Ayala, J. a. (2002). Topological characterization of the essential Escherichia coli cell division protein FtsW. *FEMS Microbiology Letters*, *216*, 23–32.

Lara, B., Mengin-Lecreulx, D., Ayala, J. a., & Van Heijenoort, J. (2005). Peptidoglycan precursor pools associated with MraY and FtsW deficiencies or antibiotic treatments. *FEMS Microbiology Letters*, *250*(2), 195–200. http://doi.org/10.1016/j.femsle.2005.07.005

Lavollay, M., Arthur, M., Fourgeaud, M., Dubost, L., Marie, A., Veziris, N., … Mainardi, J. L. (2008). The peptidoglycan of stationary-phase Mycobacterium tuberculosis predominantly contains cross-links generated by L,D-transpeptidation. *Journal of Bacteriology*, *190*(12), 4360–4366. http://doi.org/10.1128/JB.00239-08

Leaver, M., Domínguez-Cuevas, P., Coxhead, J. M., Daniel, R. a, & Errington, J. (2009). Life without a wall or division machine in Bacillus subtilis. *Nature*, *457*(7231), 849–853. http://doi.org/10.1038/nature08232

Leaver, M., & Errington, J. (2005). Roles for MreC and MreD proteins in helical growth of the cylindrical cell wall in Bacillus subtilis. *Molecular Microbiology*, *57*(5), 1196–1209. http://doi.org/10.1111/j.1365-2958.2005.04736.x

Lecoq, L., Bougault, C., Hugonnet, J.-E., Veckerlé, C., Pessey, O., Arthur, M., & Simorre, J.-P. (2012). Dynamics induced by β-lactam antibiotics in the active site of Bacillus subtilis L,D-transpeptidase. *Structure*, *20*(5), 850–61. http://doi.org/10.1016/j.str.2012.03.015

Lee, J. H., Na, Y., Song, H. E., Kim, D., Park, B. H., Rho, S. H., … Eom, S. H. (2006). Crystal structure of the Apo form of D-alanine: D-alanine ligase (Ddl) from Thermus caldophilus: A basis for the substrate-induced conformational changes. *Proteins: Structure, Function and Genetics*, *64*(4), 1078–1082. http://doi.org/10.1002/prot.20927

Lee, M., Hesek, D., Llarrull, L. I., Lastochkin, E., Pi, H., Boggess, B., & Mobashery, S. (2013). Reactions of All E. coli Lytic Transglycosylases with Bacterial Cell Wall. *Journal of the American Chemical Society*, 10–13. http://doi.org/10.1021/ja309036q

Lee, M., Hesek, D., Suvorov, M., Lee, W., & Vakulenko, S. (2003). A Mechanism-Based Inhibitor Targeting the DD -Transpeptidase Activity of Bacterial Penicillin-Binding Proteins. *J. Am. Chem. Soc.*, *125*(4), 16322–16326. http://doi.org/10.1021/ja038445l

Leger, M. M., Eme, L., Petru, M., Eliás, M., Dole, P., & Roger, A. J. (2015). An ancestral bacterial division system is widespread in eukaryotic mitochondria. *Proceedings of the National Academy of Sciences*, 1–8. http://doi.org/10.1073/pnas.1421392112

Leidenix, M. J., Jacoby, G. H., Henderson, T. a., & Young, K. D. (1989). Separation of Escherichia coli penicillin-binding proteins into different membrane vesicles by agarose electrophoresis and sizing chromatography. *Journal of Bacteriology*, *171*(10), 5680–5686.

Levengood, S. K., Beyer, W. F., & Webster, R. E. (1991). TolA: a membrane protein involved in colicin uptake contains an extended helical region. *Proceedings of the National Academy of Sciences of the United States of America*, *88*(14), 5939–5943. http://doi.org/10.1073/pnas.88.14.5939

Li, Z., Trimble, M. J., Brun, Y. V, & Jensen, G. J. (2007). The structure of FtsZ filaments in vivo suggests a force-generating role in cell division. *The EMBO Journal*, *26*(22), 4694–4708. http://doi.org/10.1038/sj.emboj.7601895

Liechti, G. W., Kuru, E., Hall, E., Kalinda, A., Brun, Y. V., VanNieuwenhze, M., & Maurelli, a T. (2014). A new metabolic cell-wall labelling method reveals peptidoglycan in Chlamydia trachomatis. *Nature*, *506*(7489), 507–10. http://doi.org/10.1038/nature12892

Liepinsh, E., Généreux, C., Dehareng, D., Joris, B., & Otting, G. (2003). NMR structure of Citrobacter freundii AmpD, comparison with bacteriophage T7 lysozyme and homology with PGRP domains. *Journal of Molecular Biology*, *327*(4), 833–842. http://doi.org/10.1016/S0022-2836(03)00185-2

Liger, D., Blanot, D., & Van Heijenoort, J. (1991). Effect of various alanine analogues on the L-alanine-adding enzyme from Escherichia coli. *FEMS Microbiology Letters*, *80*, 111–116.

Lindberg, F., Lindquist, S., & Normark, S. (1987). Inactivation of the ampD gene causes semiconstitutive overproduction of the inducible Citrobacter freundii β-lactamase. *Journal of Bacteriology*, *169*(5), 1923–1928.

Lindquist, S., Weston-Hafer, K., Schmidt, H., Pul, C., Korfmann, G., Erickson, J., … Normark, S. (1993). AmpG, a signal transducer in chromosomal beta-lactamase induction. *Molecular Microbiology*, *9*(4), 703–715.

Liu, B., Persons, L., Lee, L., & de Boer, P. A. J. (2015). Roles for both FtsA and the FtsBLQ subcomplex in FtsN-stimulated cell constriction in Escherichia coli. *Molecular Microbiology*, n/a–n/a. http://doi.org/10.1111/mmi.12906

Lloubès, R., Cascales, E., Walburger, A., Bouveret, E., Lazdunski, C., Bernadac, A., & Journet, L. (2001). The Tol-Pal proteins of the Escherichia coli cell envelope: an energized system required for outer membrane integrity? *Research in Microbiology*, *152*(6), 523–9. Retrieved from http://www.ncbi.nlm.nih.gov/pubmed/11501670

Loskill, P., Pereira, P. M., Jung, P., Bischoff, M., Herrmann, M., Pinho, M. G., & Jacobs, K. (2014). Reduction of the peptidoglycan crosslinking causes a decrease in stiffness of the Staphylococcus aureus cell envelope. *Biophysical Journal*, *107*(5), 1082–1089. http://doi.org/10.1016/j.bpj.2014.07.029

Lovering, A. L., de Castro, L. H., Lim, D., & Strynadka, N. C. J. (2007). Structural insight into the transglycosylation step of bacterial cell-wall biosynthesis. *Science*, *315*(5817), 1402–1405. http://doi.org/10.1126/science.1136611

Lovering, A. L., & Strynadka, N. C. J. (2007). High-resolution Structure of the Major Periplasmic Domain from the Cell Shape-determining Filament MreC. *Journal of Molecular Biology*, *372*(4), 1034–1044. http://doi.org/10.1016/j.jmb.2007.07.022

Low, H. H., Moncrieffe, M. C., & Löwe, J. (2004). The crystal structure of ZapA and its modulation of FtsZ polymerisation. *Journal of Molecular Biology*, *341*(3), 839–852. http://doi.org/10.1016/j.jmb.2004.05.031

Löwe, J., & Amos, L. a. (1998). Crystal structure of the bacterial cell-division protein FtsZ. *Nature*, *391*(6663), 203–206. http://doi.org/10.1038/34472

Lower, B. H., & Bazylinski, D. a. (2013). The bacterial magnetosome: A unique prokaryotic organelle. *Journal of Molecular Microbiology and Biotechnology*, *23*(1-2), 63–80. http://doi.org/10.1159/000346543

Lu, C., Reedy, M., & Erickson, H. P. (2000). Straight and curved conformations of FtsZ are regulated by GTP hydrolysis. *Journal of Bacteriology*, *182*(1), 164–170. http://doi.org/10.1128/JB.182.1.164-170.2000

Lundqvist, T., Fisher, S. L., Kern, G., Folmer, R. H. a, Xue, Y., Newton, D. T., … de Jonge, B. L. M. (2007). Exploitation of structural and regulatory diversity in glutamate racemases. *Nature*, *447*(7146), 817–822. http://doi.org/10.1038/nature05689

Lupoli, T. J., Lebar, M. D., Markovski, M., Bernhardt, T. G., Kahne, D., & Walker, S. (2014). Lipoprotein activators stimulate Escherichia coli penicillin-binding proteins by different mechanisms. *Journal of the American Chemical Society*, *136*(1), 52–5. http://doi.org/10.1021/ja410813j

Madoori, P. K., & Thunnissen, A. M. W. H. (2010). Purification, crystallization and preliminary X-ray diffraction analysis of the lytic transglycosylase MltF from Escherichia coli. *Acta Crystallographica. Section F, Structural Biology and Crystallization Communications*, *66*(Pt 5), 534–538. http://doi.org/10.1107/S1744309110010596

Magnet, S., Bellais, S., Dubost, L., Fourgeaud, M., Mainardi, J. L., Petit-Frère, S., … Gutmann, L. (2007). Identification of the L,D-transpeptidases responsible for attachment of the Braun lipoprotein to Escherichia coli peptidoglycan. *Journal of Bacteriology*, *189*(10), 3927–3931. http://doi.org/10.1128/JB.00084-07

Magnet, S., Dubost, L., Marie, A., Arthur, M., & Gutmann, L. (2008). Identification of the L,D-transpeptidases for peptidoglycan cross-linking in Escherichia coli. *Journal of Bacteriology*, *190*(13), 4782–4785. http://doi.org/10.1128/JB.00025-08

Mainardi, J. L., Fourgeaud, M., Hugonnet, J. E., Dubost, L., Brouard, J. P., Ouazzani, J., … Arthur, M. (2005). A novel peptidoglycan cross-linking enzyme for a β-lactam-resistant transpeptidation pathway. *Journal of Biological Chemistry*, *280*(46), 38146–38152. http://doi.org/10.1074/jbc.M507384200

Mainardi, J. L., Hugonnet, J. E., Rusconi, F., Fourgeaud, M., Dubost, L., Moumi, A. N., … Arthur, M. (2007). Unexpected inhibition of peptidoglycan LD-transpeptidase from Enterococcus faecium by the β-lactam imipenem. *Journal of Biological Chemistry*, *282*(42), 30414–30422. http://doi.org/10.1074/jbc.M704286200

Mainardi, J. L., Legrand, R., Arthur, M., Schoot, B., Van Heijenoort, J., & Gutmann, L. (2000). Novel mechanism of β-lactam resistance due to bypass of DD- transpeptidation in Enterococcus faecium. *Journal of Biological Chemistry*, *275*(22), 16490–16496. http://doi.org/10.1074/jbc.M909877199

Mainardi, J. L., Morel, V., Fourgeaud, M., Cremniter, J., Blanot, D., Legrand, R., … Gutmann, L. (2002). Balance between two transpeptidation mechanisms determines the expression of β-lactam resistance in Enterococcus faecium. *Journal of Biological Chemistry*, *277*(39), 35801–35807. http://doi.org/10.1074/jbc.M204319200

Manat, G., Roure, S., Auger, R., Bouhss, A., Barreteau, H., Mengin-Lecreulx, D., & Touzé, T. (2014). Deciphering the metabolism of undecaprenyl-phosphate: the bacterial cell-wall unit carrier at the membrane frontier. *Microbial Drug Resistance*, *20*(3), 199–214. http://doi.org/10.1089/mdr.2014.0035

Mansour, T. S., Caufield, C. E., Rasmussen, B., Chopra, R., Krishnamurthy, G., Morris, K. M., … Singh, G.

(2007). Naphthyl tetronic acids as multi-target inhibitors of bacterial peptidoglycan biosynthesis. *ChemMedChem*, *2*(10), 1414–1417. http://doi.org/10.1002/cmdc.200700094

Maqbool, A., Herve, M., Mengin-Lecreulx, D., Wilkinson, A., & Thomas, G. (2012). MpaA is a murein-tripeptide-specific zinc carboxypeptidase that functions as part of a catabolic pathway for peptidoglycan derived peptides in γ-proteobacteria. *Biochemical Journal*, *341*, 329–341. http://doi.org/10.1042/BJ20121164

Marcyjaniak, M., Odintsov, S. G., Sabala, I., & Bochtler, M. (2004). Peptidoglycan amidase MepA is a LAS metallopeptidase. *Journal of Biological Chemistry*, *279*(42), 43982–43989. http://doi.org/10.1074/jbc.M406735200

Marion, D. (2013). An introduction to biological NMR spectroscopy. *Molecular & Cellular Proteomics*, *12*(11), 3006–25. http://doi.org/10.1074/mcp.O113.030239

Markovski, M. (2012). *Bacterial Cell Wall Synthases Require Outer Membrane Lipoprotein Cofactors*.

Marquardt, J. ., Brown, E. D., Lane, W. ., Haley, T. ., Ichikawa, Y., Wong, C.-H., & Walsh, C. T. (1994). Kinetics, Stoichiometry, and Identification of the Reactive Thiolate in the Inactivation of UDP-GlcNAc Enolpyruvoyl Transferase by the Antibiotic Fosfomycin. *Biochemistry*, *33*(35), 10646–10651.

Marquardt, J. ., Brown, E. D., Walsh, C. T., & Anderson, K. . (1993). Isolation and structural elucidation of a tetrahedral intermediate in the UDP-N-acetylglucosamine enolpyruvoyl transferase enzymatic pathway. *Journal of the American Chemical Society*, *115*, 10398–10399.

Marteyn, B. S., Karimova, G., Fenton, A. K., Gazi, A. D., West, N., Touqui, L., … Tang, C. M. (2014). ZapE is a novel cell division protein interacting with FtsZ and modulating the Z-ring dynamics. *mBio*, *5*(2), 1–10. http://doi.org/10.1128/mBio.00022-14

Mason, O. U., Nakagawa, T., Rosner, M., van Nostrand, J. D., Zhou, J., Maruyama, A., … Giovannoni, S. J. (2010). First investigation of the microbiology of the deepest layer of ocean crust. *PLoS ONE*, *5*(11). http://doi.org/10.1371/journal.pone.0015399

Massey, T. H., Mercogliano, C. P., Yates, J., Sherratt, D. J., & Löwe, J. (2006). Double-Stranded DNA Translocation: Structure and Mechanism of Hexameric FtsK. *Molecular Cell*, *23*(4), 457–469. http://doi.org/10.1016/j.molcel.2006.06.019

Matias, V. R. F., Al-amoudi, A., Dubochet, J., & Beveridge, T. J. (2003). Cryo-Transmission Electron Microscopy of Frozen-Hydrated Sections of Escherichia coli and Pseudomonas aeruginosa. *Journal of Bacteriology*, *185*(20), 6112–6118. http://doi.org/10.1128/JB.185.20.6112

Matias, V. R. F., & Beveridge, T. J. (2005). Cryo-electron microscopy reveals native polymeric cell wall structure in Bacillus subtilis 168 and the existence of a periplasmic space. *Molecular Microbiology*, *56*(1), 240–251. http://doi.org/10.1111/j.1365-2958.2005.04535.x

Matias, V. R. F., & Beveridge, T. J. (2006). Native cell wall organization shown by cryo-electron microscopy confirms the existence of a periplasmic space in Staphylococcus aureus. *Journal of Bacteriology*, *188*(3), 1011–1021. http://doi.org/10.1128/JB.188.3.1011-1021.2006

Mauriello, E. M. F., Mouhamar, F., Nan, B., Ducret, A., Dai, D., Zusman, D. R., & Mignot, T. (2010). Bacterial motility complexes require the actin-like protein, MreB and the Ras homologue, MglA. *The EMBO Journal*, *29*(2), 315–326. http://doi.org/10.1038/emboj.2009.356

Mavrici, D., Marakalala, M. J., Holton, J. M., Prigozhin, D. M., Gee, C. L., Zhang, Y. J., … Alber, T. (2014). Mycobacterium tuberculosis FtsX extracellular domain activates the peptidoglycan hydrolase, RipC. *Proceedings of the National Academy of Sciences of the United States of America*, *111*(22), 8037–42. http://doi.org/10.1073/pnas.1321812111

Mazza, P., Noens, E. E., Schirner, K., Grantcharova, N., Mommaas, a. M., Koerten, H. K., … Wohlleben, W. (2006). MreB of Streptomyces coelicolor is not essential for vegetative growth but is required for the

integrity of aerial hyphae and spores. *Molecular Microbiology*, *60*(4), 838–852. http://doi.org/10.1111/j.1365-2958.2006.05134.x

McCoy, A. J., & Maurelli, A. T. (2005). Characterization of Chlamydia MurC-Ddl, a fusion protein exhibiting D-alanyl-D-alanine ligase activity involved in peptidoglycan synthesis and D-cycloserine sensitivity. *Molecular Microbiology*, *57*(1), 41–52. http://doi.org/10.1111/j.1365-2958.2005.04661.x

Mcpherson, D. C., & Popham, D. L. (2003). Peptidoglycan Synthesis in the Absence of Class A Penicillin-Binding Proteins in Bacillus subtilis Peptidoglycan Synthesis in the Absence of Class A Penicillin-Binding Proteins in Bacillus subtilis. *Journal of Bacteriology*, *185*(4), 1423–1431. http://doi.org/10.1128/JB.185.4.1423

Meeske, A. J., Sham, L.-T., Kimsey, H., Koo, B.-M., Gross, C. a., Bernhardt, T. G., & Rudner, D. Z. (2015). MurJ and a novel lipid II flippase are required for cell wall biogenesis in Bacillus subtilis. *Proceedings of the National Academy of Sciences*, *112*(20), 201504967. http://doi.org/10.1073/pnas.1504967112

Meisner, J., Montero Llopis, P., Sham, L. T., Garner, E., Bernhardt, T. G., & Rudner, D. Z. (2013). FtsEX is required for CwlO peptidoglycan hydrolase activity during cell wall elongation in Bacillus subtilis. *Molecular Microbiology*, *89*(6), 1069–1083. http://doi.org/10.1111/mmi.12330

Mengin-Lecreulx, D., Van Heijenoort, J., & Park, J. T. (1996). Identification of the mpl gene encoding UDP-N-acetylmuramate: L-alanyl-gamma-D-glutamyl-meso-diaminopimelate ligase in Escherichia coli and its role in recycling of cell wall peptidoglycan. *Journal of Bacteriology*, *178*(18), 5347–5352.

Mercer, K. L. N., & Weiss, D. S. (2002). The Escherichia coli cell division protein FtsW is required to recruit its cognate transpeptidase, FtsI (PBP3), to the division site. *Journal of Bacteriology*, *184*(4), 904–912. http://doi.org/10.1128/jb.184.4.904-912.2002

Meroueh, S. O., Bencze, K. Z., Hesek, D., Lee, M., Fisher, J. F., Stemmler, T. L., & Mobashery, S. (2006). Three-dimensional structure of the bacterial cell wall peptidoglycan. *Proceedings of the National Academy of Sciences of the United States of America*, *103*(12), 4404–4409. http://doi.org/10.1073/pnas.0510182103

Mertens, H. D. T., & Svergun, D. I. (2010). Structural characterization of proteins and complexes using small-angle X-ray solution scattering. *Journal of Structural Biology*, *172*(1), 128–41. http://doi.org/10.1016/j.jsb.2010.06.012

Mizyed, S., Oddone, A., Byczynski, B., Hughes, D. W., & Berti, P. J. (2005). UDP-N-acetylmuramic Acid (UDP-MurNAc) Is a Potent Inhibitor of MurA (Enolpyruvyl-UDP-GlcNAc synthase). *Biochemistry*, *44*, 4011–4017.

Modi, S. R., Collins, J. J., & Relman, D. A. (2014). Antibiotics and the gut microbiota. *The Journal of Clinical Investigation*, *124*(10), 4212–8. http://doi.org/10.1172/JCI72333.The

Mohammadi, T., Karczmarek, A., Crouvoisier, M., Bouhss, A., Mengin-Lecreulx, D., & Den Blaauwen, T. (2007). The essential peptidoglycan glycosyltransferase MurG forms a complex with proteins involved in lateral envelope growth as well as with proteins involved in cell division in Escherichia coli. *Molecular Microbiology*, *65*(4), 1106–1121. http://doi.org/10.1111/j.1365-2958.2007.05851.x

Mohammadi, T., Sijbrandi, R., Lutters, M., Verheul, J., Martin, N. I., Den Blaauwen, T., … Breukink, E. (2014). Specificity of the transport of lipid II by FtsW in Escherichia coli. *Journal of Biological Chemistry*, *289*(21), 14707–14718. http://doi.org/10.1074/jbc.M114.557371

Mohammadi, T., van Dam, V., Sijbrandi, R., Vernet, T., Zapun, A., Bouhss, A., … Breukink, E. (2011). Identification of FtsW as a transporter of lipid-linked cell wall precursors across the membrane. *The EMBO Journal*, *30*(8), 1425–1432. http://doi.org/10.1038/emboj.2011.61

Moraes, G. L., Gomes, G. C., Monteiro de Sousa, P. R., Alves, C. N., Govender, T., Kruger, H. G., … Lameira, J. (2015). Structural and functional features of enzymes of Mycobacterium tuberculosis peptidoglycan biosynthesis as targets for drug development. *Tuberculosis*, *95*(2), 95–111.

http://doi.org/10.1016/j.tube.2015.01.006

Morimoto, Y., & Minamino, T. (2014). Structure and Function of the Bi-Directional Bacterial Flagellar Motor. *Biomolecules*, *4*(1), 217–234. http://doi.org/10.3390/biom4010217

Mosyak, L., Zhang, Y., Glasfeld, E., Haney, S., Stahl, M., Seehra, J., & Somers, W. S. (2000). The bacterial cell-division protein ZipA and its interaction with an FtsZ fragment revealed by X-ray crystallography. *The EMBO Journal*, *19*(13), 3179–3191. http://doi.org/10.1093/emboj/19.13.3179

Mouilleron, S., Badet-Denisot, M. A., Badet, B., & Golinelli-Pimpaneau, B. (2011). Dynamics of glucosamine-6-phosphate synthase catalysis. *Archives of Biochemistry and Biophysics*, *505*(1), 1–12. http://doi.org/10.1016/j.abb.2010.08.008

Moy, F. J., Glasfeld, E., Mosyak, L., & Powers, R. (2000). Solution structure of ZipA, a crucial component of Escherichia coli cell division. *Biochemistry*, *39*(31), 9146–9156. http://doi.org/10.1021/bi0009690

Moynihan, P. J., & Clarke, A. J. (2010). O-acetylation of peptidoglycan in gram-negative bacteria: Identification and characterization of peptidoglycan O-acetyltransferase in Neisseria gonorrhoeae. *Journal of Biological Chemistry*, *285*(17), 13264–13273. http://doi.org/10.1074/jbc.M110.107086

Moynihan, P. J., & Clarke, A. J. (2013). Assay for peptidoglycan O-acetyltransferase: A potential new antibacterial target. *Analytical Biochemistry*, *439*(2), 73–79. http://doi.org/10.1016/j.ab.2013.04.022

Moynihan, P. J., & Clarke, A. J. (2014a). Mechanism of Action of Peptidoglycan O-Acetyltransferase B Involves a Ser-His-Asp Catalytic Triad. *Biochemistry*, *53*, 6243–6251.

Moynihan, P. J., & Clarke, A. J. (2014b). Substrate specificity and kinetic characterization of peptidoglycan O-acetyltransferase B from Neisseria gonorrhoeae. *Journal of Biological Chemistry*, *289*(24), 16748–16760. http://doi.org/10.1074/jbc.M114.567388

Moynihan, P. J., Sychantha, D., & Clarke, A. J. (2014). Chemical biology of peptidoglycan acetylation and deacetylation. *Bioorganic Chemistry*, *54*, 44–50. http://doi.org/10.1016/j.bioorg.2014.03.010Minireview

Mukherjee, a., & Lutkenhaus, J. (1994). Guanine nucleotide-dependent assembly of FtsZ into filaments. *Journal of Bacteriology*, *176*(9), 2754–2758.

Müller, H., Etzkorn, M., & Henrike, H. (2013). Solid-State NMR Spectroscopy of Proteins. In *Modern NMR Methodology* (Vol. 11, pp. 121–156). Springer. http://doi.org/10.1007/128

Mullins, L. S., Zawadzkeg, E., Walsh, T., & Raushelall, M. (1990). Kinetic evidence for the formation of D-Alanyl phosphate in the mechanism of D-Alanyl-D-Alanine ligase. *The Journal of Biological Chemistry*, *265*(16), 8993–8998.

Nakayama, H., Kurokawa, K., & Lee, B. L. (2012). Lipoproteins in bacteria: Structures and biosynthetic pathways. *FEBS Journal*. http://doi.org/10.1111/febs.12041

Nanninga, N. (1991). Cell division and peptidoglycan assembly in Escherichia coli. *Molecular Microbiology*, *5*(4), 791–795. http://doi.org/10.1111/j.1365-2958.1991.tb00751.x

Nelson, D. E., & Young, K. D. (2000). Penicillin Binding Protein 5 Affects Cell Diameter , Contour , and Morphology of Escherichia coli Penicillin Binding Protein 5 Affects Cell Diameter , Contour , and Morphology of Escherichia coli. *Journal of Bacteriology*, *182*(6), 1714–1721. http://doi.org/10.1128/JB.182.6.1714-1721.2000.Updated

Nelson, D. E., & Young, K. D. (2001). Contributions of PBP 5 and dd-Carboxypeptidase Penicillin Binding Proteins to Maintenance of Cell Shape in Escherichia coli Contributions of PBP 5 and DD -Carboxypeptidase Penicillin Binding Proteins to Maintenance of Cell Shape in Escherichia coli. *Journal of Bacteriology*, *183*(10), 3055–3064. http://doi.org/10.1128/JB.183.10.3055

Neuhaus, F. C. (1962). The enzymatic synthesis of D-alanyl-D-alanine. I. Purification and properties of D-alanyl-D-alanine synthetase. *The Journal of Biological Chemistry*, *237*(3), 778–786.

Nikolaidis, I., Favini-Stabile, S., & Dessen, A. (2014). Resistance to antibiotics targeted to the bacterial cell wall. *Protein Science*, *23*(3), 243–259. http://doi.org/10.1002/pro.2414

Nogales, E., Downing, K. H., Amos, L. a, & Löwe, J. (1998). Tubulin and FtsZ form a distinct family of GTPases. *Nature Structural Biology*, *5*(6), 451–458. http://doi.org/10.1038/nsb0698-451

O'Connell, M. R., Gamsjaeger, R., & Mackay, J. P. (2009). The structural analysis of protein-protein interactions by NMR spectroscopy. *Proteomics*, *9*(23), 5224–5232. http://doi.org/10.1002/pmic.200900303

Oberbarnscheidt, L., Taylor, E. J., Davies, G. J., & Gloster, T. M. (2007). Structure of a carbohydrate esterase from Bacillus anthracis. *Proteins: Structure, Function and Genetics*, *66*(1), 250–252. http://doi.org/10.1002/prot.21217

Oliva, M. a., Trambaiolo, D., & Löwe, J. (2007). Structural Insights into the Conformational Variability of FtsZ. *Journal of Molecular Biology*, *373*(5), 1229–1242. http://doi.org/10.1016/j.jmb.2007.08.056

Olshausen, P. V., Defeu Soufo, H. J., Wicker, K., Heintzmann, R., Graumann, P. L., & Rohrbach, A. (2013). Superresolution imaging of dynamic MreB filaments in B. subtilis - A multiple-motor-driven transport? *Biophysical Journal*, *105*(5), 1171–1181. http://doi.org/10.1016/j.bpj.2013.07.038

Orf, G. S., & Blankenship, R. E. (2013). Chlorosome antenna complexes from green photosynthetic bacteria. *Photosynthesis Research*, *116*(2-3), 315–331. http://doi.org/10.1007/s11120-013-9869-3

Osawa, M., Anderson, D. E., & Erickson, H. P. (2008). Reconstitution of contractile FtsZ rings in liposomes. *Science*, *320*(5877), 792–794. http://doi.org/10.1126/science.1154520

Paradis-Bleau, C., Markovski, M., Uehara, T., Lupoli, T. J., Walker, S., Kahne, D. E., & Bernhardt, T. G. (2010). Lipoprotein cofactors located in the outer membrane activate bacterial cell wall polymerases. *Cell*, *143*(7), 1110–20. http://doi.org/10.1016/j.cell.2010.11.037

Park, H. J., Kang, K. M., Dybvig, K., Lee, B. L., Jung, Y. W., & Lee, I. H. (2013). Interaction of cationic antimicrobial peptides with Mycoplasma pulmonis. *FEBS Letters*, *587*(20), 3321–3326. http://doi.org/10.1016/j.febslet.2013.08.016

Park, J. T., Raychaudhuri, D., Li, H., Mengin-lecreulx, D., & Normark, S. (1998). MppA , a Periplasmic Binding Protein Essential for Import of the Bacterial Cell Wall Peptidel-Alanyl- γ -d-Glutamyl- meso MppA , a Periplasmic Binding Protein Essential for Import of the Bacterial Cell Wall Peptide L -Alanyl- % - D -Glutamyl- meso -Diamin. *Journal of Bacteriology*, *180*(5), 1215–1223.

Park, J. T., & Uehara, T. (2008). How bacteria consume their own exoskeletons (turnover and recycling of cell wall peptidoglycan). *Microbiology and Molecular Biology Reviews*, *72*(2), 211–227. http://doi.org/10.1128/MMBR.00027-07

Parsons, L. M., Grishaev, A., & Bax, A. (2008). The periplasmic domain of TolR from Haemophilus influenzae forms a dimer with a large hydrophobic groove: NMR solution structure and comparison to SAXS Data. *Biochemistry*, *47*(10), 3131–3142. http://doi.org/10.1021/bi702283x

Parsons, L. M., Lin, F., & Orban, J. (2006). Peptidoglycan recognition by Pal, an outer membrane lipoprotein. *Biochemistry*, *45*(7), 2122–2128. http://doi.org/10.1021/bi052227i

Patti, G. J., Chen, J., Schaefer, J., & Gross, M. L. (2008). Characterization of Structural Variations in the Peptidoglycan of Vancomycin-Susceptible Enterococcus faecium: Understanding Glycopeptide-Antibiotic Binding Sites Using Mass Spectrometry. *Journal of the American Society for Mass Spectrometry*, *19*(10), 1467–1475. http://doi.org/10.1016/j.jasms.2008.06.020

Pazos, M., Natale, P., & Vicente, M. (2013). A specific role for the ZipA protein in cell division: Stabilization of the FtsZ protein. *Journal of Biological Chemistry*, *288*(5), 3219–3226. http://doi.org/10.1074/jbc.M112.434944

Pedersen, C. M., Figueroa-Perez, I., Boruwa, J., Lindner, B., Ulmer, A. J., Zähringer, U., & Schmidt, R. R.

(2010). Synthesis of the core structure of the lipoteichoic acid of streptococcus pneumoniae. *Chemistry - A European Journal*, *16*(42), 12627–12641. http://doi.org/10.1002/chem.201001204

Pennartz, A., Généreux, C., Parquet, C., Mengin-Lecreulx, D., & Joris, B. (2009). Substrate-induced inactivation of the Escherichia coli AmiD N-acetylmuramoyl-L-alanine amidase highlights a new strategy to inhibit this class of enzyme. *Antimicrobial Agents and Chemotherapy*, *53*(7), 2991–2997. http://doi.org/10.1128/AAC.01520-07

Percy, M. G., & Gründling, A. (2014). Lipoteichoic Acid Synthesis and Function in Gram-Positive Bacteria. *Annual Review of Microbiology*, (April), 81–100. http://doi.org/10.1146/annurev-micro-091213-112949

Perdih, A., Hrast, M., Pureber, K., Barreteau, H., Grdadolnik, S. G., Kocjan, D., … Wolber, G. (2015). Furan-based benzene mono- and dicarboxylic acid derivatives as multiple inhibitors of the bacterial Mur ligases (MurC–MurF): experimental and computational characterization. *Journal of Computer-Aided Molecular Design*, *29*(6), 541–560. http://doi.org/10.1007/s10822-015-9843-6

Perdih, A., Kotnik, M., Hodoscek, M., & Solmajer, T. (2007). Targeted molecular dynamics simulation studies of binding and conformational changes in E. coli MurD. *Proteins*, *68*(1), 243–54. http://doi.org/10.1002/prot.21374

Peters, N. T., Dinh, T., & Bernhardt, T. G. (2011). A Fail-safe mechanism in the septal ring assembly pathway generated by the sequential recruitment of cell separation amidases and their activators. *Journal of Bacteriology*, *193*(18), 4973–4983. http://doi.org/10.1128/JB.00316-11

Petoukhov, M. V., & Svergun, D. I. (2013). Applications of small-angle X-ray scattering to biomacromolecular solutions. *International Journal of Biochemistry and Cell Biology*, *45*(2), 429–437. http://doi.org/10.1016/j.biocel.2012.10.017

Pichoff, S., Du, S., & Lutkenhaus, J. (2015). The bypass of ZipA by overexpression of FtsN requires a previously unknown conserved FtsN motif essential for FtsA – FtsN interaction supporting a model in which FtsA monomers recruit late cell division proteins to the Z ring. *Molecular Microbiology*, *95*(February), 971–987. http://doi.org/10.1111/mmi.12907

Pichoff, S., & Lutkenhaus, J. (2002). Unique and overlapping roles for ZipA and FtsA in septal ring assembly in Escherichia coli. *EMBO Journal*, *21*(4), 685–693. http://doi.org/10.1093/emboj/21.4.685

Pichoff, S., & Lutkenhaus, J. (2005). Tethering the Z ring to the membrane through a conserved membrane targeting sequence in FtsA. *Molecular Microbiology*, *55*(6), 1722–1734. http://doi.org/10.1111/j.1365-2958.2005.04522.x

Pichoff, S., Shen, B., Sullivan, B., & Lutkenhaus, J. (2012). FtsA mutants impaired for self-interaction bypass ZipA suggesting a model in which FtsA's self-interaction competes with its ability to recruit downstream division proteins. *Molecular Microbiology*, *83*(1), 151–167. http://doi.org/10.1111/j.1365-2958.2011.07923.x

Pilhofer, M., Aistleitner, K., Biboy, J., Gray, J., Kuru, E., Hall, E., … Jensen, G. J. (2013). Discovery of chlamydial peptidoglycan reveals bacteria with murein sacculi but without FtsZ. *Nature Communications*, *4*, 2856. http://doi.org/10.1038/ncomms3856

Pisabarro, A. G., de Pedro, M. A., & Vazquez, D. (1985). Structural modifications in the peptidoglycan of Escherichia coli associated with changes in the state of growth of the culture. *Journal of Bacteriology*, *161*(1), 238–242.

Popp, D., Narita, A., Maeda, K., Fujisawa, T., Ghoshdastider, U., Iwasa, M., … Robinson, R. C. (2010). Filament structure, organization, and dynamics in MreB sheets. *Journal of Biological Chemistry*, *285*(21), 15858–15865. http://doi.org/10.1074/jbc.M109.095901

Potluri, L. P., Kannan, S., & Young, K. D. (2012). ZipA is required for FtsZ-dependent preseptal peptidoglycan synthesis prior to invagination during cell division. *Journal of Bacteriology*, *194*(19), 5334–5342.

http://doi.org/10.1128/JB.00859-12

Pucci, M. J., Thanassi, J. A., Ho, H.-T., Falk, P. J., & Dougherty, T. J. (1995). Staphylococcus haemolyticus contains two D-glutamic acid biosynthetic activities, a glutamate racemase and a D-amino acid transaminase. *Journal of Bacteriology*, *177*(2), 336–342.

Puchner, E. M., & Gaub, H. E. (2009). Force and function: probing proteins with AFM-based force spectroscopy. *Current Opinion in Structural Biology*, *19*(5), 605–614. http://doi.org/10.1016/j.sbi.2009.09.005

Purdy, M. D., Bennett, B. C., McIntire, W. E., Khan, A. K., Kasson, P. M., & Yeager, M. (2014). Function and dynamics of macromolecular complexes explored by integrative structural and computational biology. *Current Opinion in Structural Biology*, *27*, 138–148. http://doi.org/10.1016/j.sbi.2014.08.006

Putker, F., Bos, M. P., & Tommassen, J. (2015). Transport of lipopolysaccharide to the Gram-negative bacterial cell surface. *FEMS Microbiology Reviews*, (February), 1–18. http://doi.org/10.1093/femsre/fuv026

Rae, B. D., Long, B. M., Whitehead, L. F., Förster, B., Badger, M. R., & Price, G. D. (2013). Cyanobacterial carboxysomes: Microcompartments that facilitate CO 2 fixation. *Journal of Molecular Microbiology and Biotechnology*, *23*(4-5), 300–307. http://doi.org/10.1159/000351342

RayChaudhuri, D. (1999). ZipA is a MAP-Tau homolog and is essential for structural integrity of the cytokinetic FtsZ ring during bacterial cell division. *EMBO Journal*, *18*(9), 2372–2383. http://doi.org/10.1093/emboj/18.9.2372

Raymond, J. B., Mahapatra, S., Crick, D. C., & Pavelka, M. S. (2005). Identification of the namH Gene, Encoding the Hydroxylase Responsible for the N-Glycolylation of the Mycobacterial Peptidoglycan. *Journal of Biological Chemistry*, *280*(1), 326–333. http://doi.org/10.1074/jbc.M411006200

Reddy, M. (2007). Role of FtsEX in cell division of Escherichia coli: Viability of ftsEX mutants is dependent on functional SufI or high osmotic strength. *Journal of Bacteriology*, *189*(1), 98–108. http://doi.org/10.1128/JB.01347-06

Reimold, C., Defeu Soufo, H. J., Dempwolff, F., & Graumann, P. L. (2013). Motion of variable-length MreB filaments at the bacterial cell membrane influences cell morphology. *Molecular Biology of the Cell*, *24*(15), 2340–9. http://doi.org/10.1091/mbc.E12-10-0728

Rico, A. I., García-Ovalle, M., Mingorance, J., & Vicente, M. (2004). Role of two essential domains of Escherichia coli FtsA in localization and progression of the division ring. *Molecular Microbiology*, *53*(5), 1359–1371. http://doi.org/10.1111/j.1365-2958.2004.04245.x

Rico, A. I., Krupka, M., & Vicente, M. (2013). In the beginning, escherichia coli assembled the proto-ring: An initial phase of division. *Journal of Biological Chemistry*. http://doi.org/10.1074/jbc.R113.479519

Rocaboy, M., Herman, R., Sauvage, E., Remaut, H., Moonens, K., Terrak, M., … Kerff, F. (2013). The crystal structure of the cell division amidase amic reveals the fold of the AMIN domain, a new peptidoglycan binding domain. *Molecular Microbiology*, *90*(2), 267–277. http://doi.org/10.1111/mmi.12361

Romberg, L., Simon, M., & Erickson, H. P. (2001). Polymerization of FtsZ, a bacterial homolog of tubulin. Is assembly cooperative? *Journal of Biological Chemistry*, *276*(15), 11743–11753. http://doi.org/10.1074/jbc.M009033200

Romeis, T., & Höltje, J. V. (1994). Penicillin-binding protein 7/8 of Escherichia coli is a DD-endopeptidase. *European Journal of Biochemistry*, *224*, 597–604.

Ruiz, N. (2008). Bioinformatics identification of MurJ (MviN) as the peptidoglycan lipid II flippase in Escherichia coli. *Proceedings of the National Academy of Sciences of the United States of America*, *105*(40), 15553–15557. http://doi.org/10.1073/pnas.0808352105

Sahin, E., & Roberts, C. J. (2012). Size-exclusion chromatography with multi-angle light scattering for elucidating protein aggregation mechanisms. *Methods in Molecular Biology*, *899*, 403–423.

http://doi.org/10.1007/978-1-61779-921-1_25

Salje, J., Gayathri, P., & Löwe, J. (2010). The ParMRC system: molecular mechanisms of plasmid segregation by actin-like filaments. *Nature Reviews Microbiology*, *8*(10), 683–692. http://doi.org/10.1038/nrmicro2425

Salje, J., van den Ent, F., de Boer, P. A. J., & Löwe, J. (2011). Direct Membrane Binding by Bacterial Actin MreB. *Molecular Cell*, *43*(3), 478–487. http://doi.org/10.1016/j.molcel.2011.07.008

Samaluru, H., Saisree, L., & Reddy, M. (2007). Role of SufI (FtsP) in cell division of Escherichia coli: Evidence for its involvement in stabilizing the assembly of the divisome. *Journal of Bacteriology*, *189*(22), 8044–8052. http://doi.org/10.1128/JB.00773-07

Saraste, M., Sibbald, P. R., & Wittinghofer, a. (1990). The P-loop--a common motif in ATP- and GTP-binding proteins. *Trends in Biochemical Sciences*, *15*(11), 430–434. http://doi.org/10.1016/0968-0004(90)90281-F

Sauvage, E., Duez, C., Herman, R., Kerff, F., Petrella, S., Anderson, J. W., … Charlier, P. (2007). Crystal Structure of the Bacillus subtilis Penicillin-binding Protein 4a, and its Complex with a Peptidoglycan Mimetic Peptide. *Journal of Molecular Biology*, *371*(2), 528–539. http://doi.org/10.1016/j.jmb.2007.05.071

Sauvage, E., Kerff, F., Terrak, M., Ayala, J. A., & Charlier, P. (2008). The penicillin-binding proteins: structure and role in peptidoglycan biosynthesis. *FEMS Microbiology Reviews*, *32*(2), 234–258. http://doi.org/10.1111/j.1574-6976.2008.00105.x

Schanda, P., Triboulet, S., Laguri, C., Bougault, C. M., Ayala, I., Callon, M., … Simorre, J.-P. (2014). Atomic model of a cell-wall cross-linking enzyme in complex with an intact bacterial peptidoglycan. *Journal of the American Chemical Society*, *136*, 17852–17860. http://doi.org/10.1021/ja5105987

Schiffer, G., & Höltje, J. V. (1999). Cloning and characterization of PBP 1C, a third member of the multimodular class A penicillin-binding proteins of Escherichia coli. *Journal of Biological Chemistry*, *274*(45), 32031–32039. http://doi.org/10.1074/jbc.274.45.32031

Schlag, M., Biswas, R., Krismer, B., Kohler, T., Zoll, S., Yu, W., … Götz, F. (2010). Role of staphylococcal wall teichoic acid in targeting the major autolysin Atl. *Molecular Microbiology*, *75*(4), 864–873. http://doi.org/10.1111/j.1365-2958.2009.07007.x

Schmidt, D. M. Z., Hubbard, B. K., & Gerlt, J. A. (2001). Evolution of enzymatic activities in the enolase superfamily: Functional assignment of unknown proteins in bacillus subtilis and Escherichia coli as L-Ala-D/L-Glu epimerases. *Biochemistry*, *40*(51), 15707–15715. http://doi.org/10.1021/bi011640x

Schmidt, K. L., Peterson, N. D., Kustusch, R. J., Wissel, M. C., Graham, B., Phillips, G. J., & Weiss, D. S. (2004). A predicted ABC transporter, FtsEX , is needed for cell division in Escherichia coli. *Journal of Bacteriology*, *186*(3), 785–793. http://doi.org/10.1128/JB.186.3.785

Schönbrunn, E., Svergun, D. I., Amrhein, N., & Koch, M. H. J. (1998). Studies on the conformational changes in the bacterial cell wall biosynthetic enzyme UDP-N-acetylglucosamine enolpyruvyltransferase. *European Journal of Biochemistry*, *253*, 406–412.

Schroeder, U., Henrich, B., Fink, J., & Plapp, R. (1994). Peptidase D of Escherichia coli K-12, a metallopeptidase of low substrate specificity. *FEMS Microbiology Letters*, *123*(1-2), 153–159.

Shaik, M. M., Cendron, L., Percudani, R., & Zanotti, G. (2011). The structure of Helicobacter pylori HP0310 reveals an atypical peptidoglycan deacetylase. *PLoS ONE*, *6*(4), 1–8. http://doi.org/10.1371/journal.pone.0019207

Sham, L.-T., Barendt, S. M., Kopecky, K. E., & Winkler, M. E. (2011). Essential PcsB putative peptidoglycan hydrolase interacts with the essential FtsXSpn cell division protein in Streptococcus pneumoniae D39. *Proceedings of the National Academy of Sciences*, *108*(45), E1061–E1069. http://doi.org/10.1073/pnas.1108323108

Sham, L.-T., Butler, E. K., Lebar, M. D., Kahne, D., Bernhardt, T. G., & Ruiz, N. (2014). MurJ is the flippase of lipid-linked precursors for peptidoglycan biogenesis. *Science*, *345*(6193), 220–222. http://doi.org/10.1126/science.1254522

Shaw, J. P., Petsko, G. a, & Ringe, D. (1997). Determination of the structure of alanine racemase from Bacillus stearothermophilus at 1.9-A resolution. *Biochemistry*, *36*(6), 1329–1342. http://doi.org/10.1021/bi961856c

Shen, Y., Delaglio, F., Cornilescu, G., & Bax, A. (2009). TALOS+: A hybrid method for predicting protein backbone torsion angles from NMR chemical shifts. *Journal of Biological Chemistry*, *44*(4), 213–223. Retrieved from http://www.ncbi.nlm.nih.gov/pubmed/18554561

Shenouda, N. S., Yong, P., Schaefer, J., & Wilson, G. E. (1996). A simple solid-state NMR method for determining peptidoglycan crosslinking in Bacillus subtilis. *Biochimica et Biophysica Acta - General Subjects*, *1289*(2), 217–220. http://doi.org/10.1016/0304-4165(95)00177-8

Shi, Y. (2014). A Glimpse of Structural Biology through X-Ray Crystallography. *Cell*, *159*(5), 995–1014. http://doi.org/10.1016/j.cell.2014.10.051

Shiomi, D., Sakai, M., & Niki, H. (2008). Determination of bacterial rod shape by a novel cytoskeletal membrane protein. *The EMBO Journal*, *27*(23), 3081–3091. http://doi.org/10.1038/emboj.2008.234

Si, F., Busiek, K., Margolin, W., & Sun, S. X. (2013). Organization of FtsZ filaments in the bacterial division ring measured from polarized fluorescence microscopy. *Biophysical Journal*, *105*(9), 1976–1986. http://doi.org/10.1016/j.bpj.2013.09.030

Siewert, G., & Strominger, J. L. (1967). Bacitracin: an Inhibitor of the Dephosphorylation of Lipid Pyrophosphate, an Intermediate in the Biosynthesis of the Peptidoglycan of Bacterial Cell Walls*. *Proceedings of the National Academy of Sciences of the United States of America*, *57*(3), 767–773. http://doi.org/10.1073/pnas.57.3.767

Silhavy, T. J., Kahne, D., & Walker, S. (2010). The bacterial cell envelope. *Cold Spring Harbor Perspectives in Biology*, *2*(5), a000414. http://doi.org/10.1101/cshperspect.a000414

Silver, L. L. (2013). Viable screening targets related to the bacterial cell wall. *Annals of the New York Academy of Sciences*, *1277*(1), 29–53. http://doi.org/10.1111/nyas.12006

Sinz, A., Arlt, C., Chorev, D., & Sharon, M. (2015). Chemical Cross-Linking and Native Mass Spectrometry: A Fruitful Combination for Structural Biology. *Protein Science*, *24*, 1193–1209. http://doi.org/10.1002/pro.2696

Smith, C. a. (2006). Structure, Function and Dynamics in the mur Family of Bacterial Cell Wall Ligases. *Journal of Molecular Biology*, *362*(4), 640–655. http://doi.org/10.1016/j.jmb.2006.07.066

Sobhanifar, S., King, D. T., & Strynadka, N. C. J. (2013). Fortifying the wall: Synthesis, regulation and degradation of bacterial peptidoglycan. *Current Opinion in Structural Biology*, *23*(5), 695–703. http://doi.org/10.1016/j.sbi.2013.07.008

Söderström, B., Skoog, K., Blom, H., Weiss, D. S., von Heijne, G., & Daley, D. O. (2014). Disassembly of the divisome in Escherichia coli: Evidence that FtsZ dissociates before compartmentalization. *Molecular Microbiology*, *92*(1), 1–9. http://doi.org/10.1111/mmi.12534

Sova, M., Kovač, A., Turk, S., Hrast, M., Blanot, D., & Gobec, S. (2009). Phosphorylated hydroxyethylamines as novel inhibitors of the bacterial cell wall biosynthesis enzymes MurC to MurF. *Bioorganic Chemistry*, *37*(6), 217–222. http://doi.org/10.1016/j.bioorg.2009.09.001

Spratt, B. G., & Pardee, A. B. (1975). Penicillin-binding proteins and cell shape in E. coli. *Nature*, *254*(5500), 516–517. http://doi.org/10.1038/254516a0

Starr, J., Brown, M. F., Aschenbrenner, L., Caspers, N., Che, Y., Gerstenberger, B. S., … Han, S. (2014). Siderophore receptor-mediated uptake of lactivicin analogues in gram-negative bacteria. *Journal of*

Medicinal Chemistry, *57*(9), 3845–3855. http://doi.org/10.1021/jm500219c

Steele, V. R., Bottomley, A. L., Garcia-Lara, J., Kasturiarachchi, J., & Foster, S. J. (2011). Multiple essential roles for EzrA in cell division of Staphylococcus aureus. *Molecular Microbiology*, *80*(2), 542–555. http://doi.org/10.1111/j.1365-2958.2011.07591.x

Steiner, W., Liu, G., Donachie, W. D., & Kuempel, P. (1999). The cytoplasmic domain of FtsK protein is required for resolution of chromosome dimers. *Molecular Microbiology*, *31*(2), 579–583. http://doi.org/10.1046/j.1365-2958.1999.01198.x

Strahl, H., Bürmann, F., & Hamoen, L. W. (2014). The actin homologue MreB organizes the bacterial cell membrane. *Nature Communications*, *5*, 3442. http://doi.org/10.1038/ncomms4442

Strauss, M. P., Liew, A. T. F., Turnbull, L., Whitchurch, C. B., Monahan, L. G., & Harry, E. J. (2012). 3D-SIM Super Resolution Microscopy Reveals a Bead-Like Arrangement for FtsZ and the Division Machinery: Implications for Triggering Cytokinesis. *PLoS Biology*, *10*(9). http://doi.org/10.1371/journal.pbio.1001389

Stricker, J., Maddox, P., Salmon, E. D., & Erickson, H. P. (2002). Rapid assembly dynamics of the Escherichia coli FtsZ-ring demonstrated by fluorescence recovery after photobleaching. *Proceedings of the National Academy of Sciences of the United States of America*, *99*(5), 3171–3175. http://doi.org/10.1073/pnas.052595099

Strych, U., & Benedik, M. J. (2002). Mutant analysis shows that alanine racemases from Pseudomonas aeruginosa and Escherichia coli are dimeric. *Journal of Bacteriology*, *184*(15), 4321–4325. http://doi.org/10.1128/JB.184.15.4321-4325.2002

Stubbs, K. a., Balcewich, M., Mark, B. L., & Vocadlo, D. J. (2007). Small molecule inhibitors of a glycoside hydrolase attenuate inducible AmpC-mediated beta-lactam resistance. *Journal of Biological Chemistry*, *282*(29), 21382–21391. http://doi.org/10.1074/jbc.M700084200

Sun, Y., Rombola, C., Jyothikumar, V., & Periasamy, A. (2013). Förster Resonance Energy Transfer Microscopy and Spectroscopy for Localizing Protein – Protein Interactions in Living Cells. *Cytometry Part A, Early View*(2), 1–14. http://doi.org/10.1002/cyto.22321

Sung, M.-T., Lai, Y.-T., Huang, C.-Y., Chou, L.-Y., Shih, H.-W., Cheng, W.-C., … Ma, C. (2009). Crystal structure of the membrane-bound bifunctional transglycosylase PBP1b from Escherichia coli. *Proceedings of the National Academy of Sciences of the United States of America*, *106*(22), 8824–9. http://doi.org/10.1073/pnas.0904030106

Swulius, M. T., & Jensen, G. J. (2012). The helical mreb cytoskeleton in Escherichia coli MC1000/pLE7 is an artifact of the N-terminal yellow fluorescent protein tag. *Journal of Bacteriology*, *194*(23), 6382–6386. http://doi.org/10.1128/JB.00505-12

Szwedziak, P., & Löwe, J. (2013). Do the divisome and elongasome share a common evolutionary past? *Current Opinion in Microbiology*. http://doi.org/10.1016/j.mib.2013.09.003

Szwedziak, P., Wang, Q., Bharat, T. a M., Tsim, M., & Löwe, J. (2014). Architecture of the ring formed by the tubulin homologue FtsZ in bacterial cell division. *eLife*, *3*, 1–22. http://doi.org/10.7554/eLife.04601

Szwedziak, P., Wang, Q., Freund, S. M., & Löwe, J. (2012). FtsA forms actin-like protofilaments. *The EMBO Journal*, *31*(10), 2249–2260. http://doi.org/10.1038/emboj.2012.76

Tarry, M., Arends, S. J. R., Roversi, P., Piette, E., Sargent, F., Berks, B. C., … Lea, S. M. (2009). The Escherichia coli Cell Division Protein and Model Tat Substrate SufI (FtsP) Localizes to the Septal Ring and Has a Multicopper Oxidase-Like Structure. *Journal of Molecular Biology*, *386*(2), 504–519. http://doi.org/10.1016/j.jmb.2008.12.043

Tatar, L. D., Marolda, C. L., Polischuk, A. N., van Leeuwen, D., & Valvano, M. a. (2007). An Escherichia coli undecaprenyl-pyrophosphate phosphatase implicated in undecaprenyl phosphate recycling. *Microbiology*, *153*(8), 2518–2529. http://doi.org/10.1099/mic.0.2007/006312-0

Templin, M. F., Ursinus, A., & Höltje, J. V. (1999). A defect in cell wall recycling triggers autolysis during the stationary growth phase of Escherichia coli. *EMBO Journal*, *18*(15), 4108–4117. http://doi.org/10.1093/emboj/18.15.4108

TerBush, A. D., Yoshida, Y., & Osteryoung, K. W. (2013). FtsZ in chloroplast division: Structure, function and evolution. *Current Opinion in Cell Biology*, *25*(4), 461–470. http://doi.org/10.1016/j.ceb.2013.04.006

Terrak, M., Ghosh, T. K., Van Heijenoort, J., Van Beeumen, J., Lampilas, M., Aszodi, J., … Nguyen-Distèche, M. (1999). The catalytic, glycosyl transferase and acyl transferase modules of the cell wall peptidoglycan-polymerizing penicillin-binding protein 1b of Escherichia coli. *Molecular Microbiology*, *34*(2), 350–364. http://doi.org/10.1046/j.1365-2958.1999.01612.x

Terrak, M., Sauvage, E., Derouaux, A., Dehareng, D., Bouhss, A., Breukink, E., … Nguyen-Distèche, M. (2008). Importance of the conserved residues in the peptidoglycan glycosyltransferase module of the class A penicillin-binding protein 1b of Escherichia coli. *Journal of Biological Chemistry*, *283*(42), 28464–28470. http://doi.org/10.1074/jbc.M803223200

Tipper, D. J., & Strominger, J. L. (1965). Mechanism of action of penicillins: a proposal based on their structural similarity to acyl-D-alanyl-D-alanine. *Proceedings of the National Academy of Sciences of the United States of America*, *54*(4), 1133–1141. http://doi.org/10.1073/pnas.54.4.1133

Tortora, G. C., Funke, B. R., & Case, C. L. (2012). *Microbiology: An introduction*. (Pearson Education, Ed.) (11th ed.). Benjamin Cummings.

Treuner-Lange, a., Macia, E., Guzzo, M., Hot, E., Faure, L. M., Jakobczak, B., … Mignot, T. (2015). The small G-protein MglA connects to the MreB actin cytoskeleton at bacterial focal adhesions. *The Journal of Cell Biology*, *210*(2). http://doi.org/10.1083/jcb.201412047

Triassi, A. J., Wheatley, M. S., Savka, M. a., Gan, H. M., Dobson, R. C. J., & Hudson, A. O. (2014). L,L-diaminopimelate aminotransferase (DapL): a putative target for the development of narrow-spectrum antibacterial compounds. *Frontiers in Microbiology*, *5*(September), 1–10. http://doi.org/10.3389/fmicb.2014.00509

Triboulet, S., Bougault, C. M., Laguri, C., Hugonnet, J.-E., Arthur, M., & Simorre, J.-P. (2015). Acyl acceptor recognition by Enterococcus faecium L,D-transpeptidase Ldt fm. *Molecular Microbiology*, n/a–n/a. http://doi.org/10.1111/mmi.13104

Triboulet, S., Dubée, V., Lecoq, L., Bougault, C., Mainardi, J. L., Rice, L. B., … Arthur, M. (2013). Kinetic Features of L,D-Transpeptidase Inactivation Critical for β-Lactam Antibacterial Activity. *PLoS ONE*, *8*(7), 1–9. http://doi.org/10.1371/journal.pone.0067831

Tsang, M.-J., & Bernhardt, T. G. (2015). A role for the FtsQLB complex in cytokinetic ring activation revealed by an ftsL allele that accelerates division. *Molecular Microbiology*, *95*(January), n/a–n/a. http://doi.org/10.1111/mmi.12905

Tugarinov, V. (2013). Indirect use of deuterium in solution NMR studies of protein structure and hydrogen bonding. *Progress in Nuclear Magnetic Resonance Spectroscopy*, *77*, 49–68. http://doi.org/10.1016/j.pnmrs.2013.08.001

Turner, R. D., Hurd, A. F., Cadby, A., Hobbs, J. K., & Foster, S. J. (2013). Cell wall elongation mode in Gram-negative bacteria is determined by peptidoglycan architecture. *Nature Communications*, *4*, 1496. http://doi.org/10.1038/ncomms2503

Turner, R. D., Ratcliffe, E. C., Wheeler, R., Golestanian, R., Hobbs, J. K., & Foster, S. J. (2010). Peptidoglycan architecture can specify division planes in Staphylococcus aureus. *Nature Communications*, *1*(3), 26. http://doi.org/10.1038/ncomms1025

Turner, R. D., Vollmer, W., & Foster, S. J. (2014). Different walls for rods and balls: The diversity of peptidoglycan. *Molecular Microbiology*, *91*(5), 862–874. http://doi.org/10.1111/mmi.12513

Typas, A., Banzhaf, M., Gross, C. a, & Vollmer, W. (2012). From the regulation of peptidoglycan synthesis to bacterial growth and morphology. *Nature Reviews Microbiology*, *10*(2), 123–36. http://doi.org/10.1038/nrmicro2677

Typas, A., Banzhaf, M., van den Berg van Saparoea, B., Verheul, J., Biboy, J., Nichols, R. J., … Vollmer, W. (2010). Regulation of peptidoglycan synthesis by outer-membrane proteins. *Cell*, *143*(7), 1097–1109. http://doi.org/10.1016/j.cell.2010.11.038

Uehara, T., & Park, J. T. (2003). Identification of MpaA, an amidase in Escherichia coli that hydrolyzes the gamma-D-glutamyl-meso-diaminopimelate bond in murein peptides. *Journal of Bacteriology*, *185*(2), 679–682. http://doi.org/10.1128/JB.185.2.679-682.2003

Uehara, T., & Park, J. T. (2004). The N-Acetyl-d-Glucosamine Kinase of Escherichia coli and Its Role in Murein Recycling The N-Acetyl- D -Glucosamine Kinase of Escherichia coli and Its Role in Murein Recycling. *Journal of Bacteriology*, *186*(21), 7273–7279. http://doi.org/10.1128/JB.186.21.7273

Uehara, T., & Park, J. T. (2007). An anhydro-N-acetylmuramyl-L-alanine amidase with broad specificity tethered to the outer membrane of Escherichia coli. *Journal of Bacteriology*, *189*(15), 5634–5641. http://doi.org/10.1128/JB.00446-07

Uehara, T., Parzych, K. R., Dinh, T., & Bernhardt, T. G. (2010). Daughter cell separation is controlled by cytokinetic ring-activated cell wall hydrolysis. *The EMBO Journal*, *29*(8), 1412–1422. http://doi.org/10.1038/emboj.2010.36

Uehara, T., Suefuji, K., Valbuena, N., Donegan, M., Park, J. T., & Meehan, B. (2005). Recycling of the Anhydro-N -Acetylmuramic Acid Derived from Cell Wall Murein Involves a Two-Step Conversion to N Recycling of the Anhydro- N -Acetylmuramic Acid Derived from Cell Wall Murein Involves a Two-Step Conversion to N -Acetylglucosamine-Phosphat. *Journal of Bacteriology*, *187*(11), 3643–3649. http://doi.org/10.1128/JB.187.11.3643

Ursell, T. S., Nguyen, J., Monds, R. D., Colavin, A., Billings, G., Ouzounov, N., … Huang, K. C. (2014). Rod-like bacterial shape is maintained by feedback between cell curvature and cytoskeletal localization. *Proceedings of the National Academy of Sciences of the United States of America*. http://doi.org/10.1073/pnas.1317174111

Ursinus, A., van den Ent, F., Brechtel, S., de Pedro, M. A., Höltje, J. V., Löwe, J., & de Pedro, M. A. (2004). Murein (Peptidoglycan) Binding Property of the Essential Cell Division Protein FtsN from Escherichia coli. *Journal of Bacteriology*, *186*(20), 6728–6737. http://doi.org/10.1128/JB.186.20.6728

van Asselt, E. J., Thunnissen, A.-M. W. H., & Dijkstra, B. W. (1999). High resolution crystal structures of the Escherichia coli lytic transglycosylase Slt70 and its complex with a peptidoglycan fragment. *Journal of Molecular Biology*, *291*(4), 877–898. http://doi.org/10.1006/jmbi.1999.3013

van Dam, V., Sijbrandi, R., Kol, M., Swiezewska, E., De Kruijff, B., & Breukink, E. (2007). Transmembrane transport of peptidoglycan precursors across model and bacterial membranes. *Molecular Microbiology*, *64*(4), 1105–1114. http://doi.org/10.1111/j.1365-2958.2007.05722.x

van den Bedem, H., & Fraser, J. S. (2015). Integrative, dynamic structural biology at atomic resolution—it's about time. *Nature Methods*, *12*(4), 307–318. http://doi.org/10.1038/nmeth.3324

van den Ent, F., Amos, L. A., & Löwe, J. (2001). Prokaryotic origin of the actin cytoskeleton. *Nature*, *413*(6851), 39–44. http://doi.org/10.1038/35092500

van den Ent, F., Izoré, T., Bharat, T. a M., Johnson, C. M., & Löwe, J. (2014). Bacterial actin MreB forms antiparallel double filaments. *eLife*, *2014*(3), 1–22. http://doi.org/10.7554/eLife.02634

van den Ent, F., Johnson, C. M., Persons, L., de Boer, P. A. J., & Löwe, J. (2010). Bacterial actin MreB assembles in complex with cell shape protein RodZ. *The EMBO Journal*, *29*(6), 1081–1090. http://doi.org/10.1038/emboj.2010.9

van Den Ent, F., Leaver, M., Bendezú, F. O., Errington, J., de Boer, P. A. J., & Löwe, J. (2006). Dimeric structure of the cell shape protein MreC and its functional implications. *Molecular Microbiology*, *62*(6), 1631–1642. http://doi.org/10.1111/j.1365-2958.2006.05485.x

van den Ent, F., & Löwe, J. (2000). Crystal structure of the cell division protein FtsA from Thermotoga maritima. *The EMBO Journal*, *19*(20), 5300–5307. http://doi.org/10.1093/emboj/19.20.5300

van den Ent, F., Vinkenvleugel, T. M. F., Ind, A., West, P., Veprintsev, D., Nanninga, N., … Löwe, J. (2008). Structural and mutational analysis of the cell division protein FtsQ. *Molecular Microbiology*, *68*(1), 110–123. http://doi.org/10.1111/j.1365-2958.2008.06141.x

van der Ploeg, R., Verheul, J., Vischer, N. O. E., Alexeeva, S., Hoogendoorn, E., Postma, M., … den Blaauwen, T. (2013). Colocalization and interaction between elongasome and divisome during a preparative cell division phase in Escherichia coli. *Molecular Microbiology*, *87*(5), 1074–87. http://doi.org/10.1111/mmi.12150

van Heijenoort, J. (2001). Recent advances in the formation of the bacterial peptidoglycan monomer unit. *Natural Product Reports*, *18*(5), 503–519. http://doi.org/10.1039/a804532a

van Heijenoort, J. (2011). Peptidoglycan Hydrolases of Escherichia coli. *Microbiology and Molecular Biology Reviews*, *75*(4), 636–663. http://doi.org/10.1128/MMBR.00022-11

van Straaten, K. E., Dijkstra, B. W., Vollmer, W., & Thunnissen, A. M. W. H. (2005). Crystal structure of MltA from Escherichia coli reveals a unique lytic transglycosylase fold. *Journal of Molecular Biology*, *352*(5), 1068–1080. http://doi.org/10.1016/j.jmb.2005.07.067

van Teeffelen, S., Wang, S., Furchtgott, L., Huang, K. C., Wingreen, N. S., Shaevitz, J. W., & Gitai, Z. (2011). The bacterial actin MreB rotates, and rotation depends on cell-wall assembly. *Proceedings of the National Academy of Sciences*, *108*(38), 15822–15827. http://doi.org/10.1073/pnas.1108999108

van Teeseling, M. C. F., Mesman, R. J., Kuru, E., Espaillat, A., Cava, F., Brun, Y. V., … van Niftrik, L. (2015). Anammox Planctomycetes have a peptidoglycan cell wall. *Nature Communications*, *6*(May), 6878. http://doi.org/10.1038/ncomms7878

van Zundert, G. C. P., Rodrigues, J. P. G. L. M., Trellet, M., Schmitz, C., Kastritis, P. L., Karaca, E., … Bonvin, a. M. J. J. (2015). The HADDOCK2.2 web server: User-friendly integrative modeling of biomolecular complexes. *Journal of Molecular Biology*. http://doi.org/10.1016/j.jmb.2015.09.014

Vaughan, S., Wickstead, B., Gull, K., & Addinall, S. G. (2004). Molecular Evolution of FtsZ Protein Sequences Encoded Within the Genomes of Archaea, Bacteria, and Eukaryota. *Journal of Molecular Evolution*, *58*(1), 19–39. http://doi.org/10.1007/s00239-003-2523-5

Vázquez-laslop, N., Lee, H., Hu, R., & Alex, A. (2001). Molecular Sieve Mechanism of Selective Release of Cytoplasmic Proteins by Osmotically Shocked Escherichia coli Molecular Sieve Mechanism of Selective Release of Cytoplasmic Proteins by Osmotically Shocked Escherichia coli. *Journal of Bacteriology*, *183*(8), 2399–2404. http://doi.org/10.1128/JB.183.8.2399

Vega, D., & Ayala, J. a. (2006). The DD-carboxypeptidase activity encoded by pbp4B is not essential for the cell growth of Escherichia coli. *Archives of Microbiology*, *185*(1), 23–27. http://doi.org/10.1007/s00203-005-0057-5

Veyrier, F. J., Williams, A. H., Mesnage, S., Schmitt, C., Taha, M. K., & Boneca, I. G. (2013). De-O-acetylation of peptidoglycan regulates glycan chain extension and affects in vivo survival of Neisseria meningitidis. *Molecular Microbiology*, *87*(5), 1100–1112. http://doi.org/10.1111/mmi.12153

Vicente, M., Gomez, M. J., & Ayala, J. a. (1998). Regulation of transcription of cell division genes in the Escherichia coli dcw cluster. *Cellular and Molecular Life Sciences*, *54*(4), 317–324.

Vijayalakshmi, J., Akerley, B. J., & Saper, M. a. (2008). Structure of YraM, a protein essential for growth of Haemophilus influenzae. *Proteins*, *73*(1), 204–17. http://doi.org/10.1002/prot.22033

Vincent, F., Yates, D., Garman, E., Davies, G. J., & Brannigan, J. a. (2004). The three-dimensional structure of the N-acetylglucosamine-6-phosphate deacetylase, NagA, from Bacillus subtilis: A member of the urease superfamily. *Journal of Biological Chemistry*, *279*(4), 2809–2816. http://doi.org/10.1074/jbc.M310165200

Vischer, N. O. E., Verheul, J., Postma, M., van den Berg van Saparoea, B., Galli, E., Natale, P., … den Blaauwen, T. (2015). Cell age dependent concentration of Escherichia coli divisome proteins analyzed with ImageJ and ObjectJ. *Frontiers in Microbiology*, *6*(June), 1–18. http://doi.org/10.3389/fmicb.2015.00586

Vocadlo, D. J., Davies, G. J., Laine, R., & Withers, S. G. (2001). Catalysis by hen egg-white lysozyme proceeds via a covalent intermediate. *Nature*, *412*(6849), 835–838. http://doi.org/10.1038/35090602

Vollmer, W. (2008). Structural variation in the glycan strands of bacterial peptidoglycan. *FEMS Microbiology Reviews*, *32*(2), 287–306. http://doi.org/10.1111/j.1574-6976.2007.00088.x

Vollmer, W., Blanot, D., & de Pedro, M. A. (2008). Peptidoglycan structure and architecture. *FEMS Microbiology Reviews*, *32*(2), 149–67. http://doi.org/10.1111/j.1574-6976.2007.00094.x

Vollmer, W., & Höltje, J. V. (2004). The Architecture of the Murein (Peptidoglycan) in Gram-Negative Bacteria : Vertical Scaffold or Horizontal Layer (s)? *Journal of Bacteriology*, *186*(18), 5978–5987. http://doi.org/10.1128/JB.186.18.5978

Vollmer, W., Joris, B., Charlier, P., & Foster, S. J. (2008). Bacterial peptidoglycan (murein) hydrolases. *FEMS Microbiology Reviews*, *32*(2), 259–86. http://doi.org/10.1111/j.1574-6976.2007.00099.x

Vollmer, W., & Seligman, S. J. (2010). Architecture of peptidoglycan: more data and more models. *Trends in Microbiology*, *18*(2), 59–66. http://doi.org/10.1016/j.tim.2009.12.004

Vollmer, W., Von Rechenberg, M., & Höltje, J. V. (1999). Demonstration of molecular interactions between the murein polymerase PBP1B, the lytic transglycosylase MltA, and the scaffolding protein MipA of Escherichia coli. *Journal of Biological Chemistry*, *274*(10), 6726–6734. http://doi.org/10.1074/jbc.274.10.6726

von Rechenberg, M., Ursinus, A., & Höltje, J. V. (1996). Affinity chromatography as a means to study multienzyme complexes involved in murein synthesis. *Microbial Drug Resistance*, *2*(1), 155–157. http://doi.org/10.1089/mdr.1996.2.155

Vötsch, W., & Templin, M. F. (2000). Characterization of a β-N-acetylglucosaminidase of Escherichia coli and elucidation of its role in muropeptide recycling and β-lactamase induction. *Journal of Biological Chemistry*, *275*(50), 39032–39038. http://doi.org/10.1074/jbc.M004797200

Wang, G., Olczak, A., Forsberg, L. S., & Maier, R. J. (2009). Oxidative stress-induced Peptidoglycan deacetylase in Helicobacter pylori. *Journal of Biological Chemistry*, *284*(11), 6790–6800. http://doi.org/10.1074/jbc.M808071200

Wang, L., & Lutkenhaus, J. (1998). FtsK is an essential cell division protein that is localized to the septum and induced as part of the SOS response. *Molecular Microbiology*, *29*(3), 731–740. http://doi.org/10.1046/j.1365-2958.1998.00958.x

Wasserman, S. a., Walsh, C. T., & Botstein, D. (1983). Two alanine racemase genes in Salmonella typhimurium that differ in structure and function. *Journal of Bacteriology*, *153*(3), 1439–1450.

Watanabe, A., Yoshimura, T., Mikami, B., Hayashi, H., Kagamiyama, H., & Esaki, N. (2002). Reaction mechanism of alanine racemase from Bacillus stearothermophilus: X-ray crystallographic studies of the enzyme bound with N-(5′-phosphopyridoxyl)alanine. *Journal of Biological Chemistry*, *277*(21), 19166–19172. http://doi.org/10.1074/jbc.M201615200

Weadge, J. T., & Clarke, A. J. (2006). Identification and characterization of O-acetylpeptidoglycan esterase: A novel enzyme discovered in Neisseria gonorrhoeae. *Biochemistry*, *45*(3), 839–851. http://doi.org/10.1021/bi051679s

Weadge, J. T., Pfeffer, J. M., & Clarke, A. J. (2005). Identification of a new family of enzymes with potential O-acetylpeptidoglycan esterase activity in both Gram-positive and Gram-negative bacteria. *BMC Microbiology*, *5*, 49. http://doi.org/10.1186/1471-2180-5-49

Weidenmaier, C., & Peschel, A. (2008). Teichoic acids and related cell-wall glycopolymers in Gram-positive physiology and host interactions. *Nature Reviews Microbiology*, *6*(4), 276–287. http://doi.org/10.1038/nrmicro1861

Weiss, D. S. (2015). Last but not least: new insights into how FtsN triggers constriction during Escherichia coli cell division. *Molecular Microbiology*, *95*(6), 903–909. http://doi.org/10.1111/mmi.12925

Weiss, D. S., Pogliano, K., Carson, M., Guzman, L. M., Fraipont, C., Nguyen-Distèche, M., … Beckwith, J. (1997). Localization of the Escherichia coli cell division protein Ftsl (PBP3) to the division site and cell pole. *Molecular Microbiology*, *25*(4), 671–681.

Wheeler, R., Mesnage, S., Boneca, I. G., Hobbs, J. K., & Foster, S. J. (2011). Super-resolution microscopy reveals cell wall dynamics and peptidoglycan architecture in ovococcal bacteria. *Molecular Microbiology*, *82*(5), 1096–1109. http://doi.org/10.1111/j.1365-2958.2011.07871.x

White, C. L., Kitich, A., & Gober, J. W. (2010). Positioning cell wall synthetic complexes by the bacterial morphogenetic proteins MreB and MreD. *Molecular Microbiology*, *76*(3), 616–633. http://doi.org/10.1111/j.1365-2958.2010.07108.x

White, R. J., & Pasternak, C. a. (1967). The purification and properties of N-acetylglucosamine 6-phosphate deacetylase from Escherichia coli. *The Biochemical Journal*, *105*(1), 121–125.

Wientjes, F. B., Woldringh, C. L., & Nanninga, N. (1991). Amount of Peptidoglycan in Cell Walls of Gram-Negative Bacteria. *J Bacteriol*, *173*(23), 7684–7691.

Wild, J., Hennig, J., Lobocka, M., Walczak, W., & Klopotowski, T. (1985). Identification of the dadX gene coding for the predominant isozyme of alanine racemase in Escherichia coli K12. *MGG Molecular & General Genetics*, *198*(2), 315–322. http://doi.org/10.1007/BF00383013

Williams, A. H., Veyrier, F. J., Bonis, M., Michaud, Y., Raynal, B., Taha, M.-K., … Boneca, I. G. (2014). Visualization of a substrate-induced productive conformation of the catalytic triad of the *Neisseria meningitidis* peptidoglycan *O* -acetylesterase reveals mechanistic conservation in SGNH esterase family members. *Acta Crystallographica Section D Biological Crystallography*, *70*(10), 2631–2639. http://doi.org/10.1107/S1399004714016770

Williams, K. B., Yahashiri, A., Arends, S. J. R., Popham, D. L., Fowler, C. A., & Weiss, D. S. (2013). Nuclear magnetic resonance solution structure of the peptidoglycan-binding SPOR domain from Escherichia coli DamX: Insights into septal localization. *Biochemistry*, *52*(4), 627–639. http://doi.org/10.1021/bi301609e

Witty, M., Sanz, C., Shah, A., Grossmann, J. G., Mizuquchi, K., Perham, R. N., & Luisi, B. (2002). Structure of the periplasmic domain of Pseudomonas aeruginosa TolA: Evidence for an evolutionary relationship with the TonB transporter protein. *EMBO Journal*, *21*(16), 4207–4218. http://doi.org/10.1093/emboj/cdf417

Woese, C. R., Kandler, O., & Wheelis, M. L. (1990). Towards a natural system of organisms: proposal for the domains Archaea, Bacteria, and Eucarya. *Proceedings of the National Academy of Sciences of the United States of America*, *87*(12), 4576–4579. http://doi.org/10.1073/pnas.87.12.4576

Xia, G., Kohler, T., & Peschel, A. (2010). The wall teichoic acid and lipoteichoic acid polymers of Staphylococcus aureus. *International Journal of Medical Microbiology*, *300*(2-3), 148–154. http://doi.org/10.1016/j.ijmm.2009.10.001

Yahashiri, A., Jorgenson, M. A., & Weiss, D. S. (2015). Bacterial SPOR domains are recruited to septal peptidoglycan by binding to glycan strands that lack stem peptides. *Proceedings of the National Academy of Sciences*. http://doi.org/10.1073/pnas.1508536112

binding cassette transporter-like complex governs cell-wall hydrolysis at the bacterial cytokinetic ring. *Proceedings of the National Academy of Sciences of the United States of America*. http://doi.org/10.1073/pnas.1107780108

Yang, D. C., Tan, K., Joachimiak, A., & Bernhardt, T. G. (2012). A conformational switch controls cell wall-remodelling enzymes required for bacterial cell division. *Molecular Microbiology*, *85*(4), 768–781. http://doi.org/10.1111/j.1365-2958.2012.08138.x

Yang, J. C., van den Ent, F., Neuhaus, D., Brevier, J., & Löwe, J. (2004). Solution structure and domain architecture of the divisome protein FtsN. *Molecular Microbiology*, *52*(3), 651–660. http://doi.org/10.1111/j.1365-2958.2004.03991.x

Yao, X., Jericho, M., Pink, D., & Beveridge, T. (1999). Thickness and elasticity of gram-negative murein sacculi measured by atomic force microscopy. *Journal of Bacteriology*, *181*(22), 6865–6875.

Yoon, J., Matsuo, Y., Matsuda, S., Kasai, H., & Yokota, A. (2010). Cerasicoccus maritimus sp. nov. and Cerasicoccus frondis sp. nov., two peptidoglycan-less marine verrucomicrobial species, and description of Verrucomicrobia phyl. nov., nom. rev. *The Journal of General and Applied Microbiology*, *56*(3), 213–222. http://doi.org/10.2323/jgam.56.213

Yousif, S. Y., Broome-Smith, J. K., & Spratt, B. G. (1985). Lysis of Escherichia coli by beta-lactam antibiotics: deletion analysis of the role of penicillin-binding proteins 1A and 1B. *Journal of General Microbiology*, *131*(10), 2839–2845. http://doi.org/10.1099/00221287-131-10-2839

Yuan, Y., Barrett, D., Zhang, Y., Kahne, D., Sliz, P., & Walker, S. (2007). Crystal structure of a peptidoglycan glycosyltransferase suggests a model for processive glycan chain synthesis. *Proceedings of the National Academy of Sciences of the United States of America*, *104*(13), 5348–5353. http://doi.org/10.1073/pnas.0701160104

Zapun, A., Contreras-Martel, C., & Vernet, T. (2008). Penicillin-binding proteins and β-lactam resistance. *FEMS Microbiology Reviews*, *32*(2), 361–385. http://doi.org/10.1111/j.1574-6976.2007.00095.x

Zapun, A., Philippe, J., Abrahams, K. a., Signor, L., Roper, D. I., Breukink, E., & Vernet, T. (2013). In vitro reconstitution of peptidoglycan assembly from the gram-positive pathogen streptococcus pneumoniae. *ACS Chemical Biology*, *8*(12), 2688–2696. http://doi.org/10.1021/cb400575t

Zawadzke, L. E., Bugg, T. D., & Walsh, C. T. (1991). Existence of two D-alanine:D-alanine ligases in Escherichia coli: cloning and sequencing of the ddlA gene and purification and characterization of the DdlA and DdlB enzymes. *Biochemistry*, *30*(6), 1673–1682. http://doi.org/10.1021/bi00220a033

Zeng, X., & Lin, J. (2013). Beta-lactamase induction and cell wall metabolism in Gram-negative bacteria. *Frontiers in Microbiology*, *4*(MAY), 1–9. http://doi.org/10.3389/fmicb.2013.00128

Zijderveld, C. a L., Aarsman, M. E. G., Den Blaauwen, T., & Nanninga, N. (1991). Penicillin-binding protein 1B of Escherichia coli exists in dimeric forms. *Journal of Bacteriology*, *173*(18), 5740–5746.

Zuber, B., Chami, M., Houssin, C., Dubochet, J., Griffiths, G., & Daffé, M. (2008). Direct visualization of the outer membrane of mycobacteria and corynebacteria in their native state. *Journal of Bacteriology*, *190*(16), 5672–5680. http://doi.org/10.1128/JB.01919-07

Annexes

Annex 1: Protein-protein interactions reported in bacterial cell wall synthesis complexes

Table A.1: Non-exhaustive list of protein-protein interactions reported in the elongasome.

Proteins	Category	Partners	Techniques[a]	Organism[b]	References
MreB	Cytoskeletal-like protein	MurD	SPR	*T. maritima*	Favini-Stabile et al., Environ. Microbiol., 2013
		MurE	Dot blot, SPR	*T. maritima*	Favini-Stabile et al., Environ. Microbiol., 2013
		MurF	Dot blot, SPR	*T. maritima*	Favini-Stabile et al., Environ. Microbiol., 2013
		MurG	1: Immuno-precipitation 2: Bacterial two-hybrid 3: Dot blot, SPR	1: *E. coli* 2: *C. crescentus* 3: *T. maritima*	1: Mohammadi et al., Mol. Microbiol., 2007 2: White et al., Mol. Microbiol., 2010 3: Favini-Stabile et al., Environ. Microbiol., 2013
		MraY	Immuno-precipitation	*E. coli*	Mohammadi et al., Mol. Microbiol., 2007
		MreB (to form filaments)	Pull-down, X-ray crystallography, EM	*T. maritima*	van den Ent et al., Nature, 2001
		MreC	Bacterial two-hybrid	*E. coli*	Kruse et al., Mol. Microbiol., 2005
		RodZ	1: Bacterial two-hybrid 2: Pelleting assay, ITC, X-ray crystallography	1: *E. coli* 2: *T. maritima*	1: Bendezú et al., EMBO J., 2009 2: van den Ent et al., EMBO J., 2010
		FtsZ	Bacterial two-hybrid, *in vivo* cross-linking	*E. coli*	Fenton & Gerdes, EMBO J., 2013
MreC	Inner-membrane sub-complex	MreB	Bacterial two-hybrid	*E. coli*	Kruse et al., Mol. Microbiol., 2005
		MreC	X-ray crystallography, Bacterial two-hybrid	*B. subtilis*	van den Ent et al., Mol. Microbiol., 2006
		MreD	Bacterial two-hybrid	*E. coli*	Kruse et al., Mol. Microbiol., 2005
		RodZ	Bacterial two-hybrid	*E. coli*	Bendezú et al., EMBO J., 2009
		HMW PBPs class A and B	1: Affinity chromatography, labelled penicillin binding assay 2: Bacterial two-hybrid	1: *C. crescentus* 2: *B. subtilis*	1: Divakaruni et al., Proc. Natl. Acad. Sci. USA, 2005 2: van den Ent et al., Mol. Microbiol., 2006
		PBP2	Yeast two-hybrid, affinity chromatography, cross-liking, SPR, AUC, SAXS	*H. pylori*	El Ghachi et al., Mol.Microbiol. 2011

MreD	Inner-membrane sub-complex	MraY	Bacterial two-hybrid	*C. crescentus*	White et al., Mol. Microbiol., 2010
		MurG	Bacterial two-hybrid	*C. crescentus*	White et al., Mol. Microbiol., 2010
		MreC	Bacterial two-hybrid	*E. coli*	Kruse et al., Mol. Microbiol., 2005
		RodZ	Bacterial two-hybrid	*C. crescentus*	White et al., Mol. Microbiol., 2010
RodA	Putative fippase	RodZ	Bacterial two-hybrid	*C. crescentus*	White et al., Mol. Microbiol., 2010
RodZ	Inner-membrane sub-complex	MreB	1: Bacterial two-hybrid 2: Pelleting assay, ITC, X-ray crystallography	1: *E. coli* 2: *T. maritima*	1: Bendezú et al., EMBO J., 2009 2: van den Ent et al., EMBO J., 2010
		MreC	Bacterial two-hybrid	*E. coli*	Bendezú et al., EMBO J., 2009
		MreD	Bacterial two-hybrid	*C. crescentus*	White et al., Mol. Microbiol., 2010
		RodA	Bacterial two-hybrid	*C. crescentus*	White et al., Mol. Microbiol., 2010
		RodZ	1,2: Bacterial two-hybrid	1: *E. coli* 2: *C. crescentus*	1: Bendezú et al., EMBO J., 2009 2: White et al., Mol. Microbiol., 2010
PBP1A	Peptidoglycan synthesis	PBP2	Affinity chromatography, bacterial two-hybrid, *in vivo* cross-linking	*E. coli*	Banzhaf et al., Mol. Microbiol., 2012
		LpoA	1,2: Affinity chromatography 1: Immunoprecipitation after *in vivo* cross-linking 2: Pull-down	1, 2: *E. coli*	1: Typas et al., Cell, 2012 2: Paradis-Bleau et al., Cell, 2012
PBP2	Peptidoglycan synthesis	PBP1A	Affinity chromatography, bacterial two-hybrid, *in vivo* cross-linking	*E. coli*	Banzhaf et al., Mol. Microbiol., 2012
		PBP3	FRET	*E. coli*	van der Ploeg et al., Mol. Microbiol., 2013
		Slt70	Affinity chromatography	*E. coli*	von Rechenberg et al., Microb. Drug Resist., 1996
		MreC	Yeast two-hybrid, affinity chromatography, cross-liking, SPR, AUC, SAXS	*H. pylori*	El Ghachi et al., Mol.Microbiol. 2011
LpoA	Regulator of peptidoglycan synthesis	PBP1A	1,2: Affinity chromatography 1: Immunoprecipitation after *in vivo* cross-	1, 2: *E. coli*	1: Typas et al., Cell, 2012 2: Paradis-Bleau et al., Cell, 2012

			linking 2: Pull-down		

[a]: AUC: Analytical UltraCentriugation; EM: Electron Microscopy; FRET: Fluorescence Resonance Transfer; SAXS: Small Angle X-ray Scattering; SPR: Surface Plasmon Rsonances.
[b]: *B. subtilis*, *C. crescentus*, *E. coli*, *H. pylori*, *T. maritima*, stand for *Bacillus subtilis*, *Caulobacter crescentus*, *Escherichia coli*, *Helicobacter pylori*, *Thermotoga maritima*, respectively.

Table A.2: Non-exhaustive list of protein-protein interactions reported concerning members of the divisome and of the Tol-Pal and associated systems.

Proteins	Category	Partners	Techniques[a]	Organism[b]	References
FtsZ	Cytoskeletal-like protein	FtsZ	1: Sedimentation assay, light scattering, EM	*E. coli*	Bramhill & Thompson, Proc. Natl. Acad. Sci. USA, 1994
		ZipA	1: Affinity blotting 2: Yeast two-hybrid 3: *In vivo* point mutations 4: X-ray crystallography	1, 2, 3, 4: *E. coli*	1: Hale et al., J. Bacteriol., 1997 2: Liu et al., Mol. Microbiol., 1999 3: Ma & Margolin, J. Bacteriol, 1999 4: Mosyak et al., EMBO J., 2000
		FtsA	1: Yeast two-hybrid 2: Yeast two-hybrid, *in vivo* point mutations 3: X-ray crystallography	1: *C. crescentus* 2: *E. coli* 3: *T. maritima*	1: Din et al., Mol. Microbiol., 1998 2: Ma & Margolin, J. Bacteriol, 1999 3: Szwedziak et al., EMBO J., 2012
		ZapA	1: Affinity chromatography 2: Pelleting assay 3: FRET	1: *B. subtilis* 2: *P. aeruginosa* 3: *E. coli*	1: Gueiros-Filho & Losick, Genes Dev., 2002 2: Low et al., J. Mol. Biol., 2004 3: Alexeeva et al., Mol. Microbiol., 2010
		ZapC	1: Yeast protein-interaction platform assay, sedimentation assay 2: Yeast two-hybrid, sedimentation assay	1, 2: *E. coli*	1: Durand-Heredia et al., J. Bacteriol., 2011 2: Hale et al., J. Bacteriol, 2011
		ZapD	Yeast protein-interaction platform assay, sedimentation assay	*E. coli*	Durand-Heredia et al., J. Bacteriol., 2012
		ZapE	Bacterial two-hybrid, pulldown	*E. coli*	Marteyn et al., mBio, 2014
		FtsE	Co-immunoprecipitation, co-purification	*E. coli*	Corbin et al., J. Bacteriol., 2007
		FtsK	1, 2: Bacterial two-hybrid	1, 2: *E. coli*	1: Di Lallo et al., Microbiology, 2003 2: Grenga et al., FEMS Microbiol. Lett., 2008
		FtsQ	Bacterial two-hybrid, co-immunoprecipitation	*S. pneumoniae*	Maggi et al., Microbiology, 2008
		FtsL	Bacterial two-hybrid, co-immunoprecipitation	*S. pneumoniae*	Maggi et al., Microbiology, 2008
		FtsB	Bacterial two-hybrid, co-immunoprecipitation	*S. pneumoniae*	Maggi et al., Microbiology, 2008

		FtsW	Bacterial two-hybrid, co-immunoprecipitation	*S. pneumoniae*	Maggi et al., Microbiology, 2008
		MreB	Bacterial two-hybrid, *in vivo* cross-linking	*E. coli*	Fenton & Gerdes, EMBO J., 2013
ZipA	Membrane anchoring of the Z-ring	FtsZ	1: Affinity blotting 2: Yeast two-hybrid 3: *In vivo* point mutations 4: X-ray crystallography	1, 2, 3, 4: *E. coli*	1: Hale et al., J. Bacteriol., 1997 2: Liu et al., Mol. Microbiol., 1999 3: Ma & Margolin, J. Bacteriol, 1999 4: Mosyak et al., EMBO J., 2000
		ZipA	1: Bacterial two-hybrid 2: *in vivo* cross-linking	1,2: *E. coli*	1: Di Lallo et al., Microbiology, 2003 2: Skoog & Daley, Biochemistry, 2012
FtsA	Membrane anchoring of the Z-ring	FtsZ	1: Yeast two-hybrid 2: Yeast two-hybrid, *in vivo* point mutations 3: X-ray crystallography	1: *C. crescentus* 2: *E. coli* 3: *T. maritima*	1: Din et al., Mol. Microbiol., 1998 2: Ma & Margolin, J. Bacteriol, 1999 3: Szwedziak et al., EMBO J., 2012
		FtsA	1: Bacterial two-hybrid 2: X-ray crystallography, EM	1: *E. coli* 2: *T. maritima*	1: Di Lallo et al., Microbiology, 2003 2: Szwedziak et al., EMBO J., 2012
		FtsK	Bacterial two-hybrid, co-immunoprecipitation	*S. pneumoniae*	Maggi et al., Microbiology, 2008
		FtsL	Bacterial two-hybrid, co-immunoprecipitation	*S. pneumoniae*	Maggi et al., Microbiology, 2008
		FtsN	Affinity chromatography, bacterial two-hybrid, Far-Western assay	*E. coli*	Busiek et al., J. Bacteriol., 2012
ZapA	Stability of the Z-ring	FtsZ	1: Affinity chromatography 2: Pelleting assay 3: FRET	1: *B. subtilis* 2: *P. aeruginosa* 3: *E. coli*	1: Gueiros-Filho & Losick, Genes Dev., 2002 2: Low et al., J. Mol. Biol., 2004 3: Alexeeva et al., Mol. Microbiol., 2010
		ZapA	1: X-ray crystallography, SEC 2: FRET	1: *P. aeruginosa* 2: *E. coli*	1: Low et al., J. Mol. Biol., 2004 2: Alexeeva et al., Mol. Microbiol., 2010
		ZapB	Bacterial two-hybrid, ultracentrifugation	*E. coli*	Galli & Gerdes, Mol. Microbiol., 2010
		PBP3	FRET	*E. coli*	Alexeeva et al., Mol. Microbiol., 2010
		FtsN	FRET	*E. coli*	Alexeeva et al., Mol. Microbiol., 2010
ZapB	Stability of	ZapA	Bacterial two-hybrid,	*E. coli*	Galli & Gerdes, Mol.

	the Z-ring		ultracentrifugation		Microbiol., 2010
		ZapB	1: X-ray crystallography, EM 2: ultracentrifugation	1,2: *E. coli*	1: Ebersbach et al., Mol. Microbiol, 2008 2: Galli & Gerdes, Mol. Microbiol., 2010
ZapC	Stability of the Z-ring	FtsZ	1: Yeast protein-interaction platform assay, sedimentation assay 2: Yeast two-hybrid, sedimentation assay	1, 2: *E. coli*	1: Durand-Heredia et al., J. Bacteriol., 2011 2: Hale et al., J. Bacteriol, 2011
ZapD	Stability of the Z-ring	FtsZ	Yeast protein-interaction platform assay, sedimentation assay	*E. coli*	Durand-Heredia et al., J. Bacteriol., 2012
		ZapD	Yeast protein-interaction platform assay	*E. coli*	Durand-Heredia et al., J. Bacteriol., 2012
ZapE	Disassembly of the Z-ring	FtsZ	Bacterial two-hybrid, pulldown	*E. coli*	Merteyn et al., mBio, 2014
FtsE	Hydrolysis regulation	FtsZ	Co-immunoprecipitation, co-purification	*E. coli*	Corbin et al., J. Bacteriol., 2007
		FtsX	Co-immunoprecipitation, co-purification	*E. coli*	de Leeuw et al., Mol. Microbiol., 1999
FtsX	Hydrolysis regulation	FtsE	Co-immunoprecipitation, co-purification	*E. coli*	de Leeuw et al., Mol. Microbiol., 1999
		EnvC	Bacterial two-hybrid, pull-down	*E. coli*	Yang et al., Proc. Natl. Acad. Sci. USA, 2011
FtsK	Divisome maturation	FtsZ	Bacterial two-hybrid	*E. coli*	1: Di Lallo et al., Microbiology, 2003 2: Grenga et al., FEMS Microbiol. Lett., 2008
		FtsA	Bacterial two-hybrid, co-immunoprecipitation	*S. pneumoniae*	Maggi et al., Microbiology, 2008
		FtsK	Bacterial two-hybrid	*E. coli*	1: Di Lallo et al., Microbiology, 2003 2: Grenga et al., FEMS Microbiol. Lett., 2008
		FtsQ	1: Bacterial two-hybrid 2: Co-immunoprecipitation	*E. coli*	1: Di Lallo et al., Microbiology, 2003 2: D'Ulisse et al., Microbiology, 2007
		FtsL	Bacterial two-hybrid	*E. coli*	1: Di Lallo et al., Microbiology, 2003 2: Grenga et al., FEMS Microbiol. Lett., 2008
		FtsW	Bacterial two-hybrid, co-immunoprecipitation	*S. pneumoniae*	Maggi et al., Microbiology, 2008
		PBP3	Bacterial two-hybrid	*E. coli*	1: Di Lallo et al.,

					Microbiology, 2003 2: Grenga et al., FEMS Microbiol. Lett., 2008
FtsQ	Divisome maturation	FtsZ	Bacterial two-hybrid, co-immunoprecipitation	*S. pneumoniae*	Maggi et al., Microbiology, 2008
		FtsK	1: Bacterial two-hybrid 2: Co-immunoprecipitation	*E. coli*	1: Di Lallo et al., Microbiology, 2003 2: D'Ulisse et al., Microbiology, 2007
		FtsQ	Bacterial two-hybrid	*E. coli*	1: Di Lallo et al., Microbiology, 2003 2: Karimova et al., J. Bacteriol., 2005
		FtsL	1: Bacterial two-hybrid 2: Co-immunoprecipitation	*E. coli*	1: Di Lallo et al., Microbiology, 2003 2: Buddelmeijer, Mol. Microbiol., 2004
		FtsB	Co-immunoprecipitation	*E. coli*	Buddelmeijer, Mol. Microbiol., 2004
		FtsW	1: Bacterial two-hybrid 2: Co-immunoprecipitation	*E. coli*	1: Di Lallo et al., Microbiology, 2003 2: D'Ulisse et al., Microbiology, 2007
		PBP3	1: Bacterial two-hybrid 2: Co-immunoprecipitation	*E. coli*	1: Di Lallo et al., Microbiology, 2003 2: D'Ulisse et al., Microbiology, 2007
		FtsN	1: Bacterial two-hybrid 2: Co-immunoprecipitation	*E. coli*	1: Di Lallo et al., Microbiology, 2003 2: D'Ulisse et al., Microbiology, 2007
FtsL	Divisome maturation	FtsZ	Bacterial two-hybrid, co-immunoprecipitation	*S. pneumoniae*	Maggi et al., Microbiology, 2008
		FtsA	Bacterial two-hybrid, co-immunoprecipitation	*S. pneumoniae*	Maggi et al., Microbiology, 2008
		FtsK	Bacterial two-hybrid	*E. coli*	1: Di Lallo et al., Microbiology, 2003 2: Grenga et al., FEMS Microbiol. Lett., 2008
		FtsQ	1: Bacterial two-hybrid 2: Co-immunoprecipitation	*E. coli*	1: Di Lallo et al., Microbiology, 2003 2: Buddelmeijer, Mol. Microbiol., 2004
		FtsB	Co-immunoprecipitation	*E. coli*	Buddelmeijer, Mol. Microbiol., 2004
		FtsW	Bacterial two-hybrid	*E. coli*	Di Lallo et al., Microbiology, 2003
		PBP3	Bacterial two-hybrid	*E. coli*	Di Lallo et al., Microbiology, 2003
FtsB	Divisome maturation	FtsZ	Bacterial two-hybrid, co-	*S. pneumoniae*	Maggi et al., Microbiology, 2008

			immunoprecipitation		
		FtsL	Co-immunoprecipitation	*E. coli*	Buddelmeijer, Mol. Microbiol., 2004
		FtsQ	Co-immunoprecipitation	*E. coli*	Buddelmeijer, Mol. Microbiol., 2004
		FtsW	Bacterial two-hybrid, co-immunoprecipitation	*S. pneumoniae*	Maggi et al., Microbiology, 2008
FtsW	Putative fippase	FtsZ	Bacterial two-hybrid, co-immunoprecipitation	*S. pneumoniae*	Maggi et al., Microbiology, 2008
		FtsK	Bacterial two-hybrid, co-immunoprecipitation	*S. pneumoniae*	Maggi et al., Microbiology, 2008
		FtsQ	1: Bacterial two-hybrid 2: Co-immunoprecipitation	*E. coli*	1: Di Lallo et al., Microbiology, 2003 2: D'Ulisse et al., Microbiology, 2007
		FtsL	Bacterial two-hybrid	*E. coli*	Di Lallo et al., Microbiology, 2003
		FtsW	Bacterial two-hybrid, co-immunoprecipitation	*S. pneumoniae*	Maggi et al., Microbiology, 2008
		PBP1B	Bacterial two-hybrid	*E. coli*	Fraipont et al., Microbiology, 2011
		PBP3	1, 2: Bacterial two-hybrid 2: FRET, co-immunoprecipitation	*E. coli*	1: Di Lallo et al., Microbiology, 2003 2: Fraipont et al., Microbiology, 2011
		MtgA	Bacterial two-hybrid	*E. coli*	Derouaux et al., J. Bacteriol., 2008
		FtsN	1: Bacterial two-hybrid 2: FRET	*E. coli*	1: Di Lallo et al., Microbiology, 2003 2: Alexeeva et al., Mol. Microbiol., 2010
PBP1B	Peptidoglycan synthesis	FtsW	Bacterial two-hybrid	*E. coli*	Fraipont et al., Microbiology, 2011
		PBP1B	1: Western Blot 2: SPR 3: Affinity chromatography	*E. coli*	1: Zijderveld, J. Bacteriol, 1991 2: Bertsche et al., J. Biol. Chem., 2005 3: Müller et al., J. Biol. Chem., 2007
		PBP3	Affinity chromatography, SPR, bacterial two-hybrid, co-immunoprecipitation after *in vivo* cross-linking	*E. coli*	Bertsche et al., Mol. Microbiol. 2006
		LpoB	1,2: Affinity chromatography 1: Immunoprecipitation	*E. coli*	1: Typas et al., Cell, 2012 2: Paradis-Bleau et al., Cell, 2012

			after *in vivo* cross-linking 2: Pull-down 3: SPR, NMR		3: Egan, Jean et al., Proc. Natl. Acad. Sci. USA, 2014
		FtsN	Affinity chromatography, SPR, bacterial two-hybrid, co-immunoprecipitation after *in vivo* cross-linking	*E. coli*	Müller et al., J. Biol. Chem., 2007
		PBP1C	Affinity chromatography	*E. coli*	Schiffer & Höltje, J. Biol. Chem., 1999
		MipA	Affinity chromatography, SPR	*E. coli*	Vollmer et al., J. Biol. Chem., 1999
		CpoB	SPR, co-immunoprecipitation after *in vivo* cross-linking	*E. coli*	Gray et al., eLife, 2015
		TolA	Affinity chromatography, co-immunoprecipitation after *in vivo* cross-linking	*E. coli*	Gray et al., eLife, 2015
		Slt70	Affinity chromatography	*E. coli*	von Rechenberg et al., Microb. Drug Resist., 1996
		MltB	Affinity chromatography	*E. coli*	von Rechenberg et al., Microb. Drug Resist., 1996
PBP3 (FtsI)	Peptidoglycan synthesis	ZapA	FRET	*E. coli*	Alexeeva et al., Mol. Microbiol., 2010
		FtsQ	1: Bacterial two-hybrid 2: Co-immunoprecipitation	*E. coli*	1: Di Lallo et al., Microbiology, 2003 2: D'Ulisse et al., Microbiology, 2007
		FtsK	1,2: Bacterial two-hybrid	*E. coli*	1: Di Lallo et al., Microbiology, 2003 2: Grenga et al., FEMS Microbiol. Lett., 2008
		FtsW	1, 2: Bacterial two-hybrid 2: FRET, co-immunoprecipitation	*E. coli*	1: Di Lallo et al., Microbiology, 2003 2: Fraipont et al., Microbiology, 2011
		PBP1B	Affinity chromatography, SPR, bacterial two-hybrid, co-immunoprecipitation after *in vivo* cross-linking	*E. coli*	Bertsche et al., Mol. Microbiol. 2006
		PBP3	1: Bacterial two-hybrid 2: FRET	*E. coli*	1: Di Lallo et al., Microbiology, 2003 2: Fraipont et al., Microbiology, 2011

		FtsN	1: Bacterial two-hybrid 2: FRET	*E. coli*	1: Di Lallo et al., Microbiology, 2003 2: Alexeeva et al., Mol. Microbiol., 2010
		PBP1C	Affinity chromatography	*E. coli*	Schiffer & Höltje, J. Biol. Chem., 1999
		PBP2	FRET	*E. coli*	van der Ploeg et al., Mol. Microbiol., 2013
		MtgA	Bacterial two-hybrid	*E. coli*	Derouaux et al., J. Bacteriol., 2008
		Slt70	Affinity chromatography	*E. coli*	Romeis et Höltje, J. Biol. Chem., 1996
		MltB	Affinity chromatography	*E. coli*	von Rechenberg et al., Microb. Drug Resist., 1996
FtsN	Divisome maturation	ZapA	FRET	*E. coli*	Alexeeva et al., Mol. Microbiol., 2010
		FtsA	Affinity chromatography, bacterial two-hybrid, Far-Western assay	*E. coli*	Busiek et al., J. Bacteriol., 2012
		FtsQ	1: Bacterial two-hybrid 2: Co-immunoprecipitation	*E. coli*	1: Di Lallo et al., Microbiology, 2003 2: D'Ulisse et al., Microbiology, 2007
		FtsW	1: Bacterial two-hybrid 2: FRET	*E. coli*	1: Di Lallo et al., Microbiology, 2003 2: Alexeeva et al., Mol. Microbiol., 2010
		PBP1B	Affinity chromatography, SPR, bacterial two-hybrid, co-immunoprecipitation after *in vivo* cross-linking	*E. coli*	Müller et al., J. Biol. Chem., 2007
		PBP3	1: Bacterial two-hybrid 2: FRET	*E. coli*	1: Di Lallo et al., Microbiology, 2003 2: Alexeeva et al., Mol. Microbiol., 2010
		FtsN	1: Bacterial two-hybrid 2: FRET	*E. coli*	1: Di Lallo et al., Microbiology, 2003 2: Alexeeva et al., Mol. Microbiol., 2010
		MtgA	Bacterial two-hybrid	*E. coli*	Derouaux et al., J. Bacteriol., 2008
FtsP	Divisome maturation	?			
LpoB	Regulation of peptidoglycan synthesis	PBP1B	1,2: Affinity chromatography 1: Immunoprecipitation after *in vivo* cross-linking 2: Pull-down	1, 2, 3: *E. coli*	1: Typas et al., Cell, 2012 2: Paradis-Bleau et al., Cell, 2012 3: Egan, Jean et al., Proc. Natl. Acad. Sci. USA, 2014

			3: SPR, NMR		
EnvC	Hydrolysis regulation	FtsX	Bacterial two-hybrid, pull-down	*E. coli*	Yang et al., Proc. Natl. Acad. Sci. USA, 2011
		AmiA	Activity assays	*E. coli*	Uehara et al., EMBO J., 2010
		AmiB	Activity assays	*E. coli*	Uehara et al., EMBO J., 2010
AmiA	Hydrolysis	EnvC	Activity assays	*E. coli*	Uehara et al., EMBO J., 2010
AmiB	Hydrolysis	EnvC	Activity assays	*E. coli*	Uehara et al., EMBO J., 2010
AmiC	Hydrolysis	NlpD	Activity assays	*E. coli*	Uehara et al., EMBO J., 2010
MipA	Scaffold	PBP1B	Affinity chromatography, SPR	*E. coli*	Vollmer et al., J. Biol. Chem., 1999
		MltA	Affinity chromatography, SPR	*E. coli*	Vollmer et al., J. Biol. Chem., 1999
MltA	Hydrolysis	MipA	Affinity chromatography, SPR	*E. coli*	Vollmer et al., J. Biol. Chem., 1999
		PBP1C	Affinity chromatography	*E. coli*	Schiffer & Höltje, J. Biol. Chem., 1999
TolQ	Outer-membrane invagination	TolR	Immuno-precipitation	*E. coli*	Journet et al., J. Baceriol, 1999
		TolA	co-immunoprecipitation after *in vivo* cross-linking	*E. coli*	Derouichei et al., J. Biol. Chem., 1995
TolR	Outer-membrane invagination	TolQ	Immuno-precipitation	*E. coli*	Journet et al., J. Baceriol, 1999
		TolR	1: *in vivo* cross-linking, co-immunoprecipitation 2:Yeast two-hybrid 3: NMR, SAXS	1, 2: *E. coli* 3: *H.influenzae*	1: Journet et al., J. Baceriol, 1999 2: Walburger et al., Mol. Microbiol., 2002 3: Parsons et al., Biochemistry, 2008
		TolA	Co-immunoprecipitation after *in vivo* cross-linking	*E. coli*	Derouichei et al., J. Biol. Chem., 1995
TolA	Outer-membrane invagination	PBP1B	Affinity chromatography, co-immunoprecipitation after *in vivo* cross-linking	*E. coli*	Gray et al., eLife, 2015
		TolQ	Co-immunoprecipitation after *in vivo* cross-linking	*E. coli*	Derouichei et al., J. Biol. Chem., 1995
		TolR	Co-immunoprecipitation after *in vivo* cross-linking	*E. coli*	Derouichei et al., J. Biol. Chem., 1995
		TolB	1: Yeast two-hybrid	*E. coli*	1: Walburger et al., Mol.

			2: Cross-linking, ITC, NMR		Microbiol., 2002 2: Bonsor et al., EMBO J., 2009
		Pal	Affinity chromatography, co-immunoprecipitation after *in vivo* cross-linking	*E. coli*	Cascales et al., Mol. Microbiol., 2000
		CpoB	1: Yeast two-hybrid 2: SEC-MALLS, pull-down after cross-linking, ITC	*1, 2: E. coli* *2: S. enterica, X. campestris*	1: Walburger et al., Mol. Microbiol., 2002 2: Krachler et al., J. Mol. Biol., 2010
TolB	Outer-membrane invagination	TolA	1: Yeast two-hybrid 2: Cross-linking, ITC, NMR	1, 2: *E. coli*	1: Walburger et al., Mol. Microbiol., 2002 2: Bonsor et al., EMBO J., 2009
		TolB	Yeast two-hybrid	*E. coli*	Walburger et al., Mol. Microbiol., 2002
		Pal	1: Immunoprecipitation, *in vivo* cross-linking 2: Yeast two-hybrid 3: X-ray crystallography, ITC	*E. coli*	1: Bouveret et al., J. Biol. Chem., 1995 2: Walburger et al., Mol. Microbiol., 2002 3: Bonsor et al., J. Am. Chem. Soc., 2007
Pal	Outer-membrane invagination	TolA	Affinity chromatography, co-immunoprecipitation after *in vivo* cross-linking	*E. coli*	Cascales et al., Mol. Microbiol., 2000
		TolB	1: Immunoprecipitation, *in vivo* cross-linking 2: Yeast two-hybrid 3: X-ray crystallography, ITC	*E. coli*	1: Bouveret et al., J. Biol. Chem., 1995 2: Walburger et al., Mol. Microbiol., 2002 3: Bonsor et al., J. Am. Chem. Soc., 2007
CpoB (YbgF)	Coordination of peptidoglycan synthesis and outer membrane invagination	TolA	1: Yeast two-hybrid 2: SEC-MALLS, pull-down after cross-linking, ITC	*1,2: E. coli* *2: S. enterica, X. campestris*	1: Walburger et al., Mol. Microbiol., 2002 2: Krachler et al., J. Mol. Biol., 2010
		PBP1B	SPR, co-immunoprecipitation after *in vivo* cross-linking	*E. coli*	Gray et al., eLife, 2015
		CpoB	AUC, SEC-MALLS, cross-linking	*E. coli*	Krachler et al., Proteins, 2010

[a]: List of abbreviations AUC: Analytical Ultra-Centrifugation; EM: Electron Microscopy; FRET: Florescence Resonance Energy Transfer; ITC: Isothermal Titration Calorimetry; MALLS: Multiple Angle Laser Light Scattering; NMR: Nuclear Magnetic resonance; SAXS: Small Angle X-ray Scattering; SEC: Size Exclusion Chromatography; SPR: Surface Plasmon Resonance.

[b]: *B. subtilis*, *C. crescentus*, *E. coli*, *H. influenzae*, *P. aeruginosa*, *S. enterica*, *S. pneumoniae*, *T. maritima*, and *X. campestris* stand for *Bacillus subtilis*, *Caulobacter crescentus*, *Escherichia coli*, *Hemophilus influenzae*, *Pseudomonas aeruginosa*, *Salmonella enterica*, *Streptococcus pneumoniae*, *Thermotoga maritima*, and *Xanthomonas campestris*,

respectively.

Annex 2: Abstracts

Etudes par RMN de mécanismes de régulation de la biosynthèse de la paroi bactérienne.

Résumé

Le peptidoglycane est un biopolymère essentiel délimitant la bactérie et dont la synthèse est le produit de réactions catalysées par des complexes protéiques finement régulés spatio-temporellement. Le point culminant de ce processus est l'assemblage et l'insertion des chaînes réticulées de peptidoglycane dans la structure déjà existante par les PBPs, cibles des β-lactames. Les travaux présentées ici portent sur deux importants régulateurs peu caractérisés au niveau atomique, les Lpos (chez *Escherichia coli*), qui stimulent les activités des PBPs. En utilisant principalement la RMN, les premières structures à haute-résolution de ces protéines ont été obtenues et quelques interactions ont pu être étudiées. Les résultats présentés permettent de mieux comprendre comment ces facteurs, ancrés à la membrane externe, atteignent leur cible et régulent directement la synthèse du peptidoglycane.

Mots-clés: Peptidoglycane, Lpos, régulation, RMN

NMR studies of mechanisms regulating the biosynthesis of the bacterial cell wall.

Abstract

Peptidoglycan is an essential biopolymer which surrounds the bacterial cell. Its biosynthesis is the product of large macromolecular complexes tightly regulated in space and time. The peak of this process is the assembly and insertion of peptidoglycan reticulated chains in the existing network by Penicillin-Binding Proteins (PBPs), targets of β-lactam antibiotics. The work presented here focuses on two important regulators of peptidoglycan growth lacking atomic-scale characterization, the Lpo proteins (in *Escherichia coli*). These proteins are directly stimulating PBPs activities. Using mainly NMR, their structure was obtained, for the first time, and, for one of them, the interaction with its protein partner was investigated. The results provide new insights on how these proteins reach their targets from the outer-membrane and on how their regulatory function is determined.

Key words: Peptidoglycan, Lpos, regulation, NMR